ISSN 2307-8960 (online)

World Journal of *Clinical Cases*

World J Clin Cases 2022 April 16; 10(11): 3321-3638

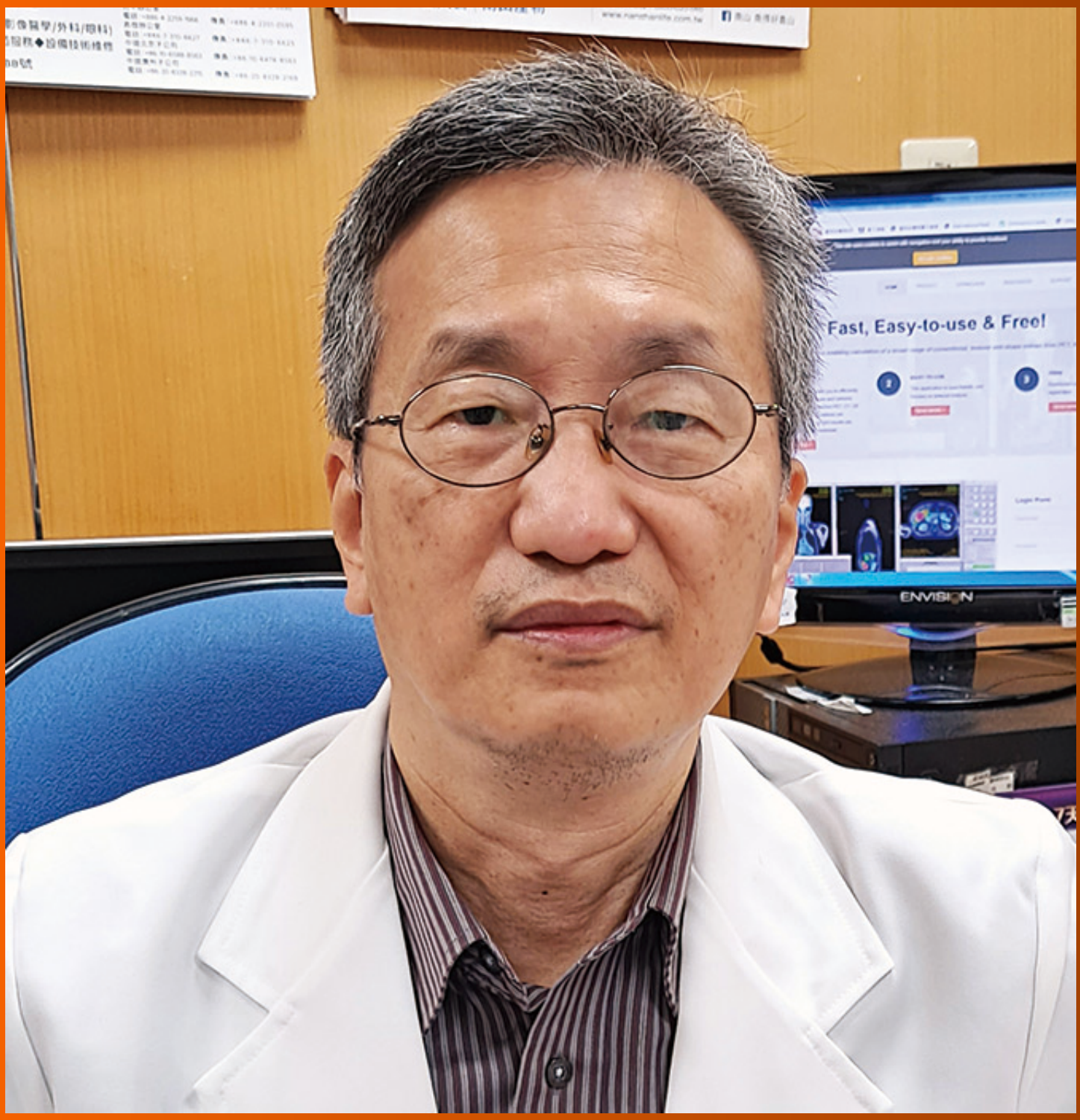

Published by Baishideng Publishing Group Inc

World Journal of Clinical Cases

Contents Thrice Monthly Volume 10 Number 11 April 16, 2022

CASE REPORT

World Journal of Clinical Cases

Thrice Monthly Volume 10 Number 11 April 16, 2022

Contents

World Journal of Clinical Cases

Thrice Monthly Volume 10 Number 11 April 16, 2022

Contents

ABOUT COVER

Editorial Board Member of *World Journal of Clinical Cases*, Chi-Yuan Yeh, MD, PhD, Assistant Professor, Chief Doctor, radiation oncology, Tungs' Taichung MetroHarbor Hospital, Taichung 43503, Taiwan. peteryeh46@gmail.com

AIMS AND SCOPE

The primary aim of *World Journal of Clinical Cases* (*WJCC*, *World J Clin Cases*) is to provide scholars and readers from various fields of clinical medicine with a platform to publish high-quality clinical research articles and communicate their research findings online.

WJCC mainly publishes articles reporting research results and findings obtained in the field of clinical medicine and covering a wide range of topics, including case control studies, retrospective cohort studies, retrospective studies, clinical trials studies, observational studies, prospective studies, randomized controlled trials, randomized clinical trials, systematic reviews, meta-analysis, and case reports.

INDEXING/ABSTRACTING

The *WJCC* is now indexed in Science Citation Index Expanded (also known as SciSearch®), Journal Citation Reports/Science Edition, Scopus, PubMed, and PubMed Central. The 2021 Edition of Journal Citation Reports® cites the 2020 impact factor (IF) for *WJCC* as 1.337; IF without journal self cites: 1.301; 5-year IF: 1.742; Journal Citation Indicator: 0.33; Ranking: 119 among 169 journals in medicine, general and internal; and Quartile category: Q3. The *WJCC*'s CiteScore for 2020 is 0.8 and Scopus CiteScore rank 2020: General Medicine is 493/793.

RESPONSIBLE EDITORS FOR THIS ISSUE

NAME OF JOURNAL

World Journal of Clinical Cases

ISSN

ISSN 2307-8960 (online)

LAUNCH DATE

April 16, 2013

FREQUENCY

Thrice Monthly

PUBLICATION DATE

April 16, 2022

World Journal of Clinical Cases

Submit a Manuscript: https://www.f6publishing.com

World J Clin Cases 2022 April 16; 10(11): 3321-3333

DOI: 10.12998/wjcc.v10.i11.3321

ISSN 2307-8960 (online)

REVIEW

Encouraging specific biomarkers-based therapeutic strategies for hepatocellular carcinoma

Min Yao, Jun-Ling Yang, De-Feng Wang, Li Wang, Ying Chen, Deng-Fu Yao

Specialty type: Gastroenterology and hepatology

Provenance and peer review: Invited article; Externally peer reviewed.

Peer-review model: Single blind

Peer-review report's scientific quality classification

Grade A (Excellent): 0
Grade B (Very good): 0
Grade C (Good): C
Grade D (Fair): 0
Grade E (Poor): 0

P-Reviewer: Li Y

Received: March 19, 2021
Peer-review started: March 19, 2021
First decision: May 1, 2021
Revised: May 10, 2021
Accepted: May 25, 2021
Article in press: May 25, 2021
Published online: April 16, 2022

Min Yao, Research Center of Clinical Medicine & Department of Immunology, Medical School of Nantong University, Nantong 226001, Jiangsu Province, China

Jun-Ling Yang, De-Feng Wang, Deng-Fu Yao, Research Center of Clinical Medicine, Affiliated Hospital of Nantong University, Nantong 226001, Jiangsu Province, China

Li Wang, Department of Medical Informatics, Medical School of Nantong University, Nantong 226001, Jiangsu Province, China

Ying Chen, Department of Oncology, Affiliated Second Hospital of Nantong University, Nantong 226001, Jiangsu Province, China

Corresponding author: Deng-Fu Yao, MD, PhD, Director, Full Professor, Research Center of Clinical Medicine, Affiliated Hospital of Nantong University, No. 20 West Temple Road, Nantong 226001, Jiangsu Province, China. yaodf@ahnmc.com

Abstract

The prevention, early discovery and effective treatment of patients with hepatocellular carcinoma (HCC) remain a global medical challenge. At present, HCC is still mainly treated by surgery, supplemented by vascular embolization, radio frequency, radiotherapy, chemotherapy and biotherapy. The application of multikinase inhibitor sorafenib, chimeric antigen receptor T cells, or PD-1/PD-L1 inhibitors can prolong the median survival of HCC patients. However, the treatment efficacy is still unsatisfactory due to HCC metastasis and postoperative recurrence. During the process of hepatocyte malignant transformation, HCC tissues can express and secrete many types of specific biomarkers, or oncogenic antigen molecules into blood, for example, alpha-fetoprotein, glypican-3, Wnt3a (one of the key signaling molecules in the Wnt/β-catenin pathway), insulin-like growth factor (IGF)-II or IGF-I receptor, vascular endothelial growth factor, secretory clusterin and so on. In addition, combining immunotherapy with non-coding RNAs might improve anti-cancer efficacy. These biomarkers not only contribute to HCC diagnosis or prognosis, but may also become molecular targets for HCC therapy under developing or clinical trials. This article reviews the progress in emerging biomarkers in basic research or clinical trials for HCC immunotherapy.

Key Words: Hepatocellular carcinoma; Immunotherapy; Carcinoembryonic proteins; Specific biomarkers; Wnt/β-catenin pathway; Signal molecules

Core Tip: Tissues in hepatocellular carcinoma (HCC) or hepatocyte malignant transformation can express and secrete a variety of molecules such as specific biomarkers or oncogenic antigens into blood. These biomarkers not only contribute to the diagnosis or prognosis of HCC, but may also become molecular targets for HCC therapy under developing or clinical trials. This article reviews the recent novel progress of some emerging biomarkers in basic studies or clinical trials for HCC immunotherapy.

Citation: Yao M, Yang JL, Wang DF, Wang L, Chen Y, Yao DF. Encouraging specific biomarkers-based therapeutic strategies for hepatocellular carcinoma. *World J Clin Cases* 2022; 10(11): 3321-3333
URL: https://www.wjgnet.com/2307-8960/full/v10/i11/3321.htm
DOI: https://dx.doi.org/10.12998/wjcc.v10.i11.3321

INTRODUCTION

The prevention, early monitoring or diagnosis and accurate or effective treatment of hepatocellular carcinoma (HCC) are still urgent medical problems[1,2]. The occurrence of HCC is mainly associated with chronic persistent infection of hepatitis B virus (HBV) or hepatitis C virus (HCV), intake of chemical carcinogens, and nonalcoholic fatty liver disease (NAFLD)[3]. In the past decade, NAFLD has become a leading cause of chronic hepatitis and liver cirrhosis, as well as an important risk factor for HCC[4]. Innate and adaptive immunity play a pivotal role in determining tumor control *vs* progression. Genomic instability and abnormal signaling in the setting of chronic liver inflammation that promotes fibrogenesis and angiogenesis lead to tumorigenesis, and it is necessary to determine how they may be exploited in the development of novel therapeutics[5]. The activation of oncogenes or HCC-related genes, inactivation of anti-oncogenes or activation of some oncogenes during the embryonic period can induce malignant transformation of hepatocytes[5], many types of specific markers can be expressed, and then secreted into blood during the process of initiation, promotion and evolution[1]. Notably, HCC oncoimmunology depends on diverse genetic and environmental factors that together shape cancer-promoting inflammation and immune dysfunction-critical processes that control HCC malignant progression and response to therapy[6,7].

Currently, HCC is still treated mainly by surgery, with auxiliary vascular embolization, radio frequency, radiotherapy, chemotherapy, and biological therapy[8,9]. Application of the multikinase inhibitor sorafenib can prolong the median survival of HCC patients. However, its efficacy in HCC treatment remains unsatisfactory due to tumor metastasis or postoperative occurrence[10,11]. Undoubtedly, the integration of data obtained from both preclinical models and human studies can help to accelerate the identification of robust predictive biomarkers of response to targeted or immune-therapy[12,13]. HCC tissues express specific antigens such as the key molecules of HCC-related signal pathways, growth factors and receptors, vascular endothelial growth factor (VEGF), and the products of oncogenes that mediated tumor progression and could be potential molecular targets for anti-cancer therapy with high specificity and application prospects[14,15]. This review presents new advances in a few promising carcinoembryonic biomarkers for HCC immunotherapy from basic studies or clinical trials.

ALPHA-FETOPROTEIN

A glycoprotein of alpha-fetoprotein (AFP) synthesized from fetal liver or HCC tissues[16], consisting of 609 single-chain amino acid polypeptides and containing 24 leading signal points (9 ~ 10 amino acid) residues located in three N-terminal domains, the major histocompatibility complex (MHC) class I or II molecules recognize these precursor signals and present them to $CD4^+$ T cells and $CD8^+$ T cells, and the activated T cells recognize the body's immunodominant or sub-immunodominant epitopes[17]. Amino acid peptide sequences and immunogenicity of human AFP epitopes are shown in Table 1. These immunogenic or sub-immunogenic AFP peptide chains could play an immunomodulatory role in humans, as they have the function and ability of a polypeptide vaccine, and could induce or stimulate anti-AFP specific immune responses.

AFP peptide chains have several fragments showing immunodominant or sub- immunodominant epitopes, which can be recognized by the MHC-I molecules, and specifically induce T cells to activate or recognize AFP antigen. AFP positive peripheral blood mononuclear cells (PBMC) containing five human leukocyte antigen (HLA)-A*24:02 restricted T cell epitopes, AFP-derived peptide induces cytotoxic T lymphocytes (CTL) to produce interferon-γ (INF-γ), which can kill AFP-positive cancer cells.

Table 1 Amino acid peptide sequences and immunogenicity of alpha-fetoprotein epitopes

No.	Starting	Numbers	Fragment	Immunogenicity
1	7	9	IFLIFLLNF	Sub-immunodominant Ag
2	137	9	PLFQVPEPV	Immunodominant Ag
3	150	9	AYEEDRETF	Sub-immunodominant Ag
4	158	9	FMNKFIYEI	Immunodominant Ag
5	218	9	LLNQHACAV	Sub-immunodominant Ag
6	235	9	FQAITVTKL	Sub-immunodominant Ag
7	249	10	KVNFTEIQKL	Immunodominant Ag
8	307	9	TTLERGQCII	Sub-immunodominant Ag
9	321	9	KPEGLSPNL	Immunodominant Ag
10	325	10	GLSPNLNRFL	Immunodominant Ag
11	357	9	EYSRRHPQL	Immunodominant Ag
12	364	10	QLAVSVILRV	Immunodominant Ag
13	403	9	KYIQESQAL	Immunodominant Ag
14	414	9	RSCGLFQKL	Immunodominant Ag
15	424	9	EYYLQNAFL	Immunodominant Ag
16	434	9	AYTKKAPQL	Immunodominant Ag
17	485	10	CIRHEMTPV	Sub-immunodominant Ag
18	492	9	PVNPGVGQC	Sub-immunodominant Ag
19	503	9	SYANRRPCF	Sub-immunodominant Ag
20	507	10	NRRPCFSSLV	Sub-immunodominant Ag
21	542	9	GVALQTMKQ	Immunodominant Ag
22	547	10	TMKQEFLINL	Sub-immunodominant Ag
23	555	9	NLVKQKPQI	Sub-immunodominant Ag
24	591	9	CFAEEGQKL	Sub-immunodominant Ag

Ag: Antigen; Fragment: Fragment of alpha-fetoprotein (AFP) peptide chain; Numbers: Amino acid numbers of AFP peptide chain; Starting: Starting point of AFP peptide chain.

Although it has been shown in clinical trials, the function of dendritic cells (DC), specific CTL, and $CD8^+$ T cell response, targeting therapy for AFP positive cancer cells remains to be studied. The T cell receptor (TCR) has been prepared by induction and screening *in vitro*, which can specifically recognize and bind AFP/HLA-A*02 antigen that is restricted to AFP158-166 peptide (FMNKFIYEI) to lay the foundation for HCC immuno-therapy[18]. A novel HLA-A*24:02 antigen was found to be more common than the HLA-A*02:01 among Asian HCC patients. Its restrictive peptide (KWVESIFLIF, AFP2-11 signal) was found to be soluble in healthy human monocyte AFP 2-11-HLA-A*24:02-specific TCR (KWV3.1). T cells could be activated specifically and kill AFP-positive T2-A24 HCC cells that contained AFP 2-11 and HLA-A*24:02$^+$ antigen, indicating that AFP$^+$HLA-A*24:02$^+$ antigen might be a new immunotherapeutic target for HCC[19].

The combination of anti-CTL-A-4 therapy (tremelimumab) together with ablation in advanced HCC cases has shown that killing tumors by direct methods can result in the immune system being activated or switched on. There are new drugs available known as immune checkpoint inhibitors (ICIs) which can enhance the anti-HCC effect. In patients treated with tremelimumab, blood $CD4^+$-HLA-DR^+, $CD4^+$PD-1^+, $CD8^+$HLA-DR^+, $CD8^+$PD-1^+, $CD4^+ICOS^+$, and $CD8^+ICOS^+$ T cells increased, the patients with higher CD^+PD-1^+ cells responded well to treatment, with increasing specific $CD8^+$PD-1 T cells for AFP and survivin, and higher $CD3^+$T cells for tumor infiltration, suggesting that tremelimumab with ablation is a novel potential method for increasing $CD8^+$ T cells and decreasing circulating HCV, and an effective therapy for advanced HCC patients[20].

ANGIOGENIC FACTORS

Most patients with HCC are diagnosed at an advanced stage of disease. Until recently, systemic treatment options that showed survival benefits in HCC have been limited to tyrosine kinase inhibitors, antibodies targeting oncogenic signaling pathways or VEGF receptors[21]. Angiogenesis plays an important role in HCC progression, and VEGF and angiopoietin (Ang) are key drivers of tumor angiogenesis. A better understanding of the relation between VEGF and angiogenesis or progression may reveal their potential as biomarkers for liver cancer diagnosis and therapy. VEGF-targeting strategies already represent an important component of today's systemic treatment for HCC, whereas targeting the Ang/Tie2 signaling pathway may harbor future potential in this context due to reported beneficial anticancer effects when targeting this pathway[22,23]. Following a decade of negative Phase III trials since the approval of sorafenib, more recently several drugs have proven efficacy both in first line *vs* sorafenib (lenvatinib) or in second line *vs* placebo (regorafenib, cabozantinib, ramucirumab/Cyramza®). A fully human anti-VEGFR-2 recombinant IgG1 monoclonal antibody (ramucirumab) has been approved as monotherapy for HCC patients with AFP levels over 400 ng/mL who have been treated with sorafenib, with significantly prolonged overall survival (OS) and progression-free survival. Its safety profile was consistent with that expected for agents targeting the VEGF/VEGFR axis. The potential clinical development of systemic treatments for HCC, focuses on combination therapies with immunotherapy and treatment sequences as a way to maximize survival benefit[24,25].

The HCC microenvironment is characterized by dysfunction of the immune system through multiple mechanisms, including accumulation of various immunosuppressive factors, recruitment of regulatory T cells and myeloid-derived suppressor cells, and induction of T cell exhaustion accompanied by the interaction between immune checkpoint ligands and receptors. ICIs interfere in this interaction and have altered the therapeutic landscape of multiple cancer types including HCC. HCC patients with different levels of liver function, tumor size, and number of lesions may all have intermediate-stage disease according to the BCLC staging system. Their treatment includes conventional or drug-eluting bead transarterial chemoembolization, yttrium-90 radioembolization, thermal ablation, bland embolization, and combination therapy with VEGF inhibitors or ICIs. Clinical evidence supports the available locoregional treatment options for intermediate-stage HCC[26]. Although optimal sequencing is an area of ongoing investigation, multiple targeted therapies have improved OS in intermediate or advanced HCC[27]. Several targeted agents including multi-tyrosine kinase inhibitors and immunotherapy agents have been approved for use beyond the frontline setting in advanced HCC patients, and combining therapeutic strategies is an evolving approach showing early promise[23,28]. The success of PD-1 monotherapy, combining regimens with PD-1/PD-L1 inhibitors plus VEGF targeted agents has shown positive results in various malignancies including HCC. These innovative approaches enhance the intensity of cancer-directed immune responses and will potentially impact the outcome of this aggressive disease[29].

GLYPICAN-3

With regard to HCC, a promising antigen appears to be glypican-3 (GPC3) which is over-expressed in HCC tissues and has been associated with worse disease-free survival and OS. GPC3 is involved in many signaling cascades that promote cell growth and invasion, including the Wnt pathway that is well-known for its role in embryogenesis. GPC3 as an oncofetal proteoglycan anchored to the cell membrane of HCC, and is normally detected in the fetal liver but not in the healthy adult liver[30,31]. However, abnormal GPC3 in tissues or sera of HCC patients is expressed as GPC3 mRNA gene transcription or protein levels, and predicts a poor prognosis of HCC. Mechanistic studies have revealed that GPC3 functions by binding to molecules such as the Wnt/β-catenin signaling or growth factors during HCC formation and progression. Moreover, specific serum GPC3 has been used as a diagnostic or prognostic serological marker, and a molecular target for molecular imaging or therapeutic intervention in HCC[32-34]. GPC3 as a molecular target for HCC immunotherapy is shown in Table 2. To date, GPC3-targeted magnetic resonance imaging, positron emission tomography, and near-infrared imaging have investigated the early stage of HCC, and immunotherapeutic protocols targeting GPC3 have been developed, including the use of humanized anti-GPC3 cytotoxic antibodies, peptide/DNA vaccines, immuno-toxin therapies, and genetic therapies.

Different synergisms have been postulated based on the potential interplay between anti-angiogenic drugs and immunotherapy, with several clinical trials currently ongoing. As the most extensively tested combination regimens for advanced HCC comprise anti-PD-1/anti-PD-L1 agents plus anti-angiogenic agents, oncogenic GPC3 is an ideal promising candidate for HCC immunotherapy as it is highly expressed in cancerous tissues but limited in normal livers. Recently, the adoptive transfer of hGPC3-specific chimeric antigen receptor T (CAR-T) cells for HCC treatment has been conducted in clinical trials. Due to rigid construction, conventional CAR-T cells have some intrinsic limitations, such as uncontrollable overactivation and inducing severe cytokine release syndrome. By using co-culturing assays and a xenograft mouse model, the *in vitro* and *in vivo* cytotoxicity and cytokine release of the split

Table 2 Glypican-3 as molecule-target for hepatocellular carcinoma immunotherapy

Group	Name	Species	Epitopes	Verifying/applying
Antibody	M18D04/19B11	Mouse	N-terminal (aa: 25-358)	Basic studies
	A1836A	Mouse	N- terminal	Basic studies
	GPC3-C02	Mouse	C- terminal	Basic studies
	GC33	Mouse	C-terminal (aa: 524-563)	Preclinical trial studies
	hGC33	Human	C- terminal (aa: 524-563)	Clinical trial-II
	HS20	Human	Heparan sulfate chain	Preclinical trial
	sGPC3	Human	–	Preclinical trial
Vaccines	$GPC3_{298-306}$	Mouse	298-306 peptide	Clinical trial-II
	$GPC3_{144-152}$	Mouse	144-152 peptide	Clinical trial-II
miRNA	miR-219-5p	Human	–	*In vitro* or *in vivo* studies
	miR-520c-3p	Human	–	*In vitro* studies
	miR-1271	Human	–	*In vitro* studies
shRNA	GPC3 shRNA	Human	–	*In vitro* or *in vivo* studies
siRNA	GPC3 siRNA	Human	–	*In vitro* or *in vivo* studies

GPC-3: Glypican-3; aa: Amino acid; miR: MicroRNA; shRNA: Small hairpin RNA; siRNA: Small interfering RNA.

anti-hGPC3 CAR-T cells were evaluated against various HCC cell lines and compared with conventional CAR-T cells. *In vitro* data demonstrated that split anti-hGPC3 CAR-T cells could recognize and lyse hGPC3-positive HepG2 or Huh7 cells in a dose-dependent manner. Impressively, the split anti-hGPC3 CAR-T cells produced and released a significantly lower amount of pro-inflammatory cytokines, including IFN-γ, TNF-α, IL-6, and GM-CSF, than conventional CAR-T cells. When injected into immune-deficient mice inoculated subcutaneously with HepG2 cells, the split anti-hGPC3 CAR-T cells could suppress HCC growth, but released significantly lower levels of cytokines than conventional CAR-T cells. The split anti-hGPC3 CAR-T cells reduced the level of cytokine release, and represent a more versatile and safer alternative to conventional CAR-T cells for HCC treatment[35,36]. The most recent data indicate novel combination strategies and targets, and a future role for molecular therapies in the treatment of advanced HCC. Current barriers in CAR-T therapy include its high production cost and the need to identify validated extracellular HCC-specific antigens[33,37].

WNT3a

Several signaling pathways involved in HCC have been studied, including STAT3- NFκB, JAK-STAT, RAS MAPK, PI3K-AKT-mTOR and Wnt-*β*-catenin. Of these, cascades involving mitogen-activated protein kinase (MAPK) emerge as key regulators of HCC. Both HBV and HCV infection can induce activation of the Wnt/β-catenin signal pathway and participate in HCC progression[38,39]. Oncogenic HBx of HBV can activate Src kinase to inhibit GSK3 activity and induce intracellular β-catenin accumulation, promote DNA methyl-transferase I expression and Wnt3a to bind and silence secreted frizzled related protein 1 and 5[40]. HBx can reduce the inhibitory role of deacetylase 1 to β-catenin, and activation of the Wnt pathway promotes HCC development[41]. Also, the core protein of HCV can promote Wnt3a expression, induce TCF dependent transcription, inhibit GSK3, increase and stabilize intracellular β-catenin to nucleus transport, and up-regulate the expression of cyclinDl, c-myc, WISP2, Wnt3a, Wnt1 and CTGF to promote HCC growth, and DNA synthesis for HCC progression[42]. Wnt3a is a critical signal molecule among the 19 mammalian Wnt proteins. A higher level of Wnt3a expression was only found in the sera or tissues of HCC patients from a cohort of cases with chronic liver diseases [43,44], and it is the first report of Wnt3a as a novel specific marker for HCC diagnosis and prognosis[45, 46].

Abnormal Wnt3a expression is involved in the development and metastasis of HCC[47], and may be a novel strategy for HBV or HCV-related HCC therapy. High hepatic LINC00662 correlated with poor survival of HCC patients[48,49], and might up-regulate Wnt3a expression by competitively binding miR-15a, miR-16 and miR-107, with tumor-associated macrophages as a major component of the HCC microenvironment, and they have been revealed to have associations with Wnt3a signaling and cancer initiation, tumor growth, metastasis, dormancy, immunity and tumor stem cell maintenance[40]. Wnt3a

is one of HCC-related Wnt signals exhibiting numerous genetic abnormalities as well as epigenetic alterations including modulation of DNA methylation. Targeted *Wnt3a* gene transcription might be an effective molecule-targeted therapy. The novel Crispr/Cas9-gsRNA lentiviral vector system with the advantages of higher targeting accuracy has been successfully used to inhibit *Wnt3a* in liver cancer cell lines at the mRNA level *in vitro* and confirmed at the protein level *in vivo* in transplanted tumor studies [44,50].

The inhibitory effect of Wnt3a on the proliferation of HCC cells or HCC xenograft growth has been demonstrated and interfering with *Wnt3a* could significantly inhibit the expression of down-stream β-catenin and related-signal molecules[51]. The xenograft model of knockout *Wnt3a* in HepG2 cells resulted in slower growth, and a significant reduction in tumor size or loss of weight. The molecular mechanism of the Wnt3a cascade reaction involving multiple targets, can block upstream GPC-3 signals and downstream β-catenin to nucleus transport[52,53], and inhibiting or delaying HCC progression can be carried out using specific antibodies (OMP-54F28, OTSA101)[54] and small size peptide SAH-BCL-9 [55]. The abnormal liver or circulating Wnt3a in HCC has provided initial evidence, and the tumor volume after intervening in Wnt3a mRNA transcription with specific shRNA was 355.0 ± 99.9 mm^3 in the intervention group which was significantly lower than that (869.4 ± 222.5 mm^3) in the negative group, and the time to tumor formation in the intervention group was longer than that in the negative group; the tumor weight (0.35 ± 0.11 g) in the intervention group was markedly lower than that (0.88 ± 0.20 g) in the negative group. Immunohistochemistry confirmed that Wnt3a was strongly inhibited in the intervention group[56], and indicated that targeted-Wnt3a signaling could result in effective inhibition of HCC growth.

CLUSTERIN

Secretory clusterin (sCLU) is a stress-induced heterodimer sulfated glycoprotein, located on chromosome 8q21-q12, which is highly conserved between species and has a cytoprotective effect. Its biological function as a small molecule partner is almost similar to that of heat shock protein[57]. Basic and clinical studies have shown that sCLU expression was low in normal liver tissues and its activation during the malignant transformation of hepatocytes was progressively over-expressed[58,59], which was closely associated with HCC progression by contributing to angiogenesis, chemo-resistance, cell survival, and metastasis[60]. The positive rate of hepatic sCLU expression was up to 73.3% in stage I HCC by immunohistochemical analysis. Its expression at the mRNA or protein level was increased with clinical staging of HCC, which indicated that sCLU could be a biomarker for differentiating benign from malignant liver diseases[61].

Recurrence and metastasis after hepatectomy are the main causes of poor prognosis of HCC[62]. Hepatic sCLU plays an important role in the proliferation, multidrug resistance, invasion and metastasis of HCC cells[63,64]. sCLU mediated the expression of MMP-2, p-AKT and E-cadherin in HCC BEL-7402 or SMMC-7721 cell lines, and down-regulating sCLU expression can significantly reduce the invasive ability of HCC cells by the selective COX-2 inhibitor meloxicam plus specific sCLU-shRNA plasmids[65, 66]. These data indicated that sCLU is a new effective target for the occurrence, invasion and metastasis of HCC, and should have a bright future in HCC immunotherapy.

INSULIN-LIKE GROWTH FACTOR AXIS

The hepatic insulin-like growth factor (IGF) axis contains ligands, receptors, substrates, and ligand binding proteins. Accumulating data have demonstrated that aberrant IGF signaling might lead to malignant transformation of hepatocytes or HCC progression, in particular, IGF-II or IGF-I receptor (IGF-IR) are key molecules in hepatocarcinogenesis[67] or rat xenograft models[68], and affect the molecular pathogenesis of HCC, thus providing the rationale for targeting the IGF axis in HCC[69]. The biological activities of IGF-II or IGF-IR not only promote HCC cell proliferation or xenograft growth, but also confer resistance to standard treatments[70]. Several strategies targeting this system including monoclonal antibodies against IGF-1R or small molecule inhibitors of the tyrosine kinase function of IGF-1R are under active investigation. For example, DX-2647, a recombinant human antibody, potently neutralizes the action of IGF-II, which is overexpressed in HCC[71] and impairs xenograft growth of the Hep3B but not HepG2 cell line with high p-STAT3 levels, suggesting that STAT3 activation is one pathway that mediates resistance to IGF-II-targeted therapy in HCC[72].

The over-expression of hepatic IGF-IR in human HCC promotes HCC cell proliferation, and attaching importance to IGF-IR might improve the prognostic or therapy of HCC[73]. Enhancer of zeste 2 polycomb repressive complex 2 subunit (EZH2) is a regulator of promoted IGF-IR induced sorafenib resistance of HCC *in vitro* by directly transcriptionally repressing a set of microRNAs including miR-101, miR-122, miR-125b, and miR-139[74-76]. A model of an EZH2-miRNAs-IGF-IR regulatory axis might provide insights into how to reverse sorafenib resistance in HCC. Silencing the IGF-IR gene by a specific shRNA to induce inhibition of cell proliferation *in vitro* or rat xenograft growth *in vivo* may be a

novel molecular-targeted therapy for HCC. Several strategies targeting this system including monoclonal antibodies against IGF-IR and inhibitors of the tyrosine kinase function of IGF-IR are under active investigation. Gene-specific shRNA against IGF-signaling molecules as well as IGF-IR selective receptor tyrosine kinase (RTK)-inhibitors (tyrphostins) may therefore offer new therapeutic options[77,78]. However, as a specific shRNA is currently not applicable in HCC therapy, selective RTK-inhibitors represent the most promising approach for future therapeutic strategies.

SYNERGY OF NON-CODING RNAS

While immunotherapy holds great promise for combating cancer, its limited efficacy due to an immunosuppressive tumor microenvironment and systemic toxicity hinder the broader application of immunotherapy[79,80]. Combinatorial immunotherapy approaches that use a highly efficient and tumor-selective gene carrier can improve anticancer efficacy and circumvent the systemic toxicity. HCC is one of the multi-genetic diseases, and multiple studies have highlighted the key roles of noncoding RNAs (ncRNAs) in the chemo-resistance of HCC such as biomarkers and functional modulation of the cellular response to sorafenib[81-83]. Targeted chemotherapeutic agent, sorafenib, is known to show a statistically significant but limited OS advantage in advanced HCC, linked with the modulation of several intracellular signaling pathways through diverse operating biomolecules including ncRNAs[84-86]. Accumulated evidence has demonstrated that ncRNAs (miRNAs, long ncRNAs or lncRNAs, and circular RNA or circRNA) could serve as biomarkers in the diagnosis, prognosis, and treatment of HCC [87,88] and have been well-documented to participate in HCC progression with promoting or inhibiting roles[89,90].

Interestingly, varied responses to miRNAs have been linked with the modulation of several intracellular signaling pathways[91]. An abnormality of miR-218 expression was investigated in human HCC tissues or HCC cell lines to evaluate its function and the underlying mechanisms of HCC. Gain-of-function and loss-of-function assays indicated forced expression of miR-218 by inhibited HCC cell migration/invasion and reversed epithelial-mesenchymal transition to mesenchymal-epithelial transition. Serpine mRNA binding protein 1 (SERBP1) is a target gene of miR-218, and targeting the miR-218/SERBP1 signal pathway that inhibits malignant phenotype formation might be a potential novel strategy for HCC therapeutics, as miR-218 functions as a HCC suppressor and is involved in many biological processes such as tumor initiation, development, and metastasis[92]. Nanotechnology-enabled dual delivery of siRNA and plasmid DNA that selectively targets and reprograms the immune-suppressive tumor microenvironment has been shown to improve HCC immunotherapy[93-95].

HCC-associated circRNAs are abundant, and their over/low expression might promote/inhibit HCC cell proliferation or tumor growth[96-98]. An abnormality of circ-homer1 in HCC cells or tissues was related to tumor size, lymph node metastasis, high clinical staging and poor prognosis. The mechanism of circ-homer1 over-expression promoted HCC growth or invasiveness *via* the mir-1322/cxc16 axis[99]; conversely, interfering with circ-homer1 activation inhibited the proliferation, migration and invasion of liver cancer cells *via* apoptosis. The circ-0051443 from circulating exosomes or HCC tissues regulated BAK1 expression by combining with mir-331-3p to promote cell apoptosis or cell cycle arrest in HCC, and inhibit the biological behavior of HCC cells *in vivo* or nude mice HCC xenografts[100]. Another interesting study also showed that has_circ_0008450 expression in HCC tissues or cells might inhibit HCC progression by regulating the mir-214-3p/ezh2 axis[101,102]. These data suggested that specific ncRNAs were useful molecular targets for HCC therapy.

CONCLUSION

In conclusion, HCC is a multi-gene variant malignant tumor with DNA methylation, microRNA, lncRNA expression and immune response[103]. Immunotherapy for HCC has begun to produce better results, and HCC-specific molecules may be combined with comprehensive interventions such as surgery, interventional therapy, radiotherapy, and chemotherapy to improve the efficacy and prolong the survival time of HCC patients[104]. Despite the rapid development of genomics and proteomics, advances in molecular pathology, pharmacology and genetic engineering, DNA splicing, gene silencing, transcription interference, and monoclonal antibodies for more specific and less side effects immune therapy techniques[105] that can directly block the signaling molecules involved in HCC growth related signaling pathways (Figure 1) or serve as molecular targets such as radionuclide, drug carriers, and immunotherapy play a unique role in the specific or comprehensive treatment of HCC.

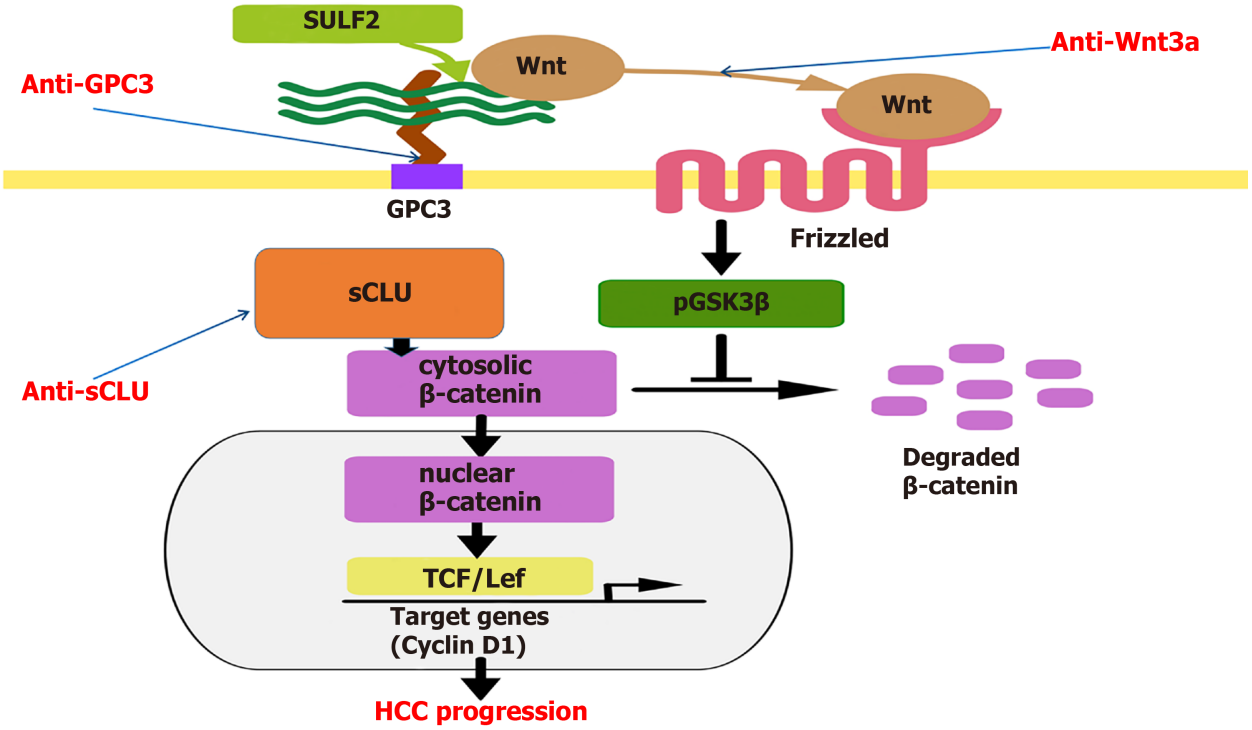

Figure 1 Some signals in the Wnt/β-catenin pathway by anti-signaling antibodies or intervening in their gene transcription to inhibit hepatocellular carcinoma growth. Using anti-signaling molecule antibodies or intervening in their gene transcription to inhibit Wnt/β-catenin pathway activation could suppress proliferation of hepatocellular carcinoma (HCC) cells or HCC growth. GPC-3: Glypican-3; HCC: Hepatocellular carcinoma; sCLU: Secretory clusterin; TCF: T-cell factor; SULF2: Sulfatase 2; pGSK3β: Phosphorylated glycogen synthase kinase 3β.

FOOTNOTES

Author contributions: Yao M, Yang JL, and Wang DF contributed equally to this work and wrote the first draft of the paper; Wang L and Chen Y performed the literature search for the manuscript; Yao M and Yao DF revised the manuscript and edited all drafts of the paper; all authors approved the final version of the manuscript.

Supported by the National Natural Science Foundation of China, No. 84673241, No. 81873915 and No. 31872738; and Nantong S&T Development Plan, No. MS12020021, and No. MS12019016.

Conflict-of-interest statement: The authors report no conflicts of interest.

Country/Territory of origin: China

ORCID number: Min Yao 0000-0002-5473-0186; Jun-Ling Yang 0000-0003- 2882-0599; De-Feng Wang 0000-0003-0033-6447; Li Wang 0000-0003-2838-9807; Ying Chen 0000-0003-3585-1289; Deng-Fu Yao 0000-0002-3448-7756.

S-Editor: Gong ZM
L-Editor: Webster JR
P-Editor: Yu HG

REFERENCES

1 **Craig AJ**, von Felden J, Garcia-Lezana T, Sarcognato S, Villanueva A. Tumour evolution in hepatocellular carcinoma. *Nat Rev Gastroenterol Hepatol* 2020; **17**: 139-152 [PMID: 31792430 DOI: 10.1038/s41575-019-0229-4]
2 **Forner A**, Reig M, Bruix J. Hepatocellular carcinoma. *Lancet* 2018; **391**: 1301-1314 [PMID: 29307467 DOI: 10.1016/S0140-6736(18)30010-2]
3 **Chen JG**, Zhu J, Zhang YH, Zhang YX, Yao DF, Chen YS, Lu JH, Ding LL, Chen HZ, Zhu CY, Yang LP, Zhu YR,

Qiang FL. Cancer survival in Qidong between 1972 and 2011: A population-based analysis. *Mol Clin Oncol* 2017; **6**: 944-954 [PMID: 28588795 DOI: 10.3892/mco.2017.1234]
4 **Negro F**. Natural history of NASH and HCC. *Liver Int* 2020; **40** Suppl 1: 72-76 [PMID: 32077608 DOI: 10.1111/liv.14362]
5 **Wang SZ**, Lee SD, Sarkar D, Lee HM, Khan A, Bhati C, Sharma A, Kumaran V, Bruno D, Cotterell A, Levy MF. Immunological characterization of hepatocellular carcinoma. *Hepatoma Res* 2021; **7**: 6 [DOI: 10.20517/2394-5079.2020.113]
6 **Hou J**, Zhang H, Sun B, Karin M. The immunobiology of hepatocellular carcinoma in humans and mice: Basic concepts and therapeutic implications. *J Hepatol* 2020; **72**: 167-182 [PMID: 31449859 DOI: 10.1016/j.jhep.2019.08.014]
7 **Rebouissou S**, Nault JC. Advances in molecular classification and precision oncology in hepatocellular carcinoma. *J Hepatol* 2020; **72**: 215-229 [PMID: 31954487 DOI: 10.1016/j.jhep.2019.08.017]
8 **Finn RS**, Zhu AX, Farah W, Almasri J, Zaiem F, Prokop LJ, Murad MH, Mohammed K. Therapies for advanced stage hepatocellular carcinoma with macrovascular invasion or metastatic disease: A systematic review and meta-analysis. *Hepatology* 2018; **67**: 422-435 [PMID: 28881497 DOI: 10.1002/hep.29486]
9 **Doycheva I**, Thuluvath PJ. Systemic Therapy for Advanced Hepatocellular Carcinoma: An Update of a Rapidly Evolving Field. *J Clin Exp Hepatol* 2019; **9**: 588-596 [PMID: 31695249 DOI: 10.1016/j.jceh.2019.07.012]
10 **D'Agnano I**, Berardi AC. Extracellular Vesicles, A Possible Theranostic Platform Strategy for Hepatocellular Carcinoma-An Overview. *Cancers (Basel)* 2020; **12** [PMID: 31973229 DOI: 10.3390/cancers12020261]
11 **Xia S**, Pan Y, Liang Y, Xu J, Cai X. The microenvironmental and metabolic aspects of sorafenib resistance in hepatocellular carcinoma. *EBioMedicine* 2020; **51**: 102610 [PMID: 31918403 DOI: 10.1016/j.ebiom.2019.102610]
12 **Reig M**, da Fonseca LG, Faivre S. New trials and results in systemic treatment of HCC. *J Hepatol* 2018; **69**: 525-533 [PMID: 29653122 DOI: 10.1016/j.jhep.2018.03.028]
13 **Casadei-Gardini A**, Orsi G, Caputo F, Ercolani G. Developments in predictive biomarkers for hepatocellular carcinoma therapy. *Expert Rev Anticancer Ther* 2020; **20**: 63-74 [PMID: 31910040 DOI: 10.1080/14737140.2020.1712198]
14 **Luo P**, Wu S, Yu Y, Ming X, Li S, Zuo X, Tu J. Current Status and Perspective Biomarkers in AFP Negative HCC: Towards Screening for and Diagnosing Hepatocellular Carcinoma at an Earlier Stage. *Pathol Oncol Res* 2020; **26**: 599-603 [PMID: 30661224 DOI: 10.1007/s12253-019-00585-5]
15 **Cheng AL**, Hsu C, Chan SL, Choo SP, Kudo M. Challenges of combination therapy with immune checkpoint inhibitors for hepatocellular carcinoma. *J Hepatol* 2020; **72**: 307-319 [PMID: 31954494 DOI: 10.1016/j.jhep.2019.09.025]
16 **Li XJ**, Shao DH, He ML, Liang GW. Association of Common Variants in HNF1A Gene with Serum AFP Level in Healthy Chinese Individuals and HCC Patients. *Dis Markers* 2019; **2019**: 6273497 [PMID: 31915469 DOI: 10.1155/2019/6273497]
17 **Docta RY**, Ferronha T, Sanderson JP, Weissensteiner T, Pope GR, Bennett AD, Pumphrey NJ, Ferjentsik Z, Quinn LL, Wiedermann GE, Anderson VE, Saini M, Maroto M, Norry E, Gerry AB. Tuning T-Cell Receptor Affinity to Optimize Clinical Risk-Benefit When Targeting Alpha-Fetoprotein-Positive Liver Cancer. *Hepatology* 2019; **69**: 2061-2075 [PMID: 30561769 DOI: 10.1002/hep.30477]
18 **Li Z**, Gong H, Liu Q, Wu W, Cheng J, Mei Y, Chen Y, Zheng H, Yu X, Zhong S, Li Y. Identification of an HLA-A* 24:02-restricted α-fetoprotein signal peptide-derived antigen and its specific T-cell receptor for T-cell immunotherapy. *Immunology* 2020; **159**: 384-392 [PMID: 31849039 DOI: 10.1111/imm.13168]
19 **Agdashian D**, ElGindi M, Xie C, Sandhu M, Pratt D, Kleiner DE, Figg WD, Rytlewski JA, Sanders C, Yusko EC, Wood B, Venzon D, Brar G, Duffy AG, Greten TF, Korangy F. The effect of anti-CTLA4 treatment on peripheral and intra-tumoral T cells in patients with hepatocellular carcinoma. *Cancer Immunol Immunother* 2019; **68**: 599-608 [PMID: 30688989 DOI: 10.1007/s00262-019-02299-8]
20 **Duffy AG**, Ulahannan SV, Makorova-Rusher O, Rahma O, Wedemeyer H, Pratt D, Davis JL, Hughes MS, Heller T, ElGindi M, Uppala A, Korangy F, Kleiner DE, Figg WD, Venzon D, Steinberg SM, Venkatesan AM, Krishnasamy V, Abi-Jaoudeh N, Levy E, Wood BJ, Greten TF. Tremelimumab in combination with ablation in patients with advanced hepatocellular carcinoma. *J Hepatol* 2017; **66**: 545-551 [PMID: 27816492 DOI: 10.1016/j.jhep.2016.10.029]
21 **Lee HW**, Cho KJ, Park JY. Current Status and Future Direction of Immunotherapy in Hepatocellular Carcinoma: What Do the Data Suggest? *Immune Netw* 2020; **20**: e11 [PMID: 32158599 DOI: 10.4110/in.2020.20.e11]
22 **Vanderborght B**, Lefere S, Vlierberghe HV, Devisscher L. The Angiopoietin/Tie2 Pathway in Hepatocellular Carcinoma. *Cells* 2020; **9** [PMID: 33143149 DOI: 10.3390/cells9112382]
23 **Saeed A**, Hildebrand H, Park R, Al-Jumayli M, Abbasi S, Melancon T, Saeed A, Al-Rajabi R, Kasi A, Baranda J, Williamson S, Sun W. Immune Checkpoint Inhibitors versus VEGF Targeted Therapy as Second Line Regimen in Advanced Hepatocellular Carcinoma (HCC): A Retrospective Study. *J Clin Med* 2020; **9** [PMID: 32824968 DOI: 10.3390/jcm9092682]
24 **Syed YY**. Ramucirumab: A Review in Hepatocellular Carcinoma. *Drugs* 2020; **80**: 315-322 [PMID: 32034692 DOI: 10.1007/s40265-020-01263-6]
25 **De Luca E**, Marino D, Di Maio M. Ramucirumab, A Second-Line Option For Patients With Hepatocellular Carcinoma: A Review Of The Evidence. *Cancer Manag Res* 2020; **12**: 3721-3729 [PMID: 32547208 DOI: 10.2147/CMAR.S216220]
26 **Chai NX**, Chapiro J. Therapy of Intermediate-Stage Hepatocellular Carcinoma: Current Evidence and Clinical Practice. *Semin Intervent Radiol* 2020; **37**: 456-465 [PMID: 33328701 DOI: 10.1055/s-0040-1719186]
27 **Lim H**, Ramjeesingh R, Liu D, Tam VC, Knox JJ, Card PB, Meyers BM. Optimizing Survival and the Changing Landscape of Targeted Therapy for Intermediate and Advanced Hepatocellular Carcinoma: A Systematic Review. *J Natl Cancer Inst* 2021; **113**: 123-136 [PMID: 32898239 DOI: 10.1093/jnci/djaa119]
28 **Mao CS**, Yin H, Ning HB, Peng Z, Li K, Ding GQ. Levels of HBx, VEGF, and CEACAM1 in HBV-related hepatocellular carcinoma and their correlation with cancer prognosis. *Eur Rev Med Pharmacol Sci* 2017; **21**: 3827-3833 [PMID: 28975984]
29 **Park R**, Eshrat F, Al-Jumayli M, Saeed A. Immuno-Oncotherapeutic Approaches in Advanced Hepatocellular Carcinoma. *Vaccines (Basel)* 2020; **8** [PMID: 32784389 DOI: 10.3390/vaccines8030447]

30 **Yao M**, Wang L, Fang M, Zheng W, Dong Z, Yao D. Advances in the study of oncofetal antigen glypican-3 expression in HBV-related hepatocellular carcinoma. *Biosci Trends* 2016; **10**: 337-343 [PMID: 27795482 DOI: 10.5582/bst.2016.01176]

31 **Zhou F**, Shang W, Yu X, Tian J. Glypican-3: A promising biomarker for hepatocellular carcinoma diagnosis and treatment. *Med Res Rev* 2018; **38**: 741-767 [PMID: 28621802 DOI: 10.1002/med.21455]

32 **Cao W**, Sharma M, Imam R, Yu J. Study on Diagnostic Values of Astrocyte Elevated Gene 1 (AEG-1) and Glypican 3 (GPC-3) in Hepatocellular Carcinoma. *Am J Clin Pathol* 2019; **152**: 647-655 [PMID: 31305883 DOI: 10.1093/ajcp/aqz086]

33 . Erratum for the Research Article: "PI4KIIIβ is a therapeutic target in chromosome 1q-amplified lung adenocarcinoma" by X. Tan, P. Banerjee, E. A. Pham, F. U. N. Rutaganira, K. Basu, N. Bota-Rabassedas, H.-F. Guo, C. L. Grzeskowiak, X. Liu, J. Yu, L. Shi, D. H. Peng, B. L. Rodriguez, J. Zhang, V. Zheng, D. Y. Duose, L. M. Solis, B. Mino, M. G. Raso, C. Behrens, I. I. Wistuba, K. L. Scott, M. Smith, K. Nguyen, G. Lam, I. Choong, A. Mazumdar, J. L. Hill, D. L. Gibbons, P. H. Brown, W. K. Russell, K. Shokat, C. J. Creighton, J. S. Glenn, J. M. Kurie. *Sci Transl Med* 2020; **12** [PMID: 32188723 DOI: 10.1126/scitranslmed.abb5995]

34 **Nishida T**, Kataoka H. Glypican 3-Targeted Therapy in Hepatocellular Carcinoma. *Cancers (Basel)* 2019; **11** [PMID: 31510063 DOI: 10.3390/cancers11091339]

35 **Liu X**, Wen J, Yi H, Hou X, Yin Y, Ye G, Wu X, Jiang X. Split chimeric antigen receptor-modified T cells targeting glypican-3 suppress hepatocellular carcinoma growth with reduced cytokine release. *Ther Adv Med Oncol* 2020; **12**: 1758835920910347 [PMID: 32215059 DOI: 10.1177/1758835920910347]

36 **Faivre S**, Rimassa L, Finn RS. Molecular therapies for HCC: Looking outside the box. *J Hepatol* 2020; **72**: 342-352 [PMID: 31954496 DOI: 10.1016/j.jhep.2019.09.010]

37 **Vormittag P**, Gunn R, Ghorashian S, Veraitch FS. A guide to manufacturing CAR T cell therapies. *Curr Opin Biotechnol* 2018; **53**: 164-181 [PMID: 29462761 DOI: 10.1016/j.copbio.2018.01.025]

38 **Piconese S**, Cammarata I, Barnaba V. Viral hepatitis, inflammation, and cancer: A lesson for autoimmunity. *J Autoimmun* 2018; **95**: 58-68 [PMID: 30509387 DOI: 10.1016/j.jaut.2018.10.021]

39 **Jiang XH**, Xie YT, Cai YP, Ren J, Ma T. Effects of hepatitis C virus core protein and nonstructural protein 4B on the Wnt/β-catenin pathway. *BMC Microbiol* 2017; **17**: 124 [PMID: 28545480 DOI: 10.1186/s12866-017-1032-4]

40 **Janda CY**, Dang LT, You C, Chang J, de Lau W, Zhong ZA, Yan KS, Marecic O, Siepe D, Li X, Moody JD, Williams BO, Clevers H, Piehler J, Baker D, Kuo CJ, Garcia KC. Surrogate Wnt agonists that phenocopy canonical Wnt and β-catenin signalling. *Nature* 2017; **545**: 234-237 [PMID: 28467818 DOI: 10.1038/nature22306]

41 **Timperi E**, Barnaba V. Viral Hepatitides, Inflammation and Tumour Microenvironment. *Adv Exp Med Biol* 2020; **1263**: 25-43 [PMID: 32588321 DOI: 10.1007/978-3-030-44518-8_3]

42 **Wang L**, Yao M, Fang M, Zheng WJ, Dong ZZ, Pan LH, Zhang HJ, Yao DF. Expression of hepatic Wnt5a and its clinicopathological features in patients with hepatocellular carcinoma. *Hepatobiliary Pancreat Dis Int* 2018; **17**: 227-232 [PMID: 29709351 DOI: 10.1016/j.hbpd.2018.03.005]

43 **Sai WL**, Yao M, Zheng WJ, Wu MN, Sun JY, Pan LH, Dong ZZ, Yao DF. [Abnormal expression of Wnt3a and inhibiting role of its molecular-targeted intervening in hepatocellular carcinoma]. *Zhonghua Gan Zang Bing Za Zhi* 2019; **27**: 866-871 [PMID: 31941241 DOI: 10.3760/cma.j.issn.1007-3418.2019.11.009]

44 **Zheng W**, Yao M, Fang M, Pan L, Wang L, Yang J, Dong Z, Yao D. Oncogenic Wnt3a: A Candidate Specific Marker and Novel Molecular Target for Hepatocellular Carcinoma. *J Cancer* 2019; **10**: 5862-5873 [PMID: 31737122 DOI: 10.7150/jca.31599]

45 **Pan L**, Yao M, Zheng W, Gu J, Yang X, Qiu L, Cai Y, Wu W, Yao D. Abnormality of Wnt3a expression as novel specific biomarker for diagnosis and differentiation of hepatocellular carcinoma. *Tumour Biol* 2016; **37**: 5561-5568 [PMID: 26577850 DOI: 10.1007/s13277-015-4413-z]

46 **Jingjing H**, Hongna H, Wenfu Z, Jianlin L, Guochu H, Yuanjia L, Songlin C, Yueqiang H. Bie Jia Jian Pill Combined with Bone Mesenchymal Stem Cells Regulates microRNA-140 to Suppress Hepatocellular Carcinoma Stem Cells. *Int J Stem Cells* 2021 [PMID: 33632990 DOI: 10.15283/ijsc20157]

47 **Lu C**, He Y, Duan J, Yang Y, Zhong C, Zhang J, Liao W, Huang X, Zhu R, Li M. Expression of Wnt3a in hepatocellular carcinoma and its effects on cell cycle and metastasis. *Int J Oncol* 2017; **51**: 1135-1145 [PMID: 28902357 DOI: 10.3892/ijo.2017.4112]

48 **Tian X**, Wu Y, Yang Y, Wang J, Niu M, Gao S, Qin T, Bao D. Long noncoding RNA LINC00662 promotes M2 macrophage polarization and hepatocellular carcinoma progression *via* activating Wnt/β-catenin signaling. *Mol Oncol* 2020; **14**: 462-483 [PMID: 31785055 DOI: 10.1002/1878-0261.12606]

49 **You Y**, Que K, Zhou Y, Zhang Z, Zhao X, Gong J, Liu Z. MicroRNA-766-3p Inhibits Tumour Progression by Targeting Wnt3a in Hepatocellular Carcinoma. *Mol Cells* 2018; **41**: 830-841 [PMID: 30145863 DOI: 10.14348/molcells.2018.0181]

50 **Abd Elhameed AG**, Helal MG, Said E, Salem HA. Saxagliptin Defers Thioacetamide-Induced Hepatocarcinogenesis in Rats; A Novel Suppressive Impact on Wnt/Hedgehog /Notch1 Signaling. *Environ Toxicol Pharmacol* 2021; 103668 [PMID: 33945853 DOI: 10.1016/j.etap.2021.103668]

51 **Li N**, Wei L, Liu X, Bai H, Ye Y, Li D, Li N, Baxa U, Wang Q, Lv L, Chen Y, Feng M, Lee B, Gao W, Ho M. A Frizzled-Like Cysteine-Rich Domain in Glypican-3 Mediates Wnt Binding and Regulates Hepatocellular Carcinoma Tumor Growth in Mice. *Hepatology* 2019; **70**: 1231-1245 [PMID: 30963603 DOI: 10.1002/hep.30646]

52 **Chen J**, Rajasekaran M, Xia H, Zhang X, Kong SN, Sekar K, Seshachalam VP, Deivasigamani A, Goh BK, Ooi LL, Hong W, Hui KM. The microtubule-associated protein PRC1 promotes early recurrence of hepatocellular carcinoma in association with the Wnt/β-catenin signalling pathway. *Gut* 2016; **65**: 1522-1534 [PMID: 26941395 DOI: 10.1136/gutjnl-2015-310625]

53 **Yang Y**, Ye YC, Chen Y, Zhao JL, Gao CC, Han H, Liu WC, Qin HY. Crosstalk between hepatic tumor cells and macrophages *via* Wnt/β-catenin signaling promotes M2-like macrophage polarization and reinforces tumor malignant behaviors. *Cell Death Dis* 2018; **9**: 793 [PMID: 30022048 DOI: 10.1038/s41419-018-0818-0]

54 **Sebio A**, Kahn M, Lenz HJ. The potential of targeting Wnt/β-catenin in colon cancer. *Expert Opin Ther Targets* 2014; **18**:

611-615 [PMID: 24702624 DOI: 10.1517/14728222.2014.906580]
55 **Takada K**, Zhu D, Bird GH, Sukhdeo K, Zhao JJ, Mani M, Lemieux M, Carrasco DE, Ryan J, Horst D, Fulciniti M, Munshi NC, Xu W, Kung AL, Shivdasani RA, Walensky LD, Carrasco DR. Targeted disruption of the BCL9/β-catenin complex inhibits oncogenic Wnt signaling. *Sci Transl Med* 2012; **4**: 148ra117 [PMID: 22914623 DOI: 10.1126/scitranslmed.3003808]
56 **Chikhaliwala P**, Rai R, Chandra S. Simultaneous voltammetric immunodetection of alpha-fetoprotein and glypican-3 using a glassy carbon electrode modified with magnetite-conjugated dendrimers. *Mikrochim Acta* 2019; **186**: 255 [PMID: 30904972 DOI: 10.1007/s00604-019-3354-4]
57 **Li Y**, Liu F, Zhou W, Zhang S, Chu P, Lin F, Wang HL. Diagnostic value of clusterin immunostaining in hepatocellular carcinoma. *Diagn Pathol* 2020; **15**: 127 [PMID: 33054843 DOI: 10.1186/s13000-020-01041-8]
58 **Zheng W**, Yao M, Qian Q, Sai W, Qiu L, Yang J, Wu W, Dong Z, Yao D. Oncogenic secretory clusterin in hepatocellular carcinoma: Expression at early staging and emerging molecular target. *Oncotarget* 2017; **8**: 52321-52332 [PMID: 28881732 DOI: 10.18632/oncotarget.13674]
59 **Udomsinprasert W**, Poovorawan Y, Chongsrisawat V, Vejchapipat P, Honsawek S. Decreased circulating clusterin reflects severe liver complications after hepatoportoenterostomy of biliary atresia. *Sci Rep* 2020; **10**: 19736 [PMID: 33184463 DOI: 10.1038/s41598-020-76875-9]
60 **Wang X**, Liu Y, Qin Q, Zheng T. Clusterin role in hepatocellular carcinoma patients treated with oxaliplatin. *Biosci Rep* 2020; **40** [PMID: 32039450 DOI: 10.1042/BSR20200071]
61 **Park JS**, Lee WK, Kim HS, Seo JA, Kim DH, Han HC, Min BH. Clusterin overexpression protects against western diet-induced obesity and NAFLD. *Sci Rep* 2020; **10**: 17484 [PMID: 33060605 DOI: 10.1038/s41598-020-73927-y]
62 **Yao M**, Sai W, Zheng W, Wang L, Dong Z, Yao D. Secretory Clusterin as a Novel Molecular-targeted Therapy for Inhibiting Hepatocellular Carcinoma Growth. *Curr Med Chem* 2020; **27**: 3290-3301 [PMID: 31232234 DOI: 10.2174/0929867326666190624161158]
63 **Fu N**, Du H, Li D, Lu Y, Li W, Wang Y, Kong L, Du J, Zhao S, Ren W, Han F, Wang R, Zhang Y, Nan Y. Clusterin contributes to hepatitis C virus-related hepatocellular carcinoma by regulating autophagy. *Life Sci* 2020; **256**: 117911 [PMID: 32504756 DOI: 10.1016/j.lfs.2020.117911]
64 **Wang X**, Zou F, Zhong J, Yue L, Wang F, Wei H, Yang G, Jin T, Dong X, Li J, Xiu P. Secretory Clusterin Mediates Oxaliplatin Resistance *via* the Gadd45a/PI3K/Akt Signaling Pathway in Hepatocellular Carcinoma. *J Cancer* 2018; **9**: 1403-1413 [PMID: 29721050 DOI: 10.7150/jca.23849]
65 **Wu B**, Shang H, Liang X, Sun Y, Jing H, Han X, Cheng W. Preparation of novel targeting nanobubbles conjugated with small interfering RNA for concurrent molecular imaging and gene therapy *in vivo*. *FASEB J* 2019; **33**: 14129-14136 [PMID: 31657628 DOI: 10.1096/fj.201900716RR]
66 **Kuo PC**, Chau IY, Li AF, Chau YP, Hsia CY, Chau GY. Clusterin expression in nontumor tissue in patients with resectable hepatocellular carcinoma related with postresectional survival. *J Chin Med Assoc* 2019; **82**: 929-934 [PMID: 31800534 DOI: 10.1097/JCMA.0000000000000195]
67 **Tai BJ**, Yao M, Zheng WJ, Shen YC, Wang L, Sun JY, Wu MN, Dong ZZ, Yao DF. Alteration of oncogenic IGF-II gene methylation status associates with hepatocyte malignant transformation. *Hepatobiliary Pancreat Dis Int* 2019; **18**: 158-163 [PMID: 30692043 DOI: 10.1016/j.hbpd.2019.01.003]
68 **Ngo MT**, Jeng HY, Kuo YC, Diony Nanda J, Brahmadhi A, Ling TY, Chang TS, Huang YH. The Role of IGF/IGF-1R Signaling in Hepatocellular Carcinomas: Stemness-Related Properties and Drug Resistance. *Int J Mol Sci* 2021; **22** [PMID: 33669204 DOI: 10.3390/ijms22041931]
69 **Wang L**, Yao M, Zheng W, Fang M, Wu M, Sun J, Dong Z, Yao D. Insulin-like Growth Factor I Receptor: A Novel Target for Hepatocellular Carcinoma Gene Therapy. *Mini Rev Med Chem* 2019; **19**: 272-280 [PMID: 30360707 DOI: 10.2174/]
70 **Hua H**, Kong Q, Yin J, Zhang J, Jiang Y. Insulin-like growth factor receptor signaling in tumorigenesis and drug resistance: a challenge for cancer therapy. *J Hematol Oncol* 2020; **13**: 64 [PMID: 32493414 DOI: 10.1186/s13045-020-00904-3]
71 **Qian J**, Yao D, Dong Z, Wu W, Qiu L, Yao N, Li S, Bian Y, Wang Z, Shi G. Characteristics of hepatic igf-ii expression and monitored levels of circulating igf-ii mRNA in metastasis of hepatocellular carcinoma. *Am J Clin Pathol* 2010; **134**: 799-806 [PMID: 20959664 DOI: 10.1309/AJCPTFDSE2V3LCZP]
72 **Greenall SA**, Donoghue J, Johns TG, Adams TE. Differential Sensitivity of Human Hepatocellular Carcinoma Xenografts to an IGF-II Neutralizing Antibody May Involve Activated STAT3. *Transl Oncol* 2018; **11**: 971-978 [PMID: 29933129 DOI: 10.1016/j.tranon.2018.05.011]
73 **Bie C**, Chen Y, Tang H, Li Q, Zhong L, Peng X, Shi Y, Lin J, Lai J, Wu S, Tang S. Insulin-Like Growth Factor 1 Receptor Drives Hepatocellular Carcinoma Growth and Invasion by Activating Stat3-Midkine-Stat3 Loop. *Dig Dis Sci* 2021 [PMID: 33559791 DOI: 10.1007/s10620-021-06862-1]
74 **Cheng Z**, Wei-Qi J, Jin D. New insights on sorafenib resistance in liver cancer with correlation of individualized therapy. *Biochim Biophys Acta Rev Cancer* 2020; **1874**: 188382 [PMID: 32522600 DOI: 10.1016/j.bbcan.2020.188382]
75 **Ghosh MK**, Patra F, Ghosh S, Hossain CM, Mukherjee B. Antisense oligonucleotides directed against insulin-like growth factor-II messenger ribonucleic acids delay the progress of rat hepatocarcinogenesis. *J Carcinog* 2014; **13**: 2 [PMID: 24737950 DOI: 10.4103/1477-3163.126761]
76 **Wei L**, Wang X, Lv L, Liu J, Xing H, Song Y, Xie M, Lei T, Zhang N, Yang M. The emerging role of microRNAs and long noncoding RNAs in drug resistance of hepatocellular carcinoma. *Mol Cancer* 2019; **18**: 147 [PMID: 31651347 DOI: 10.1186/s12943-019-1086-z]
77 **Yao N**, Yao D, Wang L, Dong Z, Wu W, Qiu L, Yan X, Yu D, Chen J, Sai W, Zhang H, Yang J. Inhibition of autocrine IGF-II on effect of human HepG2 cell proliferation and angiogenesis factor expression. *Tumour Biol* 2012; **33**: 1767-1776 [PMID: 22684773 DOI: 10.1007/s13277-012-0436-x]
78 **Mohamed YI**, Lee S, Xiao L, Hassan MM, Qayyum A, Hiatia R, Pestana RC, Haque A, George B, Rashid A, Duda DG, Elghazaly H, Wolff RA, Morris JS, Yao J, Amin HM, Kaseb AO. Insulin-like growth factor 1/Child-Turcotte-Pugh

composite score as a predictor of treatment outcomes in patients with advanced hepatocellular carcinoma treated with sorafenib. *Oncotarget* 2021; **12**: 756-766 [PMID: 33889299 DOI: 10.18632/oncotarget.27924]

79 **Kanthaje S**, Makol A, Chakraborti A. Sorafenib response in hepatocellular carcinoma: MicroRNAs as tuning forks. *Hepatol Res* 2018; **48**: 5-14 [PMID: 29055114 DOI: 10.1111/hepr.12991]

80 **Huang KW**, Hsu FF, Qiu JT, Chern GJ, Lee YA, Chang CC, Huang YT, Sung YC, Chiang CC, Huang RL, Lin CC, Dinh TK, Huang HC, Shih YC, Alson D, Lin CY, Lin YC, Chang PC, Lin SY, Chen Y. Highly efficient and tumor-selective nanoparticles for dual-targeted immunogene therapy against cancer. *Sci Adv* 2020; **6**: eaax5032 [PMID: 31998834 DOI: 10.1126/sciadv.aax5032]

81 **Niu L**, Liu L, Yang S, Ren J, Lai PBS, Chen GG. New insights into sorafenib resistance in hepatocellular carcinoma: Responsible mechanisms and promising strategies. *Biochim Biophys Acta Rev Cancer* 2017; **1868**: 564-570 [PMID: 29054475 DOI: 10.1016/j.bbcan.]

82 **Zhou B**, Yang H, Yang C, Bao YL, Yang SM, Liu J, Xiao YF. Translation of noncoding RNAs and cancer. *Cancer Lett* 2021; **497**: 89-99 [PMID: 33038492 DOI: 10.1016/j.canlet.]

83 **Gramantieri L**, Pollutri D, Gagliardi M, Giovannini C, Quarta S, Ferracin M, Casadei-Gardini A, Callegari E, De Carolis S, Marinelli S, Benevento F, Vasuri F, Ravaioli M, Cescon M, Piscaglia F, Negrini M, Bolondi L, Fornari F. MiR-30e-3p Influences Tumor Phenotype through *MDM2*/*TP53* Axis and Predicts Sorafenib Resistance in Hepatocellular Carcinoma. *Cancer Res* 2020; **80**: 1720-1734 [PMID: 32015093 DOI: 10.1158/0008-5472.CAN-19-0472]

84 **Li Y**, He X, Zhang X, Xu Y, Wu Y, Xu X. Immune-related microRNA signature for predicting prognosis and the immune microenvironment in hepatocellular carcinoma. *Life Sci* 2021; **265**: 118799 [PMID: 33220285 DOI: 10.1016/j.lfs.2020.118799]

85 **Yugawa K**, Yoshizumi T, Mano Y, Itoh S, Harada N, Ikegami T, Kohashi K, Oda Y, Mori M. Cancer-associated fibroblasts promote hepatocellular carcinoma progression through downregulation of exosomal miR-150-3p. *Eur J Surg Oncol* 2021; **47**: 384-393 [PMID: 32883551 DOI: 10.1016/j.ejso.2020.08.002]

86 **Lim LJ**, Wong SYS, Huang F, Lim S, Chong SS, Ooi LL, Kon OL, Lee CG. Roles and Regulation of Long Noncoding RNAs in Hepatocellular Carcinoma. *Cancer Res* 2019; **79**: 5131-5139 [PMID: 31337653 DOI: 10.1158/0008-5472.CAN-19-0255]

87 **Zhou Y**, Ren H, Dai B, Li J, Shang L, Huang J, Shi X. Hepatocellular carcinoma-derived exosomal miRNA-21 contributes to tumor progression by converting hepatocyte stellate cells to cancer-associated fibroblasts. *J Exp Clin Cancer Res* 2018; **37**: 324 [PMID: 30591064 DOI: 10.1186/s13046-018-0965-2]

88 **Sun C**, Xiao T, Xiao Y, Li Y. Silencing of long noncoding RNA NEAT1 inhibits hepatocellular carcinoma progression by downregulating SMO by sponging microRNA503. *Mol Med Rep* 2021; **23** [PMID: 33398379 DOI: 10.3892/mmr.2020.11807]

89 **Sukowati CHC**, Cabral LKD, Tiribelli C, Pascut D. Circulating Long and Circular Noncoding RNA as Non-Invasive Diagnostic Tools of Hepatocellular Carcinoma. *Biomedicines* 2021; **9** [PMID: 33477833 DOI: 10.3390/biomedicines9010090]

90 **Salerno D**, Chiodo L, Alfano V, Floriot O, Cottone G, Paturel A, Pallocca M, Plissonnier ML, Jeddari S, Belloni L, Zeisel M, Levrero M, Guerrieri F. Hepatitis B protein HBx binds the DLEU2 lncRNA to sustain cccDNA and host cancer-related gene transcription. *Gut* 2020; **69**: 2016-2024 [PMID: 32114505 DOI: 10.1136/gutjnl-2019-319637]

91 **Onuma AE**, Zhang H, Huang H, Williams TM, Noonan A, Tsung A. Immune Checkpoint Inhibitors in Hepatocellular Cancer: Current Understanding on Mechanisms of Resistance and Biomarkers of Response to Treatment. *Gene Expr* 2020; **20**: 53-65 [PMID: 32340652 DOI: 10.3727/105221620X15880179864121]

92 **Wang T**, Xu L, Jia R, Wei J. MiR-218 suppresses the metastasis and EMT of HCC cells *via* targeting SERBP1. *Acta Biochim Biophys Sin (Shanghai)* 2017; **49**: 383-391 [PMID: 28369267 DOI: 10.1093/abbs/gmx017]

93 **Aspichueta P**. Lipid-rich environment: a key role promoting carcinogenesis in obesity-related non-alcoholic fatty liver disease. *Gut* 2018; **67**: 1376-1377 [PMID: 29540438 DOI: 10.1136/gutjnl-2018-316047]

94 **Zayac A**, Almhanna K. Hepatobiliary cancers and immunotherapy: where are we now and where are we heading? *Transl Gastroenterol Hepatol* 2020; **5**: 8 [PMID: 32190776 DOI: 10.21037/tgh.2019.09.07]

95 **Gan L**, Liu Z, Sun C. Obesity linking to hepatocellular carcinoma: A global view. *Biochim Biophys Acta Rev Cancer* 2018; **1869**: 97-102 [PMID: 29366974 DOI: 10.1016/j.bbcan.2017.12.006]

96 **Zhang H**, Deng T, Ge S, Liu Y, Bai M, Zhu K, Fan Q, Li J, Ning T, Tian F, Li H, Sun W, Ying G, Ba Y. Exosome circRNA secreted from adipocytes promotes the growth of hepatocellular carcinoma by targeting deubiquitination-related USP7. *Oncogene* 2019; **38**: 2844-2859 [PMID: 30546088 DOI: 10.1038/s41388-018-0619-z]

97 **Zhu C**, Su Y, Liu L, Wang S, Liu Y, Wu J. Circular RNA hsa_circ_0004277 Stimulates Malignant Phenotype of Hepatocellular Carcinoma and Epithelial-Mesenchymal Transition of Peripheral Cells. *Front Cell Dev Biol* 2020; **8**: 585565 [PMID: 33511111 DOI: 10.3389/fcell.2020.585565]

98 **Wang S**, Zhang K, Tan S, Xin J, Yuan Q, Xu H, Xu X, Liang Q, Christiani DC, Wang M, Liu L, Du M. Circular RNAs in body fluids as cancer biomarkers: the new frontier of liquid biopsies. *Mol Cancer* 2021; **20**: 13 [PMID: 33430880 DOI: 10.1186/s12943-020-01298-z]

99 **Zhao M**, Dong G, Meng Q, Lin S, Li X. Circ-HOMER1 enhances the inhibition of miR-1322 on CXCL6 to regulate the growth and aggressiveness of hepatocellular carcinoma cells. *J Cell Biochem* 2020; **121**: 4440-4449 [PMID: 32037619 DOI: 10.1002/jcb.]

100 **Chen W**, Quan Y, Fan S, Wang H, Liang J, Huang L, Chen L, Liu Q, He P, Ye Y. Exosome-transmitted circular RNA hsa_circ_0051443 suppresses hepatocellular carcinoma progression. *Cancer Lett* 2020; **475**: 119-128 [PMID: 32014458 DOI: 10.1016/j.]

101 **Du Q**, Han J, Gao S, Zhang S, Pan Y. Hypoxia-induced circular RNA hsa_circ_0008450 accelerates hepatocellular cancer progression *via* the miR-431/AKAP1 axis. *Oncol Lett* 2020; **20**: 388 [PMID: 33193848 DOI: 10.3892/ol.2020.12251]

102 **Lin T**, Dai Y, Guo X, Chen W, Zhao J, Cao L, Wu Z. Silencing Of hsa_circ_0008450 Represses Hepatocellular Carcinoma Progression Through Regulation Of microRNA-214-3p/EZH2 Axis. *Cancer Manag Res* 2019; **11**: 9133-9143 [PMID: 31695501 DOI: 10.2147/CMAR.S222716]

103 **Sutti S**, Albano E. Adaptive immunity: an emerging player in the progression of NAFLD. *Nat Rev Gastroenterol Hepatol* 2020; **17**: 81-92 [PMID: 31605031 DOI: 10.1038/s41575-019-0210-2]

104 **Shen S**, Peng H, Wang Y, Xu M, Lin M, Xie X, Peng B, Kuang M. Screening for immune-potentiating antigens from hepatocellular carcinoma patients after radiofrequency ablation by serum proteomic analysis. *BMC Cancer* 2018; **18**: 117 [PMID: 29386009 DOI: 10.1186/s12885-018-4011-8]

105 **Nishida N**, Kudo M. Immune Phenotype and Immune Checkpoint Inhibitors for the Treatment of Human Hepatocellular Carcinoma. *Cancers (Basel)* 2020; **12** [PMID: 32443599 DOI: 10.3390/cancers12051274]

World Journal of Clinical Cases

Submit a Manuscript: https://www.f6publishing.com

World J Clin Cases 2022 April 16; 10(11): 3334-3351

DOI: 10.12998/wjcc.v10.i11.3334

ISSN 2307-8960 (online)

ORIGINAL ARTICLE

Clinical and Translational Research

Autophagy-related long non-coding RNA prognostic model predicts prognosis and survival of melanoma patients

Yue Qiu, Hong-Tao Wang, Xi-Fan Zheng, Xing Huang, Jin-Zhi Meng, Jun-Pu Huang, Zhen-Pei Wen, Jun Yao

Specialty type: Medicine, research and experimental

Provenance and peer review: Unsolicited article; Externally peer reviewed.

Peer-review model: Single blind

Peer-review report's scientific quality classification

Grade A (Excellent): 0
Grade B (Very good): B
Grade C (Good): 0
Grade D (Fair): 0
Grade E (Poor): 0

P-Reviewer: Wang CY

Received: August 10, 2021
Peer-review started: August 10, 2021
First decision: October 20, 2021
Revised: October 29, 2021
Accepted: January 17, 2022
Article in press: January 17, 2022
Published online: April 16, 2022

Yue Qiu, Department of Bone and Joint Surgery, The First Affiliated Hospital of Guangxi Medical University, Nanning 530000, Guangxi Zhuang Autonomous Region, China

Yue Qiu, Xi-Fan Zheng, Xing Huang, Jin-Zhi Meng, Jun-Pu Huang, Zhen-Pei Wen, Department of Bone and Joint Surgery, Guangxi Medical University, Nanning 530000, Guangxi Zhuang Autonomous Region, China

Hong-Tao Wang, Jun Yao, Department of Orthopedics, The First Affiliated Hospital of Guangxi Medical University, Guangxi Medical University, Nanning 530000, Guangxi Zhuang Autonomous Region, China

Corresponding author: Jun Yao, MD, Chief Doctor, Surgeon, Department of Orthopedics, The First Affiliated Hospital of Guangxi Medical University, Guangxi Medical University, No. 6 Shuangyong Road, Nanning 530000, Guangxi Zhuang Autonomous Region, China.
yaojun800524@126.com

Abstract

BACKGROUND

Melanomas are malignant tumors that can occur in different body parts or tissues such as the skin, mucous membrane, uvea, and pia mater. Long non-coding RNAs (lncRNAs) are key factors in the occurrence and development of many malignant tumors, and are involved in the prognosis of some patients.

AIM

To identify autophagy-related lncRNAs in melanoma that are crucial for the diagnosis, treatment, and prognosis of melanoma patients.

METHODS

We retrieved transcriptome expression profiles and clinical information of 470 melanoma patients from The Cancer Genome Atlas (TCGA) database. Then, we identified autophagy-related genes in the Human Autophagy Database. Using R, coexpression analysis of lncRNAs and autophagy-related genes was conducted to obtain autophagy-related lncRNAs and their expression levels. We also performed univariate and multivariate Cox proportional risk analyses on the obtained datasets, to systematically evaluate the prognostic value of autophagy-related lncRNAs in melanoma. Fifteen autophagy-related lncRNAs were identified and an autophagy-related prognostic signature for melanoma was established. The Kaplan-Meier and univariate and multivariate Cox regression

analyses were used to calculate risk scores. Based on the risk scores, melanoma patients were randomly divided into high- and low-risk groups. Receiver operating characteristic curve analysis, dependent on time, was performed to assess the accuracy of the prognostic model. At the same time, we also downloaded the melanoma data sets GSE65904, GSE19234, and GSE78220 from the GENE EXPRESSION OMNIBUS database for model verification. Finally, we performed Gene Set Enrichment Analysis functional annotation, which showed that the low and the high-risk groups had different enriched pathways.

RESULTS

The co-expression network for autophagy-related genes was constructed using R, and 936 lncRNAs related to autophagy were identified. Then, 52 autophagy-related lncRNAs were significantly associated with TCGA melanoma patients' survival by univariate Cox proportional risk analysis ($P < 0.01$). Further, the 52 autophagy-related lncRNAs mentioned above were analyzed by multivariate Cox analysis with R. Fifteen lncRNAs were selected: LINC01943, AC090948.3, USP30-AS1, AC068282.1, AC004687.1, AL133371.2, AC242842.1, PCED1B-AS1, HLA-DQB1-AS1, AC011374.2, LINC00324, AC018553.1, LINC00520, DBH-AS1, and ITGB2-AS1. The *P* values in all survival analyses using these 15 lncRNAs were < 0.05. These lncRNAs were used to build a risk model based on the risk score. Negative correlations were observed between risk scores and overall survival rate in melanoma patients over time. Additionally, the melanoma risk curve and scatter plot analyses showed that the death number increased along with the increase in the risk score. Overall, we identified and established a new prognostic risk model for melanoma using 15 autophagy-related lncRNAs. The risk model constructed with these lncRNAs can help and guide melanoma patient prognosis predictions and individualized treatments in the future.

CONCLUSION

Overall, the risk model developed based on the 15 autophagy-related lncRNAs can have important prognostic value and may provide autophagy-related clinical targets for melanoma treatment.

Key Words: Melanoma; Long non-coding RNAs; Autophagy; Prognosis; The Cancer Genome Atlas; Bioinformatics

Core Tip: Long non-coding ribonucleic acids (lncRNAs) are key factors in the development of many malignant tumors and are involved in the prognosis of some patients. The expression of autophagy-associated lncRNAs was associated with survival in melanoma patients. We obtained 15 autophagy-related lncRNAs and established a melanoma prognosis model, which can predict the prognosis of melanoma patients and is more accurate than TNM stage, age, gender, and other clinical indicators, and may provide autophagy-related clinical targets for the treatment of melanoma.

Citation: Qiu Y, Wang HT, Zheng XF, Huang X, Meng JZ, Huang JP, Wen ZP, Yao J. Autophagy-related long non-coding RNA prognostic model predicts prognosis and survival of melanoma patients. *World J Clin Cases* 2022; 10(11): 3334-3351

URL: https://www.wjgnet.com/2307-8960/full/v10/i11/3334.htm

DOI: https://dx.doi.org/10.12998/wjcc.v10.i11.3334

INTRODUCTION

Melanomas are malignant tumors that can occur in different body parts or tissues such as the skin, mucous membrane, uvea, and pia mater. While the incidence of many tumors is declining, the incidence of melanoma continues to increase[1]. The global prevalence of melanoma is increasing by about 3% to 7% per year[2]. Although many melanoma patients have localized tumors at diagnosis that can be completely removed by surgery, many patients present signs of metastasis[3]. Early melanoma has a good prognosis, but advanced melanoma patients have a very poor prognosis, with a 5%-10% survival rate, even with treatment[4]. Autophagy, originally considered a process of lysosomal-dependent degradation of cytoplasmic components in response to starvation, has been shown to affect multiple homeostasis aspects and to constitute a prevention barrier to malignant transformation[5]. Therefore, the combination of autophagy-related factors and pathological classification for risk stratification in melanoma patients can be crucial to prognosis and treatment response predictions.

Long non-coding RNAs (lncRNAs) are transcribed RNAs with a length of more than 200 nucleotides that are not translated into proteins[6]. Many studies have shown that noncoding RNAs can be associated with tumor pathogenesis by epigenetic regulation, as well as transcriptional and/or post-transcriptional processes. Moreover, lncRNAs can be used as sensitive and specific cancer biomarkers [7]. Previous studies have shown that melanoma pathogenesis was associated with different lncRNAs, *in vitro* and *in vivo*, and that some of them can be potential melanoma therapy targets, such as UCA1, DSCAM-AS1, and miR155HG[8,9]. However, the lncRNAs involved in autophagy and their prognostic value were not previously investigated, and many mechanisms remain unclear.

Therefore, we retrieved human clinical melanoma datasets from The Cancer Genome Atlas (TCGA) database and screened and analyzed genes associated with melanoma prognosis. Finally, 15 autophagy-related lncRNAs were identified as melanoma prognosis biomarkers. Compared to other clinical indicators, these lncRNAs had higher accuracy to predict melanoma patients' survival.

MATERIALS AND METHODS

Patient characteristics and data processing

The data of 471 melanoma patients were retrieved from the TCGA database (https://cancergenome.nih.gov/). In addition, the GSE65904, GSE19234, and GSE78220 data sets were downloaded from the GENE EXPRESSION OMNIBUS (GEO) database, including the expression data and clinical information of a total of 265 melanoma patients (https://www.ncbi.nlm.nih.gov/geo/). In this study, the lncRNA expression data in the TCGA database included complete clinical and follow-up data of 349 patients, which were finally used for analyses. Patients' clinical characteristics are detailed in Table 1. This study followed the TCGA published guidelines, and since the data used here were from the published TCGA database, Institutional Review Board approval was not required.

Autophagy-related gene acquisition and co-expression network establishment

The Human Autophagy Database was used to identify autophagy-related genes. Then, R was used to analyze the association of autophagy-related genes and lncRNAs (correlation coefficient > 0.3; $P < 0.001$), and a co-expression network was constructed. Finally, 936 melanoma autophagy-related lncRNAs were identified, and their expression levels were obtained.

Autophagy-related lncRNA signaling related to melanoma prognosis

The univariate proportional risk, Kaplan-Meier survival, and multivariate risk analyses were conducted using R to calculate patients' risk scores and to identify if these autophagy-related lncRNAs were involved in the melanoma prognosis. The risk score was calculated using the formula: Risk score = expr (lncRNA1) × coef (lncRNA1) + expr (lncRNA2) × coef (lncRNA2) + … + expr (lncRNAn) × coef (lncRNAn). Melanoma patients were divided into high- and low-risk groups, based on the median risk score. Finally, three data sets from the GEO database (GSE65904, GSE19234, and GSE78220) were used for verification analysis.

Multi-indicator receiver operating characteristic curve and independent prognostic analyses

Univariate and multivariate regression analyses were used to systematically assess the relations between prognosis, clinicopathological factors, and risk scores in melanoma patients. To evaluate and verify the predictive accuracy of the prognostic model, we conducted receiver operating characteristic (ROC) analysis on the data from the TCGA database and the GSE78220 data set from the GEO database, and drew the ROC curve.

Co-expression network and Gene Set Enrichment Analysis

A co-expression network with 15 prognostic autophagy-related genes was constructed using R (version 4.0.4). The mulberries were mapped and the network was visualized using Cytoscape. Then, survival curves were drawn for these 15 lncRNAs, and risk survival and risk curves were drawn. Then, Gene Set Enrichment Analysis (GSEA) was employed for functional annotation. The GSEA focused not only on high-score genes but also on a range of genes related to biological processes that are associated with cancer pathogenesis, including stress response, transcription, and metabolic pathways. $P < 0.05$ was considered statistically significant[10].

RESULTS

Identification of autophagy-related lncRNAs and establishment of a melanoma prognostic model

The co-expression network for autophagy-related genes was constructed using R, and 936 lncRNAs related to autophagy were identified. Then, 52 autophagy-related lncRNAs were significantly associated

Table 1 Clinical correlation analysis in melanoma patients

Variable	Group	*n*	Mean	SD	*t* value	*P* value
Age	≤ 65	228	1.25	0.788	-2.14416	0.033
	> 65	121	1.488	1.081		
Gender	Female	133	1.323	1.016	-0.1461	0.884
	Male	216	1.338	0.834		
Stage	I-II	194	1.283	0.801	-1.10172	0.272
	III-IV	155	1.394	1.022		
T	0-2	135	1.155	0.747	-3.10656	0.002
	3-4	214	1.444	0.978		
M	0	338	1.336	0.912	0.502769	0.625
	1	11	1.223	0.727		
N	0	202	1.281	0.8	-1.19357	0.234
	1-3	147	1.403	1.033		

with TCGA melanoma patients' survival by univariate Cox proportional risk analysis ($P < 0.01$). Among the 52 autophagy-related lncRNAs, four were related to a high risk (Table 2). Further, the 52 autophagy-related lncRNAs mentioned above were analyzed by multivariate Cox analysis with R. Fifteen lncRNAs were selected: LINC01943, AC090948.3, USP30-AS1, AC068282.1, AC004687.1, AL133371.2, AC242842.1, PCED1B-AS1, HLA-DQB1-AS1, AC011374.2, LINC00324, AC018553.1, LINC00520, DBH-AS1, and ITGB2-AS1 (Table 3). They were subsequently used to construct a melanoma prognostic risk model (Figure 1). Then, we assigned the enrolled melanoma patients into two groups based on their median risk scores. The *P* values in all survival analyses using these 15 lncRNAs were < 0.05 (Figure 2). To investigate the survival rates in these groups, other survival analyses were performed. Negative correlations were observed between risk scores and overall survival rate in melanoma patients over time (Figure 3A). Additionally, the melanoma risk curve and scatter plot analyses showed that the death number increased along with the increase in the risk score. Therefore, this demonstrated that the melanoma patients' mortality was related to the risk score (Figure 3B-D). The heat map produced with these 15 autophagy-related lncRNAs shows that LINC00520 and AC018553.1 were highly expressed in the high-risk group. High expression of others lncRNAs was observed in patients with a low-risk score. In order to verify the accuracy and stability of the model, we decided to use the GSE65904, GSE19234, and GSE78220 data sets from the GEO database to verify, and conduct survival, risk curve, scatter plot, and heat map analyses, and the results are basically consistent with those of the above analysis (Supplementary Figure 1). Overall, we screened 15 pairs of lncRNAs with prognostic significance in melanoma, paving the way for the subsequent melanoma prognostic model establishment.

Evaluation of the independent prognostic risk model in melanoma patients

The above analyses identified 15 lncRNAs and established a prognostic risk model for the melanoma patients. Next, multivariate and univariate Cox regression analyses were employed to confirm if this model could be used for melanoma prognosis prediction. Results showed that the hazard ratio (HR) was 1.912 in the univariate analysis and 1.715 in the multivariate. Additionally, the 95% confidence interval of the risk score was 1.643-2.226 ($P < 0.001$) and 1.467-2.005 ($P < 0.001$) in the univariate and multivariate analyses, respectively (Figure 4A and B). These results suggested that in our model, the most important prognostic factors for melanoma were not age, gender, or TMN stage, but the 15 lncRNAs. To verify the sensitivity and specificity of the risk model, ROC curves of risk scores and other clinical indicators were plotted. The area under the risk score curve (AUC) was 0.712, exceeding the AUC of the other clinical factors (Figure 4C). In addition, we also verified the above analysis in three datasets from the GEO database, and the analysis results are consistent with those of the TCGA database (Supplementary Figure 2). These results suggested that the risk model was more accurate than other clinicopathological factors in predicting melanoma patients' prognosis.

Different autophagy states in melanoma patients

GSEA software (version 4.1.0) was used for functional annotation. The differentially expressed genes of the high-risk group were mainly enriched in glyoxylate and dicarboxylate metabolism, while in the low-risk group, pathways such as antigen processing and presentation, Toll-like receptor signaling, and cytokine production positive regulation were enriched (Figure 5).

Table 2 Fifty-two lncRNAs associated with survival in melanoma patients identified by univariate Cox proportional risk analysis

LncRNA	HR	Lower limit (95%CI)	Upper limit (95%CI)	*P* value	Risk
C5orf56	0.478	0.348	0.656	0.000	Low
AC011899.2	0.588	0.437	0.792	0.000	Low
AC098613.1	0.595	0.456	0.776	0.000	Low
AC068282.1	0.617	0.448	0.851	0.003	Low
LINC01943	0.627	0.500	0.786	0.000	Low
AP002807.1	0.630	0.464	0.856	0.003	Low
AL590764.1	0.634	0.496	0.811	0.000	Low
LINC00324	0.635	0.517	0.779	0.000	Low
ZEB1-AS1	0.659	0.531	0.817	0.000	Low
VIM-AS1	0.659	0.533	0.816	0.000	Low
LINC02328	0.662	0.504	0.870	0.003	Low
MMP25-AS1	0.674	0.544	0.835	0.000	Low
AC015911.3	0.674	0.553	0.821	0.000	Low
AL662844.4	0.688	0.526	0.901	0.007	Low
AL137003.2	0.689	0.544	0.871	0.002	Low
MIAT	0.701	0.575	0.854	0.000	Low
AL133371.2	0.707	0.587	0.852	0.000	Low
AC022706.1	0.713	0.569	0.895	0.003	Low
U62317.1	0.714	0.580	0.879	0.002	Low
AC090948.3	0.727	0.574	0.921	0.008	Low
AC011374.2	0.735	0.608	0.888	0.001	Low
AC242842.1	0.741	0.639	0.859	0.000	Low
AC004918.1	0.756	0.629	0.908	0.003	Low
TRG-AS1	0.763	0.643	0.905	0.002	Low
DBH-AS1	0.777	0.664	0.910	0.002	Low
AC018755.4	0.779	0.670	0.906	0.001	Low
AC060766.7	0.782	0.658	0.929	0.005	Low
AC090559.1	0.789	0.680	0.916	0.002	Low
USP30-AS1	0.803	0.732	0.880	0.000	Low
PAXIP1-AS2	0.806	0.706	0.919	0.001	Low
AL365361.1	0.814	0.719	0.922	0.001	Low
AC012236.1	0.835	0.741	0.941	0.003	Low
HLA-DQB1-AS1	0.835	0.765	0.912	0.000	Low
TRBV11-2	0.838	0.738	0.950	0.006	Low
AC093726.1	0.844	0.772	0.923	0.000	Low
AL157871.2	0.847	0.759	0.945	0.003	Low
MIR155HG	0.848	0.775	0.928	0.000	Low
AC243960.1	0.854	0.774	0.942	0.002	Low
AC083799.1	0.871	0.817	0.927	0.000	Low
LINC02446	0.873	0.809	0.941	0.000	Low
ITGB2-AS1	0.875	0.793	0.966	0.008	Low

AC004687.1	0.881	0.813	0.955	0.002	Low
PCED1B-AS1	0.914	0.865	0.964	0.001	Low
WAC-AS1	0.916	0.876	0.959	0.000	Low
LINC01871	0.918	0.880	0.957	0.000	Low
PSMB8-AS1	0.944	0.920	0.969	0.000	Low
THCAT158	0.952	0.923	0.981	0.001	Low
HCP5	0.975	0.964	0.986	0.000	Low
KU-MEL-3	1.006	1.002	1.010	0.003	High
LINC00520	1.011	1.005	1.017	0.001	High
AC100791.3	1.186	1.067	1.318	0.001	High
AC018553.1	1.255	1.129	1.396	0.000	High

HR: Hazard ratio.

Table 3 Prognostic melanoma risk model based on multivariate Cox proportional hazards analysis

LncRNA	Coefficient	HR	Risk
LINC01943	-0.265	0.768	Low
AC090948.3	-0.282	0.754	Low
USP30-AS1	-0.206	0.814	Low
AC068282.1	-0.253	0.776	Low
AC004687.1	-0.152	0.859	Low
AL133371.2	-0.253	0.777	Low
AC242842.1	-0.209	0.812	Low
PCED1B-AS1	0.229	1.258	High
HLA-DQB1-AS1	-0.096	0.909	Low
AC011374.2	-0.218	0.804	Low
LINC00324	-0.231	0.794	Low
ITGB2-AS1	0.188	1.206	High
AC018553.1	0.121	1.128	High
LINC00520	0.01	1.01	High
DBH-AS1	0.259	1.296	High

HR: Hazard ratio.

DISCUSSION

As an aggressive tumor, melanoma has a poor prognosis and increasing incidence[11]. The main reason for the high mortality rate is late diagnosis[12]. Studies have found that the survival rate of melanoma patients with distant metastases was only 5%-10%[13]. Therefore, early detection and diagnosis of melanoma are crucial to improving the survival rate. At present, TNM staging is commonly used to evaluate the melanoma prognosis. However, some studies have found that TNM staging methods might predict different overall survival rates[14]. Increasing studies have shown that tumor TNM staging also has clinical limitations[15,16]. Therefore, new melanoma diagnosis and prognosis methods are required to improve melanoma patients' prognosis and survival rate. The promotive and suppressive effects of autophagy on the development of tumors were observed by many previous studies[17,18]. In other words, autophagy is a dual process regarding tumors. For example, Mgrditchian *et al*[19] reported that autophagy can recruit natural killer cell infiltration into tumor tissues, and subsequently reduce the melanoma growth *in vivo*[19]. Luan *et al*[20] showed that POL can downregulate miR1290, leading to BECN1 upregulation and enhanced autophagy, thereby reducing the survival of melanoma cells.

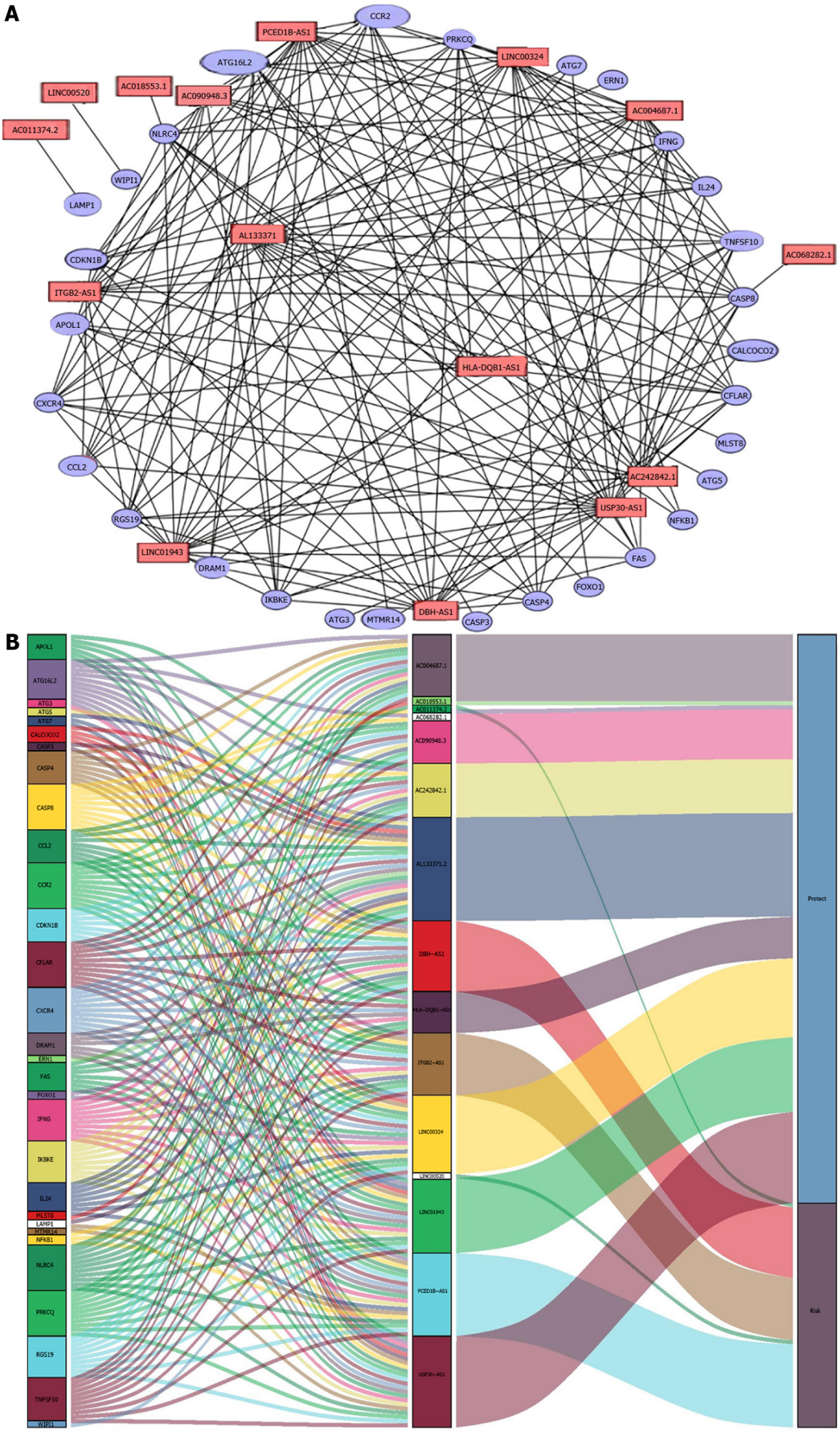

Figure 1 Co-expression network construction using 15 lncRNAs with Cytoscape. A: Cytoscape network; B: Sankey diagram for lncRNA visualization.

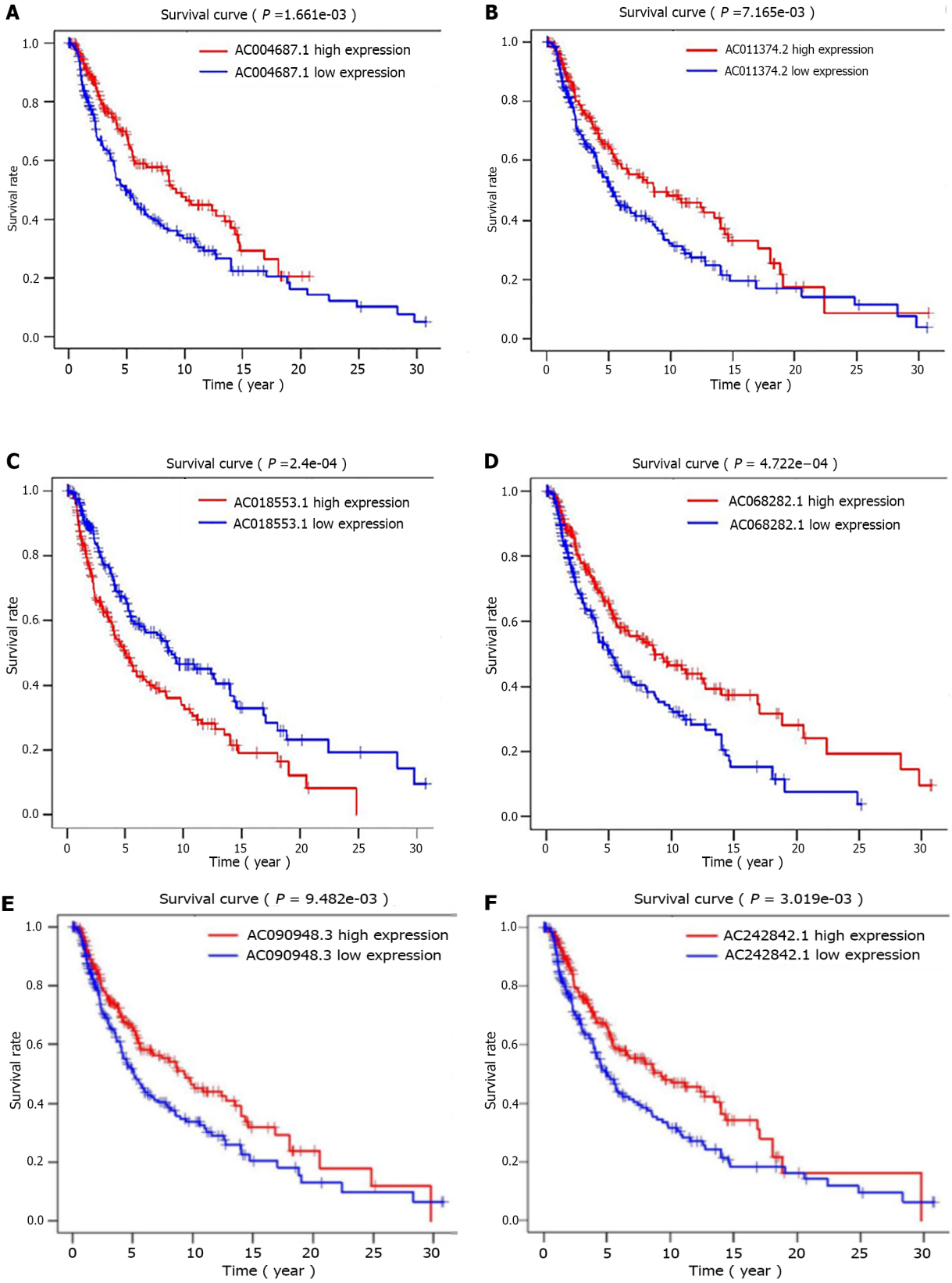
A
Survival curve (P =1.661e-03)
AC004687.1 high expression
AC004687.1 low expression
Survival rate
Time (year)
B
Survival curve (P =7.165e-03)
AC011374.2 high expression
AC011374.2 low expression
Survival rate
Time (year)
C
Survival curve (P =2.4e-04)
AC018553.1 high expression
AC018553.1 low expression
Survival rate
Time (year)
D
Survival curve (P = 4.722e−04)
AC068282.1 high expression
AC068282.1 low expression
Survival rate
Time (year)
E
Survival curve (P = 9.482e-03)
AC090948.3 high expression
AC090948.3 low expression
Survival rate
Time (year)
F
Survival curve (P = 3.019e-03)
AC242842.1 high expression
AC242842.1 low expression
Survival rate
Time (year)

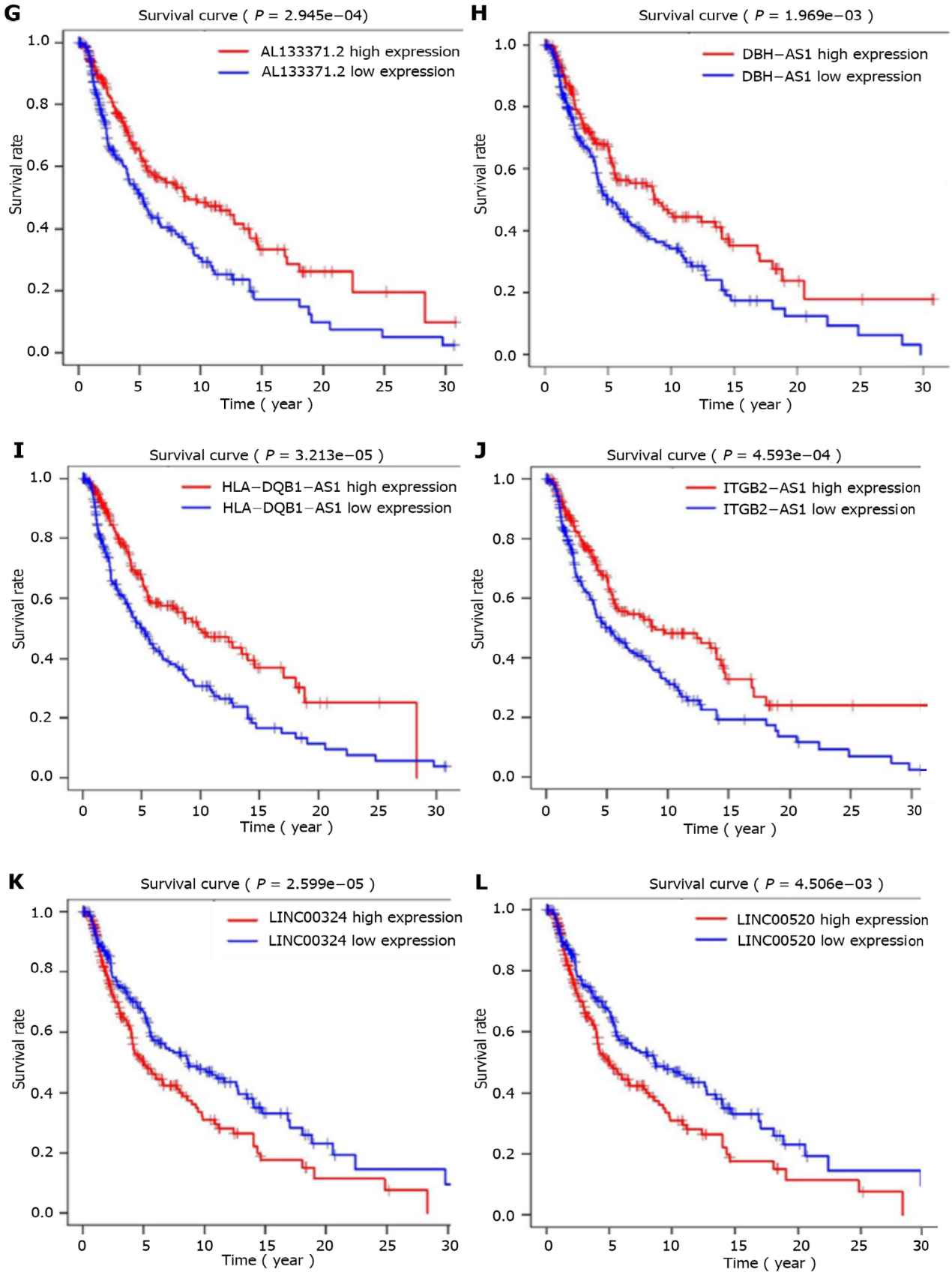
G
Survival curve (P = 2.945e−04)
AL133371.2 high expression
AL133371.2 low expression
Survival rate
Time (year)
H
Survival curve (P = 1.969e−03)
DBH−AS1 high expression
DBH−AS1 low expression
Survival rate
Time (year)
I
Survival curve (P = 3.213e−05)
HLA−DQB1−AS1 high expression
HLA−DQB1−AS1 low expression
Survival rate
Time (year)
J
Survival curve (P = 4.593e−04)
ITGB2−AS1 high expression
ITGB2−AS1 low expression
Survival rate
Time (year)
K
Survival curve (P = 2.599e−05)
LINC00324 high expression
LINC00324 low expression
Survival rate
Time (year)
L
Survival curve (P = 4.506e−03)
LINC00520 high expression
LINC00520 low expression
Survival rate
Time (year)

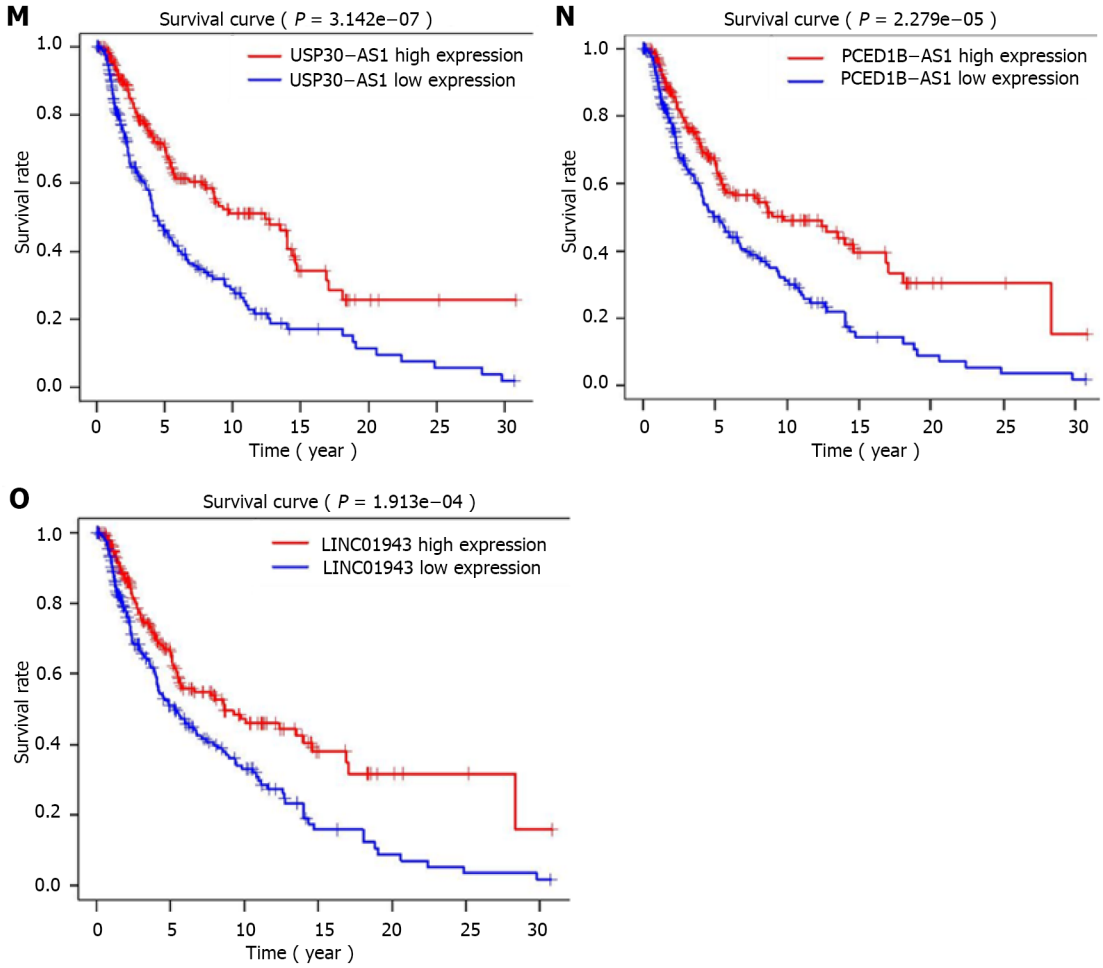

Figure 2 Survival analysis of 15 autophagy-associated lncRNAs. A: AC004687.1; B: AC011374.2; C: AC018553.1; D: AC068282; E: AC090948.3; F: AC242842.1; G: AL133371.2; H: DBH−AS1; I: HLA−DQB1−AS1; J: ITGB2−AS1; K: LINC00324; L: LINC00520; M: USP30−AS1; N: PCED1B−AS1; O: LINC01943. (Red and blue represent the high and low expression of the lncRNAs in melanoma patients, respectively).

However, Xiao *et al*[21] showed that beclin-1 expression and LC3-II/I ratio were significantly increased by miR-24-1-5p. Meanwhile, they also observed the promotive effect of miR-24-1-5p on autophagy and subsequently inhibitory function in melanoma cell proliferation[21]. The studies listed above showed both positive and negative effects of autophagy on tumor development, and that autophagy plays a crucial role in this process.

Additionally, the roles of lncRNAs in the pathogenesis of different tumors have been identified by other researchers, including breast cancer, lung cancer, and hepatocellular carcinoma[22,23]. In this study, we analyzed and identified 15 lncRNAs that can be related to melanoma survival and prognosis, and established a risk model for melanoma prognosis. We consulted many previous studies and found that only LINC00520 and DBH-AS1 have been linked to melanoma. USP30-AS1, PCED1B-AS1, LINC00324, ITGB2-AS1, LINC00520, and DBH-AS1 have also been reported in other tumors. The remaining lncRNAs (LINC01943, AC090948.3, AC068282.1, AC004687.1, AL133371.2, AC242842.1, HLA-DQB1-AS1, AC011374.2, and AC018553.1) have not yet been reported. LICN00520 can promote melanoma's proliferative and metastatic capabilities by competitively targeting miR-125b-5p and acting on the miR-125b-5p/eIF5A2 axis *in vivo*[24]. Also, LINC00520 can be involved in the progressive processes of many tumors. For example, Luan *et al*[24] pointed out that through MiR-3175 suppression, LINC00520 was involved in lung cancer progression[25]. Jin *et al*[26] found that LINC00520 can act as a miR-577 competitive suppressor to enhance HSP27 expression, leading to colorectal cancer progression [26]. Besides, LINC00520 can promote thyroid papillary carcinoma, nasopharyngeal carcinoma, breast cancer, and non-small cell lung cancer progression, being a poor prognostic factor for these tumors[27-31]. Chen *et al*[32] found that DBH-AS1 can enhance the glycolytic activity of melanoma cells, thereby blocking the miR-223-3p/EGFR/AKT axis[32]. Crucial roles of the lncRNA DBH-AS1 were also observed in osteosarcoma, diffuse large b-cell lymphoma, liver cancer, and non-small cell lung cancer [33-36]. In our analyses, both DBH-AS1 and LINC00520 were high-risk autophagy-related lncRNAs. Their elevated expression in melanoma patients indicated a poor prognosis. Through sequestering miR-229-3p and subsequently enhancing the expression of PTP4A1[37], USP30-AS1 expression can promote cervical cancer malignant progression. The lncRNA pCED1B-AS1 can activate glioma cell proliferation

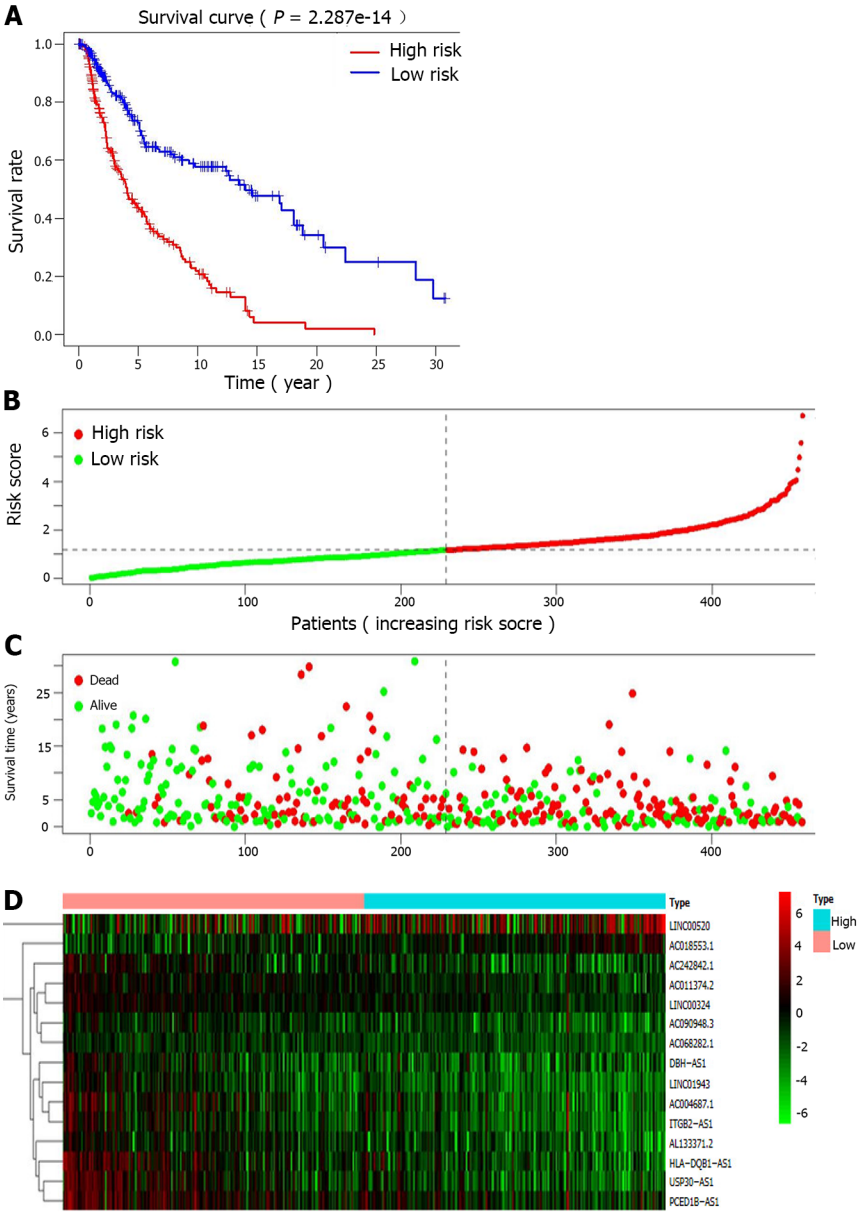

Figure 3 Prognostic value of the 15-lncRNA risk model for melanoma. A: Survival rate analysis; B: Representative risk curve showing the risk scores; C: Scatter diagram of survival state. Green dots: Surviving; red dots: Dead; D: Representative heatmap showing the expression of indicated lncRNAs in different groups. Green and red represent low and high expression, respectively.

and limit apoptosis, working with the miR-194-5p/ pCED1B axis[38]. pCED1B-AS1 can also induce hepatocellular carcinoma immunosuppression through PD-1 and PD-L1 regulation *via* sponging has-miR-1945p[39]. Other studies have shown that the lncRNA pcED1B-AS1 can also promote clear cell renal carcinoma and pancreatic ductal adenocarcinoma progression[40,41]. Important roles of the lncRNAs LINC00324 and A ITGB2-AS1 have been observed during different tumors progressions. For example, the proliferative and invasive capabilities of osteosarcoma were promoted by LINC00324 through WDR66 regulation. Also, the promotive effects of LNC00324 on papillary thyroid carcinoma progression were found, due to its regulatory effect on Notch-related pathways[42,43]. The lncRNA ITGB2-AS1 can upregulate ITGB2 and promote breast cancer cell migration and invasion. Besides, ITGB2-AS1 can also promote pancreatic ductal adenocarcinoma growth and metastasis, acting on the miR-4319/RAF1 axis[44,45].

The mechanisms of the remaining nine lncRNAs identified in our study (LINC01943, AC090948.3, AC068282.1, AC004687.1, AL133371.2, AC242842.1, HLA-DQB1-AS1, AC011374.2, and AC018553.1) have not been yet reported and remain to be explored. Five of them, including PCED1B-AS1, ITGB2-AS1, AC018553.1, LINC00520, and DBH-AS1, were risk-related lncRNAs, and their increased expression levels suggested a poor prognosis. The remaining ten lncRNAs (LINC01943, AC090948.3, USP30-AS1, AC068282.1, AC004687.1, AL133371.2, AC242842.1, HLA-DQB1-AS1, AC011374.2, and LINC00324) were protective lncRNAs, and their elevated expression levels in melanoma patients predicted a good prognosis. The survival analysis (P = 2.287e - 14) suggested a significant difference between the survival

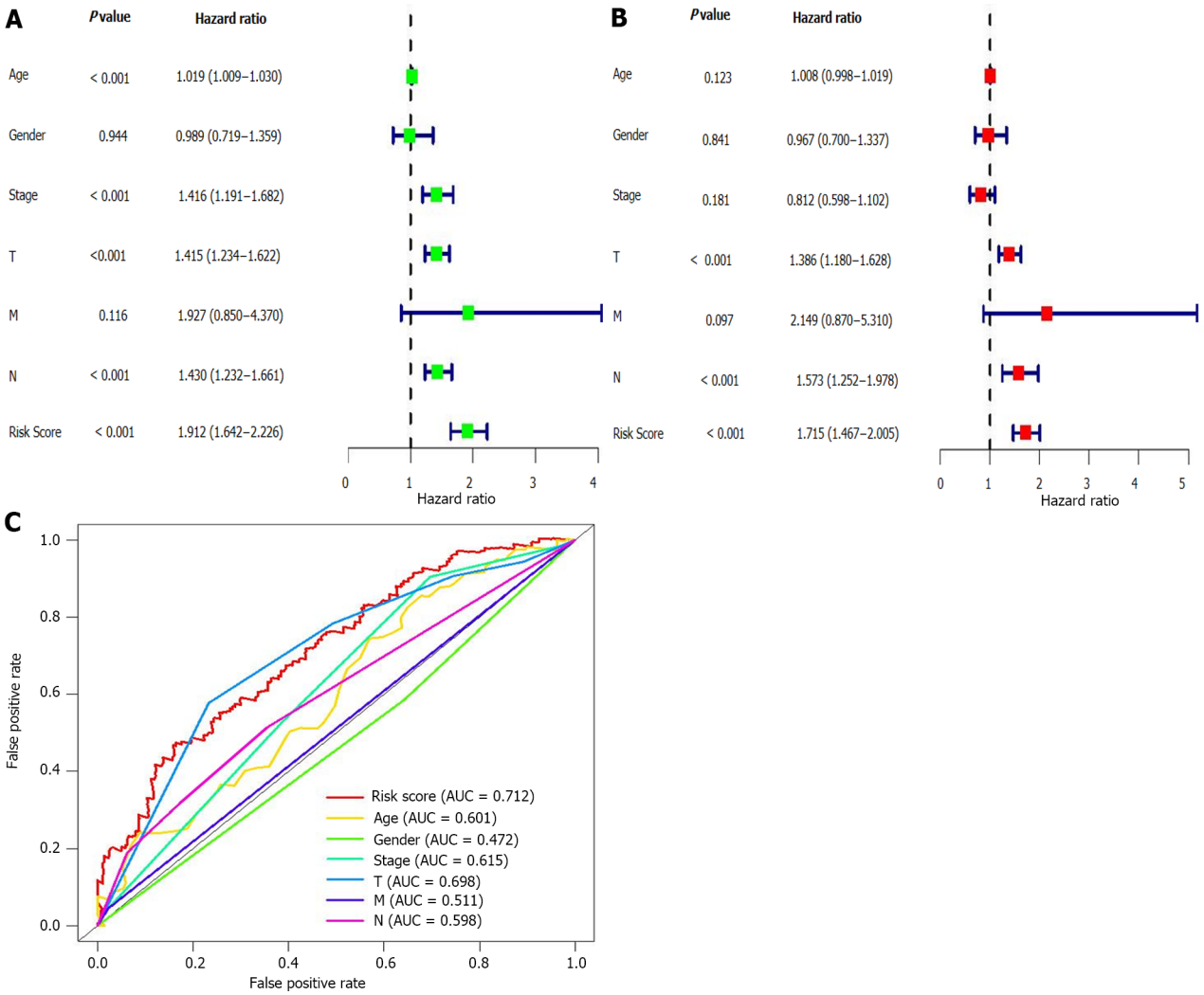

Figure 4 Melanoma risk model evaluation. A and B: Univariate and multivariate Cox regression analyses for prognostic risk scores and different clinical features; C: Receiver operating characteristic curves for risk scores and different clinical characteristics (age, gender, and TMN stage).

rate of the high- and low-risk score patients. Meanwhile, we also observed negative correlations between the risk scores and overall survival rate in melanoma patients. Finally, we constructed the ROC curve, and the AUC value was 0.712, higher than the AUC of all clinicopathological indicators analyzed. Not only that, we also downloaded 265 melanoma samples from GEO database to verify the accuracy of this model, and the results are consistent with those of the previous analysis. These results demonstrated that the prognostic model established based on autophagy-related lncRNAs in melanoma patients had a higher prognostic accuracy than other clinical indicators. Altogether, these results suggested that the risk model established based on the 15 autophagy-related lncRNAs could better predict melanoma patients' prognosis and survival.

The GSEA analysis revealed a difference in signaling pathway enrichment between the high- and low-risk melanoma patients. In low-risk populations, the main significantly enriched pathways were immune-related, such as antigen processing and presentation, Toll-like receptor signaling pathway, systemic lupus erythematosus, and autoimmune thyroid disease. The high-risk populations were mainly enriched in metabolism-related pathways, such as glyoxylate and dicarboxylate signaling pathways. These results indicated that the immunity improvement might be related to melanoma patients' prognosis improvement and that a poor prognosis can be associated with glyoxylate and dicarboxylate metabolic pathways.

Recently, increasing studies have explored the significance of lncRNAs in cell autophagy, and their functional effect in tumors have attracted researchers' attention. However, the function, mechanisms, and value of these lncRNAs in melanoma prognosis remain unclear. Our current study proposed a new melanoma risk model composed of 15 lncRNAs involved in autophagy that can be helpful for future melanoma treatment and prognosis evaluation. However, our research also has limitations. Although the data and analyses used have been verified for their accuracy in different studies, our study was not verified experimentally. The molecular mechanism of autophagy-related lncRNAs has not yet been elucidated, and some lncRNAs have never even been reported in the literature. Therefore, further

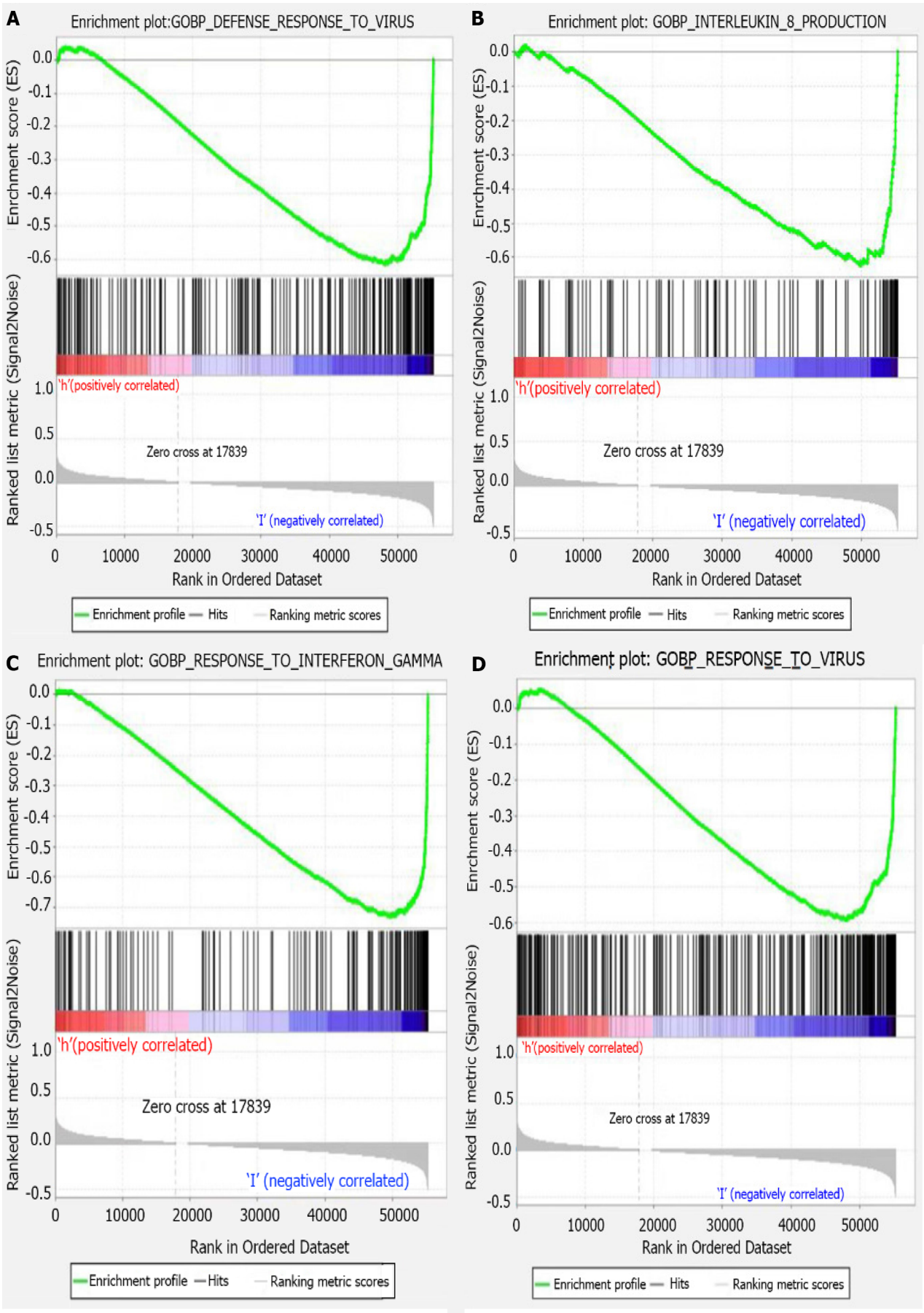
A
Enrichment plot:GOBP_DEFENSE_RESPONSE_TO_VIRUS
Enrchment score (ES)
Ranked list metric (Signal2Noise)
'h'(positively correlated)
'l' (negatively correlated)
Zero cross at 17839
Rank in Ordered Dataset
Enrichment profile
Hits
Ranking metric scores
B
Enrichment plot: GOBP_INTERLEUKIN_8_PRODUCTION
C
Enrichment plot: GOBP_RESPONSE_TO_INTERFERON_GAMMA
D
Enrichment plot: GOBP_RESPONSE_TO_VIRUS

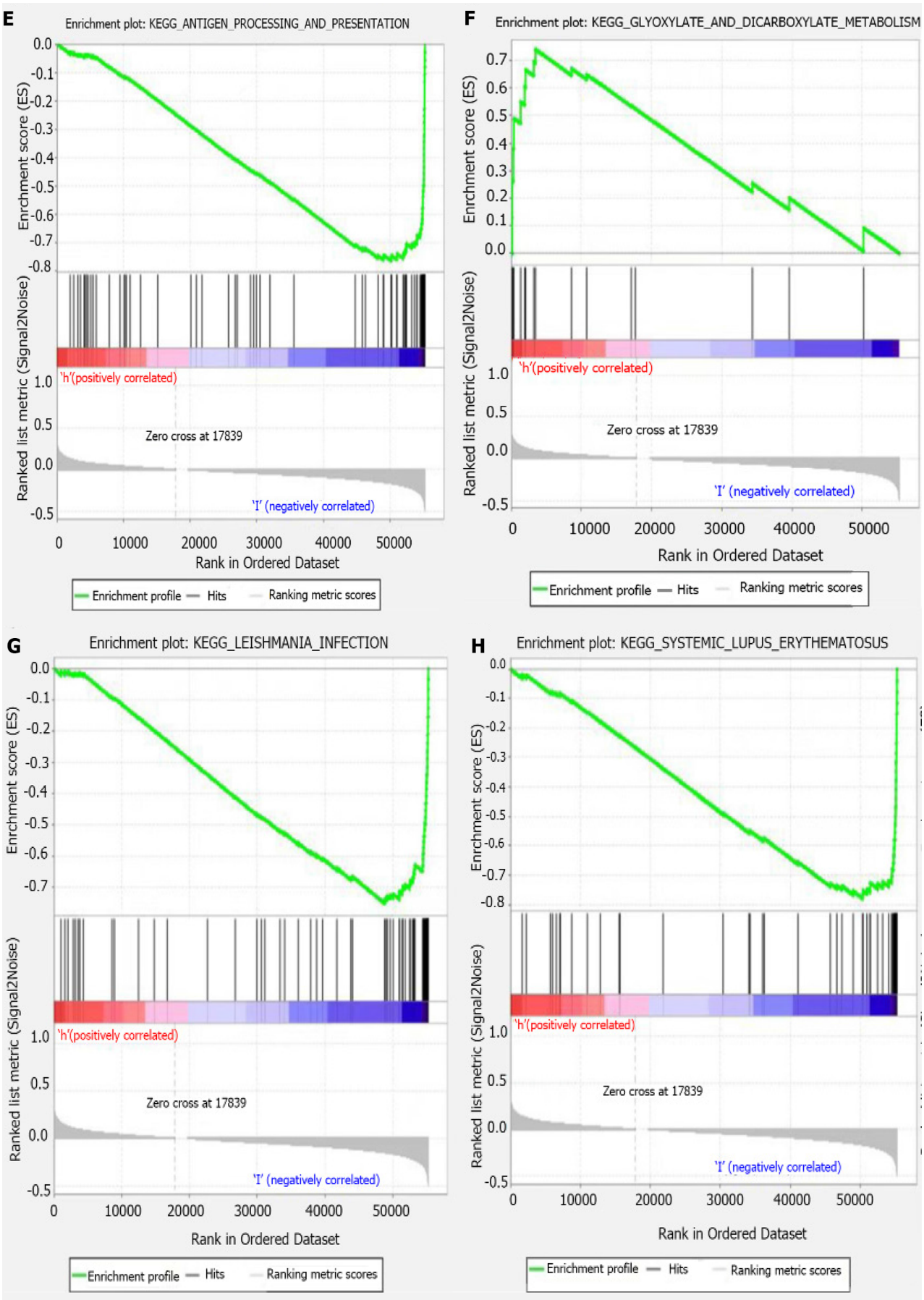
E
Enrichment plot: KEGG_ANTIGEN_PROCESSING_AND_PRESENTATION
Enrchment score (ES)
Ranked list metric (Signal2Noise)
'h'(positively correlated)
Zero cross at 17839
'I' (negatively correlated)
Rank in Ordered Dataset
Enrichment profile
Hits
Ranking metric scores
F
Enrichment plot: KEGG_GLYOXYLATE_AND_DICARBOXYLATE_METABOLISM
Enrchment score (ES)
Ranked list metric (Signal2Noise)
'h'(positively correlated)
Zero cross at 17839
'I' (negatively correlated)
Rank in Ordered Dataset
Enrichment profile
Hits
Ranking metric scores
G
Enrichment plot: KEGG_LEISHMANIA_INFECTION
Enrchment score (ES)
Ranked list metric (Signal2Noise)
'h'(positively correlated)
Zero cross at 17839
'I' (negatively correlated)
Rank in Ordered Dataset
Enrichment profile
Hits
Ranking metric scores
H
Enrichment plot: KEGG_SYSTEMIC_LUPUS_ERYTHEMATOSUS
Enrchment score (ES)
Ranked list metric (Signal2Noise)
'h'(positively correlated)
Zero cross at 17839
'I' (negatively correlated)
Rank in Ordered Dataset
Enrichment profile
Hits
Ranking metric scores

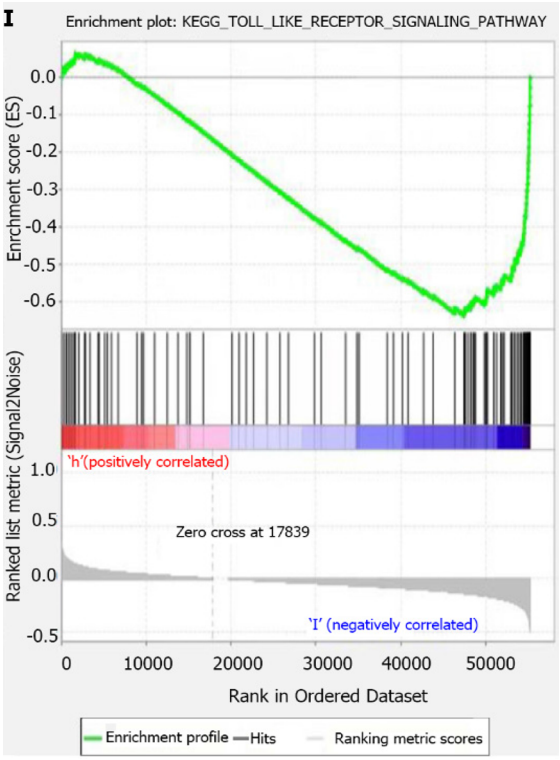

Figure 5 Gene Set Enrichment Analysis for functional enrichment analysis of 15 autophagy-related lncRNAs. Among them, Gene Ontology, KEGG pathway, and immune signal were significantly enriched in the low-risk group, while the KEGG pathway was slightly enriched in the high-risk group. A: Enrichment plot: GOBP_DEFENSE_RESPONSE_TO_VIRUS; B: GOBP_INTERLEUKIN_8_PRODUCTION; C: GOBP_RESPONSE_TO_INTERFERON_GAMMA; D: GOBP_RESPONSE_TO_VIRUS; E: KEGG_ANTIGEN_PROCESSING_AND_PRESENTATION; F: KEGG_GLYOXYLATE_AND_DICARBOXYLATE_METABOLISM; G: KEGG_LEISHMANIA_INFECTION; H: KEGG_SYSTEMIC_LUPUS_ERYTHEMATOSUS; I: KEGG_TOLL_LIKE_RECEPTOR_SIGNALING_PATHWAY.

experimental studies are required to verify our results.

CONCLUSION

Overall, we have identified and established a new prognostic risk model for melanoma using 15 autophagy-related lncRNAs: LINC01943, AC090948.3, USP30-AS1, AC068282.1, AC004687.1, AL133371.2, AC242842.1, PCED1B-AS1, HLA-DQB1-AS1, AC011374.2, LINC00324, ITGB2-AS1, AC018553.1, LINC00520, and DBH-AS1. The risk model constructed with these lncRNAs can help guide prognosis prediction and individualized treatment in melanoma patients in the future.

ARTICLE HIGHLIGHTS

Research background

At present, melanoma is mainly treated by surgical resection, but many patients have tumor metastasis. Patients with advanced melanoma have a very poor prognosis, so a new method is needed to predict and evaluate the prognosis and survival of patients. Autophagy, originally thought to be a process of lysosomal dependent degradation of cytoplasmic components in response to starvation, has been shown to influence multiple dynamic equilibria and to constitute a barrier against malignant transformation. However, long non-coding RNAs (lncRNAs) involved in autophagy and their prognostic value have not been studied before, and many mechanisms remain unclear. Therefore, risk stratification of melanoma patients based on autophagy-associated lncRNAs combined with pathological classification is crucial to predict prognosis and treatment response.

Research motivation

The main purpose of this study was to identify autophagy lncRNAs associated with melanoma prognosis and establish a risk model to predict survival and prognosis. Among the 15 autophagy-related lncRNAs analyzed in this study, the mechanisms of action of some lncRNAs are still unclear and have not been reported in the literature, so further studies are needed to explore the role of these

lncRNAs. The solution of this major problem will help us to have a deeper understanding of melanoma and make it possible to completely cure melanoma.

Research objectives

The main objective of this study was to establish a more accurate method for predicting and evaluating the prognosis and survival of melanoma patients.

Research methods

First, data from The Cancer Genome Atlas and GENE EXPRESSION OMNIBUS (GEO) databases were processed, and then R was used to analyze the correlation between autophagy-related genes and lncRNAs (correlation coefficient > 0.30; $P < 0.001$), and a co-expression network was constructed. In order to evaluate the relationship between autophagy-related lncRNAs and melanoma prognosis, univariate proportional risk, Kaplan-Meier survival, and multivariate risk analyses were performed. R software was used to calculate the risk score of each patient, and the calculation formula is as follows: Risk score = expR (lncRNA1) × COEF (lncRNA1) + expr (lncRNA2) × COEF (lncRNA2) +... + expr (lncRNAn) × COEF (lncRNAn). In order to assess the stability of risk models, univariate and multivariate regression analyses and receiver operating characteristic analyses were also performed. Finally, Gene Set Enrichment Analysis was used for functional annotation and GEO data was used for further validation to ensure the accuracy of the results.

Research results

Our current study proposed a new melanoma risk model composed of 15 lncRNAs involved in autophagy that can be helpful for future melanoma treatment and prognosis evaluation. However, our research also has limitations. Although the data and analyses used have been verified for their accuracy in different studies, our study was not verified experimentally. The molecular mechanisms of phagocytosis-related lncRNAs have not yet been elucidated, and some lncRNAs have never even been reported in the literature. Therefore, further experimental studies are required to verify our results.

Research conclusions

This study identified new and unreported lncRNAs through a series of analyses, which are closely related to the prognosis of melanoma patients, providing a new direction for future research on melanoma-related lncRNAs.

Research perspectives

In the future, we can conduct further experimental verification on these 15 lncRNAs to understand the specific mechanism of action and specific role of these 15 lncRNAs in melanoma.

FOOTNOTES

Author contributions: Qiu Y wrote the manuscript; Huang JP and Wen ZP contributed to data sorting; Qiu Y, Yao J, and Wang HT performed data analysis; Meng JZ, Zheng XF, and Huang X finalized the manuscript; Yao J read and approved the final manuscript.

Institutional review board statement: Institutional review board approval is not required since this study using the public datasets from the TCGA and GEO databases.

Conflict-of-interest statement: There are no conflicts or financial interests to disclose.

Data sharing statement: No additional data are available.

Country/Territory of origin: China

ORCID number: Yue Qiu 0000-0002-2474-8107; Hong-Tao Wang 0000-0003-4183-6368; Xi-Fan Zheng 0000-0002-6185-8778; Xing Huang 0000-0002-9211-4624; Jin-Zhi Meng 0000-0003-0601-4019; Jun-Pu Huang 0000-0002-1362-3560; Zhen-Pei Wen 0000-0001-7306-6033; Jun Yao 0000-0003-2085-1665.

S-Editor: Fan JR
L-Editor: Wang TQ

P-Editor: Cai YX

REFERENCES

1 **MacKie RM**, Hauschild A, Eggermont AM. Epidemiology of invasive cutaneous melanoma. *Ann Oncol* 2009; **20** Suppl 6: vi1-vi7 [PMID: 19617292 DOI: 10.1093/annonc/mdp252]

2 **Rigel DS**. Epidemiology of melanoma. *Semin Cutan Med Surg* 2010; **29**: 204-209 [PMID: 21277533 DOI: 10.1016/j.sder.2010.10.005]

3 **Duncan LM**. The classification of cutaneous melanoma. *Hematol Oncol Clin North Am* 2009; **23**: 501-513, ix [PMID: 19464599 DOI: 10.1016/j.hoc.2009.03.013]

4 **Ugurel S**, Röhmel J, Ascierto PA, Flaherty KT, Grob JJ, Hauschild A, Larkin J, Long GV, Lorigan P, McArthur GA, Ribas A, Robert C, Schadendorf D, Garbe C. Survival of patients with advanced metastatic melanoma: the impact of novel therapies-update 2017. *Eur J Cancer* 2017; **83**: 247-257 [PMID: 28756137 DOI: 10.1016/j.ejca.2017.06.028]

5 **Li S**, Song Y, Quach C, Guo H, Jang GB, Maazi H, Zhao S, Sands NA, Liu Q, In GK, Peng D, Yuan W, Machida K, Yu M, Akbari O, Hagiya A, Yang Y, Punj V, Tang L, Liang C. Transcriptional regulation of autophagy-lysosomal function in BRAF-driven melanoma progression and chemoresistance. *Nat Commun* 2019; **10**: 1693 [PMID: 30979895 DOI: 10.1038/s41467-019-09634-8]

6 **Fazal FM**, Chang HY. lncRNA Structure: Message to the Heart. *Mol Cell* 2016; **64**: 1-2 [PMID: 27716479 DOI: 10.1016/j.molcel.2016.09.030]

7 **Li X**, Li Y, Yu X, Jin F. Identification and validation of stemness-related lncRNA prognostic signature for breast cancer. *J Transl Med* 2020; **18**: 331 [PMID: 32867770 DOI: 10.1186/s12967-020-02497-4]

8 **Chen X**, Gao J, Yu Y, Zhao Z, Pan Y. RETRACTED: Long non-coding RNA UCA1 targets miR-185-5p and regulates cell mobility by affecting epithelial-mesenchymal transition in melanoma *via* Wnt/β-catenin signaling pathway. *Gene* 2018; **676**: 298-305 [PMID: 30144501 DOI: 10.1016/j.gene.2018.08.065]

9 **Peng L**, Chen Z, Chen Y, Wang X, Tang N. MIR155HG is a prognostic biomarker and associated with immune infiltration and immune checkpoint molecules expression in multiple cancers. *Cancer Med* 2019; **8**: 7161-7173 [PMID: 31568700 DOI: 10.1002/cam4.2583]

10 **Li X**, Jin F, Li Y. A novel autophagy-related lncRNA prognostic risk model for breast cancer. *J Cell Mol Med* 2021; **25**: 4-14 [PMID: 33216456 DOI: 10.1111/jcmm.15980]

11 **Liu N**, Liu Z, Liu X, Chen H. Comprehensive Analysis of a Competing Endogenous RNA Network Identifies Seven-lncRNA Signature as a Prognostic Biomarker for Melanoma. *Front Oncol* 2019; **9**: 935 [PMID: 31649871 DOI: 10.3389/fonc.2019.00935]

12 **Huang R**, Mao M, Lu Y, Yu Q, Liao L. A novel immune-related genes prognosis biomarker for melanoma: associated with tumor microenvironment. *Aging (Albany NY)* 2020; **12**: 6966-6980 [PMID: 32310824 DOI: 10.18632/aging.103054]

13 **Sun L**, Guan Z, Wei S, Tan R, Li P, Yan L. Identification of Long Non-coding and Messenger RNAs Differentially Expressed Between Primary and Metastatic Melanoma. *Front Genet* 2019; **10**: 292 [PMID: 31024618 DOI: 10.3389/fgene.2019.00292]

14 **Perakis SO**, Thomas JE, Pichler M. Non-coding RNAs Enabling Prognostic Stratification and Prediction of Therapeutic Response in Colorectal Cancer Patients. *Adv Exp Med Biol* 2016; **937**: 183-204 [PMID: 27573901 DOI: 10.1007/978-3-319-42059-2_10]

15 **Edge SB**, Compton CC. The American Joint Committee on Cancer: the 7th edition of the AJCC cancer staging manual and the future of TNM. *Ann Surg Oncol* 2010; **17**: 1471-1474 [PMID: 20180029 DOI: 10.1245/s10434-010-0985-4]

16 **Galon J**, Pagès F, Marincola FM, Thurin M, Trinchieri G, Fox BA, Gajewski TF, Ascierto PA. The immune score as a new possible approach for the classification of cancer. *J Transl Med* 2012; **10**: 1 [PMID: 22214470 DOI: 10.1186/1479-5876-10-1]

17 **Shintani T**, Klionsky DJ. Autophagy in health and disease: a double-edged sword. *Science* 2004; **306**: 990-995 [PMID: 15528435 DOI: 10.1126/science.1099993]

18 **White E**, DiPaola RS. The double-edged sword of autophagy modulation in cancer. *Clin Cancer Res* 2009; **15**: 5308-5316 [PMID: 19706824 DOI: 10.1158/1078-0432.CCR-07-5023]

19 **Mgrditchian T**, Arakelian T, Paggetti J, Noman MZ, Viry E, Moussay E, Van Moer K, Kreis S, Guerin C, Buart S, Robert C, Borg C, Vielh P, Chouaib S, Berchem G, Janji B. Targeting autophagy inhibits melanoma growth by enhancing NK cells infiltration in a CCL5-dependent manner. *Proc Natl Acad Sci U S A* 2017; **114**: E9271-E9279 [PMID: 29078276 DOI: 10.1073/pnas.1703921114]

20 **Luan W**, Qian Y, Ni X, Chanda TK, Xia Y, Wang J, Yan Y, Xu B. *Polygonatum odoratum* lectin promotes *BECN1* expression and induces autophagy in malignant melanoma by regulation of miR1290. *Onco Targets Ther* 2017; **10**: 4569-4577 [PMID: 29066911 DOI: 10.2147/OTT.S147406]

21 **Xiao Y**, Diao Q, Liang Y, Peng Y, Zeng K. MicroRNA 24 1 5p promotes malignant melanoma cell autophagy and apoptosis *via* regulating ubiquitin D. *Mol Med Rep* 2017; **16**: 8448-8454 [DOI: 10.3892/mmr.2017.7614]

22 **Xiong H**, Ni Z, He J, Jiang S, Li X, Gong W, Zheng L, Chen S, Li B, Zhang N, Lyu X, Huang G, Chen B, Zhang Y, He F. LncRNA HULC triggers autophagy *via* stabilizing Sirt1 and attenuates the chemosensitivity of HCC cells. *Oncogene* 2017; **36**: 3528-3540 [PMID: 28166203 DOI: 10.1038/onc.2016.521]

23 **Liu XW**, Xiao ZD, Han L, Zhang JX, Lee SW, Wang WQ, Lee H, Zhuang L, Chen JJ, Lin HK, Wang J, Liang H, Gan BY. LncRNA NBR2 engages a metabolic checkpoint by regulating AMPK under energy stress. *Nat Cell Biol* 2016; **18**: 431-442 [PMID: 26999735 DOI: 10.1038/ncb3328]

24 **Luan W**, Ding Y, Yuan H, Ma S, Ruan H, Wang J, Lu F, Bu X. Long non-coding RNA LINC00520 promotes the proliferation and metastasis of malignant melanoma by inducing the miR-125b-5p/EIF5A2 axis. *J Exp Clin Cancer Res*

2020; **39**: 96 [PMID: 32466797 DOI: 10.1186/s13046-020-01599-7]

25 **Xia G**, Li X, Chen F, Shao Z. LncRNA LINC00520 Predicts Poor Prognosis and Promotes Progression of Lung Cancer by Inhibiting MiR-3175 Expression. *Cancer Manag Res* 2020; **12**: 5741-5748 [PMID: 32801856 DOI: 10.2147/CMAR.S250631]

26 **Jin XH**, Hong YG, Li P, Hao LQ, Chen M. Long noncoding RNA LINC00520 accelerates the progression of colorectal cancer by serving as a competing endogenous RNA of microRNA-577 to increase HSP27 expression. *Hum Cell* 2020; **33**: 683-694 [PMID: 32146708 DOI: 10.1007/s13577-020-00336-8]

27 **Sun Y**, Shi T, Ma Y, Qin H, Li K. Long noncoding RNA LINC00520 accelerates progression of papillary thyroid carcinoma by serving as a competing endogenous RNA of microRNA-577 to increase Sphk2 expression. *Cell Cycle* 2020; **19**: 787-800 [PMID: 32075502 DOI: 10.1080/15384101.2020.1731062]

28 **Wang JF**, Xi ZN, Su HJ, Bao Z, Qiao YH. SP1-induced overexpression of LINC00520 facilitates non-small cell lung cancer progression through miR-577/CCNE2 pathway and predicts poor prognosis. *Hum Cell* 2021; **34**: 952-964 [PMID: 33728585 DOI: 10.1007/s13577-021-00518-y]

29 **Chen X**, Chen H, Liu M, Xiong J, Song Z. Long noncoding RNA LINC00520 accelerates lung adenocarcinoma progression *via* miR-1252-5p/FOXR2 pathway. *Hum Cell* 2021; **34**: 478-490 [PMID: 33464477 DOI: 10.1007/s13577-020-00478-9]

30 **Xie T**, Pi G, Yang B, Ren H, Yu J, Ren Q, Zhou X, Hu D, Zhang H, Zhang Q, Hu L, Li Y, Zhou F. Long non-coding RNA 520 is a negative prognostic biomarker and exhibits pro-oncogenic function in nasopharyngeal carcinoma carcinogenesis through regulation of miR-26b-3p/USP39 axis. *Gene* 2019; **707**: 44-52 [PMID: 30898716 DOI: 10.1016/j.gene.2019.02.093]

31 **Henry WS**, Hendrickson DG, Beca F, Glass B, Lindahl-Allen M, He L, Ji Z, Struhl K, Beck AH, Rinn JL, Toker A. LINC00520 is induced by Src, STAT3, and PI3K and plays a functional role in breast cancer. *Oncotarget* 2016; **7**: 81981-81994 [PMID: 27626181 DOI: 10.18632/oncotarget.11962]

32 **Chen XX**, Zhang N, Fu XF, Jiang Y, Wang MY. LncRNA DBH-AS1 facilitates the tumorigenesis of melanoma by targeting miR-233-3p *via* IGF-1R/Akt signaling. *Eur Rev Med Pharmacol Sci* 2020; **24**: 7698-7708 [PMID: 32744696 DOI: 10.26355/eurrev_202007_22272]

33 **Huang JL**, Ren TY, Cao SW, Zheng SH, Hu XM, Hu YW, Lin L, Chen J, Zheng L, Wang Q. HBx-related long non-coding RNA DBH-AS1 promotes cell proliferation and survival by activating MAPK signaling in hepatocellular carcinoma. *Oncotarget* 2015; **6**: 33791-33804 [PMID: 26393879 DOI: 10.18632/oncotarget.5667]

34 **Song Y**, Gao F, Peng Y, Yang X. Long non-coding RNA DBH-AS1 promotes cancer progression in diffuse large B-cell lymphoma by targeting FN1 *via* RNA-binding protein BUD13. *Cell Biol Int* 2020; **44**: 1331-1340 [PMID: 32091157 DOI: 10.1002/cbin.11327]

35 **Liu ZB**, Wang JA, Lv RQ. Downregulation of long non-coding RNA DBH-AS1 inhibits osteosarcoma progression by PI3K-AKT signaling pathways and indicates good prognosis. *Eur Rev Med Pharmacol Sci* 2019; **23**: 1418-1427 [PMID: 30840262 DOI: 10.26355/eurrev_201902_17098]

36 **Bao J**, Chen X, Hou Y, Kang G, Li Q, Xu Y. LncRNA DBH-AS1 facilitates the tumorigenesis of hepatocellular carcinoma by targeting miR-138 *via* FAK/Src/ERK pathway. *Biomed Pharmacother* 2018; **107**: 824-833 [PMID: 30142544 DOI: 10.1016/j.biopha.2018.08.079]

37 **Chen M**, Chi Y, Chen H, Zhao L. Long non-coding RNA USP30-AS1 aggravates the malignant progression of cervical cancer by sequestering microRNA-299-3p and thereby overexpressing PTP4A1. *Oncol Lett* 2021; **22**: 505 [PMID: 33986866 DOI: 10.3892/ol.2021.12766]

38 **Yang J**, Yu D, Liu X, Changyong E, Yu S. LncRNA PCED1B-AS1 activates the proliferation and restricts the apoptosis of glioma through cooperating with miR-194-5p/PCED1B axis. *J Cell Biochem* 2020; **121**: 1823-1833 [PMID: 31680313 DOI: 10.1002/jcb.29417]

39 **Fan F**, Chen K, Lu X, Li A, Liu C, Wu B. Dual targeting of PD-L1 and PD-L2 by PCED1B-AS1 *via* sponging hsa-miR-194-5p induces immunosuppression in hepatocellular carcinoma. *Hepatol Int* 2021; **15**: 444-458 [PMID: 33219943 DOI: 10.1007/s12072-020-10101-6]

40 **Qin J**, Zhu T, Wu W, Chen H, He Y. Long Non-Coding RNA PCED1B-AS1 Promotes the Progression of Clear Cell Renal Cell Carcinoma Through miR-484/ZEB1 Axis. *Onco Targets Ther* 2021; **14**: 393-402 [PMID: 33469315 DOI: 10.2147/OTT.S270149]

41 **Zhang Y**, Ma H, Chen C. Long non-coding RNA PCED1B-AS1 promotes pancreatic ductal adenocarcinoma progression by regulating the miR-411-3p/HIF-1α axis. *Oncol Rep* 2021; **46**: 134 [PMID: 34036383 DOI: 10.3892/or.2021.8085]

42 **Wu S**, Gu Z, Wu Y, Wu W, Mao B, Zhao S. LINC00324 accelerates the proliferation and migration of osteosarcoma through regulating WDR66. *J Cell Physiol* 2020; **235**: 339-348 [PMID: 31225659 DOI: 10.1002/jcp.28973]

43 **Wan JF**, Wan JY, Dong C, Li L. Linc00324 promotes the progression of papillary thyroid cancer *via* regulating Notch signaling pathway. *Eur Rev Med Pharmacol Sci* 2020; **24**: 6818-6824 [PMID: 32633374 DOI: 10.26355/eurrev_202006_21671]

44 **Yang M**, Qin Q, Zhu J, Guo Y, Yin T, Wu H, Wang C. Long noncoding RNA ITGB2-AS1 promotes growth and metastasis through miR-4319/RAF1 axis in pancreatic ductal adenocarcinoma. *J Cell Physiol* 2020 [PMID: 31957875 DOI: 10.1002/jcp.29471]

45 **Liu M**, Gou L, Xia J, Wan Q, Jiang Y, Sun S, Tang M, He T, Zhang Y. LncRNA ITGB2-AS1 Could Promote the Migration and Invasion of Breast Cancer Cells through Up-Regulating ITGB2. *Int J Mol Sci* 2018; **19** [PMID: 29941860 DOI: 10.3390/ijms19071866]

World Journal of Clinical Cases

Submit a Manuscript: https://www.f6publishing.com

World J Clin Cases 2022 April 16; 10(11): 3352-3368

DOI: 10.12998/wjcc.v10.i11.3352

ISSN 2307-8960 (online)

ORIGINAL ARTICLE

Clinical and Translational Research

Identification of circ_0000375 and circ_0011536 as novel diagnostic biomarkers of colorectal cancer

Teng-Fei Yin, Shi-Yu Du, Dong-Yan Zhao, Xi-Zhen Sun, Yuan-Chen Zhou, Qian-Qian Wang, Ge-Yu-Jia Zhou, Shu-Kun Yao

Specialty type: Oncology

Provenance and peer review: Unsolicited article; Externally peer reviewed.

Peer-review model: Single blind

Peer-review report's scientific quality classification

Grade A (Excellent): 0
Grade B (Very good): B, B
Grade C (Good): 0
Grade D (Fair): 0
Grade E (Poor): 0

P-Reviewer: Janvilisri T, Kołat D

Received: October 29, 2021
Peer-review started: October 29, 2021
First decision: December 27, 2021
Revised: December 30, 2021
Accepted: February 12, 2022
Article in press: February 12, 2022
Published online: April 16, 2022

Teng-Fei Yin, Shi-Yu Du, Yuan-Chen Zhou, Qian-Qian Wang, Shu-Kun Yao, Graduate School, Peking University China-Japan Friendship School of Clinical Medicine, Beijing 100029, China

Shi-Yu Du, Dong-Yan Zhao, Ge-Yu-Jia Zhou, Shu-Kun Yao, Department of Gastroenterology, China-Japan Friendship Hospital, Beijing 100029, China

Dong-Yan Zhao, Xi-Zhen Sun, Ge-Yu-Jia Zhou, Graduate School, Peking Union Medical College and Chinese Academy of Medical Sciences, Beijing 100730, China

Xi-Zhen Sun, Department of Gastroenterology, Beijing Jishuitan Hospital, Beijing 100035, China

Corresponding author: Shu-Kun Yao, MD, PhD, Doctor, Professor, Graduate School, Peking University China-Japan Friendship School of Clinical Medicine, No. 2 Yinghua East Road, Chaoyang District, Beijing 100029, China. shukunyao@126.com

Abstract

BACKGROUND

Colorectal cancer (CRC) imposes a tremendous burden on human health, with high morbidity and mortality. Circular ribonucleic acids (circRNAs), a new type of noncoding RNA, are considered to participate in cancer pathogenesis as microRNA (miRNA) sponges. However, the dysregulation and biological functions of circRNAs in CRC remain to be explored.

AIM

To identify potential circRNA biomarkers of CRC and explore their functions in CRC carcinogenesis.

METHODS

CircRNAs and miRNAs differentially expressed in CRC tissues were identified by analyzing expression profiles from the Gene Expression Omnibus (GEO) database. Circ_0000375 and circ_0011536 were selected as CRC biomarker candidates. Quantitative real-time polymerase chain reaction was utilized to evaluate the expression of these 2 circRNAs in CRC tissues, serums and cell lines. Receiver operating characteristic curves were generated to assess the diagnostic performances of these 2 circRNAs. Then, functional experiments, including cell counting kit-8, wound healing and Transwell invasion assays, were performed

after the overexpression of circ_0000375 and circ_0011536 in CRC cell lines. Furthermore, candidate target miRNAs of circ_0000375 and circ_0011536 were predicted *via* bioinformatics analysis. The expression levels of these miRNAs were explored in CRC cell lines and tissues from GEO datasets. A luciferase reporter assay was developed to examine the interactions between circRNAs and miRNAs. Based on the target miRNAs and downstream genes, functional enrichment analyses were applied to reveal the critical signaling pathways involved in CRC carcinogenesis.

RESULTS

Downregulated circ_0000375 and circ_0011536 expression was observed in CRC tissues in GSE126095, clinical CRC tissue and serum samples and CRC cell lines. The areas under the curve for circ_0000375 and circ_0011536 were 0.911 and 0.885 in CRC tissue and 0.976 and 0.982 in CRC serum, respectively. Moreover, the serum levels of these 2 circRNAs were higher in patients at 30 d postsurgery than in patients before surgery, suggesting that the serum expression of circ_0000375 and circ_0011536 is related to CRC tumorigenesis. Circ_0000375 and circ_0011536 overexpression inhibited the proliferation, migration and invasion of CRC cells. Furthermore, miR-1182 and miR-1246, which were overexpressed in CRC tissues in GSE41655, GSE49246 and GSE115513, were verified as target miRNAs of circ_0000375 and circ_0011536, respectively, by luciferase reporter assays. The downstream genes of miR-1182 and miR-1246 were enriched in some CRC-associated pathways, such as the Wnt signaling pathway.

CONCLUSION

Circ_0000375 and circ_0011536 may function as tumor suppressors in CRC progression, serving as novel biomarkers for CRC diagnosis and as promising candidates for therapeutic exploration.

Key Words: Cir_0000375; Circ_0011536; MicroRNA; Biomarker; Colorectal cancer; Tumor suppressor

Core Tip: The dysregulation and biological functions of circular ribonucleic acids (circRNAs) in colorectal cancer (CRC) have not been well elucidated. In this study, circ_0000375 and circ_0011536 were observed to be downregulated in CRC tissues, serum samples and cell lines. These 2 circRNAs were validated as biomarker candidates in tissues and serum samples with high diagnostic performance. Overexpression of circ_0000375 and circ_0011536 inhibited the growth, migration and invasion of CRC cells. Furthermore, miR-1182 and miR-1246 were upregulated in CRC tissues as target microRNA of circ_0000375 and circ_0011536, respectively. Overall, circ_0000375 and circ_0011536 may serve as diagnostic biomarkers and function as tumor suppressors in CRC.

Citation: Yin TF, Du SY, Zhao DY, Sun XZ, Zhou YC, Wang QQ, Zhou GYJ, Yao SK. Identification of circ_0000375 and circ_0011536 as novel diagnostic biomarkers of colorectal cancer. *World J Clin Cases* 2022; 10(11): 3352-3368

URL: https://www.wjgnet.com/2307-8960/full/v10/i11/3352.htm

DOI: https://dx.doi.org/10.12998/wjcc.v10.i11.3352

INTRODUCTION

Colorectal cancer (CRC) is a common malignancy worldwide, with incidence and mortality rates ranking 3th and 2nd, respectively[1]. More than 50% of CRC patients are first diagnosed at an advanced stage, which creates enormous threats to human health and imposes a social burden[2]. The 5-year overall survival rate of CRC patients in stage I can reach approximately 90%, while the rate is only 10% for stage IV patients[3], suggesting that the prognoses of patients with advanced CRC are notably poorer. The great challenges related to early diagnosis and successful therapy are attributed to the high potential for metastasis or relapse, treatment resistance, high heterogeneity and multistep initiation of CRC. Conventional tumor markers widely used in clinical practice, such as glycoprotein carcinoembryonic antigen, exhibit unsatisfactory specificity and sensitivity[4]. Thus, there is an urgent need to discover innovative and reliable diagnostic biomarkers to improve predictive accuracy, guide individualized treatment and assess clinical outcome.

Recently, an increasing number of circular ribonucleic acids (circRNAs) have been identified through bioinformatic analysis and high-throughput sequencing technology. CircRNAs have drawn widespread

attention as a class of single-stranded noncoding RNA molecules with a circular structure lacking 5′ and 3′ ends that are more stable than linear RNAs and resistant to RNA exonucleases[5]. CircRNAs are highly expressed in eukaryotes and exert diverse functions, including sponging microRNAs (miRNAs), regulating transcription and splicing in the nucleus, interacting with proteins and undergoing translation in the cytoplasm[6,7]. Accumulating evidence has demonstrated that circRNAs contain adequate miRNA-binding elements to sponge and sequester corresponding miRNAs, acting as competing endogenous RNAs at the posttranscriptional level[8,9]. Some circRNAs have been reported to be not only potential diagnostic and prognostic indicators for CRC but also regulators of carcinogenesis *via* their interactions with miRNAs and their target genes. For example, hsa_circ_0005273 (circPTK2) in CRC tissue is associated with tumor growth and metastasis as well as prognosis and might serve as a therapeutic target for CRC metastasis[10]. Serum exosomal hsa_circ_0004771 can act as a diagnostic biomarker of CRC[11]. Hsa_circ_0001955 and hsa_circ_0000977 were found to mediate the miRNA-mRNA regulatory network in CRC[12]. Collectively, circRNAs could play vital roles in the tumorigenesis of CRC and have potential as novel biomarkers for diagnosis and clinical outcome prediction.

MiRNAs are small single-stranded noncoding RNA molecules that are 19-25 nucleotides in size and mediate the posttranscriptional silencing of target genes by combining with the 3′ untranslated region of a mRNA transcript to contribute to translational inhibition and mRNA destabilization[13,14]. The miRNAs in tissue samples and cell-free biological fluids, have been reported as crucial gene regulators, promising candidate biomarkers and therapeutic targets[14,15]. Considerable miRNAs have been observed to regulate various biological and pathological processes in many diseases, especially cancer. For instance, many miRNAs differentially expressed in CRC can influence the growth, progression, autophagy, apoptosis and even microbiome of CRC cells[16-18], and act as noninvasive biomarkers of CRC[19].

The aim of this study was to identify promising circRNA biomarkers for CRC diagnosis and obtain insights into their functions in modulating the development of CRC. In the present study, we investigated the expression levels of 2 circRNAs, circ_0000375 and circ_0011536, in tissue and serum samples as well as in CRC cell lines. The biological functions of the 2 circRNAs were explored by evaluating the proliferation, migration and invasion of CRC cell lines. The expression of target miRNAs and their interactions with circRNAs were also investigated in CRC. Collectively, our findings revealed the circRNAs and their miRNA interactions that are critically important to the tumorigenesis of CRC, providing potential biomarkers for diagnosis and therapeutic options.

MATERIALS AND METHODS

Bioinformatic analysis of circRNA and miRNA profiles

The expression profiles of circRNAs and miRNAs of CRC patients and negative controls (NCs) were obtained from the Gene Expression Omnibus (GEO) database (http://www.ncbi.nlm.nih.gov/geo). The GSE126095 (10 CRCs *vs* 10 NCs) dataset was utilized for circRNA expression analysis, while GSE41655 (33 CRCs *vs* 15 NCs), GSE49246 (40 CRCs *vs* 40 NCs) and GSE115513 (750 CRCs *vs* 649 NCs) were used for miRNA analysis. The platform and series matrix files of the datasets were downloaded from the GEO database, and then the probe matrix was converted into the corresponding RNA name referring to the annotation from the platform files. The "limma" R package was used for normalization of raw data and identification of the differentially expressed circRNAs and miRNAs between CRC and NC samples. The target miRNAs were predicted with the circular RNA interactome database (CircInteractome, https://circinteractome.nia.nih.gov/). Gene Ontology and Kyoto Encyclopedia of Genes and Genomes (KEGG) analyses were employed to reveal the vital signaling pathways of miRNAs involved in the tumorigenesis of CRC using the "clusterProfiler" R package.

Human tissue and serum sample collection

In this study, patients with CRC and healthy control (HC) participants were enrolled from May 2019 to May 2021 at China-Japan Friendship Hospital. All patients included in our study were newly diagnosed with colorectal adenocarcinoma confirmed by postoperative pathological examination. Patients who had already received radiotherapy, chemotherapy or other molecular targeted therapy before surgery were screened out. Age- and sex-matched HC participants were recruited from a population of individuals without major abnormalities and with negative results after complete colonoscopy. In total, 34 tumor tissue samples from CRC patients and 24 colon tissue samples from HCs were obtained. Serum samples were collected from HCs before colonoscopy (n = 28), from CRC patients before curative surgery (n = 56) and from CRC patients at 30 d after surgery (n = 14). Demographic data and clinicopathological features, including age, gender, TNM stage, tumor size, tumor location and lymph node metastasis, were collected. Tissue samples taken from CRC patients or HCs were frozen in liquid nitrogen immediately and stored at -80 °C until further analysis. Serum specimens were immediately centrifuged at 4000 g for 10 min at 4 °C, and 1 mL of supernatant was stored at -80 °C. This study was approved by the Ethics Committee of the China-Japan Friendship Hospital (No. 2018-116-K85-1), and all

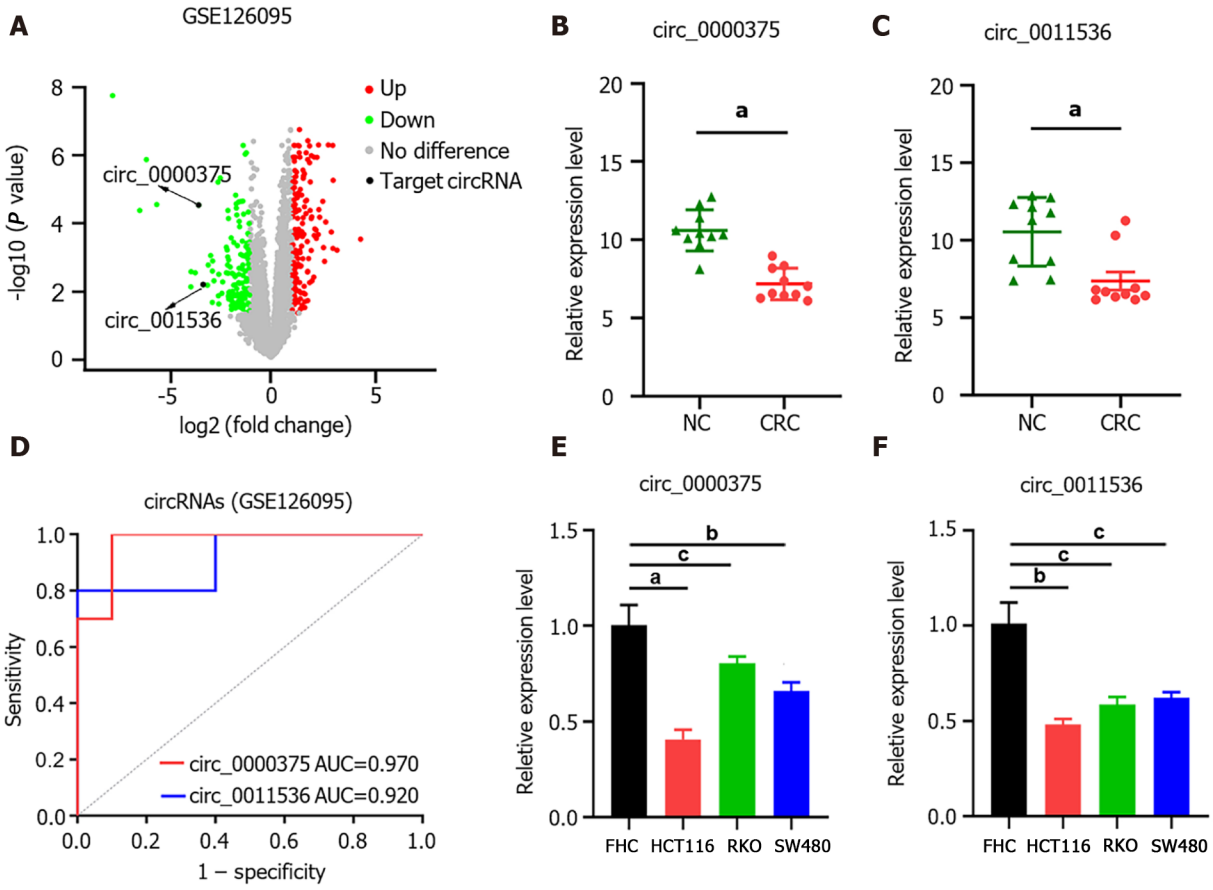

Figure 1 Expression profiles of circular ribonucleic acids in colorectal cancer tissues from GSE126095 datasets and in cell lines. A: Volcano plot of circular ribonucleic acids expression levels; B: The expression of circ_0000375 in colorectal cancer (CRC) tissues and negative control tissues; C: The expression of circ_0011536 in CRC tissues and negative control tissues; D: Receiver operating characteristic curves to evaluate the diagnostic value of circ_0000375 and circ_0011536 by assessing the area under the curve; E: The relative expression levels of circ_0000375 in a normal colon cell line (FHC) and CRC cell lines (HCT116, RKO and SW480); F: The relative expression levels of circ_0011536 in a normal colon cell line (FHC) and CRC cell lines (HCT116, RKO and SW480). $^{a}P < 0.001$; $^{b}P < 0.01$; $^{c}P < 0.05$. NC: Negative control; AUC: Area under the curve; CRC: Colorectal cancer.

participants signed written informed consent forms.

Cell culture

Three CRC cell lines (HCT, RKO, and SW480) and a human normal colonic epithelial cell line (FHC) were obtained from the American Type Culture Collection. All cell lines except RKO were cultured in Roswell Park Memorial Institute-1640 medium (RPMI-1640; Invitrogen, Carlsbad, United States), and RKO cells were cultured in Dulbecco's modified Eagle's medium (DMEM, Invitrogen). All the cell lines were supplemented with 100 IU/mL penicillin, 100 μg/mL streptomycin and 10% fetal bovine serum (FBS) and cultured at 37 °C in a humidified atmosphere with 5% CO_2.

Cell transfection

An empty pcDNA3.1 vector and overexpression plasmids for circRNAs were synthesized by GenePharma (Shanghai, China). Then, Lipofectamine 3000 Transfection Reagent (Invitrogen) was utilized to transfect HCT116 and SW480 cells with the above plasmids according to the manufacturer's instructions. 24 h later, CRC cells were collected for subsequent experiments.

Quantitative reverse transcription-polymerase chain reaction and Sanger sequencing

Total RNA was isolated from tissues, serums and cells using the RNAprep Pure Cell Kit (Solarbio, Beijing, China) following the manufacturer's protocol. Then, the isolated RNA was reverse transcribed into cDNA using the Hifair® II 1st Strand cDNA Synthesis Kit (YESEN, Shanghai, China). Then, quantitative reverse transcription-polymerase chain reaction (qRT-PCR) was conducted using Hieff® qPCR SYBR® Green Master Mix (No Rox) (YESEN). The relative expression levels of circRNAs and miRNAs were quantified by the $2^{-\Delta\Delta Ct}$ method, using *GAPDH* and *U6* as internal reference genes, respectively. The primers for qRT-PCR were synthesized by Sangon Biotech and are listed in Supplementary Table 1. To further ascertain the back-splicing and junction sequence of each circRNA, Sanger sequencing of the amplification products of circRNAs was performed by Tsingke (Beijing,

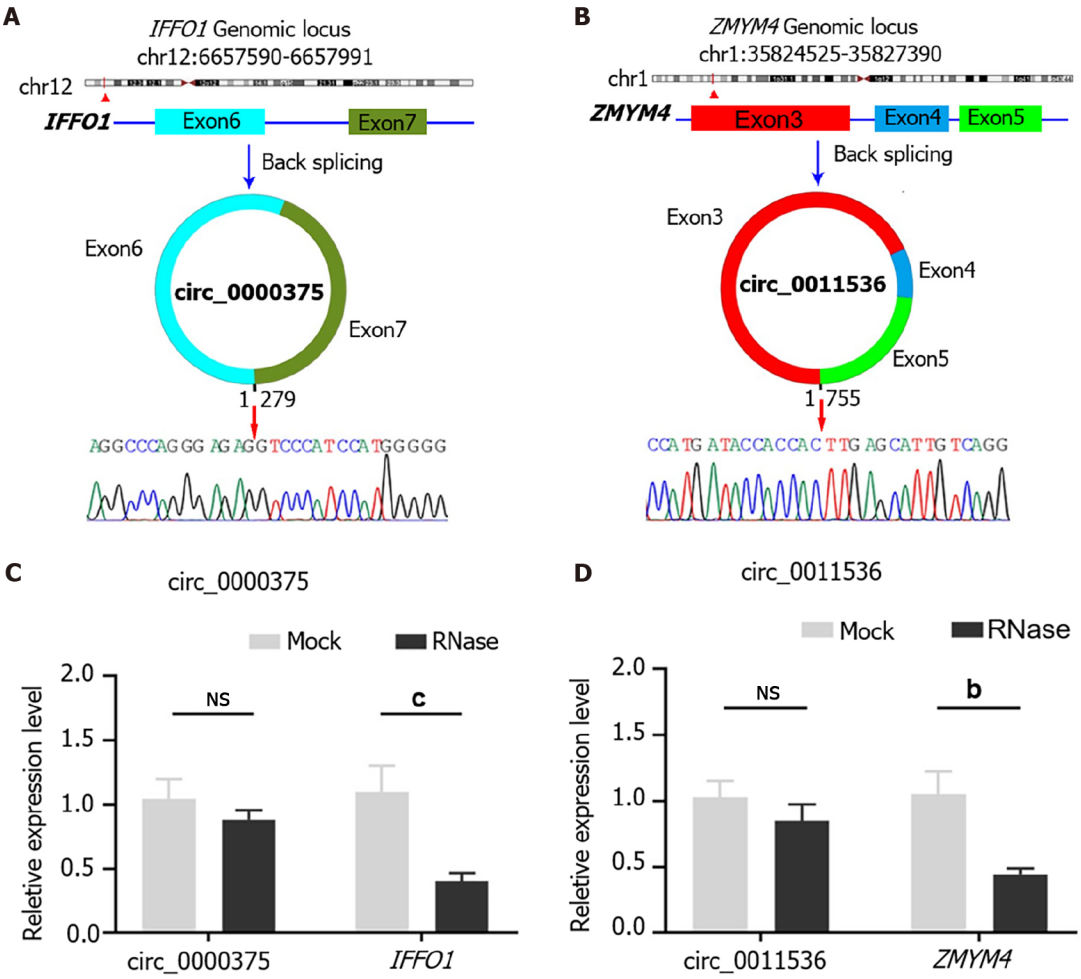

Figure 2 Characteristics of circ_0000375 and circ_0011536 in colorectal cancer tissues. A: Structures and back-splicing sequences of circ_0000375; B: Structures and back-splicing sequences of circ_0011536; C: The relative expression levels of circ_0000375 and the corresponding linear mRNA IFFO1 in colorectal cancer tissues treated with RNase R; D: The relative expression levels of circ_0011536 and ZMYM4 treated with RNase R. $^{b}P < 0.01$; $^{c}P < 0.05$. NS: Not significant.

China).

RNase R treatment

To determine the stability characteristics of circRNAs, 2 circRNAs and their corresponding linear mRNAs were digested with RNase R. A 5-μg aliquot of total RNA was incubated with or without 1 μL of 10-fold reaction buffer and 0.5 μL of RNase R (20 U/μL) for 30 min at 37 °C. Then, the expression levels of the circRNAs and their corresponding linear mRNAs were quantified by PCR.

Cell counting kit-8 proliferation assay

A total of 1500 SW480 or HCT116 cells in 100 μL of medium were seeded in each well of a 96-well plate. After 24 h, the CRC cells were transfected with oe-circRNA plasmid or vector. Then, at 0 h, 24 h, 48 h and 72 h, 10 μL of cell counting kit-8 (CCK-8) reagent (Solarbio) and 90 μL of medium were added after the previous medium was removed. Then, the cells were incubated for 1 h at 37 °C with 5% CO_2, and the optical density (OD) was detected at 450 nm using a microplate reader (BioTek Instruments, United States).

Wound healing assay

SW480 or HCT116 cells were cultured in 6-well plates for 24 h, and then, cell transfection was performed as described above. After incubation for 48 h, a wound was scratched with a 200 μL sterile pipette tip. Then, the cells were washed with PBS 3 times and incubated in serum-free medium. Representative images were captured at 0 h and 24 h after scratching. The total wound area was measured using ImageJ software, and the relative migration rate was calculated.

Transwell invasion assay

CRC cells were suspended in 200 μL of serum-free medium and seeded in the upper chambers coated with matrigel (Corning, United States). The bottom 24-well plates were filled with 600 μL of medium containing 10% FBS as a chemoattractant. After incubation for 72 h, the cells remaining in the upper chamber were gently removed with cotton swabs, and the cells on the lower surface were photographed and counted after being fixed with 4% paraformaldehyde and stained with 0.1% crystal violet.

Luciferase reporter assay

Fragments of circ_0000375 and circ_0011536 and corresponding mutant sequences were designed and inserted into a luciferase reporter vector (GP-miRGLO) to produce circ_0000375-WT, circ_0011536-WT, circ_0000375-MUT and circ_0011536-MUT, respectively (GenePharma, China). HEK293T cells obtained from the American Type Culture Collection were seeded in 12-well plates and then cotransfected with a mixture of these plasmids and miRNA mimics or mimics NC. After incubation for 24 h, firefly and Renilla luciferase activities were examined with a Dual-Luciferase Reporter Assay System (Promega, United States) in line with the manufacturer's instructions.

Statistical analysis

Statistical Program for Social Science version 26.0 (SPSS 26.0), R software (version 4.0.3) and GraphPad Prism (version 9) were used to perform statistical analysis. Quantitative data with a normal distribution are presented as the mean ± SD and were analyzed using Student's *t*-test or one-way analysis of variance, while variables with a nonnormal distribution are presented as the median and interquartile range and were compared using a Mann-Whitney *U* test or Kruskal-Wallis test. Moreover, categorical variables were analyzed by the chi-square test or a nonparametric test. Receiver operating characteristic (ROC) curves were constructed to examine the diagnostic efficiency of RNA molecules by assessing the area under the curve (AUC). A two-tailed $P < 0.05$ was considered statistically significant.

RESULTS

Identification of two circRNAs differentially expressed in CRC

In GSE126095, the expression levels of circRNAs were compared between CRC ($n = 10$) and NC ($n = 10$) samples. The circRNAs differentially expressed between CRC and NC were obtained with the criteria |log2 fold change| > 1 and *P* value < 0.05 (Figure 1A). Based on the circRNA regulatory network identified in our previous study[20], we selected 2 circRNAs, namely, hsa_circ_0000375 (circ_0000375) and hsa_circ_0011536 (circ_0011536), which were downregulated in CRC (Figure 1B and C). The AUCs of circ_0000375 and circ_0011536 were 0.970 and 0.920, respectively (Figure 1D), suggesting that these 2 circRNAs were useful as CRC biomarkers in the GSE126095 dataset. To further confirm the value of the 2 circRNAs in CRC, we investigated the expression levels of the 2 circRNAs in cell lines. Compared with the normal colonic epithelial cell line FHC, CRC cell lines (HCT, RKO and SW480) showed significantly decreased expression levels of circ_0000375 and circ_0011536 (Figure 1E and F).

Sanger sequencing and RNase R digestion to determine the characteristics of circ_0000375 and circ_0011536

Circ_0000375 originates from head-to-tail splicing of exon 6 and exon 7 in the linear mRNA *IFFO1*, which is located on chromosome 12. According to the Sanger sequencing results for PCR products, the target sequence of circ_0000375 was verified to be the head-to-tail splicing site (Figure 2A). For circ_0011536, which is generated by back-splicing of exon 3 to exon 5 of the *ZMYM4* gene, our primer covered the splicing site, so the inverse complementary sequence of the amplification products of circ_0011536 was consistent with that in the circBase database (Figure 2B). Subsequently, the expression level of circ_0000375 did not show an obvious decline after CRC tissues were degraded with RNase R, but its corresponding linear mRNA, *IFFO1*, was significantly downregulated (Figure 2C). Similar results were obtained for circ_0011536 and *ZMYM4* (Figure 2D). These results revealed that circ_0000375 and circ_0011536 were more resistant to RNase R digestion than the corresponding linear mRNAs.

Expression and diagnostic value of circ_0000375 and circ_0011536 in CRC tissue and serum samples

The clinicopathological features of CRC patients and HCs are listed in Table 1. Downregulation of circ_0000375 and circ_0011536 was validated in CRC tissues compared with HC tissues (Figure 3A and B). ROC curve analysis revealed that the AUCs of circ_0000375 and circ_0011536 were 0.911 and 0.885, respectively. Combined with both circRNAs, the AUC was 0.928, indicating possible better performance based on these 2 circRNAs (Figure 3C). Furthermore, the median expression levels of circ_0000375 and circ_0011536 in tissues were used to divide the CRC patients into low and high expression groups, which were used for subgroup analysis of the clinicopathological characteristics of the CRC patients (Table 2). The results indicated that patients with lymph node metastasis or advanced TNM stage tended to exhibit high expression of circ_0011536. However, the expression of circ_0000375 in tissue was

Table 1 Clinicopathological characteristics of participants

	Tissues		Serums		
	HC (*n* = 24)	CRC (*n* = 34)	HC (*n* = 28)	CRC (*n* = 56)	AS (*n* = 14)
Age (yr) (M) (P_{25}, P_{75})	62.0 (55.0, 69.0)	64.5 (58.8, 73.0)	63.5 (56.3, 71.8)	66.0 (60.3, 75.0)	61.0 (49.5, 68.3)
Gender					
Male	17	23	15	39	9
Female	7	11	13	17	5
TNM stage					
I		9		9	2
II		9		16	4
III		10		21	6
IV		6		10	2
Tumor size					
≤ 5 cm		20		29	9
> 5 cm		14		27	5
Tumor location					
Left colon		6		12	3
Right colon		5		9	2
Rectum		23		35	9
Lymph node metastasis					
No		19		35	6
Yes		15		21	8

HC: Healthy control; CRC: Colorectal cancer; AS: After surgery.

not related to clinicopathological indexes.

Furthermore, the expression levels of the 2 circRNAs in serum samples from CRC patients were lower than those in serum samples of HCs (Figure 3D and E). For CRC patients after surgery, the levels of circ_0000375 and circ_0011536 in the serum were elevated compared with the levels in preoperative patients but were still significantly lower than the levels in HCs significantly, indicating that circ_0000375 and circ_0011536 in the serum were closely related to CRC tumorigenesis. The AUCs of circ_0000375, circ_0011536 and combined circRNAs in CRC serum were 0.976, 0.982 and 0.997, respectively (Figure 3F), indicating that these 2 circRNAs could serve as new biomarkers for CRC diagnosis and that both circRNAs might yield better performance. The expression levels of circ_0000375 and circ_0011536 in the serum were not correlated with the clinicopathological indexes of CRC patients, which suggested the robustness of the expression of these 2 circRNAs among different subtypes of CRC patients (Supplementary Table 2).

Circ_0000375 and circ_0011536 suppressed the malignant behavior of CRC cells in vitro

To investigate the biological effects of circ_0000375 and circ_0011536 on CRC cells, SW480 and HCT116 cells were transfected with overexpression vectors for these 2 circRNAs (Figure 4A and B). CCK-8 assays revealed that upregulation of circ_0000375 or circ_0011536 remarkably inhibited the proliferation of CRC cells (Figure 4C and D), indicating that these 2 circRNAs inhibited the proliferation of CRC cells. Wound healing assays were utilized to verify the function of the 2 circRNAs related to the migration of CRC cells, suggesting that the migratory abilities of CRC cells were significantly restrained by overexpression of circ_0000375 or circ_0011536 (Figure 4E, F and I). Transwell assay results suggested that these 2 circRNAs also affected the invasion of CRC cells. Upregulation of circ_0000375 or circ_0011536 suppressed CRC cell invasion capability (Figure 4G, H and J). Therefore, circ_0000375 and circ_0011536 suppressed cell proliferation, migration and invasion in CRC cells.

Targeted miRNA predictions for circ_0000375 and circ_0011536

Given that mounting evidence has demonstrated that circRNAs serve as miRNA sponges, the miRNA binding abilities of circ_0000375 and circ_0011536 in CRC were explored using the CircInteractome

Table 2 Associations between the expressions of two Circular ribonucleic acids and clinicopathological features in colorectal cancer tissues

	n	Circ_0000375 expression		*P* value	Circ_0011536 expression		*P* value
		Low	High		Low	High	
Age (yr)				0.730			0.300
≤ 65	19	9	10		8	11	
> 65	15	8	7		9	6	
Gender				0.714			
Female	11	6	5		5	6	0.714
Male	23	11	12		12	11	
TNM stage				0.169			0.039[a]
I-II	18	11	7		12	6	
III-IV	16	6	10		5	11	
Tumor size				0.486			1.000
≤ 5 cm	20	9	11		10	10	
> 5 cm	14	8	6		7	7	
Tumor location				0.271			0.714
Colon	11	4	7		5	6	
Rectum	23	13	10		12	11	
Lymph node metastasis				0.084			0.016[a]
No	19	12	7		13	6	
Yes	15	5	10		4	11	

[a]$P < 0.05$.

database. We identified miR-1182 and miR-1246 as potential targets of circ_0000375 and circ_0011536, respectively, and then examined the interaction of these miRNAs with the circRNAs. The expression of miR-1182 was elevated in CRC cell lines compared with the FHC cell line (Figure 5A). MiR-1182 was downregulated in circ_0000375-overexpressing CRC cells (Figure 5B). Moreover, to examine the direct interaction between circ_0000375 and miR-1182, we conducted a dual-luciferase reporter assay. The results showed that the luciferase activity of circ_0000375-WT was significantly reduced in the miR-1182 mimics group compared with the mimics NC group, while no difference was observed with circ_0000375-MUT (Figure 5C). Similarly, miR-1246 was also upregulated in CRC cell lines (Figure 5D) but downregulated after overexpression of circ_0011536 (Figure 5E). MiR-1246 mimics led to decreased luciferase activity of circ_0011536-WT, but no change was found for circ_0011536-MUT (Figure 5F). Overall, circ_0000375 and circ_0011536 were confirmed to serve as sponges for miR-1182 and miR-1246, respectively, and the binding sites were uncovered in the present study.

MiR-1182 and miR-1246 were upregulated in CRC tissues in GEO datasets

We compared the miR-1182 and miR-1246 expression levels among 3 GEO datasets, GSE41655 (33 CRCs *vs* 15 NCs), GSE49246 (40 CRCs *vs* 40 NCs) and GSE115513 (750 CRCs *vs* 649 NCs). The results suggested that miR-1182 was overexpressed in CRC tissues in GSE41655, GSE49246 and GSE115513 (Figure 6A-C), supporting our discovery in vitro. Consistently, the expression of miR-1246 was also increased in CRC tissues in GSE41655, GSE49246 and GSE115513 (Figure 6D-F). The diagnostic performances of miR-1182 and miR-1246 in these 3 GEO datasets are shown in Figure 6G and H, suggesting that these miRNAs could serve as CRC indicators. These results revealed that miR-1182 and miR-1246, predicted as target miRNAs for circ_0000375 and circ_0011536 in our study, are overexpressed in CRC tissues and might act as potential biomarkers for CRC diagnosis.

Functional enrichment analysis of the downstream genes of two miRNAs

A total of 19 genes were predicted to be potential targets of miR-1182 and miR-1246 using the TargetScan, miRDB and miRTarBase databases. *MTRNR2L8, TRIM25, DIRC2, ZNF609, GTF3C4, ARID1A, DARS* and *MAVS* were recognized as downstream genes of miR-1182, and *DYRK1A, GSK3B,*

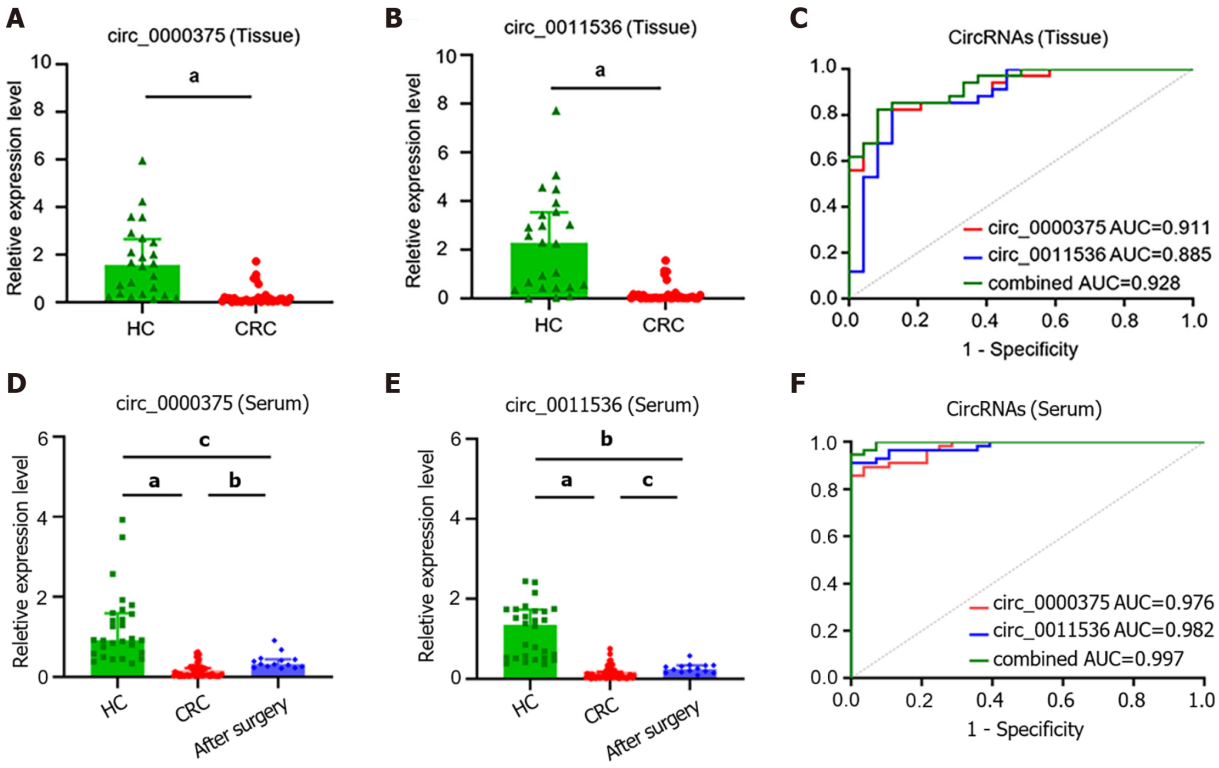

Figure 3 Circ_0000375 and circ_0011536 were downregulated in colorectal cancer tissue and serum samples. A: The expression levels of circ_0000375 in healthy control (HC) and colorectal cancer (CRC) tissue samples; B: The expression levels of circ_0011536 in HC and CRC tissue samples; C: Receiver operating characteristic curves for circ_0000375, circ_0011536 and combined circular ribonucleic acids in CRC tissues with the area under the curve calculated; D: The expression levels of circ_0000375 in serum samples of HC, preoperative CRC and CRC after surgery; E: The expression levels of circ_0011536 in serum samples of HC, preoperative CRC and CRC after surgery; F: Receiver operating characteristic curves for Circular ribonucleic acids in CRC serum samples. $^{a}P < 0.001$; $^{b}P < 0.01$; $^{c}P < 0.05$. CRC: Colorectal cancer; HC: Healthy control; AUC: Area under the curve; ROC: Receiver operating characteristic.

AXIN2, *CRADD*, *KIAA0895*, *GPATCH11*, *CALM2*, *CKS2*, *SKIL*, *RORA* and *ZNF502* were identified as targets for miR-1246 (Supplementary Table 3). Based on these 19 genes, the top 10 enrichment terms in GO analysis were revealed, including the apoptotic signaling pathway for biological processes, Wnt/beta-catenin signaling pathway and SWI/SNF complex for cellular components, beta-catenin binding and SMAD binding for molecular functions (Figure 7A). Meanwhile, KEGG analysis revealed that these genes were enriched in some tumorigenesis-associated pathways, including the signaling pathways regulating pluripotency of stem cells, the RIG-I-like receptor signaling pathway, the Hippo signaling pathway and the Wnt signaling pathway (Figure 7B). Therefore, miR-1182 and miR-1246 and their target genes might play crucial roles in CRC tumorigenesis.

DISCUSSION

Although CRC treatment has been revolutionized in recent years, the current therapeutic strategies, including surgery, chemotherapy and molecular targeted therapy, still do not satisfy the ever-rising demand for early diagnostic and prognostic improvements for patients. Under this circumstance, it is pivotal to elucidate the mechanisms underlying CRC initiation and progression and to identify useful biomarkers for the early diagnosis of CRC. In this study, we first revealed that circ_0000375 and circ_0011536 are potential biomarkers for CRC diagnosis and then explored their function as tumor suppressors in CRC progression.

Compelling evidence indicates that circRNAs play crucial roles in diverse pathological processes in various cancer types. In our study, we compared the expression profiles in GSE126095 datasets and selected circ_0000375 and circ_0011536 as biomarker candidates. The expression levels of these 2 circRNAs were downregulated in CRC cell lines compared with normal colonic mucosa cells. Furthermore, we observed low circ_0000375 and circ_0011536 expression in CRC tissues and serum samples, with high diagnostic value, respectively, or combined. Interestingly, the serum expression levels of these 2 circRNAs were elevated in CRC patients 30 d postsurgery compared with preoperative patients, further supporting our discovery. Considering that serum exosomal circRNAs are abundant, stable and easy to test, circRNAs in the serum might have substantial advantages as promising noninvasive biomarkers for accurately diagnosing CRC, assessing disease stage and predicting

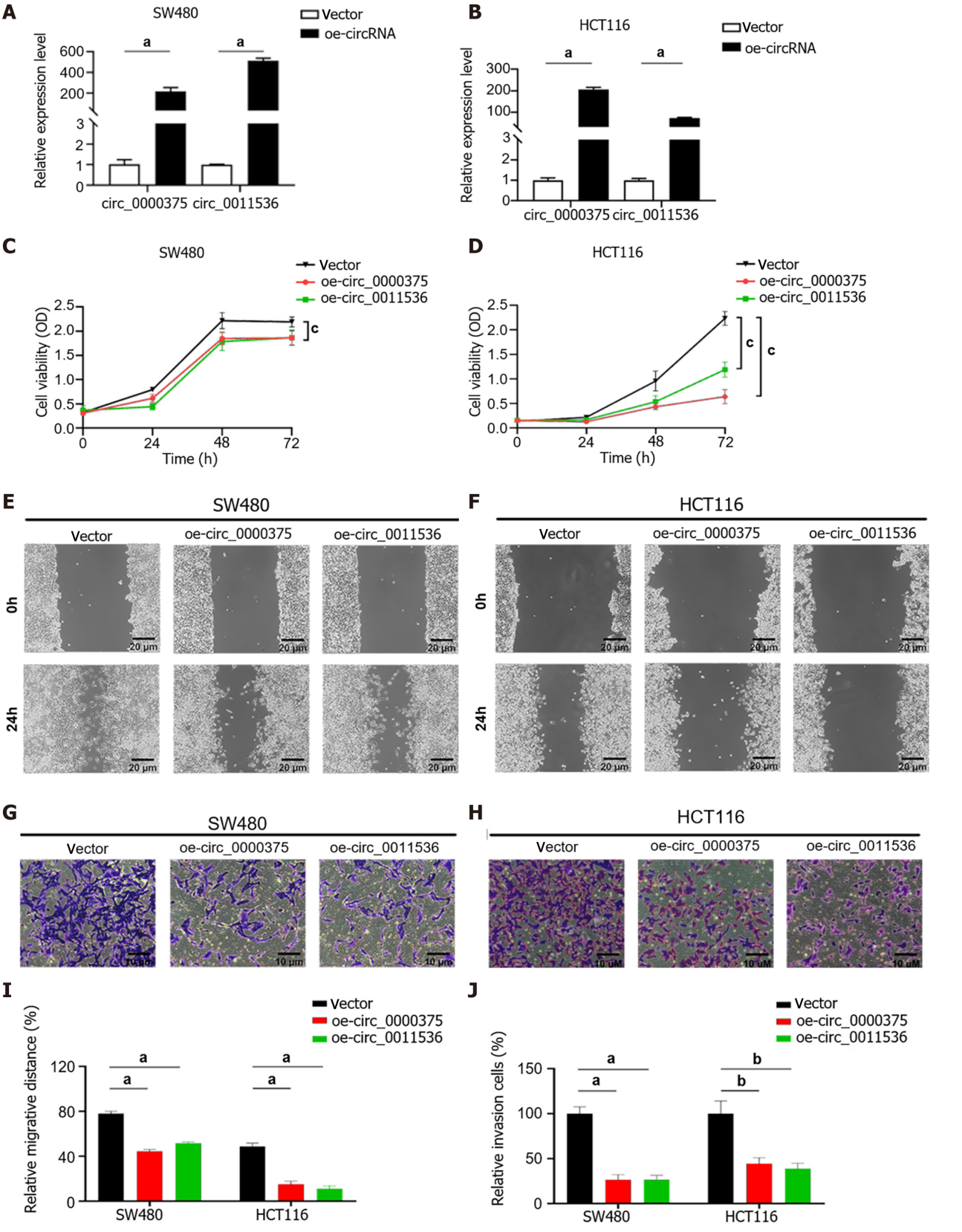

Figure 4 Overexpression of circ_0000375 and circ_0011536 suppresses proliferation, migration and invasion in colorectal cancer. A: The relative expression levels of circ_0000375 and circ_0011536 in SW480 cells transfected with overexpression plasmids; B: The relative expression levels of circ_0000375 and circ_0011536 in HCT116 cells transfected with overexpression plasmids; C: Cell counting kit-8 (CCK-8) assays were performed to determine the ability of proliferation in SW480 cells transfected with oe-circ_0000375 or oe-circ_0011536; D: CCK-8 assays were performed to determine the ability of proliferation in HCT116 cells transfected with oe-circ_0000375 or oe-circ_0011536; E: Wound healing assays were conducted to assess the cell migrative capability of SW480; F: Wound healing assays were conducted to assess the cell migrative capability of HCT116 cells; G: Transwell invasion assays were utilized to reveal the invasive ability of SW480; H: Transwell invasion assays were utilized to reveal the invasive ability of HCT116 cells; I: Results of wound healing assays of SW480 and HCT116

cell lines; J: Results of Transwell invasion assays of SW480 and HCT116 cell lines. $^{a}P < 0.001$; $^{b}P < 0.01$; $^{c}P < 0.05$.

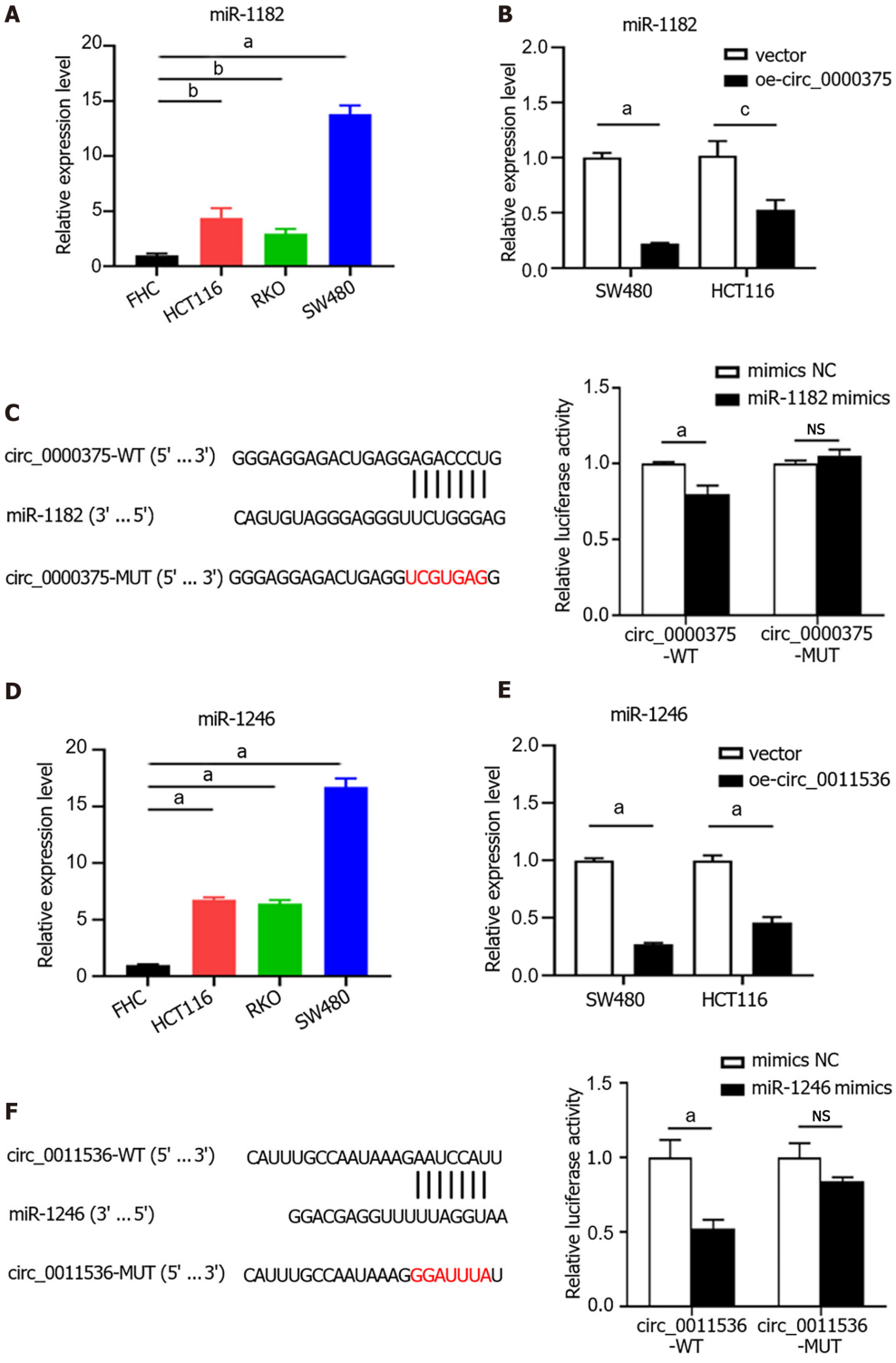

Figure 5 Circ_0000375 and circ_0011536 serve as sponges of miR-1182 and miR-1246 in colorectal cancer. A: The expression level of miR-1182 in a normal colon cell line (FHC) and colorectal cancer cell lines (HCT116, RKO and SW480); B: The relative expression level of miR-1182 in SW480 and HCT116 cells transfected with a circ_0000375 overexpression vector; C: Relative luciferase activities were detected in HEK293T cells after cotransfection with circ_0000375-WT, circ_0000375-MUT, miR-1182 mimics and negative control mimics; D: The expression level of miR-1246 in colorectal cancer cell lines; E: The relative expression level of miR-1246 in SW480 and HCT116 cells transfected with oe-circ_0011536; F: Luciferase reporter assays were performed after cotransfection with circ_0011536-WT, circ_0011536-MUT, miR-1246 mimics and negative control mimics. $^{a}P < 0.001$; $^{b}P < 0.01$; $^{c}P < 0.05$. NC: Negative control; NS: Not significant.

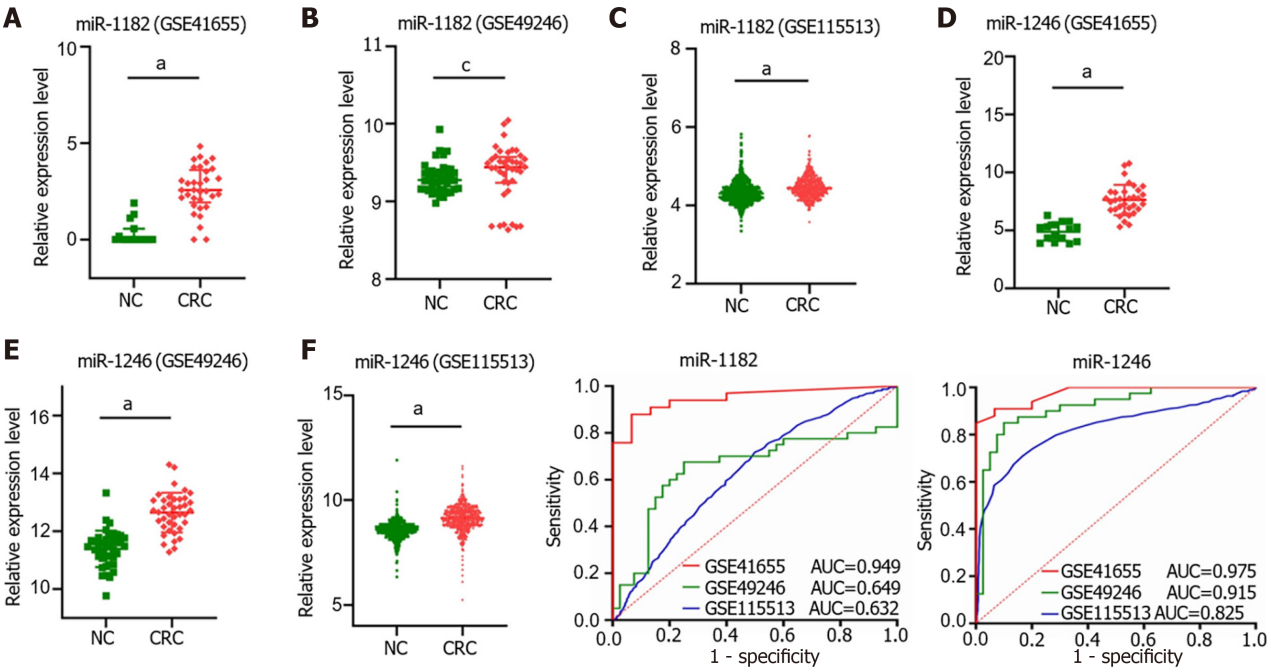

Figure 6 MiR-1182 and miR-1246 were upregulated in colorectal cancer tissues in Gene Expression Omnibus datasets. A: The expression level of miR-1182 in GSE41655; B: The expression level of miR-1182 in GSE49246; C: The expression level of miR-1182 in GSE115513; D: The expression level of miR-1246 in GSE41655; E: The expression level of miR-1246 in GSE49246; F: The expression level of miR-1246 in GSE115513; G: The diagnostic value of miR-1182 in Gene Expression Omnibus (GEO) datasets was evaluated by the area under the curve; H: The diagnostic value of miR-1246 in GEO datasets was evaluated by the area under the curve. $^{a}P < 0.001$; $^{b}P < 0.01$; $^{c}P < 0.05$. CRC: Colorectal cancer; NC: Negative control; AUC: Area under the curve.

prognosis. Previously, several circRNAs have been shown to be diagnostic biomarkers of CRC, including hsa_circ_0004771[11] and circ-PNN[21] in the serum. Metastasis and progression biomarkers of CRC have been revealed, including circPTK2[10] and circ-133[22], which might be new therapeutic targets. Four circRNAs, hsa_circ_0122319, hsa_circ_0087391, hsa_circ_0079480, and hsa_circ_0008039, were identified as reliable prognostic tools for postoperative recurrence of stage II/III CRC[23]. Furthermore, in the present study, we found that CRC patients with lymph node metastasis or advanced TNM stage tended to exhibit high circ_0011536 expression compared with patients in the early stage, suggesting that circ_0011536 is a more sensitive indicator for early CRC and that a complicated regulation system might impact the expression level of circ_0011536 in CRC tissues during CRC progression and metastasis. The expression levels of circ_0000375 in tissues and serum and circ_0011536 in serum samples from CRC patients were relatively stable and not associated with clinical features. Overall, we provide the first evidence of the potential of circ_0000375 and circ_0011536 as tumor biomarkers in tissues and serum samples from CRC patients, but the relationship of circRNA expression and clinicopathological features still needs to be confirmed by further investigation in a large cohort.

In our study, tumorigenic and metastatic properties, such as cell proliferation, migration and invasion, were suppressed by circ_0000375 and circ_0011536 overexpression in CRC cells. Next, miR-1182 and miR-1246 were predicted as target miRNAs of circ_0000375 and circ_0011536, respectively, through bioinformatics analysis, and these findings were validated by luciferase reporter assays. Furthermore, the expression levels of miR-1182 and miR-1246 in CRC cells were significantly decreased after transfection with circ_0000375 and circ_0011536 overexpression plasmids, further supporting our discovery. To date, an increasing number of studies have reported circRNAs as tumor regulators through direct binding to different miRNA molecules in CRC. For instance, CRC cell proliferation, metastasis and apoptosis can be regulated by circPACRGL *via* the miR-142-3p/miR-506-3p-TGF-β1 axis [24], and by circHIPK3 sponging of miR-7[25]. Moreover, circRNAs can play crucial roles in the therapeutic response of CRC as miRNA sponges. Hsa_circ_0005963 was reported to induce chemoresistance and modulate glycolysis in CRC through the miR-122-PKM2 axis[26]. Additionally, Liu *et al*[27] found that synthetic circRNA targeting miR-21 could efficiently inhibit cancer cell proliferation and achieve loss-of-function, revealing the enormous promise of circRNA sponges as innovative tools for molecular therapy in the future. In summary, our results described the tumor-suppressive role of circ_0000375 and circ_0011536 and identified the specific binding sites between circ_0000375 and miR-1182 and between circ_0011536 and miR-1246 for the first time, providing exploitable targets for CRC therapeutic strategies.

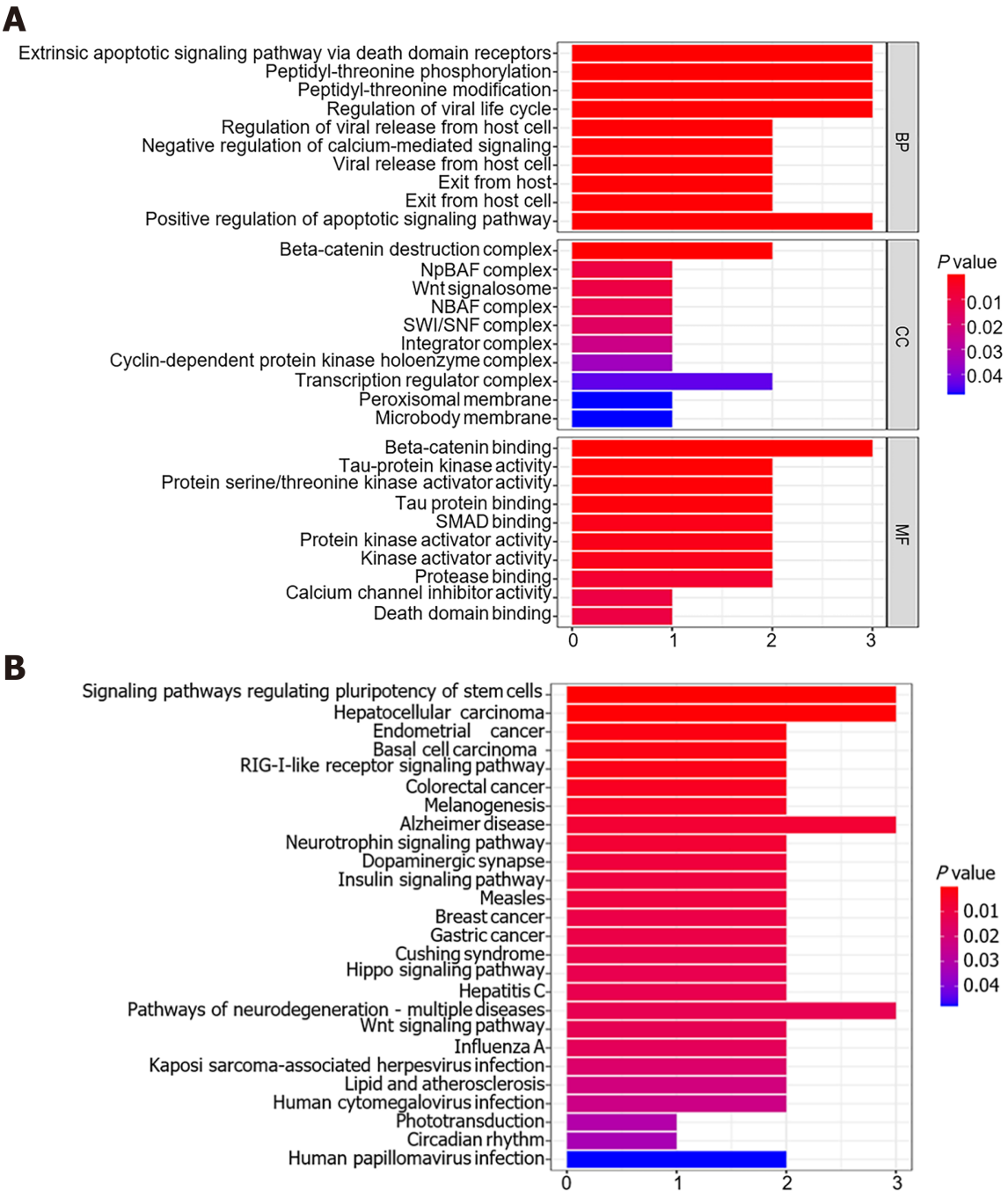

Figure 7 Enrichment analyses based on downstream genes of miR-1182 and miR-1246. A: Gene Ontology analysis of biological processes, cellular components, and molecular functions; B: Kyoto Encyclopedia of Genes and Genomes pathway analysis.

We next discovered significantly higher miR-1182 and miR-1246 expression levels in CRC cell lines than in normal colonic mucosa cells. Consistently, the expression levels of these 2 miRNAs were also upregulated in CRC tissues in three GEO datasets, GSE41655, GSE49246 and GSE115513. The critical roles of miR-1182 and miR-1246 have been investigated in some cancer types. For instance, miR-1182 was reported to attenuate proliferation and metastasis by targeting telomerase reverse transcriptase in gastric cancer[28]. Moreover, circCSPP1 in liver cancer[29], circ_0067934 in non-small cell lung cancer [30], circWHSC1 in ovarian cancer[31] and circFMN2 in CRC[32] can modulate the malignant behavior of tumors by sponging miR-1182. Moreover, miR-1246 plays an oncogenic role in metastasis by upregulating the methyltransferase METT3 in CRC[33]. Recent advances have indicated that infection with the CRC-associated bacterium *Fusobacterium nucleatum* might stimulate the generation of miR-1246/92b-3p/27a-3p-rich exosomes from tumor cells to promote the prometastatic ability of uninfected cells[34]. Mutant *P53* might reprogram macrophages into tumor-supporting macrophages with anti-inflammatory immunosuppressive activity *via* exosomal miR-1246 in colon cancer cells, which could promote the progression and metastasis of CRC[35]. In summary, miR-1182 and miR-1246 might serve as biomarkers and function as oncogenic miRNAs in CRC carcinogenesis, but the diagnostic value of miR-

1182 and miR-1246 in CRC tissues and serum samples still requires further investigation in the future.

In the present study, we also predicted the downstream genes of miR-1182 and miR-1246 as well as the potential signaling pathways involved in the regulation of these 2 miRNAs. The Wnt/beta-catenin signaling pathway is central to CRC tumorigenesis and might have promising value as a therapeutic target[36,37]. Zhao *et al*[30] found that miR-1182 might regulate the Wnt/beta-catenin pathway in lung cancer. In liver cancer, miR-1246 was reported to activate the Wnt/beta-catenin pathway in liver cancer stem cells[38] and regulate the RORalpha-Wnt/beta-catenin axis to promote liver cancer progression [39]. Moreover, miR-1246 was found to promote lung cancer metastasis and invasion through the Wnt/beta-catenin pathway by targeting *GSK3B*[40] and to induce apoptosis and overcome drug resistance by targeting *AXIN2* and *GSK3B*[41]. *DYRK1A* was also reported to be a potential target of miR-1246 because overexpression of miR-1246 induced by *P53* could downregulate the *DYRK1A* level [42]. In a nutshell, the targets of miR-1182 and miR-1246 were preliminarily identified in this study, and the Wnt/beta-catenin pathway might be involved in the regulation of these two miRNAs in CRC, which needs further exploration in the future.

In summary, we identified circ_0000375 and circ_0011536 as promising diagnostic biomarkers and tumor suppressors in CRC. To our knowledge, this is the first study to reveal the dysregulation of circ_0000375 and circ_0011536 in CRC tissues and serum samples and uncover their function in CRC pathogenesis. This is also the first study to investigate the interaction between circ_0000375 and miR-1182 and between circ_0011536 and miR-1246. However, some limitations also exist in our study. First, the robustness of these circRNAs and miRNAs as diagnostic and prognostic biomarkers should be confirmed with large-scale clinical samples. In addition, whether the tumor-suppressive effects of circ_0000375 and circ_0011536 can be counteracted by miR-1182 or miR-1246 remains unclear and should be validated through further comprehensive exploration. Finally, we tried to predict molecular mechanisms in this study, but the specific downstream genes and signaling pathways should be further elucidated later by performing experiments in vivo and in vitro.

CONCLUSION

To sum up, our findings demonstrated that circ_0000375 and circ_0011536 are downregulated in CRC cell lines, tissues and serum samples and exhibit potential diagnostic performances. Furthermore, these 2 circRNAs significantly suppress CRC cell proliferation, migration and invasion. As potential targets of circ_0000375 and circ_0011536, miR-1182 and miR-1246, respectively, are overexpressed in CRC cells and tissues. Our study not only further elucidates the mechanism of circRNA regulation in CRC cell growth and progression but also provides novel diagnostic biomarkers and promising therapeutic targets for CRC.

ARTICLE HIGHLIGHTS

Research background

Colorectal cancer (CRC) is a common tumor worldwide. Circular ribonucleic acids (circRNAs) have been reported to regulate CRC as microRNA (miRNA) sponges. However, the aberrant expression and biological functions of circRNAs in CRC remain to be further explored.

Research motivation

CircRNAs might serve as novel biomarker candidates for CRC diagnosis. Further exploration of useful biomarkers to improve CRC diagnosis and treatment is crucial.

Research objectives

This study aimed to identify circRNAs that could be potential biomarkers of CRC and explore their functions in CRC carcinogenesis.

Research methods

Cir_0000375 and circ_0011536 were selected as CRC biomarker candidates using the Gene Expression Omnibus (GEO) database. Quantitative real-time polymerase chain reaction was utilized to evaluate the expression levels of these 2 circRNAs in CRC tissues, serum samples and cell lines. Functional experiments, including cell counting kit-8 (CCK-8), wound healing and Transwell invasion assays, were carried out after overexpression of cir_0000375 and circ_0011536 in CRC cell lines. Furthermore, the expression levels of target miRNAs in CRC tissues were explored in GEO datasets and CRC cell lines. Then, the interactions of circRNAs and miRNAs and enrichment analysis of the miRNAs and target genes were further performed.

Research results

Our findings demonstrated that circ_0000375 and circ_0011536 were downregulated in CRC cell lines, tissues and serum samples and showed good diagnostic performance. Furthermore, these 2 circRNAs significantly inhibited CRC cell proliferation, migration and invasion. As potential targets of circ_0000375 and circ_0011536, miR-1182 and miR-1246, respectively, were overexpressed in CRC cells and tissues.

Research conclusions

Circ_0000375 and circ_0011536 may function as tumor suppressors and serve as novel biomarkers for CRC diagnosis and are promising candidates for therapeutic exploration.

Research perspectives

Our findings uncover the mechanisms by which 2 circRNAs, circ_0000375 and circ_0011536, suppress CRC cell growth and progression and provide novel diagnostic biomarkers and promising therapeutic targets for CRC.

ACKNOWLEDGEMENTS

We thank the Gene Expression Omnibus project for providing invaluable datasets for bioinformatic analysis.

FOOTNOTES

Author contributions: Yin TF conceived and designed the study, performed sample collection and formal analysis, and prepared the original draft; Du SY, Zhao DY and Sun XZ participated in sample acquisition, data analysis and manuscript revision; Zhou YC, Wang QQ and Zhou GYJ reviewed and edited the manuscript critically; Yao SK designed and supervised the study, revised the manuscript, and obtained the funding; all authors read and approved the final manuscript.

Supported by the National Key Development Plan for Precision Medicine Research, No. 2017YFC0910002.

Institutional review board statement: This study was approved by the Ethics Committee of China-Japan Friendship Hospital, No. 2018-116-K85-1.

Informed consent statement: All participants signed written informed consent.

Conflict-of-interest statement: There are no conflicts of interest to report.

Data sharing statement: No additional data are available.

Country/Territory of origin: China

ORCID number: Teng-Fei Yin 0000-0003-1140-8637; Shi-Yu Du 0000-0002-5482-2240; Dong-Yan Zhao 0000-0002-7026-068X; Xi-Zhen Sun 0000-0001-9967-5726; Yuan-Chen Zhou 0000-0001-6024-6246; Qian-Qian Wang 0000-0002-7709-2121; Ge-Yu-Jia Zhou 0000-0002-4196-1436; Shu-Kun Yao 0000-0002-8512-2589.

S-Editor: Guo XR
L-Editor: A
P-Editor: Yu HG

REFERENCES

1 **Sung H**, Ferlay J, Siegel RL, Laversanne M, Soerjomataram I, Jemal A, Bray F. Global Cancer Statistics 2020: GLOBOCAN Estimates of Incidence and Mortality Worldwide for 36 Cancers in 185 Countries. *CA Cancer J Clin* 2021; **71**: 209-249 [PMID: 33538338 DOI: 10.3322/caac.21660]

2 **Siegel RL**, Miller KD, Goding Sauer A, Fedewa SA, Butterly LF, Anderson JC, Cercek A, Smith RA, Jemal A. Colorectal

cancer statistics, 2020. *CA Cancer J Clin* 2020; **70**: 145-164 [PMID: 32133645 DOI: 10.3322/caac.21601]
3 **Brenner H**, Kloor M, Pox CP. Colorectal cancer. *Lancet* 2014; **383**: 1490-1502 [PMID: 24225001 DOI: 10.1016/S0140-6736(13)61649-9]
4 **Gao Y**, Wang J, Zhou Y, Sheng S, Qian SY, Huo X. Evaluation of Serum CEA, CA19-9, CA72-4, CA125 and Ferritin as Diagnostic Markers and Factors of Clinical Parameters for Colorectal Cancer. *Sci Rep* 2018; **8**: 2732 [PMID: 29426902 DOI: 10.1038/s41598-018-21048-y]
5 **Su M**, Xiao Y, Ma J, Tang Y, Tian B, Zhang Y, Li X, Wu Z, Yang D, Zhou Y, Wang H, Liao Q, Wang W. Circular RNAs in Cancer: emerging functions in hallmarks, stemness, resistance and roles as potential biomarkers. *Mol Cancer* 2019; **18**: 90 [PMID: 30999909 DOI: 10.1186/s12943-019-1002-6]
6 **Chen B**, Huang S. Circular RNA: An emerging non-coding RNA as a regulator and biomarker in cancer. *Cancer Lett* 2018; **418**: 41-50 [PMID: 29330104 DOI: 10.1016/j.canlet.2018.01.011]
7 **Han B**, Chao J, Yao H. Circular RNA and its mechanisms in disease: From the bench to the clinic. *Pharmacol Ther* 2018; **187**: 31-44 [PMID: 29406246 DOI: 10.1016/j.pharmthera.2018.01.010]
8 **Hansen TB**, Jensen TI, Clausen BH, Bramsen JB, Finsen B, Damgaard CK, Kjems J. Natural RNA circles function as efficient microRNA sponges. *Nature* 2013; **495**: 384-388 [PMID: 23446346 DOI: 10.1038/nature11993]
9 **Kristensen LS**, Andersen MS, Stagsted LVW, Ebbesen KK, Hansen TB, Kjems J. The biogenesis, biology and characterization of circular RNAs. *Nat Rev Genet* 2019; **20**: 675-691 [PMID: 31395983 DOI: 10.1038/s41576-019-0158-7]
10 **Yang H**, Li X, Meng Q, Sun H, Wu S, Hu W, Liu G, Yang Y, Chen R. CircPTK2 (hsa_circ_0005273) as a novel therapeutic target for metastatic colorectal cancer. *Mol Cancer* 2020; **19**: 13 [PMID: 31973707 DOI: 10.1186/s12943-020-1139-3]
11 **Pan B**, Qin J, Liu X, He B, Wang X, Pan Y, Sun H, Xu T, Xu M, Chen X, Xu X, Zeng K, Sun L, Wang S. Identification of Serum Exosomal hsa-circ-0004771 as a Novel Diagnostic Biomarker of Colorectal Cancer. *Front Genet* 2019; **10**: 1096 [PMID: 31737058 DOI: 10.3389/fgene.2019.01096]
12 **Ding B**, Yao M, Fan W, Lou W. Whole-transcriptome analysis reveals a potential hsa_circ_0001955/hsa_circ_0000977-mediated miRNA-mRNA regulatory sub-network in colorectal cancer. *Aging (Albany NY)* 2020; **12**: 5259-5279 [PMID: 32221048 DOI: 10.18632/aging.102945]
13 **Bushati N**, Cohen SM. microRNA functions. *Annu Rev Cell Dev Biol* 2007; **23**: 175-205 [PMID: 17506695 DOI: 10.1146/annurev.cellbio.23.090506.123406]
14 **Lu TX**, Rothenberg ME. MicroRNA. *J Allergy Clin Immunol* 2018; **141**: 1202-1207 [PMID: 29074454 DOI: 10.1016/j.jaci.2017.08.034]
15 **Marcuello M**, Vymetalkova V, Neves RPL, Duran-Sanchon S, Vedeld HM, Tham E, van Dalum G, Flügen G, Garcia-Barberan V, Fijneman RJ, Castells A, Vodicka P, Lind GE, Stoecklein NH, Heitzer E, Gironella M. Circulating biomarkers for early detection and clinical management of colorectal cancer. *Mol Aspects Med* 2019; **69**: 107-122 [PMID: 31189073 DOI: 10.1016/j.mam.2019.06.002]
16 **Long J**, He Q, Yin Y, Lei X, Li Z, Zhu W. The effect of miRNA and autophagy on colorectal cancer. *Cell Prolif* 2020; **53**: e12900 [PMID: 32914514 DOI: 10.1111/cpr.12900]
17 **Savardashtaki A**, Shabaninejad Z, Movahedpour A, Sahebnasagh R, Mirzaei H, Hamblin MR. miRNAs derived from cancer-associated fibroblasts in colorectal cancer. *Epigenomics* 2019; **11**: 1627-1645 [PMID: 31702390 DOI: 10.2217/epi-2019-0110]
18 **Dong J**, Tai JW, Lu LF. miRNA-Microbiota Interaction in Gut Homeostasis and Colorectal Cancer. *Trends Cancer* 2019; **5**: 666-669 [PMID: 31735285 DOI: 10.1016/j.trecan.2019.08.003]
19 **Ren A**, Dong Y, Tsoi H, Yu J. Detection of miRNA as non-invasive biomarkers of colorectal cancer. *Int J Mol Sci* 2015; **16**: 2810-2823 [PMID: 25633103 DOI: 10.3390/ijms16022810]
20 **Yin TF**, Zhao DY, Zhou YC, Wang QQ, Yao SK. Identification of the circRNA-miRNA-mRNA regulatory network and its prognostic effect in colorectal cancer. *World J Clin Cases* 2021; **9**: 4520-4541 [PMID: 34222420 DOI: 10.12998/wjcc.v9.i18.4520]
21 **Xie Y**, Li J, Li P, Li N, Zhang Y, Binang H, Zhao Y, Duan W, Chen Y, Wang Y, Du L, Wang C. RNA-Seq Profiling of Serum Exosomal Circular RNAs Reveals Circ-PNN as a Potential Biomarker for Human Colorectal Cancer. *Front Oncol* 2020; **10**: 982 [PMID: 32626660 DOI: 10.3389/fonc.2020.00982]
22 **Yang H**, Zhang H, Yang Y, Wang X, Deng T, Liu R, Ning T, Bai M, Li H, Zhu K, Li J, Fan Q, Ying G, Ba Y. Hypoxia induced exosomal circRNA promotes metastasis of Colorectal Cancer *via* targeting GEF-H1/RhoA axis. *Theranostics* 2020; **10**: 8211-8226 [PMID: 32724467 DOI: 10.7150/thno.44419]
23 **Ju HQ**, Zhao Q, Wang F, Lan P, Wang Z, Zuo ZX, Wu QN, Fan XJ, Mo HY, Chen L, Li T, Ren C, Wan XB, Chen G, Li YH, Jia WH, Xu RH. A circRNA signature predicts postoperative recurrence in stage II/III colon cancer. *EMBO Mol Med* 2019; **11**: e10168 [PMID: 31475771 DOI: 10.15252/emmm.201810168]
24 **Shang A**, Gu C, Wang W, Wang X, Sun J, Zeng B, Chen C, Chang W, Ping Y, Ji P, Wu J, Quan W, Yao Y, Zhou Y, Sun Z, Li D. Exosomal circPACRGL promotes progression of colorectal cancer *via* the miR-142-3p/miR-506-3p- TGF-β1 axis. *Mol Cancer* 2020; **19**: 117 [PMID: 32713345 DOI: 10.1186/s12943-020-01235-0]
25 **Zeng K**, Chen X, Xu M, Liu X, Hu X, Xu T, Sun H, Pan Y, He B, Wang S. CircHIPK3 promotes colorectal cancer growth and metastasis by sponging miR-7. *Cell Death Dis* 2018; **9**: 417 [PMID: 29549306 DOI: 10.1038/s41419-018-0454-8]
26 **Wang X**, Zhang H, Yang H, Bai M, Ning T, Deng T, Liu R, Fan Q, Zhu K, Li J, Zhan Y, Ying G, Ba Y. Exosome-delivered circRNA promotes glycolysis to induce chemoresistance through the miR-122-PKM2 axis in colorectal cancer. *Mol Oncol* 2020; **14**: 539-555 [PMID: 31901148 DOI: 10.1002/1878-0261.12629]
27 **Liu X**, Abraham JM, Cheng Y, Wang Z, Zhang G, Ashktorab H, Smoot DT, Cole RN, Boronina TN, DeVine LR, Talbot CC Jr, Liu Z, Meltzer SJ. Synthetic Circular RNA Functions as a miR-21 Sponge to Suppress Gastric Carcinoma Cell Proliferation. *Mol Ther Nucleic Acids* 2018; **13**: 312-321 [PMID: 30326427 DOI: 10.1016/j.omtn.2018.09.010]
28 **Zhang D**, Xiao YF, Zhang JW, Xie R, Hu CJ, Tang B, Wang SM, Wu YY, Hao NB, Yang SM. miR-1182 attenuates gastric cancer proliferation and metastasis by targeting the open reading frame of hTERT. *Cancer Lett* 2015; **360**: 151-159 [PMID: 25662441 DOI: 10.1016/j.canlet.2015.01.044]

29 **Jia N**, Song Z, Chen B, Cheng J, Zhou W. A Novel Circular RNA circCSPP1 Promotes Liver Cancer Progression by Sponging miR-1182. *Onco Targets Ther* 2021; **14**: 2829-2838 [PMID: 33935503 DOI: 10.2147/OTT.S292320]

30 **Zhao M**, Ma W, Ma C. Circ_0067934 promotes non-small cell lung cancer development by regulating miR-1182/KLF8 axis and activating Wnt/β-catenin pathway. *Biomed Pharmacother* 2020; **129**: 110461 [PMID: 32768951 DOI: 10.1016/j.biopha.2020.110461]

31 **Zong ZH**, Du YP, Guan X, Chen S, Zhao Y. CircWHSC1 promotes ovarian cancer progression by regulating MUC1 and hTERT through sponging miR-145 and miR-1182. *J Exp Clin Cancer Res* 2019; **38**: 437 [PMID: 31666098 DOI: 10.1186/s13046-019-1437-z]

32 **Li Y**, Li C, Xu R, Wang Y, Li D, Zhang B. A novel circFMN2 promotes tumor proliferation in CRC by regulating the miR-1182/hTERT signaling pathways. *Clin Sci (Lond)* 2019; **133**: 2463-2479 [PMID: 31738400 DOI: 10.1042/CS20190715]

33 **Peng W**, Li J, Chen R, Gu Q, Yang P, Qian W, Ji D, Wang Q, Zhang Z, Tang J, Sun Y. Upregulated METTL3 promotes metastasis of colorectal Cancer *via* miR-1246/SPRED2/MAPK signaling pathway. *J Exp Clin Cancer Res* 2019; **38**: 393 [PMID: 31492150 DOI: 10.1186/s13046-019-1408-4]

34 **Guo S**, Chen J, Chen F, Zeng Q, Liu WL, Zhang G. Exosomes derived from *Fusobacterium nucleatum*-infected colorectal cancer cells facilitate tumour metastasis by selectively carrying miR-1246/92b-3p/27a-3p and CXCL16. *Gut* 2020 [PMID: 33172926 DOI: 10.1136/gutjnl-2020-321187]

35 **Cooks T**, Pateras IS, Jenkins LM, Patel KM, Robles AI, Morris J, Forshew T, Appella E, Gorgoulis VG, Harris CC. Mutant p53 cancers reprogram macrophages to tumor supporting macrophages *via* exosomal miR-1246. *Nat Commun* 2018; **9**: 771 [PMID: 29472616 DOI: 10.1038/s41467-018-03224-w]

36 **Bian J**, Dannappel M, Wan C, Firestein R. Transcriptional Regulation of Wnt/β-Catenin Pathway in Colorectal Cancer. *Cells* 2020; **9** [PMID: 32961708 DOI: 10.3390/cells9092125]

37 **Cheng X**, Xu X, Chen D, Zhao F, Wang W. Therapeutic potential of targeting the Wnt/β-catenin signaling pathway in colorectal cancer. *Biomed Pharmacother* 2019; **110**: 473-481 [PMID: 30530050 DOI: 10.1016/j.biopha.2018.11.082]

38 **Chai S**, Ng KY, Tong M, Lau EY, Lee TK, Chan KW, Yuan YF, Cheung TT, Cheung ST, Wang XQ, Wong N, Lo CM, Man K, Guan XY, Ma S. Octamer 4/microRNA-1246 signaling axis drives Wnt/β-catenin activation in liver cancer stem cells. *Hepatology* 2016; **64**: 2062-2076 [PMID: 27639189 DOI: 10.1002/hep.28821]

39 **Huang JL**, Fu YP, Gan W, Liu G, Zhou PY, Zhou C, Sun BY, Guan RY, Zhou J, Fan J, Yi Y, Qiu SJ. Hepatic stellate cells promote the progression of hepatocellular carcinoma through microRNA-1246-RORα-Wnt/β-Catenin axis. *Cancer Lett* 2020; **476**: 140-151 [PMID: 32061951 DOI: 10.1016/j.canlet.2020.02.012]

40 **Yang F**, Xiong H, Duan L, Li Q, Li X, Zhou Y. MiR-1246 Promotes Metastasis and Invasion of A549 cells by Targeting GSK-3β–Mediated Wnt/β-Catenin Pathway. *Cancer Res Treat* 2019; **51**: 1420-1429 [PMID: 30913872 DOI: 10.4143/crt.2018.638]

41 **Xie B**, Li L, Zhang Z, Zhao L, Cheng J, Zhou C, Yan J, Chen J, Yi J, Wang B, Jin S, Wei H. MicroRNA-1246 by Targeting AXIN2 and GSK-3β Overcomes Drug Resistance and Induces Apoptosis in Chemo-resistant Leukemia Cells. *J Cancer* 2021; **12**: 4196-4208 [PMID: 34093820 DOI: 10.7150/jca.58522]

42 **Zhang Y**, Liao JM, Zeng SX, Lu H. p53 downregulates Down syndrome-associated DYRK1A through miR-1246. *EMBO Rep* 2011; **12**: 811-817 [PMID: 21637297 DOI: 10.1038/embor.2011.98]

World Journal of Clinical Cases

Submit a Manuscript: https://www.f6publishing.com

World J Clin Cases 2022 April 16; 10(11): 3369-3378

DOI: 10.12998/wjcc.v10.i11.3369

ISSN 2307-8960 (online)

ORIGINAL ARTICLE

Retrospective Study

Echocardiography in the diagnosis of Shone's complex and analysis of the causes for missed diagnosis and misdiagnosis

Ye-Dan Li, Hong Meng, Kun-Jing Pang, Mu-Zi Li, Nan Xu, Hao Wang, Shou-Jun Li, Jun Yan

Specialty type: Cardiac and Cardiovascular Systems

Provenance and peer review: Unsolicited article; Externally peer reviewed.

Peer-review model: Single blind

Peer-review report's scientific quality classification

Grade A (Excellent): 0
Grade B (Very good): B
Grade C (Good): 0
Grade D (Fair): D
Grade E (Poor): 0

P-Reviewer: Gulel O, Turkey; Ong LT, Malaysia

Received: September 3, 2021
Peer-review started: September 3, 2021
First decision: October 25, 2021
Revised: December 23, 2021
Accepted: February 27, 2022
Article in press: February 27, 2022
Published online: April 16, 2022

Ye-Dan Li, Hong Meng, Kun-Jing Pang, Mu-Zi Li, Nan Xu, Hao Wang, Department of Echocardiography, Fuwai Hospital, Beijing 100037, China

Shou-Jun Li, Jun Yan, Department of Cardiovascular Surgery, Fuwai Hospital, Beijing 100037, China

Corresponding author: Hong Meng, MD, Doctor, Department of Echocardiography, Fuwai Hospital, No. 167 North Lishi Road, Xicheng District, Beijing 100037, China.
597330958@qq.com

Abstract

BACKGROUND

Shone's complex is a rare syndrome characterized by congenital left heart defects that can differ among the patients.

AIM

To use echocardiography in the diagnosis of Shone's complex and analyze the causes of missed diagnosis and misdiagnosis.

METHODS

This was a retrospective study of patients who underwent echocardiography and repair surgery from February 14, 2008, to November 22, 2019. The patients were followed once a year at the outpatient clinic after surgery.

RESULTS

Sixty-six patients were included. The patients were 2.7 (0.8-5.6) years of age, and 54.5% were male. Ten (15.2%) had a history of heart surgery. The most common heart defect was the Annulo-Leaflet mitral ring (ALMR) (50/66, 75.8%), followed by coarctation of the aorta (CoA) (43/66, 65.2%). The patients had a variety of combinations of defects. Only two (3.0%) patients had all four defects. None of the patients had a family history of congenital heart disease. The preoperative echocardiographic findings were examined against the intraoperative findings. Echocardiography missed an ALMR in 31 patients (47.0%), a parachute mitral valve (PMV) in one patient (1.5%), subaortic stenosis in one patient (1.5%), and CoA in two patients (3.0%).

CONCLUSION

Echocardiography is an effective method to diagnose the Shone's complex. Due to

this disease's complexity and interindividual variability, Improving the understanding of the disease can reduce misdiagnosis and missed diagnosis.

Key Words: Shone's syndrome; Congenital heart disease; Mitral valve; Echocardiography; Left heart; Misdiagnosis

Core Tip: This was a retrospective study with the largest sample size which aimed to examine the use of echocardiography in the diagnosis of Shone's complex and to analyze the possible causes of missed diagnosis and misdiagnosis. Sixty-six patients were included. The preoperative echocardiographic findings were examined against the intraoperative findings. Echocardiography missed an Annulo-Leaflet mitral ring in 31 patients, a parachute mitral valve in one patient, subaortic stenosis in one patient, and coarctation of the aorta in two patients. Due to this disease's complexity and interindividual variability, echocardiography missed diagnosis can occur. Combining the results of echocardiography, computed tomography, magnetic resonance imaging might be helpful.

Citation: Li YD, Meng H, Pang KJ, Li MZ, Xu N, Wang H, Li SJ, Yan J. Echocardiography in the diagnosis of Shone's complex and analysis of the causes for missed diagnosis and misdiagnosis. *World J Clin Cases* 2022; 10(11): 3369-3378
URL: https://www.wjgnet.com/2307-8960/full/v10/i11/3369.htm
DOI: https://dx.doi.org/10.12998/wjcc.v10.i11.3369

INTRODUCTION

Shone's complex is a rare congenital heart disease characterized by multiple left heart obstructive defects, including coarctation of the aorta (CoA), valvular stenosis, and mitral stenosis[1-4]. Those defects interfere with the normal flow of oxygenated blood from the left heart. There are complete and incomplete forms of the syndrome, as well as possible combinations with other heart defects such as patent ductus arteriosus, interrupted aortic arch, bicuspid aortic valve, atrial septal defect, and ventricular septal defect[5]. The spectrum of symptoms, treatments, and outcomes will vary according to the number of defects[6-10]. Shone's complex represent about 0.7% of the patients with congenital heart disease[11] or 0.03% of echocardiography examinations[12]. The long-term prognosis is poor, and the perioperative mortality rates are 24%-27%[13,14].

Echocardiography is a non-invasive imaging modality that provides hemodynamic information in a short period and at the patient bedside. It can be used to reveal abnormal left ventricular wall motions, right ventricle dilation, an intimal flap in the ascending aorta, pericardial effusion, left ventricular ejection fraction[15-19]. It is a non-invasive, rapid, inexpensive diagnostic modality for a number of heart conditions such as pericardial tamponade, acute coronary syndrome, cardiomyopathy, pulmonary embolism, and Stanford type A aortic dissection[19,20]. It can also be used for the diagnosis, follow-up, and management of congenital heart diseases[21-23].

The studies about the use of echocardiography for the diagnosis of Shone's complex are mainly limited to case reports[5,24-26] or small case series[12,27,28]. Nevertheless, a study suggested that echocardiography is invaluable in the characterization of the left heart defects found in Shone's complex, but that diagnosis is complicated by the high variability of the possible combinations of defects[27]. This could result in a missed diagnosis or misdiagnosis. Additional studies are necessary to determine the exact value of echocardiography in the diagnosis of Shone's complex.

Therefore, this study aims to examine the use of echocardiography in the diagnosis of Shone's complex and to analyze the possible causes of missed diagnosis and misdiagnosis. The results could support the use of echocardiography for the diagnosis of Shone's complex.

MATERIALS AND METHODS

Study design and patients

This was a retrospective study of patients who underwent echocardiography and repair surgery at Fuwai Hospital (Beijing, China) from February 14, 2008, to November 22, 2019. The study was approved by the ethics committee of Fuwai Hospital, Beijing, China (2016YFC1302000). The requirement for informed consent was waived by the committee because of the retrospective study nature.

The inclusion criteria were: (1) Surgically confirmed Shone's complex; and (2) Underwent echocardiography, and qualified images were available. Patients with incomplete clinical data were excluded.

Diagnostic criteria

In 1963, Shone *et al*[29] reported the feature of Shone's syndrome, which includes Annulo-Leaflet mitral ring (ALMR), parachute mitral valve (PMV), subaortic stenosis (subAS), and CoA. Shone's syndrome is a rare form of congenital heart disease that consists of several heart defects, including ALMR, PMV, subAS, and CoA. The corresponding pathological changes are as follows: ALMR occurs in the septum of the region above the annulus of the mitral valve. PMV is a form of congenital mitral stenosis where the main pathological change is papillary muscle fusion, which involves mitral chordae tendineae attaching to a single dominant papillary muscle, leading to the inability of the mitral valve to fully open during ventricular diastole. There are two common types of subAS: (1) Limited subaortic stenosis includes fibromuscular septum inferior stenosis and septum inferior aortic stenosis, which is caused by 1.0 - 1.5 cm fibrous septums below the aortic valve; and (2) Diffuse subaortic stenosis is tubular stenosis caused by diffuse thickening of the outflow tract muscle in the left ventricle. Coarctation of the aorta is a local or diffuse narrowing of the aorta that results in reduced blood flow.

When only two or three of the abnormalities are present, Shone's complex is diagnosed as the incomplete form. Delmo *et al*[30] believe that a mitral valve abnormality of the inflow tract is the main factor that affected surgical effects. Therefore, when there are outflow abnormalities complicated with ALMR or mitral stenosis, Shone's complex can be diagnosed as the incomplete form.

Echocardiography

Echocardiography was performed within one week before surgery. The ultrasonic examinations of all children were performed by a sonographer with more than 5 years of working experience.

In addition to providing unified technical training and consistent examination conditions, we employed skilled sonographers to minimize bias and strictly controlled objective indicators, thus facilitating diagnoses according to diagnostic criteria. The equipment included Philips IE33 and EPIQ 7C systems, with the S8-3 (3-8 MHz) and S5-1 (1-5 MHz) probes (Philips, Best, The Netherlands). If the children did not cooperate with the examination, a 0.5 mL/kg chloral hydrate solution was orally administrated for sedation. The children were in the horizontal or left lateral position, and echocardiography was performed in the order of subxiphoid, parasternal area, cardiac apex, and suprasternal fossa. The diagnosis was made using the three-segment method, paying special attention to the subxiphoid four-chamber view, parasternal left ventricular long-axis view, parasternal four-chamber view, parasternal left ventricular short-axis view, apical four/five-chamber view, and suprasternal fossa view.

Surgery

The patients underwent repair surgeries according to different combinations of defects under general anesthesia, including mitral valvuloplasty, resection of supravalvular septum, patch angioplasty for CoA, and CoA resection and end-to-end anastomosis.

Follow-up

The patients were followed once a year at the outpatient clinic after surgery. Echocardiography was performed to observe the forward flow velocity and regurgitation of the mitral valve, forward flow velocity and regurgitation of the aortic valve, and the descending aortic flow velocity, and determine the presence or absence of postoperative re-obstruction (defined as descending aortic flow velocity of < 2 m/s).

Statistical analysis

Only descriptive statistics were used. Age was presented as median (range), and categorical variables were presented as prequencies and percentages.

The statistical methods of this study were reviewed by Ye-Dan Li, Kun-Jing Pang, Mu-Zi Li, Nan Xu, Hao Wang, Shou-Jun Li and Jun Yan from State Key Laboratory of Cardiovascular Disease, Fuwai Hospital, National Center for Cardiovascular Diseases, Chinese Academy of Medical Sciences and Peking Union Medical College.

RESULTS

Characteristics of the patients

The characteristics of the 66 patients are shown in Table 1. The patients were 2.7 (0.8-5.6) years of age, and 54.5% (36/66) were male. Twenty (30.3%) were born by cesarean section, and 10 (15.2%) had a history of heart surgery. The most common heart defect was an ALMR (50/66, 75.8%), followed by CoA (43/66, 65.2%). None of the patients showed signs of cyanosis, while only one patient displayed

Table 1 Characteristics of the patients (*n* = 66)

Characteristics	Median (range) / *n* (%)
Age (yr)	2.7 (0.8-5.6)
Sex (male)	36 (54.5%)
Cesarean section	20 (30.3%)
History of heart surgery	10 (15.2%)
Shone's complex	
ALMR	50 (75.8%)
CoA	43 (65.2%)
subAS	25 (37.9%)
PMV	20 (30.3%)
Other defects	
PDA	30 (45.5%)
VSD	24 (36.4%)
MS	23 (34.8%)
MR	18 (27.3%)
BAV	18 (27.3%)
AS	13 (19.7%)
HAA	11 (16.7%)
supraAS	8 (12.1%)

ALMR: Annulo-Leaflet mitral ring; CoA: Coarctation of the aorta; subAS: Subaortic stenosis; PMV: Parachute mitral valve; PDA: Patent ductus arteriosus; VSD: Ventriculap septal defect; MS: Mitral stenosis; MR: Mitral regurgitation; BAV: Bicuspid aortic valve; AS: Aortic stenosis; HAA: Hypoplastic aortic arch; supraAS: Supra-aortic stenosis.

symptoms of dyspnea and left heart failure (1/66, 1.5%). The patients had a variety of combinations of defects (Table 1). Only two (3.0%) patients had all four defects. None of the patients had a family history of congenital heart disease.

Missed diagnoses

The preoperative echocardiographic findings were examined against the intraoperative findings. Echocardiography missed an ALMR in 31 patients (47.0%), a PMV in one patient (1.5%), subaortic stenosis in one patient (1.5%), and CoA in two patients (3.0%). Figures 1-4 present typical echocardiography images of Shone's complex.

DISCUSSION

Shone's complex is a rare syndrome characterized by congenital left heart defects that can differ among the patients. This retrospective study aims to examine the use of echocardiography in the diagnosis of Shone's complex and to analyze the possible causes of missed diagnosis and misdiagnosis. The results suggest that echocardiography is an effective, non-invasive, and low-cost method to diagnose the heart defects of Shone's complex. Due to this disease's complexity and interindividual variability, missed diagnosis and misdiagnosis can occur. Combining the results of echocardiography, computed tomography, and/or magnetic resonance imaging might be helpful.

Some case reports examined the use of echocardiography in some patients[5,24-26], and small case series are available[12,27,28]. Ma *et al*[27] reported 38 patients with Shone's complex that were evaluated by echocardiography. They reported a wide variety of combinations of defects among their patients, as in the present study, and concluded that echocardiography is important in the diagnosis of Shone's complex, but they did not examine the misdiagnoses. Kumar *et al*[28] reported five patients with Shone's complex and transesophageal echocardiographic evaluation and highlighted the usefulness of transesophageal echocardiography. Zucker *et al*[12] suggested that ultrasound is crucial to discriminate between Shone's complex and hypoplastic left ventricle, influencing the physician's management.

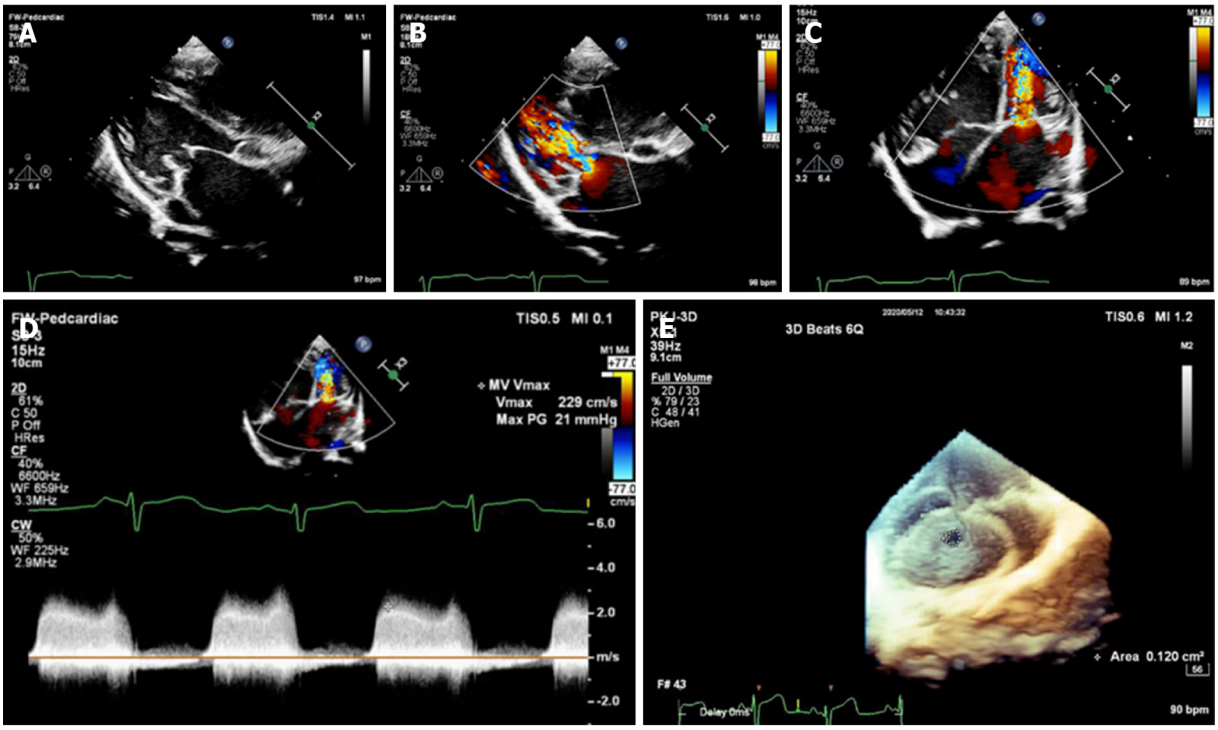

DOI: 10.12998/wjcc.v10.i11.3369

Figure 1 A case of Annulo-Leaflet mitral ring. A: Two-dimensional ultrasonography at the parasternal left ventricular long-axis view revealed thickened mitral valve and a mitral ring adhered to the anterior and posterior leaflets of the mitral valve, restricting the opening of the valve leaflets and causing mitral valve inflow tract obstruction; B: Color Doppler ultrasonography at the parasternal left ventricular long-axis view revealed that blood flow velocity increased at the mitral annulus, and the forward flow velocity of the mitral valve was increased; C: Color Doppler ultrasonography at the apical four-chamber view revealed that blood flow velocity increased at the mitral annulus, and the forward flow velocity of the mitral valve was increased; D: The forward flow velocity of the mitral valve was increased significantly, at 2.29 m/s; E: Real-time three-dimensional echocardiography showed a narrow mitral valve orifice.

An innovation of the present study is the validation of the preoperative echographic findings with the intraoperative findings. A surprising result is that echocardiography missed an ALMR in 47.0% of the patients or 62.0% of the patients with an ALMR, while PMV (1.5% of the patients or 5.0% of the PMVs), subaortic stenosis (1.5% of the patients or 4.0% of the subaortic stenoses), and CoA (3.0% of the patients or 4.7% of the CoAs) were missed in smaller proportions of patients. Various reasons might be involved. The mitral ring is very small. Sometimes, only the ridge adhered to the mitral valve, or only to the anterior and posterior leaflets or annulus of the mitral valve, or did not adhere to the mitral valve but was very close to it. In these cases, it was difficult to identify an ALMR on echocardiography. The mitral valve leaflets can also be thickened and enhancing the echo, which can easily cover the supravalvular ring on the images. If the sonographer is inexperienced, the ALMR might be missed without further careful observation when PMV and mitral stenosis were found. Regarding PMV. If the left ventricular short-axis papillary muscle is not carefully checked, the anomaly of the papillary muscle can be missed. The flow velocity can be increased in the presence of mitral stenosis. If the sonographer considered the increase in flow velocity as a result of mitral stenosis, PMV might be missed due to not paying further attention. Subaortic stenosis is classified as the membranous type and fibromuscular type (isolated and diffuse stenosis). Usually, the manifestation of fibromuscular stenosis is obvious, and it cannot be missed. On the other hand, the membranous type is easy to be missed, because the subvalvular septum is sometimes very small, or the septum is close to the aortic valve. CoA can be classified as two types according to the different positions of the arterial duct: preductual and postductal. If the color Doppler and spectral Doppler images of the descending aortic arch on the suprasternal fossa view are not carefully observed, CoA can be missed. CoA patients are often accompanied by post-stenotic dilation of the descending aorta, which may suggest CoA. When children develop left ventricular wall hypertrophy or decreased left ventricular systolic function, the presence of CoA can be considered. In addition, many patients with anomalies of the bicuspid aortic valve have CoA and should be carefully screened.

Subaortic stenosis was misdiagnosed as aortic stenosis in one case. Because the subaortic septum is often very close to the aortic valve, subaortic stenosis caused by the subaortic septum is commonly mistaken for aortic stenosis. Therefore, it is easy to misdiagnose the condition if the clinician lacks experience or does not make careful observations.

In addition, 10 children in this study had a history of heart surgery, but misdiagnosis or missed diagnosis still occurred because previous surgical procedures were also planned based on the results of

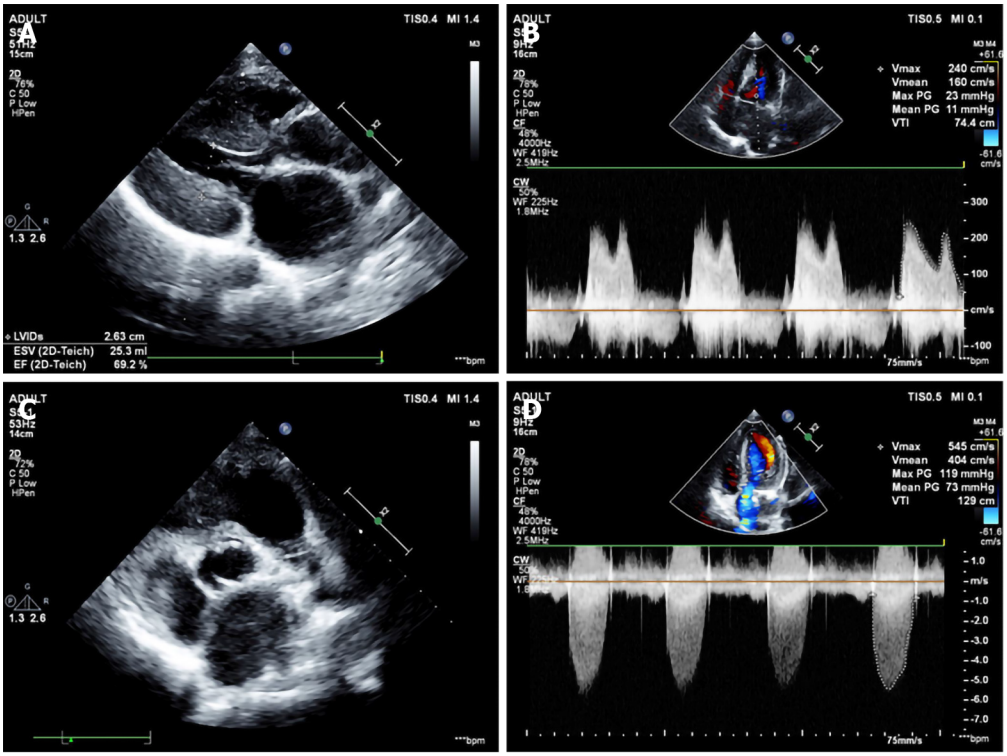

DOI: 10.12998/wjcc.v10.i11.3369

Figure 2 Image of a patient with incomplete Shone's complex. Echocardiography missed the ALMR. Intraoperative exploration revealed that the mitral valve adhered to the anterior leaflet, close to the anterior leaflet of the mitral valve. A: The parasternal left ventricular long-axis view showed a significant thickening of the left ventricular wall; B: The forward flow velocity at the mitral valve was increased significantly, at 2.4 m/s, and the mean transvalvular pressure gradient was 11 mmHg; C: The aortic valve was bicuspid and arranged on the left and right; D: The flow velocity of the aortic valve was increased significantly, at 5.45 m/s, and the mean transvalvular pressure gradient was 73 mmHg.

echocardiography. For example, if only a mitral valve defect was found and CoA was missed at that time, only the mitral valve was treated during surgery, and the CoA was still missed.

The prognosis of patients after surgery was as follows: one patient developed a third-degree atrioventricular block and had a permanent pacemaker installed. Another case had cyanosis and dyspnea and underwent mitral and tricuspid valve repair. One patient had severe mitral insufficiency in the early stage and received a mechanical mitral valve replacement three days after the operation. Besides, one case underwent ALMR resection nine years after the first operation. There were no instances of in-hospital deaths.

Patients were treated with torasemide tablets and potassium citrate granules after surgery. Surgical methods of inflow tract obstruction mainly included ALMR removal, chordae tendineae release, papillary muscle incision, and mitral valve replacement. Approaches for outflow tract obstruction primarily involved aortic coarctation resection, end-to-end anastomosis, subvalvular septum removal, *etc.* Among the 66 patients, seven underwent secondary surgery. Besides, there were four cases of complete Shone's syndrome and 62 cases of incomplete Shone's syndrome.

This study has limitations. Most previous studies are either case reports or small case series, and the present study is probably the largest series so far, with $n = 66$, but it is still a small series to draw firm conclusions. All patients were from a single center, and future studies should include multiple hospitals. Indeed, the disease is rare, and collective research efforts should be undertaken. Finally, the available data were limited to those available in the charts.

CONCLUSION

In conclusion, echocardiography is an effective, non-invasive, and low-cost method to diagnose the heart defects of Shone's complex. Due to the complexity and interindividual variability of the syndrome, missed diagnosis and misdiagnosis may easily occur. Future studies should examine the combination of multiple imaging modalities, including echocardiography, computed tomography, and magnetic resonance imaging.

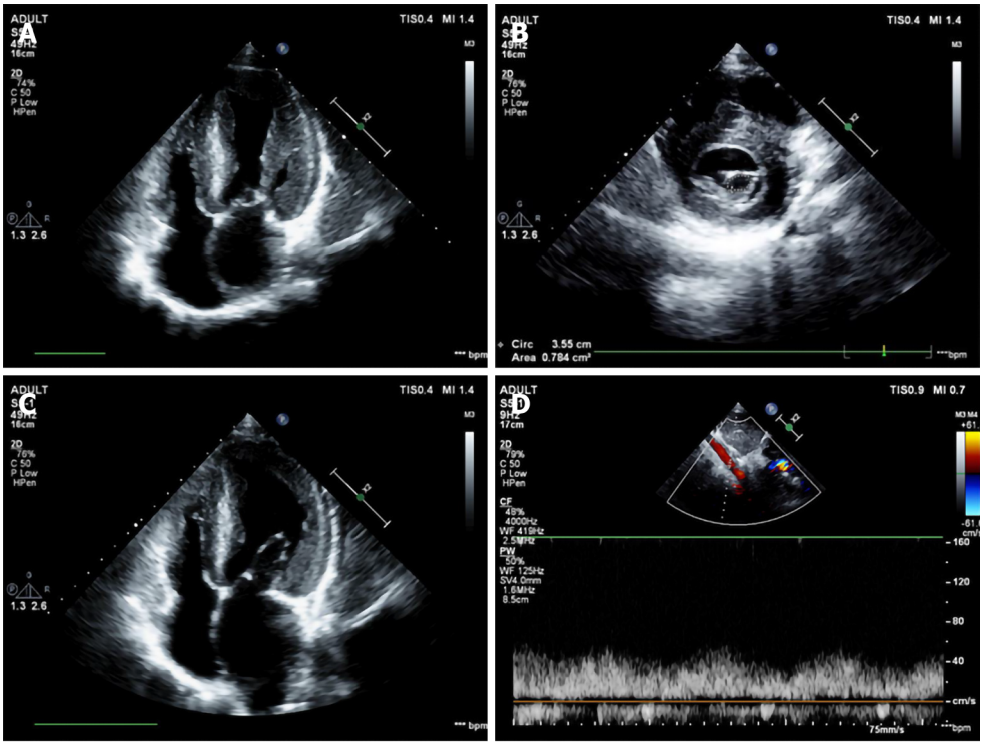

DOI: 10.12998/wjcc.v10.i11.3369 **Copyright** © The Author(s) 2022.

Figure 3 A case in which the Annulo-Leaflet mitral ring was missed by echocardiography at the outpatient. Intraoperative exploration revealed that the supramitral ring was adhered to the anterior and posterior leaflets, close to the anterior and posterior leaflets of the mitral valve. A: The parasternal mitral short-axis view showed a significant reduction in the area of the mitral valve orifice, which was only 0.78 cm^2; B: Two-dimensional ultrasonography at the apical four-chamber view showed thickened mitral valve with restricted opening; C: There are both annulo-leaflet mitral ring and parachute mitral valve. Preoperative echocardiography after admission showed a tiny septum on the anterior leaflet of the mitral valve; D: Spectral Doppler of the abdominal aorta showed low velocity and low resistance, suggesting coarctation of the aorta.

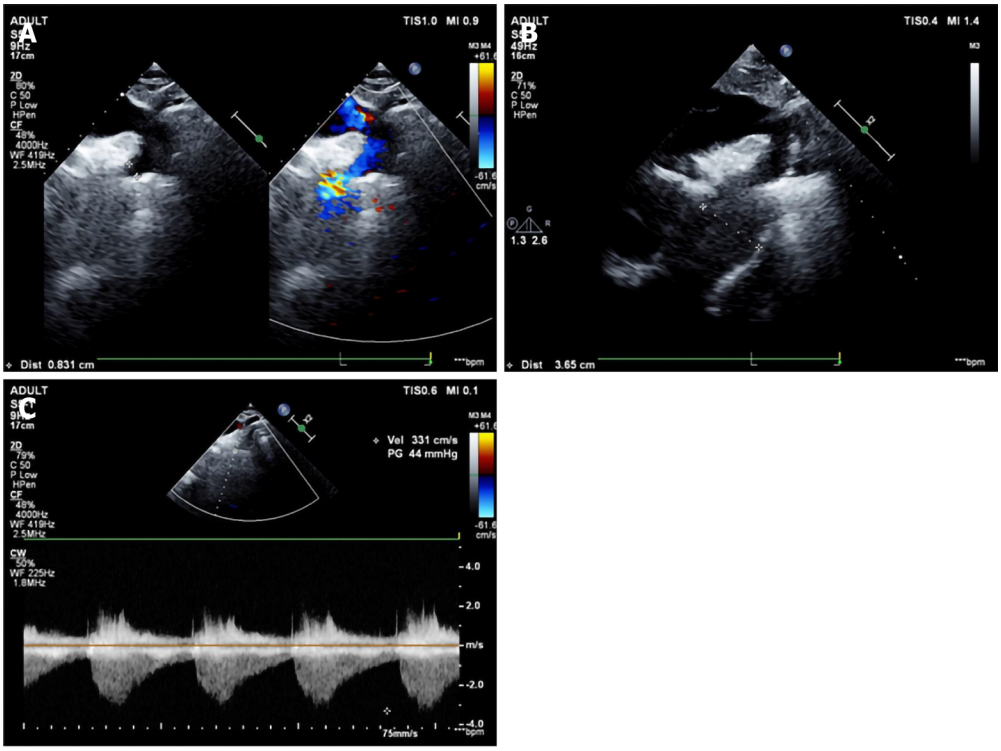

DOI: 10.12998/wjcc.v10.i11.3369 **Copyright** © The Author(s) 2022.

Figure 4 The long-axis view of the aortic arch of the suprasternal fossa showed coarctation of the aorta.

ARTICLE HIGHLIGHTS

Research background

Shone's complex is a rare syndrome characterized by congenital left heart defects that can differ among the patients.

Research motivation

To use echocardiography in the diagnosis of Shone's complex and analyze the causes of missed diagnosis and misdiagnosis.

Research objectives

Sixty-six patients were included.

Research methods

This was a retrospective study of patients who underwent echocardiography and repair surgery from February 14, 2008, to November 22, 2019. The patients were followed once a year at the outpatient clinic after surgery.

Research results

Sixty-six patients were included. The patients were 2.7 (0.8-5.6) years of age, and 54.5% were male. Ten (15.2%) had a history of heart surgery. The most common heart defect was the Annulo-Leaflet mitral ring (ALMR) (50/66, 75.8%), followed by coarctation of the aorta (CoA) (43/66, 65.2%).

Research conclusions

Echocardiography is an effective method to diagnose the Shone's complex. Due to this disease's complexity and interindividual variability, Improving the understanding of the disease can reduce misdiagnosis and missed diagnosis.

Research perspectives

This was a retrospective study with the largest sample size which aimed to examine the use of echocardiography in the diagnosis of Shone's complex and to analyze the possible causes of missed diagnosis and misdiagnosis. Sixty-six patients were included. The preoperative echocardiographic findings were examined against the intraoperative findings. Echocardiography missed an ALMR in 31 patients, a parachute mitral valve in one patient, subaortic stenosis in one patient, and CoA in two patients. Due to this disease's complexity and interindividual variability, echocardiography missed diagnosis can occur. Combining the results of echocardiography, computed tomography, magnetic resonance imaging might be helpful.

ACKNOWLEDGEMENTS

The authors thank all the medical workers at the Ultrasound Department of Fuwai Hospital, Chinese Academy of Medical Sciences, for their help in this study.

FOOTNOTES

Author contributions: Li YD, Xu N and Li MZ carried out the studies, participated in collecting data, and drafted the manuscript; Li YD, Meng H, Pang KJ and Wang H performed the statistical analysis and participated in its design; Li YD, Li SJ, and Yan J participated in acquisition, analysis, or interpretation of data and draft the manuscript; all authors read and approved the final manuscript.

Institutional review board statement: The study was approved by the ethics committee of Fuwai Hospital, Beijing, China (2016YFC1302000).

Informed consent statement: The requirement for informed consent was waived by the committee because of the retrospective study nature.

Conflict-of-interest statement: We have no financial relationships to disclose.

Data sharing statement: No additional data are available.

Country/Territory of origin: China

ORCID number: Ye-Dan Li 0000-0002-3992-2972; Hong Meng 0000-0002-2028-4018; kun-Jing Pang 0000-0003-0605-2680; Mu-Zi Li 0000-0001-8997-3682; Nan Xu 0000-0003-4746-7655; Hao Wang 0000-0003-0780-248X; Shou-Jun Li 0000-0002-6878-8733; Jun Yan 0000-0002-9380-8695.

S-Editor: Ma YJ
L-Editor: A
P-Editor: Ma YJ

REFERENCES

1 **Ahmed M**, Aziz H, Jiang L. Severe aortic complications in a patient with variant Shone's complex and bicuspid aortic valve. *BMJ Case Rep* 2017; **2017** [PMID: 28790051 DOI: 10.1136/bcr-2017-221348]
2 **Bobylev D**, Meschenmoser L, Boethig D, Horke A. Surgical repair of Shone's complex with anomalous origin of the left coronary artery arising from the right pulmonary artery. *Interact Cardiovasc Thorac Surg* 2015; **20**: 439-442 [PMID: 25535179 DOI: 10.1093/icvts/ivu422]
3 **Elmahrouk AF**, Ismail MF, Arafat AA, Dohain AM, Helal AM, Hamouda TE, Galal M, Edrees AM, Al-Radi OO, Jamjoom AA. Outcomes of biventricular repair for shone's complex. *J Card Surg* 2021; **36**: 12-20 [PMID: 33032391 DOI: 10.1111/jocs.15090]
4 **Escárcega RO**, Michelena HI, Bove AA. Bicuspid aortic valve: a neglected feature of Shone's complex? *Pediatr Cardiol* 2014; **35**: 186-187 [PMID: 24078196 DOI: 10.1007/s00246-013-0804-3]
5 **Ganju NK**, Kandoria A, Thakur S, Ganju SA. A Constellation of Cardiac Anomalies: Beyond Shone's Complex. *Heart Views* 2016; **17**: 23-26 [PMID: 27293526 DOI: 10.4103/1995-705X.182643]
6 **Ikemba CM**, Eidem BW, Fraley JK, Eapen RS, Pignatelli R, Ayres NA, Bezold LI. Mitral valve morphology and morbidity/mortality in Shone's complex. *Am J Cardiol* 2005; **95**: 541-543 [PMID: 15695151 DOI: 10.1016/j.amjcard.2004.10.030]
7 **Narvencar KP**, Jaques e Costa AK, Patil VR. Shone's complex. *J Assoc Physicians India* 2009; **57**: 415-416 [PMID: 19634293]
8 **Nicholson GT**, Kelleman MS, De la Uz CM, Pignatelli RH, Ayres NA, Petit CJ. Late outcomes in children with Shone's complex: a single-centre, 20-year experience. *Cardiol Young* 2017; **27**: 697-705 [PMID: 27456367 DOI: 10.1017/S1047951116001104]
9 **Pizzuto MF**, Zampi JD. Left main coronary artery atresia in an infant with Shone's complex. *Cardiol Young* 2016; **26**: 991-992 [PMID: 26898109 DOI: 10.1017/S1047951116000019]
10 **Yang LT**, Foley TA, Eidem BW, Crestanello JA, Michelena HI. Double-orifice mitral valve associated and bicuspid aortic valve: forme fruste of Shone's complex? *Eur Heart J Cardiovasc Imaging* 2020; **21**: 118 [PMID: 31302682 DOI: 10.1093/ehjci/jez195]
11 **Aslam S**, Khairy P, Shohoudi A, Mercier LA, Dore A, Marcotte F, Miró J, Avila-Alonso P, Ibrahim R, Asgar A, Poirier N, Mongeon FP. Shone Complex: An Under-recognized Congenital Heart Disease With Substantial Morbidity in Adulthood. *Can J Cardiol* 2017; **33**: 253-259 [PMID: 27956040 DOI: 10.1016/j.cjca.2016.09.005]
12 **Zucker N**, Levitas A, Zalzstein E. Prenatal diagnosis of Shone's syndrome: parental counseling and clinical outcome. *Ultrasound Obstet Gynecol* 2004; **24**: 629-632 [PMID: 15517547 DOI: 10.1002/uog.1753]
13 **Bolling SF**, Iannettoni MD, Dick M 2nd, Rosenthal A, Bove EL. Shone's anomaly: operative results and late outcome. *Ann Thorac Surg* 1990; **49**: 887-893 [PMID: 2369186 DOI: 10.1016/0003-4975(90)90861-y]
14 **Brauner RA**, Laks H, Drinkwater DC Jr, Scholl F, McCaffery S. Multiple left heart obstructions (Shone's anomaly) with mitral valve involvement: long-term surgical outcome. *Ann Thorac Surg* 1997; **64**: 721-729 [PMID: 9307464 DOI: 10.1016/s0003-4975(97)00632-2]
15 **Arntfield R**, Pace J, Hewak M, Thompson D. Focused Transesophageal Echocardiography by Emergency Physicians is Feasible and Clinically Influential: Observational Results from a Novel Ultrasound Program. *J Emerg Med* 2016; **50**: 286-294 [PMID: 26508495 DOI: 10.1016/j.jemermed.2015.09.018]
16 **Nazerian P**, Vanni S, Castelli M, Morello F, Tozzetti C, Zagli G, Giannazzo G, Vergara R, Grifoni S. Diagnostic performance of emergency transthoracic focus cardiac ultrasound in suspected acute type A aortic dissection. *Intern Emerg Med* 2014; **9**: 665-670 [PMID: 24871637 DOI: 10.1007/s11739-014-1080-9]
17 **Lang RM**, Badano LP, Mor-Avi V, Afilalo J, Armstrong A, Ernande L, Flachskampf FA, Foster E, Goldstein SA, Kuznetsova T, Lancellotti P, Muraru D, Picard MH, Rietzschel ER, Rudski L, Spencer KT, Tsang W, Voigt JU. Recommendations for cardiac chamber quantification by echocardiography in adults: an update from the American Society of Echocardiography and the European Association of Cardiovascular Imaging. *Eur Heart J Cardiovasc Imaging* 2015; **16**: 233-270 [PMID: 25712077 DOI: 10.1093/ehjci/jev014]
18 **Kennedy Hall M**, Coffey EC, Herbst M, Liu R, Pare JR, Andrew Taylor R, Thomas S, Moore CL. The "5Es" of emergency physician-performed focused cardiac ultrasound: a protocol for rapid identification of effusion, ejection, equality, exit, and entrance. *Acad Emerg Med* 2015; **22**: 583-593 [PMID: 25903585 DOI: 10.1111/acem.12652]
19 **Herbst MK**, Velasquez J, O'Rourke MC. Cardiac Ultrasound. StatPearls. Treasure Island (FL), 2020

20 **Arntfield RT**, Millington SJ. Point of care cardiac ultrasound applications in the emergency department and intensive care unit--a review. *Curr Cardiol Rev* 2012; **8**: 98-108 [PMID: 22894759 DOI: 10.2174/157340312801784952]

21 **Simpson JM**, van den Bosch A. EDUCATIONAL SERIES IN CONGENITAL HEART DISEASE: Three-dimensional echocardiography in congenital heart disease. *Echo Res Pract* 2019; **6**: R75-R86 [PMID: 31026813 DOI: 10.1530/ERP-18-0074]

22 **Alghamdi MH**, Ismail MI, Yelbuz TM, Alhabshan F. Do We Need More Than a Transthoracic Echocardiography When Evaluating Children with Congenital Heart Disease before Cardiac Surgery? *Congenit Heart Dis* 2016; **11**: 262-269 [PMID: 26560082 DOI: 10.1111/chd.12312]

23 **Moodie DS**. Diagnosis and management of congenital heart disease in the adult. *Cardiol Rev* 2001; **9**: 276-281 [PMID: 11520451 DOI: 10.1097/00045415-200109000-00007]

24 **Popescu BA**, Jurcut R, Serban M, Parascan L, Ginghina C. Shone's syndrome diagnosed with echocardiography and confirmed at pathology. *Eur J Echocardiogr* 2008; **9**: 865-867 [PMID: 18621780 DOI: 10.1093/ejechocard/jen200]

25 **Shehatha JS**, Taha AY, Mizra AJ. Late Shone complex: A case report and literature review. *J Egypt Soc Cardio-Thoracic Surg* 2018; **26**: 133-135

26 **Nkoke C**, Lekoubou A, Yonta EW, Dzudie A, Kengne AP. Shone's anomaly: a report of one case in sub-Saharan Africa. *Cardiovasc Diagn Ther* 2014; **4**: 495-498 [PMID: 25610807 DOI: 10.3978/j.issn.2223-3652.2014.12.04]

27 **Ma XJ**, Huang GY, Liang XC, Liu XQ, Jia B. Atypical Shone's complex diagnosed by echocardiography. *Pediatr Cardiol* 2011; **32**: 442-448 [PMID: 21279339 DOI: 10.1007/s00246-011-9886-y]

28 **Kumar A**, Bhat IH, Kumar B, T Shyam KS. Role of perioperative echocardiography in repair of incomplete shone complex: A case series. *Ann Card Anaesth* 2019; **22**: 444-448 [PMID: 31621686 DOI: 10.4103/aca.ACA_80_18]

29 **SHONE JD**, SELLERS RD, ANDERSON RC, ADAMS P Jr, LILLEHEI CW, EDWARDS JE. The developmental complex of "parachute mitral valve," supravalvular ring of left atrium, subaortic stenosis, and coarctation of aorta. *Am J Cardiol* 1963; **11**: 714-725 [PMID: 13988650 DOI: 10.1016/0002-9149(63)90098-5]

30 **Delmo Walter EM**, Komoda T, Siniawski H, Miera O, Van Praagh R, Hetzer R. Long-term surgical outcome of mitral valve repair in infants and children with Shone's anomaly. *Eur J Cardiothorac Surg* 2013; **43**: 473-81; discussion 481 [PMID: 22922555 DOI: 10.1093/ejcts/ezs325]

World Journal of Clinical Cases

Submit a Manuscript: https://www.f6publishing.com

World J Clin Cases 2022 April 16; 10(11): 3379-3388

DOI: 10.12998/wjcc.v10.i11.3379

ISSN 2307-8960 (online)

ORIGINAL ARTICLE

Retrospective Study

Predictors and prognostic impact of post-operative atrial fibrillation in patients with hip fracture surgery

Seong Jun Bae, Chang Hee Kwon, Tae-Young Kim, Haseong Chang, Bum Sung Kim, Sung Hea Kim, Hyun-Joong Kim

Specialty type: Cardiac and cardiovascular systems

Provenance and peer review: Unsolicited article; Externally peer reviewed.

Peer-review model: Single blind

Peer-review report's scientific quality classification

Grade A (Excellent): 0
Grade B (Very good): B, B
Grade C (Good): 0
Grade D (Fair): 0
Grade E (Poor): 0

P-Reviewer: Sawalha K, United States; Xie M, China

Received: October 15, 2021
Peer-review started: October 15, 2021
First decision: December 17, 2021
Revised: December 18, 2021
Accepted: February 17, 2022
Article in press: February 27, 2022
Published online: April 16, 2022

Seong Jun Bae, Chang Hee Kwon, Haseong Chang, Bum Sung Kim, Sung Hea Kim, Hyun-Joong Kim, Department of Internal Medicine, Konkuk University Medical Center, Seoul 05030, South Korea

Tae-Young Kim, Department of Orthopaedic Surgery, Konkuk University Medical Center, Seoul 05030, South Korea

Corresponding author: Chang Hee Kwon, MD, PhD, Assistant Professor, Internal Medicine, Konkuk University Medical Center, 120-1 Neungdong-ro, Gwangjin-gu, Seoul 05030, South Korea. vertex_77@naver.com

Abstract

BACKGROUND

Atrial fibrillation (AF) is the most common arrhythmia developing in post-operative patients. Limited data are available regarding pre-operative risk factors and prognostic impact of post-operative AF (POAF) following hip fracture surgery (HFS) in Korean population.

AIM

We aimed to investigate the incidence, predictors, and hospital prognosis of POAF in HFS patients.

METHODS

This study included 245 patients without history of AF who underwent HFS between August 2014 and November 2016. POAF was defined as new-onset AF that occurred during hospitalization after HFS.

RESULTS

Twenty patients (8.2%) experienced POAF after HFS. POAF developed on median post-operative day 2 (interquartile range, 1–3). Multivariable logistic regression analysis showed that age [odds ratio (OR), 1.111; 95% confidence interval (CI), 1.022–1.209], chronic obstructive pulmonary disease (COPD) (OR, 6.352; 95%CI, 1.561–25.841) and E/e' ratio (OR, 1.174; 95%CI, 1.002–1.376) were significant predictors of POAF. Patients with POAF had a significantly higher intensive care unit admission rate (55.0% *vs* 14.7%, $P < 0.001$) and incidence of congestive heart failure (45.0% *vs* 10.7%, $P < 0.001$). In multivariable logistic regression analysis, POAF was significantly associated with increased incidence of congestive heart

failure (OR, 4.856; 95%CI, 1.437–16.411) and intensive care unit admission (OR, 6.615; 95%CI, 2.112–20.718).

CONCLUSION

POAF was frequently developed in elderly patients following HFS. Age, COPD and elevated E/e' ratio were found as significant predictors of POAF in HFS patients. Patients with POAF significantly experienced intensive care unit admission and incident congestive heart failure during hospitalization.

Key Words: Atrial fibrillation; Post-operative; Predictor; Prognosis; Hip fracture surgery

Core Tip: This study is a retrospective study to evaluate the predictors and prognosis of post-operative atrial fibrillation (POAF) following hip fracture surgery (HFS) in elderly patients. Atrial fibrillation (AF) was developed in 8.2% following HFS. Patients with older age, COPD, or elevated E/e' ratio were shown as high risk of suffering POAF following HFS. Moreover, Patients with POAF significantly experienced intensive care unit admission and incident heart failure rather than those without POAF. Therefore, physicians have to carefully observe the occurrence of AF after HFS in elderly patients.

Citation: Bae SJ, Kwon CH, Kim TY, Chang H, Kim BS, Kim SH, Kim HJ. Predictors and prognostic impact of post-operative atrial fibrillation in patients with hip fracture surgery. *World J Clin Cases* 2022; 10(11): 3379-3388
URL: https://www.wjgnet.com/2307-8960/full/v10/i11/3379.htm
DOI: https://dx.doi.org/10.12998/wjcc.v10.i11.3379

INTRODUCTION

Atrial fibrillation (AF) is the most common cardiac arrhythmia and is independently associated with increased risks of mortality and morbidity[1,2] Incidence of post-operative AF (POAF) has been reported as 15%–45% of patients after cardiac surgery[3,4], and 0.4%–3% after non-cardiac surgery[5,6]. POAF after cardiac surgery is associated with increased length of hospital stay, early stroke risk, morbidity, and 30-d mortality[7-9]. In addition, a recent study has shown that patients with POAF after non-cardiac surgery have a significantly higher risk of stroke, myocardial infarction, and death at 1 year than patients without developing POAF[10].

Approximately 300000 individuals are hospitalized with hip fractures in the United States per year, and about one-third of these patients go on to receive a hip fracture surgery (HFS)[11,12]. Hip fractures occur frequently with aging in patients older than 65 years[13], and substantially increase the risk of death and major morbidity in elderly patients[14,15]. Moreover, HFS is associated with post-operative cardiovascular complications including AF[16-18]. Therefore, we aimed to investigate the incidence, predictors, and clinical impact of POAF in HFS patients.

MATERIALS AND METHODS

Study patients

This retrospective study involved 435 patients who underwent HFS in the Konkuk University Medical Center between August 2014 and November 2016. We excluded 190 patients who met the following exclusion criteria: (1) Patients with preoperative acute coronary syndrome (ACS) or acute decompensated congestive heart failure (CHF) (n = 18); (2) Patients with AF documented in a preoperative evaluation (n = 35); and (3) Patients with insufficient preoperative clinical or laboratory data (n = 138). Finally, 245 patients were included in this analysis. We evaluated the occurrence of POAF during hospitalization after HFS.

Ethics statement

The present study protocol was reviewed and approved by the Institutional Review Board of the Konkuk University Medical Center (protocol No. KUMC 2019-07-053). The requirement for informed consent was waived because de-identified information was retrieved retrospectively.

Study outcomes and definitions

The primary outcome was the new-onset POAF during hospitalization after HFS. POAF was defined as AF of any duration on 12-lead electrocardiography (ECG) during the post-operative period. We evaluated the incidence of clinical adverse events including ACS, CHF, pulmonary thromboembolism, and death according to the occurrence of POAF. Post-operative ACS was defined as the appearance of appropriate clinical symptoms representing unstable angina or evidence of myocardial infarction defined as creatine kinase-myocardial band levels that increased to > 2 times the upper normal limit in association with at least one of the following ECG findings: New Q wave (≥ 30 ms in 2 continuous leads), persistent significant ST elevation or depression, or a new regional wall motion abnormality. Post-operative CHF was defined as the appearance of appropriate clinical symptoms and signs of CHF that required diuretics or post-operative ventilation regardless of left ventricular ejection fraction. Pulmonary thromboembolism was diagnosed if there was a thrombus in the pulmonary arteries on computed tomographic angiography. We also compared the incidence of transfusion, admission duration, and rate of intensive care unit admission according to the occurrence of POAF.

Statistical analysis

Statistical analyses were performed using SPSS 17 software (SPSS Inc., Chicago, IL, the United States). The data were expressed as the mean ± SD for continuous variables and as frequencies with percentages for categorical variables. Continuous variables were compared by using a Student's *t*-test or Mann–Whitney test, and categorical variables using a chi-square test or Fisher's exact test. The associations of clinical, echocardiographic, or laboratory variables with the development of POAF were assessed by using univariable and multivariable logistic regression models. All variables with *P* values < 0.10 in univariable analysis were included in the multivariable analysis. A multivariable logistic regression model with stepwise backward elimination was used to test the independent correlations of these variables with POAF. Significant predictors for incident heart failure and intensive care unit admission were assessed by using univariable and multivariable logistic regression models. All *P* values were two-tailed, and a $P < 0.05$ was considered statistically significant.

RESULTS

Figure 1 shows incidence, risk factors, and prognostic impact of POAF following HFS. The mean age of the study patients was 76.4 ± 13.1 years, and 64.9% were female. Among the 245 HFS patients enrolled in this analysis, POAF developed in 20 patients (8.2%) during post-operative hospitalization. POAF occurred on median post-operative day 2 (interquartile range[1-3]). Baseline characteristics of the patients according to occurrence of POAF are shown in Table 1. Patients with POAF were more likely to be older, to have history of previous myocardial infarction, previous CHF, or chronic obstructive pulmonary disease (COPD), and to have higher e/e' ratio levels significantly.

In the univariable logistic regression analysis, age, previous myocardial infarction, previous CHF, and COPD were significantly associated with development of POAF after HFS (Table 2). However, in multivariable logistic regression analysis with stepwise backward elimination, age, COPD, and E/e' ratio level were left as significant predictors of POAF (Table 2).

Table 3 shows clinical adverse events during hospitalization according to occurrence of POAF. Patients with POAF required more transfusion and longer hospitalization than those without POAF, but the difference was not statistically significant. The incidences of intensive care unit admission and CHF were significantly increased in patients with POAF. Median time of CHF incidence was post-operative day 3 (interquartile range[2-4]). The incidences of pulmonary thromboembolism, ACS, or death during hospitalization were not different significantly between two groups. All death events were developed in patients without POAF. Two patients died from cardiac arrest and one patient died from hypovolemic shock.

Table 4 shows the results of logistic regression analyses to evaluate independent predictors of incident CHF following HFS. Lower hemoglobin levels and POAF were found as significant predictors of incident CHF following HFS in multivariable analysis. Independent predictors of intensive care unit admission following HFS are shown in Table 5. History of previous stroke, elevated creatinine levels, and POAF were significantly associated with intensive care unit admission following HFS.

DISCUSSION

The major findings of the present study are as follows: (1) The incidence of POAF was 20 (8.2%) among 245 patients with HFS; (2) Age, COPD, and elevated E/e' ratio were significant predictors of POAF in these patients; (3) Incidences of intensive care unit admission and CHF during hospitalization were significantly higher in patients with POAF; and (4) POAF was significantly associated with intensive care unit admission and incident CHF following HFS.

Table 1 Baseline characteristics of study patients according to occurrence of post-operative atrial fibrillation

Variables	Sinus rhythm (*n* = 225)	POAF (*n* = 20)	*P* value
Age (yr)	75.3 ± 13.3	84.3 ± 5.7	< 0.001
Male	79 (35.1)	7 (35.0)	0.992
Medical history			
Hypertension	153 (68.0)	14 (70.0)	0.854
Diabetes	68 (30.2)	5 (25.0)	0.625
Chronic kidney disease	30 (13.3)	5 (25.0)	0.153
Coronary artery disease	15 (6.7)	3 (15.0)	0.171
Previous MI	6 (2.7)	3 (15.0)	0.005
Previous CHF	9 (4.0)	3 (15.0)	0.029
Previous stroke	27 (12.0)	1 (5.0)	0.346
COPD	14 (6.2)	6 (30.0)	< 0.001
Echocardiographic parameter			
LVEF, %	59.1 ± 6.9	56.3 ± 9.2	0.096
LVEF < 50%	18 (8.0)	2 (10.0)	0.754
E/e'	10.9 ± 3.2	12.6 ± 2.8	0.047
Laboratory parameter			
Hemoglobin, g/dL	11.8 ± 2.0	11.2 ± 2.1	0.227
Creatinine, mg/dL	1.0 ± 1.1	1.2 ± 0.8	0.634
CK-MB, ng/mL	2.9 ± 3.9	2.8 ± 4.3	0.863
hsTn-I, ng/L	30.3 ± 155.2	24.1 ± 29.1	0.858
NT-proBNP, pg/dL	598.8 ± 1923.4	1172.7 ± 1844.5	0.251

Data are expressed as the mean ± standard deviation, or as a number (percentage). CHF: Congestive heart failure; CK-MB: Creatine kinase-myocardial band; COPD: Chronic obstructive pulmonary disease; hsTn-I: High-sensitivity troponin I; LVEF: Left ventricular ejection fraction; MI: Myocardial infarction; NT-proBNP: N-terminal pro-brain natriuretic peptide; and POAF: Post-operative atrial fibrillation.

The 8.2% incidence of POAF was consistent with previous results[5,6,10]. Among various types of non-cardiac surgery, abdominal, thoracic and vascular surgeries have been associated with higher incidence rates of POAF[5,10,19]. Although HFS is orthopedic surgery, most patients with hip fractures are elderly and commonly have impaired functional status and medical comorbidities[15,20]. Moreover, in elderly patients receiving HFS, perioperative atrial arrhythmias were reported to be common (5.6%) and to be associated with greater mortality[21]. Rhythm monitoring might be used only for selected patients after surgery, and patients do not always feel AF symptoms. Therefore, the incidence of POAF in this study might be underestimated. So, we have to monitor rhythm status actively in elderly patients as having high risk of POAF during the perioperative period.

In this analysis, age, COPD, and elevated e/e' ratio were significant predictors of POAF after HFS. Old age, pre-existing AF, CHF, ischemic heart disease, hypertension, chronic renal failure, sepsis, shock, asthma, and valvular heart disease are associated with increased risk of POAF[5,22-24]. The pathophysiology of the development of POAF after non-cardiac surgery is not fully understood. Potential mechanisms may be explained by a combination of multiple factors including increased sympathetic activity, autonomic stimulation, electrolyte imbalance, anemia, underlying cardiac disease, metabolic alterations, hypothermia, inflammation, hypoxia, and intraoperative adverse events like hypotension[25]. The prevalence and incidence of AF are elevated among patients with COPD[26,27]. Although we did not evaluate lung function in this study, patients with COPD history might have reduced lung function compared to those without COPD. Therefore, these patients are more likely to experience hypoxia in stress situations caused by surgery, which may cause hypoxia-driven POAF. In addition, E/e' ratio is well known marker for high left ventricular filling pressure[28]. In this analysis, elevated E/e' ratio was a significant predictor of POAF. Elevated E/e' ratio has been reported as significant predictor of POAF following non-cardiac surgery[29-31]. Elevated E/e' ratio presents left ventricular diastolic dysfunction, which is related to increased left atrial filling pressures. With increasing pressure in left atrium, pathological changes including increased atrial afterload, myocyte

Table 2 Independent predictors of post-operative atrial fibrillation following hip fracture surgery

Variables	Unadjusted OR (95%CI)	*P* value	Adjusted OR (95%CI)	*P* value
Age (yr)	1.100 (1.031-1.172)	0.004	1.111 (1.022-1.209)	0.014
Male	0.995 (0.382-2.596)	0.992		
Hypertension	1.098 (0.405-2.974)	0.854		
Diabetes mellitus	0.770 (0.269-2.202)	0.625		
Chronic kidney disease	2.167 (0.734-6.397)	0.162		
Coronary artery disease	0.405 (0.107-1.537)	0.184		
Previous MI	6.441 (1.479-28.046)	0.013		
Previous CHF	4.235 (1.048-17.120)	0.043		
Previous stroke	0.386 (0.050-3.000)	0.363		
COPD	6.459 (2.153-19.380)	0.001	6.352 (1.561-25.841)	0.010
LVEF (%)	0.952 (0.899-1.009)	0.098		
E/e′	1.151 (0.999-1.327)	0.051	1.174 (1.002-1.376)	0.047
Hemoglobin (g/dL)	0.870 (0.694-1.091)	0.228		
Creatinine (mg/dL)	1.083 (0.778-1.506)	0.636		
CK-MB (ng/mL)	0.988 (0.872-1.120)	0.853		
hsTn-I (ng/L)	1.000 (0.996-1.003)	0.859		
NT-proBNP (pg/dL)	1.000 (1.000-1.000)	0.279		

CHF: Congestive heart failure; CK-MB: Creatine kinase-myocardial band; COPD: Chronic obstructive pulmonary disease; hsTn-I: High-sensitivity troponin I; LVEF: Left ventricular ejection fraction; MI: myocardial infarction; NT-proBNP: N-terminal pro-brain natriuretic peptide; and OR: Odds ratio.

Table 3 Clinical adverse events during hospitalization according to occurrence of post-operative atrial fibrillation

	Sinus rhythm (*n* = 225)	POAF (*n* = 20)	*P* value
Transfusion	190 (84.4)	19 (95.0)	0.201
Transfused packed RBC count	3.4 ± 4.4	4.1 ± 2.4	0.508
Admission day	23.0 ± 33.8	29.6 ± 18.4	0.391
Intensive care unit admission	33 (14.7)	11 (55.0)	< 0.001
Congestive heart failure	24 (10.7)	9 (45.0)	< 0.001
Pulmonary thromboembolism	4 (1.8)	0 (0.0)	0.548
Acute coronary syndrome	7 (3.1)	2 (10.0)	0.117
Death	3 (1.3)	0 (0.0)	0.548

Data are expressed as the mean ± SD, or as a number (percentage). POAF: Post-operative atrial fibrillation; RBC: Red blood cell.

stretch, and atrial wall stress are developed[32]. This consequent left atrial remodeling is believed as main mechanism of POAF following HFS.

Patients with POAF required a longer hospital stay, had a higher intensive care unit admission, and experienced more development of CHF during hospitalization. Our results are consistent with previous findings that POAF leads to increased length of hospital stay and subsequently elevated health care costs[22,23,33]. Moreover, recent cohort including large number (*n* = 2922) of patients underwent HFS reported that patients with POAF experienced not only higher length of hospital stay but also higher 1-year mortality in comparison to control group[34]. The present study only showed significant association between POAF and in-hospital complications, but this study revealed poor long-term prognosis of POAF patients. AF and CHF often occur together, and each can precede and follow the other[35]. In this study, POAF occurred on median day 2 after surgery, but CHF developed on median post-operative day 3. Thus, CHF might not result in POAF in these patients. Even then, we cannot

Table 4 Independent predictors of incident congestive heart failure following hip fracture surgery

Variables	Unadjusted OR (95%CI)	*P* value	Adjusted OR (95%CI)	*P* value
Age (yr)	1.060 (1.015-1.107)	0.008		
Male	1.238 (0.583-2.629)	0.579		
Hypertension	0.924 (0.424-2.015)	0.843		
Diabetes mellitus	0.724 (0.310-1.690)	0.455		
Chronic kidney disease	3.917 (1.692-9.066)	0.001	2.570 (0.946-6.980)	0.064
Coronary artery disease	1.951 (0.601-6.333)	0.266		
Previous MI	5.710 (1.450-22.495)	0.013		
Previous CHF	5.230 (1.554-17.602)	0.008		
Previous stroke	1.080 (0.350-3.339)	0.893		
COPD	5.333 (1.989-14.303)	0.001	3.408 (0.898-12.934)	0.072
LVEF (%)	0.971 (0.925-1.020)	0.243		
E/e′	1.088 (0.967-1.224)	0.159		
Hemoglobin (g/dL)	0.688 (0.565-0.838)	< 0.001	0.753 (0.597-0.949)	0.016
Creatinine (mg/dL)	1.266 (0.997-1.608)	0.053		
CK-MB (ng/mL)	1.042 (0.969-1.121)	0.268		
hsTn-I (ng/L)	1.001 (0.999-1.003)	0.334		
NT-proBNP (pg/dL)	1.000 (1.000-1.000)	0.050		
Post-operative AF	6.852 (2.579-18.209)	< 0.001	4.856 (1.437-16.411)	0.011

AF: Atrial fibrillation; CHF: Congestive heart failure; CK-MB: Creatine kinase-myocardial band; COPD: Chronic obstructive pulmonary disease; hsTn-I: High-sensitivity troponin I; LVEF: Left ventricular ejection fraction; MI: Myocardial infarction; NT-proBNP: N-terminal pro-brain natriuretic peptide; and OR: Odds ratio.

conclude that POAF directly causes CHF after surgery. Because patients with POAF had more chronic comorbidities like COPD and CKD, the poor outcomes might be the consequence of their comorbidities rather than the result of POAF. Even we cannot explain complex mechanism between POAF and post-operative CHF development, we need to pay more attention to the development of CHF when patients experience POAF following surgery.

Limitations

This study had several inherent limitations. First, the study design was retrospective and observational, and thus we could not adjust potential confounding factors. Second, evaluation of 12-lead ECG after HFS was not consistent and uniform because it was left to the discretion of attending physician. Third, diagnosis of POAF was based only on 12-lead ECG. Therefore, the incidence of new-onset POAF might have been underestimated because paroxysmal AF, especially asymptomatic episodes, could not be diagnosed. Fourth, a large population (n = 138) with insufficient laboratory data including high-sensitivity troponin I and/or N-terminal pro-brain natriuretic peptide were excluded from this study because pre-operative biomarker evaluation was not performed in all patients. Therefore, there would be a selection bias associated with this factor. Fifth, frailty is a strong indication for mortality, intensive care unit admission, and AF. But, we could not incorporate frailty score in our analysis. Finally, because study patients and incident POAF patients (n = 20) were relatively small, the statistical power for the predictors of POAF might have been low. Moreover, for this reason, we only evaluated the association between POAF and in-hospital complications, but not long-term prognosis of POAF. Despite these limitations, the present study may have clinical significance because this analysis showed real-world observational results in elderly Korean patients who underwent HFS.

CONCLUSION

The incidence of POAF was 8.2% in patients with HFS. Age, COPD and elevated E/e′ ratio were potential predictors of POAF in these patients. Patients with POAF significantly experienced intensive care unit admission and incident CHF during hospitalization. POAF was revealed as significant

Table 5 Independent predictors of intensive care unit admission following hip fracture surgery

Variables	Unadjusted OR (95%CI)	*P* value	Adjusted OR (95%CI)	*P* value
Age (yr)	1.017 (0.989-1.046)	0.242		
Male	0.836 (0.417-1.678)	0.615		
Hypertension	0.781 (0.394-1.546)	0.477		
Diabetes mellitus	1.444 (0.727-2.868)	0.295		
Chronic kidney disease	2.458 (1.100-5.496)	0.028		
Coronary artery disease	1.336 (0.418-4.271)	0.626		
Previous MI	2.378 (0.571-9.900)	0.234		
Previous CHF	5.132 (1.571-16.763)	0.007	3.295 (0.860-12.632)	0.082
Previous stroke	2.463 (1.030-5.889)	0.043	3.718 (1.326-10.420)	0.013
COPD	2.109 (0.762-5.837)	0.151		
LVEF (%)	0.979 (0.937-1.024)	0.358		
E/e'	1.032 (0.928-1.148)	0.557		
Hemoglobin (g/dL)	0.853 (0.724-1.004)	0.057		
Creatinine (mg/dL)	1.348 (1.054-1.725)	0.018	1.416 (1.085-1.848)	0.011
CK-MB (ng/mL)	1.033 (0.963-1.108)	0.368		
hsTn-I (ng/L)	1.002 (1.000-1.004)	0.112		
NT-proBNP (pg/dL)	1.000 (1.000-1.000)	0.019		
Post-operative AF	7.111 (2.736-18.484)	<0.001	6.615 (2.112-20.718)	0.001

AF: Atrial fibrillation; CHF: Congestive heart failure; CK-MB: Creatine kinase-myocardial band; COPD: Chronic obstructive pulmonary disease; hsTn-I: High-sensitivity troponin I; LVEF: Left ventricular ejection fraction; MI: Myocardial infarction; NT-proBNP: N-terminal pro-brain natriuretic peptide; and OR: Odds ratio.

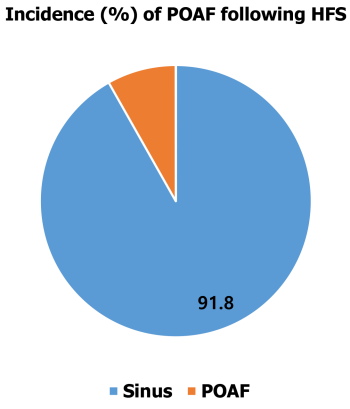

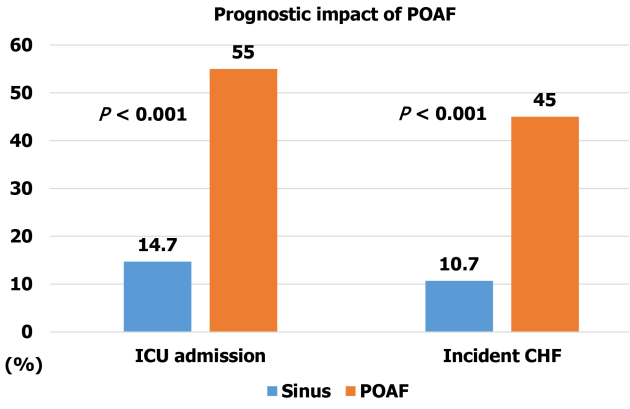

Risk factors of POAF

	Adjusted OR (95%CI)	*P* value
Age (yr)	1.111 (1.022–1.209)	0.014
COPD	6.352 (1.561–25.841)	0.010
E/e' ratio	1.174 (1.002–1.376)	0.047

Prognostic impact of POAF

	ICU admission	Incident CHF
Adjusted OR (95%CI)	6.615 (2.112–20.718)	4.856 (1.437–16.411)

DOI: 10.12998/wjcc.v10.i11.3379

Figure 1 Incidence, risk factors, and prognostic impact of post-operative atrial fibrillation following hip fracture surgery. POAF: Post-operative atrial fibrillation; COPD: Chronic obstructive pulmonary disease; CHF: Congestive heart failure; ICU: Intensive care unit.

predictor of intensive care unit admission and incident CHF. Therefore, physicians have to observe closely the incidence of POAF in old HFS patients.

ARTICLE HIGHLIGHTS

Research perspectives

Physicians have to carefully observe the occurrence of atrial fibrillation (AF) after hip fracture surgery (HFS) in elderly patients.

Research conclusions

Age, chronic obstructive pulmonary disease (COPD) and elevated E/e' ratio were found as significant predictors of post-operative AF (POAF) in HFS patients. Patients with POAF significantly experienced intensive care unit admission and incident congestive heart failure during hospitalization.

Research results

The major findings of the present study are as follows: (1) The incidence of POAF was 20 (8.2%) among 245 patients with HFS; (2) Age, chronic obstructive pulmonary disease, and elevated E/e' ratio were significant predictors of POAF in these patients; (3) Incidences of intensive care unit admission and congestive heart failure during hospitalization were significantly higher in patients with POAF; and (4) POAF was significantly associated with intensive care unit admission and incident congestive heart failure following HFS.

Research methods

This retrospective study involved 245 patients who underwent HFS in the Konkuk University Medical Center between August 2014 and November 2016. We evaluated the incidence, risk factors, and prognosis impact during hospitalization following HFS.

Research objectives

We aimed to investigate the incidence, predictors, and hospital prognosis of POAF in HFS patients.

Research motivation

People are getting older, and many elderly patients have been undergoing HFS. Atrial fibrillation is the most common arrhythmia developing in post-operative patients. So, we was wondering if POAF may affect in-hospital outcomes in patients underwent HFS.

Research background

Limited data are available regarding pre-operative risk factors and prognostic impact of post-operative atrial fibrillation following hip fracture surgery in Korean population.

FOOTNOTES

Author contributions: Kwon CH conceptioned and designed the research study; Bae SJ acquisitioned the data; Bae SJ and Kwon CH analysised and interpreted the data; Bae SJ and Kwon CH prepared the manuscript; Kwon CH, Bae SJ, Kim TY, Chang H, Kim BS, Kim SH, and Kim HJ revised the manuscript.

Institutional review board statement: The present study protocol was reviewed and approved by the Institutional Review Board of the Konkuk University Medical Center (protocol No. KUMC 2019-07-053). The requirement for informed consent was waived because de-identified information was retrieved retrospectively.

Conflict-of-interest statement: The authors declare that there is no conflict of interest.

Country/Territory of origin: South Korea

ORCID number: Seong Jun Bae 0000-0001-8345-5366; Chang Hee Kwon 0000-0001-8716-1146; Tae-Young Kim 0000-0003-2028-0460; Haseong Chang 0000-0001-5463-4699; Bum Sung Kim 0000-0002-3864-419X; Sung Hea Kim 0000-0001-5809-7958; Hyun-Joong Kim 0000-0003-1636-0193.

S-Editor: Xing YX
L-Editor: A
P-Editor: Xing YX

REFERENCES

1 **Benjamin EJ**, Wolf PA, D'Agostino RB, Silbershatz H, Kannel WB, Levy D. Impact of atrial fibrillation on the risk of death: the Framingham Heart Study. *Circulation* 1998; **98**: 946-952 [PMID: 9737513 DOI: 10.1161/01.cir.98.10.946]
2 **Krahn AD**, Manfreda J, Tate RB, Mathewson FA, Cuddy TE. The natural history of atrial fibrillation: incidence, risk factors, and prognosis in the Manitoba Follow-Up Study. *Am J Med* 1995; **98**: 476-484 [PMID: 7733127 DOI: 10.1016/S0002-9343(99)80348-9]
3 **Mathew JP**, Fontes ML, Tudor IC, Ramsay J, Duke P, Mazer CD, Barash PG, Hsu PH, Mangano DT; Investigators of the Ischemia Research and Education Foundation; Multicenter Study of Perioperative Ischemia Research Group. A multicenter risk index for atrial fibrillation after cardiac surgery. *JAMA* 2004; **291**: 1720-1729 [PMID: 15082699 DOI: 10.1001/jama.291.14.1720]
4 **Ahlsson AJ**, Bodin L, Lundblad OH, Englund AG. Postoperative atrial fibrillation is not correlated to C-reactive protein. *Ann Thorac Surg* 2007; **83**: 1332-1337 [PMID: 17383336 DOI: 10.1016/j.athoracsur.2006.11.047]
5 **Bhave PD**, Goldman LE, Vittinghoff E, Maselli J, Auerbach A. Incidence, predictors, and outcomes associated with postoperative atrial fibrillation after major noncardiac surgery. *Am Heart J* 2012; **164**: 918-924 [PMID: 23194493 DOI: 10.1016/j.ahj.2012.09.004]
6 **Butt JH**, Olesen JB, Havers-Borgersen E, Gundlund A, Andersson C, Gislason GH, Torp-Pedersen C, Køber L, Fosbøl EL. Risk of Thromboembolism Associated With Atrial Fibrillation Following Noncardiac Surgery. *J Am Coll Cardiol* 2018; **72**: 2027-2036 [PMID: 30336826 DOI: 10.1016/j.jacc.2018.07.088]
7 **LaPar DJ**, Speir AM, Crosby IK, Fonner E, Jr. , Brown M, Rich JB, Quader M, Kern JA, Kron IL, Ailawadi G. Postoperative atrial fibrillation significantly increases mortality, hospital readmission, and hospital costs. *Ann Thorac Surg* 2014; **98**: 527-533; discussion 533 [PMID: 25087786 DOI: 10.1016/j.athoracsur.2014.03.039]
8 **Saxena A**, Dinh DT, Smith JA, Shardey GC, Reid CM, Newcomb AE. Usefulness of postoperative atrial fibrillation as an independent predictor for worse early and late outcomes after isolated coronary artery bypass grafting (multicenter Australian study of 19,497 patients). *Am J Cardiol* 2012; **109**: 219-225 [PMID: 22011556 DOI: 10.1016/j.amjcard.2011.08.033]
9 **Steinberg BA**, Zhao Y, He X, Hernandez AF, Fullerton DA, Thomas KL, Mills R, Klaskala W, Peterson ED, Piccini JP. Management of postoperative atrial fibrillation and subsequent outcomes in contemporary patients undergoing cardiac surgery: insights from the Society of Thoracic Surgeons CAPS-Care Atrial Fibrillation Registry. *Clin Cardiol* 2014; **37**: 7-13 [PMID: 24353215 DOI: 10.1002/clc.22230]
10 **Conen D**, Alonso-Coello P, Douketis J, Chan MTV, Kurz A, Sigamani A, Parlow JL, Wang CY, Villar JC, Srinathan SK, Tiboni M, Malaga G, Guyatt G, Sivakumaran S, Rodriguez Funes MV, Cruz P, Yang H, Dresser GK, Alvarez-Garcia J, Schricker T, Jones PM, Drummond LW, Balasubramanian K, Yusuf S, Devereaux PJ. Risk of stroke and other adverse outcomes in patients with perioperative atrial fibrillation 1 year after non-cardiac surgery. *Eur Heart J* 2020; **41**: 645-651 [PMID: 31237939 DOI: 10.1093/eurheartj/ehz431]
11 **Brauer CA**, Coca-Perraillon M, Cutler DM, Rosen AB. Incidence and mortality of hip fractures in the United States. *JAMA* 2009; **302**: 1573-1579 [PMID: 19826027 DOI: 10.1001/jama.2009.1462]
12 **Dy CJ**, McCollister KE, Lubarsky DA, Lane JM. An economic evaluation of a systems-based strategy to expedite surgical treatment of hip fractures. *J Bone Joint Surg Am* 2011; **93**: 1326-1334 [PMID: 21792499 DOI: 10.2106/JBJS.I.01132]
13 **Karagas MR**, Lu-Yao GL, Barrett JA, Beach ML, Baron JA. Heterogeneity of hip fracture: age, race, sex, and geographic patterns of femoral neck and trochanteric fractures among the US elderly. *Am J Epidemiol* 1996; **143**: 677-682 [PMID: 8651229 DOI: 10.1093/oxfordjournals.aje.a008800]
14 **Wolinsky FD**, Fitzgerald JF, Stump TE. The effect of hip fracture on mortality, hospitalization, and functional status: a prospective study. *Am J Public Health* 1997; **87**: 398-403 [PMID: 9096540 DOI: 10.2105/ajph.87.3.398]
15 **Bentler SE**, Liu L, Obrizan M, Cook EA, Wright KB, Geweke JF, Chrischilles EA, Pavlik CE, Wallace RB, Ohsfeldt RL, Jones MP, Rosenthal GE, Wolinsky FD. The aftermath of hip fracture: discharge placement, functional status change, and mortality. *Am J Epidemiol* 2009; **170**: 1290-1299 [PMID: 19808632 DOI: 10.1093/aje/kwp266]
16 **Chiang CH**, Liu CJ, Chen PJ, Huang CC, Hsu CY, Chen ZY, Chan WL, Huang PH, Chen TJ, Chung CM, Lin SJ, Chen JW, Leu HB. Hip fracture and risk of acute myocardial infarction: a nationwide study. *J Bone Miner Res* 2013; **28**: 404-411 [PMID: 22836505 DOI: 10.1002/jbmr.1714]
17 **Sathiyakumar V**, Avilucea FR, Whiting PS, Jahangir AA, Mir HR, Obremskey WT, Sethi MK. Risk factors for adverse cardiac events in hip fracture patients: an analysis of NSQIP data. *Int Orthop* 2016; **40**: 439-445 [PMID: 26194916 DOI: 10.1007/s00264-015-2832-5]
18 **Kim BS**, Kim TH, Oh JH, Kwon CH, Kim SH, Kim HJ, Hwang HK, Chung SM. Association between preoperative high sensitive troponin I levels and cardiovascular events after hip fracture surgery in the elderly. *J Geriatr Cardiol* 2018; **15**: 215-221 [PMID: 29721000 DOI: 10.11909/j.issn.1671-5411.2018.03.002]
19 **Brathwaite D**, Weissman C. The new onset of atrial arrhythmias following major noncardiothoracic surgery is associated with increased mortality. *Chest* 1998; **114**: 462-468 [PMID: 9726731 DOI: 10.1378/chest.114.2.462]
20 **Sennerby U**, Melhus H, Gedeborg R, Byberg L, Garmo H, Ahlbom A, Pedersen NL, Michaëlsson K. Cardiovascular diseases and risk of hip fracture. *JAMA* 2009; **302**: 1666-1673 [PMID: 19843901 DOI: 10.1001/jama.2009.1463]
21 **Gupta BP**, Steckelberg RC, Gullerud RE, Huddleston PM, Kirkland LL, Wright RS, Huddleston JM. Incidence and 1-Year Outcomes of Perioperative Atrial Arrhythmia in Elderly Adults After Hip Fracture Surgery. *J Am Geriatr Soc* 2015; **63**:

2269-2274 [PMID: 26503010 DOI: 10.1111/jgs.13789]
22 **Polanczyk CA**, Goldman L, Marcantonio ER, Orav EJ, Lee TH. Supraventricular arrhythmia in patients having noncardiac surgery: clinical correlates and effect on length of stay. *Ann Intern Med* 1998; **129**: 279-285 [PMID: 9729180 DOI: 10.7326/0003-4819-129-4-199808150-00003]
23 **Sohn GH**, Shin DH, Byun KM, Han HJ, Cho SJ, Song YB, Kim JH, On YK, Kim JS. The incidence and predictors of postoperative atrial fibrillation after noncardiothoracic surgery. *Korean Circ J* 2009; **39**: 100-104 [PMID: 19949595 DOI: 10.4070/kcj.2009.39.3.100]
24 **La Manna G**, Boriani G, Capelli I, Marchetti A, Grandinetti V, Spazzoli A, Dalmastri V, Todeschini P, Rucci P, Stefoni S. Incidence and predictors of postoperative atrial fibrillation in kidney transplant recipients. *Transplantation* 2013; **96**: 981-986 [PMID: 23924775 DOI: 10.1097/TP.0b013e3182a2b492]
25 **Danelich IM**, Lose JM, Wright SS, Asirvatham SJ, Ballinger BA, Larson DW, Lovely JK. Practical management of postoperative atrial fibrillation after noncardiac surgery. *J Am Coll Surg* 2014; **219**: 831-841 [PMID: 25127508 DOI: 10.1016/j.jamcollsurg.2014.02.038]
26 **Xiao X**, Han H, Wu C, He Q, Ruan Y, Zhai Y, Gao Y, Zhao X, He J. Prevalence of Atrial Fibrillation in Hospital Encounters With End-Stage COPD on Home Oxygen: National Trends in the United States. *Chest* 2019; **155**: 918-927 [PMID: 30684473 DOI: 10.1016/j.chest.2018.12.021]
27 **Buch P**, Friberg J, Scharling H, Lange P, Prescott E. Reduced lung function and risk of atrial fibrillation in the Copenhagen City Heart Study. *Eur Respir J* 2003; **21**: 1012-1016 [PMID: 12797497 DOI: 10.1183/09031936.03.00051502]
28 **Andersen OS**, Smiseth OA, Dokainish H, Abudiab MM, Schutt RC, Kumar A, Sato K, Harb S, Gude E, Remme EW, Andreassen AK, Ha JW, Xu J, Klein AL, Nagueh SF. Estimating Left Ventricular Filling Pressure by Echocardiography. *J Am Coll Cardiol* 2017; **69**: 1937-1948 [PMID: 28408024 DOI: 10.1016/j.jacc.2017.01.058]
29 **Nagatsuka Y**, Sugimura K, Miyata H, Shinnno N, Asukai K, Hara H, Hasegawa S, Yamada D, Yamamoto K, Haraguchi N, Nishimura J, Motoori M, Wada H, Takahashi H, Yasui M, Omori T, Ohue M, Yano M. Predictive value of preoperative echocardiographic assessment for postoperative atrial fibrillation after esophagectomy for esophageal cancer. *Esophagus* 2021; **18**: 496-503 [PMID: 33511516 DOI: 10.1007/s10388-020-00804-y]
30 **Brecher O**, Gulati H, Roistacher N, Zhang H, Shi W, Thaler HT, Amar D. Preoperative Echocardiographic Indices of Diastolic Dysfunction and Brain Natriuretic Peptide in Predicting Postoperative Atrial Fibrillation After Noncardiac Surgery. *Anesth Analg* 2017; **124**: 1099-1104 [PMID: 27918330 DOI: 10.1213/ANE.0000000000001471]
31 **Nojiri T**, Maeda H, Takeuchi Y, Funakoshi Y, Maekura R, Yamamoto K, Okumura M. Predictive value of preoperative tissue Doppler echocardiographic analysis for postoperative atrial fibrillation after pulmonary resection for lung cancer. *J Thorac Cardiovasc Surg* 2010; **140**: 764-768 [PMID: 20691999 DOI: 10.1016/j.jtcvs.2009.11.073]
32 **Rosenberg MA**, Manning WJ. Diastolic dysfunction and risk of atrial fibrillation: a mechanistic appraisal. *Circulation* 2012; **126**: 2353-2362 [PMID: 23129702 DOI: 10.1161/CIRCULATIONAHA.112.113233]
33 **Seguin P**, Signouret T, Laviolle B, Branger B, Mallédant Y. Incidence and risk factors of atrial fibrillation in a surgical intensive care unit. *Crit Care Med* 2004; **32**: 722-726 [PMID: 15090953 DOI: 10.1097/01.ccm.0000114579.56430.e0]
34 **Rostagno C**, Cartei A, Rubbieri G, Ceccofiglio A, Polidori G, Curcio M, Civinini R, Prisco D. Postoperative atrial fibrillation is related to a worse outcome in patients undergoing surgery for hip fracture. *Intern Emerg Med* 2021; **16**: 333-338 [PMID: 32440983 DOI: 10.1007/s11739-020-02372-6]
35 **Santhanakrishnan R**, Wang N, Larson MG, Magnani JW, McManus DD, Lubitz SA, Ellinor PT, Cheng S, Vasan RS, Lee DS, Wang TJ, Levy D, Benjamin EJ, Ho JE. Atrial Fibrillation Begets Heart Failure and Vice Versa: Temporal Associations and Differences in Preserved Versus Reduced Ejection Fraction. *Circulation* 2016; **133**: 484-492 [PMID: 26746177 DOI: 10.1161/CIRCULATIONAHA.115.018614]

World Journal of Clinical Cases

Submit a Manuscript: https://www.f6publishing.com

World J Clin Cases 2022 April 16; 10(11): 3389-3400

DOI: 10.12998/wjcc.v10.i11.3389

ISSN 2307-8960 (online)

ORIGINAL ARTICLE

Retrospective Study

Added value of systemic inflammation markers for monitoring response to neoadjuvant chemotherapy in breast cancer patients

Zi-Rui Ke, Wei Chen, Man-Xiu Li, Shun Wu, Li-Ting Jin, Tie-Jun Wang

Specialty type: Oncology

Provenance and peer review: Unsolicited article; Externally peer reviewed.

Peer-review model: Single blind

Peer-review report's scientific quality classification

Grade A (Excellent): A
Grade B (Very good): B
Grade C (Good): 0
Grade D (Fair): 0
Grade E (Poor): 0

P-Reviewer: Fang S, China; Nath J, India

Received: October 25, 2021
Peer-review started: October 25, 2021
First decision: December 17, 2021
Revised: December 23, 2021
Accepted: February 27, 2022
Article in press: February 27, 2022
Published online: April 16, 2022

Zi-Rui Ke, Wei Chen, Man-Xiu Li, Shun Wu, Li-Ting Jin, Tie-Jun Wang, Department of Breast Surgery, Hubei Cancer Hospital, Tongji Medical College, Huazhong University of Science and Technology and Hubei Provincial Clinical Research Center for Breast Cancer, Wuhan 430079, Hubei Province, China

Corresponding author: Tie-Jun Wang, MD, Chief Doctor, Department of Breast Surgery, Hubei Cancer Hospital, Tongji Medical College, Huazhong University of Science and Technology and Hubei Provincial Clinical Research Center for Breast Cancer, No. 116 Zhuodaoquan South Road, Hongshan District, Wuhan 430079, Hubei Province, China. tiejunwanghp@163.com

Abstract

BACKGROUND

Complete response after neoadjuvant chemotherapy (rNACT) elevates the surgical outcomes of patients with breast cancer, however, non-rNACT have a higher risk of death and recurrence.

AIM

To establish novel machine learning (ML)-based predictive models for predicting probability of rNACT in breast cancer patients who intends to receive NACT.

METHODS

A retrospective analysis of 487 breast cancer patients who underwent mastectomy or breast-conserving surgery and axillary lymph node dissection following neoadjuvant chemotherapy at the Hubei Cancer Hospital between January 1, 2013, and October 1, 2021. The study cohort was divided into internal training and testing datasets in a 70:30 ratio for further analysis. A total of twenty-four variables were included to develop predictive models for rNACT by multiple ML-based algorithms. A feature selection approach was used to identify optimal predictive factors. These models were evaluated by the receiver operating characteristic (ROC) curve for predictive performance.

RESULTS

Analysis identified several significant differences between the rNACT and non-rNACT groups, including total cholesterol, low-density lipoprotein, neutrophil-to-lymphocyte ratio, body mass index, platelet count, albumin-to-globulin ratio, platelet-to-lymphocyte ratio, and lymphocyte-to-monocyte ratio. The areas under the curve of the six models ranged from 0.81 to 0.96. Some ML-based models performed better than models using conventional statistical methods in both ROC

curves. The support vector machine (SVM) model with twelve variables introduced was identified as the best predictive model.

CONCLUSION

By incorporating pretreatment serum lipids and serum inflammation markers, it is feasible to develop ML-based models for the preoperative prediction of rNACT and therefore facilitate the choice of treatment, particularly the SVM, which can improve the prediction of rNACT in patients with breast cancer.

Key Words: Breast cancer; Neoadjuvant chemotherapy; Clinical response; Machine learning; Prediction

Core Tip: For predicting response after neoadjuvant chemotherapy (rNACT), some machine learning-based models performed better than models using conventional methods, and the support vector machine model performed best. Preoperative serum lipids and serum inflammation markers have contributed to predicting rNACT in breast cancer patients. These results suggested the need to raise awareness of the importance of minimally-invasive approaches for monitoring breast cancer patients who intended to undergo neoadjuvant chemotherapy. However, the current study needs to be validated with caution and require external validation in the future.

Citation: Ke ZR, Chen W, Li MX, Wu S, Jin LT, Wang TJ. Added value of systemic inflammation markers for monitoring response to neoadjuvant chemotherapy in breast cancer patients. *World J Clin Cases* 2022; 10(11): 3389-3400

URL: https://www.wjgnet.com/2307-8960/full/v10/i11/3389.htm

DOI: https://dx.doi.org/10.12998/wjcc.v10.i11.3389

INTRODUCTION

Worldwide, breast cancer is a major cause of human suffering and high mortality among women[1]. Neoadjuvant chemotherapy (NACT) as a treatment for early breast cancer, can make breast conserving surgery more feasible, and may achieve more than the same chemotherapy after surgery to eradicate micrometastasis[2]. More than 65% of the patients treated with NACT have a response, and more than 15% have achieved a complete clinical response. Although some trials use the old chemotherapy regimen, more than 15% of the patients have undergone partial chemotherapy[2-4]. In other words, most patients who cannot achieve a complete pathological response after NACT may face a higher risk of death and recurrence. Therefore, it is necessary to develop a practical, convenient and efficient tool to predict the pathological response of patients with NACT breast cancer.

Machine learning (ML)-based integrated analysis is a new computer-based method, which has been widely used in medical data management in the past decade[5]. It appears at the intersection of statistics and computer science. The former attempts to learn relationships from data, while the latter emphasizes efficient computational algorithms[6,7]. Compared with traditional statistical prediction models such as logistic regression (LR), ML depends on a predetermined model. It can potentially find the interaction between variables and iteratively learn the update algorithm from the data[8,9]. Previously, several conventional predictive models have been made for predicting after NACT in breast cancer patients, including LR, GLM[10-14]. However, few reports have incorporated multiple ML-based ensemble analyses for predicting response after NACT (rNACT).

In this study, we aimed to develop a rNACT risk prediction model for breast cancer patients that utilizes pretreatment serum lipids and serum inflammation markers to stratify patients by rNACT risk on admission. We then analyzed the predictive performance of these ML-based models in a deviation cohort and then verified performance in an internal and external validation cohort.

MATERIALS AND METHODS

Patients

Between January 1, 2013 and October 1, 2021, we retrospectively collated data from consecutive patients who had been diagnosed with breast cancer at the Hubei Cancer Hospital. All patients had received NACT before surgery. This study was approved by the Institutional Ethics Committee of the Hubei

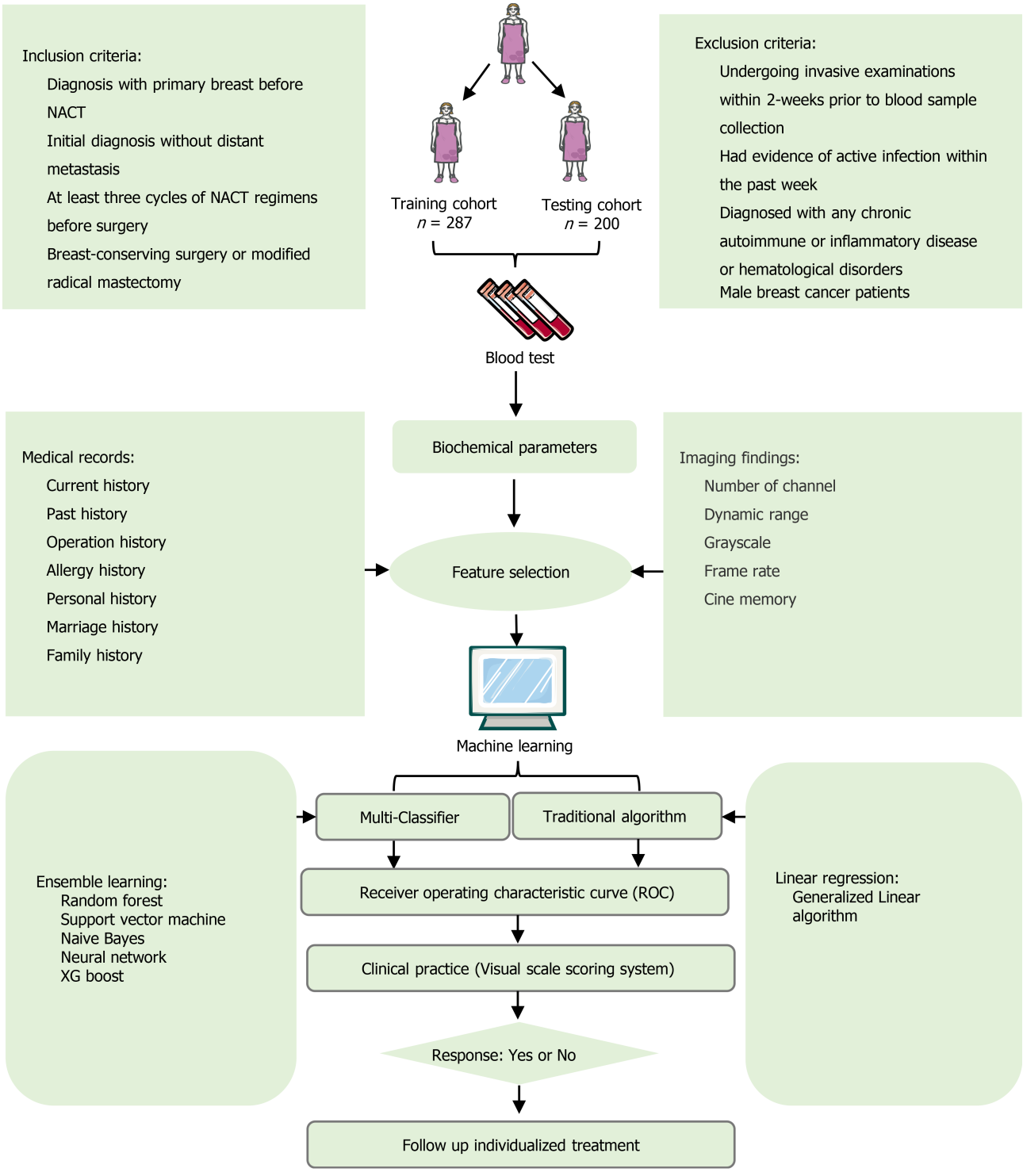

DOI: 10.12998/wjcc.v10.i11.3389

Figure 1 The flow chart of patient selection and data process. NACT: Neoadjuvant chemotherapy; ROC: Receiver operating characteristic.

Cancer Hospital (Reference: LLHBCH2021YN-021), in compliance with the Declaration of Helsinki. Written informed consent was obtained from all participants before any treatment. We confirmed that the data from all the patients were anonymized in this study. The inclusion and exclusion criteria were summarized in Figure 1. The study cohort was divided into internal training and testing datasets in a 70:30 ratio for further analysis.

Blood data collection

The blood samples of all patients were taken from the fasting state before chemotherapy, and the blood tests were operated by professional personnel to ensure that the blood test results were not biased. The results of the blood test are as follows: Blood routine, liver and kidney function, electrolytes, and blood lipids.

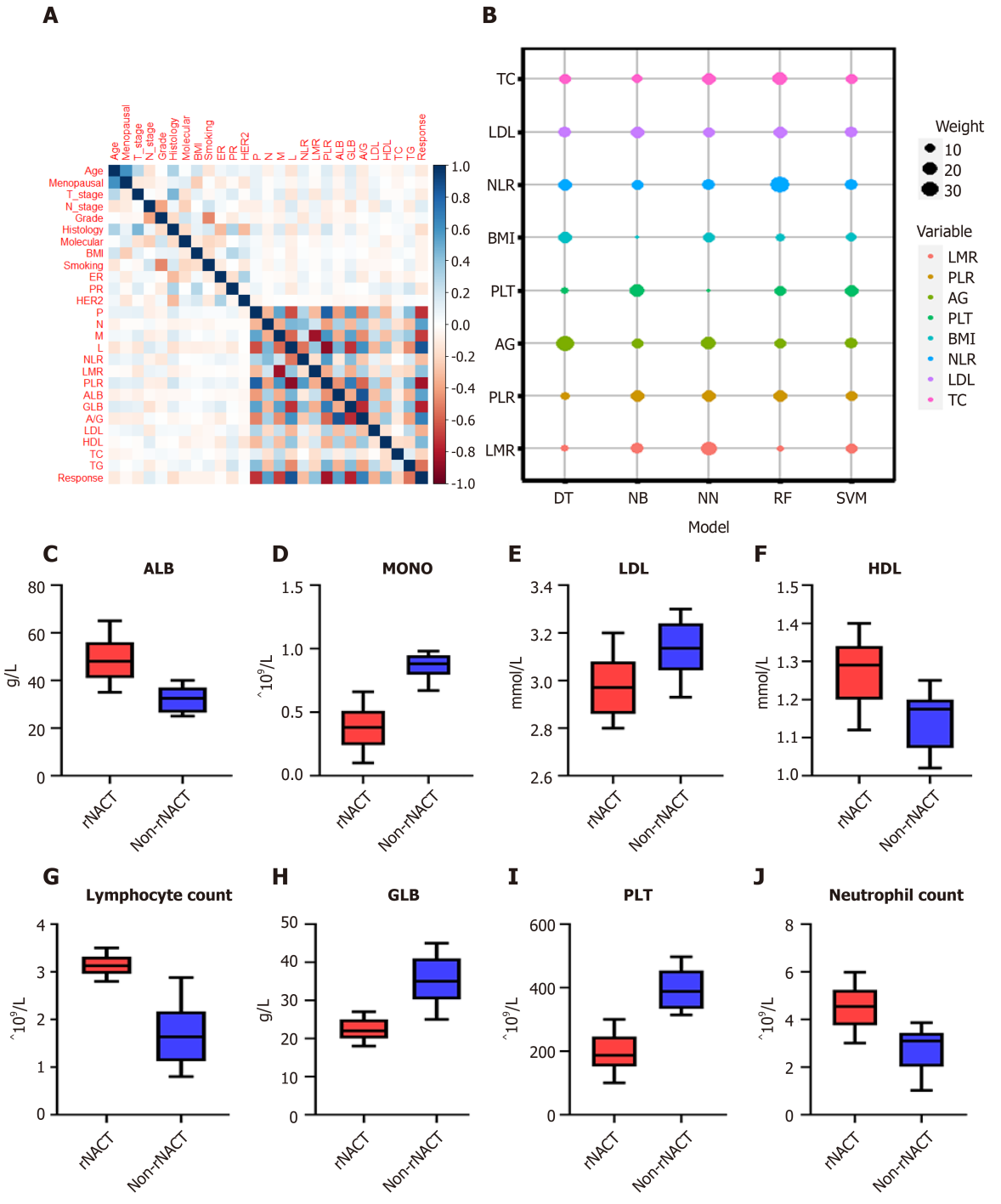

DOI: 10.12998/wjcc.v10.i11.3389

Figure 2 Statistical analysis of features included in machine learning based models. A: Heatmap representing the correlation between candidate variables included in predictive models using Spearman's correlation coefficient; B: Scaled importance rank of all features included in predictive models for identifying risk of response after neoadjuvant chemotherapy (rNACT) in breast cancer patients; C-J: Box and jitter plots showing distribution of continuous features included in predictive models between rNACT and non-rNACT groups. BMI: Body mass index; PR: Partial response; NLR: Neutrophil-to-lymphocyte ratio; LMR: Lymphocyte-to-monocyte ratio; PLR: Platelet-to-lymphocyte ratio; A/G: Albumin-to-globulin ratio; LDL: Low-density lipoprotein; HDL: High-density lipoprotein; TC: Total cholesterol; TG: Triglyceride.

Evaluating the safety and efficacy of NACT

According to RECIST (version 1.1) criteria[15], the efficacy of NACT is defined as follows: (1) Cardiol Res. The tumor is disappeared completely; (2) Partial response (PR). The diameter of the tumor is reduced (≥ 30%); (3) Progressive disease (PD). The diameter of the tumor was reduced (≥ 20%); and (4) Stable disease (SD). The diameter of the tumor was altered between PR and PD. Collectively, patients were considered to be responsive to NACT provided that they were evaluated as CR or PR after NACT treatment. On the contrary, patients with SD or PD were regarded as non-responsive to NACT.

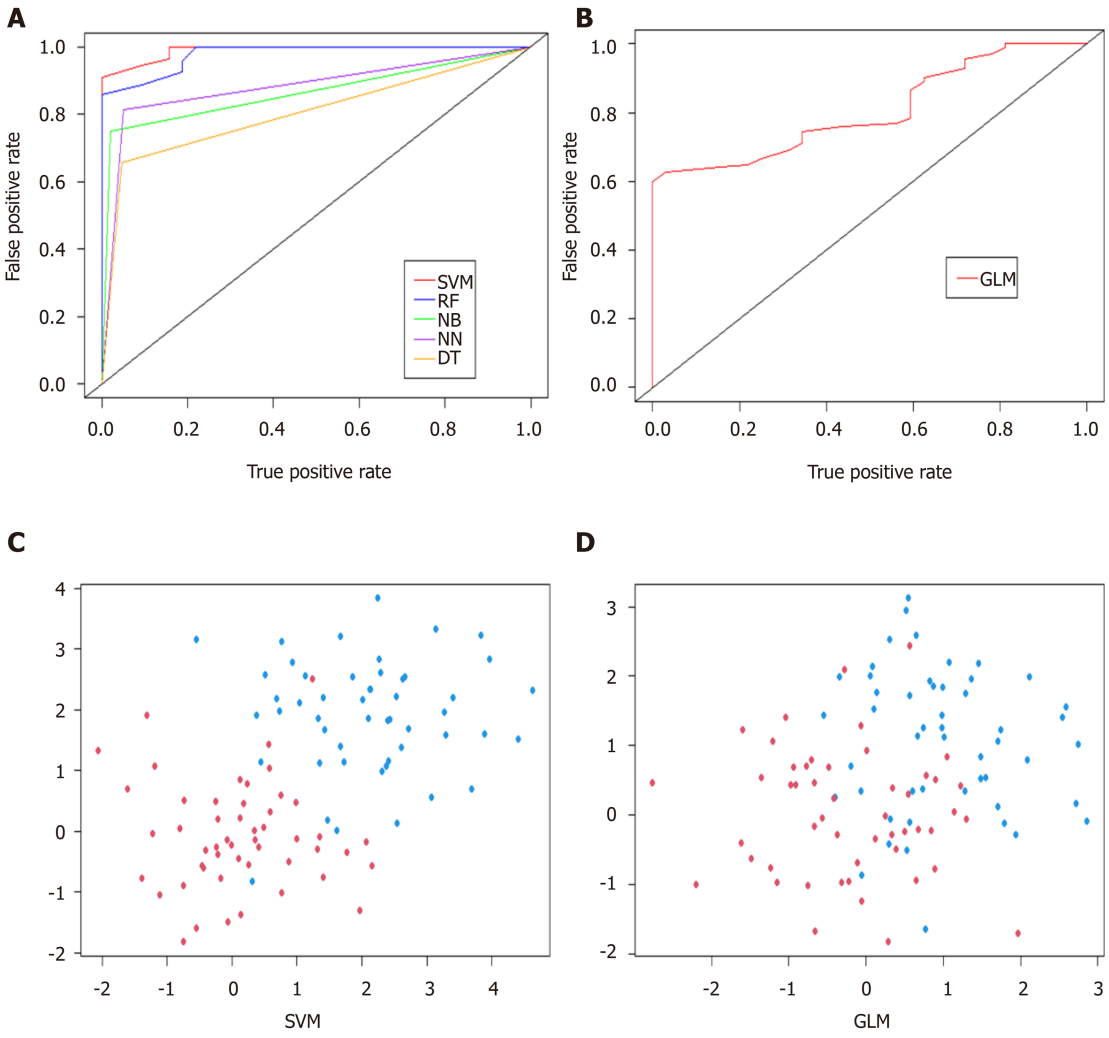

DOI: 10.12998/wjcc.v10.i11.3389

Figure 3 Validation and comparison of the predictive model. A: Area under the receiver operating characteristic curve (AUC) to assess the performance of response after neoadjuvant chemotherapy (rNACT) risk prediction of machine learning based models; B: AUC to assess the performance of rNACT risk prediction of generalized linear model (GLM); C: Discriminative evaluation of support vector machine in predicting rNACT; D: Discriminative evaluation of GLM in predicting rNACT. SVM: Support vector machine; GLM: Generalized linear model.

Development and validation of ML-based models

Four ML-based algorithms were performed to build predictive models, we used the *caret* package to randomly divide the data set into two parts, 70% for model training and 30% for model testing. A total of 6 ML-based algorithms were executed to establish the predictive model. According to the principle of "two-step estimation"[16], We obtained the prediction model through variable screening and algorithm, as follows: M is the intersection of M3 and M4.The characteristic variable is marked as X and the target variable is marked as Y. The X and Y were evenly divided into two parts, namely X1, Y1, and X2, Y2. Through univariate screening, the variable quantum set M1was screened on X1 and Y1, and M2was filtered by X2 and Y2. Then, a lasso was used to fit the model again, and the filtered variables were marked asM3 and M4 Briefly, by sorting the intersection of variable sets, the optimal subset modeling is obtained. The model was evaluated by inspection, discrimination, and calibration.The receiver operating characteristic (ROC) curve was used to evaluate the recognition ability of the prediction model in the training data set and the test data set; The discrimination ability of each model was quantified by the area under the ROC curve (AUC), decision curve analysis, and clinical impact curve (CIC).

Statistical analysis

Continuous variables are expressed as mean ± SD and compared using the two-tailed *t*-test or the Mann-Whitney test. Categorical variables were compared using the chi-square test or Fisher's exact test. Univariate and multivariate logistic analyses were used to explore the risk factors for rNACT. Several ML-based algorithms were applied to predict rNACT, including support vector machine (SVM), random forest (RF), Naive Bayes (NB), neural network (NN), decision tree (DT), and generalized linear

model (GLM)[17,18]. Among all 6 algorithms, the GLM is considered conventional methods, and the others are representative supervised ML-based algorithms. The prediction ability of the 6 models was first evaluated by the ROC curve. All analysis was performed using the Python programming language (version 3.9.2, Python Software Foundation, https://www.python.org/) and R Project for Statistical Computing (version 4.0.4, http://www.r-project.org/). Statistical analyses were performed using a two-tailed Student's t-test in PRISM software (GraphPad 6 Software) to compare the differences between rNACT and non-rNACT groups assuming equal variance. All *P* values were two-tailed, and $P < 0.05$ was considered statistically significant.

RESULTS

Clinicopathological characteristics

During the period of enrollment, 287 consecutive patients with breast cancer underwent mastectomy or breast-conserving surgery and axillary lymph node dissection following NACT. Besides, 201 patients were validated as external data sets for the prediction model. Demographics and baseline data were summarized in Table 1. According to the RECIST (version 1.1) criteria, rNACT was identified in 255 (88.9%) and 32 (11.1%) patients with non-rNACT in the internal whole cohort. In the external cohort, 176 (88.0%) patients were confirmed to have rNACT, and 24 (12.0%) patients represented non-rNACT. Overall, most patients with breast cancer presenting with rNACT were positively associated with pretreatment serum lipids and serum inflammation markers. No statistically significant difference was detected between two cohorts with regard to age, menopause, grade, smoking, estrogen receptor (ER), progesterone receptor (PR), and human epidermal growth factor receptor 2 (HER2) ($P \geq 0.05$).

Variable importance and candidate features selection

By feature selection, the twenty-four variables for each algorithm were screened by their predictive importance. As depicted in Figure 2A, only twelve of the candidate features were eventually chosen for modeling, among which eight features had a positive association with rNACT, including PLT, monocyte count (MONO), neutrophil-to-lymphocyte ratio (NLR), lymphocyte-to-monocyte ratio (LMR), platelet-to-lymphocyte ratio (PLR), low-density lipoprotein (LDL), A/G, and total cholesterol (TC). Four features were negatively correlated with rNACT, including high-density lipoprotein (HDL), triglyceride (TG), BMI, and age. The weight of the top eight variables was shown in Figure 2B. The pretreatment serum lipids and serum inflammation markers also showed significant differences between rNACT and non-rNACT groups (Figure 2C-J). Multivariable logistic analysis using raw data of the candidate features proved that the features selected by stepwise analysis exhibited similar risk implications (Supplementary Table 1). Based on our results, NLR (OR: 1.02, 95%CI: 0.78-1.26), LMR (OR: 1.44, 95%CI: 1.32-1.56), PLR (OR:2.54, 95%CI: 1.81-6.94), PLT (OR:1.87, 95%CI: 1.76-1.98), LDL (OR:1.01, 95%CI: 0.89-1.13), BMI (OR:1.23, 95%CI: 0.78-1.68), A/G (OR:1.69, 95%CI: 1.24-2.14), TC (OR:0.71, 95%CI: 0.26-1.16), and TG (OR:0.42, 95%CI: 0.17-0.68) were positively correlated with rNACT.

Comparison Between ML-Based Models

A total of twelve preoperative variables were used to develop predictive models for rNACT based on six algorithms. The predictive performance of all models was shown in Figure 3A and B and Table 2. The best performance was observed in the SVM model (AUC = 0.96, 95%CI: 0.91-1.01), which performed similarly to RF model (AUC = 0.94, 95%CI: 0.87-1.01), superior than NB model (AUC = 0.86, 95%CI: 0.79-0.93), NN model (AUC = 0.88, 95%CI: 0.82-0.94), DT model (AUC = 0.83, 95%CI: 0.77-0.89), and GLM (AUC = 0.81, 95%CI: 0.71-0.91). All ML-based models were better than conventional model. Furthermore, the optimal model SVM showed superior to the traditional linear model in discrimination (Figure 3C and D).

Internal and external validation of the optimal predictive model

To further validate the performance of the SVM model, we also adopted CIC to evaluate the prediction efficiency, as illustrated in Figure 4A, the CIC demonstrated that the stratification of rNACT could be distinguished in the training cohorts. These results were also parallel to risk factors of rNACT delineated in the validation cohorts (Figure 4B), indicating that the selected features were highly relevant to rNACT.

DISCUSSION

Reliable markers of chemosensitivity help select patients who most benefit from NACT[19]. Previous studies on the candidate predictors of NACT efficacy in breast cancer patients are discordant, suggesting that the potential predictors to predict efficacy is insufficient[20-23]. In addition, whilst many studies report the predictive outcomes of breast cancer patients who have received NACT, however,

Table 1 Demographics and baseline characteristics of the breast cancer patients undergoing neoadjuvant chemotherapy

Variables	Dummy variables	Training cohort				Testing cohort			
		Overall (*n* = 287)	Yes (*n* = 255)	No (*n* = 32)	*P* value	Overall (*n* = 200)	Yes (*n* = 176)	No (*n* = 24)	*P* value
Age [median (IQR)],yr		61.00 (55.00, 70.00)	61.00 (54.00, 70.00)	64.00 (58.75, 69.25)	0.11	61.00 (55.75, 70.25)	61.00 (55.00, 70.25)	64.00 (57.75, 70.25)	0.28
Menopausal (%)	Yes	35 (12.2)	30 (11.8)	5 (15.6)	0.73	28 (14.0)	24 (13.6)	4 (16.7)	0.93
	No	252 (87.8)	225 (88.2)	27 (84.4)		172 (86.0)	152 (86.4)	20 (83.3)	
T stage (%)	T1-2	216 (75.3)	196 (76.9)	20 (62.5)	0.12	156 (78.0)	140 (79.5)	16 (66.7)	0.24
	T3-4	71 (24.7)	59 (23.1)	12 (37.5)		44 (22.0)	36 (20.5)	8 (33.3)	
N stage (%)	N0-1	71 (24.7)	58 (22.7)	13 (40.6)	0.04	52 (26.0)	40 (22.7)	12 (50.0)	0.01
	N2-3	216 (75.3)	197 (77.3)	19 (59.4)		148 (74.0)	136 (77.3)	12 (50.0)	
Grade (%)	I-II	195 (67.9)	175 (68.6)	20 (62.5)	0.61	134 (67.0)	118 (67.0)	16 (66.7)	0.11
	III	92 (32.1)	80 (31.4)	12 (37.5)		66 (33.0)	58 (33.0)	8 (33.3)	
Histology (%)	IDC	111 (38.7)	106 (41.6)	5 (15.6)	0.02	80 (40.0)	77 (43.8)	3 (12.5)	0.03
	ILC	91 (31.7)	79 (31.0)	12 (37.5)		61 (30.5)	51 (29.0)	10 (41.7)	
	IMC	48 (16.7)	41 (16.1)	7 (21.9)		36 (18.0)	29 (16.5)	7 (29.2)	
	Others	37 (12.9)	29 (11.4)	8 (25.0)		23 (11.5)	19 (10.8)	4 (16.7)	
Molecular subtyping (%)	HER2-LuB	108 (37.6)	100 (39.2)	8 (25.0)	< 0.01	76 (38.0)	71 (40.3)	5 (20.8)	0.01
	HER2+	71 (24.7)	66 (25.9)	5 (15.6)		53 (26.5)	50 (28.4)	3 (12.5)	
	HER2+LuB	29 (10.1)	24 (9.4)	5 (15.6)		18 (9.0)	15 (8.5)	3 (12.5)	
	LuA	54 (18.8)	41 (16.1)	13 (40.6)		37 (18.5)	25 (14.2)	12 (50.0)	
	TN	25 (8.7)	24 (9.4)	1 (3.1)		16 (8.0)	15 (8.5)	1 (4.2)	
BMI (%)	≤ 18	21 (7.3)	21 (8.2)	0 (0.0)	0.22	11 (5.5)	11 (6.2)	0 (0.0)	0.42
	≥ 27	36 (12.5)	31 (12.2)	5 (15.6)		27 (13.5)	23 (13.1)	4 (16.7)	
	18 - 27	230 (80.1)	203 (79.6)	27 (84.4)		162 (81.0)	142 (80.7)	20 (83.3)	
Smoking (%)	No	258 (89.9)	231 (90.6)	27 (84.4)	0.43	182 (91.0)	161 (91.5)	21 (87.5)	0.79
	Yes	29 (10.1)	24 (9.4)	5 (15.6)		18 (9.0)	15 (8.5)	3 (12.5)	
ER (%)	Negative	103 (35.9)	91 (35.7)	12 (37.5)	0.99	73 (36.5)	66 (37.5)	7 (29.2)	0.56
	Positive	184 (64.1)	164 (64.3)	20 (62.5)		127 (63.5)	110 (62.5)	17 (70.8)	
PR (%)	Negative	165 (57.5)	141 (55.3)	24 (75.0)	0.05	109 (54.5)	91 (51.7)	18 (75.0)	0.05
	Positive	122 (42.5)	114 (44.7)	8 (25.0)		91 (45.5)	85 (48.3)	6 (25.0)	
HER2 (%)	Negative	157 (54.7)	140 (54.9)	17 (53.1)	0.99	110 (55.0)	96 (54.5)	14 (58.3)	0.89
	Positive	130 (45.3)	115 (45.1)	15 (46.9)		90 (45.0)	80 (45.5)	10 (41.7)	
PLT [median (IQR)] × 10^9/L		200.00 (154.50, 268.50)	187.00 (152.50, 245.50)	388.00 (334.50, 454.00)	< 0.01	202.50 (158.75, 267.25)	190.50 (154.00, 246.50)	377.00 (332.50, 443.50)	< 0.01
Neutrophil [median (IQR)] × 10^9/L		4.35 (3.52, 5.13)	4.54 (3.76, 5.23)	3.09 (2.02, 3.39)	< 0.01	4.44 (3.50, 5.21)	4.60 (3.78, 5.27)	3.09 (2.02, 3.35)	< 0.01
MONO [median (IQR)] × 10^9/L		0.40 (0.25, 0.57)	0.38 (0.24, 0.50)	0.88 (0.80, 0.94)	< 0.01	0.41 (0.25, 0.58)	0.37 (0.23, 0.49)	0.86 (0.75, 0.91)	< 0.01
Lymphocyte [median (IQR)] × 10^9/L		3.09 (2.92, 3.30)	3.13 (2.96, 3.32)	1.64 (1.14, 2.16)	< 0.01	3.08 (2.92, 3.30)	3.12 (2.98, 3.32)	1.67 (1.14, 2.16)	< 0.01
NLR [median (IQR)]		1.43 (1.20, 1.67)	1.42 (1.20, 1.64)	1.56 (1.21, 2.68)	0.03	1.48 (1.20, 1.70)	1.47 (1.20, 1.67)	1.56 (1.22, 2.75)	< 0.01
LMR [median (IQR)]		7.62 (5.59,	8.51 (6.18,	1.86 (1.51,	< 0.01	7.59 (5.60,	8.53 (6.26,	1.87 (1.59,	< 0.01

	12.96)	13.31)	2.47)		13.07)	13.46)	2.52)	
PLR [median (IQR)]	64.45 (49.59, 85.43)	61.99 (47.81, 78.50)	237.76 (189.53, 342.96)	< 0.01	65.33 (50.30, 85.89)	62.36 (49.02, 78.10)	226.10 (189.53, 305.51)	< 0.01
ALB [median (IQR)],g/L	47.00 (39.00, 55.00)	48.00 (41.00, 56.00)	32.50 (27.50, 37.00)	< 0.01	47.00 (39.00, 55.25)	49.00 (41.00, 56.00)	31.50 (27.50, 37.00)	< 0.01
GLB [median (IQR)],g/L	23.00 (20.00, 26.00)	22.00 (20.00, 25.00)	35.00 (30.75, 41.00)	< 0.01	23.00 (20.00, 26.00)	23.00 (20.00, 25.00)	35.50 (30.75, 41.25)	< 0.01
A/G [median (IQR)]	2.11 (1.76, 2.53)	2.18 (1.88, 2.57)	0.88 (0.82, 1.03)	< 0.01	2.11 (1.71, 2.50)	2.18 (1.85, 2.55)	0.88 (0.82, 1.03)	< 0.01
LDL [median (IQR)],mmol/L	3.00 (2.88, 3.10)	2.97 (2.87, 3.08)	3.13 (3.05, 3.24)	< 0.01	3.00 (2.90, 3.08)	2.97 (2.88, 3.07)	3.13 (3.04, 3.22)	< 0.01
HDL [median (IQR)],mmol/L	1.26 (1.19, 1.33)	1.29 (1.20, 1.34)	1.17 (1.08, 1.20)	< 0.01	1.25 (1.18, 1.32)	1.28 (1.20, 1.33)	1.15 (1.08, 1.19)	0.02
TC [median (IQR)], mmol/L	0.52 (0.49, 0.56)	0.52 (0.48, 0.56)	0.56 (0.52, 0.58)	< 0.01	0.52 (0.48, 0.56)	0.52 (0.48, 0.56)	0.56 (0.52, 0.57)	< 0.01
TG [median (IQR)], mmol/L	1.82 (1.61, 2.15)	1.78 (1.59, 2.04)	2.34 (2.27, 2.39)	< 0.01	1.85 (1.60, 2.15)	1.79 (1.59, 2.04)	2.34 (2.27, 2.39)	< 0.01

rNACT: Response to neoadjuvant chemotherapy; Non-rNACT: None response to neoadjuvant chemotherapy; IQR: Interquartile range; ER: Estrogen receptor; PR: Progesterone receptor. HER2: Human epidermal growth factor receptor 2; IDC: Invasive ductal carcinoma; ILC: Invasive lobular carcinoma; IMC: Invasive mammary carcinoma; BMI: Body mass index; PLT: Platelet count; MONO: Monocyte count; NLR: Neutrophil-to-lymphocyte ratio; LMR: Lymphocyte-to-monocyte ratio; PLR: Platelet-to-lymphocyte ratio; ALB: Albumin; GLB: Globulin; A/G: Albumin-to-globulin ratio; LDL: Low density lipoprotein; HDL: High density lipoprotein; TC: Total cholesterol; TG: Triglyceride.

Table 2 Performance for response to neoadjuvant chemotherapy risk prediction of models in breast cancer patients

Model	AUC (95%CI)	Sensitivity	Specificity	PPV	NPV	Kappa	Brier
SVM	0.96 (0.91-1.01)	96.58	45.28	88.63	75.00	0.68	0.06
RF	0.94 (0.87-1.01)	94.44	68.75	86.67	68.75	0.65	0.07
NB	0.86 (0.79-0.93)	96.36	35.80	83.14	75.00	0.62	0.07
NN	0.88 (0.82-0.94)	93.15	25.00	93.15	53.15	0.62	0.07
DT	0.83 (0.77-0.89)	94.50	24.14	74.12	65.63	0.59	0.07
GLM	0.81 (0.71-0.91)	95.70	23.76	69.80	75.00	0.57	0.08

AUC: Area under the curve.area under the receiver operating characteristics curve; PPV: Positive predictive value; NPV: Negative predictive value, 95%CI: 95% confidence interval; SVM: Support vector machine; RF: Random forest; NB: Naive bayes ; NN: Neural network; DT: Decision tree; GLM: Generalized linear model.

relatively few have investigated the individual contribution of multiple models to accuracy, especially prediction efficiency[24-27]. Whilst this study indicates that ML-based predictive algorithms should be included in NACT risk assessments in breast cancer patients, it also highlights the importance of conducting newly predictive models for clinical management.

Supervised ML algorithms have been a dominant method in the data mining field[17]. In recent years, ML-based algorithms were widely used for the evaluation of disease prognosis[28-30]. In this study, extensive variables were made to identify those predictive that applied more than one supervised ML algorithm on rNACT prediction. Based on the ML algorithm, we employed a variety of statistical, probabilistic, and optimization methods to learn from experience and detect useful patterns from large, unstructured, and complex datasets. To sum up, we extracted the data from the patient's medical records as much as possible. With the help of different algorithms, such as automated text categorisation [31], network intrusion detection[32], optimizing manufacturing process[33], *etc.*, we finally obtained meaningful candidate variables. Given the growing applicability and effectiveness of supervised ML algorithms on predictive disease modeling. Interestingly, we found that the SVM algorithm is applied most robust in predicting rNACT, which denotes superior performance than the conventional linear prediction model. Besides, the remaining machine prediction models are better than GLM. Therefore, our research demonstrated that, compared with the traditional model, machine learning modeling prediction rNACT could obtain better prediction performance.

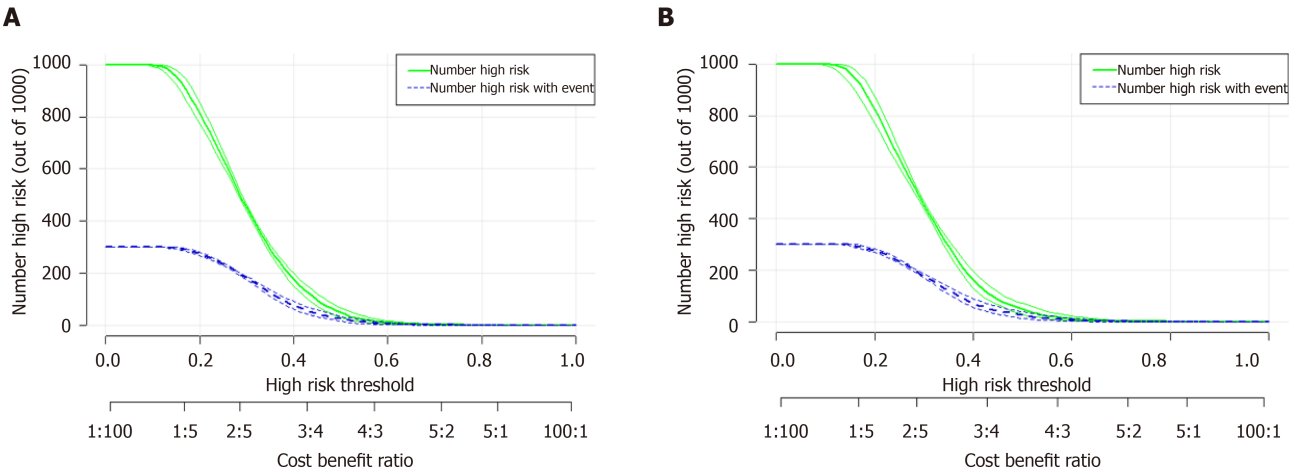

DOI: 10.12998/wjcc.v10.i11.3389

Figure 4 Prediction performance of support vector machine model *via* clinical impact curve. A: Training set; B: Validation set. The green line predicts the probability of poor response after neoadjuvant chemotherapy (rNACT), and the blue line shows how many patients will be at high risk of non-rNACT.

Inflammation is associated with the development and malignant progression of most cancers[34]. Inflammatory blood markers have emerged as potential prognostic factors in various cancers, such as NLR, LMR, and PLR. Activated inflammatory cells are sources of reactive oxygen species and reactive nitrogen intermediates that can promote cancer initiation[35]. In breast cancer, pretreatment NLR values are associated with patient prognosis[36]. Similarly, our study indicated that NLR, LMR, and PLR values can be reliably used to predict breast patient responses to NACT treatment, which can effectively stratify patients based upon their likelihood of achieving rNACT. Besides, we also found that pretreatment abnormal A/G ratio, which might be attributable to rNACT. Indeed, a low pretreatment A/G ratio is associated with poor prognosis in human cancers[37]. The importance of lipids in tumor progression, invasion, and metastasis has been described in the previous studies[38]. High triglycerides and low levels of HDL are observed to promote tumor growth[39]. In the present study, we observed that LDL, TC, and BMI were highly associated with rNACT, consistent with previous studies[37,38]. Collectively, clinicians can more effectively weigh the relative costs and benefits of pretreatment serum lipids and serum inflammation markers to ensure that they act in the optimal choice of breast cancer patients.

There are multiple strengths to this study. First, our observations were limited to retrospective studies from a single-center, these findings need further multi-institutional validation with larger sample size. Second, our nomograms were merely validated *via* an internal training set, external verification using independent patient set is necessary. Third, this is a retrospective study that could not completely avoid missing data and measurement biases, more candidate useful biomarkers may be needed to develop predictive models in the future.

CONCLUSION

In summary, for predicting rNACT, some ML-based models performed better than models using conventional methods, and the SVM model performed best. Preoperative serum lipids and serum inflammation markers have contributed to predicting rNACT in breast cancer patients. These results suggested the need to raise awareness of the importance of minimally-invasive approaches for monitoring breast cancer patients who intended to undergo NACT. However, the current study needs to be validated with caution and require external validation in the future.

ARTICLE HIGHLIGHTS

Research background

Complete response after neoadjuvant chemotherapy (rNACT) elevates the surgical outcomes of patients with breast cancer, however, non-rNACT have a higher risk of death and recurrence.

Research motivation

In this study, we aimed to develop an rNACT risk prediction model for breast cancer patients that

utilizes pretreatment serum lipids and serum inflammation markers to stratify patients by rNACT risk on admission. We then analyzed the predictive performance of these ML-based models in a deviation cohort and then verified performance in an internal and external validation cohort.

Research objectives

In this study, we aimed to develop an rNACT risk prediction model for breast cancer patients that utilizes pretreatment serum lipids and serum inflammation markers to stratify patients by rNACT risk on admission. We then analyzed the predictive performance of these ML-based models in a deviation cohort and then verified performance in an internal and external validation cohort.

Research methods

A retrospective analysis of 487 breast cancer patients who underwent mastectomy or breast-conserving surgery and axillary lymph node dissection following NACT at the Hubei Cancer Hospital between January 1, 2013, and October 1, 2021. The study cohort was divided into internal training and testing datasets in a 70:30 ratio for further analysis. A total of twenty-four variables were included to develop predictive models for rNACT by multiple ML-based algorithms. A feature selection approach was used to identify optimal predictive factors. These models were evaluated by the receiver operating characteristic (ROC) curve for predictive performance.

Research results

Analysis identified several significant differences between the rNACT and non-rNACT groups, including total cholesterol, low-density lipoprotein, neutrophil-to-lymphocyte ratio, body mass index, platelet count, albumin-to-globulin ratio (A/G), platelet-to-lymphocyte ratio, and lymphocyte-to-monocyte ratio. The areas under the curve of the six models ranged from 0.81 to 0.96. Some ML-based models performed better than models using conventional statistical methods in both ROC curves. The support vector machine (SVM) model with twelve variables introduced was identified as the best predictive model.

Research conclusions

By incorporating pretreatment serum lipids and serum inflammation markers, it is feasible to develop ML-based models for the preoperative prediction of rNACT and therefore facilitate the choice of treatment, particularly the SVM, which can improve the prediction of rNACT in patients with breast cancer.

Research perspectives

For predicting rNACT, some ML-based models performed better than models using conventional methods, and the SVM model performed best. Preoperative serum lipids and serum inflammation markers have contributed to predicting rNACT in breast cancer patients. These results suggested the need to raise awareness of the importance of minimally-invasive approaches for monitoring breast cancer patients who intended to undergo NACT. However, the current study needs to be validated with caution and require external validation in the future.

ACKNOWLEDGEMENTS

The authors gratefully acknowledge all of our participants for sharing their medical records. The authors also wish to thank the staff members at Hubei Cancer Hospital for their assistance with data collection.

FOOTNOTES

Author contributions: Ke ZR and Chen W originated the idea, data analysis and writing; Li MX, Wu S, Jin LT and Wang TJ contributed to the data analysis and writing; all authors have read and approved the manuscript.

Institutional review board statement: This study was approved by the Institutional Ethics Committee of the Hubei Cancer Hospital (Reference: LLHBCH2021YN-021), in compliance with the Declaration of Helsinki.

Informed consent statement: Patients were not required to give informed consent to the study because the analysis used anonymous clinical data that were obtained after each patient agreed to treatment by written consent.

Conflict-of-interest statement: None of the authors have any conflicts of interest to declare.

Data sharing statement: No additional data are available.

Country/Territory of origin: China

ORCID number: Zi-Rui Ke 0000-0003-1207-0791; Wei Chen 0000-0003-1056-0211; Man-Xiu Li 0000-0003-1068-0128; Shun Wu 0000-0003-1123-0298; Li-Ting Jin 0000-0003-1278-0237; Tie-Jun Wang 0000-0003-1244-0794.

S-Editor: Xing YX
L-Editor: A
P-Editor: Xing YX

REFERENCES

1 **Coughlin SS**. Epidemiology of Breast Cancer in Women. *Adv Exp Med Biol* 2019; **1152**: 9-29 [PMID: 31456177 DOI: 10.1007/978-3-030-20301-6_2]
2 **Early Breast Cancer Trialists' Collaborative Group (EBCTCG)**. Long-term outcomes for neoadjuvant versus adjuvant chemotherapy in early breast cancer: meta-analysis of individual patient data from ten randomised trials. *Lancet Oncol* 2018; **19**: 27-39 [PMID: 29242041 DOI: 10.1016/S1470-2045(17)30777-5]
3 **Wolmark N**, Wang J, Mamounas E, Bryant J, Fisher B. Preoperative chemotherapy in patients with operable breast cancer: nine-year results from National Surgical Adjuvant Breast and Bowel Project B-18. *J Natl Cancer Inst Monogr* 2001; 96-102 [PMID: 11773300 DOI: 10.1093/oxfordjournals.jncimonographs.a003469]
4 **Powles TJ**, Hickish TF, Makris A, Ashley SE, O'Brien ME, Tidy VA, Casey S, Nash AG, Sacks N, Cosgrove D. Randomized trial of chemoendocrine therapy started before or after surgery for treatment of primary breast cancer. *J Clin Oncol* 1995; **13**: 547-552 [PMID: 7884414 DOI: 10.1200/JCO.1995.13.3.547]
5 **Thrall JH**, Li X, Li Q, Cruz C, Do S, Dreyer K, Brink J. Artificial Intelligence and Machine Learning in Radiology: Opportunities, Challenges, Pitfalls, and Criteria for Success. *J Am Coll Radiol* 2018; **15**: 504-508 [PMID: 29402533 DOI: 10.1016/j.jacr.2017.12.026]
6 **Deo RC**. Machine Learning in Medicine. *Circulation* 2015; **132**: 1920-1930 [PMID: 26572668 DOI: 10.1161/CIRCULATIONAHA.115.001593]
7 **O'Mahony C**, Jichi F, Pavlou M, Monserrat L, Anastasakis A, Rapezzi C, Biagini E, Gimeno JR, Limongelli G, McKenna WJ, Omar RZ, Elliott PM; Hypertrophic Cardiomyopathy Outcomes Investigators. A novel clinical risk prediction model for sudden cardiac death in hypertrophic cardiomyopathy (HCM risk-SCD). *Eur Heart J* 2014; **35**: 2010-2020 [PMID: 24126876 DOI: 10.1093/eurheartj/eht439]
8 **Waljee AK**, Higgins PD. Machine learning in medicine: a primer for physicians. *Am J Gastroenterol* 2010; **105**: 1224-1226 [PMID: 20523307 DOI: 10.1038/ajg.2010.173]
9 **Austin PC**, Merlo J. Intermediate and advanced topics in multilevel logistic regression analysis. *Stat Med* 2017; **36**: 3257-3277 [PMID: 28543517 DOI: 10.1002/sim.7336]
10 **Davis J Jr**, Hoskin TL, Day CN, Wickre M, Piltin MA, Caudle AS, Boughey JC. Performance and Clinical Utility of Models Predicting Eradication of Nodal Disease in Patients with Clinically Node-Positive Breast Cancer Treated with Neoadjuvant Chemotherapy by Tumor Biology. *Ann Surg Oncol* 2020; **27**: 4678-4686 [PMID: 32729046 DOI: 10.1245/s10434-020-08885-w]
11 **Zhang J**, Xiao L, Pu S, Liu Y, He J, Wang K. Can We Reliably Identify the Pathological Outcomes of Neoadjuvant Chemotherapy in Patients with Breast Cancer? *Ann Surg Oncol* 2021; **28**: 2632-2645 [PMID: 33095360 DOI: 10.1245/s10434-020-09214-x]
12 **Kim WH**, Kim HJ, Park HY, Park JY, Chae YS, Lee SM, Cho SH, Shin KM, Lee SY. Axillary Pathologic Complete Response to Neoadjuvant Chemotherapy in Clinically Node-Positive Breast Cancer Patients: A Predictive Model Integrating the Imaging Characteristics of Ultrasound Restaging with Known Clinicopathologic Characteristics. *Ultrasound Med Biol* 2019; **45**: 702-709 [PMID: 30567630 DOI: 10.1016/j.ultrasmedbio.2018.10.026]
13 **Hwang HW**, Jung H, Hyeon J, Park YH, Ahn JS, Im YH, Nam SJ, Kim SW, Lee JE, Yu JH, Lee SK, Choi M, Cho SY, Cho EY. A nomogram to predict pathologic complete response (pCR) and the value of tumor-infiltrating lymphocytes (TILs) for prediction of response to neoadjuvant chemotherapy (NAC) in breast cancer patients. *Breast Cancer Res Treat* 2019; **173**: 255-266 [PMID: 30324273 DOI: 10.1007/s10549-018-4981-x]
14 **Matsuda N**, Hayashi N, Ohde S, Yagata H, Kajiura Y, Yoshida A, Suzuki K, Nakamura S, Tsunoda H, Yamauchi H. A nomogram for predicting locoregional recurrence in primary breast cancer patients who received breast-conserving surgery after neoadjuvant chemotherapy. *J Surg Oncol* 2014; **109**: 764-769 [PMID: 24647874 DOI: 10.1002/jso.23586]
15 **Eisenhauer EA**, Therasse P, Bogaerts J, Schwartz LH, Sargent D, Ford R, Dancey J, Arbuck S, Gwyther S, Mooney M, Rubinstein L, Shankar L, Dodd L, Kaplan R, Lacombe D, Verweij J. New response evaluation criteria in solid tumours: revised RECIST guideline (version 1.1). *Eur J Cancer* 2009; **45**: 228-247 [PMID: 19097774 DOI: 10.1016/j.ejca.2008.10.026]
16 **Fan J**, Lv J. A Selective Overview of Variable Selection in High Dimensional Feature Space. *Stat Sin* 2010; **20**: 101-148 [PMID: 21572976]
17 **Uddin S**, Khan A, Hossain ME, Moni MA. Comparing different supervised machine learning algorithms for disease

prediction. *BMC Med Inform Decis Mak* 2019; **19**: 281 [PMID: 31864346 DOI: 10.1186/s12911-019-1004-8]
18 **Christodoulou E**, Ma J, Collins GS, Steyerberg EW, Verbakel JY, Van Calster B. A systematic review shows no performance benefit of machine learning over logistic regression for clinical prediction models. *J Clin Epidemiol* 2019; **110**: 12-22 [PMID: 30763612 DOI: 10.1016/j.jclinepi.2019.02.004]
19 **Pu S**, Wang K, Liu Y, Liao X, Chen H, He J, Zhang J. Nomogram-derived prediction of pathologic complete response (pCR) in breast cancer patients treated with neoadjuvant chemotherapy (NCT). *BMC Cancer* 2020; **20**: 1120 [PMID: 33213397 DOI: 10.1186/s12885-020-07621-7]
20 **Fayanju OM**, Ren Y, Thomas SM, Greenup RA, Plichta JK, Rosenberger LH, Tamirisa N, Force J, Boughey JC, Hyslop T, Hwang ES. The Clinical Significance of Breast-only and Node-only Pathologic Complete Response (pCR) After Neoadjuvant Chemotherapy (NACT): A Review of 20,000 Breast Cancer Patients in the National Cancer Data Base (NCDB). *Ann Surg* 2018; **268**: 591-601 [PMID: 30048319 DOI: 10.1097/SLA.0000000000002953]
21 **Corbeau I**, Jacot W, Guiu S. Neutrophil to Lymphocyte Ratio as Prognostic and Predictive Factor in Breast Cancer Patients: A Systematic Review. *Cancers (Basel)* 2020; **12** [PMID: 32295078 DOI: 10.3390/cancers12040958]
22 **Machireddy A**, Thibault G, Tudorica A, Afzal A, Mishal M, Kemmer K, Naik A, Troxell M, Goranson E, Oh K, Roy N, Jafarian N, Holtorf M, Huang W, Song X. Early Prediction of Breast Cancer Therapy Response using Multiresolution Fractal Analysis of DCE-MRI Parametric Maps. *Tomography* 2019; **5**: 90-98 [PMID: 30854446 DOI: 10.18383/j.tom.2018.00046]
23 **Cho N**, Im SA, Park IA, Lee KH, Li M, Han W, Noh DY, Moon WK. Breast cancer: early prediction of response to neoadjuvant chemotherapy using parametric response maps for MR imaging. *Radiology* 2014; **272**: 385-396 [PMID: 24738612 DOI: 10.1148/radiol.14131332]
24 **Gu J**, Polley EC, Denis M, Carter JM, Pruthi S, Gregory AV, Boughey JC, Fazzio RT, Fatemi M, Alizad A. Early assessment of shear wave elastography parameters foresees the response to neoadjuvant chemotherapy in patients with invasive breast cancer. *Breast Cancer Res* 2021; **23**: 52 [PMID: 33926522 DOI: 10.1186/s13058-021-01429-4]
25 **Zhang J**, Sun M, Chang E, Lu CY, Chen HM, Wu SY. Pathologic response as predictor of recurrence, metastasis, and survival in breast cancer patients receiving neoadjuvant chemotherapy and total mastectomy. *Am J Cancer Res* 2020; **10**: 3415-3427 [PMID: 33163280]
26 **Iwasa H**, Kubota K, Hamada N, Nogami M, Nishioka A. Early prediction of response to neoadjuvant chemotherapy in patients with breast cancer using diffusion-weighted imaging and gray-scale ultrasonography. *Oncol Rep* 2014; **31**: 1555-1560 [PMID: 24535214 DOI: 10.3892/or.2014.3025]
27 **Maier AM**, Heil J, Harcos A, Sinn HP, Rauch G, Uhlmann L, Gomez C, Stieber A, Funk A, Barr RG, Hennigs A, Riedel F, Schäfgen B, Hug S, Marmé F, Sohn C, Golatta M. Prediction of pathological complete response in breast cancer patients during neoadjuvant chemotherapy: Is shear wave elastography a useful tool in clinical routine? *Eur J Radiol* 2020; **128**: 109025 [PMID: 32371182 DOI: 10.1016/j.ejrad.2020.109025]
28 **Heo J**, Yoon JG, Park H, Kim YD, Nam HS, Heo JH. Machine Learning-Based Model for Prediction of Outcomes in Acute Stroke. *Stroke* 2019; **50**: 1263-1265 [PMID: 30890116 DOI: 10.1161/STROKEAHA.118.024293]
29 **Kalafi EY**, Nor NAM, Taib NA, Ganggayah MD, Town C, Dhillon SK. Machine Learning and Deep Learning Approaches in Breast Cancer Survival Prediction Using Clinical Data. *Folia Biol (Praha)* 2019; **65**: 212-220 [PMID: 32362304]
30 **Peiffer-Smadja N**, Rawson TM, Ahmad R, Buchard A, Georgiou P, Lescure FX, Birgand G, Holmes AH. Machine learning for clinical decision support in infectious diseases: a narrative review of current applications. *Clin Microbiol Infect* 2020; **26**: 584-595 [PMID: 31539636 DOI: 10.1016/j.cmi.2019.09.009]
31 **Lee Y**, Ragguett RM, Mansur RB, Boutilier JJ, Rosenblat JD, Trevizol A, Brietzke E, Lin K, Pan Z, Subramaniapillai M, Chan TCY, Fus D, Park C, Musial N, Zuckerman H, Chen VC, Ho R, Rong C, McIntyre RS. Applications of machine learning algorithms to predict therapeutic outcomes in depression: A meta-analysis and systematic review. *J Affect Disord* 2018; **241**: 519-532 [PMID: 30153635 DOI: 10.1016/j.jad.2018.08.073]
32 **Dutta V**, Choraś M, Pawlicki M, Kozik R. A Deep Learning Ensemble for Network Anomaly and Cyber-Attack Detection. *Sensors (Basel)* 2020; **20** [PMID: 32824187 DOI: 10.3390/s20164583]
33 **Sadeghi Aghili SA**, Fatahi Valilai O, Haji A, Khalilzadeh M. Dynamic mutual manufacturing and transportation routing service selection for cloud manufacturing with multi-period service-demand matching. *PeerJ Comput Sci* 2021; **7**: e461 [PMID: 33981835 DOI: 10.7717/peerj-cs.461]
34 **Todoric J**, Antonucci L, Karin M. Targeting Inflammation in Cancer Prevention and Therapy. *Cancer Prev Res (Phila)* 2016; **9**: 895-905 [PMID: 27913448 DOI: 10.1158/1940-6207.CAPR-16-0209]
35 **Singh R**, Mishra MK, Aggarwal H. Inflammation, Immunity, and Cancer. *Mediators Inflamm* 2017; **2017**: 6027305 [PMID: 29234189 DOI: 10.1155/2017/6027305]
36 **Guo W**, Lu X, Liu Q, Zhang T, Li P, Qiao W, Deng M. Prognostic value of neutrophil-to-lymphocyte ratio and platelet-to-lymphocyte ratio for breast cancer patients: An updated meta-analysis of 17079 individuals. *Cancer Med* 2019; **8**: 4135-4148 [PMID: 31197958 DOI: 10.1002/cam4.2281]
37 **Lv GY**, An L, Sun XD, Hu YL, Sun DW. Pretreatment albumin to globulin ratio can serve as a prognostic marker in human cancers: a meta-analysis. *Clin Chim Acta* 2018; **476**: 81-91 [PMID: 29170102 DOI: 10.1016/j.cca.2017.11.019]
38 **Hashemi SA**, Bathaie SZ, Mohagheghi MA. Crocetin and crocin decreased cholesterol and triglyceride content of both breast cancer tumors and cell lines. *Avicenna J Phytomed* 2020; **10**: 384-397 [PMID: 32850295]
39 **Lofterød T**, Mortensen ES, Nalwoga H, Wilsgaard T, Frydenberg H, Risberg T, Eggen AE, McTiernan A, Aziz S, Wist EA, Stensvold A, Reitan JB, Akslen LA, Thune I. Impact of pre-diagnostic triglycerides and HDL-cholesterol on breast cancer recurrence and survival by breast cancer subtypes. *BMC Cancer* 2018; **18**: 654 [PMID: 29902993 DOI: 10.1186/s12885-018-4568-2]

World Journal of Clinical Cases

Submit a Manuscript: https://www.f6publishing.com

World J Clin Cases 2022 April 16; 10(11): 3401-3413

DOI: 10.12998/wjcc.v10.i11.3401

ISSN 2307-8960 (online)

ORIGINAL ARTICLE

Retrospective Study

Washed microbiota transplantation reduces serum uric acid levels in patients with hyperuricaemia

Jin-Rong Cai, Xin-Wen Chen, Yu-Jian He, Bin Wu, Min Zhang, Li-Hao Wu

Specialty type: Gastroenterology and hepatology

Provenance and peer review: Unsolicited article; Externally peer reviewed.

Peer-review model: Single blind

Peer-review report's scientific quality classification

Grade A (Excellent): 0
Grade B (Very good): 0
Grade C (Good): C, C, C
Grade D (Fair): 0
Grade E (Poor): 0

P-Reviewer: Innocenti T, Italy; Patel VJ, India; Rothschild B, United States

Received: October 27, 2021
Peer-review started: October 27, 2021
First decision: December 27, 2021
Revised: January 8, 2022
Accepted: February 17, 2022
Article in press: February 27, 2022
Published online: April 16, 2022

Jin-Rong Cai, Xin-Wen Chen, Yu-Jian He, Bin Wu, School of Clinical Medicine, Guangdong Pharmaceutical University, Guangzhou 510030, Guangdong Province, China

Min Zhang, Department of Epidemiology and Health Statistics, Guangdong Pharmaceutical University, Guangzhou 510220, Guangdong Province, China

Li-Hao Wu, Department of Gastroenterology, The First Affiliated Hospital of Guangdong Pharmaceutical University, Guangzhou 510030, Guangdong Province, China

Li-Hao Wu, Research Center, Engineering Techniques of Microbiota-Targeted Therapies of Guangdong Province, Guangzhou 510030, Guangdong Province, China

Corresponding author: Li-Hao Wu, MD, Associate Professor, Department of Gastroenterology, The First Affiliated Hospital of Guangdong Pharmaceutical University, No. 19 Nonglinxia Road, Yuexiu District, Guangzhou 510030, Guangdong Province, China.
wulihao888@126.com

Abstract

BACKGROUND

Previous studies have found that hyperuricaemia (HUA) is closely related to intestinal flora imbalance.

AIM

The current study investigated the effects and safety of washed microbiota transplantation (WMT) on serum uric acid (SUA) levels in different populations.

METHODS

A total of 144 patients who received WMT from July 2016 to April 2020 in the First Affiliated Hospital of Guangdong Pharmaceutical University and had SUA data before treatment were selected. Changes in SUA levels before and after treatment were retrospectively reviewed based on short-term and mid-term effects of WMT regimens. SUA levels measured in the last test within 3 mo after the first WMT represented the short-term effect, and SUA levels measured in the last test within 3-6 mo after the first WMT represented the mid-term effect. The patients were divided into an HUA group (SUA > 416 μM) and a normal uric acid (NUA) group (SUA ≥ 202 μM to ≤ 416 μM) based on pretreatment SUA levels.

RESULTS

Average short-term SUA levels in the HUA group decreased after WMT (481.00 ± 99.85 *vs* 546.81 ± 109.64 μM, n = 32, P < 0.05) in 25/32 patients and returned to normal in 10/32 patients. The short-term level of SUA reduction after treatment moderately correlated with SUA levels before treatment (r = 0.549, R^2 = 0.300, P < 0.05). Average SUA levels decreased after the first and second courses of WMT (469.74 ± 97.68 *vs* 540.00 ± 107.16 μM, n = 35, and 465.57 ± 88.88 *vs* 513.19 ± 78.14 μM, n = 21, P < 0.05). Short-term and mid-term SUA levels after WMT and SUA levels after the first, second and third courses of WMT were similar to the levels before WMT in the NUA group (P > 0.05). Only 1/144 patients developed mild diarrhea after WMT.

CONCLUSION

WMT reduces short-term SUA levels in patients with HUA with mild side effects but has no obvious effect on SUA levels in patients with NUA.

Key Words: Washed microbiota transplantation; Hyperuricaemia; Intestinal flora; Effect; Safety; Retrospective study

Core Tip: In this study, we demonstrate that washed microbiota transplantation (WMT) can lower serum uric acid (SUA) levels in patients with hyperuricaemia in the short term with only mild side effects but that WMT has no obvious effect on the SUA levels of people with normal uric acid levels.

Citation: Cai JR, Chen XW, He YJ, Wu B, Zhang M, Wu LH. Washed microbiota transplantation reduces serum uric acid levels in patients with hyperuricaemia. *World J Clin Cases* 2022; 10(11): 3401-3413
URL: https://www.wjgnet.com/2307-8960/full/v10/i11/3401.htm
DOI: https://dx.doi.org/10.12998/wjcc.v10.i11.3401

INTRODUCTION

Nutrition-related diseases caused by changes in people's diet are gradually increasing, and hyperuricaemia (HUA) has gradually developed into a global public health problem. HUA is a common disease in China. The prevalence of HUA in the Chinese population is 13%[1]. HUA is a metabolic syndrome related to obesity, insulin resistance, diabetes, coronary artery disease and hypertension, but it is also a pathological state that causes uric acid (UA) crystal deposition in bones, joints and kidneys, which may lead to gout, urolithiasis and UA nephropathy[2,3].

The traditional treatment methods for HUA include maintaining a healthy lifestyle, UA-lowering drugs, alkalizing urine, and traditional Chinese medicine. Existing drugs for the treatment of HUA include xanthine oxidase inhibitors (alopurinol) to inhibit UA production, benzbromarone, which promotes UA excretion, and UA enzymes that promote UA decomposition[4,5]. However, these drugs have adverse reactions, such as gastrointestinal discomfort, diarrhoea, and rash, and some patients have poor tolerance. Patients also need to take drugs regularly for a long time, which causes a long-term burden for patients and their families because the existing UA-lowering drugs are associated with a withdrawal and rebound phenomenon[4,5]. Due to the limitations of drug use, novel therapeutic approaches are needed in the treatment of HUA.

The functional status of the intestines and kidneys is critical to the metabolism of UA. The daily production and excretion of UA in the human body is 600-700 mg. Approximately two-thirds of this amount is excreted by the kidneys, and one-third is excreted through the intestines. The intestinal pathway compensates in cases of renal damage and becomes the main pathway for urate elimination [6]. The imbalance between probiotics and pathogenic bacteria affects the expression of intestinal tight junction proteins, which increases the permeability of the intestinal mucosa barrier, leads to gut-derived lipopolysaccharide (LPS) translocation and causes kidney damage *via* blood circulation. These changes induce renal UA excretion disorder, reduce UA excretion and increase serum UA (SUA) levels[7,8]. The intestinal flora also regulates adenosine triphosphate-binding cassette superfamily G member 2 (ABCG2), solute carrier family 2 member 9 (SLC2A9) and other UA transporters of the intestinal epithelium[9,10].

Faecal microbiota transplantation (FMT) recently emerged as a treatment strategy for HUA. FMT relate to the transplantation of the functional flora of a healthy individual into the gastrointestinal tract of a patient to establish a new intestinal microbiota for the treatment of intestinal and extraintestinal diseases. FMT technology was first used for treating refractory *Clostridium difficile* infection in 2013[11]. FMT also aids in inducing the remission of ulcerative colitis and improving hepatic encephalopathy and

insulin sensitivity[12-14]. Washed microbiota transplantation (WMT), the generation of bacterial solutions *via* automatic purification systems, is respected in clinic. WMT reduces the adverse events caused by traditional faecal suspension preparations and greatly improves the treatment efficacy[15,16].

Previous studies have found that HUA is closely associated with an intestinal flora imbalance[17,18]. Manipulation of gut dysbiosis with probiotics relieves fructose-induced hyperuricaemia in mice and enhances intestinal barrier function[19]. A pilot study[20] found that all patients (n = 11) exhibited a reduction in SUA levels on day 28 post-FMT (P < 0.05). Our study expanded the sample size to retrospectively examine the short-term and mid-term effects and safety of WMT on SUA levels in patients with HUA and normal UA (NUA) levels.

MATERIALS AND METHODS

Participants

A total of 144 patients who received WMT treatment from July 2016 to April 2020 in the First Affiliated Hospital of Guangdong Pharmaceutical University and had SUA data before treatment were selected. All Patients in this study provided informed consent. Patients who received WMT treatment were divided into an HUA group and an NUA group based on their SUA levels before treatment. The inclusion criterion for the HUA group was an SUA > 416 μM. The inclusion criterion for the NUA group was an SUA ≥ 202 μM to ≤ 416 μM.

Inclusion and exclusion criteria

Patients included in the study met the following criteria: (1) Aged 18-85 years; (2) received WMT treatment; and (3) had SUA data before and after treatment (Figure 1). The following exclusion criteria were used: (1) Gastrointestinal infection, cardiopulmonary failure or serious liver and kidney diseases; (2) pregnancy; (3) malignant tumours; (4) rejection to transendoscopic enteral tubing; (5) rejection or failure to complete the follow-ups; and (6) a high-purine diet.

WMT

All the patients were treated with WMT. Mixed multi-donor faeces were used as the source of the bacterial suspension for WMT. Healthy young men aged 18-25 years was one of requirements of the donors. The donors underwent health examinations to exclude metabolic diseases, genetic diseases, infectious diseases, digestive tract diseases, malignant tumours, and other associated diseases. The donors did not take antibiotics or drugs that affected alimentary canal dynamics and/or caused gut microecological disorders in the previous 3 mo. Utilizing an automatic purification system (GenFMTer; FMT Medical, Nanjing, Jiangsu Province, China), bacterial solution (200 mL) was isolated and injected into the sick's gut through the lower or middle alimentary canal within 30 min. Two transplantation routes were available for use. One route was the middle alimentary canal route in which transendoscopic enteral tubing was placed in the jejunum under gastroscopy, and proton pump inhibitors were administered intravenously 1 h before the injection. This procedure was performed to lower the inactivation of bacteria when moving through the stomach. Metoclopramide hydrochloride (10 mg) was injected intramuscularly to decrease side effects, like abdominal distension or vomiting, resulted from stimulus of the digestive tract by the fresh faecal liquid. The sick was placed in a sitting position during injection of the fresh faecal liquid. The injection procedure was mild and slow, and needed at least 30 min for 200 mL of the fresh faecal liquid. After the injection, the patient sustained standing or seated not less than 2 h. The other method was the lower alimentary canal route in which transendoscopic enteral tubing was placed into the caecum by means of enteroscopy. During injection of the fresh faecal liquid, the sick was placed in the right sided position, and this process lasted for 30 min. Completed this procedure, the sick rested in the right sided position for at least 2 h. One course was administered once daily for 3 d. Four courses were administered at one course per month in the first month, second month, third month, and sixth month.

Outcome measures

The main outcome was the changes in SUA levels before and after WMT treatment. The SUA measured in the last test within 3 mo after the first WMT represented the short-term effect, and the SUA measured in the last test within 3-6 mo after the first WMT was the mid-term effect. The secondary outcomes included the WMT course and occurrence of adverse events (AEs) after WMT. In accordance with the National Cancer Institute Common Terminology Criteria for Adverse Events version 5.0, We graded the AEs and classified the relationship between AEs and WMT as unrelated and possibly, probably and definitely related.

Statistical analysis

Statistical product and service solutions version 26.0 were used for data analyses. Categorical data are expressed as the frequency and percentage, and numerical data are expressed as the mean ± SD

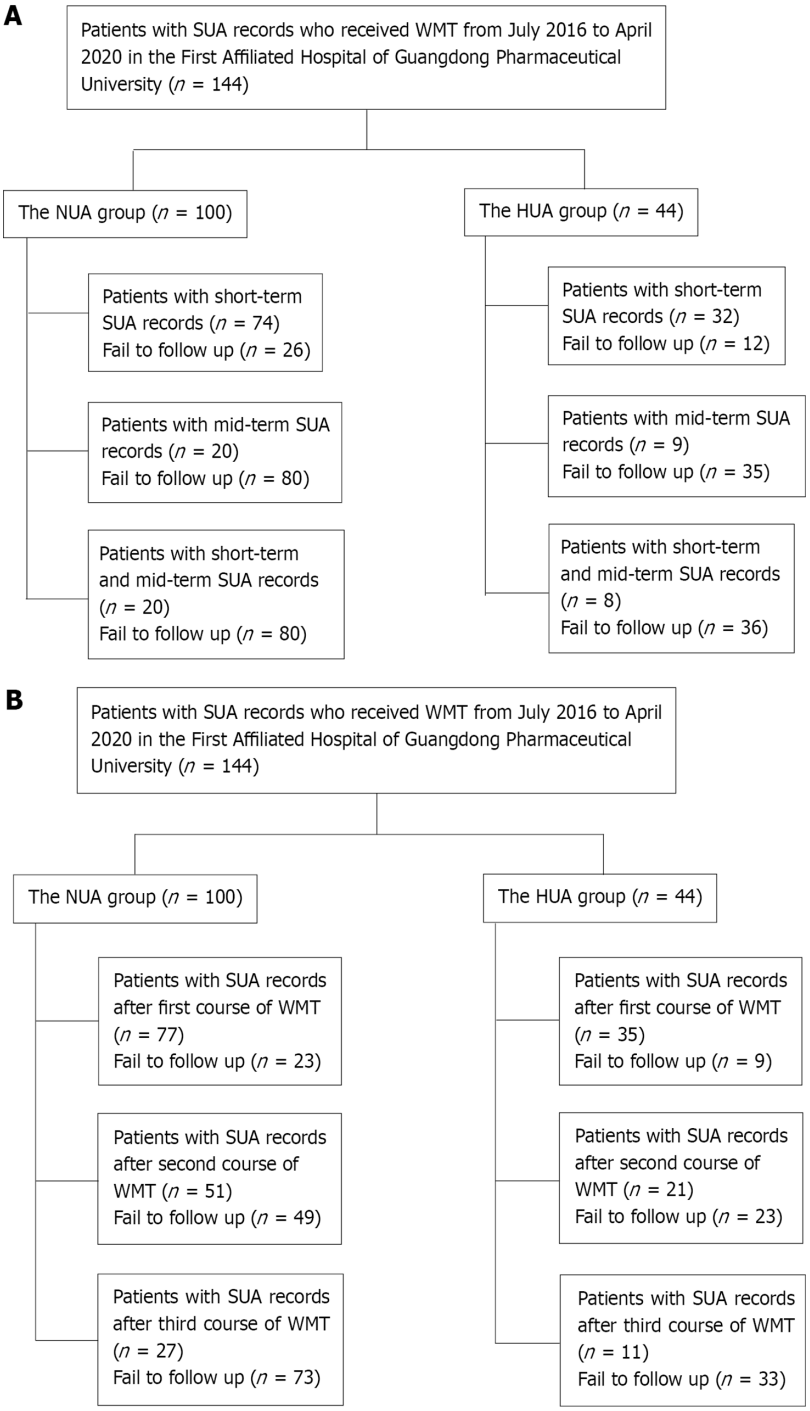

DOI: 10.12998/wjcc.v10.i11.3401

Figure 1 Flow chart of patient inclusion for analysis effects of washed microbiota transplantation on serum uric acid levels. A: Flow chart of patient inclusion for analysis of the short-term and mid-term effects of washed microbiota transplantation (WMT) on serum uric acid (SUA) levels; B: Flow chart of patient inclusion for analysis of the effects of the course of WMT on SUA levels. HUA: Hyperuricaemia; NUA: Normal uric acid; SUA: Serum uric acid; WMT: Washed microbiota transplantation.

deviation. If a normal distribution was observed, Student's *t* test was used for comparison between groups. Otherwise, the Wilcoxon signed rank test was used. Differences were defined as statistically significant when $P < 0.05$.

RESULTS

Baseline data of the patients

Most of the patients were not treated with WMT due to HUA (Table 1). The patients received different

Table 1 Main diagnosis of 144 patients receiving washed microbiota transplantation

Main diagnosis	*n* (%)
Irritable bowel syndrome	32 (22.22)
Functional constipation	22 (15.28)
Ulcerative colitis	14 (9.72)
Gastroesophageal reflux disease	14 (9.72)
Nonalcoholic fatty liver disease	11 (7.64)
Childhood autism	9 (6.25)
Functional enteropathy	5 (3.47)
Functional diarrhea	5 (3.47)
Gout	5 (3.47)
Cirrhosis after hepatitis	3 (2.08)
Functional abdominal pain syndrome	3 (2.08)
Radiation colitis	2 (1.39)
Chronic viral hepatitis B	2 (1.39)
Other	16 (11.11)

short- and mid-term courses of WMT in the HUA group and the NUA group (Table 2).

Analysis of the short-term and mid-term effects of WMT on SUA levels

The short-term average SUA level after WMT treatment in the HUA group was lower than that before treatment (481.00 ± 99.85 *vs* 546.81 ± 109.64 μM, $n = 32$, $P < 0.05$; Table 3 and Figure 2A). The mid-term average SUA level after WMT treatment was lower than that before treatment, but the difference was not statistically significant (483.00 ± 101.21 *vs* 504.00 ± 100.30 μM, $n = 9$, $P > 0.05$; Table 3 and Figure 2A). The mid-term average SUA level after WMT treatment decreased compared with the short-term SUA level after treatment, but the difference was not statistically significant (485.88 ± 107.80 *vs* 528.12 ± 111.89 μM, $n = 8$, $P > 0.05$; Table 3 and Figure 2A). The average short-term and mid-term SUA levels after treatment in the NUA group were similar to the levels before treatment ($P > 0.05$; Table 3 and Figure 2B).

SUA levels decreased in the short term after treatment in 25 patients in the HUA group (78.12%), and SUA levels returned to normal in 10 patients (31.25%). A total of 55.56% (5/9) of patients had a decrease in SUA levels in the mid-term after treatment, and the SUA levels of 22.22% (2/9) of these patients returned to normal (Figure 3).

Correlation analysis between the short-term SUA reduction level after WMT treatment and SUA before treatment

The relationship between the short-term SUA reduction level after WMT treatment and the SUA level before treatment in the HUA group showed $r = 0.549$ and $R^2 = 0.300$ ($P < 0.05$), which suggested that the short-term SUA reduction level after WMT treatment and the SUA level before treatment were moderately correlated (Figure 4).

Analysis of the effects of the course of WMT on SUA levels

The average SUA level of the patients in the HUA group decreased after the first course of WMT compared with that before treatment (469.74 ± 97.68 *vs* 540.00 ± 107.16 μM, $n = 35$, $P < 0.05$; Table 4 and Figure 5A). The average SUA level of the patients in the HUA group was lower after the second course of WMT than before treatment (465.57 ± 88.88 *vs* 513.19 ± 78.14 μM, $n = 21$, $P < 0.05$; Table 4 and Figure 5A). The average SUA level of the patients in the HUA group after the third course of WMT was decreased compared with that before treatment, but the difference was not statistically significant (417.36 ± 92.84 *vs* 526.73 ± 111.30 μM, $n = 11$, $P > 0.05$; Table 4 and Figure 5A). The average SUA level of the patients in the NUA group ($n = 100$) after receiving different courses of WMT was similar to that before treatment ($P > 0.05$; Table 4 and Figure 5B).

Analysis of the short-term and mid-term effects of WMT on serum creatinine levels

The average short-term and mid-term serum creatinine levels after treatment were similar to those before treatment in both groups ($P > 0.05$; Table 5).

Table 2 Short-term (within 3 mo) and mid-term (within 3-6 mo) washed microbiota transplantation treatment courses in the hyperuricaemia group and normal uric acid group

Time	Group	*n*	1 course	2 courses	3 courses	4 courses
Short-term						
	HUA group	32	1	21	10	-
	NUA group	74	1	51	22	-
Mid-term						
	HUA group	9	-	1	6	2
	NUA group	20	-	-	15	5

HUA: Hyperuricaemia; NUA: Normal uric acid.

Table 3 Changes in short-term (within 3 mo) and mid-term (within 3-6 mo) serum uric acid levels before and after washed microbiota transplantation treatment

Group	SUA levels (μM)		*P* value	SUA levels (μM)		*P* value	SUA levels (μM)		*P* value
	Before treatment	Short-term effect after treatment		Before treatment	Mid-term effect after treatment		Short-term effect after treatment	Mid-term effect after treatment	
HUA group (*n* = 44)	546.81 ± 109.64 (*n* = 32)	481.00 ± 99.85 (*n* = 32)	0.001	504.0 ± 100.3 (*n* = 9)	483.00 ± 101.21 (*n* = 9)	0.596	528.12 ± 111.89 (*n* = 8)	485.88 ± 107.80 (*n* = 8)	0.276
NUA group (*n* = 100)	322.8 ± 52.0 (*n* = 74)	326.62 ± 63.30 (*n* = 74)	0.500	308.30 ± 70.28 (*n* = 20)	325.50 ± 101.03 (*n* = 20)	0.350	309.10 ± 68.32 (*n* = 20)	325.50 ± 101.03 (*n* = 20)	0.301

SUA: Serum uric acid; HUA: Hyperuricaemia; NUA: Normal uric acid.

Table 4 Changes in serum uric acid before and after treatment in patients receiving different courses of washed microbiota transplantation

Group	SUA levels (μM)		*P* value	SUA levels (μM)		*P* value	SUA levels (μM)		*P* value
	Before treatment	After first course of WMT		Before treatment	After second course of WMT		Before treatment	After third course of WMT	
HUA group (*n* = 44)	540.00 ± 107.16 (*n* = 35)	469.74 ± 97.68 (*n* = 35)	0.001	513.19 ± 78.14 (*n* = 21)	465.57 ± 88.88 (*n* = 21)	0.026	526.73 ± 111.30 (*n* = 11)	417.36 ± 92.84 (*n* = 11)	0.101
NUA group (*n* = 100)	320.55 ± 52.73 (*n* = 77)	328.86 ± 71.91 (*n* = 77)	0.184	317.29 ± 57.44 (*n* = 51)	323.18 ± 68.06 (*n* = 51)	0.442	333.00 ± 55.49 (*n* = 27)	328.59 ± 73.52 (*n* =27)	0.628

HUA: Hyperuricaemia; NUA: Normal uric acid; WMT: Washed microbiota transplantation.

Analysis of the safety of WMT

No serious adverse reactions occurred during WMT treatment in the 144 treated patients. Only one patient developed mild diarrhea during the second WMT treatment, which gradually returned to normal within 3 d. This AE was classified as possibly related to WMT.

DISCUSSION

HUA is closely related to intestinal flora imbalance. A bacterial disorder was observed in patients with HUA that manifested as an increase in the total count of aerobes, *Escherichia coli* and *Bacteroides* and a decrease in the number of *Lactobacillus* and *Bifidobacteria*[17]. The composition of the intestinal flora also changed in animal models of HUA caused by a high-fat diet, a high-glucose diet, a high-fructose diet, and a high-oxalic-acid diet[18,21,22]. Liu *et al*[23] transplanted the faecal flora of HUA rats into recipient

Table 5 Changes in short-term (within 3 mo) and mid-term (within 3-6 mo) serum creatinine levels before and after washed microbiota transplantation treatment

Group	SCR levels (μM)		*P* value	SCR levels (μM)		*P* value
	Before treatment	Short-term effect after treatment		Before treatment	Mid-term effect after treatment	
HUA group (*n* = 44)	73.00 ± 20.17 (*n* = 29)	72.07 ± 17.27 (*n* = 29)	0.575	68.44 ± 14.67 (*n* = 9)	67.78 ± 13.03 (*n* = 9)	0.798
NUA group (*n* = 100)	64.85 ± 13.74 (*n* = 73)	64.67 ± 13.22 (*n* = 73)	0.791	66.3 ± 14.6 (*n* = 20)	66.10 ± 14.02 (*n* = 20)	0.890

HUA: Hyperuricaemia; NUA: Normal uric acid.

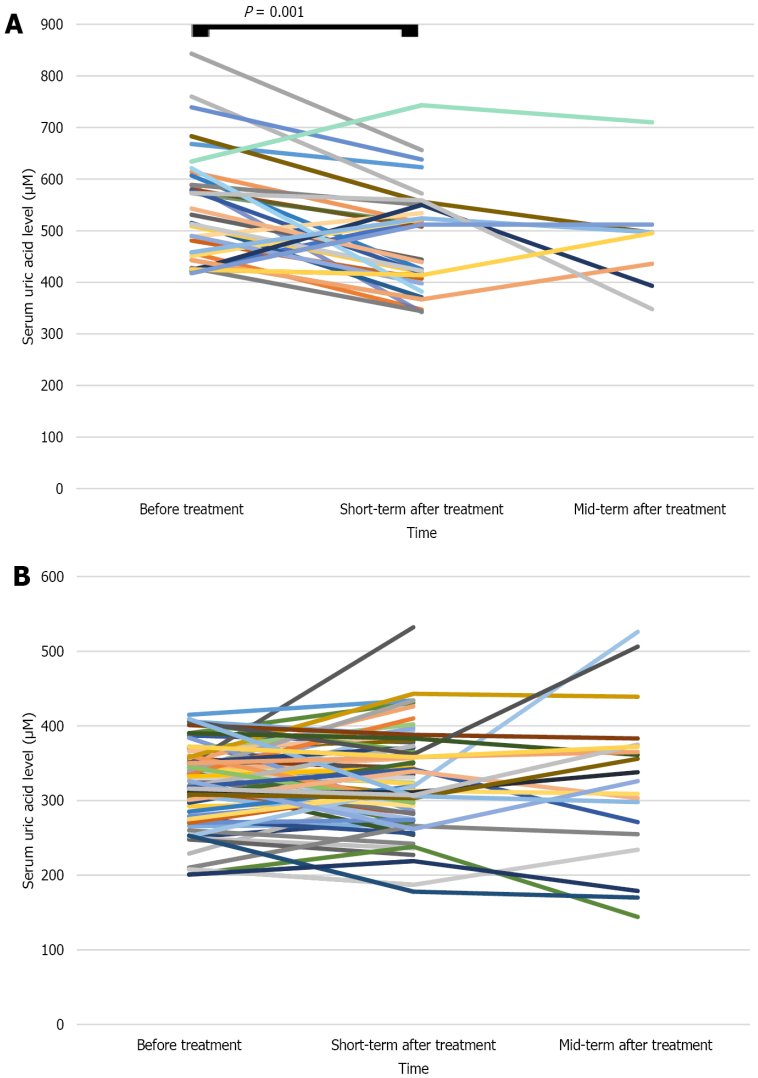

DOI: 10.12998/wjcc.v10.i11.3401

Figure 2 Changes in short-term (within 3 mo) and mid-term (within 6 mo) serum uric acid levels. A: Hyperuricaemia group (*n* = 32) before and after washed microbiota transplantation (WMT) treatment. Short-term after treatment and before treatment: 481.00 ± 99.85 *vs* 546.81 ± 109.64 μM, *P* = 0.001. Mid-term after treatment and before treatment: 483.00 ± 101.21 *vs* 504.00 ± 100.30, *P* = 0.596. Short-term after treatment and mid-term after treatment: 485.88 ± 107.80 *vs* 528.12 ± 111.89, *P* = 0.276; B: Normal uric acid group (*n* = 100) before and after WMT treatment. Short-term after treatment and before treatment: 326.62 ± 63.30 *vs* 322.80 ± 52.00 μM, *P* = 0.500. Mid-term after treatment and before treatment: 325.50 ± 101.03 *vs* 308.30 ± 70.28, *P* = 0.350. Short-term after treatment and mid-term after treatment: 325.50 ± 101.03 *vs* 309.10 ± 68.32, *P* = 0.301.

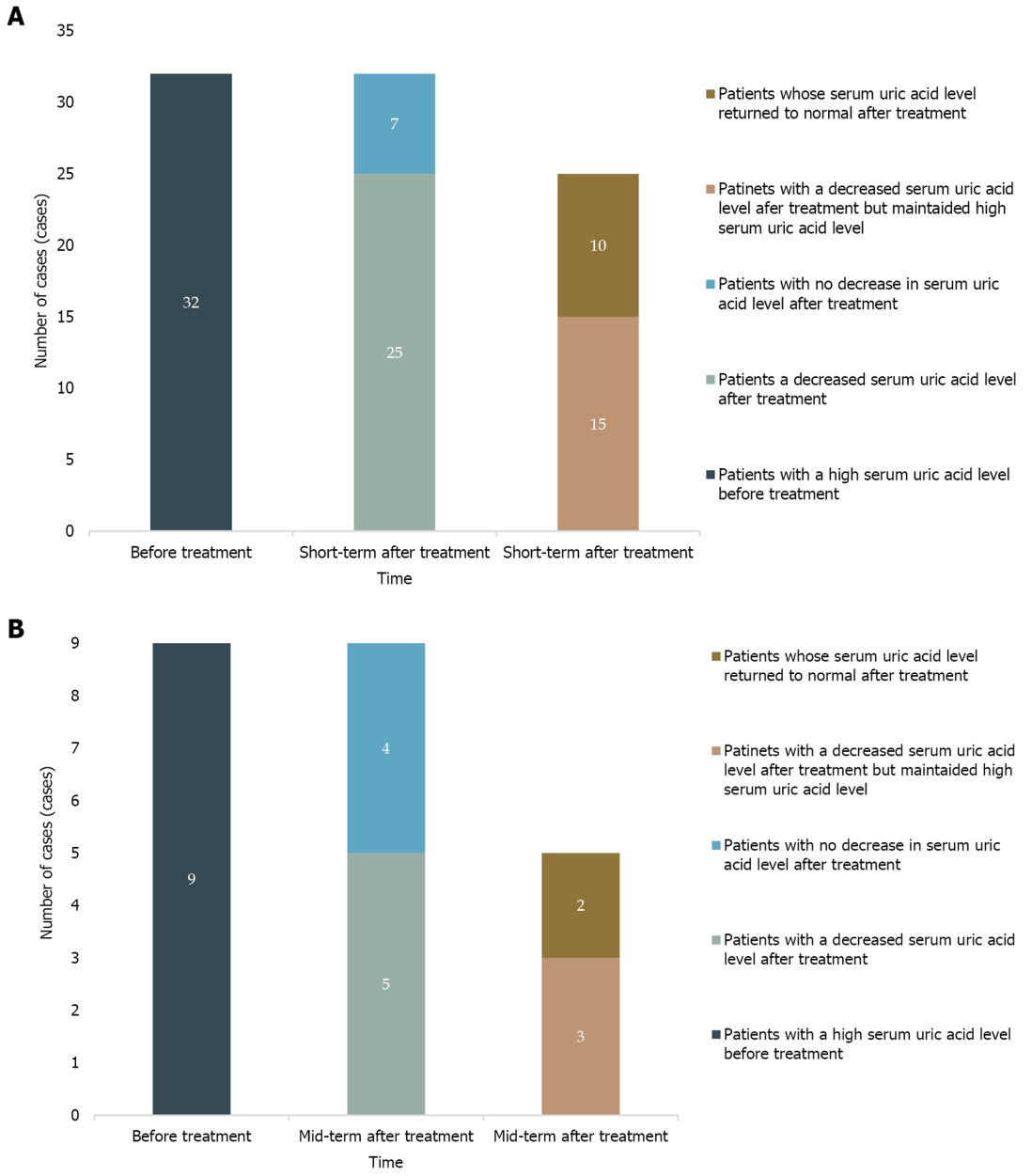

DOI: 10.12998/wjcc.v10.i11.3401

Figure 3 The number of cases serum uric acid level reduction after washed microbiota transplantation treatment in the hyperuricaemia group. A: The number of cases with short-term (within 3 mo) serum uric acid level reduction after washed microbiota transplantation (WMT) treatment in the hyperuricaemia (HUA) group; B: The number of cases with mid-term (within 6 mo) serum uric acid level reduction after WMT treatment in the HUA group.

rats. After 3 wk, the diversity and richness of the intestinal flora of recipient rats changed, and UA levels of recipient rats also increased.

Previous studies have shown that probiotics effectively treat HUA[24,25]. However, one study demonstrated that symbiotic and probiotic interventions had no effect on SUA levels after 12 wk of intervention[26]. A meta-analysis showed that UA levels were significantly increased in the intervention group compared to a control group[27].

These studies have clarified the differences in the intestinal flora between patients with HUA and healthy individuals, but controversy over the role of probiotics in reducing SUA remains. WMT significantly improves intestinal bacterial disorders and is currently recognized as the most effective method to restore the intestinal microecological balance. A pilot study[20] found that all patients (n = 11) had a reduction in SUA levels on day 28 post-FMT ($P < 0.05$). However, this study did not examine the short- and mid-term effects of WMT on patients with NUA levels or the mid-term effect of WMT on patients with HUA and had a relatively small sample size.

The average SUA level in the HUA group decreased within 3 mo after WMT in our study ($P < 0.05$). Short-term SUA levels decreased in 25 patients (78.12%) after treatment, and SUA levels returned to normal in 10 patients (31.25%). The mechanism of WMT treatment in the reduction of UA may involve

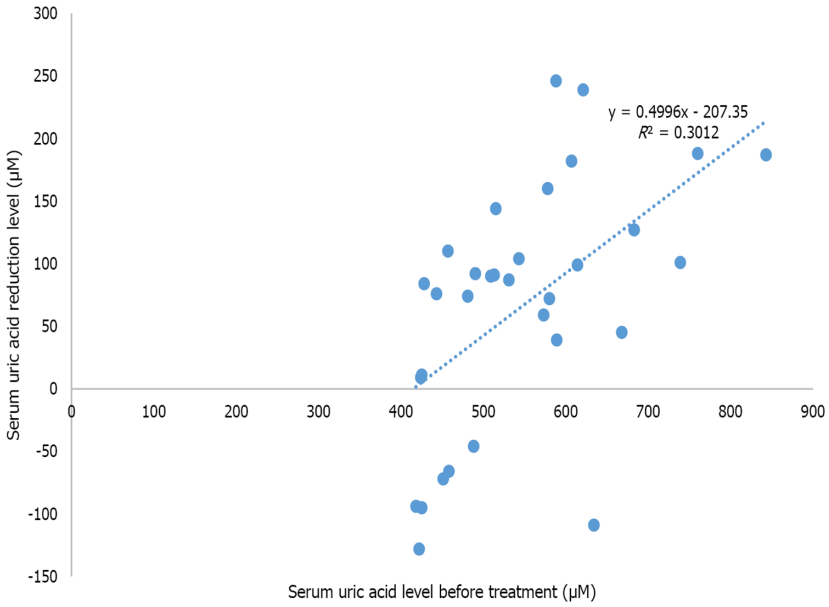

DOI: 10.12998/wjcc.v10.i11.3401

Figure 4 The linear relationship between the short-term (within 3 mo) uric acid reduction level after washed microbiota transplantation treatment and the serum uric acid level before treatment in the hyperuricaemia group (*n* = 32).

two pathways, promotion of UA decomposition and excretion. The intestinal flora degrade UA into allantoin[28]. The intestinal flora also affect the metabolism of UA by regulating ABCG2, SLC2A9 and other UA transporters of the intestinal epithelium[9,10]. Some scholars[7,8] have hypothesised a "metabolic endotoxemia", wherein changes in the structure of the intestinal flora can increase the permeability of the intestinal tract and cause microbial metabolites, such as endotoxins or LPS, to increase in the host circulatory system. LPS forms an immune complex with its receptor CD14, which is recognized by Toll-like receptor 4 on the surface of immune cells and causes kidney damage through blood circulation. These effects subsequently lead to renal UA excretion disorders and reduced UA excretion, which increase SUA levels. Wang *et al*[19] treated mice with fructose-induced HUA with isolated *Lactobacillus brevis* DM9218. The results showed that DM9218 decreased SUA levels, hepatic xanthine oxidase activity and liver LPS in fructose-fed mice. Diamine oxidase and endotoxin levels decreased after FMT in a clinical study ($P < 0.05$)[20]. Because our study was a retrospective study, further studies are needed to explore the mechanism of WMT reduction of SUA. The SUA levels of some patients in the HUA group did not decrease. The high SUA levels in these patients may not be the result of an intestinal flora imbalance, and WMT had no obvious effect, or it interfered with other factors, such as a high-purine diet. Therefore, we should clarify that the role of WMT in HUA results from different causes in further studies.

After WMT in the HUA group, SUA levels at the mid-term observation point were reduced compared with those before treatment and at the short-term observation point. However, there was no significant difference ($P > 0.05$). It may be associated with the small sample included in the mid-term observation. Alternatively, WMT may have no effect on mid-term SUA levels in HUA. Follow-up studies should further expand the sample size and extend follow-up time to clarify the mid-term and long-term effects of WMT treatment.

There was a difference in the number of courses of WMT in the evaluation of short-term and long-term effects (Table 2). Therefore, we further analysed the effect of WMT on SUA in different populations based on the number of treatment courses. After one and two courses of WMT in the HUA group, the average SUA level decreased ($P < 0.05$), which indicated that the first and second courses of WMT played a significant impact on reducing SUA levels in patients with HUA. After three courses, the average SUA level decreased compared with that before treatment, but the difference was not statistically significant ($P > 0.05$). This finding may be related to the small sample size or may suggest that the third course of WMT cannot reduce SUA levels. Follow-up researches with a larger sample capacity are needed to elucidate the effect on SUA level of the third course of treatment. Because of the limited number of patients in this study with complete UA data before treatment and after each treatment, it was difficult to further analyse the relationship between the number of courses of treatment and the effect of WMT. Future research should investigate the optimal course of treatment for HUA.

The average SUA level in the NUA group was similar to that before treatment, and the difference was not statistically significant. This finding suggests that WMT treatment does not interfere with normal UA metabolism. These results also provide evidence to support the safety of WMT treatment from the perspective of UA metabolism.

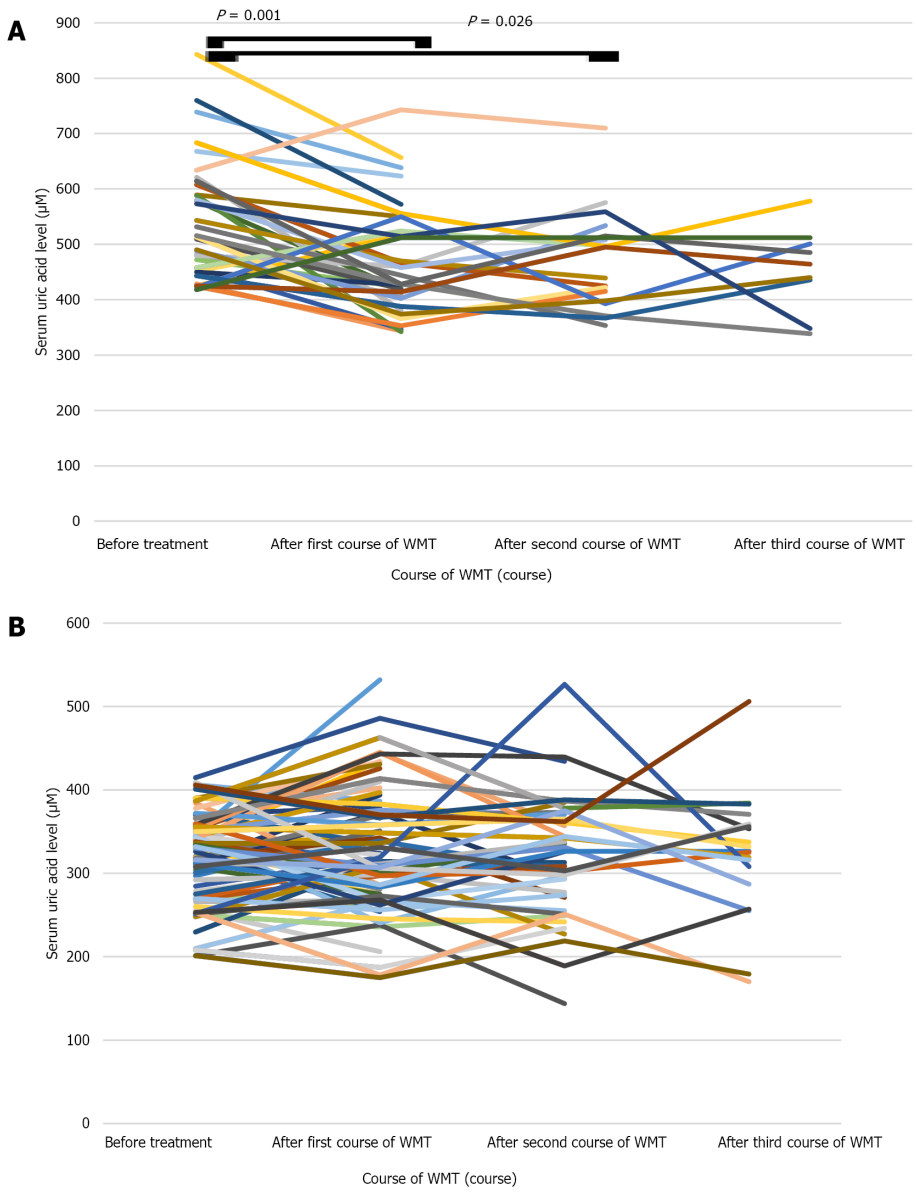

DOI: 10.12998/wjcc.v10.i11.3401

Figure 5 Changes in the serum uric acid level before and after different courses of washed microbiota transplantation. A: Hyperuricaemia group (*n* = 44). After the first course of washed microbiota transplantation (WMT) and before treatment: 469.74 ± 97.68 *vs* 540.00 ± 107.16, *P* = 0.001. After the second course of WMT and before treatment: 465.57 ± 88.88 *vs* 513.19 ± 78.14, *P* = 0.026. After the third course of WMT and before treatment: 417.36 ± 92.84 *vs* 526.73 ± 111.30, *P* = 0.101; B: Normal uric acid group (*n* = 100). After the first course of WMT and before treatment: 328.86 ± 71.91 *vs* 320.55 ± 52.73, *P* = 0.184. After the second course of WMT and before treatment: 323.18 ± 68.06 *vs* 317.29 ± 57.44, *P* = 0.442. After the third course of WMT and before treatment: 328.59 ± 73.52 *vs* 333 ± 55.49, *P* = 0.628. WMT: Washed microbiota transplantation.

The safety of WMT is noteworthy. Only one patient developed mild diarrhea during the second WMT treatment, which gradually returned to normal within 3 d. A systematic review analysed the FMT-related AEs reported in 129 studies worldwide from 2000 to 2020, and the results showed that the total incidence of FMT-related AEs was 19%[29]. The low number of adverse reactions in the current study may be related to the use of WMT instead of FMT or the small sample size. Due to the short follow-up time, the current study could not clarify the long-term safety of WMT for the treatment of HUA.

The current study also has the following limitations: (1) No analysis of the effects of WMT on the improvement of gout flares in people with HUA; (2) no placebo control group or UA-lowering drug group; and (3) a single-centre design, which may lead to regional and genetic background bias.

CONCLUSION

WMT reduces SUA levels of patients with HUA in the short term with mild side effects but has no obvious effect on the SUA level of patients with NUA.

ARTICLE HIGHLIGHTS

Research background

Hyperuricaemia (HUA) pathogenesis is closely associated with intestinal bacteria.

Research motivation

Current treatments for HUA have failed to obtained satisfactory clinical results.

Research objectives

To investigate the effect and safety of washed microbiota transplantation (WMT) on serum uric acid (SUA) levels in different populations.

Research methods

A total of 144 patients who received WMT from July 2016 to April 2020 in the First Affiliated Hospital of Guangdong Pharmaceutical University and had SUA data before treatment were selected. The changes in SUA levels before and after treatment were retrospectively reviewed. According to the pretreatment SUA level, the patients were divided into a hyperuricaemia group (HUA group: SUA > 416 μM) and a normal uric acid group (NUA group: SUA ≥ 202 μM to ≤ 416 μM). Statistical product and service solutions 26.0 was used to analyse the data.

Research results

The average short-term SUA levels in the HUA group decreased after WMT (481.00 ± 99.85 *vs* 546.81 ± 109.64 μM, n = 32, P < 0.05). The levels decreased in 25/32 patients and returned to normal in 10/32 patients. The short-term level of SUA reduction after treatment moderately correlated with the SUA levels before treatment (r = 0.549, R^2 = 0.300, P < 0.05). The average SUA levels decreased after the first and second courses of WMT (469.74 ± 97.68 *vs* 540.00 ± 107.16 μM, n = 35, 465.57 ± 88.88 *vs* 513.19 ± 78.14 μM, n = 21, P < 0.05). Short-term and mid-term SUA levels in the NUA group after WMT and SUA levels after the first, second and third courses of WMT were similar to those before WMT (P > 0.05). Only 1/144 patients developed mild diarrhoea after WMT.

Research conclusions

WMT can lower the SUA level in patients with HUA in the short term with mild side effects, but WMT has no obvious effect on the SUA level of patients with NUA.

Research perspectives

WMT may be a novel treatment for HUA.

ACKNOWLEDGEMENTS

We thank the information department and medical records room of the First Affiliated Hospital of Guangdong Pharmaceutical University for their help on data collection and patients follow-up from the bottom of our heart. We honestly acknowledge Zheng YM at the First Affiliated Hospital of Guangdong Pharmaceutical University for her guidance during the submission process. We truly thank Fu SL, Wang XH, Zhu JW and Guo JD at the Inner Mongolia Ewenki Autonomous Banner People's Hospital for their help on patients follow-up. We also sincerely thank the patients for their enthusiastic participation in our study.

FOOTNOTES

Author contributions: Cai JR, Chen XW, He YJ and Wu B jointly analysed the data, wrote the manuscript, and contributed equally to this article; Zhang M provided statistical advice; Wu LH designed the study and revised the manuscript; all authors read and approved the manuscript.

Supported by the Innovation and Entrepreneurship Training Program for College Students of Guangdong Province, No. S201910573028.

Institutional review board statement: This study was reviewed and approved by the Ethics Committee of Guangdong Pharmaceutical University, No. 68.

Informed consent statement: All participants signed written informed consent.

Conflict-of-interest statement: We have no financial relationships to disclose.

Data sharing statement: No additional data are available.

Country/Territory of origin: China

ORCID number: Jin-Rong Cai 0000-0003-3514-1703; Xin-Wen Chen 0000-0003-4452-9523; Yu-Jian He 0000-0002-2962-1199; Bin Wu 0000-0002-6058-3127; Min Zhang 0000-0002-3792-8668; Li-Hao Wu 0000-0003-4674-8287.

S-Editor: Guo XR
L-Editor: A
P-Editor: Guo XR

REFERENCES

1 **Wu J**, Qiu L, Cheng XQ, Xu T, Wu W, Zeng XJ, Ye YC, Guo XZ, Cheng Q, Liu Q, Liu L, Xu CL, Zhu GJ. Hyperuricemia and clustering of cardiovascular risk factors in the Chinese adult population. *Sci Rep* 2017; **7**: 5456 [PMID: 28710367 DOI: 10.1038/s41598-017-05751-w]
2 **Joosten LAB**, Crişan TO, Bjornstad P, Johnson RJ. Asymptomatic hyperuricaemia: a silent activator of the innate immune system. *Nat Rev Rheumatol* 2020; **16**: 75-86 [PMID: 31822862 DOI: 10.1038/s41584-019-0334-3]
3 **Yamanaka H**; Japanese Society of Gout and Nucleic Acid Metabolism. Japanese guideline for the management of hyperuricemia and gout: second edition. *Nucleosides Nucleotides Nucleic Acids* 2011; **30**: 1018-1029 [PMID: 22132951 DOI: 10.1080/15257770.2011.596496]
4 **Pisaniello HL**, Fisher MC, Farquhar H, Vargas-Santos AB, Hill CL, Stamp LK, Gaffo AL. Efficacy and safety of gout flare prophylaxis and therapy use in people with chronic kidney disease: a Gout, Hyperuricemia and Crystal-Associated Disease Network (G-CAN)-initiated literature review. *Arthritis Res Ther* 2021; **23**: 130 [PMID: 33910619 DOI: 10.1186/s13075-021-02416-y]
5 **Strilchuk L**, Fogacci F, Cicero AF. Safety and tolerability of available urate-lowering drugs: a critical review. *Expert Opin Drug Saf* 2019; **18**: 261-271 [PMID: 30915866 DOI: 10.1080/14740338.2019.1594771]
6 **Dalbeth N**, Choi HK, Joosten LAB, Khanna PP, Matsuo H, Perez-Ruiz F, Stamp LK. Gout. *Nat Rev Dis Primers* 2019; **5**: 69 [PMID: 31558729 DOI: 10.1038/s41572-019-0115-y]
7 **Anhê FF**, Roy D, Pilon G, Dudonné S, Matamoros S, Varin TV, Garofalo C, Moine Q, Desjardins Y, Levy E, Marette A. A polyphenol-rich cranberry extract protects from diet-induced obesity, insulin resistance and intestinal inflammation in association with increased Akkermansia spp. population in the gut microbiota of mice. *Gut* 2015; **64**: 872-883 [PMID: 25080446 DOI: 10.1136/gutjnl-2014-307142]
8 **Xu D**, Lv Q, Wang X, Cui X, Zhao P, Yang X, Liu X, Yang W, Yang G, Wang G, Wang P, Wang Z, Li Z, Xing S. Hyperuricemia is associated with impaired intestinal permeability in mice. *Am J Physiol Gastrointest Liver Physiol* 2019; **317**: G484-G492 [PMID: 31369290 DOI: 10.1152/ajpgi.00151.2019]
9 **Hosomi A**, Nakanishi T, Fujita T, Tamai I. Extra-renal elimination of uric acid *via* intestinal efflux transporter BCRP/ABCG2. *PLoS One* 2012; **7**: e30456 [PMID: 22348008 DOI: 10.1371/journal.pone.0030456]
10 **DeBosch BJ**, Kluth O, Fujiwara H, Schürmann A, Moley K. Early-onset metabolic syndrome in mice lacking the intestinal uric acid transporter SLC2A9. *Nat Commun* 2014; **5**: 4642 [PMID: 25100214 DOI: 10.1038/ncomms5642]
11 **Surawicz CM**, Brandt LJ, Binion DG, Ananthakrishnan AN, Curry SR, Gilligan PH, McFarland LV, Mellow M, Zuckerbraun BS. Guidelines for diagnosis, treatment, and prevention of Clostridium difficile infections. *Am J Gastroenterol* 2013; **108**: 478-98; quiz 499 [PMID: 23439232 DOI: 10.1038/ajg.2013.4]
12 **Lima SF**, Gogokhia L, Viladomiu M, Chou L, Putzel G, Jin WB, Pires S, Guo CJ, Gerardin Y, Crawford CV, Jacob V, Scherl E, Brown SE, Hambor J, Longman RS. Transferable Immunoglobulin A-Coated Odoribacter splanchnicus in Responders to Fecal Microbiota Transplantation for Ulcerative Colitis Limits Colonic Inflammation. *Gastroenterology* 2022; **162**: 166-178 [PMID: 34606847 DOI: 10.1053/j.gastro.2021.09.061]
13 **Bloom PP**, Tapper EB, Young VB, Lok AS. Microbiome therapeutics for hepatic encephalopathy. *J Hepatol* 2021; **75**: 1452-1464 [PMID: 34453966 DOI: 10.1016/j.jhep.2021.08.004]
14 **Mocanu V**, Zhang Z, Deehan EC, Kao DH, Hotte N, Karmali S, Birch DW, Samarasinghe KK, Walter J, Madsen KL. Fecal microbial transplantation and fiber supplementation in patients with severe obesity and metabolic syndrome: a randomized double-blind, placebo-controlled phase 2 trial. *Nat Med* 2021; **27**: 1272-1279 [PMID: 34226737 DOI: 10.1038/s41591-021-01399-2]

15 **Zhang T**, Lu G, Zhao Z, Liu Y, Shen Q, Li P, Chen Y, Yin H, Wang H, Marcella C, Cui B, Cheng L, Ji G, Zhang F. Washed microbiota transplantation vs. manual fecal microbiota transplantation: clinical findings, animal studies and in vitro screening. *Protein Cell* 2020; **11**: 251-266 [PMID: 31919742 DOI: 10.1007/s13238-019-00684-8]

16 . Nanjing consensus on methodology of washed microbiota transplantation. *Chin Med J (Engl)* 2020; **133**: 2330-2332 [PMID: 32701590 DOI: 10.1097/CM9.0000000000000954]

17 **Ren KY**, Yong CM, JIN YC, Cao B, Wei LZ. Analysis of intestinal flora in patients with hyperuricemia in Qindao District. *Zhongguo Yishi Zazhi* 2014; **16**: 1649-1651; 1656

18 **Yu Y**, Liu Q, Li H, Wen C, He Z. Alterations of the Gut Microbiome Associated With the Treatment of Hyperuricaemia in Male Rats. *Front Microbiol* 2018; **9**: 2233 [PMID: 30283432 DOI: 10.3389/fmicb.2018.02233]

19 **Wang H**, Mei L, Deng Y, Liu Y, Wei X, Liu M, Zhou J, Ma H, Zheng P, Yuan J, Li M. Lactobacillus brevis DM9218 ameliorates fructose-induced hyperuricemia through inosine degradation and manipulation of intestinal dysbiosis. *Nutrition* 2019; **62**: 63-73 [PMID: 30852460 DOI: 10.1016/j.nut.2018.11.018]

20 **Xie WR**, Yang XY, Deng ZH, Zheng YM, Zhang R, Wu LH, Cai JY, Kong LP, Xia HH, He XX. Effects of washed microbiota transplantation on serum uric acid levels, symptoms and intestinal barrier function in patients with acute and recurrent gout: a pilot study. *Dig Dis* 2021; In press

21 **Silva JCP**, Mota M, Martins FO, Nogueira C, Gonçalves T, Carneiro T, Pinto J, Duarte D, Barros AS, Jones JG, Gil AM. Intestinal Microbial and Metabolic Profiling of Mice Fed with High-Glucose and High-Fructose Diets. *J Proteome Res* 2018; **17**: 2880-2891 [PMID: 29923728 DOI: 10.1021/acs.jproteome.8b00354]

22 **García-Arroyo FE**, Gonzaga G, Muñoz-Jiménez I, Blas-Marron MG, Silverio O, Tapia E, Soto V, Ranganathan N, Ranganathan P, Vyas U, Irvin A, Ir D, Robertson CE, Frank DN, Johnson RJ, Sánchez-Lozada LG. Probiotic supplements prevented oxonic acid-induced hyperuricemia and renal damage. *PLoS One* 2018; **13**: e0202901 [PMID: 30142173 DOI: 10.1371/journal.pone.0202901]

23 **Liu X**, Lv Q, Ren H, Gao L, Zhao P, Yang X, Yang G, Xu D, Wang G, Yang W, Wang P, Wang Z, Xing S. The altered gut microbiota of high-purine-induced hyperuricemia rats and its correlation with hyperuricemia. *PeerJ* 2020; **8**: e8664 [PMID: 32185104 DOI: 10.7717/peerj.8664]

24 **Yamanaka H**, Taniguchi A, Tsuboi H, Kano H, Asami Y. Hypouricaemic effects of yoghurt containing Lactobacillus gasseri PA-3 in patients with hyperuricaemia and/or gout: A randomised, double-blind, placebo-controlled study. *Mod Rheumatol* 2019; **29**: 146-150 [PMID: 29446654 DOI: 10.1080/14397595.2018.1442183]

25 **Szulińska M**, Łoniewski I, van Hemert S, Sobieska M, Bogdański P. Dose-Dependent Effects of Multispecies Probiotic Supplementation on the Lipopolysaccharide (LPS) Level and Cardiometabolic Profile in Obese Postmenopausal Women: A 12-Week Randomized Clinical Trial. *Nutrients* 2018; **10** [PMID: 29914095 DOI: 10.3390/nu10060773]

26 **Haghighat N**, Mohammadshahi M, Shayanpour S, Haghighizadeh MH. Effect of Synbiotic and Probiotic Supplementation on Serum Levels of Endothelial Cell Adhesion Molecules in Hemodialysis Patients: a Randomized Control Study. *Probiotics Antimicrob Proteins* 2019; **11**: 1210-1218 [PMID: 30293208 DOI: 10.1007/s12602-018-9477-9]

27 **Firouzi S**, Haghighatdoost F. The effects of prebiotic, probiotic, and synbiotic supplementation on blood parameters of renal function: A systematic review and meta-analysis of clinical trials. *Nutrition* 2018; **51-52**: 104-113 [PMID: 29626749 DOI: 10.1016/j.nut.2018.01.007]

28 **Sorensen LB**. Degradation of uric acid in man. *Metabolism* 1959; **8**: 687-703 [PMID: 13832881]

29 **Marcella C**, Cui B, Kelly CR, Ianiro G, Cammarota G, Zhang F. Systematic review: the global incidence of faecal microbiota transplantation-related adverse events from 2000 to 2020. *Aliment Pharmacol Ther* 2021; **53**: 33-42 [PMID: 33159374 DOI: 10.1111/apt.16148]

World Journal of Clinical Cases

Submit a Manuscript: https://www.f6publishing.com

World J Clin Cases 2022 April 16; 10(11): 3414-3425

DOI: 10.12998/wjcc.v10.i11.3414

ISSN 2307-8960 (online)

ORIGINAL ARTICLE

Clinical Trials Study

Concurrent chemoradiotherapy using gemcitabine and nedaplatin in recurrent or locally advanced head and neck squamous cell carcinoma

Rui-Xue Huo, Ying-Ying Jin, Yong-Xue Zhuo, Xiao-Tong Ji, Yu Cui, Xiao-Jing Wu, Yi-Jia Wang, Long Zhang, Wen-Hua Zhang, Yu-Mei Cai, Cheng-Cheng Zheng, Rui-Xue Cui, Qian-Ye Wang, Zhen Sun, Feng-Wei Wang

Specialty type: Oncology

Provenance and peer review: Unsolicited article; Externally peer reviewed.

Peer-review model: Single blind

Peer-review report's scientific quality classification

Grade A (Excellent): 0
Grade B (Very good): B
Grade C (Good): C
Grade D (Fair): 0
Grade E (Poor): 0

P-Reviewer: Hamaya Y, Japan; Marickar F, India

Received: September 20, 2021
Peer-review started: September 20, 2021
First decision: January 10, 2022
Revised: January 14, 2022
Accepted: March 6, 2022
Article in press: March 6, 2022
Published online: April 16, 2022

Rui-Xue Huo, Yu Cui, Long Zhang, Wen-Hua Zhang, Yu-Mei Cai, Cheng-Cheng Zheng, Rui-Xue Cui, Qian-Ye Wang, Zhen Sun, Feng-Wei Wang, Department of Oncology, Tianjin Union Medical Center, Tianjin 300000, China

Ying-Ying Jin, Yong-Xue Zhuo, Xiao-Tong Ji, School of Medicine, Nankai University, Tianjin 300000, China

Xiao-Jing Wu, Yi-Jia Wang, Laboratory of Oncologic Molecular Medicine, Tianjin Union Medical Center, Tianjin 300000, China

Corresponding author: Feng-Wei Wang, MD, PhD, Chief Doctor, Department of Oncology, Tianjin Union Medical Center, No. 190 jieyuan Road, Hongqiao District, Tianjin 300000, China. wfengwei2004@163.com

Abstract

BACKGROUND

Patients with recurrent or locally advanced head and neck squamous cell carcinoma (HNSCC) typically have limited treatment options and poor prognosis.

AIM

To evaluate the efficacy and safety of two drugs with potent radio-sensitization properties including gemcitabine and nedaplatin as concurrent chemoradiotherapy regimens in treating HNSCC.

METHODS

This single-arm prospective study enrolled patients with HNSCC to receive gemcitabine on days 1 and 8 and nedaplatin on days 1 to 3 for 21 days. Intensity-modulated radiation therapy with a conventional fraction was delivered 5 days per week. Objective response rate (ORR), disease control rate, and toxicity were observed as primary endpoints. Overall survival (OS) and progression free survival were recorded and analyzed as secondary endpoints.

RESULTS

A total of 24 patients with HNSCC were enrolled. During the median 22.4-mo follow-up, both ORR and disease control rate were 100%. The one-year OS was

75%, and one-year progression-free survival (PFS) was 66.7% (median PFS was 15.1 mo). Recurrent HNSCC patients had a poorer prognosis than the treatment-naïve patients, and patients who achieved complete response had better survival than those in the PR group (all $P < 0.05$). The most common grade 1-4 (100%) or grade 3-4 toxicities (75%) were hematological, and the most common grade 3-4 non-hematological toxicity was mucositis in 17 (71%) patients.

CONCLUSION
Gemcitabine plus nedaplatin with concurrent chemoradiotherapy is a therapeutic option for HNSCC with predictable tolerability. Considering the high adverse event rate, the optimized dose and schedule must be further explored.

Key Words: Chemoradiotherapy; Gemcitabine; Nedaplatin; Head and neck cancer; Recurrent; Locally advanced

Core Tip: Our article focuses on the comprehensive treatments of head and neck squamous cell carcinoma, especially for recurred tumors after surgery or tumor lesions that could not be surgically removed.

Citation: Huo RX, Jin YY, Zhuo YX, Ji XT, Cui Y, Wu XJ, Wang YJ, Zhang L, Zhang WH, Cai YM, Zheng CC, Cui RX, Wang QY, Sun Z, Wang FW. Concurrent chemoradiotherapy using gemcitabine and nedaplatin in recurrent or locally advanced head and neck squamous cell carcinoma. *World J Clin Cases* 2022; 10(11): 3414-3425
URL: https://www.wjgnet.com/2307-8960/full/v10/i11/3414.htm
DOI: https://dx.doi.org/10.12998/wjcc.v10.i11.3414

INTRODUCTION

Head and neck cancers including lip, oral cavity, pharynx, nasopharynx and cervical esophagus cancer, generally have similar biological characteristics and utilize the same therapies. Of these, head and neck squamous cell carcinoma (HNSCC) is the most common cancer type, accounting for 85% of these cases. Annually, there are over 550000 new patients and 380000 deaths globally due to the disease[1]. In China, the annual incidence and mortality of head and neck cancer are 586600 and 431200 patients, respectively [2]. Smoking and drinking increase the risk of morbidity[1]. The cure rate is high for early-stage patients who undergo the main therapies including surgery, radiation, and/or chemotherapy. The 5-year survival rate of patients with oral cavity and pharynx cancer is approximately 80%[2]. Most cases, however, are diagnosed in advanced stages where locoregional recurrences and distant metastases lead to poor survival rates, and where therapeutic options are limited[3]. The median overall survival (OS) rate for patients with recurrent or metastatic HNSCC (RMHNSCC) is approximately 6 months, and the 1-year survival rate is approximately 20%[4]. Potential disfigurement and functional loss require careful deliberation when considering surgical resection, while the continued development of chemoradiotherapy approaches provide further options[5].

The standard management of locally advanced head and neck squamous cell carcinoma has evolved [6]. Radiation, especially combined with chemotherapy, is the standard treatment for organ and functional preservation and effectiveness[7]. A high-dose cisplatin regimen (100 mg/m^2) or carboplatin/fluorouracil combination regimen demonstrates superior OS to that of standard radiotherapy[6,8,9]. The Radiation Therapy Oncology Group (RTOG) 97-03 study demonstrated that in the context of concurrent radiation and chemotherapy, the 2-year disease-free survival and OS rates were significantly better in the TP (docetaxel/cisplatin) group than those in the PF group[10]. Neuropathy or anaphylaxis caused by docetaxel and hyperglycemia or hypertension connected with dexamethasone limit the application of docetaxel-based chemotherapy. Cisplatin (DDP), a common radiotherapy sensitizer, is highly emetic and may increase the risk of malnutrition in HNSCC patients. Though cetuximab, a representative targeted therapy, is regarded as a less toxic alternative, no prospective large trials have compared cetuximab to cisplatin in combination with radiotherapy. Recently, anti-PD-1 immunotherapy has been approved for the treatment of platinum-refractory recurrent and/or metastatic HNC based on an associated increase in OS and a decrease in toxicities[5]. However, due to their high costs and the rare but fatal adverse effects associated with their use, anti-PD-1 drugs are not extensively used. Therefore, new chemotherapy drugs with high efficacy and acceptable toxicity in treating HNSCC need to be explored.

Gemcitabine (GEM) (dFdC) is an antimetabolite that mechanistically functions *via* the incorporation of dFdC triphosphate adducts into DNA, resulting in chain termination and inhibition of DNA synthesis. The primary mechanism of GEM-induced radiosensitization is depletion of dATP caused by inhibition of ribonucleotide reductase[11]. In a phase II trial, single-agent GEM in patients with RMHNSCC resulted in a response rate (RR) of 13% amongst 54 patients[12]. In 110 Locally advanced HNSCC patients receiving weekly low-dose GEM with concomitant radiotherapy, the response rate was 78%, and the therapy was tolerated[13]. Additionally, GEM has demonstrated favorable safety and efficacy to treat esophageal squamous cell carcinoma. A phase II clinical trial evaluated weekly GEM and docetaxel regimens as secondline treatments in patients with metastatic esophageal squamous cell carcinoma (ESCC). The disease control rate (DCR) was 88%, with an overall response rate (ORR) of 30% [14]. Of note, GEM has synergistic action with cisplatin. In another phase II trial of triweekly GEM and cisplatin in patients with metastatic or recurrent advanced ESCC, the overall response rate was 42.1% [15]. In a Phase II multicenter clinical trial, the efficacy of a nedaplatin-based regimen, which led to less gastrointestinal reaction, was not significantly different from that of the cisplatin-based regimen for HNSCC[16]. Furthermore, nedaplatin showed excellent antitumor activity and low toxicity with concurrent chemoradiotherapy in treating HNSCC patients[17,18]. However, few studies have been conducted to explore the dosage and safety of GEM in combination with nedaplatin as the concomitant chemoradiotherapy regimen.

Our study explored the efficacy and safety of GEM in combination with nedaplatin as the concomitant chemoradiotherapy regimen for the treatment of patients with recurrent or locally advanced squamous cell carcinoma of the head and neck.

MATERIALS AND METHODS

Patients

Patients with recurrent or locally advanced head and neck squamous cell carcinoma who presented at Department of Oncology, Tianjin Union Medicine Centre, China, between July 2017 and July 2020 were recruited for enrollment. Eligible patients provided written informed consent prior to the onset of study activities. The study was registered at Chinese Clinical Trial Registry (http://www.chictr.org.cn) (ChiCTR2000034141) and was approved by China Ethics Committee of Registering Clinical Trials (ChiECRCT20170178).

Eligibility criteria was: (1) Confirmed recurrent or locally advanced head and neck squamous cell carcinoma by histology; (2) no previous treatment with GEM; (3) aged 18-70 years; (4) Eastern Cooperative Oncology Group (ECOG) performance status of 0-2; (5) at least one measurable lesion by the RECIST 1.1 criteria; (6) no other active malignancies; (7) previous organ-sparing surgery allowed; (8) life expectancy of at least 3 mo, with adequate bone marrow and normal organ function (renal, heart and hepatic function); (9) at least 4 week treatment-free; (10) at least one year since the last radiotherapy; (11) no other distant organ metastasis; (12) no other serious medical complications; and (13) willing to provide written informed consent. Pregnant women and women with childbearing potential and without access to contraception were excluded. Drop-out criteria was: (1) Did not receive concurrent chemoradiotherapy (asynchronous chemoradiotherapy); (2) received less than two cycles of chemotherapy; and (3) lost to follow-up.

Treatment

The pre-treatment evaluation included a medical history and physical examination, blood tests (including complete blood count, renal and liver function tests), electrocardiograph, echocardiography, chest and abdominal CT scan, and enhanced CT or Magnetic Resonance Imaging (MRI) of the head and neck. In addition, laryngoscopy or nasopharyngoscopy and biopsy were performed, if deemed necessary. Blood testing continued weekly throughout the study period.

Radiotherapy schemes were determined based upon individual carcinomas. Intensity-modulated radiation therapy as delivered once per day on a linear accelerator with 6 MV energy 5 days per week. The average dose was 2 Gy per fraction. Concurrent chemotherapy was given 2 hours prior to radiotherapy. Patients received intravenous GEM (600 mg/m^2) over 30 min on days 1 and 8, and intravenous nedaplatin (25 mg/m^2) over 1 h per day on days 1 to 3 for 21 days. Most patients received 2-4 cycles of subsequent chemotherapy after concomitant chemoradiation according to residual disease and their condition. During the subsequent treatment, the dose of GEM was increased to 1000 mg/m^2, and the dose of nedaplatin remained unchanged. The dose of GTV was within the range of 64-74 Gy based upon the lesion, Clinical Target Volume was 66-70 Gy, and PTV was 54-60 Gy. The preventive radiotherapy dose to the lymphatic drainage area was 54-60 Gy, after which a shrinking field administration with locally increased dose was given to the focal area. To those who received postoperative radiotherapy previously (60-66 Gy), the second radiotherapy Gross Target Volume dose was not more than 70 Gy after adjustment (64-70 Gy).

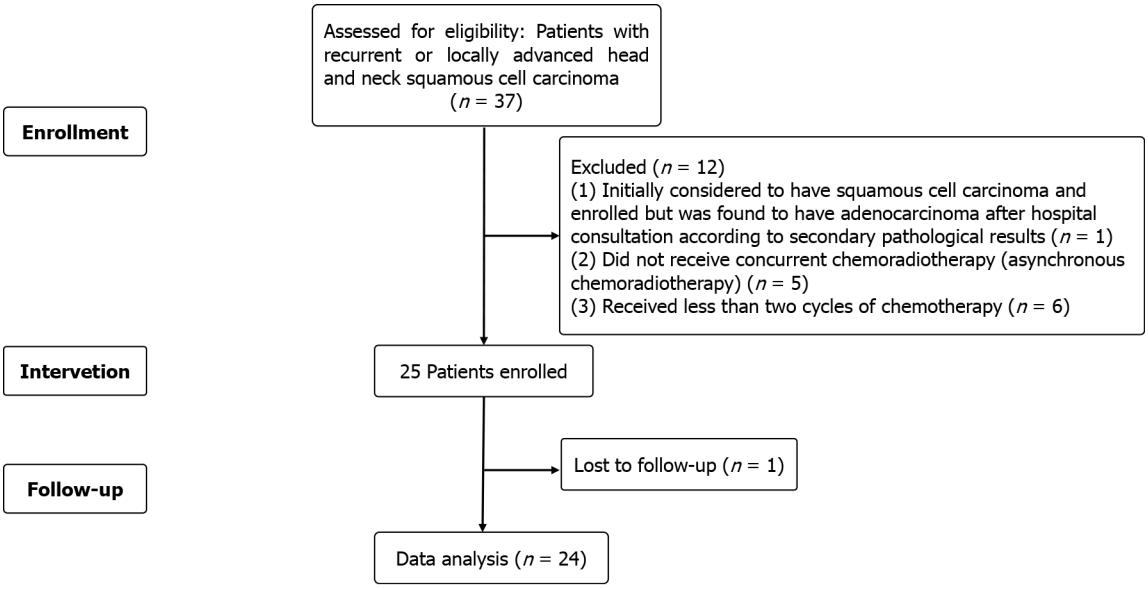

DOI: 10.12998/wjcc.v10.i11.3414

Figure 1 Patient screening flow chart.

Data collection and efficacy evaluation

Demographic and clinical indices were collected, which included age, sex, social history of smoking or drinking, primary tumor site, T stage, N stage, AJCC stage, degree of differentiation, type of tumor (recurrence/Local advancement), ECOG PS, regression ratio of tumor diameter, progression-free survival (PFS) and OS. PFS was defined as the time from enrollment to the first progression of disease or death. OS was defined as the time from patients' enrollment to death from any cause. Therapeutic evaluation was conducted according to the RECIST V1.1 criteria. Complete response (CR) was defined as the disappearance of all evidence of disease, with the minor axis of metastatic lymph shrinking to < 1 cm by physical examination, CT/MRI, or direct endoscopy. Partial response (PR) was defined as a reduction in the largest axis diameters of measurable disease (or the minor axis of metastatic lymph node) by 30%, with no progression to other lesions and no new lesions. Tumor progression (PD) was defined as an increase in the largest axis diameter of measurable disease (or the minor axis of metastatic lymph node) by 20% or the appearance of new lesions. Stable disease (SD) was defined as a disease status between PR and PD. The ORR was calculated as the number of patients achieving CR or PR divided by the number of all enrolled patients. DCR was calculated as the number of patients who reached CR or PR or SD divided by the total number of enrolled patients.

The primary endpoints of this study were ORR, DCR and toxicity. The secondary endpoints were PFS and OS.

Safety assessment

Toxicity was evaluated according to the RTOG Acute Radiation Injury Scoring Criteria and the National Cancer Institute Common Toxicity Criteria (NCI-CTC) scale version 4.0. If severe adverse reactions (grade 4 hematological toxicity, grade 3-4 non-hematological toxicity) occurred or if PS worsened, the therapy was delayed, and the dose was decreased by approximately 25% in the subsequent course. Any required supportive therapy was determined by the treating physician.

Follow-up

Follow up was conducted monthly either by telephone, in-patient admission or outpatient chart review. Data collected included disease progression, short-term and long-term adverse reactions, and imaging and laboratory findings. Imaging exam was performed 1 mo after radiotherapy, then every 2 chemotherapy cycles, and finally every 3-6 mo.

Statistical analysis

The data were analyzed in per-protocol set by excluding the participants who dropped out of the study and failed to comply with the study protocol. Demographic data was analyzed *via* descriptive statistics SPSS Version 23 (SPSS Inc., Chicago, IL, United States). Data were presented as mean ± standard deviation. Qualitative data were described as frequency and proportion. Univariate analysis of prognostic factors, including sex, age, T stage, N stage, AJCC stage, differentiation degree, smoking and drinking history, was performed, and data were compared using the log rank test. Survival curves were drawn by the Kaplan-Meier method. Statistical significance was considered when the P value was ≤

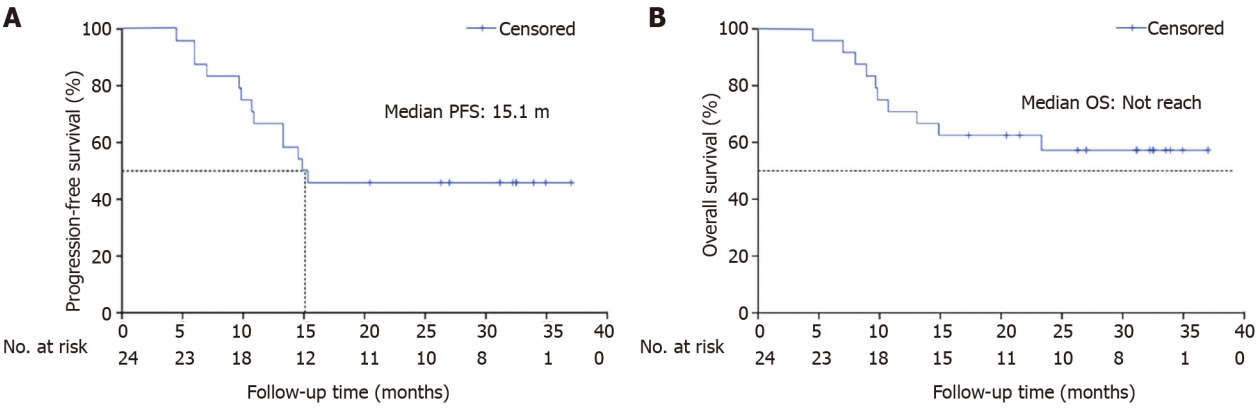

DOI: 10.12998/wjcc.v10.i11.3414

Figure 2 Survival curves of all enrolled patients. A: Survival curves of progression free survival; B: Survival curves of overall survival. PFS: Progression free survival; OS: Overall survival.

0.05.

RESULTS

Patients' characteristics

A total of 37 patients was screened for enrollment (Figure 1). Of these, 1 patient, initially considered to have squamous cell carcinoma and enrolled, was found to have adenocarcinoma after hospital consultation according to secondary pathological results, and was excluded from study participation. During treatment, 5 patients did not receive concurrent chemoradiotherapy (asynchronous chemoradiotherapy), 6 patients received less than two cycles of chemotherapy, and one patient was lost to follow-up. Thus, a total of 24 people was included in the statistical analysis.

Patients demographics and disease characteristics are described in Table 1. The male-to-female ratio was 2:1. All patients had stage III-IV with the majority having poorly differentiated squamous cell carcinoma and the most common site being the nasopharynx (37.5%). The majority of patients smoked (70.8%) or consumed alcohol (87.5%). At enrollment, 10 patients (41.7%) had recurrent disease after surgery, four of whom received postoperative radiotherapy with the GTV range of 60-66 Gy. Most (79.2%) patients had not previously received chemotherapy. A minority of patients received subsequent paclitaxel-containing salvage chemotherapy after tumor progression.

Efficacy evaluation

All 24 patients were followed up for a median period of 22.4 months (IQR 4.5-37.0). Eight of 24 evaluable cases (33.3%) achieved a CR confirmed by enhanced CT or enhanced MRI and endoscopy, and a PR was observed in sixteen (66.7%) cases with an ORR of 100% and a DCR of 100% (Table 2).

Regression ratios of tumor diameter are shown in Figure 3A. The one-year OS rate was 70.8%, and one-year PFS rate was 66.7%. The median PFS was 15.1 months, while the median OS was not attained. Fourteen patients remained alive at the end of this study, including 11 patients without disease progression (Figure 2).

A subgroup comparison was conducted for the recurrent and the treatment-naïve groups. The median PFS and OS of the recurrent group were both 10.3 months and those for treatment-naïve group had not reached (P_{PFS}=0.069, P_{OS}=0.01). The one-year PFS rates of the recurrent and treatment-naïve groups were 37.5% and 81.3%, respectively, and the one-year OS rates of the two groups were 37.5% and 87.5%, respectively (Figure 3B and C).

Another subgroup analysis for the CR and PR groups revealed additional differences (Figure 3D and E). In the PR group, the median PFS and OS time were 13.9 mo and 16.1 months, respectively, and those in the CR group were not reached with the P values in the PFS and OS analysis being 0.067 and 0.059, respectively. The one-year PFS rates of the CR and PR group were 87.5% and 56.3%, respectively, and the one-year OS rate was 87.5% *vs* 62.5%. In the CR group, one patient died of nasal hemorrhage and one with tumor recurrence *in situ*; all others remained alive and tumor-free. In the PR group, recurrence *in situ* was observed in 7 patients (41.2%), and one had distant metastases. Of the 9 patients who died, 3 died from oral and nasal hemorrhage.

Univariate analysis demonstrated no correlation of PFS or OS with age, sex, T stage, N stage, AJCC stage, differentiation degree, smoking or drinking history.

Table 1 Baseline and clinical characteristics of patients

Characteristics	Number (n)	Percentage (%)	Characteristics	Number (n)	Percentage (%)
Age, yr			Sex		
Mean	59.8 ± 8.08		Male	16	0.67
Range	37.1-66.2		Female	8	0.33
T stage			N stage		
1	1	0.042	1	5	0.208
2	9	0.375	2	17	0.708
3	4	0.167	3	2	0.083
4	10	0.417	Differentiation		
Smoking history			High	1	0.042
Nonsmoker	7	0.292	Moderately	3	0.125
20-30 yr	11	0.458	Low	12	0.5
30-39 yr	1	0.042	Uncertain	8	0.333
> 40 yr	5	0.208	Primary tumor site		
History of alcohol use			Nasopharynx	9	0.375
Nondrinker	3	0.125	Larynx	5	0.208
Infrequent (< once/wk)	8	0.333	Hypopharynx	3	0.125
Light (< 3 times/wk)	2	0.083	Oral Cavity	2	0.083
Moderate (> 3 times/wk but < once/d)	6	0.25	Tongue	2	0.083
Heavy (> once/d)	5	0.208	Esophagus	2	0.083
Disease situation			Nasal cavity	1	0.042
Recurrence	10	0.417	AJCC stage		
Local advancement	14	0.583	III	8	0.333
ECOG PS			IVA	13	0.542
0	0	0	IVB	3	0.125
1	22	0.917	Pre-treatment		
2	2	0.083	Surgery	10	0.417
			Radiotherapy	20	0.167
			Chemotherapy	5	0.208

ECOG PS: Eastern cooperative oncology group performance status; AJCC: American joint committee on cancer.

Adverse event

Adverse events were assessed over the course of the study. All patients showed some level of hematological toxicities, most of which required cell-stimulating factor support and/or blood transfusion treatments. Commonly observed adverse events included mucositis, fatigue, nausea, pain, infection, electrolyte disturbances, and dermatitis. Due to grade 3-4 hematological toxicities, only about 25% of patients completed the designed concomitant chemoradiotherapy protocol without interruption. Grade 3-4 toxicities included hematological toxicities (75%), including leukopenia in 18 (75%) patients, neutropenia in 10 (42%) patients, thrombocytopenia in 13 (54%) patients and anemia in 4 (17%) patients. The most common grade 3-4 non-hematological toxicity seen were mucositis in 17 (71%) patients, followed by pain in 5 (21%) patients, electrolyte disturbances in 4 (17%) patients, cardiotoxicity in 3 (12.5%) patients, infection in 3 (12.5%), patients and hemorrhage in 3 (12.5%) patients. Less common long-term adverse events included neuropathy, cervical stenosis and fibrosis (difficulty opening the mouth). Eighteen patients (75%) needed intravenous nutritional support (Table 3).

Table 2 Therapeutic evaluation

Indexes	Number (n)	Percentage (%)
CR	8	33.3
PR	16	66.7
SD	0	0
ORR	24	100
DCR	24	100

CR: Complete response; PR: Partial response; SD: Stable disease; ORR: Objective response rate; DCR: Disease control rate.

Table 3 Adverse event (*n* = 24)

Adverse events	Grade					
	1	2	3	4	1-4	3-4
Hematologic	2	5	7	11	24 (100%)	18 (75%)
Leukopenia	1	5	14	4	24 (100%)	18 (75%)
Neutropenia	7	4	9	1	21 (87.5%)	10 (41.7%)
Thrombocytopenia	6	3	6	7	22 (91.7%)	13 (54.2%)
Anemia	10	10	4	0	24 (100%)	4 (16.7%)
Mucositis	0	4	2	15	21 (87.5%)	17 (70.8%)
Fatigue	10	9	0	0	19 (79.2%)	0 (0%)
Nausea	2	10	0	0	12 (50%)	0 (0%)
Pain	1	8	3	0	12 (50%)	3 (12.5%)
Infection	4	6	2	0	12 (50%)	2 (8.3%)
Electrolyte disturbance	6	2	4	0	12 (50%)	4 (16.7%)
Dermatitis	8	1	0	2	11 (45.8%)	2 (8.3%)
Constipation	10	2	0	0	12 (50%)	0 (0%)
Hemorrhage	1	0	2	1	4 (16.7%)	3 (12.5%)
Hepatotoxicity	14	4	1	0	19 (79.2%)	1 (4.2%)
Renal toxicity	2	0	0	0	2 (8.3%)	0 (0%)
Cardiotoxicity	0	0	2	4	6 (25%)	6 (25%)
Xerostomia	4	0	0	0	4 (16.7%)	0 (0%)
Neuropathy	5	1	0	0	6 (25%)	0 (0%)

DISCUSSION

The results of this study showed that both ORR and DCR of patients with HNSCC who received concurrent chemoradiotherapy using gemcitabine and nedaplatin were 100%. The one-year OS rate was 75%, and one-year PFS rate was 66.7%. Recurrent HNSCC patients had a poorer prognosis than treatment-naïve patients, and patients who achieved CR had better survival than those who achieved PR. Both the most common grade 1-4 (100%) or grade 3-4 toxicities (75%) were hematological disorders, and the most common grade 3-4 non-hematological toxicity was mucositis in 17 (71%) patients. Although gemcitabine plus nedaplatin with concurrent chemoradiotherapy for HNSCC is a therapeutic option with predictable tolerability, considering the high adverse event rate, the optimized dose and schedule must be further explored.

GEM is widely applied in induction chemotherapy, concomitant chemoradiotherapy and salvage chemotherapy in treating HNSCC[13,19,20]. GEM has been thought to have radiosensitizing and synergistic action with cisplatin[11] and demonstrates effective cytotoxicity in HNSCC cell lines[8,21]. In our study, we explored the efficiency and safety of GEM combined with nedaplatin in concurrent

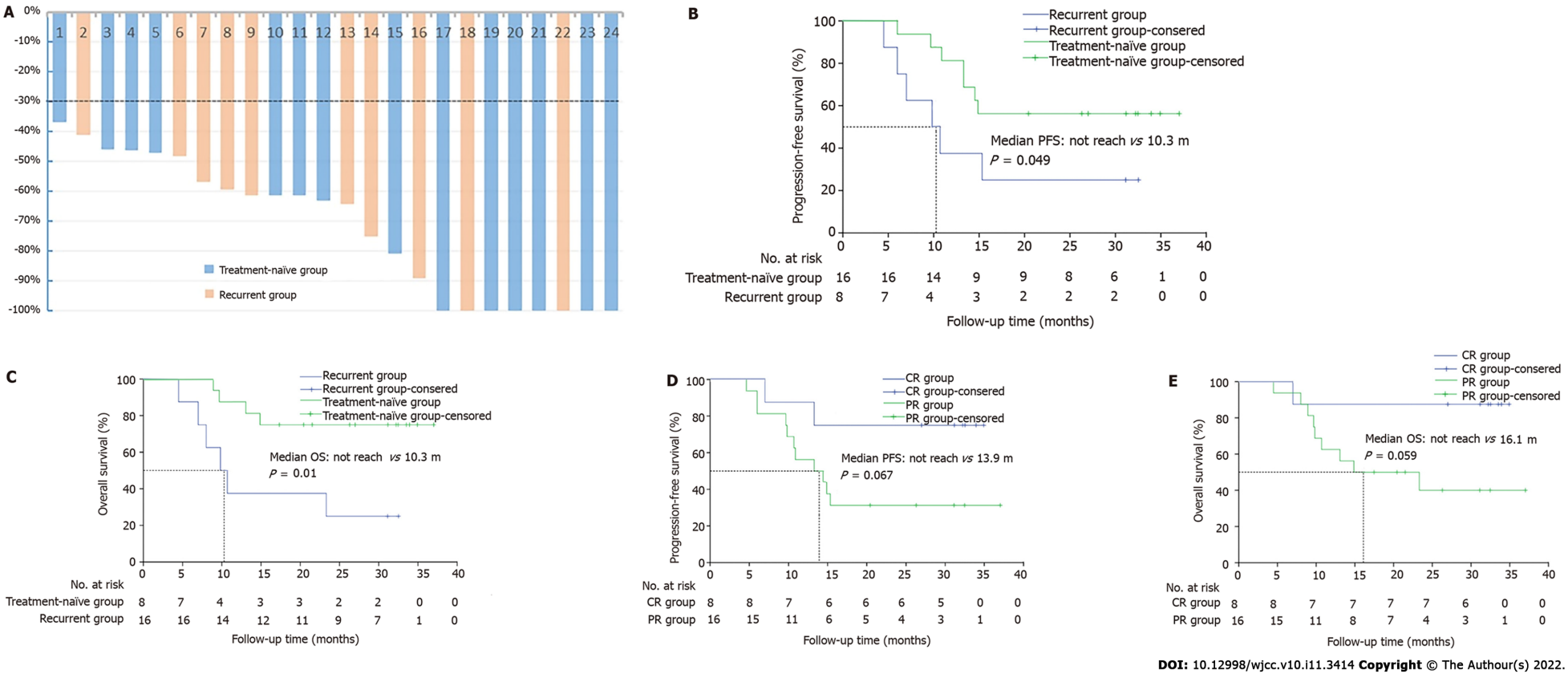

DOI: 10.12998/wjcc.v10.i11.3414

Figure 3 Subgroup analysis. A: Regression ratio of tumor diameter per case; B and C: Kaplan–Meier curve of progressionfree survival (PFS) (B) and overall survival (C) between recurrent subgroup and treatment-naïve subgroup; D and C: Kaplan–Meier curve of PFS (D) and OS (E) between complete response subgroup and partial response subgroup.

chemoradiotherapy. Although all patients had stage III or IV disease, it was encouraging to see an ORR of 100% and a DCR of 100%, which were higher and more promising than the values shown in similar studies[13,22]. However, the one-year survival rate was 70.8%, and the one-year PFS rate was 66.7%, which were slightly lower than those reported in other studies[13,22].

Although the median OS has not been reached, we estimated that the median OS would be more than 2 years. There was no significant difference between our PFS and OS survival figures and those reported in similar concomitant chemoradiation studies[2]. Our CR rate was 33.3%, with a PR rate of 66.7%, compared with a CR rate of 55%-83% reported in other studies[11,24,25]. We posited that these results reflected the prognosis of eight patients who experienced tumor recurrence after surgery and chemotherapy, among whom four patients had received radiotherapy before enrollment. This patient

subgroup that made up 33.3% of total patients was more refractory to treatment than others. In subgroup analysis, the recurrent group had a poorer prognosis than the treatment-naïve group. In the relapsed subgroup, we still observed a 37.5% CR rate, a 62.5% PR rate, a 100% ORR and a 37.5% one-year survival rate. Because of the small sample size, statistical significance was not reached. A similar CCRT study reported that the one-year OS was 43%, and the ORR was 54.5% in recurrent HNSCC patients [26]. Similar results were obtained in locoregional failure research on HNSCC; the one-year OS was 50%, with a 66.6% ORR in the CCRT subset[27].

In another subgroup analysis, patients who achieved CR appeared to achieve longer PFS and OS time than the PR-achieving group. The reason might be that the tumor biological behavior in the CR group was more sensitive to chemotherapy and radiotherapy, suggesting that CR was a better prognostic factor. Because most patients (75%) in our study received subsequent chemotherapy after concomitant chemoradiation, only one case experienced distant metastasis at the cut-off point.

The most common grade 3-4 treatment-related adverse events (75% hematologic toxicities and 70.8% mucositis) necessitated active treatment with G-CSF, IL-11, TPO, blood infusion and oral/intravenous nutritional support. Considering the higher dose of GEM, the hematologic toxicities were more serious than those described in related studies[7,13,20,25]. The grade 1-2 adverse events detected were anemia, fatigue and hepatotoxicity, all of which were relatively easy to treat. Some rare late adverse events were observed, including xerostomia, open mouth difficulty, radiation myelitis, cervical stenosis and fibrosis. Notably, 4 patients (16.7%) died of mouth or nose hemorrhage without obvious disease progression. The hemorrhage was probably due to carotid blowout syndrome (CBS), of which the incidence was 3% to 4.5% in all postoperative patients and 4.5% to 21.1% in patients who received reirradiation[28]. The mortality of CBS was as high as 75%[29]. Two of the four patients received surgery and second radiotherapy, which were both independent risk factors for CBS[30]. There was no chemotherapy-related deaths occurred in our study. Although there were death cases in both groups, the patients died after completion of treatment and in a period of time after discharge, which could not directly prove that the death was related to treatment. Tumor progression and invasion of blood vessels might also lead to death. Therefore, the death event was not considered as a grade 5 adverse event.

Our exploratory study had several limitations. First, the sample number was too small to conduct a deeper analysis and present a more thorough discussion. Second, the follow-up period was not long enough to adequately evaluate OS data or long-term adverse events. Third, the chemotherapeutic drug doses utilized in this study were not optimized and needed to be explored in future studies in order to reduce severe adverse events.

CONCLUSION

In summary, the data presented here demonstrated the efficacy and predictable tolerability of GEM plus nedaplatin in concurrent chemoradiotherapy in the treatment of HNSCC. These data served to add to the compendium of treatment modalities regarding first-line treatment for HNSCC patients with recurrent or locally advanced disease. Nevertheless, further studies are required to optimize the dose and schedule of GEM-based chemoradiotherapy to achieve better disease control and survival while minimizing related adverse events.

ARTICLE HIGHLIGHTS

Research background

As one of the most common malignant tumors, head and neck squamous cell carcinoma (HNSCC) seriously affects the survival and quality of life of patients. At present, in addition to surgery, chemoradiotherapy is the main treatment modality. However, the chemotherapy regimens of concurrent chemoradiotherapy are limited. The activity of gemcitabine and nedaplatin in treating HNSCC has been confirmed.

Research motivation

Our study focused on the efficacy and safety of gemcitabine combined with nedaplatin in concurrent chemoradiotherapy for the treatment of recurrent or metastatic HNSCC. This study provided another therapeutic option of concurrent chemoradiotherapy for HNSCC in the future.

Research objectives

The main objective of this study was to evaluate the effect of gemcitabine combined with nedaplatin on PFS and overall survival (OS) in HNSCC patients who received concurrent radiochemotherapy, and to explore the most suitable dose. The protocol and dose used in our study have proved to be effective and safe for these patients. These results can provide reference for concurrent chemoradiotherapy in the future.

Research methods

This study was a prospective single arm clinical trial. In this study, GN regimen chemotherapy and concurrent radiotherapy were used, imaging and laboratory examination were performed regularly, and RECIST 1.1 was used to evaluate treatment efficacy. The adverse effects were recorded simultaneously. The efficacy evaluation indexes included objective response rate (ORR), disease control rate (DCR), OS and progression free survival (PFS). Kaplan-Meier method was used for survival analysis by SPSS Version 23. These methods can truly and effectively reflect the effectiveness and safety of treatment schemes and are common methods in the world currently. The main objective of this study was to evaluate the effect of gemcitabine combined with nedaplatin on PFS and OS in HNSCC patients who received concurrent radiochemotherapy, and to explore the most suitable dose. The protocol and dose used in our study have proved to be effective and safe for these patients. These results can provide reference for concurrent chemoradiotherapy in the future.

Research results

The ORR and DCR were both 100%. The one-year OS was 75%, and one-year PFS was 66.7%. The most common toxicities were hematological diseases, and the most common non-hematological toxicity was mucositis. The results showed the treatment regimen in this trial was effective and the safety was acceptable, which might provide new choice for HNSCC treatment. However, the results need more large-scale randomized clinical trial to confirm.

Research conclusions

This study provided a new chemotherapy regimen (GN) in concurrent radiochemotherapy for HNSCC.

Research perspectives

It is necessary to explore more effective and safer chemoradiotherapy regimens for the treatment of HNSCC in the future.

ACKNOWLEDGEMENTS

We thank Tianjin Union Medical Center for support during the study.

FOOTNOTES

Author contributions: Wang FW contributed to the conception of the study; Huo RX performed the Clinical trial; Jin JY, Zhuo YX, and Ji XT contributed significantly to follow-up, analysis and manuscript preparation; Cui Y, Wu XJ, Wang YJ, Zhang L, Zhang WH, and Cai YM performed the data analyses and wrote the manuscript; Zheng CC, Cui RX, Wang QY, and Sun Z helped perform the analysis with constructive discussions.

Supported by Tianjin Science and Technology Plan Project, No. 19YFZCSY00170; Tianjin Union Medical center, No. 2019YJ007; and Beijing medical and health foundation, No. F1814B.

Institutional review board statement: The study was reviewed and approved by the China Ethics Committee of Registering Clinical Trials (No. ChiECRCT20170178).

Conflict-of-interest statement: The authors have no conflict of interests to disclose.

Data sharing statement: Technical appendix, statistical code, and dataset are available from the corresponding author at wfengwei2004@163.com. Participants gave informed consent for data sharing.

Country/Territory of origin: China

ORCID number: Rui-Xue Huo 0000-0001-5755-4934; Ying-Ying Jin 0000-0001-9618-0269; Yong-Xue Zhuo 0000-0002-7692-0503; Xiao-Tong Ji 0000-0003-0833-7209; Yu Cui 0000-0002-6942-5985; Xiao-Jing Wu 0000-0002-7638-1888; Yi-Jia Wang 0000-0002-4026-9245; Long Zhang 0000-0003-3151-5093; Wen-Hua Zhang 0000-0003-3730-0501; Yu-Mei Cai 0000-0003-0803-884X; Cheng-Cheng Zheng 0000-0001-8801-7584; Rui-Xue Cui 0000-0002-8588-556X; Qian-Ye Wang 0000-0001-7284-5828; Zhen Sun 0000-0001-5441-0951; Feng-Wei Wang 0000-0001-9522-3183.

Corresponding Author's Membership in Professional Societies: The Standing Committee of Sarcoma Professional Committee of China Anti Cancer Association; The Standing Committee of Tumor Standardized Treatment Committee of Chinese Medical Association; The Standing Committee of Tianjin Radiotherapy Professional Committee; The Tianjin Integrated Traditional Chinese and Western Medicine.

S-Editor: Ma YJ
L-Editor: A
P-Editor: Ma YJ

REFERENCES

1 **Hayes RB**, Ahn J, Fan X, Peters BA, Ma Y, Yang L, Agalliu I, Burk RD, Ganly I, Purdue MP, Freedman ND, Gapstur SM, Pei Z. Association of Oral Microbiome With Risk for Incident Head and Neck Squamous Cell Cancer. *JAMA Oncol* 2018; **4**: 358-365 [PMID: 29327043 DOI: 10.1001/jamaoncol.2017.4777]
2 **Chen W**, Zheng R, Baade PD, Zhang S, Zeng H, Bray F, Jemal A, Yu XQ, He J. Cancer statistics in China, 2015. *CA Cancer J Clin* 2016; **66**: 115-132 [PMID: 26808342 DOI: 10.3322/caac.21338]
3 **Siegel RL**, Miller KD, Jemal A. Cancer Statistics, 2017. *CA Cancer J Clin* 2017; **67**: 7-30 [PMID: 28055103 DOI: 10.3322/caac.21387]
4 **Leemans CR**, Braakhuis BJ, Brakenhoff RH. The molecular biology of head and neck cancer. *Nat Rev Cancer* 2011; **11**: 9-22 [PMID: 21160525 DOI: 10.1038/nrc2982]
5 **Algazi AP**, Grandis JR. Head and neck cancer in 2016: A watershed year for improvements in treatment? *Nat Rev Clin Oncol* 2017; **14**: 76-78 [PMID: 27922045 DOI: 10.1038/nrclinonc.2016.196]
6 **Forastiere AA**, Zhang Q, Weber RS, Maor MH, Goepfert H, Pajak TF, Morrison W, Glisson B, Trotti A, Ridge JA, Thorstad W, Wagner H, Ensley JF, Cooper JS. Long-term results of RTOG 91-11: a comparison of three nonsurgical treatment strategies to preserve the larynx in patients with locally advanced larynx cancer. *J Clin Oncol* 2013; **31**: 845-852 [PMID: 23182993 DOI: 10.1200/JCO.2012.43.6097]
7 **Aguilar-Ponce J**, Granados-García M, Villavicencio V, Poitevin-Chacón A, Green D, Dueñas-González A, Herrera-Gómez A, Luna-Ortiz K, Alvarado A, Martínez-Said H, Castillo-Henkel C, Segura-Pacheco B, De la Garza J. Phase II trial of gemcitabine concurrent with radiation for locally advanced squamous cell carcinoma of the head and neck. *Ann Oncol* 2004; **15**: 301-306 [PMID: 14760126 DOI: 10.1093/annonc/mdh071]
8 **Maseki S**, Ijichi K, Nakanishi H, Hasegawa Y, Ogawa T, Murakami S. Efficacy of gemcitabine and cetuximab combination treatment in head and neck squamous cell carcinoma. *Mol Clin Oncol* 2013; **1**: 918-924 [PMID: 24649271 DOI: 10.3892/mco.2013.159]
9 **Denis F**, Garaud P, Bardet E, Alfonsi M, Sire C, Germain T, Bergerot P, Rhein B, Tortochaux J, Calais G. Final results of the 94-01 French Head and Neck Oncology and Radiotherapy Group randomized trial comparing radiotherapy alone with concomitant radiochemotherapy in advanced-stage oropharynx carcinoma. *J Clin Oncol* 2004; **22**: 69-76 [PMID: 14657228 DOI: 10.1200/JCO.2004.08.021]
10 **Garden AS**, Harris J, Vokes EE, Forastiere AA, Ridge JA, Jones C, Horwitz EM, Glisson BS, Nabell L, Cooper JS, Demas W, Gore E. Preliminary results of Radiation Therapy Oncology Group 97-03: a randomized phase ii trial of concurrent radiation and chemotherapy for advanced squamous cell carcinomas of the head and neck. *J Clin Oncol* 2004; **22**: 2856-2864 [PMID: 15254053 DOI: 10.1200/JCO.2004.12.012]
11 **Vanderveken OM**, Szturz P, Specenier P, Merlano MC, Benasso M, Van Gestel D, Wouters K, Van Laer C, Van den Weyngaert D, Peeters M, Vermorken J. Gemcitabine-Based Chemoradiation in the Treatment of Locally Advanced Head and Neck Cancer: Systematic Review of Literature and Meta-Analysis. *Oncologist* 2016; **21**: 59-71 [PMID: 26712958 DOI: 10.1634/theoncologist.2015-0246]
12 **Saddoughi SA**, Garrett-Mayer E, Chaudhary U, O'Brien PE, Afrin LB, Day TA, Gillespie MB, Sharma AK, Wilhoit CS, Bostick R, Senkal CE, Hannun YA, Bielawski J, Simon GR, Shirai K, Ogretmen B. Results of a phase II trial of gemcitabine plus doxorubicin in patients with recurrent head and neck cancers: serum C_{18}-ceramide as a novel biomarker for monitoring response. *Clin Cancer Res* 2011; **17**: 6097-6105 [PMID: 21791630 DOI: 10.1158/1078-0432.CCR-11-0930]
13 **Halim AA**, Wahba HA, El-Hadaad HA, Abo-Elyazeed A. Concomitant chemoradiotherapy using low-dose weekly gemcitabine *vs* low-dose weekly paclitaxel in locally advanced head and neck squamous cell carcinoma: a phase III study. *Med Oncol* 2012; **29**: 279-284 [PMID: 21279703 DOI: 10.1007/s12032-010-9811-x]
14 **Lee MY**, Jung KS, Kim HS, Lee JY, Lim SH, Kim M, Jung HA, Kim SM, Sun JM, Ahn MJ, Lee J, Park SH, Yi SY, Hwang IG, Lee SC, Ahn HK, Lim DH, Lee SI, Park KW. Weekly docetaxel and gemcitabine in previously treated metastatic esophageal squamous cell carcinoma. *World J Gastroenterol* 2015; **21**: 4268-4274 [PMID: 25892878 DOI: 10.3748/wjg.v21.i14.4268]
15 **Huang J**, Fan QX, Chen L, Liu AN, Cai RG, Hao XZ, Wang JW, Sun Y. Long-term outcomes of gemcitabine and cisplatin in patients with recurrent or metastatic esophageal squamous cell carcinoma: a phase II trial. *Chin Med J (Engl)* 2011; **124**: 4012-4017 [PMID: 22340334]
16 **Zhang P**, Feng FY, Wu LY, Hu Y, Liu JW, Gao YJ, Guan XQ, Nan KJ, Suo AL, Wang XW, Zhang MH, Zhang WD, Li CW, Zhang Y, Zhao JB. [Phase II multicenter clinical trial of nedaplatin in the treatment of malignant tumors]. *Zhonghua Zhong Liu Za Zhi* 2006; **28**: 230-234 [PMID: 16875614]
17 **Fuwa N**, Kodaira T, Furutani K, Tachibana H, Nakamura T, Daimon T. Chemoradiation therapy using radiotherapy, systemic chemotherapy with 5-fluorouracil and nedaplatin, and intra-arterial infusion using carboplatin for locally advanced head and neck cancer - Phase II study. *Oral Oncol* 2007; **43**: 1014-1020 [PMID: 17258494 DOI:

10.1016/j.oraloncology.2006.11.019]
18 **Lai PC**, Chiu TH, Huang YT. Overexpression of BDNF and TrkB in human bladder cancer specimens. *Oncol Rep* 2010; **24**: 1265-1270 [PMID: 20878119 DOI: 10.3892/or_00000981]
19 **Zhang L**, Huang Y, Hong S, Yang Y, Yu G, Jia J, Peng P, Wu X, Lin Q, Xi X, Peng J, Xu M, Chen D, Lu X, Wang R, Cao X, Chen X, Lin Z, Xiong J, Xie C, Li Z, Pan J, Li J, Wu S, Lian Y, Yang Q, Zhao C. Gemcitabine plus cisplatin *vs* fluorouracil plus cisplatin in recurrent or metastatic nasopharyngeal carcinoma: a multicentre, randomised, open-label, phase 3 trial. *Lancet* 2016; **388**: 1883-1892 [PMID: 27567279 DOI: 10.1016/S0140-6736(16)31388-5]
20 **El Deen DA**, Toson EA, El Morsy SM. Gemcitabine-based induction chemotherapy and concurrent with radiation in advanced head and neck cancer. *Med Oncol* 2012; **29**: 3367-3373 [PMID: 22678924 DOI: 10.1007/s12032-012-0269-x]
21 **Zhu MH**, Ji SL, Zhang CY, Cui L, Xiong L, Zheng HL. DNA microarray reveals ZNF195 and SBF1 are potential biomarkers for gemcitabine sensitivity in head and neck squamous cell carcinoma cell lines. *Int J Clin Exp Pathol* 2014; **7**: 1514-1523 [PMID: 24817947]
22 **Ali EM**, Abdelraheem AG. Concurrent radiotherapy and chemotherapy for locally advanced squamous cell carcinoma of the head and neck. *Head Neck Oncol* 2011; **3**: 48 [PMID: 22085617 DOI: 10.1186/1758-3284-3-48]
23 **Specenier PM**, Van den Weyngaert D, Van Laer C, Weyler J, Van den Brande J, Huizing MT, Dyck J, Schrijvers D, Vermorken JB. Phase II feasibility study of concurrent radiotherapy and gemcitabine in chemonaive patients with squamous cell carcinoma of the head and neck: long-term follow up data. *Ann Oncol* 2007; **18**: 1856-1860 [PMID: 17823386 DOI: 10.1093/annonc/mdm346]
24 **Iqbal H**, Jamshed A, Bhatti AB, Hussain R, Jamshed S, Irfan M, Hameed N, Illyas A. Five-year follow-up of concomitant accelerated hypofractionated radiation in advanced squamous cell carcinoma of the buccal mucosa: a retrospective cohort study. *Biomed Res Int* 2015; **2015**: 963574 [PMID: 26075278 DOI: 10.1155/2015/963574]
25 **Chauhan A**, Singh H, Sharma T, Manocha KK. Gemcitabine concurrent with radiation therapy for locally advanced head and neck carcinomas. *Afr Health Sci* 2008; **8**: 149-155 [PMID: 19357741]
26 **Villaflor VM**, Haraf D, Salama JK, Kocherginsky M, Langerman A, Gomez-Abuin G, Beniwal P, Blair EA, Stenson KM, Portugal L, Seiwert T, Williams RD, Dekker AJ, Witt ME, Vokes EE, Cohen EEW. Phase II trial of pemetrexed-based induction chemotherapy followed by concomitant chemoradiotherapy in previously irradiated patients with squamous cell carcinoma of the head and neck. *Ann Oncol* 2011; **22**: 2501-2507 [PMID: 21385883 DOI: 10.1093/annonc/mdq785]
27 **Datta NR**, Nagar YS, Singh S, Naryan L. Loco-regional failures in head and neck cancer: can they be effectively salvaged by nonsurgical therapeutic modalities? *Int J Clin Oncol* 2003; **8**: 31-39 [PMID: 12601540 DOI: 10.1007/s101470300004]
28 **Suárez C**, Fernández-Alvarez V, Hamoir M, Mendenhall WM, Strojan P, Quer M, Silver CE, Rodrigo JP, Rinaldo A, Ferlito A. Carotid blowout syndrome: modern trends in management. *Cancer Manag Res* 2018; **10**: 5617-5628 [PMID: 30519108 DOI: 10.2147/CMAR.S180164]
29 **Alterio D**, Turturici I, Volpe S, Ferrari A, Russell-Edu SW, Vischioni B, Mardighian D, Preda L, Gandini S, Marvaso G, Augugliaro M, Durante S, Arculeo S, Patti F, Boccuzzi D, Casbarra A, Starzynska A, Santoni R, Jereczek-Fossa BA. Carotid blowout syndrome after reirradiation for head and neck malignancies: a comprehensive systematic review for a pragmatic multidisciplinary approach. *Crit Rev Oncol Hematol* 2020; **155**: 103088 [PMID: 32956946 DOI: 10.1016/j.critrevonc.2020.103088]
30 **Chiesa Estomba CM**, Betances Reinoso FA, Osorio Velasquez A, Castro Macia O, Gonzalez Cortés MJ, Araujo Nores J. Carotid blowout syndrome in patients treated by larynx cancer. *Braz J Otorhinolaryngol* 2017; **83**: 653-658 [PMID: 27789194 DOI: 10.1016/j.bjorl.2016.08.013]

World Journal of Clinical Cases

Submit a Manuscript: https://www.f6publishing.com

World J Clin Cases 2022 April 16; 10(11): 3426-3435

DOI: 10.12998/wjcc.v10.i11.3426

ISSN 2307-8960 (online)

META-ANALYSIS

Effect of enhanced recovery after surgery on inflammatory bowel disease surgery: A meta-analysis

Dong Peng, Yu-Xi Cheng, Wei Tao, Hua Tang, Guang-Yan Ji

Specialty type: Gastroenterology and hepatology

Provenance and peer review: Unsolicited article; Externally peer reviewed.

Peer-review model: Single blind

Peer-review report's scientific quality classification

Grade A (Excellent): A
Grade B (Very good): 0
Grade C (Good): 0
Grade D (Fair): 0
Grade E (Poor): 0

P-Reviewer: Surlin VM, Romania

Received: August 20, 2021
Peer-review started: August 20, 2021
First decision: November 11, 2021
Revised: November 12, 2021
Accepted: February 27, 2022
Article in press: February 27, 2022
Published online: April 16, 2022

Dong Peng, Yu-Xi Cheng, Wei Tao, Hua Tang, Guang-Yan Ji, Department of Gastrointestinal Surgery, The First Affiliated Hospital of Chongqing Medical University, Chongqing 400016, China

Corresponding author: Guang-Yan Ji, PhD, Doctor, Department of Gastrointestinal Surgery, The First Affiliated Hospital of Chongqing Medical University, No.1 Youyi Road, Yuanjiagang District, Chongqing 400016, China. jiguangyan168@163.com

Abstract

BACKGROUND

The purpose of enhanced recovery after surgery (ERAS) was to reduce surgical pressure and accelerate postoperative functional recovery. Although the application of biologics in treating inflammatory bowel disease (IBD) has changed treatment strategies, most patients with IBD still require surgery.

AIM

To evaluate the advantage of ERAS in IBD surgery.

METHODS

The PubMed, EMBASE and Cochrane Library databases were searched from inception to March 21, 2021 to find eligible studies. The primary outcome was postoperative complications, and the secondary outcomes included operation time, time to first flatus, time to bowel movement, postoperative hospital stay and readmission. The PROSPERO registration ID of this meta-analysis is CRD42021238052.

RESULTS

A total of eight studies involving 1939 patients were included in this meta-analysis. There were no differences in baseline information between the ERAS group and the non-ERAS group. After pooling up all of the data, no significant difference was found between the ERAS group and the non-ERAS group in terms of postoperative overall complications [odds ratio = 0.82, 95% confidence interval (CI) = 0.66 to 1.02, P = 0.08]. The ERAS group had a lower prevalence of anastomotic fistula (odds ratio = 0.36, 95%CI = 0.13 to 0.95, P = 0.04), less time to first flatus [mean difference (MD) = -2.03, 95%CI = -3.89 to -0.17, P = 0.03], less time to bowel movement (MD = -1.08, 95%CI = -1.60 to -0.57, P < 0.01) and shorter postoperative hospital stays (MD = -1.99, 95%CI = -3.27 to -0.71, P < 0.01) than the non-ERAS group.

CONCLUSION
ERAS was effective for the quicker recovery in IBD surgery and did not lead to increased complications.

Key Words: Enhanced recovery after surgery; Inflammatory bowel disease; Meta-analysis

Core Tip: The purpose of this meta-analysis was to evaluate the safety and efficacy of enhanced recovery after surgery in inflammatory bowel disease surgery. In conclusion, enhanced recovery after surgery was effective for the quicker recovery in inflammatory bowel disease surgery and did not lead to increased complications.

Citation: Peng D, Cheng YX, Tao W, Tang H, Ji GY. Effect of enhanced recovery after surgery on inflammatory bowel disease surgery: A meta-analysis. *World J Clin Cases* 2022; 10(11): 3426-3435
URL: https://www.wjgnet.com/2307-8960/full/v10/i11/3426.htm
DOI: https://dx.doi.org/10.12998/wjcc.v10.i11.3426

INTRODUCTION

Enhanced recovery after surgery (ERAS) or fast-track surgery programs were first proposed by Kehlet [1], and the purpose of ERAS was to reduce surgical pressure and accelerate postoperative functional recovery[2]. The ERAS protocol involves a series of interventions during the perioperative period, including preoperative short fasting, intraoperative epidural anesthesia, minimally invasive surgery, postoperative pain management and nutritional care[3-5]. Due to its significant advantages and safety, ERAS has developed rapidly over the past decade[6]. In recent years, ERAS has been applied to various surgical fields, including gastrectomy[7], cardiac surgery[8], esophageal cancer surgery and colorectal surgery[9,10].

Although the application of biologics in treating inflammatory bowel disease has changed treatment strategies, most patients with inflammatory bowel disease (IBD) still require surgery[11,12]. IBD patients are often malnourished and immunosuppressed, which increases the risk of postoperative complications and prolongs the postoperative hospital stay[13]. In addition, reoperation was required in a large population of IBD patients, which might not be suitable for minimally invasive surgery[14]. Furthermore, patients with IBD might experience prolonged postoperative intestinal obstruction due to chronic inflammation of the intestinal wall[15]. Therefore, the application of ERAS in IBD surgery might be limited in these high-risk situations.

A few studies suggest the feasibility of ERAS for IBD patients[16]; however, work comparing the efficiency of ERAS in IBD and non-IBD patients is scant[17]. Therefore, the purpose of this meta-analysis was to evaluate the safety and efficacy of ERAS in IBD surgery.

MATERIALS AND METHODS

This meta-analysis was conducted in accordance with the Preferred Reporting Items for Systematic Reviews and Meta-Analyses (PRISMA) statement[18]. The PROSPERO registration ID is CRD42021238052, and the link is as follows: https://www.crd.york.ac.uk/prospero/display_record.php?ID=CRD42021238052.

Literature search strategy

The PubMed, EMBASE and Cochrane Library databases were searched by two authors independently. The literature search was conducted on March 21, 2021. The search strategy focused on two key words: ERAS and IBD. The search strategy for ERAS was as follows: "enhanced recovery protocol" OR "enhanced recovery after surgery" OR "enhanced recovery" OR "fast track surgery" OR "fast track rehabilitation" OR "fast track" OR "FTS" OR "ERAS". The search strategy for IBD was as follows: "inflammatory bowel disease" OR "Crohn's" OR "Crohn disease" OR "Crohn's disease" OR "ulcerative colitis" OR "colitis" OR "IBD" OR "CD" OR "UC". Then, we used "AND" to combine these two search strategies, and the publication language was restricted to English in this search.

Inclusion and exclusion criteria

The inclusion criteria were as follows: 1, patients who underwent surgery for CD or UC; 2, the ERAS and non-ERAS protocols were both reported; and 3, reported at least one of the surgical outcomes, including operation time, complications, time to first flatus, time to bowel movement, postoperative hospital stay and readmission. The exclusion criteria were as follows: 1, reviews, letters, case reports, comments or conferences; and 2, publications with insufficient data that could not be extracted. For studies with overlapping patient groups, the most recent study or the study with the larger sample size were included. Disagreement regarding inclusion and exclusion were resolved by discussion between the two authors.

Study selection

The databases were searched by the two authors. First, the titles and abstracts were screened for relevant studies. Second, the full texts were evaluated based on the inclusion and exclusion criteria. Disagreements were discussed, and a final judgment was made by a third author if disagreement occurred.

Data extraction

The data were extracted and cross-checked by two authors. The extracted data included first author, study date, study design, country, publishing year, patients' baseline information, sample size, operation time, complications, time to first flatus, time to bowel movement, postoperative hospital stay and readmission.

Outcomes

The primary outcome of the current meta-analysis was postoperative complications, which were graded based on the Clavien-Dindo classification[19]. Secondary outcomes included operation time, time to first flatus, time to bowel movement, postoperative hospital stays and readmission.

Quality assessment

The Newcastle-Ottawa Scale was used to evaluate the quality of the included studies[20]. High-quality studies are indicated by a score of 9 points, medium-quality studies have scores from 7-8 points, and low-quality studies have scores less than 7 points[21].

Statistical analysis

In the current meta-analysis, continuous variables are presented as the mean ± standard deviation, and categorical variables are presented as proportions. For dichotomous and continuous variables, odds ratios (ORs) and mean differences (MDs) were calculated, and 95% confidence intervals (CIs) were calculated. The I^2 value and the results of the chi-squared test were used to assess the statistical heterogeneity[22,23]. High heterogeneity was considered when $I^2 > 50\%$; in such cases, the random effects model was used, and $P < 0.1$ was considered statistically significant. The fixed effects model was used when $I^2 \leq 50\%$, and $P < 0.05$ was considered statistically significant. This meta-analysis was performed with RevMan 5.3 (The Cochrane Collaboration, London, United Kingdom).

RESULTS

Study selection

A total of 602 studies (138 studies in PubMed, 332 studies in EMBASE and 132 studies in the Cochrane Library) were retrieved in the initial search, and 483 studies were screened after excluding duplicated records. The titles and abstracts were screened, and then, 52 studies were left for full-text assessment. Finally, a total of eight studies[16,24-30] that compared the surgical outcomes of IBD patients between ERAS and non-ERAS protocols were included (Figure 1).

Patient characteristics and quality assessment of the included studies

A total of eight studies including 1939 patients were included in this meta-analysis. The publication years ranged from 2012- 2021, and the study dates ranged from 2000-2019. There were six retrospective studies, one observational study and one randomized controlled trial (RCT). Three studies were conducted in United States, two studies were conducted in Italy, one study was conducted in China, one study was conducted in France and one study was conducted in the United Kingdom. The sample size and the scores of the Newcastle-Ottawa Scale of each study are shown in Table 1.

Baseline information

The baseline information, including age, sex, body mass index, American Society of Anesthesia and surgical methods, was pooled, and no differences were found between the ERAS group and the non-

Table 1 Characteristics of the studies included in the meta-analysis

Ref.	Year	Study date	Study design	Single/Multi center	Disease type	Country	Sample size	NOS
Spinelli *et al*[24]	2012	January 2008 to September 2011	Retrospective	Multi center	CD	Italy	90	7
Mineccia *et al*[25]	2020	May 2007 to December 2018	Observational	Single center	CD	Italy	94	8
Liska *et al*[26]	2019	January 2015 to April 2017	Retrospective	Single center	CD and UC	United States	671	8
D'Andrea *et al*[27]	2020	January 2013 to December 2018	Retrospective	Single center	CD and UC	United States	753	8
Zhu *et al*[28]	2018	December 2015 to December 2016	RCT	Single center	CD	China	32	8
Vrecenak *et al*[29]	2014	December 2000 to December 2010	Retrospective	Single center	CD	United States	71	7
West *et al*[30]	2013	January 2005 to January 2011	Retrospective	Multi center	CD and UC	United Kingdom	68	8
Meunier *et al*[16]	2021	November 2015 to December 2019	Retrospective	Multi center	Unknown	France	160	8

CD: Crohn's disease; RCT: Randomized controlled trial; UC: Ulcerative colitis; NOS: Newcastle-Ottawa scale.

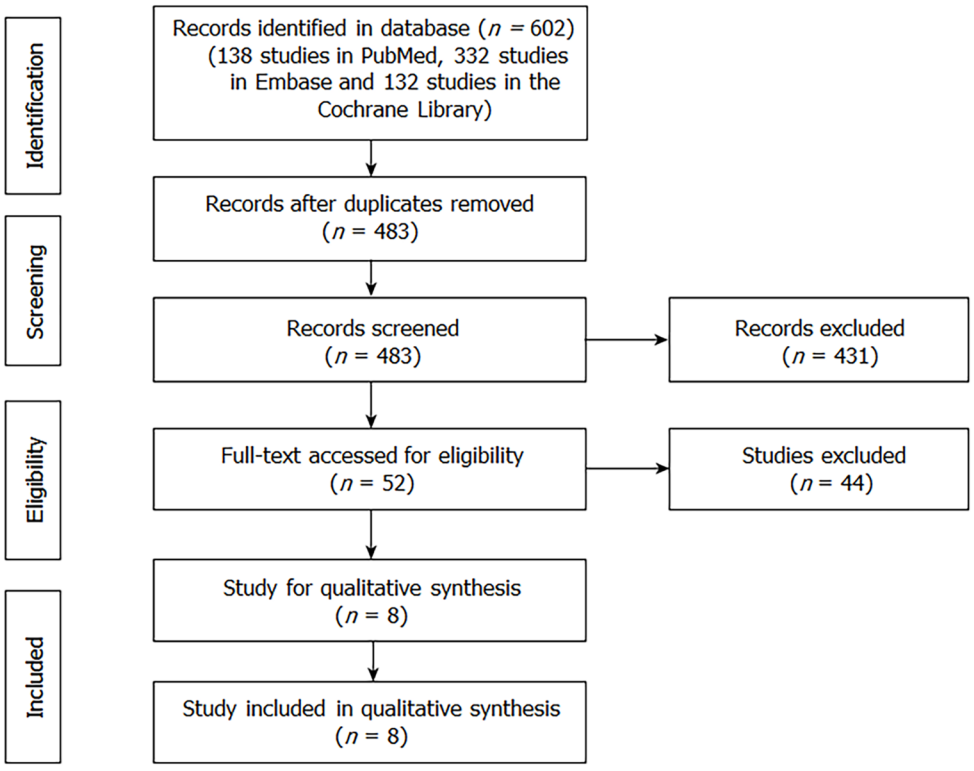

DOI: 10.12998/wjcc.v10.i11.3426

Figure 1 Flowchart of study selection.

ERAS group. The summary meta-analysis of baseline information in each study is shown in Table 2.

Complications

Data regarding overall complications were extracted from the eight studies. After pooling all of the data, no significance was found between the ERAS group and the non-ERAS group (OR = 0.82, 95%CI = 0.66 to 1.02, P = 0.08) (Figure 2). To analyze differences in minor and major complications, we conducted subgroup analysis. However, there were no significant differences between the ERAS group and the non-ERAS group in terms of minor complications (OR = 1.13, 95%CI = 0.83 to 1.55, P = 0.43) (Figure 3A) or major complications (OR = 0.64, 95%CI = 0.34 to 1.20, P = 0.16) (Figure 3B).

Table 2 Summary of characteristics between enhanced recovery after surgery group and non-enhanced recovery after surgery group

Characteristics	Studies	Participants, ERAS/Non-ERAS	Odds ratio/mean difference (95%CI)	Heterogeneity
Baseline information				
Age, yr	2	256/587	0.35 (-1.72, 2.78); P = 0.65	I^2 = 0%; P = 0.59
Male	7	644/1135	1.20 (0.98, 1.46); P = 0.08	I^2 = 0%; P = 0.74
BMI, kg/m^2	3	272/603	-0.56 (-1.19, 0.06); P = 0.08	I^2 = 12%; P = 0.32
ASA 1-2	4	549/1059	0.91 (0.73, 1.14); P = 0.41	I^2 = 0%; P = 0.77
ASA 3-4	4	510/1059	1.10 (0.88, 1.37); P = 0.41	I^2 = 0%; P = 0.77
Laparoscopic surgery	4	563/1023	1.47 (0.90, 2.38); P = 0.12	I^2 = 62%; P = 0.05
Open surgery	4	460/1023	0.68 (0.42, 1.11); P = 0.12	I^2 = 62%; P = 0.05
Surgical outcomes				
Operation time	2	256/587	-0.17 (-23.45, 23.10); P = 0.99	I^2 = 78%; P = 0.03
Time to first flatus	2	36/86	-2.03 (-3.89, -0.17); P = 0.03	I^2 = 94%; P < 0.01
Time to bowel movement	3	81/112	-1.08 (-1.60, -0.57); P < 0.01	I^2 = 71%; P = 0.03
Post-operative hospital stay	4	317/629	-1.99 (-3.27, -0.71); P < 0.01	I^2 = 89%; P < 0.01
Anastomotic fistula	6	639/1200	0.36 (0.13, 0.95); P = 0.04	I^2 = 0%; P = 0.70
Bleeding	4	358/568	1.16 (0.48, 2.76); P = 0.75	I^2 = 0%; P = 0.80
Readmission rate	7	673/1234	0.72 (0.51, 1.00); P = 0.05	I^2 = 0%; P = 0.87

ASA: American Association of Anesthesiologists; BMI: Body mass index; CI: Confidence interval; ERAS: Enhanced recovery after surgery.

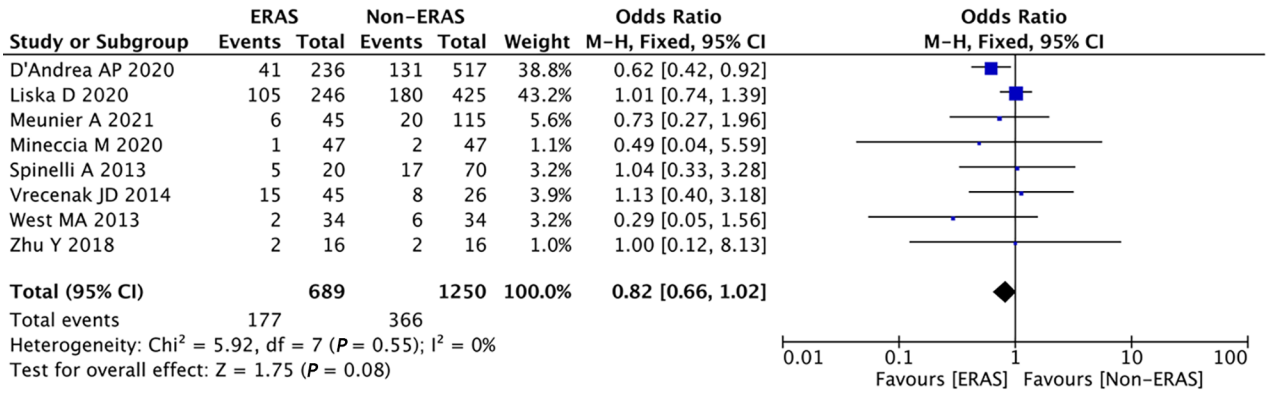

DOI: 10.12998/wjcc.v10.i11.3426

Figure 2 Comparison of postoperative overall complications between the enhanced recovery after surgery group and the non-enhanced recovery after surgery group. CI: Confidence interval; ERAS: Enhanced recovery after surgery.

Other surgical outcomes

Other surgical outcomes were compared between the two groups as well. After pooling all of the data, the ERAS group had less time to first flatus (MD = -2.03, 95%CI = -3.89 to -0.17, P = 0.03), less time to bowel movement (MD = -1.08, 95%CI = -1.60 to -0.57, P < 0.01), less anastomotic fistula (OR = 0.36, 95%CI = 0.13 to 0.95, P = 0.04) and less postoperative hospital stay (MD = -1.99, 95%CI = -3.27 to -0.71, P < 0.01) than the non-ERAS group. However, no significant difference was found in operation time (MD = -0.17, 95%CI = -23.45 to 23.10, P = 0.99), bleeding (OR = 1.16, 95%CI = 0.48 to 2.76, P = 0.75) or readmission rate (OR = 0.72, 95%CI = 0.51 to 1.00, P = 0.05) (Table 2).

Publication bias

Repeated meta-analysis was performed by excluding one study at a time, and the exclusion of any one study did not significantly alter the results. Publication bias for the included studies was based on a visual inspection of the funnel plot. The funnel plot was symmetrical, and no obvious publication bias was found (Figure 4).

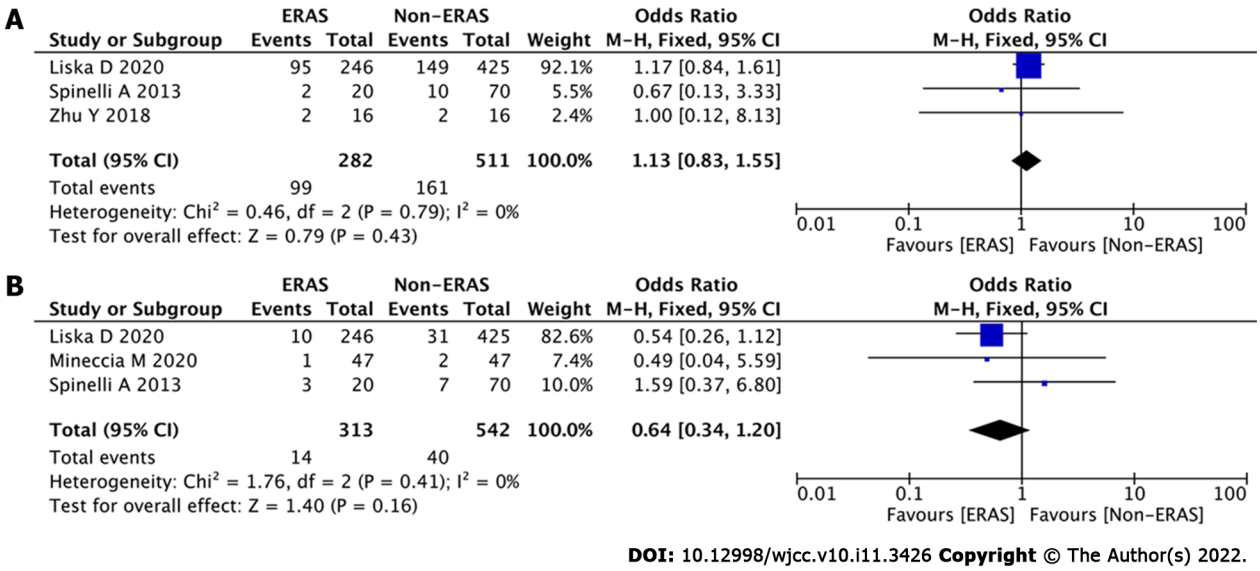

DOI: 10.12998/wjcc.v10.i11.3426

Figure 3 Subgroup analysis of minor and major complications between the enhanced recovery after surgery group and the non-enhanced recovery after surgery group. A: Minor complications; B: Major complications. CI: Confidence interval; ERAS: Enhanced recovery after surgery.

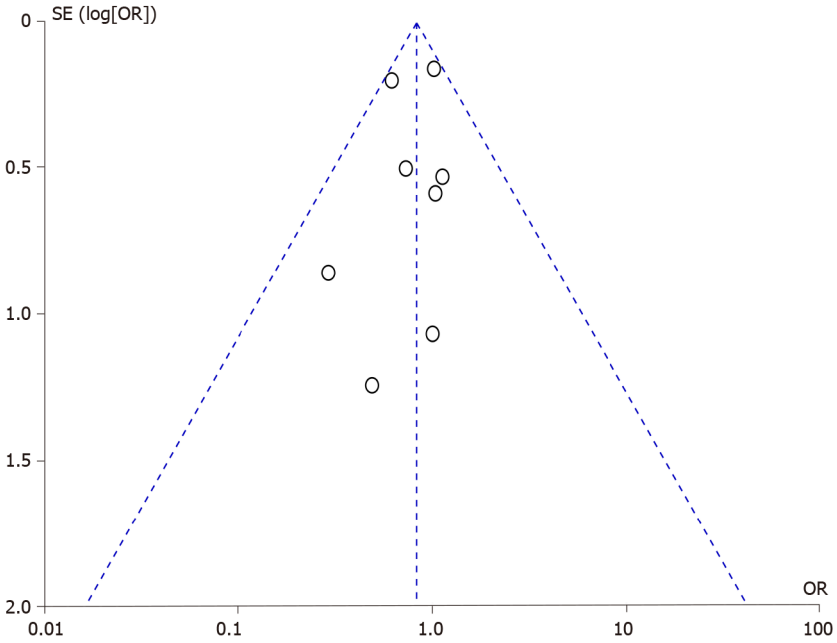

DOI: 10.12998/wjcc.v10.i11.3426

Figure 4 Funnel plot of postoperative complications.

DISCUSSION

A total of eight studies with 1939 patients were included in this meta-analysis. There were no differences between the ERAS group and the non-ERAS group regarding baseline information. After pooling all of the data, no significance was found between the ERAS group and the non-ERAS group in terms of postoperative complications. However, the ERAS group had a lower prevalence of anastomotic fistula, less time to first flatus, less time to bowel movement and shorter postoperative hospital stays than the non-ERAS group.

IBD patients were at a higher risk of complications due to frequent malnutrition, immunosuppression, intra-abdominal abscess, anemia, fistula and intestinal obstruction than patients without IBD [27]. IBD patients who underwent surgery were more likely to have longer hospital stay, increased postoperative wound infections and higher readmission rates[15,31]. Furthermore, a longer pain relief time and a higher incidence of postoperative intestinal obstruction occurred in IBD patients[15]. Therefore, the ERAS protocol seemed to be a challenging task in IBD patients.

In this meta-analysis, we observed that no significance was found between the ERAS group and the non-ERAS group in terms of postoperative complications, and the results were similar to those of previous studies[24-26]. ERAS did not increase the complications after IBD surgery, so ERAS was considered a safe protocol. On the other hand, the ERAS group had a lower likelihood of anastomotic fistula, less time to first flatus, less time to bowel movement and shorter postoperative hospital stays than the non-ERAS group. ERAS might be an effective protocol after IBD surgery. The reduction in hospital stay brings cost savings and reduces the lost work time of family members, improves patient comfort and reduces exposure to hospital-acquired infections at the same time[17]. Moreover, the likelihood anastomotic fistula was significantly reduced in the ERAS group, which confirmed the safety of the ERAS protocol.

A reduction in hospital expenses in ERAS has been reported in other surgeries, including gastric cancer[7], colorectal cancer and esophagus cancer[9,10]. A previous study reported a reduction in hospital expenses; however, the number of studies was not sufficient to be included in this meta-analysis[28]. There was a lack of analgesic use, which required more follow-up studies confirming the beneficial details of ERAS.

A recent study reported that cancer patients undergoing laparoscopic surgery and ERAS treatment might have an immunological advantage[32]. Although no present studies evaluated the immune status of IBD patients undergoing the ERAS protocol, it is interesting to see whether similar benefits could be observed in the future. The success of ERAS depended on the patient's compliance and motivation, and this was important for IBD patients, who were mostly young and often had an active lifestyle[33,34]. Such preferred patients require rapid recovery in order to return to work and social activities quickly. It was also important to involve the patient's caregivers, as they could play an important role in identifying any signs and symptoms after the patient was discharged[24].

There were some certain limitations in the current meta-analysis. First, only eight studies (one RCT and seven non-RCTs) were included. Second, the number of subgroup analyses of time to first flatus, time to bowel movement, operation time and postoperative hospital stay were relatively small, therefore, the results were not robust, and larger studies are needed. Third, differences might occur between primary or recurrent IBD patients who underwent surgery, and furthermore, the outcomes might differ from CD and UC. Fourth, the use of steroids and biologics might affect the surgical outcomes. Therefore, multicenter, multiregional, prospective and high-quality RCTs should be carried out in the future.

CONCLUSION

In conclusion, ERAS was effective for the quicker recovery in IBD surgery and did not lead to increased complications.

ARTICLE HIGHLIGHTS

Research background

To reduce surgical pressure and accelerate postoperative functional recovery, enhanced recovery after surgery (ERAS) has been recommended. Although the application of biologics in treating inflammatory bowel disease has changed treatment strategies, most patients with inflammatory bowel disease (IBD) still require surgery.

Research motivation

Many patients with IBD require surgery. The motivation of this meta-analysis was to examine the effect of ERAS in IBD surgery.

Research objectives

The aim of this meta-analysis was to evaluate the advantage of ERAS in IBD surgery.

Research methods

The PubMed, EMBASE and Cochrane Library databases were searched from inception to March 21, 2021 to find eligible studies. The primary outcome was the postoperative complications. The secondary outcomes included operation time, time to first flatus, time to bowel movement, postoperative hospital stay and readmission.

Research results

A total of eight studies involving 1939 patients were included in this meta-analysis. There was no difference in baseline information between the ERAS group and the non-ERAS group. No significant

difference was found between the ERAS group and the non-ERAS group in terms of postoperative overall complications. The ERAS group had a lower prevalence of anastomotic fistula, less time to first flatus, less time to bowel movement and shorter postoperative hospital stays than the non-ERAS group.

Research conclusions

ERAS was effective for the quicker recovery in IBD surgery and did not lead to increased complications.

Research perspectives

This meta-analysis provided a preliminary conclusion on the effect of ERAS in IBD surgery. Therefore, multicenter, multiregional, prospective and high-quality randomized controlled trials should be carried out in the future.

FOOTNOTES

Author contributions: Tang H and Ji GY are co-corresponding authors; Peng D, Tang H and Ji GY contributed to the quality assessments; Cheng YX and Tao W contributed to data extraction; Peng D, Tao W and Cheng YX contributed to data analysis; Peng D contributed to writing the original draft; Peng D, Tang H and Ji GY contributed to writing and editing; All authors read and approved the final manuscript.

Conflict-of-interest statement: The authors declare that they have no competing interests.

PRISMA 2009 Checklist statement: The authors have read the PRISMA 2009 Checklist, and the manuscript was prepared and revised according to the PRISMA 2009 Checklist.

Country/Territory of origin: China

ORCID number: Dong Peng 0000-0003-4050-4337; Yu-Xi Cheng 0000-0002-9220-7855; Wei Tao 0000-0002-3149-0642; Hua Tang 0000-0001-5068-1391; Guang-Yan Ji 0000-0003-4088-9636.

S-Editor: Ma YJ
L-Editor: Filipodia
P-Editor: Ma YJ

REFERENCES

1 **Kehlet H**. Multimodal approach to control postoperative pathophysiology and rehabilitation. *Br J Anaesth* 1997; **78**: 606-617 [PMID: 9175983 DOI: 10.1093/bja/78.5.606]
2 **Wilmore DW**, Kehlet H. Management of patients in fast track surgery. *BMJ* 2001; **322**: 473-476 [PMID: 11222424 DOI: 10.1136/bmj.322.7284.473]
3 **Lassen K**, Soop M, Nygren J, Cox PB, Hendry PO, Spies C, von Meyenfeldt MF, Fearon KC, Revhaug A, Norderval S, Ljungqvist O, Lobo DN, Dejong CH; Enhanced Recovery After Surgery (ERAS) Group. Consensus review of optimal perioperative care in colorectal surgery: Enhanced Recovery After Surgery (ERAS) Group recommendations. *Arch Surg* 2009; **144**: 961-969 [PMID: 19841366 DOI: 10.1001/archsurg.2009.170]
4 **Kehlet H**. Fast-track colonic surgery: status and perspectives. *Recent Results Cancer Res* 2005; **165**: 8-13 [PMID: 15865015 DOI: 10.1007/3-540-27449-9_2]
5 **Ramírez JM**, Blasco JA, Roig JV, Maeso-Martínez S, Casal JE, Esteban F, Lic DC; Spanish working group on fast track surgery. Enhanced recovery in colorectal surgery: a multicentre study. *BMC Surg* 2011; **11**: 9 [PMID: 21489315 DOI: 10.1186/1471-2482-11-9]
6 **Kehlet H**, Wilmore DW. Evidence-based surgical care and the evolution of fast-track surgery. *Ann Surg* 2008; **248**: 189-198 [PMID: 18650627 DOI: 10.1097/SLA.0b013e31817f2c1a]
7 **Wang LH**, Zhu RF, Gao C, Wang SL, Shen LZ. Application of enhanced recovery after gastric cancer surgery: An updated meta-analysis. *World J Gastroenterol* 2018; **24**: 1562-1578 [PMID: 29662294 DOI: 10.3748/wjg.v24.i14.1562]
8 **Jawahar K**, Scarisbrick AA. Parental perceptions in pediatric cardiac fast-track surgery. *AORN J* 2009; **89**: 725-731 [PMID: 19348820 DOI: 10.1016/j.aorn.2008.11.029]
9 **Triantafyllou T**, Olson MT, Theodorou D, Schizas D, Singhal S. Enhanced recovery pathways vs standard care pathways in esophageal cancer surgery: systematic review and meta-analysis. *Esophagus* 2020; **17**: 100-112 [PMID: 31974853 DOI: 10.1007/s10388-020-00718-9]
10 **Ni X**, Jia D, Chen Y, Wang L, Suo J. Is the Enhanced Recovery After Surgery (ERAS) Program Effective and Safe in

Laparoscopic Colorectal Cancer Surgery? *J Gastrointest Surg* 2019; **23**: 1502-1512 [PMID: 30859422 DOI: 10.1007/s11605-019-04170-8]

11 **Milsom JW**. Laparoscopic surgery in the treatment of Crohn's disease. *Surg Clin North Am* 2005; **85**: 25-34; vii [PMID: 15619526 DOI: 10.1016/j.suc.2004.10.002]

12 **Sokol H**, Seksik P, Cosnes J. Complications and surgery in the inflammatory bowel diseases biological era. *Curr Opin Gastroenterol* 2014; **30**: 378-384 [PMID: 24840000 DOI: 10.1097/MOG.0000000000000078]

13 **Sica GS**, Biancone L. Surgery for inflammatory bowel disease in the era of laparoscopy. *World J Gastroenterol* 2013; **19**: 2445-2448 [PMID: 23674844 DOI: 10.3748/wjg.v19.i16.2445]

14 **Aytac E**, Stocchi L, Remzi FH, Kiran RP. Is laparoscopic surgery for recurrent Crohn's disease beneficial in patients with previous primary resection through midline laparotomy? *Surg Endosc* 2012; **26**: 3552-3556 [PMID: 22648125 DOI: 10.1007/s00464-012-2361-x]

15 **Dai X**, Ge X, Yang J, Zhang T, Xie T, Gao W, Gong J, Zhu W. Increased incidence of prolonged ileus after colectomy for inflammatory bowel diseases under ERAS protocol: a cohort analysis. *J Surg Res* 2017; **212**: 86-93 [PMID: 28550927 DOI: 10.1016/j.jss.2016.12.031]

16 **Meunier A**, Sorce G, Hardy PY, Coimbra C, Decker E, Joris J. Comparison of outcome after right colectomy with an enhanced recovery programme in patients with inflammatory bowel disease and patients operated on for other conditions: a monocentric retrospective study. *Int J Colorectal Dis* 2021; **36**: 757-763 [PMID: 33423143 DOI: 10.1007/s00384-020-03830-5]

17 **Grass F**, Zhu E, Brunel C, Hübner M, Schoepfer A, Demartines N, Hahnloser D. Crohn's versus Cancer: Comparison of Functional and Surgical Outcomes after Right-Sided Resections. *Dig Dis* 2021; **39**: 106-112 [PMID: 32599599 DOI: 10.1159/000509748]

18 **McInnes MDF**, Moher D, Thombs BD, McGrath TA, Bossuyt PM; and the PRISMA-DTA Group, Clifford T, Cohen JF, Deeks JJ, Gatsonis C, Hooft L, Hunt HA, Hyde CJ, Korevaar DA, Leeflang MMG, Macaskill P, Reitsma JB, Rodin R, Rutjes AWS, Salameh JP, Stevens A, Takwoingi Y, Tonelli M, Weeks L, Whiting P, Willis BH. Preferred Reporting Items for a Systematic Review and Meta-analysis of Diagnostic Test Accuracy Studies: The PRISMA-DTA Statement. *JAMA* 2018; **319**: 388-396 [PMID: 29362800 DOI: 10.1001/jama.2017.19163]

19 **Dindo D**, Demartines N, Clavien PA. Classification of surgical complications: a new proposal with evaluation in a cohort of 6336 patients and results of a survey. *Ann Surg* 2004; **240**: 205-213 [PMID: 15273542 DOI: 10.1097/01.sla.0000133083.54934.ae]

20 **Stang A**. Critical evaluation of the Newcastle-Ottawa scale for the assessment of the quality of nonrandomized studies in meta-analyses. *Eur J Epidemiol* 2010; **25**: 603-605 [PMID: 20652370 DOI: 10.1007/s10654-010-9491-z]

21 **Wells GA**, Shea BJ, O'Connell D, Peterson J, Tugwell P. The Newcastle-Ottawa scale (NOS) for assessing the quality of nonrandomized studies in meta-analyses. 2011. [cited November 1, 2011] Available from: https://www.researchgate.net/publication/261773681_The_Newcastle-Ottawa_Scale_NOS_for_Assessing_the_Quality_of_Non-Randomized_Studies_in_Meta-Analysis

22 **Ioannidis JP**. Interpretation of tests of heterogeneity and bias in meta-analysis. *J Eval Clin Pract* 2008; **14**: 951-957 [PMID: 19018930 DOI: 10.1111/j.1365-2753.2008.00986.x]

23 **Higgins JP**, Thompson SG, Deeks JJ, Altman DG. Measuring inconsistency in meta-analyses. *BMJ* 2003; **327**: 557-560 [PMID: 12958120 DOI: 10.1136/bmj.327.7414.557]

24 **Spinelli A**, Bazzi P, Sacchi M, Danese S, Fiorino G, Malesci A, Gentilini L, Poggioli G, Montorsi M. Short-term outcomes of laparoscopy combined with enhanced recovery pathway after ileocecal resection for Crohn's disease: a case-matched analysis. *J Gastrointest Surg* 2013; **17**: 126-32; discussion p.132 [PMID: 22948838 DOI: 10.1007/s11605-012-2012-5]

25 **Mineccia M**, Menonna F, Germani P, Gentile V, Massucco P, Rocca R, Ferrero A. A retrospective study on efficacy of the ERAS protocol in patients undergoing surgery for Crohn disease: A propensity score analysis. *Dig Liver Dis* 2020; **52**: 625-629 [PMID: 32085992 DOI: 10.1016/j.dld.2020.01.006]

26 **Liska D**, Bora Cengiz T, Novello M, Aiello A, Stocchi L, Hull TL, Steele SR, Delaney CP, Holubar SD. Do Patients With Inflammatory Bowel Disease Benefit from an Enhanced Recovery Pathway? *Inflamm Bowel Dis* 2020; **26**: 476-483 [PMID: 31372647 DOI: 10.1093/ibd/izz172]

27 **D'Andrea AP**, Khetan P, Miller R, Sylla P, Divino CM. Outcomes After Bowel Resection for Inflammatory Bowel Disease in the Era of Surgical Care Bundles and Enhanced Recovery. *J Gastrointest Surg* 2020; **24**: 123-131 [PMID: 31468328 DOI: 10.1007/s11605-019-04362-2]

28 **Zhu Y**, Xiang J, Liu W, Cao Q, Zhou W. Laparoscopy Combined with Enhanced Recovery Pathway in Ileocecal Resection for Crohn's Disease: A Randomized Study. *Gastroenterol Res Pract* 2018; **2018**: 9648674 [PMID: 30534152 DOI: 10.1155/2018/9648674]

29 **Vrecenak JD**, Mattei P. Fast-track management is safe and effective after bowel resection in children with Crohn's disease. *J Pediatr Surg* 2014; **49**: 99-102; discussion 102 [PMID: 24439590 DOI: 10.1016/j.jpedsurg.2013.09.038]

30 **West MA**, Horwood JF, Staves S, Jones C, Goulden MR, Minford J, Lamont G, Baillie CT, Rooney PS. Potential benefits of fast-track concepts in paediatric colorectal surgery. *J Pediatr Surg* 2013; **48**: 1924-1930 [PMID: 24074669 DOI: 10.1016/j.jpedsurg.2013.02.063]

31 **Ban KA**, Berian JR, Liu JB, Ko CY, Feldman LS, Thacker JKM. Effect of Diagnosis on Outcomes in the Setting of Enhanced Recovery Protocols. *Dis Colon Rectum* 2018; **61**: 847-853 [PMID: 29878952 DOI: 10.1097/DCR.0000000000001102]

32 **Veenhof AA**, Vlug MS, van der Pas MH, Sietses C, van der Peet DL, de Lange-de Klerk ES, Bonjer HJ, Bemelman WA, Cuesta MA. Surgical stress response and postoperative immune function after laparoscopy or open surgery with fast track or standard perioperative care: a randomized trial. *Ann Surg* 2012; **255**: 216-221 [PMID: 22241289 DOI: 10.1097/SLA.0b013e31824336e2]

33 **Feroci F**, Kröning KC, Lenzi E, Moraldi L, Borrelli A, Scatizzi M. [The development of a fast track surgery program after laparoscopic colonic surgery in a General Surgery Unit]. *Minerva Chir* 2010; **65**: 127-136 [PMID: 20548268]

34 **Ahmed J**, Khan S, Lim M, Chandrasekaran TV, MacFie J. Enhanced recovery after surgery protocols - compliance and

variations in practice during routine colorectal surgery. *Colorectal Dis* 2012; **14**: 1045-1051 [PMID: 21985180 DOI: 10.1111/j.1463-1318.2011.02856.x]

World Journal of Clinical Cases

Submit a Manuscript: https://www.f6publishing.com

World J Clin Cases 2022 April 16; 10(11): 3436-3448

DOI: 10.12998/wjcc.v10.i11.3436

ISSN 2307-8960 (online)

META-ANALYSIS

Accuracy of ultrasound elastography for predicting breast cancer response to neoadjuvant chemotherapy: A systematic review and meta-analysis

Wei Chen, Li-Xiang Fang, Hai-Lan Chen, Jian-Hua Zheng

Specialty type: Medicine, research and experimental

Provenance and peer review: Unsolicited article; Externally peer reviewed.

Peer-review model: Single blind

Peer-review report's scientific quality classification

Grade A (Excellent): A
Grade B (Very good): 0
Grade C (Good): C
Grade D (Fair): 0
Grade E (Poor): 0

P-Reviewer: Cheungpasitporn W, Sun C

Received: September 12, 2021
Peer-review started: September 12, 2021
First decision: October 25, 2021
Revised: November 9, 2021
Accepted: January 13, 2022
Article in press: January 13, 2022
Published online: April 16, 2022

Wei Chen, Li-Xiang Fang, Hai-Lan Chen, Jian-Hua Zheng, Department of Ultrasound, The Affiliated Hospital of Putian University, Putian 351100, Fujian Province, China

Corresponding author: Jian-Hua Zheng, MD, Doctor, Department of Ultrasound, The Affiliated Hospital of Putian University, No. 999 Dongzhen East Road, Putian 351100, Fujian Province, China. zhengjh0328@sina.com

Abstract

BACKGROUND

Several studies have reported the prognostic value of ultrasound elastography (UE) in patients receiving neoadjuvant chemotherapy (NACT) for breast cancer. However, the assessment of parameters differed between shear-wave elastography and strain elastography in terms of measured elasticity parameter and mode of imaging. It is important, therefore, to assess the accuracy of the two modes of elastography.

AIM

To assess the accuracy of UE for predicting the pathologic complete response (pCR) in breast cancer patients following NACT.

METHODS

A comprehensive and systematic search was performed in the databases of MEDLINE, EMBASE, SCOPUS, PubMed Central, CINAHL, Web of Science and Cochrane library from inception until December 2020. Meta-analysis was performed using STATA software "Midas" package.

RESULTS

A total of 14 studies with 989 patients were included. The pooled sensitivities were 86% [95% confidence interval (CI): 76%-92%] for UE, 77% (95%CI: 68%-84%) for shear-wave elasto-graphy, and 92% (95%CI: 73%-98%) for strain-wave elastography. The pooled score specificities were 86% (95%CI: 80%-90%) for UE, 84% (95%CI: 72%-91%) for shear-wave elasticity, and 87% (95%CI: 81%-92%) for strain-wave elastography. A significant heterogeneity was found among studies based on the chi-square test results and an I^2 statistic > 75%.

CONCLUSION

Strain-wave type of UE can accurately predict the pCR following NACT amongst

breast cancer patients. Studies exploring its accuracy in different ethnic populations are required to strengthen the evidence.

Key Words: Breast cancer; Chemotherapy; Meta-analysis; Ultrasonography validation studies

Core Tip: Several studies have reported the prognostic value of ultrasound elastography (UE) in patients receiving neoadjuvant chemotherapy (NACT) for breast cancer. However, the assessment of parameters differed between shear-wave elastography and strain elastography in terms of measured elasticity parameter and mode of imaging. It is important, therefore, to assess the accuracy of the two modes of elastography. We assessed the accuracy of UE for predicting the pathologic complete response (pCR) in breast cancer patients following NACT. Strain-wave type of UE can accurately predict the pCR following NACT amongst breast cancer patients. Studies exploring its accuracy in different ethnic populations are required to strengthen the evidence.

Citation: Chen W, Fang LX, Chen HL, Zheng JH. Accuracy of ultrasound elastography for predicting breast cancer response to neoadjuvant chemotherapy: A systematic review and meta-analysis. *World J Clin Cases* 2022; 10(11): 3436-3448
URL: https://www.wjgnet.com/2307-8960/full/v10/i11/3436.htm
DOI: https://dx.doi.org/10.12998/wjcc.v10.i11.3436

INTRODUCTION

Neoadjuvant chemotherapy (NACT) has been established as the standard mode of treatment for inflammatory or locally advanced breast cancer. Pathologic complete response (pCR) has been utilized as a surrogate marker for detecting the prognosis or long-term survival following NACT in breast cancer patients[1], with several studies showing a response rate of almost 70% and pCR rate of about 30%[1,2]. Some factors were found to be associated with an increased risk of developing resistance to chemotherapy[3]. Hence, early prediction of the response to NACT in patients with breast cancer is critical.

Ultrasonic elastography (UE) is one of the most commonly used non-invasive imaging methods based on the mechanical properties of the tissue to assess the differences in breast lesion stiffness and elasticity (both quantitatively and qualitatively)[4]. It detects and quantifies the differences in tissue stiffness. Therefore, it can be used as an excellent imaging technique to differentiate benign and malignant breast masses[4]. There are two types of UE employed currently for examining the breast lesions, *i.e.*, shear-wave elastography and strain elastography. Both techniques characterize the breast lesions based on the level of stiffness. Mean stiffness can be used as an effective preoperative predictor of progression of the disease in invasive breast cancer, and maximal stiffness has been used as a predictor of histopathological severity of breast lesions[4].

Breast cancer treatment with NACT might increase the probability of down-staging of the tumors. However, pCR to NACT is highly variable, and the current protocols to predict pCR to NACT are not sensitive enough. Formulating a tailored strategy using validated biomarkers to predict the degree of response to NACT has become a priority nowadays in the research of breast cancer. Several studies have reported the prognostic value of UE in patients receiving NACT for breast cancer. Breast masses with higher aggressive pathological properties can have higher stiffness value, suggesting that UE might provide very useful information to determine the prognosis of the patient[5]. However, the assessment of parameters is different for shear-wave elastography and strain elastography in terms of measured elasticity parameter and mode of imaging. To the best of our knowledge, no meta-analysis has yet assessed the accuracy of the two modes of elastography in predicting the response to NACT in breast cancer patients. The aim of the current study was to systematically search the literature for all studies assessing the accuracy of UE for predicting response to NACT in breast cancer, and pool the data for meta-analysis.

MATERIALS AND METHODS

Inclusion and exclusion criteria

The inclusion criteria were as follows: Studies evaluating the predictive accuracy of UE for pCR

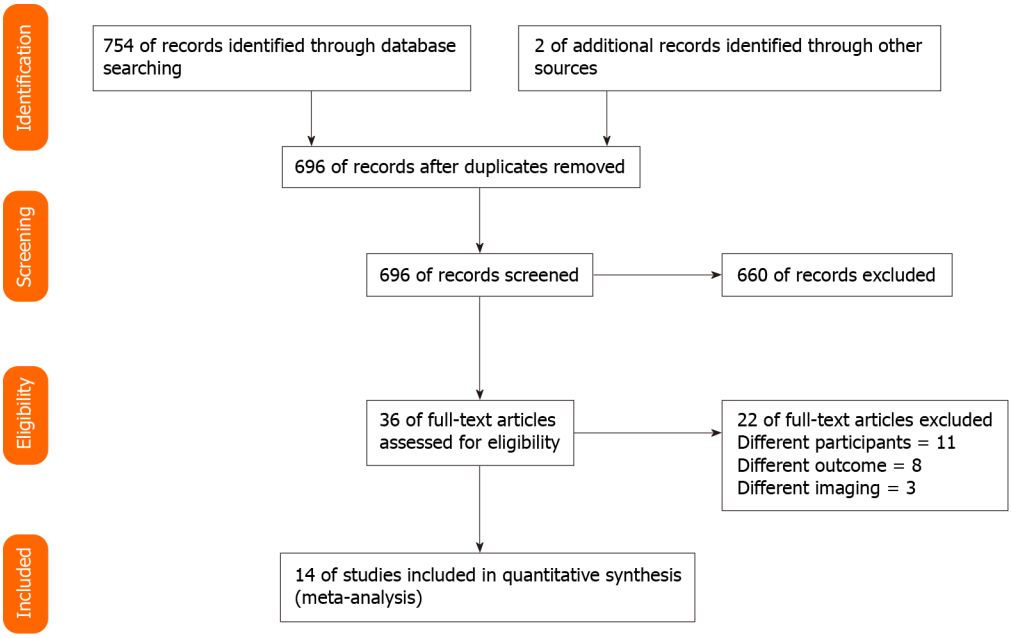

Figure 1 Search strategy.

following NACT in breast cancer patients; studies using histopathological examination as the reference standards for finding the pCR for inclusion in our review; prospective and retrospective studies.

The exclusion criteria were as follows: Studies not reporting the values necessary for pooling the sensitivity and specificity; unpublished studies.

Search strategy

We had a comprehensive search strategy to screen the databases such as MEDLINE, EMBASE, SCOPUS, PubMed Central, CINAHL, Web of Science, and Cochrane library. We did not have any language restriction and time limit for the search was between the inception of database till December 2020. The following search terms were used: "Ultrasound Elastography", "Neoadjuvant Chemotherapy", "Breast Cancer", "Breast Carcinoma", "Validation Studies", "Diagnostic Accuracy Studies", "Pathologic Complete Response", and "Remission". We also hand-searched the bibliographies of the included studies and checked for any missed-out studies matching our eligibility criteria. The details for different search strategies employed for different databases are provided in the Supplementary Material.

Study selection process

Two investigators (LF and HC) were responsible for performing the primary search of the articles by screening the title and abstract, and downloading the relevant full-text publications. The same set of investigators also independently read the retrieved full-texts and checked whether the studies were meeting the eligibility criteria of our review. Disagreements were resolved with assistance from a third author (WC), which helped in reaching a consensus for study selection. We achieved an overall agreement of 97% with a kappa statistic of 0.87.

Data extraction

The responsibility of data extraction from the final included full-text articles was assigned to the primary investigator. Data was extracted using a structured pre-defined form and directly transferred to the STATA software (StataCorp, CollegeStation, TX, United States). This data extraction form consists of the following components: Author and year of publication, country, design, participants, total sample size, study setting, details of UE, reference test, average age, cut-off (mean stiffness/strain ratio), sensitivity, and specificity. The third investigator ensured the data quality by double-checking data entries before performing the meta-analysis.

Risk of bias assessment

Two independent investigators (LF and HC) rated the included studies based on the level of bias risk using the quality assessment of diagnostic accuracy studies-2 (QUADAS-2) tool. The studies were rated for the following domains: Patient selection, conduct & interpretation of the index and reference tests, and flow and timing of outcome assessment[6]. Discrepancies and disagreements during the rating of studies were resolved by the third investigator who helped in achieving the consensus and rated all the studies as unclear, low, or high quality (based on the risk of bias).

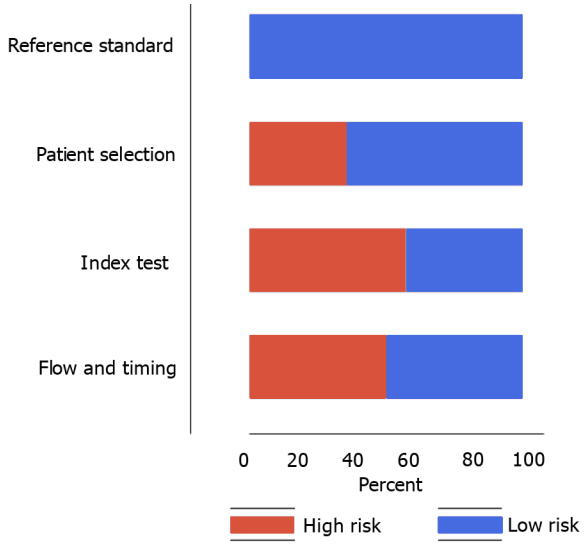

Figure 2 Quality assessment of the included studies based on quality assessment of diagnostic accuracy studies-2 tool (*n* = 19).

Statistical analysis

Meta-analysis was performed using the STATA version 14 software (StataCorp, TX, United States). Sensitivity and specificity were pooled by bivariate method for predicting the pCR following NACT in breast cancer patients using UE. We also estimated other important accuracy parameters such as positive and negative likelihood ratios (LRP and LRN, respectively) and diagnostic odds ratio (DOR) for the predictive utility of UE. We also reported these results separately for shear wave and strain wave elastography. We have reported these results using the following plots: Forest plot to depict pooled specificity and sensitivity, LR scattergram to depict the LRP and LRN, and Fagan plot to depict the pre- and post-test probabilities. LR scattergram consists of the following four quadrants with its interpretation: Left upper quadrant (LRP value > 10, LRN value < 0.1) indicative of confirmation & exclusion diagnostic criterion, right upper quadrant (LRP value > 10, LRN value > 0.1) indicative of confirmation diagnostic criterion, left lower quadrant (LRP value < 10, LRN value < 0.1) indicative of exclusion diagnostic criterion, and right lower quadrant (LRP value < 10, LRN value > 0.1) indicative of neither confirmation nor exclusion diagnostic criterion. "*Summary receiver operator characteristic curve*" (sROC) was used to report the summary predictive accuracy of UE for pCR.

Evaluation of heterogeneity was done by chi-square and I^2 statistic. It is represented graphically by a bivariate box plot. Additional meta-regression analysis was performed to identify the source of the high heterogeneity found in our results. The covariates used in the meta-regression were study design, sample size, mean age, shear or strain wave UE, country, cut-off, and quality related factors. Deeks' test was performed to assess the possibility of publication bias and it is graphically represented by funnel plot.

RESULTS

Study selection

We found a total of 754 records, amongst which 36 were found to be relevant for the full-text retrieval. Full-texts of two additional articles were retrieved after going through the bibliography of the selected articles. Finally, 14 studies with 989 participants have met the eligibility criteria and were included in our review (Figure 1)[7-20].

Characteristics of the studies included

Of 14 studies included in the analysis, 12 were prospective in nature. Six studies were conducted in China. The average age of the patients was 39 to 55 years. We analyzed data from 989 patients to assess the predictive accuracy of UE for pCR after receiving NACT (samples size of individual studies ranged from 15 to 134 patients). In total, seven studies assessed the accuracy of only shear wave elastography, six assessed the accuracy of only strain wave elastography, while only one assessed the accuracy of both shear wave and strain wave elastography. All the studies performed histopathological examination following surgical resection as the reference standard (Table 1).

Table 1 Characteristics of the included studies (*n* = 14)

No	Ref.	Country	Study design	Sample size	Study participants	Type of ultrasound elastography	Cut-off	Reference standard	Mean age (in years)
1	Evans *et al* [7], 2018	United Kingdom	Prospective	64	Patients with breast cancer receiving NACT	Shear wave elastography	Mean stiffness = 50 kPA	Assessment of any invasive cancer cells in the tumour bed at surgical resection after 6 cycles of NACT and an assessment of nodal metastases at axillary surgery	52
2	Evans *et al* [8], 2018	United Kingdom	Prospective	80	Patients with breast cancer receiving NACT	Shear wave elastography	Mean stiffness = 83 kPA	Assessment of any invasive cancer cells in the tumour bed at surgical resection after 6 cycles of NACT and an assessment of nodal metastases at axillary surgery	53
3	Falou *et al* [9], 2013	Canada	Prospective	15	Locally advanced breast cancer patients receiving NACT	Strain wave elastography	Mean strain ratio = 81	Histopathological examination following mastectomy	45
4	Fang *et al* [10], 2019	China	Prospective	60	Breast cancer patients with stage IIa-IIIc (T1-T4; N0-N3; M0) and underwent surgery after receiving NACT	Strain wave elastography	Mean strain ratio = 5.4	Pathological examination after surgical resection	39
5	Fernandes *et al*[11], 2019	Canada	Prospective	92	Patients with biopsy confirmed locally advanced breast cancer receiving NACT	Strain wave elastography	Elastography score = 4	Histopathological examination	55
6	Hayashi *et al*[12], 2012	Japan	Retrospective	55	Histologically confirmed invasive breast cancer before NACT, and they underwent surgery after completion of NACT	Strain wave elastography	Elastography score = 4	Pathologic response was assessed in surgical specimens of the breast with reference to the standards of the Japanese Breast Cancer Society	52
7	Jing *et al* [13], 2016	China	Prospective	62	Patients with diagnosis of breast carcinoma by ultrasound-guided core needle biopsy who received neoadjuvant chemotherapy followed by surgical excision	Shear wave elastography	Stiffness threshold-36.1%	Pathologic assessments involved a 2-step process. First, samples from core needle biopsies were examined to record the histologic and biologic characteristics of the tumours. These findings were usually combined with the clinical features of the patients to predict the response to neoadjuvant chemotherapy. Second, pathologic responses to neoadjuvant chemotherapy were evaluated according to the Miller-Payne grading criteria	49
8	Katyan *et al* [14], 2019	India	Prospective	86	TNM stage III and T3N0 subset of stage IIb breast cancer patients receiving NACT	Strain wave elastography	Strain ratio = 0.1	Histopathological examination	NA
9	Lee *et al* [15], 2015	Korea	Retrospective	71	Women with stage II-III invasive breast cancers who received NACT	Shear wave elastography	Mean stiffness = 98.1 kPA	Histopathological examination	NA
10	Ma *et al* [16], 2017	China	Prospective	71	Women confirmed with invasive breast cancer by ultrasound guided core needle biopsy and underwent NACT and subsequent surgical excision	Shear and strain wave eastography	Stiffness threshold-30.4%; Strain ratio = 6.7	Histopathological examination	47.3
11	Ma *et al* [17], 2020	China	Prospective	43	Breast cancer patients who were confirmed to be HER-2 positive by biopsy and puncture and underwent NACT	Shear wave elastography	Mean stiffness = 30 kPA	Histopathological examination after surgical resection	NA

12	Maier *et al* [18], 2020	Germany	Prospective	134	Histologically confirmed unilateral or bilateral breast cancer and indication for NACT	Shear wave elastography	Shear wave velocity = 3.35	Pathological examinations and immunohistochemistry from the core-cut biopsy before and from the surgical specimen after NACT	52.1
13	Wang *et al* [19], 2019	China	Prospective	65	Patients confirmed *via* biopsy to have breast cancer prior to receiving NACT treatment and they received no other treatment	Strain wave elastography	Strain ratio = 8	Histopathology results of the lesion samples isolated in the surgery were compared with those of the biopsy specimens obtained prior to treatment to determine the response to NACT	48.3
14	Zhang *et al* [20], 2020	China	Prospective	91	Patients diagnosed with invasive breast cancer by ultrasound-guided core needle biopsy and received NACT and subsequent surgical intervention	Shear wave elastography	Stiffness threshold–41.4%	Histopathological examination	46.9

HER: Human epidermal growth factor receptor; kPA: Kilopascals; NA: Not available; NACT: Neoadjuvant chemotherapy; TNM: Tumour node metastasis.

Risk of bias assessment

Risk of bias according to the QUADAS tool is shown in Figure 2. Five out of fourteen studies had a high risk with respect to patient selection domain, eight had a high risk of conduct and interpretation of index test bias, and seven had a high risk of patient flow and interval between index tests and reference standards bias. None of the studies had a high risk of bias with respect to the conduct and interpretation of reference standard.

Predictive accuracy of UE for pCR following NACT

As shown in Figures 3 and 4, the pooled sensitivity and specificity of UE for pCR amongst patients with breast cancer following NACT were 86% [95% confidence interval (CI): 76%-92%] and 86% (95%CI: 80%-90%), respectively. The DOR was 37 (95%CI: 17-77). The LRP was 6 (95%CI: 4-9) and the LRN 0.16 (0.09-0.30). The LRP and LRN in the right lower quadrant of the LR scattergram (Figure 5) indicate that UE cannot be used for confirmation or exclusion of pCR following NACT. As shown in Fagan's nomogram (Figure 6), UE had a good clinical utility for predicting pCR following NACT (positive = 74%; negative = 7%), as it differs significantly from the pre-test probability (32%). Significant heterogeneity was found with a chi-square $P < 0.001$ and $I^2 > 75\%$. Bivariate box plot further confirmed the presence of heterogeneity (Figure 7).

Deek's test for publication bias indicated the absence of publication bias ($P = 0.59$). This was further confirmed by the symmetrically shaped funnel plot (Figure 8). Meta-regression analysis was performed to assess the source of heterogeneity using the covariates. As shown in Figure 9, in the sensitivity model, patient selection ($P < 0.05$) ($P < 0.05$) could be a source of heterogeneity. Patient selection ($P < 0.05$) as well as flow and timing of tests ($P < 0.001$) were potential sources of heterogeneity in the specificity model, and the mean age was responsible for heterogeneity in the joint model ($P < 0.001$).

We next performed a subgroup analysis based on the type of elastography used for predicting pCR after NACT. Eight studies used shear-wave elastography for assessing its prognostic utility. Our results show a pooled sensitivity of 77% and pooled specificity of 84% with a DOR of 17, LRP of 4.8, and LRN of 0.27. Seven studies used strain-wave elastography for assessing its prognostic utility. Our results

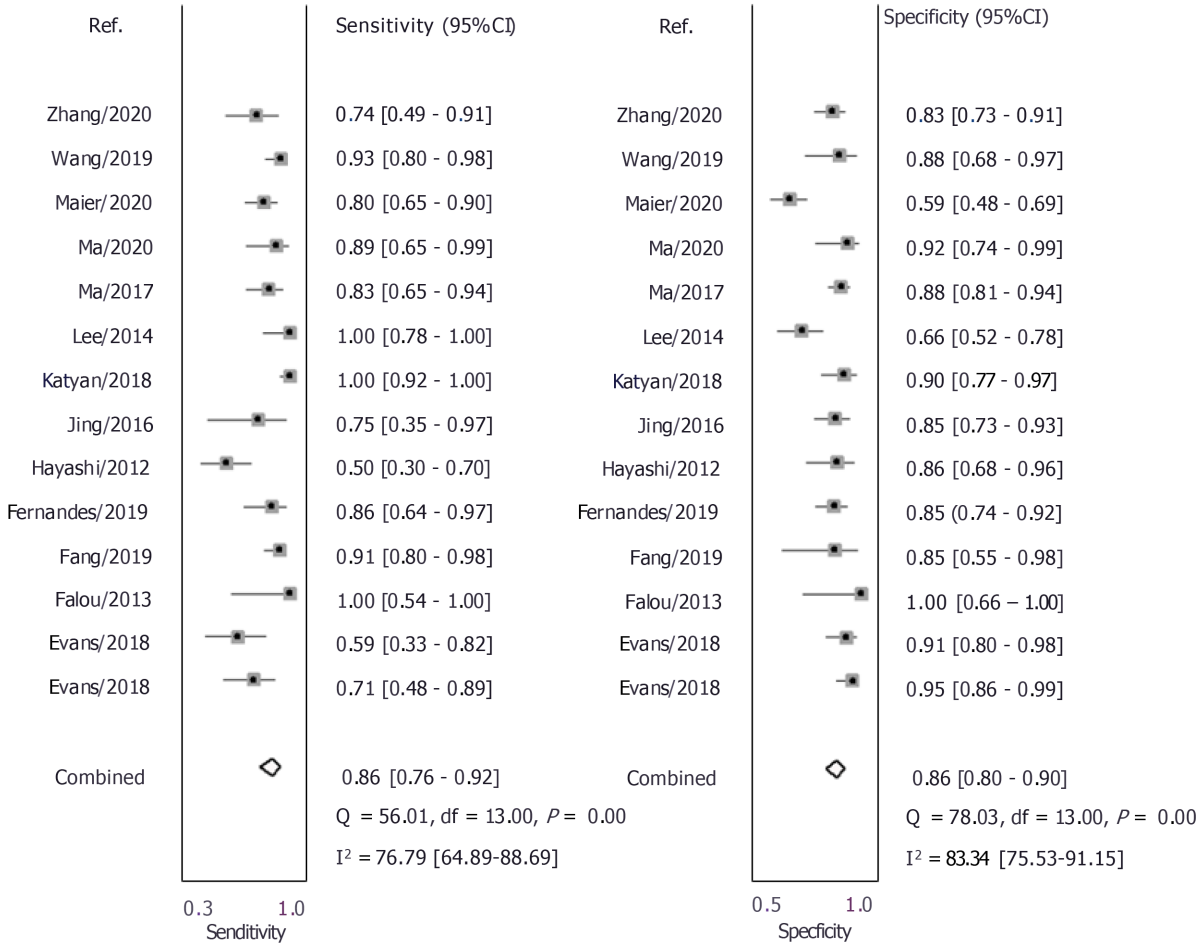

Figure 3 Forest plot showing pooled sensitivity and specificity of ultrasound elastography for predicting pathological complete response following neoadjuvant chemotherapy amongst breast cancer patients. Q: Q statistic; df: Degree of freedom; I^2: I^2 statistic for heterogeneity; CI: Confidence interval.

indicate a pooled sensitivity of 93% and pooled specificity of 87% with a DOR of 87, LRP of 7.4, and LRN of 0.08.

DISCUSSION

Major objectives of performing the NACT are to attain operability, and ensure breast conservation and historical prognostic information. In recent years, the approach shifted towards personalization of the therapy, investigation of new therapies, and identification of response biomarkers. More advanced and accurate prediction of pCR will allow to identify high-risk groups and prevent adverse outcomes by providing more specific management. Developing a fast, easy, and effective screening tool will reduce the financial burden on healthcare system, prevent life-threatening complications, and reduce mortality. However, the utility of UE has not been synthesized to predict the risk of pCR. The main goal of this review was to determine the predictive performance of shear and strain wave ultrasound elastography for the pCR.

A total of 14 studies reporting the utility of UE for predicting pCR following NACT were identified by our systematic search strategy. Most of the studies were prospective and had a low risk of bias. UE had an equal pooled sensitivity and specificity of 86%. Other diagnostic accuracy parameters also were moderate. LR scattergram showed that, since LRN and LRP occupied the right lower quadrant, UE cannot be used for confirming or excluding SAP. The clinical utility of UE was relatively acceptable, with a significant rise in the post-imaging probability compared to the pre-imaging probability on Fagan's nomogram.

Since there are two techniques of UE (shear and strain wave elastography), we determined the better technique by performing a separate subgroup analysis and calculating pooled sensitivity and specificity for each of them. We found strain wave elastography as the better technique with a pooled sensitivity of 93% and specificity of 87% compared to shear wave elastography (77% and 84%). This means that strain elastography can help in effectively ruling out the pCR patients correctly as it had a sensitivity more

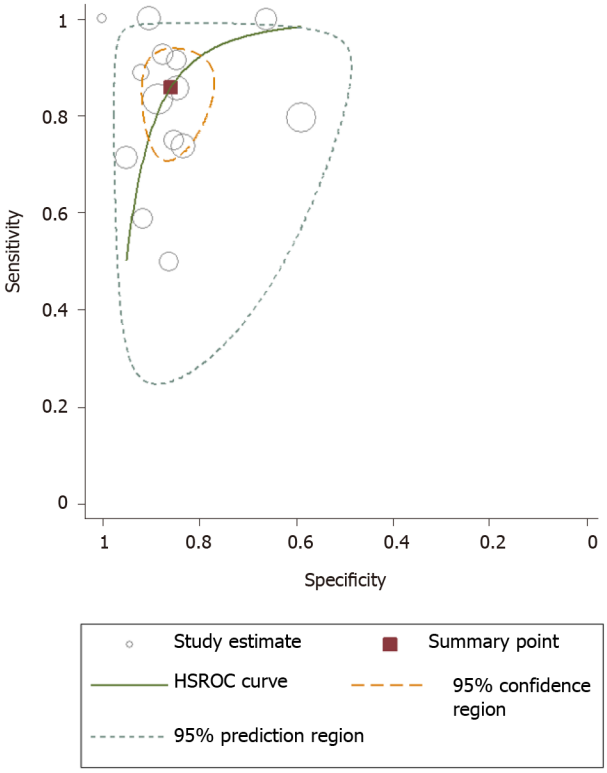

Figure 4 Summary receiver operator characteristic curve of ultrasound elastography for predicting pathological complete response following neoadjuvant chemotherapy amongst breast cancer patients.

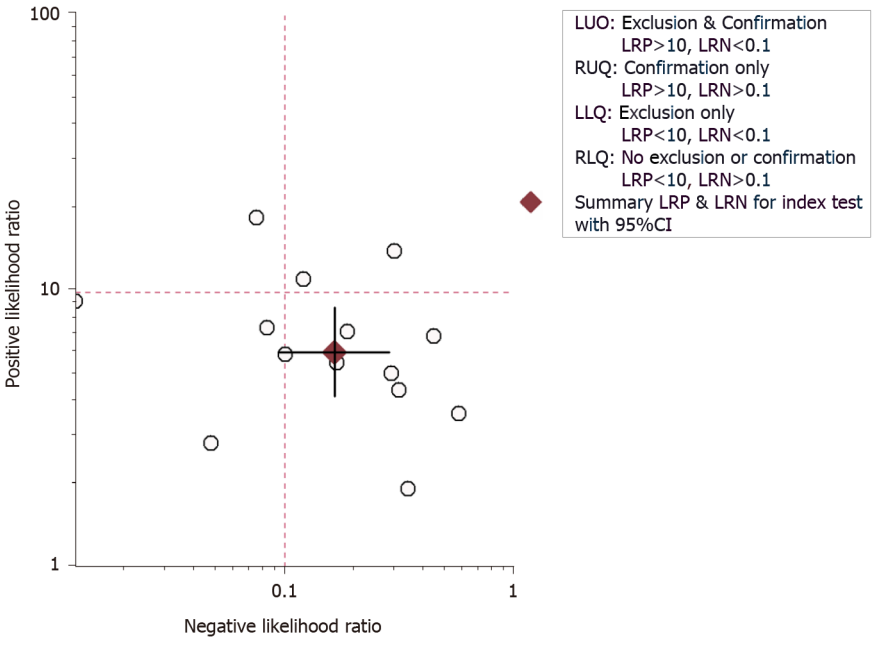

Figure 5 Likelihood scattergram of ultrasound elastography.

than 90%. Strain elastography, therefore, has a major advantage over shear wave elastography, as studies report its good predictive performance for ruling out the patients with pCR.

The accuracy parameters obtained in this review could not be compared, since no similar reviews were conducted in the past. Nevertheless, our results are almost similar to the accuracy of UE in predicting malignant liver lesions or axillary lesions[21,22]. There is a need for additional studies comparing the prognostic performance of this imaging technique with magnetic resonance imaging and other forms of ultrasonography, in order to identify the method with the highest accuracy that can be

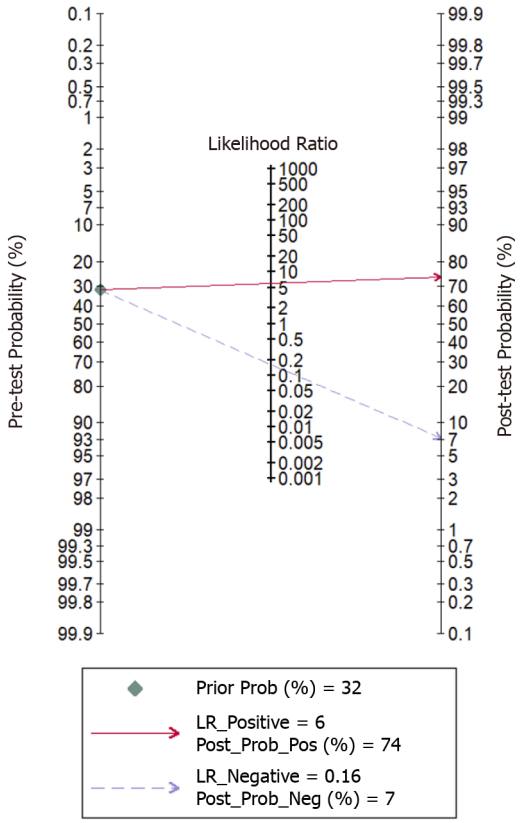

Figure 6 Fagan nomogram of ultrasound elastography.

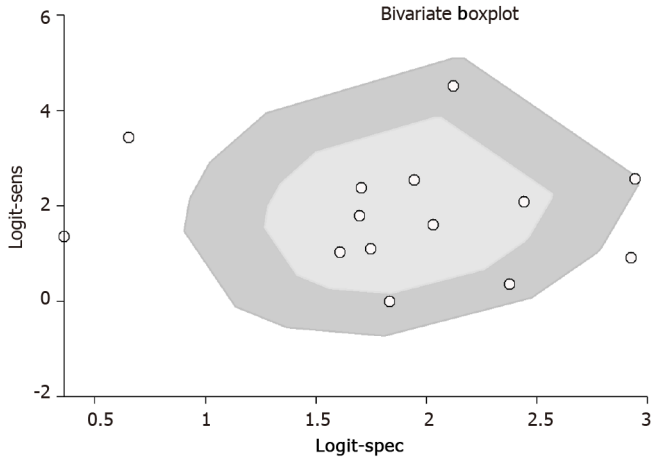

Figure 7 Bivariate boxplot of the sensitivity and specificity of ultrasound elastography.

used in the clinical practice. Further large-scale longitudinal studies are also needed to assess the predictive accuracy of strain wave elastography as only few studies reported this outcome.

It is important to interpret these results with caution, as there are several differences in the methods and quality of our included studies, which can ultimately affect the final pooled estimates. First, we evaluated and found a significant heterogeneity (significant chi-square test and higher I^2 statistic values). Hence, we performed meta-regression and found the factors responsible for this higher heterogeneity. Quality related factors and mean age were found to be the significant covariates responsible for such heterogeneity. We confirmed that there was no publication bias in the studies reporting our study outcome using Deek's test and funnel plot.

Our study has certain strengths. This is the first meta-analysis assessing the predictive ability of UE for pCR amongst breast cancer patients, with a larger number of studies (14 studies) included. Lack of significant publication bias adds credibility of the results in the meta-analysis. However, there are several limitations to our study. First, there was a significant between-study variability in our analysis. This can limit the prospect to infer or interpret the pooled findings. However, we explored the source of

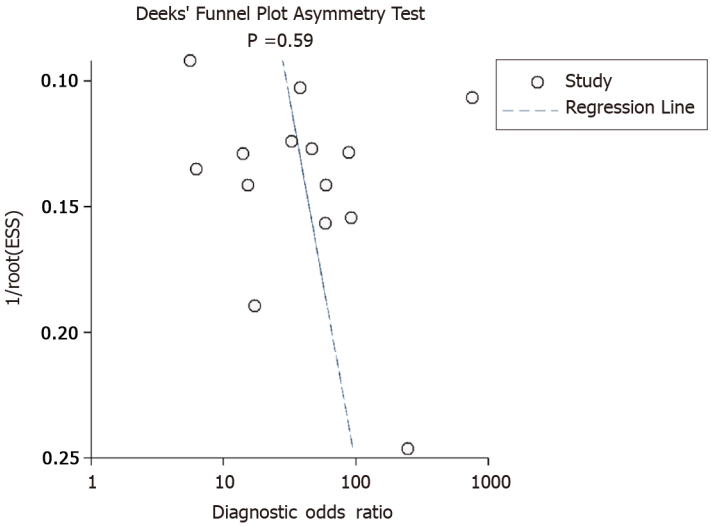

Figure 8 Funnel plot for publication bias.

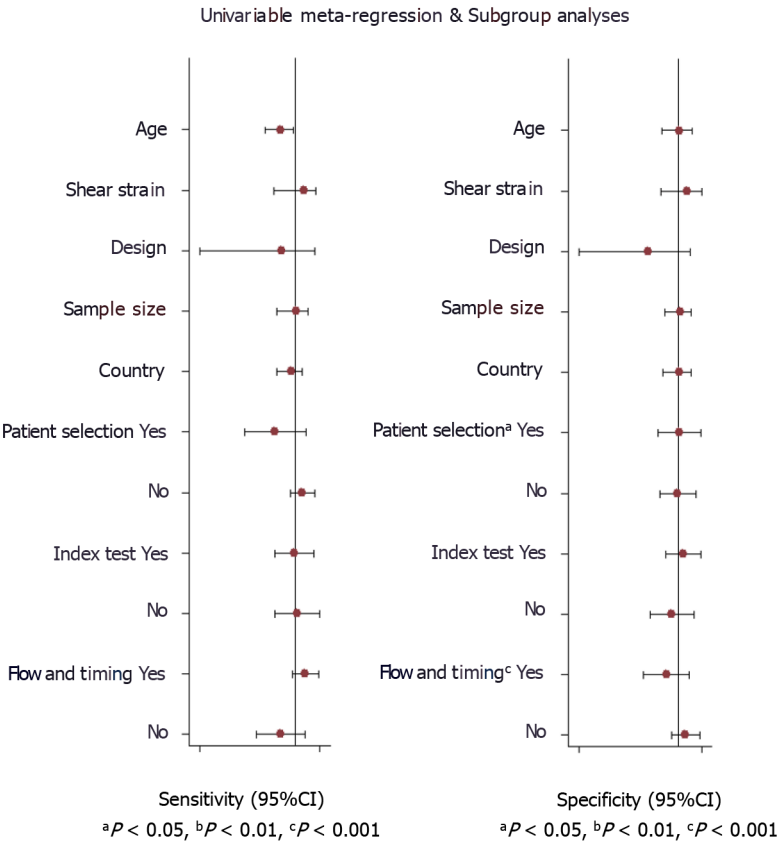

Figure 9 Univariable and multivariable meta-regression results for ultrasound elastography for predicting pathological complete response following neoadjuvant chemotherapy amongst breast cancer patients. CI: Confidence interval.

heterogeneity using meta-regression analysis to overcome this limitation. Second, the predictive accuracy of UE depends on several other factors such as the ethnicity, timing of the index test and outcome assessment, and disease severity. However, we could not evaluate their influence in our analysis. We have also not pre-registered this review online. Finally, the number of subjects/participants included was relatively small.

CONCLUSION

Despite these limitations, our study findings provide useful information for the clinicians and oncologists and may have significant implications for developing treatment strategies for breast cancer patients following NACT. Although UE had moderate sensitivity and specificity, strain-wave type of UE had a very high accuracy to rule out the patients with pCR. It should be useful, therefore, as an effective prognostic tool following the administration of NACT, because it may allow for identification of the patients at risk of developing incomplete pathological response. Applying this imaging technique could reduce the time spent undertaking various invasive diagnostic procedures and could also reduce the healthcare costs involved in the process. However, ultrasonography-based imaging techniques have substantial overlap between benign and malignant features, mainly for small lesions. A palpation imaging technique could help compensate for this deficiency by comprehensively analyzing the 2-D and 3-D tumor characteristics[23]. At the same time, it may be difficult to diagnose intraductal lesions and calcification in breast masses using palpation imaging. This, in turn, can be overcome *via* ultrasound or mammography. Hence, future studies perhaps should attempt to combine palpation imaging, ultrasonography, and mammography to analyze ambiguous clinical cases in order to improve breast lesion diagnosis. Additional large-scale setting-specific longitudinal studies are merited to establish the best imaging methods to assess all the patients administered with NACT.

ARTICLE HIGHLIGHTS

Research background

Several studies have reported the prognostic value of ultrasound elastography (UE) in patients receiving neoadjuvant chemotherapy (NACT) for breast cancer. However, the assessment of parameters is different for shear-wave elastography and strain elastography in terms of measured elasticity parameter and mode of imaging.

Research motivation

To the best of our knowledge, no meta-analysis has been conducted to assess the accuracy of the two modes of elastography in predicting the response to NACT.

Research objectives

The aim of the current study was to systematically search the literature for all studies assessing the accuracy of UE for predicting response to NACT in breast cancer, and pool the data for meta-analysis.

Research methods

A comprehensive and systematic search was performed in the databases of MEDLINE, EMBASE, SCOPUS, PubMed Central, CINAHL, Web of Science, and Cochrane library from inception until December 2020.

Research results

We found that UE had an equal pooled sensitivity and specificity of 86% for predicting the pathologic complete response (pCR) in breast cancer patients following NACT. We also found that strain wave elastography was the better technique with a pooled sensitivity of 93% and specificity of 87% compared to shear wave elastography (77% and 84%). This means that strain elastography can help in effectively ruling out the patients correctly as it had a sensitivity more than 90%.

Research conclusions

Strain-wave type of UE can accurately predict the pCR following NACT amongst breast cancer patients.

Research perspectives

Additional large-scale setting-specific longitudinal studies are merited to establish the best imaging methods to assess all the patients administered with NACT.

FOOTNOTES

Author contributions: Chen W and Zheng JH conceived and designed the study; Fang LX, Chen HL, and Zheng JH were involved in literature search and data collection; Chen W analyzed the data and wrote the paper; Zheng JH reviewed and edited the manuscript; all authors read and approved the final manuscript.

Conflict-of-interest statement: The authors deny any conflict of interest.

PRISMA 2009 Checklist statement: The authors have read the PRISMA 2009 checklist and the manuscript was prepared and revised according to the PRISMA 2009 checklist.

Country/Territory of origin: China

ORCID number: Wei Chen 0000-0003-1693-6797; Li-Xiang Fang 0000-0003-1759-9577; Hai-Lan Chen 0000-0001-8531-484X; Jian-Hua Zheng 0000-0002-8336-1113.

S-Editor: Fan JR
L-Editor: Wang TQ
P-Editor: Wu RR

REFERENCES

1 **Cortazar P**, Zhang L, Untch M, Mehta K, Costantino JP, Wolmark N, Bonnefoi H, Cameron D, Gianni L, Valagussa P, Swain SM, Prowell T, Loibl S, Wickerham DL, Bogaerts J, Baselga J, Perou C, Blumenthal G, Blohmer J, Mamounas EP, Bergh J, Semiglazov V, Justice R, Eidtmann H, Paik S, Piccart M, Sridhara R, Fasching PA, Slaets L, Tang S, Gerber B, Geyer CE Jr, Pazdur R, Ditsch N, Rastogi P, Eiermann W, von Minckwitz G. Pathological complete response and long-term clinical benefit in breast cancer: the CTNeoBC pooled analysis. *Lancet* 2014; **384**: 164-172 [PMID: 24529560 DOI: 10.1016/S0140-6736(13)62422-8]

2 **Crippa F**, Agresti R, Sandri M, Mariani G, Padovano B, Alessi A, Bianchi G, Bombardieri E, Maugeri I, Rampa M, Carcangiu ML, Trecate G, Pascali C, Bogni A, Martelli G, de Braud F. ^{18}F-FLT PET/CT as an imaging tool for early prediction of pathological response in patients with locally advanced breast cancer treated with neoadjuvant chemotherapy: a pilot study. *Eur J Nucl Med Mol Imaging* 2015; **42**: 818-830 [PMID: 25673053 DOI: 10.1007/s00259-015-2995-8]

3 **Pavlopoulou A**, Oktay Y, Vougas K, Louka M, Vorgias CE, Georgakilas AG. Determinants of resistance to chemotherapy and ionizing radiation in breast cancer stem cells. *Cancer Lett* 2016; **380**: 485-493 [PMID: 27450721 DOI: 10.1016/j.canlet.2016.07.018]

4 **Hayashi M**, Yamamoto Y, Iwase H. Clinical imaging for the prediction of neoadjuvant chemotherapy response in breast cancer. *Chin Clin Oncol* 2020; **9**: 31 [PMID: 32594748 DOI: 10.21037/cco-20-15]

5 **Youk JH**, Gweon HM, Son EJ. Shear-wave elastography in breast ultrasonography: the state of the art. *Ultrasonography* 2017; **36**: 300-309 [PMID: 28513127 DOI: 10.14366/usg.17024]

6 **Whiting PF**, Rutjes AW, Westwood ME, Mallett S, Deeks JJ, Reitsma JB, Leeflang MM, Sterne JA, Bossuyt PM; QUADAS-2 Group. QUADAS-2: a revised tool for the quality assessment of diagnostic accuracy studies. *Ann Intern Med* 2011; **155**: 529-536 [PMID: 22007046 DOI: 10.7326/0003-4819-155-8-201110180-00009]

7 **Evans A**, Whelehan P, Thompson A, Purdie C, Jordan L, Macaskill J, Henderson S, Vinnicombe S. Identification of pathological complete response after neoadjuvant chemotherapy for breast cancer: comparison of greyscale ultrasound, shear wave elastography, and MRI. *Clin Radiol* 2018; **73**: 910.e1-910.e6 [PMID: 29980324 DOI: 10.1016/j.crad.2018.05.030]

8 **Evans A**, Whelehan P, Thompson A, Purdie C, Jordan L, Macaskill J, Waugh S, Fuller-Pace F, Brauer K, Vinnicombe S. Prediction of Pathological Complete Response to Neoadjuvant Chemotherapy for Primary Breast Cancer Comparing Interim Ultrasound, Shear Wave Elastography and MRI. *Ultraschall Med* 2018; **39**: 422-431 [PMID: 28934812 DOI: 10.1055/s-0043-111589]

9 **Falou O**, Sadeghi-Naini A, Prematilake S, Sofroni E, Papanicolau N, Iradji S, Jahedmotlagh Z, Lemon-Wong S, Pignol JP, Rakovitch E, Zubovits J, Spayne J, Dent R, Trudeau M, Boileau JF, Wright FC, Yaffe MJ, Czarnota GJ. Evaluation of neoadjuvant chemotherapy response in women with locally advanced breast cancer using ultrasound elastography. *Transl Oncol* 2013; **6**: 17-24 [PMID: 23418613 DOI: 10.1593/tlo.12412]

10 **Fang C**, Yang TWYZJXW. Value of tissue elastography in the prediction of efficacy of neoadjuvant chemotherapy in breast cancer. *J BUON* 2019; **24**: 555-559 [PMID: 31128005]

11 **Fernandes J**, Sannachi L, Tran WT, Koven A, Watkins E, Hadizad F, Gandhi S, Wright F, Curpen B, El Kaffas A, Faltyn J, Sadeghi-Naini A, Czarnota G. Monitoring Breast Cancer Response to Neoadjuvant Chemotherapy Using Ultrasound Strain Elastography. *Transl Oncol* 2019; **12**: 1177-1184 [PMID: 31226518 DOI: 10.1016/j.tranon.2019.05.004]

12 **Hayashi M**, Yamamoto Y, Ibusuki M, Fujiwara S, Yamamoto S, Tomita S, Nakano M, Murakami K, Iyama K, Iwase H. Evaluation of tumor stiffness by elastography is predictive for pathologic complete response to neoadjuvant chemotherapy in patients with breast cancer. *Ann Surg Oncol* 2012; **19**: 3042-3049 [PMID: 22476757 DOI: 10.1245/s10434-012-2343-1]

13 **Jing H**, Cheng W, Li ZY, Ying L, Wang QC, Wu T, Tian JW. Early Evaluation of Relative Changes in Tumor Stiffness by Shear Wave Elastography Predicts the Response to Neoadjuvant Chemotherapy in Patients With Breast Cancer. *J Ultrasound Med* 2016; **35**: 1619-1627 [PMID: 27302898 DOI: 10.7863/ultra.15.08052]

14 **Katyan A**, Mittal MK, Mani C, Mandal AK. Strain wave elastography in response assessment to neo-adjuvant chemotherapy in patients with locally advanced breast cancer. *Br J Radiol* 2019; **92**: 20180515 [PMID: 31045431 DOI: 10.1259/bjr.20180515]

15 **Lee SH**, Chang JM, Han W, Moon HG, Koo HR, Gweon HM, Kim WH, Noh DY, Moon WK. Shear-Wave Elastography for the Detection of Residual Breast Cancer After Neoadjuvant Chemotherapy. *Ann Surg Oncol* 2015; **22** Suppl 3: S376-S384 [PMID: 26297209 DOI: 10.1245/s10434-015-4828-1]
16 **Ma Y**, Zhang S, Li J, Kang Y, Ren W. Comparison of strain and shear-wave ultrasounic elastography in predicting the pathological response to neoadjuvant chemotherapy in breast cancers. *Eur Radiol* 2017; **27**: 2282-2291 [PMID: 27752835 DOI: 10.1007/s00330-016-4619-5]
17 **Ma BX**, Fan ZN, Wu G. [The application of 3-dimensional shear wave elastography in the therapeutic effect evaluation of neoadjuvant chemotherapy for Her-2 positive breast cancer patients]. *Zhonghua Zhong Liu Za Zhi* 2020; **42**: 1049-1054 [PMID: 33342163 DOI: 10.3760/cma.j.cn112152-20190828-00552]
18 **Maier AM**, Heil J, Harcos A, Sinn HP, Rauch G, Uhlmann L, Gomez C, Stieber A, Funk A, Barr RG, Hennigs A, Riedel F, Schäfgen B, Hug S, Marmé F, Sohn C, Golatta M. Prediction of pathological complete response in breast cancer patients during neoadjuvant chemotherapy: Is shear wave elastography a useful tool in clinical routine? *Eur J Radiol* 2020; **128**: 109025 [PMID: 32371182 DOI: 10.1016/j.ejrad.2020.109025]
19 **Wang B**, Jiang T, Huang M, Wang J, Chu Y, Zhong L, Zheng S. Evaluation of the response of breast cancer patients to neoadjuvant chemotherapy by combined contrast-enhanced ultrasonography and ultrasound elastography. *Exp Ther Med* 2019; **17**: 3655-3663 [PMID: 30988749 DOI: 10.3892/etm.2019.7353]
20 **Zhang J**, Tan X, Zhang X, Kang Y, Li J, Ren W, Ma Y. Efficacy of shear-wave elastography *vs* dynamic optical breast imaging for predicting the pathological response to neoadjuvant chemotherapy in breast cancer. *Eur J Radiol* 2020; **129**: 109098 [PMID: 32559591 DOI: 10.1016/j.ejrad.2020.109098]
21 **Hu X**, Huang X, Chen H, Zhang T, Hou J, Song A, Ding L, Liu W, Wu H, Meng F. Diagnostic effect of shear wave elastography imaging for differentiation of malignant liver lesions: a meta-analysis. *BMC Gastroenterol* 2019; **19**: 60 [PMID: 31023234 DOI: 10.1186/s12876-019-0976-2]
22 **Tang GX**, Xiao XY, Xu XL, Yang HY, Cai YC, Liu XD, Tian J, Luo BM. Diagnostic value of ultrasound elastography for differentiation of benign and malignant axillary lymph nodes: a meta-analysis. *Clin Radiol* 2020; **75**: 481.e9-481.e16 [PMID: 32291079 DOI: 10.1016/j.crad.2020.03.021]
23 **Ding Y**, Sun C, Zhou Q, Cheng C, Yan C, Wang B. Use of Palpation Imaging in Diagnosis of Breast Diseases: A Way to Improve the Detection Rate. *Med Sci Monit* 2020; **26**: e927553 [PMID: 33247894 DOI: 10.12659/MSM.927553]

World Journal of Clinical Cases

Submit a Manuscript: https://www.f6publishing.com

World J Clin Cases 2022 April 16; 10(11): 3449-3460

DOI: 10.12998/wjcc.v10.i11.3449

ISSN 2307-8960 (online)

META-ANALYSIS

Association of chronic obstructive pulmonary disease with mild cognitive impairment and dementia risk: A systematic review and meta-analysis

Li-Ying Zhao, Xue-Lai Zhou

Specialty type: Medicine, research and experimental

Provenance and peer review: Unsolicited article; Externally peer reviewed.

Peer-review model: Single blind

Peer-review report's scientific quality classification

Grade A (Excellent): 0
Grade B (Very good): B, B
Grade C (Good): 0
Grade D (Fair): 0
Grade E (Poor): 0

P-Reviewer: Biondi A, Byeon H

Received: November 10, 2021
Peer-review started: November 10, 2021
First decision: January 11, 2022
Revised: January 25, 2022
Accepted: February 23, 2022
Article in press: February 23, 2022
Published online: April 16, 2022

Li-Ying Zhao, Department of Geriatrics, Traditional Chinese Medical Hospital of Zhuji, Zhuji 311800, Zhejiang Province, China

Xue-Lai Zhou, Department of Respiratory Medicine, Traditional Chinese Medical Hospital of Zhuji, Zhuji 311800, Zhejiang Province, China

Corresponding author: Xue-Lai Zhou, MD, Deputy Director, Department of Respiratory Medicine, Traditional Chinese Medical Hospital of Zhuji, No. 521 Donger Road, Zhuji 311800, Zhejiang Province, China. zxl13626883598@163.com

Abstract

BACKGROUND

Chronic obstructive pulmonary disease (COPD) is a common public health issue that has been linked to cognitive dysfunction.

AIM

To investigate the relationship between COPD and a risk of mild cognitive impairment (MCI) and dementia.

METHODS

A comprehensive literature search of the PubMed, Embase, Google Scholar, and Cochrane Library electronic databases was conducted. Pooled odds ratios (OR) and mean differences (MD) with 95% confidence intervals (CIs) were calculated using a random or fixed effects model. Studies that met the inclusion criteria were assessed for quality using the Newcastle Ottawa Scale.

RESULTS

Twenty-seven studies met all the inclusion criteria. Meta-analysis yielded a strong association between COPD and increased risk of MCI incidence (OR = 2.11, 95%CI: 1.32-3.38). It also revealed a borderline trend for an increased dementia risk in COPD patients (OR = 1.16, 95%CI: 0.98-1.37). Pooled hazard ratios (HR) using adjusted confounders also showed a higher incidence of MCI (HR = 1.22, 95%CI: -1.18 to -1.27) and dementia (HR = 1.32, 95%CI: -1.22 to -1.43) in COPD patients. A significant lower mini-mental state examination score in COPD patients was noted (MD = -1.68, 95%CI: -2.66 to -0.71).

CONCLUSION

Our findings revealed an elevated risk for the occurrence of MCI and dementia in COPD patients. Proper clinical management and attention are required to prevent and control MCI and dementia incidence in COPD patients.

Key Words: Mild cognitive impairment; Chronic obstructive pulmonary disease; Dementia; Meta-analysis

Core Tip: Chronic obstructive pulmonary disease (COPD) is a common public health issue that has been linked to cognitive dysfunction. The current meta-analysis was performed to investigate the relationship between COPD and mild cognitive impairment (MCI) and dementia risk. Twenty-seven studies met all the inclusion criteria. Meta-analysis yielded a strong association between COPD and an increased risk of MCI incidence (odds ratio = 2.11, 95% confidence interval: 1.32-3.38). Our findings revealed an elevated risk for the occurrence of MCI and dementia in COPD patients. Proper clinical management and attention are required to prevent and control MCI and dementia incidence in COPD patients.

Citation: Zhao LY, Zhou XL. Association of chronic obstructive pulmonary disease with mild cognitive impairment and dementia risk: A systematic review and meta-analysis. *World J Clin Cases* 2022; 10(11): 3449-3460
URL: https://www.wjgnet.com/2307-8960/full/v10/i11/3449.htm
DOI: https://dx.doi.org/10.12998/wjcc.v10.i11.3449

INTRODUCTION

Chronic obstructive pulmonary disease (COPD) is a progressive multicomponent lung disease that occurs more commonly in the elderly[1]. It is characterised by a partially irreversible chronic obstruction of lung airflow resulting in an abnormal decrease in blood oxygen levels, potentially leading to cognitive dysfunction[2]. Various studies have estimated that the prevalence of cognitive impairment in COPD patients ranges from 16% to 57%[3,4]. A prior review of 17 individual studies by Yohannes *et al* [5] showed that 32% of COPD patients showed some signs of cognitive dysfunction, with no less than 25% of patients showing at least mild cognitive impairment (MCI).

Cognitive impairment in COPD patients may compromise their capability to self-care and adhere to treatment regimens, making the relationship between COPD and cognitive impairment important for devising therapeutic approaches for COPD[6,7]. Some studies have focused on the relationship between COPD and neurologic function, but with inconsistent conclusions[8]. Data based on the Atherosclerosis Risk in Communities study showed that reduced lung function was associated with poor cognitive performance and higher risk of dementia hospitalization[9]. Data based on Taiwanese National Health Insurance Research Database showed that COPD patients exhibited a 1.27-fold higher risk of developing dementia[10].

To our knowledge, there has only been one published meta-analysis investigating the statistical association of COPD with cognition dysfunction. Zhang *et al*[11] concluded that COPD patients had an elevated risk of cognitive dysfunction. Similarly, only one single meta-analysis has looked at the relationship between COPD and dementia. Pooling data from three studies, Wang *et al*[12] showed that COPD patients faced a higher risk of developing dementia. However, these important clinical questions have not been investigated in a more thorough and conclusive manner. As such, we conducted a comprehensive systematic review and meta-analysis to investigate the association between COPD and the risk of MCI and dementia.

MATERIALS AND METHODS

Search strategy

Our meta-analysis was performed according to the Preferred Reporting Items for Systematic Reviews and Meta-analysis (PRISMA) guidelines[13]. We conducted a comprehensive search using PubMed, Embase, Google Scholar, and Cochrane Library online databases for articles published prior to March 31, 2021. The following key terms were used: "Chronic Obstructive Pulmonary Disease" OR "COPD" OR "Chronic Obstructive Airway Disease" OR "COAD" AND "Mild Cognitive impairment" OR "MCI" OR "Cognitive dysfunction" OR "Cognitive decline" AND "Dementia". Studies cited by articles that met the inclusion criteria were manually searched to identify additional eligible studies. Study eligibility

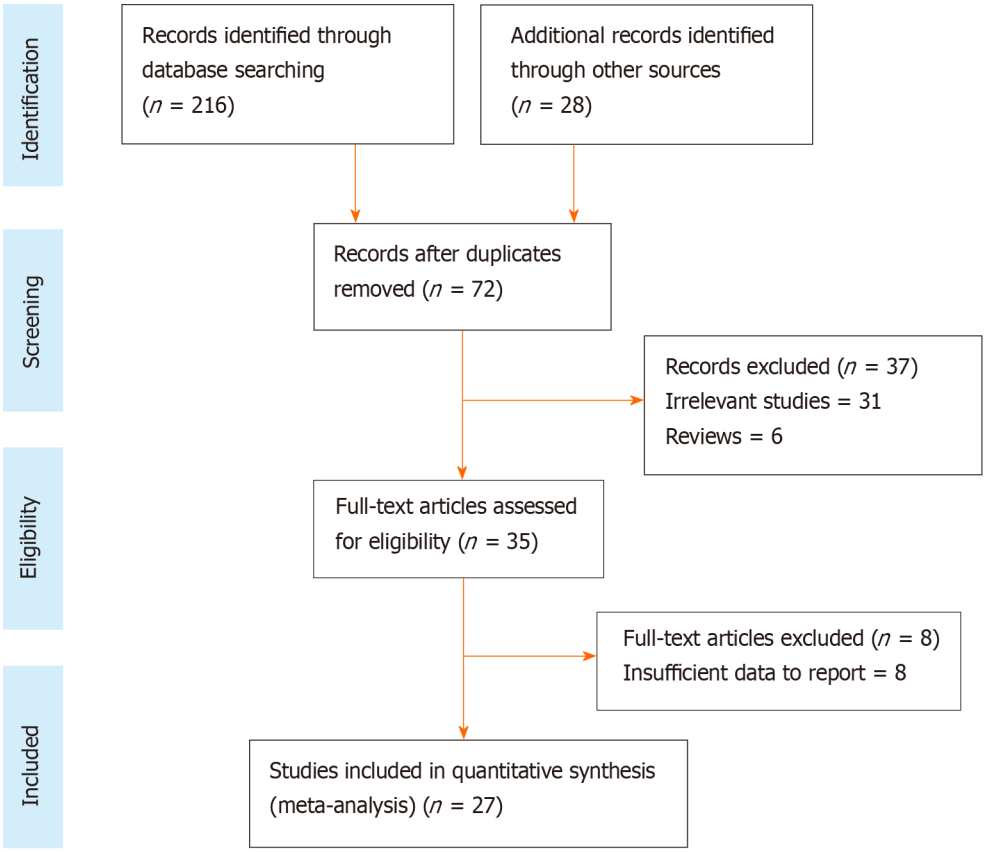

DOI: 10.12998/wjcc.v10.i11.3449

Figure 1 Flow diagram for study selection.

was not restricted based on language, sex, or publication year. Systematic reviews, conference abstracts, and editorials were excluded due to insufficient data presentation details.

Eligibility criteria

Inclusion criteria: We included studies that: (1) Investigated the association between COPD and a risk of MCI or dementia; (2) adopted a definite outcome of cognitive impairment or dementia in COPD and non-COPD subjects; (3) reported raw values necessary to calculate odds ratios (OR) or hazard ratios (HRs) for the incidence of cognitive impairment or dementia; (4) contained case controls, were prospective or retrospective-cohort, or had a cross-sectional design; and (5) compared the association between COPD and non-COPD patients.

Exclusion criteria: We excluded studies that: (1) Did not report relevant outcomes; or (2) were full-text inaccessible.

Data collection and analysis

All eligible studies were separately screened by two reviewers to determine whether they met the inclusion criteria. Screening was first conducted at the abstract content level, with relevant studies further investigated at the full-text level. Articles published in languages other than English were machine-translated using Google Translate, with the translated version reviewed. The following information was extracted from the included studies for summarization and analysis: Author, year, study design type, group investigated, sample size, diagnostic criteria for COPD, adjusted confounder for calculating pooled ratio, MCI prevalence, dementia prevalence, and scales used for cognitive assessment.

Quality assessment

Study quality was assessed independently by two separate reviewers using the Newcastle-Ottawa Scale (NOS)[14], which examined three components: Selection, comparability, and ascertainment of outcome. Disagreements were resolved through discussion.

Publication bias

Publication bias was assessed using Funnel plot analysis and Egger's regression test[15,16].

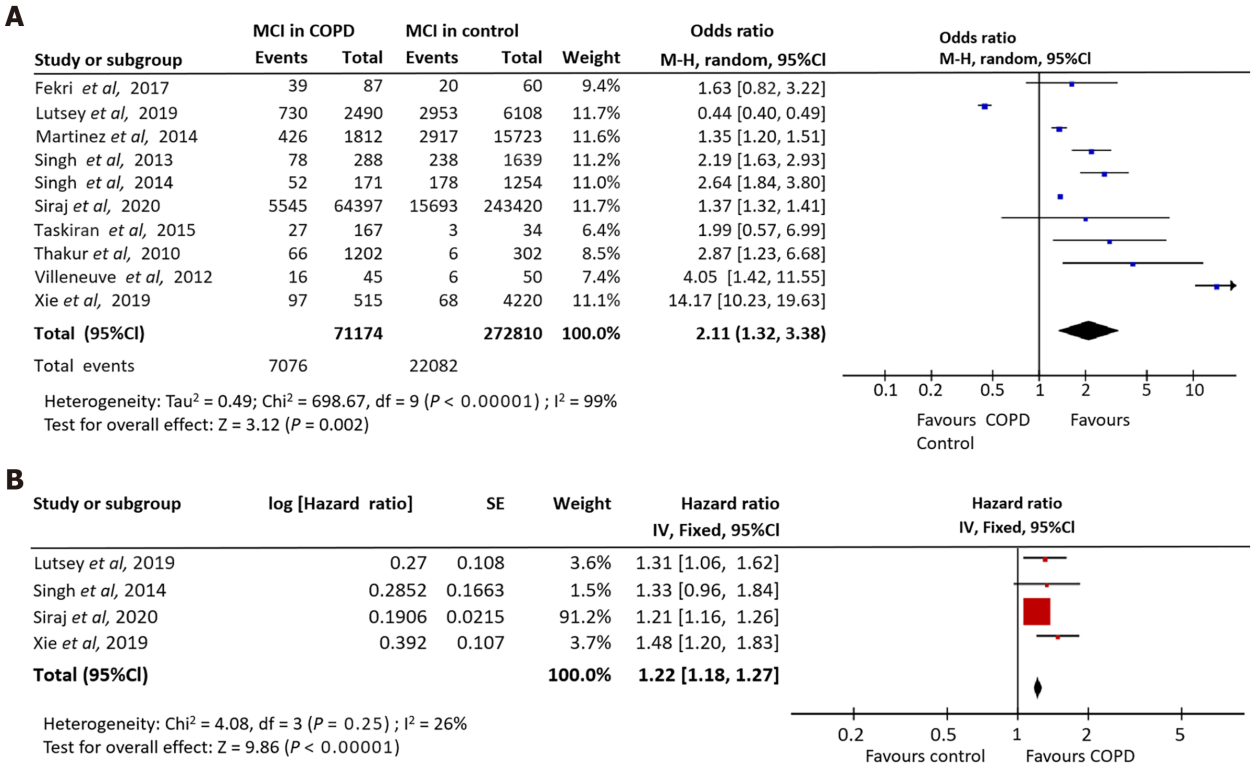

DOI: 10.12998/wjcc.v10.i11.3449

Figure 2 Forest plot examining the association of chronic obstructive pulmonary disease with mild cognitive impairment risk. A: Odds ratios; B: Hazard ratios.

Statistical analysis

Mean differences (MDs) with 95% confidence intervals (CIs) were calculated for continuous outcomes. For categorical outcomes, ORs and HRs with 95%CIs were calculated to estimate pooled findings. Heterogeneity between studies (measurable heterogeneity) was evaluated using I^2 statistics. If I^2 values > 50%, a random-effects model was applied, otherwise a fixed-effect model was applied. Statistical analyses were performed using Review Manager software (Version 5.3, Copenhagen: The Nordic Cochrane Centre, The Cochrane Collaboration 2014).

RESULTS

Literature search

Preliminary screening of PubMed, Embase, Google Scholar, and Cochrane Library databases yielded 234 results (Figure 1). Review of article title and abstract resulted in 72 remaining studies. Full-text review further excluded 45, leaving 27 studies[3,4,10,17-40] that were ultimately included in the meta-analysis.

Properties and characteristics of included studies

Relevant study data, including the diagnostic criteria for COPD, sample size, and disease assessment scales for all the 27 included studies[3,4,10,17-40] are shown in Table 1. The included studies were published between 1996 and 2020, and study sample sizes ranged from 20 to 243420 subjects. Ten studies[17,19-22,28,29,34,35,39] were case-controlled, ten were cross-sectional[3,4,24-26,32,36-38,40], four were prospective-cohort[18,27,30,31], and three were retrospective-cohort[10,23,33]. Seventeen studies[4,17-22,25,31,32,34-40] reported cognitive impairment data based on the mini-mental state examination (MMSE) scoring system. Twenty-two studies used the GOLD criteria, three[10,23,33] reported the ICD-9 CM criteria, and two[3,26] followed the standardized guidelines for COPD diagnosis. The quality score was high in twelve studies, medium in seven, and low in six (Supplementary Table 1). The assessment criteria involving the NOS uses three broad criteria: Selection, comparability, and exposure, where the selection defines and analyses the cases and control subjects included in the study, comparability defines the matching or comparison of cases and control subjects for better empirical investigation, and exposure determines whether the study was conducted in a blinded or unbiased manner along with the response of the subjects.

Table 1 Baseline and clinical characteristics of included studies

No.	Ref.	Country or region	Study design	Groups investigated	Age	Diagnostic criteria	Assessment scales	Adjusted variables	MCI (%)	Dementia (%)	NOS quality score
1	Mermit Çilingir *et al*[17], 2020	Turkey	Case Control	COPD-E (*n* = 30); COPD-S (*n* = 54); Control (*n* = 37)	COPD-E-71.8 ± 12.3; COPD-S- 62 ± 10.2; Control-65.9 ± 12.8	GOLD	MMSE; RCS	NA	NA	NA	7
2	Xie *et al*[18], 2019	China	Prospective Cohort	COPD (*n* = 515); No COPD (*n* = 4220)	COPD-82.9 ± 9.7	GOLD	MMSE	Age, gender, marital status, education level, alcohol drinking, current exercise, BMI, baseline prevalence of HTN, DM, and stroke	18.8; 14.6	2.9; 1.6	8
3	Samareh Fekri *et al*[19], 2017	Iran	Case Control	COPD (*n* = 87); Control (*n* = 60)	COPD-60.4 ± 9.8; Control-58.1 ± 9.8	GOLD	MMSE	Age and sex	51.7; 36.6	NA	7
4	Gupta *et al*[20], 2013	India	Case Control	COPD-(*n* = 40); Control (*n* = 40)	COPD-57.2 ± 9.1; Control-56.9 ± 9.2	GOLD	MMSE	Age	NA	NA	5
5	Li *et al*[21], 2013	China	Case Control	Mild COPD-(*n* = 27); Severe COPD-(*n* = 35); Control (*n* = 27)	Mild COPD-70.4 ± 7.7; Severe COPD-68.2 ± 7.8; Control-66.2 ± 7.1	GOLD	MMSE	Age, sex, education level, BMI, smoking status, and CVD	NA	NA	6
6	Li *et al*[22], 2013	China	Case Control	Mild COPD-(*n* = 37); Severe COPD-(*n* = 48); Control (*n* = 37)	Mild COPD-69.2 ± 8.1; Severe COPD-67.6 ± 7.6; Control-66.5 ± 6.9	GOLD	MMSE	Age, sex, education level, BMI, smoking status, and CVD	NA	NA	8
7	Liao *et al*[23], 2015	Taiwan	Retrospective Cohort	COPD (*n* = 20492); No COPD (*n* = 40765)	COPD-68.2 ± 12.4; No COPD-67 ± 12.5	ICD-9CM	NA	Age and sex	NA	13.29.11	**7**
8	Martinez *et al* [24], 2014	Michigan	Cross-sectional	COPD (*n* = 1812); No COPD (*n* = 15723)	COPD-70.3 ± 9.0; No COPD-68.7 ± 9.9	GOLD	ADL	Baseline cognition	16.5; 12.4	3.9; 3.1	8
9	Dal Negro *et al* [25], 2015	Italy	Cross-sectional	COPD with LTOT (*n* = 73); COPD without LTOT (*n* = 73)	COPD with LTOT-70.9 ± 8.9; No COPD with LTOT-71.2 ± 9.1	GOLD	MMSEMRC; CAT	Age, gender, smoking history, BMI, dyspnoea score, ABG, and lung function	32.8	NA	6
10	Singh *et al*[26], 2013	United States	Cross-sectional	COPD (*n* = 288); No COPD (*n* = 1639)	MCI-82.7 ± 11.2; Normal Cognition-79.7 ± 12.5	Standard criteria	BDI; CDR	BDI-II Depression, history of stroke, APOEe4 genotype, DM, HTN, CAD, and BMI	14.6; 27.1	NA	7
11	Singh *et al*[3], 2014	United States	Cross-sectional	Total COPD (*n* = 1425); COPD (*n* = 171); No COPD (*n* = 1254)	COPD-80.8 ± 7.5; No COPD-79.1 ± 7.5	Standard criteria	BDI	BDI-II depression, history of stroke, APOEe4 genotype, smoking, DM, HTN, CAD, z-scores, and BMI	NA	NA	7

12	Lutsey *et al*[27], 2019	United States	Prospective Cohort	COPD (n = 2490); No COPD (n = 6108)	COPD-55.1 ± 5.8; No COPD-53.9 ± 5.7	GOLD	NA	Age, sex, education level, race, center, cigarette smoking and pack-years of smoking, physical activity, BMI, systolic BP, BP medication use, diabetes, HDL, LDL lipid-lowering medications, CAD, heart failure, stroke, apolipoprotein E genotype, and fibrinogen	NA	NA	6
13	Siraj *et al*[28], 2020	United Kingdom	Case Control	COPD (n = 64397); No COPD (n = 243420)	COPD-66.4 ± 10.9; No COPD-65.7 ± 11	Standard criteria	NA	Age, sex, GP, BMI, smoking status, modified CCI, CV disease, corticosteroid use, and socioeconomic class	NA	NA	7
14	Villeneuve *et al* [29], 2012	Canada	Case Control	Total COPD (n = 45); Control (n = 50)	COPD-68.4 ± 8.7; Control-67.4 ± 8.7	GOLD	MMSE; MoCA	Age and education	36.0; 12.0	NA	5
15	Yeh *et al*[30], 2018	Taiwan	Prospective Cohort	COPD (n = 10260); No COPD (n = 20513)	COPD-65.6 ± 11.8; No COPD-65.5 ± 11.9	GOLD	NA	Age, sex, each comorbidity, inhaled corticosteroid, and oral steroids	NA	11.1; 8.81	4
16	Ozge *et al*[31], 2006	Turkey	Prospective cohort	COPD (n = 54); Control (n = 24)	COPD-64.6 ± 8.5; Control-62.4 ± 8.4	GOLD	MMSE,BDS, CDR, IADL	Age and sex	NA	NA	6
17	Favalli *et al*[32], 2008	Turkey	Cross-sectional	COPD (n = 21); Control (n = 20)	COPD-74.6 ± 5.4; Control-73.7 ± 4.5	GOLD	MMSE; GDS	NA	NA	NA	5
18	Liao *et al*[10], 2015	Taiwan	Retrospective Cohort	COPD (n = 8640); No COPD (n = 17280)	COPD-68.7 ± 10.7; No COPD-68.7 ± 10.7	ICD-9CM	Self-administered questionnaire	Age and sex	NA	5.22; 7.06	6
19	Thakur *et al*[33], 2010	United States	Retrospective Cohort	COPD (n = 1202); Control (n = 302)	COPD-58.2 ± 6.2; Control-58.5 ± 6.2	ICD-9CM	MRC; BODE index; MMSE	Age, sex, race, educational attainment, and smoking history	5.5; 2.0	NA	7
20	Zhou *et al*[34], 2012	China	Case Control	COPD (n = 110); Control (n = 110)	COPD-80.9 ± 1.7; Control-80.8 ± 1.5	GOLD	CDR; MMSE	Age and education	NA	NA	6
21	Dodd *et al*[4], 2013	United Kingdom	Cross-sectional	COPD-E (n = 30); COPD-S (n = 50); Control (n = 30)	COPD-E-70 ± 11; COPD-S-69 ± 8; Control-65 ± 8	GOLD	MMSE	Age	NA	NA	7
22	Isoaho *et al*[35], 1996	Finland	Case Control	COPD (n = 81); Control (n = 245)	COPD-70.4 ± 4.8; Control-71.3 ± 5.9	GOLD	MMSE	Age and sex	17.0; 13.0	7.1; 3.2	6
23	Lima *et al*[36], 2007	Brazil	Cross-sectional	COPD (n = 30); Control (n = 34)	COPD-65 ± 8; Control-66 ± 8	GOLD	MMSE; DSM-IV	NA	NA	NA	5
24	Ozyemisci-Taskiran *et al* [37], 2015	Turkey	Cross-sectional	COPD-E (n = 133); COPD-S (n = 34); Control (n = 34)	COPD-E-69.3 ± 8.9; COPD-S-67.5 ± 8.9; Control-68.3 ± 8.8	GOLD	MMSE; HAD; BODE	Age and sex	22.6	NA	6
25	Salik *et al*[38], 2007	Turkey	Cross-sectional	COPD (n = 32); Control (n = 26)	COPD-66.7 ± 2.5; Control-65.7 ± 7.3	GOLD	MMSE; MCS	NA	NA	NA	5
26	Sarınç Ulaşlı *et al* [39], 2013	Turkey	Case Control	COPD (n = 112); Control (n = 44)	COPD-65 ± 7.6; Control-64 ± 9	GOLD	MMSE	Age and sex	NA	NA	5

27	Tomruk *et al* [40], 2015	Turkey	Cross-sectional	COPD (n = 35); Control (n = 36)	COPD-62.9 ± 6.3; Control-60.8 ± 6.2	GOLD	MMSE	Age	NA	NA	4

COPD: Chronic obstructive pulmonary disease; S: Stable; E: Exacerbation; GOLD: Global Initiative for Chronic Obstructive Lung Disease; CAT: COPD Assessment Test; MMSE: Mini-Mental State Examination; COPD: Chronic obstructive pulmonary disease; LTOT: Long-term oxygen treatment; HAD: Hospital Anxiety and Depression; BODE: (B) BMI, (O) the severity of airflow obstruction (FEV1), (D) severity of dyspnea (modified Medical Research Council Dyspnea Scale), (E) exercise capacity; ICD-9CM: International Classification of Diseases, Ninth Revision, Clinical Modification; BDI: Beck Depression Inventory; IADL: Instrumental activities of daily living scale; CDR: Clinical dementia rating; BMI: Body mass index; CVD: Cardiovascular Disease; GP: General practice; DM: Diabetes mellitus; ABG: Arterial blood gas; HTN: Hypertension; CAD: Coronary artery disease; HDL: High Density lipoprotein; LDL: Low density lipoprotein; NA: Not applied.

Association of COPD with MCI risk

Ten studies[3,18,19,24,26-29,33,37] detailing 71174 COPD patients and 22082 control subjects investigated the association of COPD with MCI risk. Our meta-analysis indicated a strong association between COPD and an increased MCI incidence risk (OR = 2.11, 95%CI: 1.32-3.38). A significant degree of heterogeneity was observed (I^2 = 99%). Using a random effects model, we demonstrated that COPD patients were 1.26 times more susceptible to MCI compared to non-COPD controls (Figure 2A).

Adjusted HRs for MCI risk in COPD patients

Pooling adjusted HRs from four studies[3,18,27,28] investigating the relationship between COPD and MCI incidence revealed a significant association (HR = 1.22, 95%CI: -1.18 to -1.27; I^2 = 26%] (Figure 2B).

Association of COPD with risk of dementia

Seven studies[10,18,23,24,27,28,30] involving 108606 COPD patients and 347939 control subjects, investigated the relationship between COPD and dementia risk. Pooling these data showed a borderline trend for an increased dementia risk in COPD patients compared to non-COPD control patients (OR = 1.16, 95%CI: 0.98-1.37). A high degree of heterogeneity was observed (I^2 = 94%). Our meta-analysis showed that COPD patients were more susceptible to dementia (Figure 3A).

Adjusted HRs for dementia risk in COPD patients

Pooling adjusted HRs from six studies[10,18,23,27,28,30] investigating the relationship between COPD and dementia incidence revealed a significant association (HR = 1.32, 95%CI: -1.22 to -1.43; I^2: 99%) (Figure 3B).

MMSE score in COPD and non-COPD patients

Seventeen studies[4,17-22,32,35-40,25,31,34] involving 1392 COPD patients and 5097 control subjects, reported mean MMSE score data for both COPD and non-COPD patients. Pooling these results showed a significant lower MMSE score in COPD patients compared to controls (MD = -1.68, 95%CI: -2.66 to -0.71] (Figure 4). A high degree of heterogeneity among these seventeen studies was observed (I^2 = 96%).

Publication bias

Egger's tests did not show any significant publication bias for the examined comparisons. Figure 5 shows the funnel plot of the studies included in each comparison. However, no significant publication

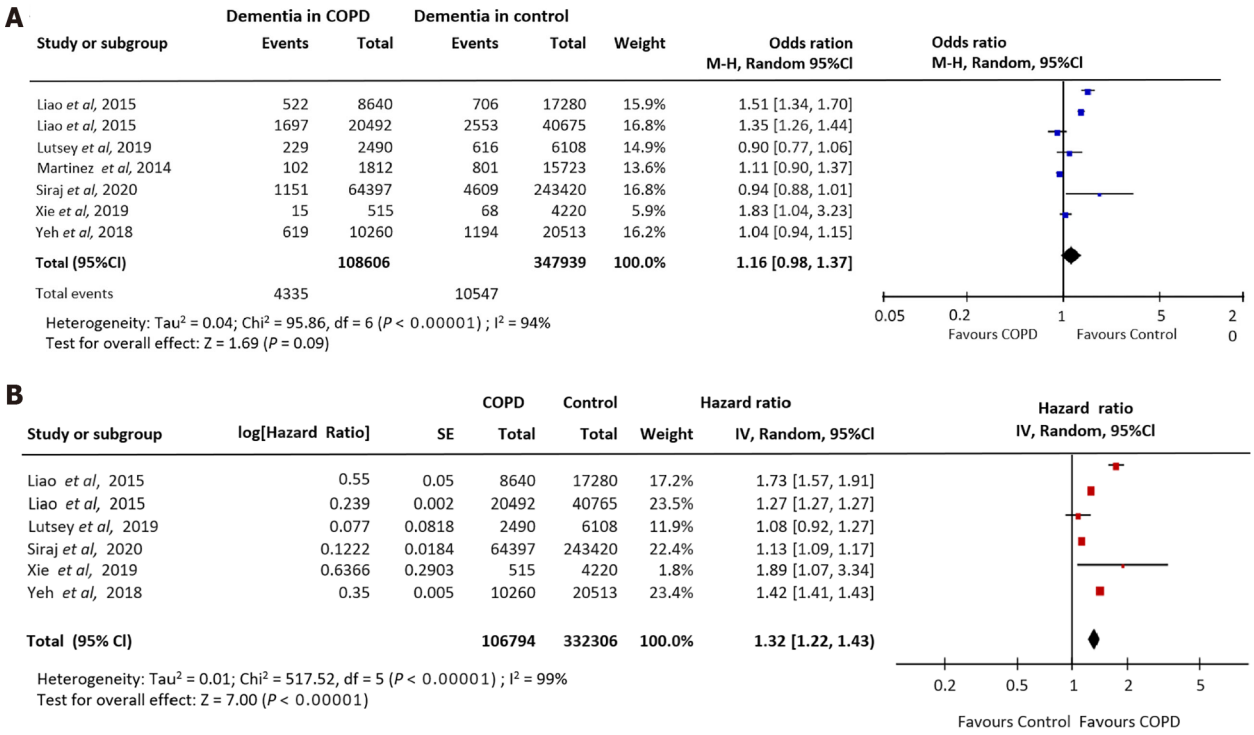

DOI: 10.12998/wjcc.v10.i11.3449

Figure 3 Forest plot examining the association of chronic obstructive pulmonary disease with dementia risk. A: Odds ratios; B: Hazard ratios.

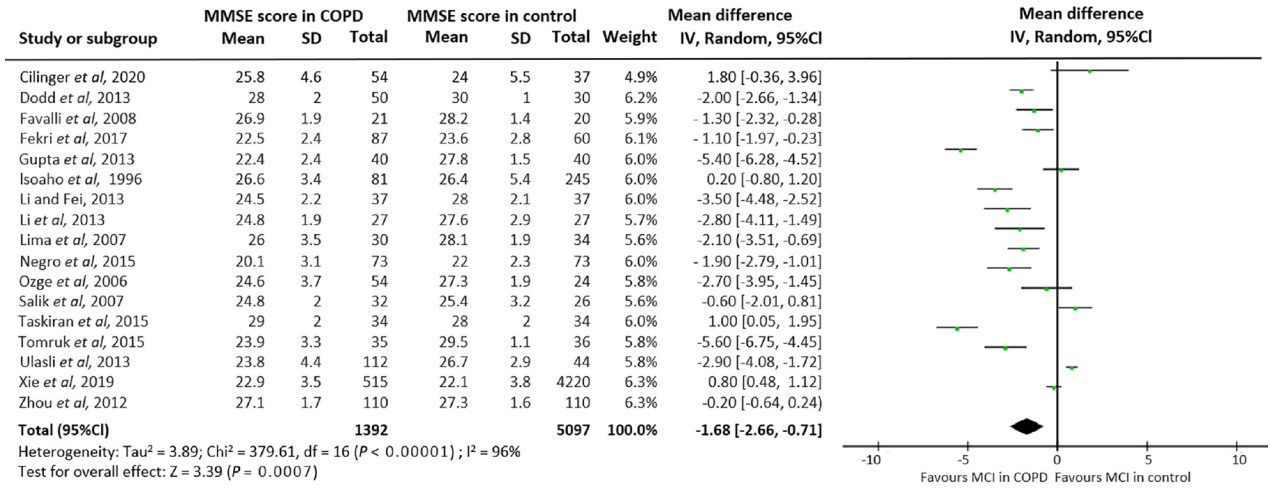

DOI: 10.12998/wjcc.v10.i11.3449

Figure 4 Forest plot examining mini-mental state examination score differences between chronic obstructive pulmonary disease and control groups.

biases were observed for the association of COPD with risk of MCI and dementia, MCI risk in COPD patients, dementia risk in COPD patients, and comparison of MMSE score between the COPD and control groups.

DISCUSSION

This study is the first systematic review and meta-analysis examining the association between COPD and the risk of MCI and dementia. We found that patients with COPD are 2.11 times more susceptible to MCI and 1.16 times more susceptible to dementia. Moreover, lower MMSE scores were observed in COPD patients, indicating greater cognitive impairment.

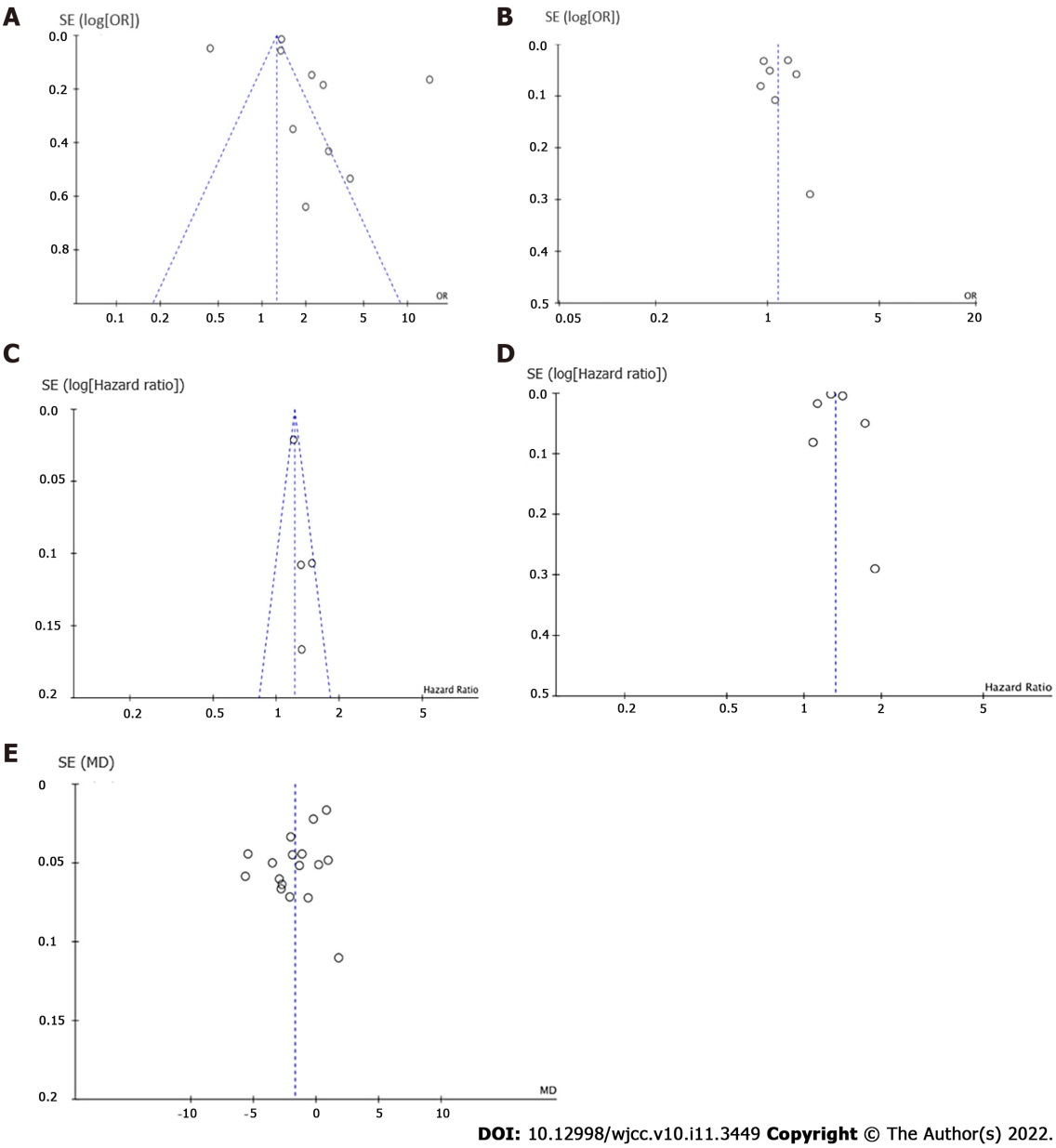

DOI: 10.12998/wjcc.v10.i11.3449

Figure 5 Funnel plot. A: Mild cognitive impairment (MCI); B: Dementia; C: MCI risk in chronic obstructive pulmonary disease (COPD) patients; D: Dementia risk in COPD patients; E: Comparison of mini-mental state examination score between COPD and control groups.

COPD-associated neurological impairment and dementia put a great burden on the patients and the healthcare system. In particular, declining cognition leads to COPD patients requiring more assistance for daily activities[41]. Our analysis was performed based on the reported adjustments within individual studies for confounding factors such as age, sex, smoking, body mass index, education level, diabetes mellitus, and previous history of stroke or cardiovascular disease[10,23,27,28,30]. Studies by Thakur *et al*[33], Singh *et al*[26], and Martinez *et al*[24] reported data as ORs for adjusted confounders and therefore were not included in the calculations for pooled incidence for MCI or dementia.

From a clinical approach, COPD can lead to pulmonary encephalopathy, hypoxemia, and inflammation, all of which may impact brain function[42]. Indeed, COPD patients exhibit a unique neurophysiological profile stemming from neurotoxicity featuring deficits of attention, motor, memory, and cognitive domain executive function[4]. Interestingly, the relationship between COPD and dementia persists even after accounting for the presence of vascular disease, suggesting that COPD is an independent predictor of dementia.

Our findings are consistent with the previous literature[5,11,12,42,43]. However, the available literature on the relationship between dementia and COPD remains limited, as only seven studies were found for this meta-analysis. Our study also had several other limitations. The included studies had different designs, which may be one of the leading causes of heterogeneity. Additional sources of heterogeneity may include different geographical population, variation in the diagnostic criteria of COPD, and diversity in the factors undertaken for the multivariate analysis of each included studies.

The included studies also lacked long-term follow-up data, as well as data that would facilitate subgroup analysis based on co-morbidities, age, and gender. Finally, different studies varied on how they assessed and diagnosed COPD and cognitive impairment.

CONCLUSION

Our meta-analysis revealed an elevated risk for MCI and dementia in COPD patients. Proper clinical management and attention are necessary to prevent or mitigate the incidence of MCI and dementia in COPD patients.

ARTICLE HIGHLIGHTS

Research background

Chronic obstructive pulmonary disease (COPD) is a common public health issue that has been linked to cognitive dysfunction. No clear evidence is available for the relationship between COPD and mild cognitive impairment (MCI) and dementia risk.

Research motivation

To our knowledge, there has only been one published meta-analysis with limited number studies investigating the statistical association of COPD with cognition dysfunction.

Research objectives

The current meta-analysis was performed to investigate the relationship between COPD and MCI and dementia risk.

Research methods

A comprehensive search was performed using PubMed, Embase, Google Scholar, and Cochrane Library online databases for articles published prior to March 31, 2021.

Research results

Twenty-seven studies met all the inclusion criteria. Meta-analysis yielded a strong association between COPD and an increased risk of MCI incidence. It also revealed a borderline trend for an increased dementia risk in COPD patients. A significant lower MMSE score in COPD patients was noted.

Research conclusions

Our findings revealed an elevated risk for the occurrence of MCI and dementia in COPD patients. Proper clinical management and attention are required to prevent and control MCI and dementia incidence in COPD patients.

Research perspectives

Further large prospective observational studies are needed to strengthen the evidence on this important subject.

FOOTNOTES

Author contributions: Zhao LY conceived and designed the study; Zhao LY and Zhou XL were involved in literature search and data collection; Zhao LY analyzed the data; Zhao LY and Zhou XL wrote the paper; Zhao LY edited the manuscript; all authors read and approved the final manuscript.

Conflict-of-interest statement: The authors deny any conflict of interest for this article.

PRISMA 2009 Checklist statement: The authors have read the PRISMA 2009 Checklist, and manuscript was prepared and revised according to the PRISMA 2009 Checklist.

Country/Territory of origin: China

ORCID number: Li-Ying Zhao 0000-0002-8106-609X; Xue-Lai Zhou 0000-0002-6652-7038.

S-Editor: Fan JR
L-Editor: Wang TQ
P-Editor: Yu HG

REFERENCES

1 **Singh D**, Agusti A, Anzueto A, Barnes PJ, Bourbeau J, Celli BR, Criner GJ, Frith P, Halpin DMG, Han M, López Varela MV, Martinez F, Montes de Oca M, Papi A, Pavord ID, Roche N, Sin DD, Stockley R, Vestbo J, Wedzicha JA, Vogelmeier C. Global Strategy for the Diagnosis, Management, and Prevention of Chronic Obstructive Lung Disease: the GOLD science committee report 2019. *Eur Respir J* 2019; **53** [PMID: 30846476 DOI: 10.1183/13993003.00164-2019]

2 **Ranzini L**, Schiavi M, Pierobon A, Granata N, Giardini A. From Mild Cognitive Impairment (MCI) to Dementia in Chronic Obstructive Pulmonary Disease. Implications for Clinical Practice and Disease Management: A Mini-Review. *Front Psychol* 2020; **11**: 337 [PMID: 32184750 DOI: 10.3389/fpsyg.2020.00337]

3 **Singh B**, Mielke MM, Parsaik AK, Cha RH, Roberts RO, Scanlon PD, Geda YE, Christianson TJ, Pankratz VS, Petersen RC. A prospective study of chronic obstructive pulmonary disease and the risk for mild cognitive impairment. *JAMA Neurol* 2014; **71**: 581-588 [PMID: 24637951 DOI: 10.1001/jamaneurol.2014.94]

4 **Dodd JW**, Charlton RA, van den Broek MD, Jones PW. Cognitive dysfunction in patients hospitalized with acute exacerbation of COPD. *Chest* 2013; **144**: 119-127 [PMID: 23349026 DOI: 10.1378/chest.12-2099]

5 **Yohannes AM**, Chen W, Moga AM, Leroi I, Connolly MJ. Cognitive Impairment in Chronic Obstructive Pulmonary Disease and Chronic Heart Failure: A Systematic Review and Meta-analysis of Observational Studies. *J Am Med Dir Assoc* 2017; **18**: 451.e1-451.e11 [PMID: 28292570 DOI: 10.1016/j.jamda.2017.01.014]

6 **Chang SS**, Chen S, McAvay GJ, Tinetti ME. Effect of coexisting chronic obstructive pulmonary disease and cognitive impairment on health outcomes in older adults. *J Am Geriatr Soc* 2012; **60**: 1839-1846 [PMID: 23035917 DOI: 10.1111/j.1532-5415.2012.04171.x]

7 **Campbell NL**, Boustani MA, Skopelja EN, Gao S, Unverzagt FW, Murray MD. Medication adherence in older adults with cognitive impairment: a systematic evidence-based review. *Am J Geriatr Pharmacother* 2012; **10**: 165-177 [PMID: 22657941 DOI: 10.1016/j.amjopharm.2012.04.004]

8 **Schou L**, Østergaard B, Rasmussen LS, Rydahl-Hansen S, Phanareth K. Cognitive dysfunction in patients with chronic obstructive pulmonary disease--a systematic review. *Respir Med* 2012; **106**: 1071-1081 [PMID: 22579108 DOI: 10.1016/j.rmed.2012.03.013]

9 **Pathan SS**, Gottesman RF, Mosley TH, Knopman DS, Sharrett AR, Alonso A. Association of lung function with cognitive decline and dementia: the Atherosclerosis Risk in Communities (ARIC) Study. *Eur J Neurol* 2011; **18**: 888-898 [PMID: 21244584 DOI: 10.1111/j.1468-1331.2010.03340.x]

10 **Liao WC**, Lin CL, Chang SN, Tu CY, Kao CH. The association between chronic obstructive pulmonary disease and dementia: a population-based retrospective cohort study. *Eur J Neurol* 2015; **22**: 334-340 [PMID: 25303726 DOI: 10.1111/ene.12573]

11 **Zhang X**, Cai X, Shi X, Zheng Z, Zhang A, Guo J, Fang Y. Chronic Obstructive Pulmonary Disease as a Risk Factor for Cognitive Dysfunction: A Meta-Analysis of Current Studies. *J Alzheimers Dis* 2016; **52**: 101-111 [PMID: 26967208 DOI: 10.3233/JAD-150735]

12 **Wang Y**, Li X, Wei B, Tung TH, Tao P, Chien CW. Association between Chronic Obstructive Pulmonary Disease and Dementia: Systematic Review and Meta-Analysis of Cohort Studies. *Dement Geriatr Cogn Dis Extra* 2019; **9**: 250-259 [PMID: 31543892 DOI: 10.1159/000496475]

13 **Moher D**, Liberati A, Tetzlaff J, Altman DG; PRISMA Group. Preferred reporting items for systematic reviews and meta-analyses: the PRISMA statement. *Ann Intern Med* 2009; **151**: 264-269, W64 [PMID: 19622511 DOI: 10.7326/0003-4819-151-4-200908180-00135]

14 **Stang A**. Critical evaluation of the Newcastle-Ottawa scale for the assessment of the quality of nonrandomized studies in meta-analyses. *Eur J Epidemiol* 2010; **25**: 603-605 [PMID: 20652370 DOI: 10.1007/s10654-010-9491-z]

15 **Egger M**, Davey Smith G, Schneider M, Minder C. Bias in meta-analysis detected by a simple, graphical test. *BMJ* 1997; **315**: 629-634 [PMID: 9310563 DOI: 10.1136/bmj.315.7109.629]

16 **Begg CB**, Mazumdar M. Operating characteristics of a rank correlation test for publication bias. *Biometrics* 1994; **50**: 1088-1101 [PMID: 7786990]

17 **Mermit Çilingir B**, Günbatar H, Çilingir V. Cognitive dysfunction among patients in chronic obstructive pulmonary disease: Effects of exacerbation and long-term oxygen therapy. *Clin Respir J* 2020; **14**: 1137-1143 [PMID: 32772486 DOI: 10.1111/crj.13250]

18 **Xie F**, Xie L. COPD and the risk of mild cognitive impairment and dementia: a cohort study based on the Chinese Longitudinal Health Longevity Survey. *Int J Chron Obstruct Pulmon Dis* 2019; **14**: 403-408 [PMID: 30863040 DOI: 10.2147/COPD.S194277]

19 **Samareh Fekri M**, Hashemi-Bajgani SM, Naghibzadeh-Tahami A, Arabnejad F. Cognitive Impairment among Patients with Chronic Obstructive Pulmonary Disease Compared to Normal Individuals. *Tanaffos* 2017; **16**: 34-39 [PMID: 28638422]

20 **Gupta PP**, Sood S, Atreja A, Agarwal D. A comparison of cognitive functions in non-hypoxemic chronic obstructive pulmonary disease (COPD) patients and age-matched healthy volunteers using mini-mental state examination questionnaire

and event-related potential, P300 analysis. *Lung India* 2013; **30**: 5-11 [PMID: 23661909 DOI: 10.4103/0970-2113.106119]
21 **Li J**, Huang Y, Fei GH. The evaluation of cognitive impairment and relevant factors in patients with chronic obstructive pulmonary disease. *Respiration* 2013; **85**: 98-105 [PMID: 23207572 DOI: 10.1159/000342970]
22 **Li J**, Fei GH. The unique alterations of hippocampus and cognitive impairment in chronic obstructive pulmonary disease. *Respir Res* 2013; **14**: 140 [PMID: 24359080 DOI: 10.1186/1465-9921-14-140]
23 **Liao KM**, Ho CH, Ko SC, Li CY. Increased Risk of Dementia in Patients With Chronic Obstructive Pulmonary Disease. *Medicine (Baltimore)* 2015; **94**: e930 [PMID: 26061317 DOI: 10.1097/MD.0000000000000930]
24 **Martinez CH**, Richardson CR, Han MK, Cigolle CT. Chronic obstructive pulmonary disease, cognitive impairment, and development of disability: the health and retirement study. *Ann Am Thorac Soc* 2014; **11**: 1362-1370 [PMID: 25285360 DOI: 10.1513/AnnalsATS.201405-187OC]
25 **Dal Negro RW**, Bonadiman L, Bricolo FP, Tognella S, Turco P. Cognitive dysfunction in severe chronic obstructive pulmonary disease (COPD) with or without Long-Term Oxygen Therapy (LTOT). *Multidiscip Respir Med* 2015; **10**: 17 [PMID: 25932326 DOI: 10.1186/s40248-015-0013-4]
26 **Singh B**, Parsaik AK, Mielke MM, Roberts RO, Scanlon PD, Geda YE, Pankratz VS, Christianson T, Yawn BP, Petersen RC. Chronic obstructive pulmonary disease and association with mild cognitive impairment: the Mayo Clinic Study of Aging. *Mayo Clin Proc* 2013; **88**: 1222-1230 [PMID: 24182702 DOI: 10.1016/j.mayocp.2013.08.012]
27 **Lutsey PL**, Chen N, Mirabelli MC, Lakshminarayan K, Knopman DS, Vossel KA, Gottesman RF, Mosley TH, Alonso A. Impaired Lung Function, Lung Disease, and Risk of Incident Dementia. *Am J Respir Crit Care Med* 2019; **199**: 1385-1396 [PMID: 30433810 DOI: 10.1164/rccm.201807-1220OC]
28 **Siraj RA**, McKeever TM, Gibson JE, Gordon AL, Bolton CE. Risk of incident dementia and cognitive impairment in patients with chronic obstructive pulmonary disease (COPD): A large UK population-based study. *Respir Med* 2020; **177**: 106288 [PMID: 33401149 DOI: 10.1016/j.rmed.2020.106288]
29 **Villeneuve S**, Pepin V, Rahayel S, Bertrand JA, de Lorimier M, Rizk A, Desjardins C, Parenteau S, Beaucage F, Joncas S, Monchi O, Gagnon JF. Mild cognitive impairment in moderate to severe COPD: a preliminary study. *Chest* 2012; **142**: 1516-1523 [PMID: 23364388 DOI: 10.1378/chest.11-3035]
30 **Yeh JJ**, Wei YF, Lin CL, Hsu WH. Effect of the asthma-chronic obstructive pulmonary disease syndrome on the stroke, Parkinson's disease, and dementia: a national cohort study. *Oncotarget* 2018; **9**: 12418-12431 [PMID: 29552322 DOI: 10.18632/oncotarget.23811]
31 **Ozge C**, Ozge A, Unal O. Cognitive and functional deterioration in patients with severe COPD. *Behav Neurol* 2006; **17**: 121-130 [PMID: 16873924 DOI: 10.1155/2006/848607]
32 **Favalli A**, Miozzo A, Cossi S, Marengoni A. Differences in neuropsychological profile between healthy and COPD older persons. *Int J Geriatr Psychiatry* 2008; **23**: 220-221 [PMID: 17562525 DOI: 10.1002/gps.1847]
33 **Thakur N**, Blanc PD, Julian LJ, Yelin EH, Katz PP, Sidney S, Iribarren C, Eisner MD. COPD and cognitive impairment: the role of hypoxemia and oxygen therapy. *Int J Chron Obstruct Pulmon Dis* 2010; **5**: 263-269 [PMID: 20856825 DOI: 10.2147/copd.s10684]
34 **Zhou G**, Liu J, Sun F, Xin X, Duan L, Zhu X, Shi Z. Association of chronic obstructive pulmonary disease with cognitive decline in very elderly men. *Dement Geriatr Cogn Dis Extra* 2012; **2**: 219-228 [PMID: 22719748 DOI: 10.1159/000338378]
35 **Isoaho R**, Puolijoki H, Huhti E, Laippala P, Kivelä SL. Chronic obstructive pulmonary disease and cognitive impairment in the elderly. *Int Psychogeriatr* 1996; **8**: 113-125 [PMID: 8805092 DOI: 10.1017/s1041610296002517]
36 **Lima OM**, Oliveira-Souza Rd, Santos Oda R, Moraes PA, Sá LF, Nascimento OJ. Subclinical encephalopathy in chronic obstructive pulmonary disease. *Arq Neuropsiquiatr* 2007; **65**: 1154-1157 [PMID: 18345421 DOI: 10.1590/s0004-282x2007000700012]
37 **Ozyemisci-Taskiran O**, Bozkurt SO, Kokturk N, Karatas GK. Is there any association between cognitive status and functional capacity during exacerbation of chronic obstructive pulmonary disease? *Chron Respir Dis* 2015; **12**: 247-255 [PMID: 26071384 DOI: 10.1177/1479972315589748]
38 **Salik Y**, Ozalevli S, Cimrin AH. Cognitive function and its effects on the quality of life status in the patients with chronic obstructive pulmonary disease (COPD). *Arch Gerontol Geriatr* 2007; **45**: 273-280 [PMID: 17343931 DOI: 10.1016/j.archger.2006.12.002]
39 **Sarınç Ulaşlı S**, Oruç S, Günay E, Aktaş O, Akar O, Koyuncu T, Ünlü M. [Effects of COPD on cognitive functions: a case control study]. *Tuberk Toraks* 2013; **61**: 193-199 [PMID: 24298960 DOI: 10.5578/tt.5841]
40 **Soysal Tomruk M**, Ozalevli S, Dizdar G, Narin S, Kilinc O. Determination of the relationship between cognitive function and hand dexterity in patients with chronic obstructive pulmonary disease (COPD): a cross-sectional study. *Physiother Theory Pract* 2015; **31**: 313-317 [PMID: 25625565 DOI: 10.3109/09593985.2015.1004768]
41 **Dulohery MM**, Schroeder DR, Benzo RP. Cognitive function and living situation in COPD: is there a relationship with self-management and quality of life? *Int J Chron Obstruct Pulmon Dis* 2015; **10**: 1883-1889 [PMID: 26392762 DOI: 10.2147/COPD.S88035]
42 **Baird C**, Lovell J, Johnson M, Shiell K, Ibrahim JE. The impact of cognitive impairment on self-management in chronic obstructive pulmonary disease: A systematic review. *Respir Med* 2017; **129**: 130-139 [PMID: 28732820 DOI: 10.1016/j.rmed.2017.06.006]
43 **van Beers M**, Janssen DJA, Gosker HR, Schols AMWJ. Cognitive impairment in chronic obstructive pulmonary disease: disease burden, determinants and possible future interventions. *Expert Rev Respir Med* 2018; **12**: 1061-1074 [PMID: 30296384 DOI: 10.1080/17476348.2018.1533405]

World Journal of Clinical Cases

Submit a Manuscript: https://www.f6publishing.com

World J Clin Cases 2022 April 16; 10(11): 3461-3471

DOI: 10.12998/wjcc.v10.i11.3461

ISSN 2307-8960 (online)

CASE REPORT

Circulating tumor DNA genomic profiling reveals the complicated olaparib-resistance mechanism in prostate cancer salvage therapy: A case report

Fang Yuan, Nan Liu, Ming-Zhen Yang, Xiao-Tian Zhang, Hong Luo, Hong Zhou

Specialty type: Medicine, research and experimental

Provenance and peer review: Unsolicited article; Externally peer reviewed.

Peer-review model: Single blind

Peer-review report's scientific quality classification

Grade A (Excellent): 0
Grade B (Very good): B, B
Grade C (Good): 0
Grade D (Fair): 0
Grade E (Poor): 0

P-Reviewer: Hazafa A, Pakistan; Yamaguchi K, Japan

Received: November 27, 2020
Peer-review started: November 30, 2020
First decision: September 28, 2021
Revised: October 12, 2021
Accepted: February 25, 2022
Article in press: February 25, 2022
Published online: April 16, 2022

Fang Yuan, Nan Liu, Hong Luo, Hong Zhou, Chongqing Key Laboratory of Translational Research for Cancer Metastasis and Individualized Treatment, Chongqing University Cancer Hospital, Chongqing 400044, China

Ming-Zhen Yang, Department of Clinical Biochemistry, College of Medical Laboratory, Army Military Medical University, Chongqing 400038, China

Xiao-Tian Zhang, Department of Medicine, BGI Genomics, Shenzhen 518083, Guangdong Province, China

Corresponding author: Hong Zhou, MD, Professor, Surgical Oncologist, Chongqing Key Laboratory of Translational Research for Cancer Metastasis and Individualized Treatment, Chongqing University Cancer Hospital, No. 181 Hanyu Road, Shapingba, Chongqing 400044, China. zhouhongcqch@126.com

Abstract

BACKGROUND

The poly (ADP-ribose) polymerase (PARP) inhibitor olaparib has displayed superior clinical effect in metastatic castration-resistant prostate cancer (mCRPC) patients with the homologous recombination repair (*HRR*) genes mutations. However, when a patient's tumor tissue volume is insufficient for genomic profiling of *HRR* gene mutations, circulating tumor DNA (ctDNA) may be useful in helping to determine and monitor the efficacy of olaparib, as well as in abiraterone-combination treatment, and for understanding any resistance mechanism related to such mutations.

CASE SUMMARY

A 61-year-old man who was diagnosed with metastatic prostate adenocarcinoma was initially hormone sensitivity, showing high Gleason score (5 + 5 = 10) and absolute positive rate (14/14 biopsied specimens). Following failure of several standard therapies, the patient progressed to mCRPC. Surprisingly, the patient showed good response to olaparib-abiraterone-prednisone combination treatment (an androgen-deprivation therapy, provided as the 'final choice' in China). Serum total prostate-specific antigen (TPSA) level reduced and symptoms remitted for 4 months. However, thereafter, serum TPSA levels began slowly increasing, indicating development of olaparib resistance. Subsequent comprehensive

genomic profiling of ctDNA, screening 508 cancer-related genes by next-generation sequencing, identified 10 somatic variants as well as 3 copy number alterations. Two identified reverse missense mutations in partner and localizer of BRCA2 (*PALB2*) may have recovered the reading frame, restoring function of the primary germline *PALB2* mutation and causing resistance to the PARP inhibitor olaparib.

CONCLUSION

Reverse mutations in *PALB2*, discovered *via* genomic profiling of ctDNA, may represent a potential resistance mechanism against olaparib in mCRPC.

Key Words: mCRPC; Olaparib; Circulating tumor DNA; Partner and localizer of BRCA2; Resistance mechanism; Reverse missense mutations

Core Tip: This case report describes the poly (ADP-ribose) polymerase inhibitor olaparib treatment response in a patient with metastatic castration-resistant prostate cancer (mCRPC). The patient's course of response to 'final choice' therapy (olaparib-abiraterone-prednisone combination treatment), consisting of serum total prostate-specific antigen (TPSA) level reduction and symptom remission for 4 months followed by TPSA rise, prompted comprehensive genomic profiling of circulating tumor (ct)DNA, which revealed reverse missense mutations in the partner and localizer of BRCA2 gene. Timely multigene testing by ctDNA, especially in mCRPC, can determine the most appropriate and accurate therapeutic approach and explore the resistance mechanism.

Citation: Yuan F, Liu N, Yang MZ, Zhang XT, Luo H, Zhou H. Circulating tumor DNA genomic profiling reveals the complicated olaparib-resistance mechanism in prostate cancer salvage therapy: A case report. *World J Clin Cases* 2022; 10(11): 3461-3471

URL: https://www.wjgnet.com/2307-8960/full/v10/i11/3461.htm

DOI: https://dx.doi.org/10.12998/wjcc.v10.i11.3461

INTRODUCTION

The International Agency for Research on Cancer produced an update on global cancer burden using the GLOBOCAN 2020 estimates of cancer incidence and mortality[1]. With an estimated almost 1.4 million new cases and 375000 deaths worldwide, prostate cancer was ranked as the second most frequent cancer and the fifth leading cause of cancer death among men. Asia is traditionally considered a low-incidence area for this type of cancer, but the incidence and mortality rates are rapidly increasing across the continent[2]. In mainland China[3], prostate cancer is now the sixth most commonly occurring malignant tumor. According to the 2020 estimates of global burden, prostate cancer accounted for 120000 of new cases, ranking as the ninth most frequent cancer in China[1]. Patients who progress to metastatic castration-resistant prostate cancer (mCRPC) considered the most serious stage usually suffer from unfavorable clinical prognosis combined with poor quality of life[4].

Treatment options during the disease progression to mCRPC are limited and mainly consist of continued androgen-deprivation therapy (ADT) combined with one of the new endocrine drugs such as abiraterone acetate plus prednisone or with docetaxel chemotherapy plus prednisone. Poly (ADP-ribose) polymerase (PARP) inhibitors, such as olaparib, rucaparib, niraparib or talazoparib, have displayed promising clinical results, with prolonged survival duration and improved life quality in patients with mutations in the homologous recombination repair (*HRR*) gene who are suffering from various cancers, including ovarian[5], breast[6], pancreatic[7], and prostate[8,9]. Recent studies have also shown the potential therapeutic effect of the PARP inhibitor olaparib in mCRPC patients with deleterious mutations in genes belonging to the DNA damage repair (*DDR*). Thereinto, harmful mutation of *BRCA2* may act as a particularly useful marker for therapeutic response to PARP inhibitor. Indeed, the published results from the study named PROfound indicate a holpful clinical effect with olaparib treatment in patients with *BRCA1/2* or *ATM* deleterious mutations[10]. For patients without *DDR* deleterious mutations, it is reported that olaparib combining with abiraterone plus prednisone could be the effective treatment options[11].

The sub-population of mCRPC patients with *HRR* gene partner and localizer of BRCA2 (*PALB2*) mutation has been reported to have the good objective response and prostate-specific antigen (PSA) response[8], but due to the relatively low mutation frequency of *PALB2*, there are limited reports of clinical benefit. Moreover, the Food and Drug Administration has approved olaparib for adult patients

with germline or somatic *HRR* gene-mutated mCRPC, who have progressed following prior treatment with enzalutamide, abiraterone or docetaxel chemotherapy. The evaluation of patients' *HRR* gene mutation was based on tumor tissue, but in routine clinical practice, especially for mCRPC patients, it is a challenge to acquire metastatic tumor tissue biopsies and of sufficient volume for evaluative processing.

Circulating tumor (ct)DNA can be obtained as a 'liquid biopsy' in a minimally invasive manner and as such can serve as a surrogate tumor specimen, providing a real-time snapshot of a patient's overall tumor burden. To date, however, the impact of ctDNA on clinical decision-making for prostate cancer remains unclear and there is a lack of prospective studies in the literature to advance this important topic.

CASE PRESENTATION

Chief complaints

A 61-year-old man presented to Chongqing University Cancer Hospital with complaint of continuous lumbosacral pain that had lasted for 3 mo.

History of present illness

The patient reported a 3 mo history of lumbosacral pain.

History of past illness

The patient had no past illness.

Personal and family history

The patient had no personal and family history.

Physical examination

The patient had stable vital signs with no edema in both lower limbs. Digital rectal examination revealed a hard prostate with many nodules and without tenderness.

Laboratory examinations

The patient showed a markedly increased level of serum total (T)PSA (787 ng/mL; normal: < 4 ng/mL) but normal neuron-specific enolase (4.32 ng/mL).

Imaging examinations

Multiple bone lesions were firstly found by the lumbar magnetic resonance imaging (MRI) (Figure 1A). Then, these lesions and other bones were revealed to have high metabolic activity by bone scanning (Figure 1B). The prostate MRI showed that the seminal vesicle and bladder wall were invaded and pelvic lymph nodes were metastasized (Figure 1C). Computed tomography showed no metastasis in lung.

HISTOLOGICAL EXAMINATIONS

Ultrasound-guided transperineal prostate needle biopsies were obtained (14 specimens in total), and histology confirmed the diagnosis of prostate adenocarcinoma. The specimens showed the Gleason score was highest (5 + 5 = 10) together with an absolute positive rate (14/14). The biopsied tissues tested through immunohistochemistry staining of serial sections excluded a neuroendocrine component [PSA (+), CK-L (+), P504S (+), AR (++) > 95%, NKX3.1 (+), Ki-67 30% (+), Syn (-), CK34βE12 (-), CgA (-), CD56 (-), P63 (-)] (Figure 1D).

MULTIDISCIPLINARY EXPERT CONSULTATION

The definite diagnosis and all treatments were performed by Department of Urology, Department of Tumor Radiotherapy, Department of Imaging, and Department of Pathology in Chongqing University Cancer Hospital.

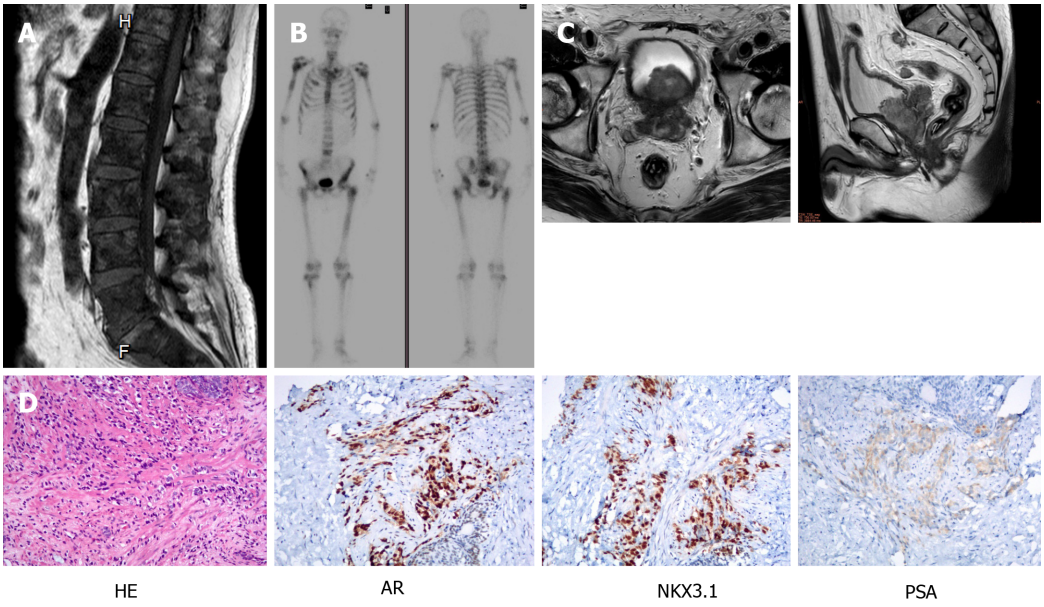

DOI: 10.12998/wjcc.v10.i11.3461

Figure 1 Radiological and immunohistochemical results showing metastatic hormone-sensitive prostate cancer. A: Sagittal magnetic resonance imaging (MRI) showed multiple lumbar vertebrate metastases; B: Bone scanning displayed the high metabolic activity of bone lesions; C: Cross (left) and sagittal (right) sections of MRI scanning (T2WI) displayed invasion of the prostate malignant lesion into the bladder wall as well as the seminal vesicle; D: Hematoxylin-eosinstaining and immunohistochemistry results for androgen receptor, NKX3.1, and periodic Schiff Acid staining. Original magnification: 100 ×; scale bar: 100 μm. HE: Hematoxylin-eosin; AR: Androgen receptor; PSA: Periodic Schiff Acid.

FINAL DIAGNOSIS

Metastatic hormone-sensitive prostate cancer (mHSPC) of pT4N1M1b type and stage IV.

TREATMENT

First-line treatment and outcome

ADT therapy (triptorelin, an LHRH agonist) in combination with docetaxel (three weekly doses of 75 mg/m^2) without prednisolone, was applied as the initial treatment[12-14] fitting with the patient's mHSPC diagnosis and high tumor burden[15]. Two cycles of this therapeutic intervention led to significant relief in the patient's self-reported pain as well as a substantial drop in TPSA level to 0.45 ng/mL (Figure 2A). However, at that point, the docetaxel had to be stopped due to severe bone marrow inhibition and liver toxicity. Therefore, ADT was continued as monotherapy.

Second-line treatment and outcome

After 5 months, the patient developed lumbosacral pain and showed a rebound of increased TPSA. Testosterone levels remained suppressed throughout entire treatment period, indicating disease progression to mCRPC. To determine the new endocrine therapy resistance or sensitivity, he was investigated the classification and respective number of circulating tumor cells (CTCs) along with the expression of AR-V7 mRNA[16]. Based on the negative findings, we had confidence in the decision for abiraterone-prednisone administration as maintenance therapy (Figure 2B and C). After 6 months of this treatment, the patient showed a decreased TPSA level (3.02 ng/mL; Figure 2A). Fortunately, the disease remained effectively controlled by this therapy for nearly 1 year.

Third-line treatment and outcome

The re-emergence of an elevated TPSA level to 69.57 ng/mL manifested disease progression again (Figure 2A). At the time, the patient's CTCs number was increased together with AR-V7 mRNA overexpressions, which confirmed that he had developed abiraterone resistance (Figure 2B and C). Then, he was deemed eligible for a phase III double-blind, randomized, placebo-controlled, multicenter clinical trial to assess the safety and efficacy of proxalutamide (a new androgen receptor[AR] antagonist) in patients with mCRPC who failed abiraterone acetate and docetaxel therapy. Of note, as of the writing of this report, the trial is ongoing. Unfortunately, the patient's disease progressed rapidly during this treatment, as reflected by TPSA level increased to 601 ng/mL (Figure 2A) with somnolence and severe bilateral lower limb edema.

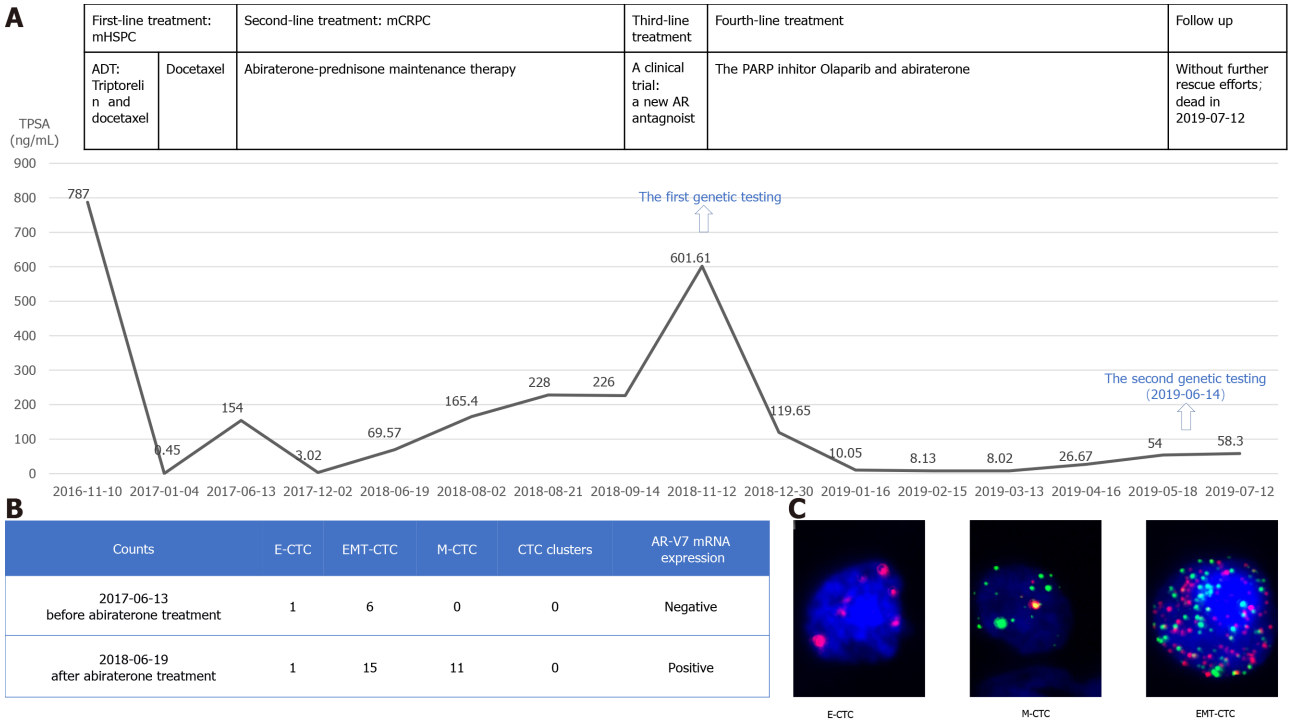

Counts	E-CTC	EMT-CTC	M-CTC	CTC clusters	AR-V7 mRNA expression
2017-06-13 before abiraterone treatment	1	6	0	0	Negative
2018-06-19 after abiraterone treatment	1	15	11	0	Positive

DOI: 10.12998/wjcc.v10.i11.3461

Figure 2 Circulating tumor cells and dynamic change of serum total prostate-specific antigen level. A: Dynamic change of serum total prostate-specific antigen level during the overall treatment with various therapeutic approaches (androgen-deprivation therapy; docetaxel; abiraterone; clinical trial; the PARP inhibitor, olaparib); B: The epithelial-circulating tumor cell (E-CTC), mesenchymal-CTC (M-CTC) and epithelial mesenchymal transition-CTC (EMT-CTC) counts and change before (2017-06-13) and after (2018-06-19) abiraterone treatment. Expression of AR-V7 mRNA was detected in these CTCs; C: Representative graphs displaying the E-CTC, M-CTC and EMT-CTC. Red signal: Probe mixture for detection of mRNA of EpCAM, CK8, CK18, and CK19; Green signal: Probe mixture for detection of mRNA of vimentin and Twist. CTC: Circulating tumor cell.

Fourth-line treatment and outcome

The first genetic testing, performed with the patient's peripheral blood leukocytes, had detected no germline *BRCA1/2* deleterious mutations (Figure 2A). Therefore, we chose to re-challenge the tumor by administration of abiraterone together with the PARP inhibitor olaparib. After only 1 mo of the combined treatment, the patient's TPSA level began to decrease rapidly (from 601.61 ng/mL to 119.65 ng/mL), and in the months thereafter he maintained a low level (8.02 ng/mL) (Figure 2A). Electrocorticography (commonly known as ECOG) findings and the patient's mental state were significantly improved. The patient also reported decreased pain and required a reduced amount of morphine dosage (30 mg, q12h, p.o.). After 5 mo, however, the TPSA level began to rise again and the patient reported increasing carcinomatous pain.

OUTCOME AND FOLLOW-UP

When the disease progressed the third time and we sought to reperform a second comprehensive genomic profile assessment, we chose to use peripheral ctDNA samples due to the difficulty of obtaining a tumor tissue biopsy (Figure 2A). A total of 508 cancer-related genes were sequenced by next-generation sequencing. The *HRR* gene *PALB2* germline pathogenic mutation and two somatic mutations were discovered (Figure 3, Table 1). *PALB2*, as a tumor suppressor belonging to the *HRR* gene, physically interacts with BRCA2 leading to the subsequent recruitment of proteins to DNA breaks and plays a crucial role in repairing double-strand breaks through homologous recombination[17]. Some studies have associated *PALB2* harmful mutations with therapeutic benefit attained from PARP inhibitors[8,18]. For example, the TOPARP-B study has shown that patients with mutations of *PALB2* or somatic cell dysfunction can benefit from olaparib therapy[8].

Meanwhile, 10 somatic variants genes were found: *AR*, *PTEN*, *TP53*, *CHD1*, *NOTCH2*, *FGFR1*, *LHCGR*, *PIK3C2G*, *FLT4* and *CDC25C* (Table 1). In particular, two reverse missense mutations in *PALB2* were suspected as functioning to recover a truncated polypeptide chain translated from the germline *PALB2* mutation (Table 1, Figure 3). Two somatic missense mutations of *PALB2* which were c.751_752delCAinsTT and c.751_753delCAGinsTAC (Figure 3) shared the same loci with the germline deleterious variant c.751C>T. Bringing about the in-frame deletion and insertion variants, the *PALB2*

Table 1 Summary of 13 gene alterations in circulating tumor DNA detected from our patient upon olaparib resistance

Gene	Base change	Amino acid variation	Exon	Variant frequency	Transcript
PTEN	c.136_137del	p.Y46Qfs*5	EX2	59.47%	NM_000314.4
AR			Copy number gain		
CHD1			Copy number loss		
FGFR1			Copy number gain		
TP53	c.665_672*11del	-	EX6-IVS6	36.13%	NM_000546.5
NOTCH2	c.5311-1G>A	-	IVS29	1.28%	NM_024408.3
PIK3C2G	c.2143A>G	p.R715G	EX15	40.23%	NM_004570.4
LHCGR	c.143C>T	p.T48M	EX1	23.39%	NM_000233.3
PALB2	c.751_752delCAinsTT	p.Q251L	EX4	7.31%	NM_024675.3
PALB2	c.751_753delCAGinsTAC	p.Q251Y	EX4	3.79%	NM_024675.3
PALB2	c.751C>T	p.Q251*	EX4	Germline	NM_024675.3
CDC25C	c.1150_1151delGGinsCC	p.G384P	EX12	2.35%	NM_001790.3
FLT4	c.376G>A	p.A126T	EX3	1.15%	NM_002020.4

Bold texts indicate the three *PALB2* mutations detected in the patient.

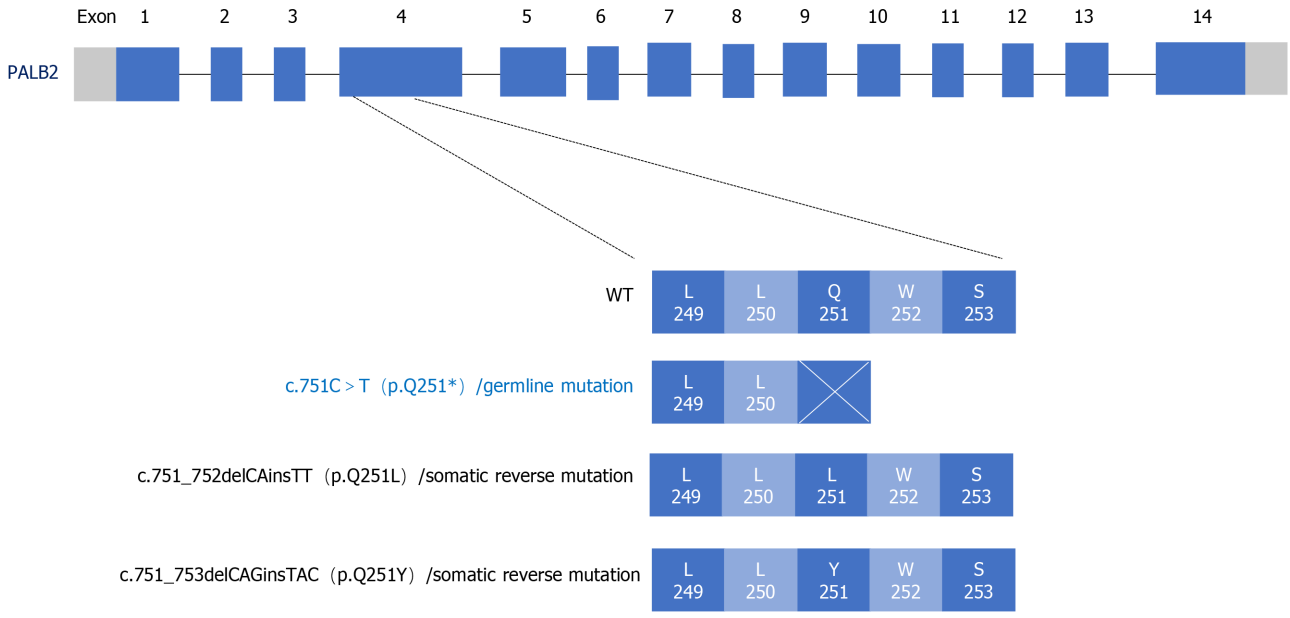

DOI: 10.12998/wjcc.v10.i11.3461

Figure 3 Diagram of the predicted *homologous recombination repair* gene *PALB2* protein sequence changes caused by the germline mutation (c.751C>T) and the two somatic reverse mutations (c.751_752delCAinsTT and c.751_753delCAGinsTAC) on the same loci detected in ctDNA from the patient presenting with resistance of olaparib PAPR inhibitor in combination with abiraterone. HRR: Homologous recombination repair; PALB2: Partner and localizer of BRCA2; WT: Wild-type. Stop codon; nonsense mutation.

mutations would contribute to restoring the entire reading frame and to supporting the correct functioning to repair DNA double-stranded breaks *via* the HRR pathway. Therefore, we reasoned that these two reversing mutations of *PALB2* may represent the mechanism of resistance to olaparib and abiraterone in this patient. In the future, functional assays are needed to validate this potential drug-resistance mechanism as indicated by these ctDNA profile findings.

Finally, the patient's ECOG scale increased and he attained a score of 4. The patient showed clouding of consciousness and developed pain throughout the body, and he died without further rescue efforts.

DISCUSSION

In the case described herein, a mCRPC patient who had undergone treatment by many differing therapy achieved surprisingly clinical response to combination therapy of olaparib and abiraterone-prednisone. Next-generation sequencing of the patient's ctDNA revealed 13 relevant gene mutations, including in the *HRR* gene *PALB2*. Intriguingly, a subgroup of prostate cancer patients who benefit from the treatment of PARP inhibitors have been identified, and these individuals show a trend towards loss-of-function mutations in the *HRR* gene[8,9,18,19]. In the TOPARP-A, TOPARP-B and PROfound studies, olaparib monotherapy was shown to exert antitumor activity against mCRPC with *HRR* or *DDR* gene alterations. The PROfound study[20] indicated that radiologic progression-free survival (rPFS) was significantly longer in the olaparib group than in the group treated with the physician's choice of enzalutamide or abiraterone (median: 7.4 mo *vs* 3.6 mo in patients with *BRCA1/2* and *ATM* mutations; 5.8 mo *vs* 3.5 mo in patients with all 15 *HRR* genes' mutations). Similarly, the TOPARP-A study showed mCRPC patients carrying the *HRR* gene mutation had a median rPFS of 9.8 mo, being 6.1 mo longer than that of mCRPC patients with wild-type *HRR* gene. The TOPARP-B study showed that the mCRPC patients with *PALB2* mutation had a median rPFS of 5.3 mo in response to treatment with olaparib. The gene scope of our first genetic testing was limited to the *BRCA1* and *BRCA2* genes, and indicated that the patient did not carry the germline *BRCA1* or *BRCA2* mutation. Based on the conclusion from the Study 08 (NCT01972217)[11] that olaparib in combination with abiraterone provided efficacious clinical benefit for patients with mCRPC compared to abiraterone alone and regardless of *HRR* mutation status, we chose the olaparib and abiraterone-prednisone combination therapy for our patient. In detail, the Study 08 revealed that olaparib and abiraterone provided median rPFS of 13.8 mo in and intention-to-treat population and 17.8 mo in an *HRR* mutation-positive subgroup.

Our patient achieved rPFS of 5 mo with the PARP inhibitor olaparib and abiraterone-prednisone combination therapy. This response time was overall consistent with olaparib single-drug use previously reported in the literature but was relatively worse than that with the olaparib and abiraterone-prednisone combination therapy. The reason for this may be that our patient had received the abiraterone treatment and developed resistance to such before the olaparib. It is important to note here that Study 08 had recruited patients who had not received prior abiraterone treatment, only having received docetaxel. In addition, there is a dual model of synergy between PARP inhibitor and ADT[21, 22]. PARP is involved in AR-dependent transcription and PARP inhibitor impairs this process, at the same time, the AR regulates transcription of DNA repair genes and androgen depletion impairs *HRR*, which might produce a so-called "BRCA-ness" phenotype that renders susceptibility to PARP inhibitor. Amplification of the *AR* gene, as observed *via* ctDNA profiling of our patient, would lead to continuous activation of downstream signaling pathway(s), overcoming the extrinsic androgen inhibition[23,24] and precluding triggering of the "BRCA-ness" phenotype. The synergy between PARP inhibitor and ADT would not be able to be established in such a patient, which would explain why our patient's clinical response was worse.

The *PALB2* reverse mutations are another important feature of our patient. There was a research about mCRPC patient who achieved 9 mo clinical effect by olaparib with germline *PALB2* p.L253Ifs*2 mutation. During that patient's disease progression, two reverse somatic mutations in *PALB2* were found by ctDNA[25]. Similarly, we detected two somatic reverse mutations and a germline p.Q251* nonsense mutation in *PALB2* at our patient, which may have restored the reading frame and the homologous recombinational function. Once the repair function of homologous recombination is restored, the synthetic lethality on which PARP inhibitors work will be broken, and patient will inevitably be resistant to PARP inhibitor therapy.

Our case also emphasizes the importance of blood-based liquid biopsies and genomic profiling by means of ctDNA. Tumor tissue can be much more difficult to obtain for this evaluative purpose, particularly from advanced cancer patients who are at higher risk in or counter-indicated for surgery or patients who cannot tolerate biopsy for other reasons; another complication is that tumor tissues, in general, may show negative pathological results if the patient has already started or undergone treatment. CtDNA is thus an attractive, minimally invasive alternative, which can used as a practical tool to profile tumor dynamics over time, elucidating features with tumor progression and overcoming spatial heterogeneity of tumors. For our patient, the genetic testing of ctDNA indicated a complicated mechanism of disease response and progression. First, the discovered *HRR* gene *PALB2* germline mutation could explain the rapid response of to the PARP inhibitor olaparib. Second, the two *PALB2* somatic reverse mutations and *AR* gene amplification could underlie the relative shorter response time. Gogola *et al*[26] had reported on activation of the PI3K-AKT–mTOR signal transduction pathway as a mechanism of resistance. These activated oncogenic pathways may cause the expression of homologous recombination genes, which were compensating for DNA double-breaks. By the way,the activated signaling pathways can accelerate the progression of cell cycle or allow cells to evade apoptosis[27]. Because our patient carried mutations in the *PTEN* and *FGFR1* genes, it is intriguing to consider that *FGFR1* amplification with a loss-of-function mutation in *PTEN* can directly or indirectly activate the RAS-RAF-MAPK/ERK signaling pathway as well as that of PI3K-AKT-mTOR[28]. Further validation at the functional level is warranted. According to the patient's ctDNA sequencing results, we were able to evaluate the patient's treatment and response course thoroughly.

Several limits to this clinical evaluative approach still need to be addressed. First, with full respect to the patient's willingness, comprehensive genomic profiling is typically performed only when resistance to olaparib presents. Owing to our patient's rapid disease progression, we were unable to adjust the treatment strategy based on the ctDNA sequencing result. Second, we were unable to distinguish whether the two somatic *PALB2* mutations discovered had been present originally or resulted from the abiraterone combination treatment. If the ctDNA comprehensive sequencing (of 508 genes) had been performed earlier, in lieu of sequencing only the *BRCA1* and *BRCA2* genes, then the abiraterone combination treatment may have been started earlier. In that situation, the detection of germline *PALB2* aberration at a relatively early stage in the disease course may have allowed for the patient to receive olaparib monotherapy, while not being enrolled into the proxalutamide clinical trial, or the abiraterone combination treatment. Third, *PALB2* as a cancer susceptibility gene increases the hazard of breast cancer (absolute risk: 41%-61%). The National Comprehensive Cancer Network (commonly known as NCCN) Genetic/Familial High-Risk assessment: Breast, Ovarian and Pancreatic (Version 1.2022) recommends that the *PALB2* germline mutation carrier should start annual mammograms, with consideration of tomosynthesis and breast MRI with contrast, at age of 30 years and that the healthcare team open discussions into the option of risk-reducing mastectomy. *PALB2* gene mutations are also associated with susceptibility to cancers of the ovary (absolute risk: 3%-5%), pancreas (absolute risk: 5%-10%), and breast in males. The NCCN: Prostate cancer (Version 1.2022) also recommends germline multigene testing that includes (at least) *BRCA1/2* and *PALB2* in its testing panel. Our patient carried a *PALB2* germline pathogenic variation, so that his offspring would carry a 50% likelihood of harboring the same variation. As such, we would suggest that first- and second-degree relatives visit a genetic counselor to further evaluate whether they carry the proband's same *PALB2* mutation; if so, the relative should receive genetic counseling to gain a sufficient understanding of the correlative cancer risk, further screening options and risk-reduction strategies. This will allow the positive carrier to better protect against the onset of related cancers or at least promote their ability to suspect and seek timely assessment to detect a cancer much earlier. Although we made such suggestions to our patient's relatives, none have accepted our suggestion as of the writing of this case report; nonetheless, this is part of our routine strategy of care and we will continue such efforts in the future.

CONCLUSION

Herein, we have described a comprehensive genomic profiling of ctDNA in a mCRPC patient which revealed *HRR* gene germline *PALB2* mutation, including reverse mutations and others affecting known cancer-related signaling pathways. Using the ctDNA sequencing results, we were able to analyze the intrinsic mechanism underlying the patient's rapid response and resistance to the PARP inhibitor and abiraterone combination therapy. On one hand, our case demonstrated that a patient with *HRR* gene *PALB2* mutation can benefit from PAPR inhibitor treatment. On the other hand, the case showed the feasibility of ctDNA sequencing to guide treatment, indicate prognosis and analyze resistance and its underlying mechanisms, with ctDNA serving as a surrogate for limited or unavailable tumor tissue. Overall, though, the case provides a real-world example of how timely multigene testing can be of great importance for selecting the most precise therapeutic approach for cancer patients, especially for those with mCRPC.

FOOTNOTES

Author contributions: Yuan F, Liu N and Yang MZ collected the patient's clinical data and drafted the paper; Yuan F and Luo H provided the patient's clinical treatment; Zhang XT performed the molecular genetic studies; Zhou H designed and coordinated the study and participated in preparation of the draft; all authors read and approved the final manuscript.

Supported by the Natural Science Foundation of Chongqing, No. cstc2018jcyjAX0781; the Major Project of Chongqing Health Committee, No. cstc2016 shmszx130033031; the National Natural Science Foundation of China, No. 81302316; and the Chongqing technological innovation and application development - Major theme projects, No. cstc2019jscx-fxydx0008.

Informed consent statement: Informed written consent was obtained from the patient for publication of this report and any accompanying images.

Conflict-of-interest statement: The authors declare that they have no conflicts of interest.

CARE Checklist (2016) statement: The authors have read the CARE Checklist (2016), and the manuscript was prepared and revised according to the CARE Checklist (2016).

Country/Territory of origin: China

ORCID number: Fang Yuan 0000-0003-2516-5090; Nan Liu 0000-0001-9011-9803; Ming-Zhen Yang 0000-0001-9389-723X; Xiao-Tian Zhang 0000-0003-0230-4860; Hong Luo 0000-0002-9228-1334; Hong Zhou 0000-0003-2526-8153.

Corresponding Author's Membership in Professional Societies: Chinese Anti-Cancer Association - Medical Ethics Professional Committee; the Chinese Society of Clinical Oncology (CSCO) Big Data Expert Committee.

S-Editor: Wang LL
L-Editor: A
P-Editor: Wang LL

REFERENCES

1 **Sung H**, Ferlay J, Siegel RL, Laversanne M, Soerjomataram I, Jemal A, Bray F. Global Cancer Statistics 2020: GLOBOCAN Estimates of Incidence and Mortality Worldwide for 36 Cancers in 185 Countries. *CA Cancer J Clin* 2021; **71**: 209-249 [PMID: 33538338 DOI: 10.3322/caac.21660]

2 **Zhu Y**, Mo M, Wei Y, Wu J, Pan J, Freedland SJ, Zheng Y, Ye D. Epidemiology and genomics of prostate cancer in Asian men. *Nat Rev Urol* 2021; **18**: 282-301 [PMID: 33692499 DOI: 10.1038/s41585-021-00442-8]

3 **Zheng RS**, Sun KX, Zhang SW, Zeng HM, Zou XN, Chen R, Gu XY, Wei WW, He J. [Report of cancer epidemiology in China, 2015]. *ZhonghuaZhong Liu ZaZhi* 2019; **41**: 19-28 [PMID: 30678413 DOI: 10.3760/cma.j.issn.0253-3766.2019.01.005]

4 **Robinson D**, Van Allen EM, Wu YM, Schultz N, Lonigro RJ, Mosquera JM, Montgomery B, Taplin ME, Pritchard CC, Attard G, Beltran H, Abida W, Bradley RK, Vinson J, Cao X, Vats P, Kunju LP, Hussain M, Feng FY, Tomlins SA, Cooney KA, Smith DC, Brennan C, Siddiqui J, Mehra R, Chen Y, Rathkopf DE, Morris MJ, Solomon SB, Durack JC, Reuter VE, Gopalan A, Gao J, Loda M, Lis RT, Bowden M, Balk SP, Gaviola G, Sougnez C, Gupta M, Yu EY, Mostaghel EA, Cheng HH, Mulcahy H, True LD, Plymate SR, Dvinge H, Ferraldeschi R, Flohr P, Miranda S, Zafeiriou Z, Tunariu N, Mateo J, Perez-Lopez R, Demichelis F, Robinson BD, Schiffman M, Nanus DM, Tagawa ST, Sigaras A, Eng KW, Elemento O, Sboner A, Heath EI, Scher HI, Pienta KJ, Kantoff P, de Bono JS, Rubin MA, Nelson PS, Garraway LA, Sawyers CL, Chinnaiyan AM. Integrative clinical genomics of advanced prostate cancer. *Cell* 2015; **161**: 1215-1228 [PMID: 26000489 DOI: 10.1016/j.cell.2015.05.001]

5 **DiSilvestro P**, Colombo N, Scambia G, Kim BG, Oaknin A, Friedlander M, Lisyanskaya A, Floquet A, Leary A, Sonke GS, Gourley C, Banerjee S, Oza A, González-Martín A, Aghajanian CA, Bradley WH, Mathews CA, Liu J, Lowe ES, Bloomfield R, Moore KN. Efficacy of Maintenance Olaparib for Patients With Newly Diagnosed Advanced Ovarian Cancer With a BRCA Mutation: Subgroup Analysis Findings From the SOLO1 Trial. *J Clin Oncol* 2020; **38**: 3528-3537 [PMID: 32749942 DOI: 10.1200/JCO.20.00799]

6 **Robson M**, Im SA, Senkus E, Xu B, Domchek SM, Masuda N, Delaloge S, Li W, Tung N, Armstrong A, Wu W, Goessl C, Runswick S, Conte P. Olaparib for Metastatic Breast Cancer in Patients with a Germline BRCA Mutation. *N Engl J Med* 2017; **377**: 523-533 [PMID: 28578601 DOI: 10.1056/NEJMoa1706450]

7 **Golan T**, Hammel P, Reni M, Van Cutsem E, Macarulla T, Hall MJ, Park JO, Hochhauser D, Arnold D, Oh DY, Reinacher-Schick A, Tortora G, Algül H, O'Reilly EM, McGuinness D, Cui KY, Schlienger K, Locker GY, Kindler HL. Maintenance Olaparib for Germline *BRCA*-Mutated Metastatic Pancreatic Cancer. *N Engl J Med* 2019; **381**: 317-327 [PMID: 31157963 DOI: 10.1056/NEJMoa1903387]

8 **Mateo J**, Porta N, Bianchini D, McGovern U, Elliott T, Jones R, Syndikus I, Ralph C, Jain S, Varughese M, Parikh O, Crabb S, Robinson A, McLaren D, Birtle A, Tanguay J, Miranda S, Figueiredo I, Seed G, Bertan C, Flohr P, Ebbs B, Rescigno P, Fowler G, Ferreira A, Riisnaes R, Pereira R, Curcean A, Chandler R, Clarke M, Gurel B, Crespo M, Nava Rodrigues D, Sandhu S, Espinasse A, Chatfield P, Tunariu N, Yuan W, Hall E, Carreira S, de Bono JS. Olaparib in patients with metastatic castration-resistant prostate cancer with DNA repair gene aberrations (TOPARP-B): a multicentre, open-label, randomised, phase 2 trial. *Lancet Oncol* 2020; **21**: 162-174 [PMID: 31806540 DOI: 10.1016/S1470-2045(19)30684-9]

9 **Mateo J**, Carreira S, Sandhu S, Miranda S, Mossop H, Perez-Lopez R, Nava Rodrigues D, Robinson D, Omlin A, Tunariu N, Boysen G, Porta N, Flohr P, Gillman A, Figueiredo I, Paulding C, Seed G, Jain S, Ralph C, Protheroe A, Hussain S, Jones R, Elliott T, McGovern U, Bianchini D, Goodall J, Zafeiriou Z, Williamson CT, Ferraldeschi R, Riisnaes R, Ebbs B, Fowler G, Roda D, Yuan W, Wu YM, Cao X, Brough R, Pemberton H, A'Hern R, Swain A, Kunju LP, Eeles R, Attard G, Lord CJ, Ashworth A, Rubin MA, Knudsen KE, Feng FY, Chinnaiyan AM, Hall E, de Bono JS. DNA-Repair Defects and Olaparib in Metastatic Prostate Cancer. *N Engl J Med* 2015; **373**: 1697-1708 [PMID: 26510020 DOI: 10.1056/NEJMoa1506859]

10 **de Bono J**, Mateo J, Fizazi K, Saad F, Shore N, Sandhu S, Chi KN, Sartor O, Agarwal N, Olmos D, Thiery-Vuillemin A, Twardowski P, Mehra N, Goessl C, Kang J, Burgents J, Wu W, Kohlmann A, Adelman CA, Hussain M. Olaparib for Metastatic Castration-Resistant Prostate Cancer. *N Engl J Med* 2020; **382**: 2091-2102 [PMID: 32343890 DOI: 10.1056/NEJMoa1911440]

11 **Clarke N**, Wiechno P, Alekseev B, Sala N, Jones R, Kocak I, Chiuri VE, Jassem J, Fléchon A, Redfern C, Goessl C, Burgents J, Kozarski R, Hodgson D, Learoyd M, Saad F. Olaparib combined with abiraterone in patients with metastatic castration-resistant prostate cancer: a randomised, double-blind, placebo-controlled, phase 2 trial. *Lancet Oncol* 2018; **19**: 975-986 [PMID: 29880291 DOI: 10.1016/S1470-2045(18)30365-6]

12 **Lavaud P**, Gravis G, Foulon S, Joly F, Oudard S, Priou F, Latorzeff I, Mourey L, Soulié M, Delva R, Krakowski I, Laguerre B, Théodore C, Ferrero JM, Beuzeboc P, Habibian M, Rolland F, Deplanque G, Pouessel D, Zanetta S, Berdah JF, Dauba J, Baciuchka M, Platini C, Linassier C, Tubiana-Mathieu N, Machiels JP, Kouri CE, Ravaud A, Suc E, Eymard JC, Hasbini A, Bousquet G, Culine S, Boher JM, Tergemina-Clain G, Legoupil C, Fizazi K. Anticancer Activity and Tolerance of Treatments Received Beyond Progression in Men Treated Upfront with Androgen Deprivation Therapy With or Without Docetaxel for Metastatic Castration-naïve Prostate Cancer in the GETUG-AFU 15 Phase 3 Trial. *EurUrol* 2018; **73**: 696-703 [PMID: 29074061 DOI: 10.1016/j.eururo.2017.09.022]

13 **James ND**, Sydes MR, Clarke NW, Mason MD, Dearnaley DP, Spears MR, Ritchie AW, Parker CC, Russell JM, Attard G, de Bono J, Cross W, Jones RJ, Thalmann G, Amos C, Matheson D, Millman R, Alzouebi M, Beesley S, Birtle AJ, Brock S, Cathomas R, Chakraborti P, Chowdhury S, Cook A, Elliott T, Gale J, Gibbs S, Graham JD, Hetherington J, Hughes R, Laing R, McKinna F, McLaren DB, O'Sullivan JM, Parikh O, Peedell C, Protheroe A, Robinson AJ, Srihari N, Srinivasan R, Staffurth J, Sundar S, Tolan S, Tsang D, Wagstaff J, Parmar MK; STAMPEDE investigators. Addition of docetaxel, zoledronic acid, or both to first-line long-term hormone therapy in prostate cancer (STAMPEDE): survival results from an adaptive, multiarm, multistage, platform randomised controlled trial. *Lancet* 2016; **387**: 1163-1177 [PMID: 26719232 DOI: 10.1016/S0140-6736(15)01037-5]

14 **Kyriakopoulos CE**, Chen YH, Carducci MA, Liu G, Jarrard DF, Hahn NM, Shevrin DH, Dreicer R, Hussain M, Eisenberger M, Kohli M, Plimack ER, Vogelzang NJ, Picus J, Cooney MM, Garcia JA, DiPaola RS, Sweeney CJ. Chemohormonal Therapy in Metastatic Hormone-Sensitive Prostate Cancer: Long-Term Survival Analysis of the Randomized Phase III E3805 CHAARTED Trial. *J Clin Oncol* 2018; **36**: 1080-1087 [PMID: 29384722 DOI: 10.1200/JCO.2017.75.3657]

15 **Gravis G**, Boher JM, Chen YH, Liu G, Fizazi K, Carducci MA, Oudard S, Joly F, Jarrard DM, Soulie M, Eisenberger MJ, Habibian M, Dreicer R, Garcia JA, Hussain MHM, Kohli M, Vogelzang NJ, Picus J, DiPaola R, Sweeney C. Burden of Metastatic Castrate Naive Prostate Cancer Patients, to Identify Men More Likely to Benefit from Early Docetaxel: Further Analyses of CHAARTED and GETUG-AFU15 Studies. *EurUrol* 2018; **73**: 847-855 [PMID: 29475737 DOI: 10.1016/j.eururo.2018.02.001]

16 **Armstrong AJ**, Halabi S, Luo J, Nanus DM, Giannakakou P, Szmulewitz RZ, Danila DC, Healy P, Anand M, Rothwell CJ, Rasmussen J, Thornburg B, Berry WR, Wilder RS, Lu C, Chen Y, Silberstein JL, Kemeny G, Galletti G, Somarelli JA, Gupta S, Gregory SG, Scher HI, Dittamore R, Tagawa ST, Antonarakis ES, George DJ. Prospective Multicenter Validation of Androgen Receptor Splice Variant 7 and Hormone Therapy Resistance in High-Risk Castration-Resistant Prostate Cancer: The PROPHECY Study. *J Clin Oncol* 2019; **37**: 1120-1129 [PMID: 30865549 DOI: 10.1200/JCO.18.01731]

17 **Xia B**, Sheng Q, Nakanishi K, Ohashi A, Wu J, Christ N, Liu X, Jasin M, Couch FJ, Livingston DM. Control of BRCA2 cellular and clinical functions by a nuclear partner, PALB2. *Mol Cell* 2006; **22**: 719-729 [PMID: 16793542 DOI: 10.1016/j.molcel.2006.05.022]

18 **Abida W**, Campbell D, Patnaik A, Shapiro JD, Sautois B, Vogelzang NJ, Voog EG, Bryce AH, McDermott R, Ricci F, Rowe J, Zhang J, Piulats JM, Fizazi K, Merseburger AS, Higano CS, Krieger LE, Ryan CJ, Feng FY, Simmons AD, Loehr A, Despain D, Dowson M, Green F, Watkins SP, Golsorkhi T, Chowdhury S. Non-BRCA DNA Damage Repair Gene Alterations and Response to the PARP Inhibitor Rucaparib in Metastatic Castration-Resistant Prostate Cancer: Analysis From the Phase II TRITON2 Study. *Clin Cancer Res* 2020; **26**: 2487-2496 [PMID: 32086346 DOI: 10.1158/1078-0432.CCR-20-0394]

19 **Niraparib Shrinks**. *BRCA*-Mutated Prostate Tumors. *Cancer Discov* 2019; **9**: OF7 [PMID: 30824427 DOI: 10.1158/2159-8290.CD-NB2019-030]

20 **M Hussain JM**, K Fizazi, F Saad, ND Shore, S Sandhu, KN Chi, O Sartor, N Agarwal, D Olmos, A Thiery-Vuillemin, P Twardowski, N Mehra, C Goessl, J Kang, J Burgents, W Wu, A Kohlmann, CA Adelman, J de Bono. Profound: Phase 3 Study of Olaparib Versus Enzalutamide or Abiraterone for Metastatic Castration-Resistant Prostate Cancer (Mcrpc) with Homologous Recombination Repair (Hrr) Gene Alterations. *Annals of Oncology* 2019; 851-934

21 **Asim M**, Tarish F, Zecchini HI, Sanjiv K, Gelali E, Massie CE, Baridi A, Warren AY, Zhao W, Ogris C, McDuffus LA, Mascalchi P, Shaw G, Dev H, Wadhwa K, Wijnhoven P, Forment JV, Lyons SR, Lynch AG, O'Neill C, Zecchini VR, Rennie PS, Baniahmad A, Tavaré S, Mills IG, Galanty Y, Crosetto N, Schultz N, Neal D, Helleday T. Synthetic lethality between androgen receptor signalling and the PARP pathway in prostate cancer. *Nat Commun* 2017; **8**: 374 [PMID: 28851861 DOI: 10.1038/s41467-017-00393-y]

22 **Li L**, Karanika S, Yang G, Wang J, Park S, Broom BM, Manyam GC, Wu W, Luo Y, Basourakos S, Song JH, Gallick GE, Karantanos T, Korentzelos D, Azad AK, Kim J, Corn PG, Aparicio AM, Logothetis CJ, Troncoso P, Heffernan T, Toniatti C, Lee HS, Lee JS, Zuo X, Chang W, Yin J, Thompson TC. Androgen receptor inhibitor-induced "BRCAness" and PARP inhibition are synthetically lethal for castration-resistant prostate cancer. *Sci Signal* 2017; **10** [PMID: 28536297 DOI: 10.1126/scisignal.aam7479]

23 **Seitz AK**, Thoene S, Bietenbeck A, Nawroth R, Tauber R, Thalgott M, Schmid S, Secci R, Retz M, Gschwend JE, Ruland J, Winter C, Heck MM. AR-V7 in Peripheral Whole Blood of Patients with Castration-resistant Prostate Cancer: Association with Treatment-specific Outcome Under Abiraterone and Enzalutamide. *EurUrol* 2017; **72**: 828-834 [PMID: 28818355 DOI: 10.1016/j.eururo.2017.07.024]

24 **De Laere B**, Rajan P, Grönberg H, Dirix L, Lindberg J; CORE-ARV-CTC and ProBIO Investigators. Androgen Receptor Burden and Poor Response to Abiraterone or Enzalutamide in TP53 Wild-Type Metastatic Castration-Resistant Prostate Cancer. *JAMA Oncol* 2019; **5**: 1060-1062 [PMID: 31046065 DOI: 10.1001/jamaoncol.2019.0869]

25 **Goodall J**, Mateo J, Yuan W, Mossop H, Porta N, Miranda S, Perez-Lopez R, Dolling D, Robinson DR, Sandhu S, Fowler G, Ebbs B, Flohr P, Seed G, Rodrigues DN, Boysen G, Bertan C, Atkin M, Clarke M, Crespo M, Figueiredo I, Riisnaes R, Sumanasuriya S, Rescigno P, Zafeiriou Z, Sharp A, Tunariu N, Bianchini D, Gillman A, Lord CJ, Hall E, Chinnaiyan AM,

Carreira S, de Bono JS; TOPARP-A investigators. Circulating Cell-Free DNA to Guide Prostate Cancer Treatment with PARP Inhibition. *Cancer Discov* 2017; **7**: 1006-1017 [PMID: 28450425 DOI: 10.1158/2159-8290.CD-17-0261]

26 **Gogola E**, Rottenberg S, Jonkers J. Resistance to PARP Inhibitors: Lessons from Preclinical Models of BRCA-Associated Cancer. *Annual Review of Cancer Biology* 2019; **3**: 235-254 [DOI: 10.1146/annurev-cancerbio-030617-050232]

27 **Pilié PG**, Tang C, Mills GB, Yap TA. State-of-the-art strategies for targeting the DNA damage response in cancer. *Nat Rev Clin Oncol* 2019; **16**: 81-104 [PMID: 30356138 DOI: 10.1038/s41571-018-0114-z]

28 **Corn PG**, Wang F, McKeehan WL, Navone N. Targeting fibroblast growth factor pathways in prostate cancer. *Clin Cancer Res* 2013; **19**: 5856-5866 [PMID: 24052019 DOI: 10.1158/1078-0432.CCR-13-1550]

World Journal of Clinical Cases

Submit a Manuscript: https://www.f6publishing.com

World J Clin Cases 2022 April 16; 10(11): 3472-3477

DOI: 10.12998/wjcc.v10.i11.3472

ISSN 2307-8960 (online)

CASE REPORT

Difference and similarity between type A interrupted aortic arch and aortic coarctation in adults: Two case reports

Si-Xie Ren, Qian Zhang, Pan-Pan Li, Xiao-Dong Wang

Specialty type: Cardiac and cardiovascular systems

Provenance and peer review: Unsolicited article; Externally peer reviewed.

Peer-review model: Single blind

Peer-review report's scientific quality classification

Grade A (Excellent): 0
Grade B (Very good): B
Grade C (Good): 0
Grade D (Fair): 0
Grade E (Poor): 0

P-Reviewer: Wierzbicka A, Poland

Received: July 12, 2021
Peer-review started: July 12, 2021
First decision: November 19, 2021
Revised: December 2, 2021
Accepted: February 27, 2022
Article in press: February 27, 2022
Published online: April 16, 2022

Si-Xie Ren, Pan-Pan Li, Department of Radiology, Chengdu Second People's Hospital, Chengdu 610000, Sichuan Province, China

Qian Zhang, Department of Radiology, First Hospital of Shanxi Medical University, Taiyuan 030000, Shanxi Province, China

Xiao-Dong Wang, Department of Radiology, Sichuan Cancer Hospital, Chengdu 610000, Sichuan Province, China

Corresponding author: Xiao-Dong Wang, MM, Doctor, Department of Radiology, Sichuan Cancer Hospital, Sichuan Cancer Hospital, No. 55 Section 4, South Renmin Road, Chengdu 610000, Sichuan Province, China. 287238197@qq.com

Abstract

BACKGROUND

Aortic coarctation (CoA) is usually confused with interrupted aortic arch (IAA), especially adult type A interrupted aortic arch, due to their similar anatomical location. Although the main difference between them is whether arterial lumen exhibits continuity or not, the clinical manifestations are similar and connection exists between them. Adult type A IAA is considered as an extreme form of CoA, which is complete discontinuity of aortic function and lumen caused by degenerative arterial coarctation. This paper reports two cases (interrupted aortic arch and severe aortic coarctation) to analyze the difference and similarity between them.

CASE SUMMARY

The two cases of patients presented with hypertension for many years. Computed tomography angiography showed that the aortic arch and descending aorta were discontinuous or significantly narrowed with extensive collateral flow. The IAA patient refused surgical treatment and blood pressure could be controlled with drugs. While the CoA patient underwent stent implantation because of uncontrollable hypertension, the blood flow recovered smoothly and the blood pressures at both ends of the stenosis returned to normal after surgery.

CONCLUSION

Adult type A IAA and CoA have difference and similarity, and type A IAA is associated with CoA to a certain extent. The treatment method should be chosen based on the patient's clinical symptoms rather than the severity of the lesion.

Key Words: Interrupted aortic arch; Aortic coarctation; Computed tomography Angiogram; Case report

Core Tip: According to the characteristics of aortic coarctation and interrupted aortic arch, this paper highlights the difference and similarity between them. The treatment method should be based on the patient's clinical symptoms rather than the severity of the lesion.

Citation: Ren SX, Zhang Q, Li PP, Wang XD. Difference and similarity between type A interrupted aortic arch and aortic coarctation in adults: Two case reports. *World J Clin Cases* 2022; 10(11): 3472-3477
URL: https://www.wjgnet.com/2307-8960/full/v10/i11/3472.htm
DOI: https://dx.doi.org/10.12998/wjcc.v10.i11.3472

INTRODUCTION

Interrupted aortic arch (IAA) is a congenital malformation disease with loss of continuity between the aortic arch and descending aorta, accounting for about 1% of congenital heart diseases[1]. According to the location of the dissection, it is divided into three types[2]: The dissection located at the distal to the left subclavian artery origin (type A); that located between the left common carotid artery and the left subclavian artery (type B); and that between the brachiocephalic trunk and the left common carotid artery (type C). Type A accounts for approximately 79% of adult IAA cases[3], without the complications associated with type B such as ventricular septal defects and patent ductus arteriosus[1,4-6]. Coarctation of the aorta (CoA) is defined as a discrete stenosis of the aorta usually located in the area of the ligamentum arteriosum, with a higher incidence of 6%-8% than IAA[3]. To investigate if there are any difference and similarity between adult type A IAA and CoA, cases of both types were reported in this study.

CASE PRESENTATION

Chief complaints

A 54-year-old woman presented to the hospital with chief complaints of discomfort in right waist and abdominal pain for 1 wk. And a 61-year-old female patient, with tiredness and dizziness, was diagnosed with CoA during physical examination 1 year ago.

History of present illness

The medical history was notable for hypertension and the right renal cyst in Case 1. And the described patient in Case 2 was diagnosed with CoA during physical examination 1 year ago with tiredness and dizziness.

History of past illness

The first woman in Case 1 had hypertension for 8 years. The second patient in Case 2 with a history of hypertension for 30 years had the highest blood pressure of 190/100 mmHg, and a clear medical history of thyroidectomy and coronary artery stenosis.

Physical examination

In Case 1, continuous murmurs were heard on the chest and back during auscultation. The blood pressure was monitored after taking the medication, and the left upper and left lower limb blood pressure was 145/77 mmHg and 120/64 mmHg, respectively. The dorsalis pedis arteries were thin and weak. In Case 2, the upper limb pressure was higher than the lower limb pressure.

Laboratory examinations

Laboratory examination indicated the following in Case 1: Uric acid, 412 μmol/L; triacylglycerol 1.95mmol/L.; and glucose, 5.5 mmol/L.

Laboratory examination indicated the following in Case 2: Urea, 3.25 mmol/L; creatinine, 50.8 μmol/L; cholesterol, 3.94 mmol/L; alanine aminotransferase, 19 U/L; aspartate aminotransferase, 23 U/L; and glucose, 4.81 mmol/L.

Urinalysis, coagulation tests, complete blood count, and infection marker tests did not reveal any obvious abnormalities in either patient.

Imaging examinations

Case 1: Electrocardiogram (ECG) showed complete right bundle branch block and T wave change. Color Doppler echocardiography displayed a normal right atrium and right ventricle, and an enlarged left atrium and left ventricle. The aortic arch and the distal to the left subclavian artery were discontinuous, and numerous collateral branches existed around the descending aorta. The flow of the abdominal aorta showed a small slow wave.

Abdominal computed tomography (CT) examination revealed multiple tortuous vascular shadows in the paravertebral column and bilateral chest wall areas. To further clarify the diagnosis, thoracic and abdominal computed tomography angiography (CTA) was performed, which showed that the aortic arch and descending aorta were discontinuous, and the disconnection was located at the distal to the left subclavian artery (type A IAA) (Figure 1A). The ascending aorta was dilated with normal curvature and aneurysm formation in the descending aorta (Figure 1A and B). Bilateral internal mammary arteries, intercostal arteries, thoracoabdominal wall arteries, and multiple arterial branches tortuously expanded to supply blood to distal vessels and organs. For example, the bilateral internal mammary arteries were connected to the external iliac arteries (Figure 1C), and the blood of the abdominal trunk came from the intercostal artery and the inferior phrenic artery.

Case 2: ECG showed first degree atrioventricular block and abnormal Q wave in V1-V3 leads. Color Doppler echocardiography indicated no obvious enlargement in the atria or ventricles of the heart.

CTA examination showed that the lumen of the aortic isthmus was significantly narrowed (Figure 2A), the normal curvature of the ascending aorta was maintained, and the proximal descending aorta was slightly enlarged (Figure 2A). The bilateral internal mammary arteries were connected with the distal external iliac arteries (Figure 2B).

Medication History

The maximum systolic pressure was acceptably controlled in the past with valsartan, hydrochlorothiazide tablets, and levamlodipine besylate tablets in Case 1. Oral administration of nifedipine controlled-release tablets (Bai Xintong), candesartan cilexetil, and indapamide sustained release tablets did not control blood pressure well in Case 2.

FINAL DIAGNOSIS

Based on the images of Figure 1 and 2, we diagnosed the two patients as having type A IAA and CoA with extensive collateral flow, respectively.

TREATMENT

Without other positive symptoms, the first patient only required treatment of the relevant symptoms. The blood pressure controlled with antihypertensive drugs was acceptable during the follow-up period.

Due to uncontrollable hypertension, the second patient was admitted to the hospital and received aortic angiography and stent implantation under general anesthesia. The angiography indicated severe narrowing of the descending aorta 15 mm distal to the left subclavian artery, with a length of 10 mm. Before stent placement, the blood pressure at both ends of the constriction was 185/73 mmHg and 110/65 mmHg, respectively. After stent placement, the blood flow recovered smoothly, and the blood pressure at both ends of the stent was 127/62 mmHg and 122/62 mmHg, respectively.

OUTCOME AND FOLLOW-UP

Both of the patients have remained stable.

DISCUSSION

The difference between type A IAA and CoA in adults is the absence or presence of continuity of the arterial lumen. As shown in Case 1, there was no anatomical continuity between the distal to the left subclavian artery and descending aorta (type A IAA). In contrast, no obvious anatomical interruption was detected in CoA case with the narrowing between the above-mentioned arteries. According to

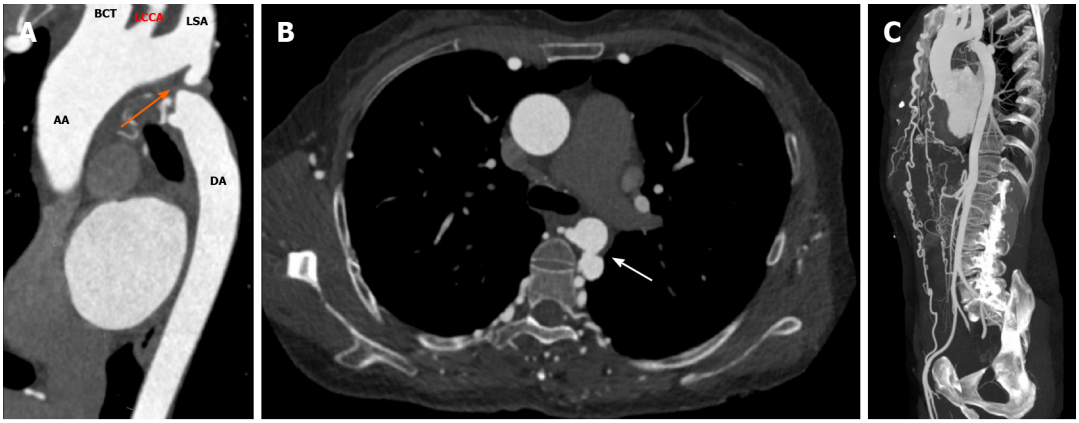

DOI: 10.12998/wjcc.v10.i11.3472 **Copyright** © The Author(s) 2022.

Figure 1 Type A IAA in a 54-year-old woman. A: Reformatted oblique sagittal image of the aorta shows interruption of the aorta just distal to the subclavian artery origin (orange arrow). Note the maintenance of curvature of the ascending aorta and the extension of the interrupted aorta beyond the left subclavian artery several centimeters; B: Aneurysm formation in the descending aorta (white arrow); C: Maximum intensity projection shows a massive aorta which included two full-fledged collateral networks ensuring blood circulation to the distal aorta. AA: Ascending aorta; DA: Descending aorta; BCT: Brachiocephalic trunk; LCCA: Left common carotid artery; LSA: Left subclavian artery.

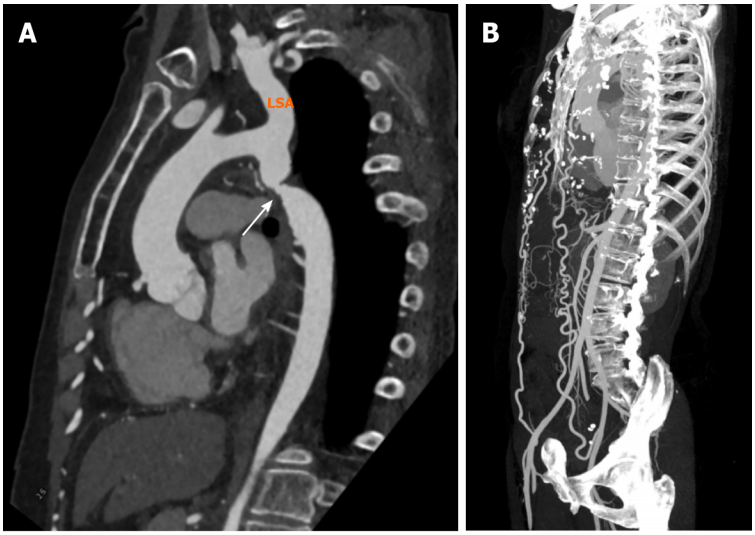

DOI: 10.12998/wjcc.v10.i11.3472 **Copyright** © The Author(s) 2022.

Figure 2 Severe coarctation in a 61-year-old woman. A: Reformatted oblique sagittal image of the aorta shows coarctation of the aorta just distal to the subclavian artery origin (white arrow) and slight enlargement of the proximal descending aorta. The ascending aorta maintains normal curvature and the narrowing is a few centimeters away from the subclavian artery; B: Maximum intensity projection shows collateral flow which included two full-fledged collateral networks ensuring blood circulation to the distal aorta. LSA: Left subclavian artery.

previous reports, although the definitions of type A IAA and CoA were different, the clinical manifestations were similar in increased blood pressure, which was higher in the upper limbs than in the lower limbs[7-12]. The manifestations of Cases 1 and 2 in this study were consistent with these reports. The pathophysiological changes are: (1) Imbalanced distribution of blood flow and blood pressure in the upper and lower limbs is caused by increased mechanical resistance resulting from interruption or stenosis of the arterial lumen; and (2) hypoperfusion in lower bodies results in the activation of the renin-angiotensin-aldosterone system[12]. Typical symptoms were not observed in the lower extremities of the two cases due to the fact that extensive collateral circulation was established to supply blood flow to the distal organs in both cases. As aggravation of the narrowing, upper limb blood pressure can be significantly increased, which may cause a series of symptoms such as upper limb pain, headache, dizziness, angina, and lower limb chills and claudication.

The mechanism of IAA in adults is different from that in infancy[1]. The most common type in infancy is the type B IAA which is closely related to congenital developmental abnormalities and may be concurrent with other anomalies including patent ductus arteriosus, aneurysm, ventricular septal defect, *etc.*[1,9]. While type A IAA in adults is similar to CoA in diseased anatomical position which is located between the left subclavian artery and the ductus arteriosus[13], type A IAA in adults may be

the result of regression or atrophy of the diseased arterial segment as this segment can be narrowed, atretic, fibrotic, or completely absent[2]. Some researchers[9,13] believed that in CoA, the ascending aorta maintained normal curvature, the narrowing was located several centimeters away from the left subclavian artery, and distal to the coarctation was enlarged or formed aneurysm because increased velocity of blood flow at the region damaged the vessel wall[6,14]. These findings were seen in Case 1, which strongly suggested that adult type A IAA is the final stage of aortic coarctation degeneration. The IAA cases caused by severe CoA have also been reported in the literature[15,16]. The patients initially showed aorta narrowing. Over time, the complete obstruction of the narrowed lumens led to aortic interruption, which was eventually treated by surgical intervention.

The blood pressure of the patient with type A IAA in Case 1 could be controlled with drugs, so surgical intervention was not performed. Generally, the main treatment for IAA is to reconstruct the blood flow at both ends of the interrupted arteries, which can be achieved by surgical means (such as end-to-end anastomosis, graft interposition, or extra-anastomotic bypass) and percutaneous approach [1]. At present, there is still a lack of long-term follow-up data on adult patients with type A IAA repaired, and postoperative complications in these patients require continuous attention. The goal of surgery in CoA is the same as that in type A IAA, which is to reestablish the lesion to enable appropriate blood flow. Surgical methods for the treatment of CoA are mainly balloon angioplasty and stent placement[17]. The patient with severe CoA in Case 2 was treated by stent placement because of uncontrollable hypertension. Blood pressure at both ends of the stenosis returned to normal after surgery, and long-term follow-up observation will be essential for a series of complications after CoA is repaired, such as restenosis, hypertension, coronary artery disease, aortic rupture, and aneurysm formation[3,11,17].

CONCLUSION

Adult type A IAA and CoA have difference and similarity. The difference lies in the absence or presence of continuity of the arterial lumen, while the similarity is that they are accompanied by secondary hypertension with extensive collateral circulation. In conclusion, type A IAA is associated with CoA to a certain extent, and it can be considered that the arterial lumen is completely interrupted between the aortic arch and descending aorta with the degeneration or atrophy of arterial narrowing.

FOOTNOTES

Author contributions: Ren SX and Li PP reviewed the literature and contributed to manuscript drafting; Zhang Q provided the image processing and interpretation and contributed to manuscript drafting; Wang XD was responsible for revising the manuscript for important intellectual content; all authors provided final approval for the version to be submitted.

Informed consent statement: Informed written consent was obtained from the patients for publication of this report and any accompanying images.

Conflict-of-interest statement: The authors declare that they have no conflict of interest to disclose.

CARE Checklist (2016) statement: The authors have read the CARE Checklist (2016), and the manuscript was prepared and revised according to the CARE Checklist (2016).

Country/Territory of origin: China

ORCID number: Si-Xie Ren 0000-0003-0915-9491; Qian Zhang 0000-0001-5275-9412; Pan-Pan Li 0000-0003-1043-5334; Xiao-Dong Wang 0000-0002-9270-4640.

S-Editor: Ma YJ
L-Editor: Wang TQ
P-Editor: Ma YJ

REFERENCES

1 **Pérez TM**, García SM, Velasco ML, Sánchez AP. Interrupted aortic arch diagnosis by computed tomography angiography and 3-D reconstruction: A case report. *Radiol Case Rep* 2018; **13**: 35-38 [PMID: 29552241 DOI: 10.1016/j.radcr.2017.10.001]

2 **CELORIA GC**, PATTON RB. Congenital absence of the aortic arch. *Am Heart J* 1959; **58**: 407-413 [PMID: 13808756 DOI: 10.1016/0002-8703(59)90157-7]

3 **John AS**, Schaff HV, Drew T, Warnes CA, Ammash N. Adult presentation of interrupted aortic arch: case presentation and a review of the medical literature. *Congenit Heart Dis* 2011; **6**: 269-275 [PMID: 21435185 DOI: 10.1111/j.1747-0803.2011.00486.x.]

4 **Vaideeswar P**, Marathe S, Singaravel S, Anderson RH. Discontinuity of the arch beyond the origin of the left subclavian artery in an adult: Interruption or coarctation? *Ann Pediatr Cardiol* 2018; **11**: 92-96 [PMID: 29440839 DOI: 10.4103/apc.APC_91_17]

5 **Borgohain S**, Gupta A, Grover V, Gupta VK. Isolated interrupted aortic arch in an 18-year-old man. *Tex Heart Inst J* 2013; **40**: 79-81 [PMID: 23467322]

6 **Franconeri A**, Ballati F, Pin M, Carone L, Danesino GM, Valentini A. Interrupted aortic arch: A case report. *Indian J Radiol Imaging* 2020; **30**: 81-83 [PMID: 32476755 DOI: 10.4103/ijri.IJRI_273_19]

7 **Xiang XR**, Chen ZX, Zhang L, Lei JQ, Guo SL. Interrupted aortic arch with multiple vascular malformations. *Chin Med J (Engl)* 2019; **132**: 2386-2387 [PMID: 31567374 DOI: 10.1097/CM9.0000000000000438]

8 **Rencuzogullari I**, Ozcan IT, Cirit A, Ayhan S. Isolated interrupted aortic arch in adulthood: A case report. *Herz* 2015; **40**: 549-551 [PMID: 24343603 DOI: 10.1007/s00059-013-4023-8]

9 **Patel DM**, Maldjian PD, Lovoulos C. Interrupted aortic arch with post-interruption aneurysm and bicuspid aortic valve in an adult: a case report and literature review. *Radiol Case Rep* 2015; **10**: 5-8 [PMID: 26649108 DOI: 10.1016/j.radcr.2015.06.001]

10 **Zhou JM**, Liu XW, Yang Y, Wang BZ, Wang JA. Secondary hypertension due to isolated interrupted aortic arch in a 45-year-old person: A case report. *Medicine (Baltimore)* 2017; **96**: e9122 [PMID: 29245349 DOI: 10.1097/MD.0000000000009122]

11 **Canniffe C**, Ou P, Walsh K, Bonnet D, Celermajer D. Hypertension after repair of aortic coarctation--a systematic review. *Int J Cardiol* 2013; **167**: 2456-2461 [PMID: 23041096 DOI: 10.1016/j.ijcard.2012.09.084]

12 **Agasthi P**, Pujari SH, Tseng A, Graziano JN, Marcotte F, Majdalany D, Mookadam F, Hagler DJ, Arsanjani R. Management of adults with coarctation of aorta. *World J Cardiol* 2020; **12**: 167-191 [PMID: 32547712 DOI: 10.4330/wjc.v12.i5.167]

13 **Vriend JW**, Lam J, Mulder BJ. Complete aortic arch obstruction: interruption or aortic coarctation? *Int J Cardiovasc Imaging* 2004; **20**: 393-396 [PMID: 15765862 DOI: 10.1023/b:caim.0000041965.64150.bb]

14 **Skandalakis JE**, Edwards BF, Gray SW, Davis BM, Hopkins WA. Coarctation of the aorta with aneurysm. *Int Abstr Surg* 1960; **111**: 307-326 [PMID: 13858730]

15 **Kaneda T**, Miyake S, Kudo T, Ogawa T, Inoue T, Matsumoto T, Onoe M, Nakamoto S, Kitayama H, Saga T. Obstructed coarctation in a right aortic arch in an adult female. *Thorac Cardiovasc Surg* 2003; **51**: 350-352 [PMID: 14669135 DOI: 10.1055/s-2003-45430]

16 **Hudsmith LE**, Thorne SA, Clift PF, de Giovanni J. Acquired thoracic aortic interruption: percutaneous repair using graft stents. *Congenit Heart Dis* 2009; **4**: 42-45 [PMID: 19207403 DOI: 10.1111/j.1747-0803.2008.00230.x]

17 **Hu ZP**, Wang ZW, Dai XF, Zhan BT, Ren W, Li LC, Zhang H, Ren ZL. Outcomes of surgical *vs* balloon angioplasty treatment for native coarctation of the aorta: a meta-analysis. *Ann Vasc Surg* 2014; **28**: 394-403 [PMID: 24200137 DOI: 10.1016/j.avsg.2013.02.026]

World Journal of Clinical Cases

Submit a Manuscript: https://www.f6publishing.com

World J Clin Cases 2022 April 16; 10(11): 3478-3484

DOI: 10.12998/wjcc.v10.i11.3478

ISSN 2307-8960 (online)

CASE REPORT

Combination therapy (toripalimab and lenvatinib)-associated toxic epidermal necrolysis in a patient with metastatic liver cancer: A case report

Kai-Kai Huang, Shan-Shan Han, Li-Ya He, Lin-Lin Yang, Bao-Ying Liang, Qing-Yu Zhen, Zi-Bo Zhu, Cai-Yun Zhang, Hong-Yi Li, Ying Lin

Specialty type: Oncology

Provenance and peer review: Unsolicited article; Externally peer reviewed.

Peer-review model: Single blind

Peer-review report's scientific quality classification

Grade A (Excellent): 0
Grade B (Very good): 0
Grade C (Good): C, C
Grade D (Fair): 0
Grade E (Poor): 0

P-Reviewer: Bhargava S, Nath L

Received: July 25, 2021
Peer-review started: July 25, 2021
First decision: December 27, 2021
Revised: January 15, 2022
Accepted: February 27, 2022
Article in press: February 27, 2022
Published online: April 16, 2022

Kai-Kai Huang, Shan-Shan Han, Li-Ya He, Lin-Lin Yang, Bao-Ying Liang, Qing-Yu Zhen, Zi-Bo Zhu, Hong-Yi Li, Ying Lin, Department of Dermatology, the Second Affiliated Hospital of Guangzhou University of Chinese Medicine, Guangzhou 510120, Guangdong Province, China

Cai-Yun Zhang, Department of Dermatology, the Second Clinical Medical College of Guangzhou University of Chinese Medicine, Guangzhou 510120, Guangdong Province, China

Ying Lin, Guangdong Provincial Key Laboratory of Chinese Medicine for Prevention and Treatment of Refractory Chronic Diseases, Guangzhou 510120, Guangdong Province, China

Corresponding author: Ying Lin, MD, Chief Physician, Department of Dermatology, The Second Affiliated Hospital of Guangzhou University of Chinese Medicine, No. 111 Dade Road, Yuexiu District, Guangzhou 510120, Guangdong Province, China. lin19791226@gzucm.edu.cn

Abstract

BACKGROUND

Both programmed cell death-1 (PD-1) inhibitors and lenvatinib, which have a synergistic effect, are promising drugs for tumor treatment. It is generally believed that combination therapy with a PD-1 inhibitor and lenvatinib is safe and effective. However, we report a case of toxic epidermal necrolysis (TEN), a grade 4 toxicity, after this combination therapy.

CASE SUMMARY

A 39-year-old male presented with erythema, blisters and erosions on the face, neck, trunk and limbs 1 wk after receiving combination therapy with lenvatinib and toripalimab, a PD-1 inhibitor. The skin injury covered more than 70% of the body surface area. He was previously diagnosed with liver cancer with cervical vertebra metastasis. Histologically, prominent necrotic keratinocytes, hyperkeratosis, liquefaction of basal cells and acantholytic bullae were observed in the epidermis. Blood vessels in the dermis were infiltrated by lymphocytes and eosinophils. Direct immunofluorescence staining was negative. Thus, the diagnosis was confirmed to be TEN (associated with combination therapy with toripalimab and lenvatinib). Full-dose and long-term corticosteroids, high-dose intravenous immunoglobulin and targeted antibiotic drugs were administered. The rashes gradually faded; however, as expected, the tumor progressed.

Therefore, sorafenib and regorafenib were given in succession, and the patient was still alive at the 10-mo follow-up.

CONCLUSION
Cautious attention should be given to rashes that develop after combination therapy with PD-1 inhibitors and lenvatinib. Large-dose and long-course glucocorticoids may be crucial for the treatment of TEN associated with this combination treatment.

Key Words: Toxic epidermal necrolysis; Toripalimab; Lenvatinib; Programmed cell death-1 inhibitor; Liver cancer; Case report

Core Tip: Both programmed cell death-1 (PD-1) inhibitors and lenvatinib, which exhibit a synergistic effect, are promising drugs for tumor treatment. However, we encountered a patient who presented with erythema, blisters and erosions on the face, neck, trunk and limbs 1 wk after combination therapy with lenvatinib and toripalimab, a PD-1 inhibitor. Skin biopsy was performed, and the diagnosis was confirmed as toxic epidermal necrolysis (TEN). We are the first group to report the occurrence of TEN, a grade 4 toxicity, after this combination therapy. Full-dose and long-term corticosteroids were administered, and the rashes gradually faded.

Citation: Huang KK, Han SS, He LY, Yang LL, Liang BY, Zhen QY, Zhu ZB, Zhang CY, Li HY, Lin Y. Combination therapy (toripalimab and lenvatinib)-associated toxic epidermal necrolysis in a patient with metastatic liver cancer: A case report. *World J Clin Cases* 2022; 10(11): 3478-3484
URL: https://www.wjgnet.com/2307-8960/full/v10/i11/3478.htm
DOI: https://dx.doi.org/10.12998/wjcc.v10.i11.3478

INTRODUCTION

Toripalimab, also known as JS001 or TAB001, is a humanized immunoglobulin G4 monoclonal antibody against programmed cell death-1 (PD-1)[1,2]. PD-1 inhibitors help to enhance the ability of the immune system to defeat tumor cells, but immune-related adverse events (irAEs) occur in many cases[3]. Toxic epidermal necrolysis (TEN) is a rare type of irAE caused by PD-1 inhibitors, with a mortality rate of up to 60%[4]. Lenvatinib is an antiangiogenic tyrosine kinase inhibitor (TKI) and shows synergism with PD-1 inhibitors in solid tumors[5,6]. There have been no case reports on TEN associated with toripalimab or lenvatinib[7]. However, we encountered a patient with metastatic liver cancer who developed TEN after combination therapy with toripalimab and lenvatinib. We are the first group to report this severe cutaneous adverse event following combination therapy with a PD-1 inhibitor and lenvatinib. This case report demonstrates that cautious attention should be given to rashes that develop following this combination treatment. The successful treatment of our case also demonstrated the significance of large-dose and long-course glucocorticoid application for this special type of TEN.

CASE PRESENTATION

Chief complaints

Erythema, blisters and erosions appeared on the face, neck, trunk and limbs 1 wk after combination therapy with toripalimab and lenvatinib.

History of present illness

Four weeks prior to presentation, a 39-year-old male began to receive combination therapy with toripalimab and lenvatinib, as well as radiotherapy, after being diagnosed with liver cancer with cervical vertebra metastasis. The oral administration dose of lenvatinib was 12 mg once daily. Toripalimab (240 mg) was administered intravenously every two weeks. One week prior to presentation, erythema, blisters and erosions began to appear on the face and neck, along with pain and fever. Rashes soon spread to the trunk and limbs, as well as the scrotum and oral mucosa. Therefore, the patient was admitted to the Dermatology Department of the Second Affiliated Hospital of Guangzhou University of Chinese Medicine.

History of past illness

The patient experienced neck pain 2 mo prior to presentation at our clinic. The diagnosis of liver cancer with cervical vertebral metastasis was ultimately confirmed by PET-CT. Hepatitis B virus (HBV) infection was diagnosed at the same time, and the patient was then treated with entecavir. The patient had no other medical history, such as diabetes or hypertension.

Personal and family history

The patient had no history of exposure to industrial poisonous substances and reported no habit of smoking or drinking alcohol. The family history was unremarkable.

Physical examination

The patient presented with typical erythema multiforme, slack bullae and epidermal peeling on the face, neck, trunk and limbs. Nikolsky's sign was positive. Scrotal and oral mucosal erosion was observed. Skin injury covered more than 70% of the body surface area (BSA) (Figure 1A and B). The patient weighed 71 kg.

Laboratory examinations

Skin biopsy was performed. Prominent necrotic keratinocytes, hyperkeratosis, liquefaction of basal cells and acantholytic bullae were observed in the epidermis. Blood vessels in the dermis were infiltrated by lymphocytes and eosinophils (Figure 2A-C). Direct immunofluorescence (DIF) staining was negative.

Serum albumin decreased to 33.6 g/L. CRP and procalcitonin slightly increased to 20.9 mg/L and 0.09 ng/mL, respectively. Random blood glucose was 11.23 mmol/L. Quantitative analysis of HBV DNA yielded a value of 3.57×10^3 IU/mL. The AFP value was 1497 ng/mL. The results of routine blood, blood coagulation function, liver and kidney function, routine stool, and routine urine tests, as well as of electrocardiography and chest radiography, were normal. *Staphylococcus aureus*, *Escherichia coli*, and *Klebsiella aerogenes* were cultured from the sites of skin erosion.

FINAL DIAGNOSIS

The diagnosis was confirmed to be TEN (associated with combination therapy with toripalimab and lenvatinib) according to the patient's medical history, typical lesion morphologies, and typical pathological findings.

TREATMENT

The patient ceased treatment with toripalimab and lenvatinib. Methylprednisolone was administered at an initial dose of 80 mg/d. The rashes continued to worsen; thus, 3 days later, the dosage of methylprednisolone was increased to 120 mg/d. Blood pressure and blood glucose were monitored, and insulin was used to control secondary hyperglycemia. The patient received high-dose intravenous immunoglobulin (IVIG) at 0.4 g/kg/d for 5 days. Targeted antibiotic drugs, such as piperacillin-tazobactam and cefuroxime, were chosen in succession based on the drug sensitivity tests in pathogenic bacteria. A potassium permanganate solution bath and compound polymyxin B ointment were administered for external use. The ocular, scrotal and oral mucosa were also carefully treated with topical medication. Oxycontin was administered to relieve the cancer-related pain.

OUTCOME AND FOLLOW-UP

Interestingly, the rashes began to improve on the face and neck and progressed on the trunk and edge of the limbs at a much lower speed when the methylprednisolone dose was adjusted to 120 mg/d. This course lasted for 2 wk, and we did not reduce the dosage of methylprednisolone until we observed remarkable improvements in erythema, blisters and erosions (Figure 1C and D).

At the 2-mo follow-up for glucocorticoid therapy, the dosage of methylprednisolone was gradually reduced to 8 mg/d, and the rashes did not recur. Enhanced computed tomography (CT) scans showed that the size of the primary liver cancer focus increased, and rib metastasis and portal vein tumor thrombosis were noticed. The patient was then treated by transcatheter arterial chemoembolization (TACE).

At the 4-mo follow-up, enhanced CT scans showed that portal vein tumor thrombosis improved, while rib metastasis progressed. Thus, ultrasound-guided microwave ablation and radiotherapy were conducted in succession. Oral sorafenib was also administered, and no cutaneous adverse drug reactions were observed.

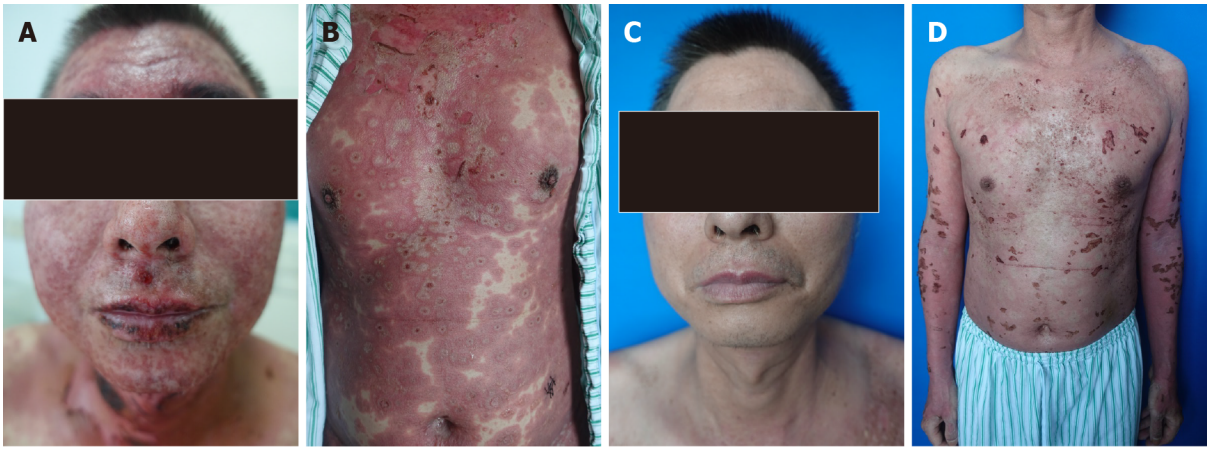

DOI: 10.12998/wjcc.v10.i11.3478

Figure 1 Clinical images before and after treatment. A: Erythema, blisters and erosions appeared on the face and neck, as well as the oral mucosa; B: Typical erythema multiforme, slack bullae and epidermal peeling could be seen and covered more than 70% of the body surface area; C and D: The rashes gradually faded after 3 wk of treatment.

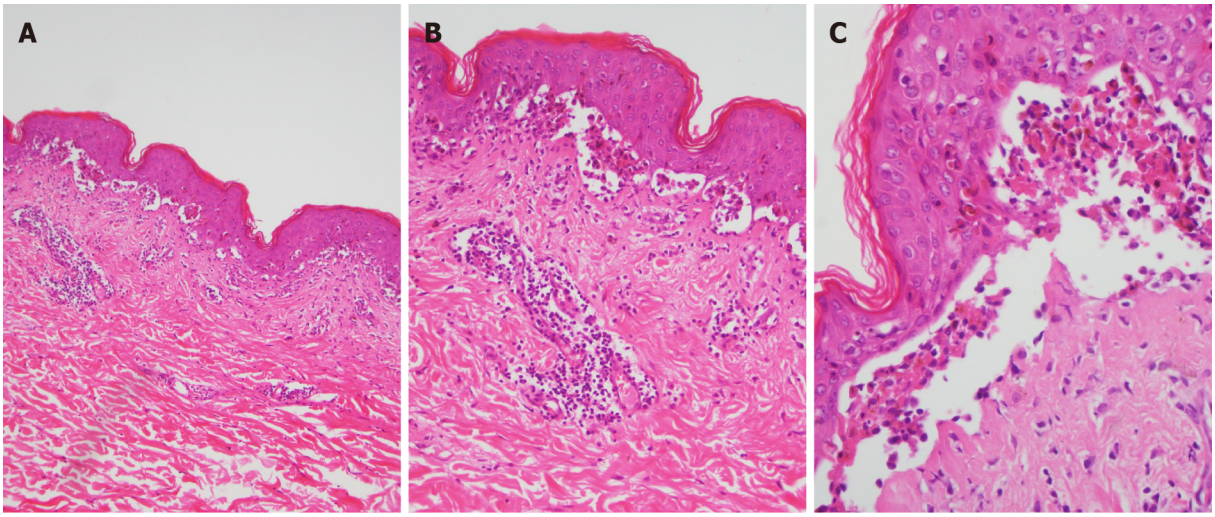

DOI: 10.12998/wjcc.v10.i11.3478

Figure 2 Pathological biopsy of the lesion. A: Acantholytic bullae were observed in the epidermis [hematoxylin-eosin staining (HE) × 40]; B: Hyperkeratosis and liquefaction of basal cells could be seen in the epidermis. Blood vessels in the dermis were infiltrated by lymphocytes and eosinophils (HE × 100); C: Prominent necrotic keratinocytes were identified in the epidermis (HE × 400).

At the 6-mo follow-up, the patient reported paraplegia, which was possibly due to the intraspinal metastatic tumors revealed on the contrast-enhanced magnetic resonance imaging scan. Emission computed tomography (ECT) revealed metastasis of the occipital bone, cervical vertebra, ribs and femur. The patient was experiencing severe pain and agreed to take the risk of the rash recurring to receive additional combination treatment with immunotherapy and targeted therapy. Due to the poor therapeutic effect of sorafenib, the therapeutic regimen was adjusted to 120 mg regorafenib once daily in combination with sintilimab, another PD-1 inhibitor, in addition to toripalimab[8]. A maculopapular rash developed on the trunk 2 wk later; thus, sintilimab was stopped. The rashes were not as severe as the initial rashes and vanished after a small dose of methylprednisolone was administered.

The patient continued taking regorafenib, and disease progression seemed to decrease. At the 10-mo follow-up, the patient was still alive.

DISCUSSION

TEN and Stevens Johnson syndrome (SJS) are two ends of a spectrum of rare severe adverse cutaneous drug reactions, typically with a clinical presentation of erythema multiforme, slack bullae and epidermal peeling[9]. They are distinguished only by their extent of skin detachment (< 10% BSA: SJS,

10%-30% BSA: SJS/TEN, > 30% BSA: TEN)[9]. Histopathologically, widespread necrosis in the epidermis aids in the diagnosis. DIF staining should be negative to rule out certain autoimmune blistering diseases. Specific drugs, such as allopurinol, carbamazepine, phenytoin, phenobarbital and some antibiotics, increase the risk of developing SJS/TEN[9]. The average mortality rate of TEN is 25-35%[9].

Immune checkpoint inhibitors, including monoclonal antibodies targeting PD-1, programmed death ligand 1 (PD-L1) or cytotoxic T lymphocyte-associated antigen-4 (CTLA-4), represent a major breakthrough in tumor therapy[10]. Physiologically, the CTLA-4 and PD-1 immune checkpoint pathways play a central role in maintaining peripheral tolerance by downregulating T cell activation[3]. However, tumor cells may take advantage of this peripheral tolerance to evade the host immune system [3]. Immune checkpoint inhibitors can restore antitumor immune responses, achieving long-term benefits for tumor treatment[3]. Pruritic maculopapular rashes, the majority of which are self-limiting, represent the most frequent cutaneous irAE, occurring in more than 1/3 of patients who receive immunotherapy[10]. There are few cases of TEN associated with PD-1 inhibitors, such as nivolumab and pembrolizumab[11-13]. Toripalimab was introduced into practice in recent years and widely adopted, especially in China, while no cases of TEN associated with toripalimab have been reported in association with any cancer condition.

Recently, a systematic review summarized 5 cases of TEN-like reactions associated with checkpoint inhibitors and reported a median time to onset of 4 wk (average of 5.38 wk) from checkpoint inhibitor initiation[4]. Two patients also developed morbilliform rashes that gradually progressed for 2-4 wk before evolving into TEN, and the mortality rate reached up to 60%[4]. The incubation period in our case was approximately 3 wk, in accordance with previously reported cases. Interestingly, we found that the rashes in our case progressed/improved at different sites at the same time. This characteristic may be explained by the pharmacokinetic patterns and long half-lives of checkpoint inhibitors. For example, nivolumab and pembrolizumab have half-lives of 25 and 23 days, respectively; thus, their peak concentrations are not reached until late in the course of treatment[4]. The PD-1/PD-L1 interaction plays an important role in peripheral tolerance by sustaining Tregs and inhibiting T cell activation. Anti-PD-1 treatment allows autoreactive CD8+ T cells targeting keratinocytes to become activated and proliferate, contributing to the apoptosis of epidermal keratinocytes[14].

Lenvatinib is an antiangiogenic TKI that is widely used in multiple solid tumors[5]. Both lenvatinib and sorafenib are recommended as the first-line treatment for unresectable hepatocellular carcinoma in the guidelines[15]. In a global randomized phase 3 trial, lenvatinib was demonstrated to be non-inferior to sorafenib for overall survival, and it led to greater improvements in progression-free survival, time to progression, objective response and quality-of-life assessments compared with sorafenib[16]. In addition, a synergistic effect has been found between lenvatinib and immune checkpoint inhibitors[6]. The combination of lenvatinib/pembrolizumab is promising in several solid tumors, such as endometrial, lung, hepatocellular and gastrointestinal malignancies[5]. Thus, the patient received combination therapy with toripalimab and lenvatinib. Some dermatological adverse events associated with the application of lenvatinib have been noted, the most common of which are hand-foot skin reactions[7]. SJS/TEN induced by TKIs is rather rare, and no case of TEN associated with lenvatinib has been reported in association with any cancer condition[7,17]. However, we are the first group to report TEN, a grade 4 toxicity, after combination therapy with a PD-1 inhibitor and lenvatinib. Since this was a single case, there is still not sufficient evidence to conclude that combination therapy with a PD-1 inhibitor and lenvatinib increases the risk of TEN compared with a PD-1 inhibitor alone.

Despite the high mortality rate of the limited cases of TEN associated with checkpoint inhibitors, whether they should be managed differently from classic cases of TEN[4] (*e.g.*, the application of corticosteroids[11]) is controversial. In our case, the rashes continued to worsen with the initial methylprednisolone dose of 80 mg/d but improved as the dosage increased later. Considering the long half-life of toripalimab, methylprednisolone was sustained for a long time, and the rashes did not recur. Successful treatment of the case above demonstrates the importance of full-dose and long-term corticosteroids in TEN associated with checkpoint inhibitors. High-dose IVIG may help to boost the immune system and prevent opportunistic infection caused by corticosteroids. Other treatments, such as anti-infection regimens, mucosal protection, anti-HBV drugs and maintaining homeostasis of the internal environment (*e.g.*, blood glucose), also contributed to the patient's recovery.

It is understandable that a tumor would progress rapidly after ceasing antineoplastic drugs due to severe adverse effects. Thus, it is important for patients to restart antitumor therapy as soon as the rashes are controlled. Based on the follow-up of our case, we found that different types of PD-1 inhibitors or targeted drugs do not necessarily cause the same dermatological adverse events. After weighing the pros and cons, other types of PD-1 inhibitors or targeted drugs are still worthy of investigation.

CONCLUSION

In conclusion, we are the first group to report TEN following combination therapy with a PD-1 inhibitor

and lenvatinib. Cautious attention should be given to rashes that develop after this combination treatment. Large-dose and long-course glucocorticoid application may be crucial for the treatment of this special type of TEN.

FOOTNOTES

Author contributions: Huang KK, Han SS, and Zhang CY contributed to the treatment, literature search; Huang KK, He LY and Zhen QY contributed to manuscript writing; Lin Y, Yang LL, and Liang BY contributed to the treatment and manuscript revision; Zhu ZB and Li HY provided comments to this literature; informed consent was conducted by Huang KK; all authors have read and approved the final manuscript.

Supported by Guangdong Provincial Key Laboratory of Chinese Medicine for Prevention and Treatment of Refractory Chronic Diseases, No. 2018B030322012.

Informed consent statement: Consent was obtained from the relatives of the patient for publication of this report and any accompanying results.

Conflict-of-interest statement: The authors declare that they have no conflicts of interest.

CARE Checklist (2016) statement: The authors have read the CARE Checklist (2016), and the manuscript was prepared and revised according to the CARE Checklist (2016).

Country/Territory of origin: China

ORCID number: Kai-Kai Huang 0000-0001-8010-7737; Shan-Shan Han 0000-0001-5779-8701; Li-Ya He 0000-0002-7477-5189; Lin-Lin Yang 0000-0002-7963-2777; Bao-Ying Liang 0000-0003-2824-4448; Qing-Yu Zhen 0000-0003-2866-7897; Zi-Bo Zhu 0000-0002-3295-0989; Cai-Yun Zhang 0000-0003-1841-3674; Hong-Yi Li 0000-0003-0099-5776; Ying Lin 0000-0003-2473-7851.

S-Editor: Ma YJ
L-Editor: A
P-Editor: Ma YJ

REFERENCES

1 **Tang B**, Yan X, Sheng X, Si L, Cui C, Kong Y, Mao L, Lian B, Bai X, Wang X, Li S, Zhou L, Yu J, Dai J, Wang K, Hu J, Dong L, Song H, Wu H, Feng H, Yao S, Chi Z, Guo J. Safety and clinical activity with an anti-PD-1 antibody JS001 in advanced melanoma or urologic cancer patients. *J Hematol Oncol* 2019; **12**: 7 [PMID: 30642373 DOI: 10.1186/s13045-018-0693-2]

2 **Sheng X**, Yan X, Chi Z, Si L, Cui C, Tang B, Li S, Mao L, Lian B, Wang X, Bai X, Zhou L, Kong Y, Dai J, Wang K, Tang X, Zhou H, Wu H, Feng H, Yao S, Flaherty KT, Guo J. Axitinib in Combination With Toripalimab, a Humanized Immunoglobulin G_4 Monoclonal Antibody Against Programmed Cell Death-1, in Patients With Metastatic Mucosal Melanoma: An Open-Label Phase IB Trial. *J Clin Oncol* 2019; **37**: 2987-2999 [PMID: 31403867 DOI: 10.1200/JCO.19.00210]

3 **Buchbinder EI**, Desai A. CTLA-4 and PD-1 Pathways: Similarities, Differences, and Implications of Their Inhibition. *Am J Clin Oncol* 2016; **39**: 98-106 [PMID: 26558876 DOI: 10.1097/COC.0000000000000239]

4 **Maloney NJ**, Ravi V, Cheng K, Bach DQ, Worswick S. Stevens-Johnson syndrome and toxic epidermal necrolysis-like reactions to checkpoint inhibitors: a systematic review. *Int J Dermatol* 2020; **59**: e183-e188 [PMID: 32052409 DOI: 10.1111/ijd.14811]

5 **Hao Z**, Wang P. Lenvatinib in Management of Solid Tumors. *Oncologist* 2020; **25**: e302-e310 [PMID: 32043789 DOI: 10.1634/theoncologist.2019-0407]

6 **Makker V**, Rasco D, Vogelzang NJ, Brose MS, Cohn AL, Mier J, Di Simone C, Hyman DM, Stepan DE, Dutcus CE, Schmidt EV, Guo M, Sachdev P, Shumaker R, Aghajanian C, Taylor M. Lenvatinib plus pembrolizumab in patients with advanced endometrial cancer: an interim analysis of a multicentre, open-label, single-arm, phase 2 trial. *Lancet Oncol* 2019; **20**: 711-718 [PMID: 30922731 DOI: 10.1016/S1470-2045(19)30020-8]

7 **Rimassa L**, Danesi R, Pressiani T, Merle P. Management of adverse events associated with tyrosine kinase inhibitors: Improving outcomes for patients with hepatocellular carcinoma. *Cancer Treat Rev* 2019; **77**: 20-28 [PMID: 31195212 DOI: 10.1016/j.ctrv.2019.05.004]

8 **Zhang L**, Mai W, Jiang W, Geng Q. Sintilimab: A Promising Anti-Tumor PD-1 Antibody. *Front Oncol* 2020; **10**: 594558

[PMID: 33324564 DOI: 10.3389/fonc.2020.594558]

9 **Harr T**, French LE. Toxic epidermal necrolysis and Stevens-Johnson syndrome. *Orphanet J Rare Dis* 2010; **5**: 39 [PMID: 21162721 DOI: 10.1186/1750-1172-5-39]

10 **Sibaud V**. Dermatologic Reactions to Immune Checkpoint Inhibitors : Skin Toxicities and Immunotherapy. *Am J Clin Dermatol* 2018; **19**: 345-361 [PMID: 29256113 DOI: 10.1007/s40257-017-0336-3]

11 **Griffin LL**, Cove-Smith L, Alachkar H, Radford JA, Brooke R, Linton KM. Toxic epidermal necrolysis (TEN) associated with the use of nivolumab (PD-1 inhibitor) for lymphoma. *JAAD Case Rep* 2018; **4**: 229-231 [PMID: 29687056 DOI: 10.1016/j.jdcr.2017.09.028]

12 **Logan IT**, Zaman S, Hussein L, Perrett CM. Combination Therapy of Ipilimumab and Nivolumab-associated Toxic Epidermal Necrolysis (TEN) in a Patient With Metastatic Melanoma: A Case Report and Literature Review. *J Immunother* 2020; **43**: 89-92 [PMID: 31651559 DOI: 10.1097/CJI.0000000000000302]

13 **Robinson S**, Saleh J, Curry J, Mudaliar K. Pembrolizumab-Induced Stevens-Johnson Syndrome/Toxic Epidermal Necrolysis in a Patient With Metastatic Cervical Squamous Cell Carcinoma: A Case Report. *Am J Dermatopathol* 2020; **42**: 292-296 [PMID: 31567395 DOI: 10.1097/DAD.0000000000001527]

14 **Goldinger SM**, Stieger P, Meier B, Micaletto S, Contassot E, French LE, Dummer R. Cytotoxic Cutaneous Adverse Drug Reactions during Anti-PD-1 Therapy. *Clin Cancer Res* 2016; **22**: 4023-4029 [PMID: 26957557 DOI: 10.1158/1078-0432.CCR-15-2872]

15 **Heimbach JK**, Kulik LM, Finn RS, Sirlin CB, Abecassis MM, Roberts LR, Zhu AX, Murad MH, Marrero JA. AASLD guidelines for the treatment of hepatocellular carcinoma. *Hepatology* 2018; **67**: 358-380 [PMID: 28130846 DOI: 10.1002/hep.29086]

16 **Kudo M**, Finn RS, Qin S, Han KH, Ikeda K, Piscaglia F, Baron A, Park JW, Han G, Jassem J, Blanc JF, Vogel A, Komov D, Evans TRJ, Lopez C, Dutcus C, Guo M, Saito K, Kraljevic S, Tamai T, Ren M, Cheng AL. Lenvatinib *vs* sorafenib in first-line treatment of patients with unresectable hepatocellular carcinoma: a randomised phase 3 non-inferiority trial. *Lancet* 2018; **391**: 1163-1173 [PMID: 29433850 DOI: 10.1016/S0140-6736(18)30207-1]

17 **Doesch J**, Debus D, Meyer C, Papadopoulos T, Schultz ES, Ficker JH, Brueckl WM. Afatinib-associated Stevens-Johnson syndrome in an EGFR-mutated lung cancer patient. *Lung Cancer* 2016; **95**: 35-38 [PMID: 27040849 DOI: 10.1016/j.lungcan.2016.02.015]

World Journal of Clinical Cases

Submit a Manuscript: https://www.f6publishing.com

World J Clin Cases 2022 April 16; 10(11): 3485-3489

DOI: 10.12998/wjcc.v10.i11.3485

ISSN 2307-8960 (online)

CASE REPORT

Unusual glomus tumor of the lower leg: A case report

Han-Yu Wang, Ping Duan, Hui Chen, Zhen-Yu Pan

Specialty type: Peripheral vascular disease

Provenance and peer review: Unsolicited article; Externally peer reviewed.

Peer-review model: Single blind

Peer-review report's scientific quality classification

Grade A (Excellent): 0
Grade B (Very good): B, B
Grade C (Good): 0
Grade D (Fair): 0
Grade E (Poor): 0

P-Reviewer: Ghannam WM, Egypt; Raj R, United States

Received: July 25, 2021
Peer-review started: July 25, 2021
First decision: October 25, 2021
Revised: November 4, 2021
Accepted: February 27, 2022
Article in press: February 27, 2022
Published online: April 16, 2022

Han-Yu Wang, Ping Duan, Hui Chen, Zhen-Yu Pan, Department of Orthopedics, Zhongnan Hospital of Wuhan University, Wuhan 430000, Hubei Province, China

Corresponding author: Zhen-Yu Pan, MD, PhD, Chief Physician, Professor, Department of Orthopedics, Zhongnan Hospital of Wuhan University, No. 169 Donghu Road, Wuchang District, Wuhan 430000, Hubei Province, China. soloistp@126.com

Abstract

BACKGROUND

Glomus tumors are rare neoplasms, usually found on the fingers or toes. Glomus tumours that occur in the lower leg are even rarer and is likely to be misdiagnosed or underdiagnosed. This article will document the diagnosis, treatment, and follow-up of a rare glomus tumor of the lower leg, which had been misdiagnosed for up to 15 years.

CASE SUMMARY

The patient was a A 36-year-old woman who had suffered from localized pain in her left lower leg for 15 years. After a complete physical examination, a glomus tumor on her lower leg was considered and removed surgically. The specimen was pathologically diagnosed as a glomus tumor. There was no relapse at a 4-year follow-up.

CONCLUSION

Correct diagnosis and complete removal of the glomus tumor is important.

Key Words: Glomus tumor; Pain; Lower leg; Case report

Core Tip: A 36-year-old woman who had suffered from localized pain in her left lower leg had been misdiagnosed for up to 15 years. She was eventually diagnosed with glomus tumor and underwent surgical treatment. The patient recovered well with no recurrence observed at a 4-year follow-up.

Citation: Wang HY, Duan P, Chen H, Pan ZY. Unusual glomus tumor of the lower leg: A case report. *World J Clin Cases* 2022; 10(11): 3485-3489
URL: https://www.wjgnet.com/2307-8960/full/v10/i11/3485.htm
DOI: https://dx.doi.org/10.12998/wjcc.v10.i11.3485

INTRODUCTION

Glomus tumor (GT), a rare neoplasm caused by degenerated smooth muscle cells in a neuro-arterial adenoma, regulates body temperature through arteriovenous shunting of blood[1,2]. Most GTs are benign, with few malignant cases reported[3,4]. The characteristic clinical manifestations of GT are spontaneous lancinating pain, extreme pain with the slightest touch, and intolerance to temperature changes[5]. It usually presents as a well-defined, blue or red nodule, often located on the fingers or toes, especially in the nail bed, and uncommon elsewhere[6]. Individual literatures have reported GTs occurring in rare sites such as sinonasal location, but more evidences are needed to verify this[7]. We reviewed the literature and found that GT was infrequently reported in the lower leg, thus, it is likely to be misdiagnosed or underdiagnosed. In this article, we report the diagnosis, treatment and follow-up of a rare case of GT of the lower leg, which was misdiagnosed for up to 15 years because of its small number of favored sites and size. The tumor was removed surgically and the patient had complete remission after surgery. This case can enhance our understanding of the rare location of GTs to decrease misdiagnosis and missed diagnosis.

CASE PRESENTATION

Chief complaints

A 36-year-old Asian woman was admitted to our hospital on April 25, 2016 with localized pain in the left anterior tibial region for 15 years.

History of present illness

The patient had visited several hospitals in the past 15 years but was diagnosed with venous thrombosis, which did not improve with conservative treatment such as analgetics. Over the past three years, the patient's pain had progressively worsened, and was exacerbated by touch, temperature changes and mood swings. In addition, the patient often had a poor sleep at night because of the pain.

History of past illness

No special history of past illness.

Personal and family history

There was no personal history of GT or any other family medical history.

Physical examination

Physical examination revealed mildly localized swelling on the on left leg along with tenderness in a 50 mm × 30 mm area of skin on the anterior medial aspect of her left lower extremity, with no ulceration or warmth.

Laboratory examinations

No obvious abnormality was found in laboratory examination.

FINAL DIAGNOSIS

After careful consideration of the patient's medical history and physical examination findings, including spontaneous tingling, minimal tenderness and intolerance to temperature changes, we made a tentative diagnosis of GT.

TREATMENT

After a thorough preoperative examination and confirming no surgical contraindications, the patient underwent soft tissue lesion resection, biopsy and flap transposition on April 27, 2016 (Figure 1A). Intra-operative examination showed an oval tumor with a light red colour, firm texture, intact envelope and clear contours under the skin of her lower leg.

We completely removed the tumor and the surrounding normal soft tissue, which was approximately 10 mm in thickness and 50 mm × 30 mm in size, for pathological diagnosis (Figure 1B). Because of the skin and soft-tissue defect, we designed a lateral gastrocnemius nutrition flap of the left lower limb to cover it (Figure 1C).

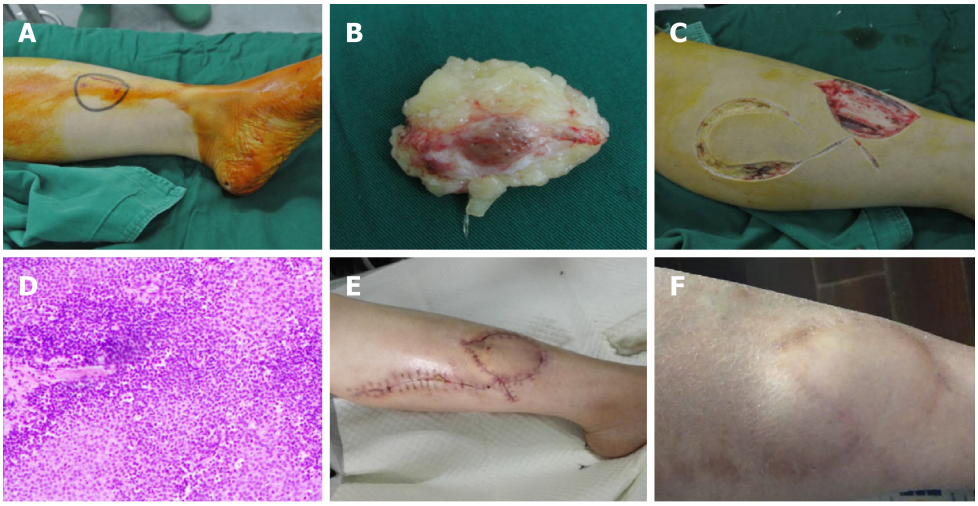

DOI: 10.12998/wjcc.v10.i11.3485

Figure 1 The imaging of case. A: Surgical field: The appearance of the medial left lower leg; B: The appearance of excised tissue in operation. Ellipsoid red soft tissue be covered with adipose tissue, about 50 mm × 30 mm ×10 mm in size; C: Designing and harvesting the lateral gastrocnemius nutrition flap of the left lower leg to cover the tumor's resection site during the surgery; D: Pathologic examination shows a glomus tumor with chronic inflammatory cell infiltrates; E: The appearance of the anteromedial incision of the left lower leg two weeks after the surgery. The incision suture had been removed. The flap survived well, and the incision recovered well with no infection; F: The anteromedial appearance of the left lower leg four years after the surgery. The pain did not relapse.

OUTCOME AND FOLLOW-UP

The pathological examination at our hospital showed a spindle cell tumor (Figure 1D). The results of immunohistochemistry were as follows: Ki-67 (3%, partially up to 10%), Caldesmon(+), CK(-), P63(-), S-100(-), SMA(part+), VIMENTIN(+), GFAP(-), CD31(-), CD34(-), HMB45(-). The examination results at two other tertiary hospitals confirmed it to be a GT. Suturing was performed two weeks after surgery. The wound healed well, and the survival of the skin flap was satisfactory (Figure 1E). There was no abnormality in blood flow, sensation and movement of her left lower limb. At the one-month follow up, the wound was well healed and patient was pain free. No recurrence of pain was observed during a 4-year follow-up (Figure 1F).

DISCUSSION

GTs were firstly reported by Wood in 1812 as "painful subcutaneous tubercle"[8]. It was not until 1924 that Masson *et al* named it GT after pathological analysis[5]. GTs are most commonly encountered on the fingers[9]. It has been reported to be very rare, accounting for 1% to 2% of all soft tissue tumors, most of which are benign[3,4,10]. The characteristic clinical manifestations of GTs are subcutaneous blue or red nodules, firm and smooth, usually no more than 10 mm in diameter. Pain is the most obvious symptom of the disease, usually presenting as spontaneous tingling, extreme pain with the slightest touch, and intolerance to temperature changes[5,11]. In addition to these obvious symptoms, uncommon presentations such as tumor-induced osteomalacia were also reported, but more evidences are needed to support this discovery[12]. The disease diagnosis depends on clinical tests such as the Love test (point tenderness) and Hildreth's sign (decreased pain on exsanguination of the limb and application of a tourniquet)[13]. In addition to qualitative diagnosis, characteristic pain can also be used to localize the lesion. Magnetic resonance imaging (MRI) is occasionally helpful, and hyperenhanced lesions on T2 weighted and short time inversion recovery sequence imaging may illustrate the vascular appearance of GT. Other imaging examinations may include plain radiography, computed tomography and colour Doppler ultrasonography. However, all of the above may be negative and exploration of the painful location should be considered if a GT is suspected even if the MRI findings are negative[14].

In the present case, the tumor was located in the left anterior tibial region, which is relatively rare, so it had been misdiagnosed as venous thrombosis or sciatica resulting in chronic pain for up to 15 years. On the one hand, the initial symptom was pain, which would be easily confused with skin disease, thrombotic diseases, *etc*., when the disease is located in the lower leg. On the other hand, the huge size of this tumor is extremely rare in this disease. A study of 138 cases suggested that the median size of superficial GT was 8 mm, with none exceeding 45 mm[1], while the size of the tumor in our case was up to 50 mm in size.

Once diagnosed, surgical resection is an effective method for the treatment of GT. It should still be noted that recurrence may occur due to incomplete resection. We should therefore remove the tumor completely during surgery *via* avoiding residuals and expanding the resection area when conditions permit[15]. In previous case reports, a simple excisional approach has generally been used. In our case, we used an innovative combination of extended tumor resection and flap transposition due to the large volume of the tumor to avoid soft tissue defects while resecting the tumor completely. The patient recovered well after the surgery with no recurrence observed during the 4 years of follow-up. The patient was satisfied with the surgery and recovered well.

CONCLUSION

The patient with glomus tumor had visited many specialists and underwent numerous examinations before receiving a correct diagnosis. Correct diagnosis and surgical treatment eventually healed her. Remaining alert to rare diseases can be an effective way to avoid them.

FOOTNOTES

Author contributions: Pan ZY completed the operation and completed the revision of the manuscript; Wang HY and Duan P completed the follow-up and wrote the manuscript; and Chen H collected the data; all authors read and approved the final manuscript.

Informed consent statement: The patient agreed the doctors could use and publish her disease related article with personal information deleted.

Conflict-of-interest statement: The authors declare no conflict of interests.

CARE Checklist (2016) statement: The authors have read the CARE Checklist (2016), and the manuscript was prepared and revised according to the CARE Checklist (2016).

Country/Territory of origin: China

ORCID number: Han-Yu Wang 0000-0002-6922-5158; Ping Duan 0000-0001-7833-9651; Hui Chen 0000-0002-8102-6178; Zhen-Yu Pan 0000-0002-1649-2957.

S-Editor: Xing YX
L-Editor: A
P-Editor: Xing YX

REFERENCES

1 **Mravic M**, LaChaud G, Nguyen A, Scott MA, Dry SM, James AW. Clinical and histopathological diagnosis of glomus tumor: an institutional experience of 138 cases. *Int J Surg Pathol* 2015; **23**: 181-188 [PMID: 25614464 DOI: 10.1177/1066896914567330]
2 **Singh D**, Garg RS, Vikas, Garg Y, Arora V. Glomus Tumor - A Rarity; M.R.I- A big help in early Diagnosis. *J Orthop Case Rep* 2016; **6**: 38-39 [PMID: 28116265 DOI: 10.13107/jocr.2250-0685.494]
3 **McDermott EM**, Weiss AP. Glomus tumors. *J Hand Surg Am* 2006; **31**: 1397-1400 [PMID: 17027805 DOI: 10.1016/j.jhsa.2006.05.018]
4 **Folpe AL**, Fanburg-Smith JC, Miettinen M, Weiss SW. Atypical and malignant glomus tumors: analysis of 52 cases, with a proposal for the reclassification of glomus tumors. *Am J Surg Pathol* 2001; **25**: 1-12 [PMID: 11145243 DOI: 10.1097/00000478-200101000-00001]
5 **Abou Jaoude JF**, Roula Farah A, Sargi Z, Khairallah S, Fakih C. Glomus tumors: report on eleven cases and a review of the literature. *Chir Main* 2000; **19**: 243-252 [PMID: 11079182 DOI: 10.1016/s1297-3203(00)73487-1]
6 **Gombos Z**, Zhang PJ. Glomus tumor. *Arch Pathol Lab Med* 2008; **132**: 1448-1452 [PMID: 18788860 DOI: 10.5858/2008-132-1448-GT]
7 **Raj R**, Hasanzadeh S, Dashtizadeh M, Kalantarhormozi M, Vahdat K, Dabbaghmanesh MH, Nabipour I, Ravanbod M, Assadi M, Hashemi B, Asadipooya K. Oncogenic osteomalacia secondary to glomus tumor. *Endocrinol Diabetes Metab Case Rep* 2021; **2021** [PMID: 34196273 DOI: 10.1530/EDM-20-0202]

8 **Gombos Z**, Fogt F, Zhang PJ. Intraosseous glomus tumor of the great toe: a case report with review of the literature. *J Foot Ankle Surg* 2008; **47**: 299-301 [PMID: 18590892 DOI: 10.1053/j.jfas.2008.04.003]

9 **Takase K**. Intraosseous glomus tumour in the distal phalanx of the index finger. *J Hand Surg Eur Vol* 2011; **36**: 74-76 [PMID: 21169304 DOI: 10.1177/1753193410381035]

10 **Tuncali D**, Yilmaz AC, Terzioglu A, Aslan G. Multiple occurrences of different histologic types of the glomus tumor. *J Hand Surg Am* 2005; **30**: 161-164 [PMID: 15680574 DOI: 10.1016/j.jhsa.2004.09.008]

11 **Heys SD**, Brittenden J, Atkinson P, Eremin O. Glomus tumour: an analysis of 43 patients and review of the literature. *Br J Surg* 1992; **79**: 345-347 [PMID: 1315603 DOI: 10.1002/bjs.1800790423]

12 **Dehghani M**, Dabbaghmanesh MH, Khalafi-Nezhad A, Riazmontazer N, Dehghanian A, Vojdani R, Sasani M. Glomus tumor as a cause of oncogenic osteomalacia. *Clin Cases Miner Bone Metab* 2017; **14**: 359-362 [PMID: 29354168 DOI: 10.11138/ccmbm/2017.14.3.359]

13 **Giele H**. Hildreth's test is a reliable clinical sign for the diagnosis of glomus tumours. *J Hand Surg Br* 2002; **27**: 157-158 [PMID: 12027491 DOI: 10.1054/jhsb.2001.0724]

14 **Al-Qattan MM**, Al-Namla A, Al-Thunayan A, Al-Subhi F, El-Shayeb AF. Magnetic resonance imaging in the diagnosis of glomus tumours of the hand. *J Hand Surg Br* 2005; **30**: 535-540 [PMID: 16085343 DOI: 10.1016/j.jhsb.2005.06.009]

15 **Giugale JM**, Fowler JR. Glomus Tumors: A Review of Preoperative Magnetic Resonance Imaging to Detect Satellite Lesions. *Orthopedics* 2015; **38**: e888-e890 [PMID: 26488783 DOI: 10.3928/01477447-20151002-55]

World Journal of Clinical Cases

Submit a Manuscript: https://www.f6publishing.com

World J Clin Cases 2022 April 16; 10(11): 3490-3495

DOI: 10.12998/wjcc.v10.i11.3490

ISSN 2307-8960 (online)

CASE REPORT

Pulmonary *Cladosporium* infection coexisting with subcutaneous *Corynespora cassiicola* infection in a patient: A case report

Wei-Yi Wang, Hong-Bin Luo, Jun-Qi Hu, Hui-Hua Hong

Specialty type: Respiratory system

Provenance and peer review: Unsolicited article; Externally peer reviewed.

Peer-review model: Single blind

Peer-review report's scientific quality classification

Grade A (Excellent): 0
Grade B (Very good): 0
Grade C (Good): C
Grade D (Fair): 0
Grade E (Poor): 0

P-Reviewer: Kamimura K, Japan

Received: July 31, 2021
Peer-review started: July 31, 2021
First decision: October 22, 2021
Revised: October 30, 2021
Accepted: February 27, 2022
Article in press: February 27, 2022
Published online: April 16, 2022

Wei-Yi Wang, Jun-Qi Hu, Hui-Hua Hong, Department of Respiratory Medicine, The First Affiliated Hospital of Zhejiang Chinese Medical University (Zhejiang Provincial Hospital of Traditional Chinese Medicine), Hangzhou 310006, Zhejiang Province, China

Hong-Bin Luo, Department of Dermatology, The First Affiliated Hospital of Zhejiang Chinese Medical University (Zhejiang Provincial Hospital of Traditional Chinese Medicine), Hangzhou 310006, Zhejiang Province, China

Corresponding author: Hui-Hua Hong, MD, Chief Physician, Department of Respiratory Medicine, The First Affiliated Hospital of Zhejiang Chinese Medical University (Zhejiang Provincial Hospital of Traditional Chinese Medicine), No. 54 Youdian Road, Hangzhou 310006, Zhejiang Province, China. hhjoe999@163.com

Abstract

BACKGROUND

Cladosporium and *Corynespora cassiicola* (*C. cassiicola*) infections rarely occur in humans. Mutations in human caspase recruitment domain protein 9 (CARD9) are reported to be associated with fungal diseases. Pulmonary *Cladosporium* infection coexisting with subcutaneous *C. cassiicola* infection in a patient with a CARD9 mutation has not been reported in the literature.

CASE SUMMARY

A 68-year-old male patient was hospitalized for hypertrophic erythema and deep ulcers on the left upper extremity. He was diagnosed with pneumonia caused by *Cladosporium*, as identified through bronchoalveolar lavage fluid analysis, and deep dermatophytosis caused by *C. cassiicola*, as identified through morphological characteristics of the wound secretion culture. He underwent antifungal therapy (voriconazole) and recovered successfully. He carried two mutations in CARD9 (chr9:139266425 and chr9:139262240) and was therefore susceptible to fungal infections.

CONCLUSION

This case study is the first to report the coexistence of pulmonary *Cladosporium* infection and subcutaneous *C. cassiicola* infection in a patient with CARD9 mutation. Our findings will be helpful in enriching the phenotypic spectrum of fungal infections underlying CARD9 deficiency.

Key Words: *Cladosporium*; *Corynespora cassiicola*; Caspase recruitment domain protein

9; Lung lesion; Dermatosis; Case report

Core Tip: The genus *Cladosporium* and *Corynespora cassiicola* (*C. cassiicola*) rarely cause human infections. Patient with caspase recruitment domain protein 9 (CARD9) mutation is reported to be more susceptible to fungal infections. Our case study is the first to report the coexistence of pulmonary *Cladosporium* infection and subcutaneous *C. cassiicola* infection in a patient with CARD9 mutation. Multiple fungal infections in patients with CARD9 mutation are worth clinicians' attention.

Citation: Wang WY, Luo HB, Hu JQ, Hong HH. Pulmonary *Cladosporium* infection coexisting with subcutaneous *Corynespora cassiicola* infection in a patient: A case report. *World J Clin Cases* 2022; 10(11): 3490-3495
URL: https://www.wjgnet.com/2307-8960/full/v10/i11/3490.htm
DOI: https://dx.doi.org/10.12998/wjcc.v10.i11.3490

INTRODUCTION

Cladosporium and *Corynespora cassiicola* (*C. cassiicola*), which are common plant pathogens existing in both indoor and outdoor environments, rarely cause illness in humans[1,2]. Pulmonary *Cladosporium* infection and subcutaneous *C. cassiicola* infection have been separately documented in the literature[3,4]. Thus far, however, there have been no reports on the coexistence of pulmonary *Cladosporium* infection and subcutaneous *C. cassiicola* infection in humans. Mutations in human caspase recruitment domain protein 9 (CARD9) lead to an autosomal recessive primary immunodeficiency disorder, resulting in the development of a wide spectrum of fungal infections[5]. Herein, we present a case of pulmonary *Cladosporium* coexisting with subcutaneous *C. cassiicola* infection with CARD9 deficiency in a patient who was successfully treated with voriconazole.

CASE PRESENTATION

Chief complaints

A 68-year-old male farmer who was a non-smoker was admitted to the hospital for hypertrophic erythema and deep ulcers on the left upper extremity (Figure 1A) on 18 July 2019.

History of present illness

The patient had a six-month history of red, itchy rash on the left upper extremity.

History of past illness

The patient had a ten-year history of hypertension and a six-month history of sleep disorder.

Personal and family history

The patient had no remarkable personal or family history.

Physical examination

Initial medical examination showed a heart rate of 77 beats/min, respiratory rate of 18 breaths/min, body temperature of 36.8 °C, and blood pressure of 137/94 mmHg.

Laboratory examinations

Routine blood test results were normal (white blood cell count in serum of 5.1 × 10^9/L, absolute neutrophil count of 3.4 × 10^9/L, C-reactive protein of 1 mg/L). Serum cryptococcal antigen, antineutrophil cytoplasmic antibodies, antinuclear antibodies, human immunodeficiency virus antibody tests, HIV antibodies, and syphilis antibody tests were negative. The serum IgE level of *Aspergillus fumigatus* was low (0.1 KU/L). A skin biopsy was performed 4 d after hospital admission, which showed partial squamous hyperplasia with a dermal granulomatous lesion (Figure 1E). *C. cassiicola* was identified according to the morphological characteristics of the wound secretion culture (Figure 1C). The patient underwent bronchoscopy 6 d after admission, with a positive result for the bronchoalveolar lavage fluid (BALF) galactomannan test (with a value of 2.16), and BALF culture revealed the presence of *Cladosporium* (Figure 1D). Two mutations in CARD9 were detected by ChIP-seq using high-throughput

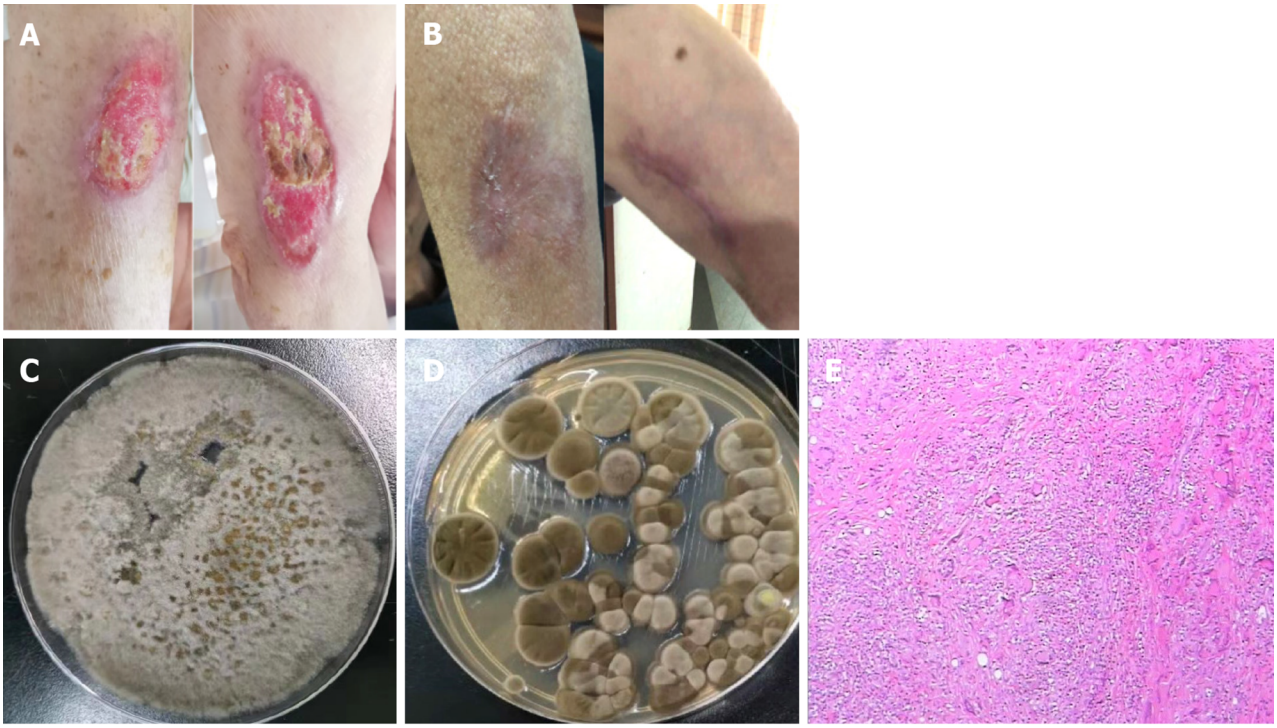

DOI: 10.12998/wjcc.v10.i11.3490

Figure 1 Symptoms, culture and pathology. A: Hypertrophic erythema and deep ulcers on the left upper extremity; B: The ulcer on the left upper extremity had completely healed after treatment; C: Wound secretion culture revealed *Corynespora cassiicola*; D: Bronchoalveolar lavage fluid culture analysis revealed the presence of *Cladosporium*; E: Skin biopsy showed a partial squamous hyperplasia with a dermal granulomatous lesion.

sequencing (detection region: exon region of approximately 20000 genes in the human genome; detection strategy: the explicit disease-causing genes included in OMIM database "2018.11" were analyzed) in the present case: (1) chromosomal location: chr9:139266425; nucleotide change: c.106C>T; and (2) chromosomal location: chr9:139262240; nucleotide change: c.1118G>C.

Imaging examinations

Chest computed tomography revealed the presence of multiple nodules with multiple patchy areas in both lungs (Figure 2).

FINAL DIAGNOSIS

We made a final diagnosis of pneumonia caused by *Cladosporium* as well as deep dermatophytosis caused by *C. cassiicola*.

TREATMENT

Piperacillin-tazobactam 3.375 g intravenous drip was administered every 8 h for 7 d, and then antifungal therapy (voriconazole: 200 mg twice daily for 3 mo) was initiated. The ulcer on the left upper extremity healed completely after one month of treatment (Figure 1B).

OUTCOME AND FOLLOW-UP

Follow-up imaging after 3 mo revealed very good resolution of the lesions in the lung (Figure 2). The lung lesions continued to shrink for 5 mo after antifungal therapy was discontinued (Figure 2).

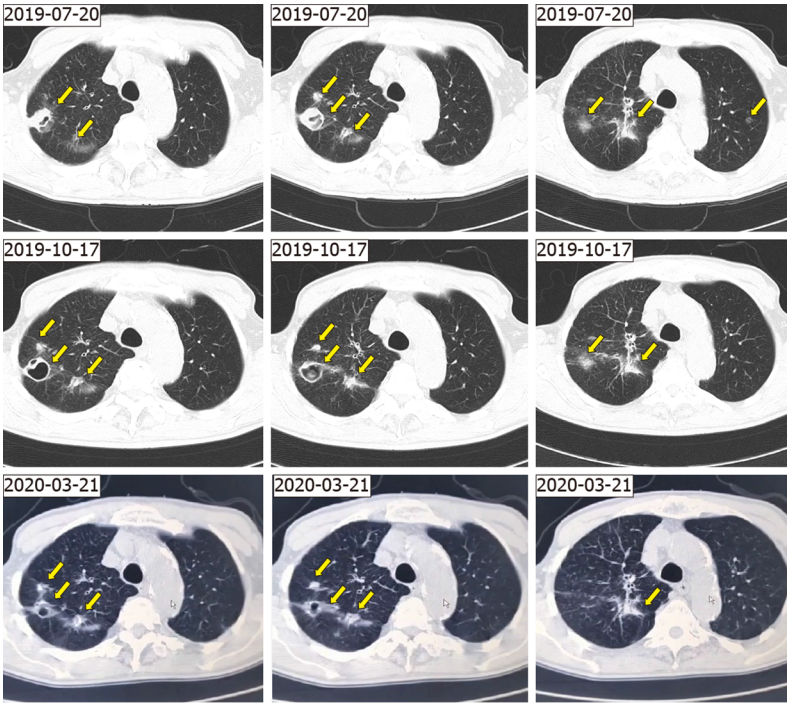

DOI: 10.12998/wjcc.v10.i11.3490

Figure 2 Imaging. A chest computed tomography scan showing multiple nodules with multiple patchy areas in both lungs (arrow).

DISCUSSION

Our case involved coexistence of pulmonary *Cladosporium* infection and subcutaneous *C. cassiicola* infection in a patient with CARD9 mutation.

The genus *Cladosporium* has been reported to cause several different types of opportunistic infections, including subcutaneous and deep infections, in humans and animals[1]. *Cladosporium* spores, which potentially lead to the development of respiratory allergy problems such as asthma, rarely cause pulmonary infection[6]. *Cladosporium* can affect the lungs, bronchi, and pulmonary artery branches, as revealed by our literature review[3,7-10]. *Cladosporium* spores can reach the lungs by inhalation[11]. The patient in the present case was a farmer; therefore, it is highly likely he was infected by *Cladosporium* via inhalation.

C. cassiicola, a member of *Pleosporales*, is a common plant pathogen[12]. Subcutaneous *C. cassiicola* infection in humans is extremely rare, and only six cases have been reported thus far[4,13-16]. In these cases, erythaematous change, ulcer, plaque, nodule, and erosion were clinical symptoms of all cases, and the face or extremities were the infection sites. Antifungal therapy has resulted in successful treatment outcomes in most cases, though two patients with CARD9 mutations did not respond well[4, 13-16].

As a member of the CARD protein family, CARD9 plays an important role in the activation of antifungal mechanisms[17]. It is a key adaptor that can mediate Dectin-1-, Dectin-2-, and Mincle-induced activation of transcription factors through formation of the CARD9–B cell lymphoma/leukaemia-10–mucosa-associated lymphoid tissue lymphoma translocation protein 1 complex in response to fungal infection[5]. These activated transcription factors mediate translation of key cytokines such as nuclear factor κB, which promotes T-helper cell (Th)1/Th17 differentiation, stimulating antifungal mechanisms in innate cells[18]. CARD9 mutation is a rare inborn error of immunity and probably leads to impaired protection against fungal infections[19]. However, detailed and comprehensive reports on CARD9 deficiency susceptibility to fungal infection, clinical characteristics, diagnostic methods, and prognosis are still lacking. Human CARD9 deficiency is reported to be responsible for the spontaneous development of persistent and severe fungal infections (such as infections caused by *Candida albicans, Candida dubliniensis*, *Phialophora verrucosa*, *Trichophyton violaceum*, *Candida sp.*, *Trichophyton mentagrophytes*, *Exophiala sp.*, *Trichophyton rubrum*, and *Corynespora cassiicola*)[17, 20]. Conversely, *Cladosporium* infection has not been reported.

The appropriate antifungal therapy for CARD9 deficiency is mostly empirical. Antifungal agents itraconazole and voriconazole have been used for the treatment of pulmonary *Cladosporium* infection, whereas amphotericin B, voriconazole, posaconazole, liposomes, and itraconazole have been used to treat subcutaneous *Corynespora cassiicola* infection[13-16]. Voriconazole had a very good therapeutic effect in our case. However, there is still no definitive conclusion on the antifungal treatment of these two diseases, including suitable medicine, reasonable dose, and course, which warrants further

research.

CONCLUSION

A good prognosis for fungal infection is associated with prompt identification and proper treatment. Given the findings of our case and the results of our literature review, multiple fungal infections in patients with CARD9 mutations are worthy of clinicians' attention. Further study into the clinical characteristics and pathogenesis of CARD9 deficiency will yield new insight into therapeutic measures for protecting humans from these devastating fungal diseases.

ACKNOWLEDGEMENTS

We acknowledge the contributions of Mr. Jun-Min Cao for the research assistance.

FOOTNOTES

Author contributions: Hong HH performed the postoperative evaluation and diagnosis; Wang WY reviewed the literature and contributed to manuscript drafting; Luo HB and Hu JQ collected the medical data; and all authors issued final approval for the submitted version.

Informed consent statement: Informed written consent was obtained from the patient for publication of this report and any accompanying images.

Conflict-of-interest statement: The authors declare that they have no conflict of interest.

CARE Checklist (2016) statement: The authors have read the CARE Checklist (2016), and the manuscript was prepared and revised according to the CARE Checklist (2016).

Country/Territory of origin: China

ORCID number: Wei-Yi Wang 0000-0003-2563-6294; Hong-Bin Luo 0000-0002-7308-3439; Jun-Qi Hu 0000-0002-6100-4609; Hui-Hua Hong 0000-0001-8431-7379.

S-Editor: Zhang H
L-Editor: A
P-Editor: Zhang H

REFERENCES

1 **Sandoval-Denis M**, Gené J, Sutton DA, Wiederhold NP, Cano-Lira JF, Guarro J. New species of Cladosporium associated with human and animal infections. *Persoonia* 2016; **36**: 281-298 [PMID: 27616793 DOI: 10.3767/003158516X691951]
2 **Yamada H**, Takahashi N, Hori N, Asano Y, Mochizuki K, Ohkusu K, Nishimura K. Rare case of fungal keratitis caused by Corynespora cassiicola. *J Infect Chemother* 2013; **19**: 1167-1169 [PMID: 23494266 DOI: 10.1007/s10156-013-0579-8]
3 **Kwon-Chung KJ**, Schwartz IS, Rybak BJ. A pulmonary fungus ball produced by Cladosporium cladosporioides. *Am J Clin Pathol* 1975; **64**: 564-568 [PMID: 1239189 DOI: 10.1093/ajcp/64.4.564]
4 **Xie Z**, Wu W, Meng D, Zhang Q, Ma Y, Liu W, Chen J. A case of Phaeohyphomycosis caused by Corynespora cassiicola infection. *BMC Infect Dis* 2018; **18**: 444 [PMID: 30170557 DOI: 10.1186/s12879-018-3342-z]
5 **De Bruyne M**, Hoste L, Bogaert DJ, Van den Bossche L, Tavernier SJ, Parthoens E, Migaud M, Konopnicki D, Yombi JC, Lambrecht BN, van Daele S, Alves de Medeiros AK, Brochez L, Beyaert R, De Baere E, Puel A, Casanova JL, Goffard JC, Savvides SN, Haerynck F, Staal J, Dullaers M. A *CARD9* Founder Mutation Disrupts NF-κB Signaling by Inhibiting BCL10 and MALT1 Recruitment and Signalosome Formation. *Front Immunol* 2018; **9**: 2366 [PMID: 30429846 DOI: 10.3389/fimmu.2018.02366]
6 **Rick EM**, Woolnough K, Pashley CH, Wardlaw AJ. Allergic Fungal Airway Disease. *J Investig Allergol Clin Immunol* 2016; **26**: 344-354 [PMID: 27996940 DOI: 10.18176/jiaci.0122]
7 **Castro AS**, Oliveira A, Lopes V. Pulmonary phaeohyphomycosis: a challenge to the clinician. *Eur Respir Rev* 2013; **22**:

187-188 [PMID: 23728874 DOI: 10.1183/09059180.00007512]
8 **Keyser A**, Schmid FX, Linde HJ, Merk J, Birnbaum DE. Disseminated Cladophialophora bantiana infection in a heart transplant recipient. *J Heart Lung Transplant* 2002; **21**: 503-505 [PMID: 11927230 DOI: 10.1016/s1053-2498(01)00357-6]
9 **Brenner SA**, Morgan J, Rickert PD, Rimland D. Cladophialophora bantiana isolated from an AIDS patient with pulmonary infiltrates. *J Med Vet Mycol* 1996; **34**: 427-429 [PMID: 8971633 DOI: 10.1080/02681219680000751]
10 **Arango-Franco CA**, Moncada-Vélez M, Beltrán CP, Berrío I, Mogollón C, Restrepo A, Trujillo M, Osorio SD, Castro L, Gómez LV, Muñoz AM, Molina V, Del Río Cobaleda DY, Ruiz AC, Garcés C, Alzate JF, Cabarcas F, Orrego JC, Casanova JL, Bustamante J, Puel A, Arias AA, Franco JL. Early-Onset Invasive Infection Due to Corynespora cassiicola Associated with Compound Heterozygous CARD9 Mutations in a Colombian Patient. *J Clin Immunol* 2018; **38**: 794-803 [PMID: 30264381 DOI: 10.1007/s10875-018-0549-0]
11 **Ismail MA**. Deterioration and spoilage of peanuts and desiccated coconuts from two sub-Saharan tropical East African countries due to the associated mycobiota and their degradative enzymes. *Mycopathologia* 2001; **150**: 67-84 [PMID: 11407493 DOI: 10.1023/a:1010863507652]
12 **Chen C**, Li Q, Fu R, Wang J, Fan Z, Chen X, Lu D. Characterization of the complete mitochondrial genome of *Corynespora cassiicola* (Pleosporales: Dothideomycetes), with its phylogenetic analysis. *Mitochondrial DNA B Resour* 2019; **4**: 2938-2939 [PMID: 33365801 DOI: 10.1080/23802359.2019.1662753]
13 **Grava S**, Lopes FA, Cavallazzi RS, Grassi MF, Svidzinski TI. A rare case of hemorrhagic pneumonia due to Cladosporium cladosporioides. *J Bras Pneumol* 2016; **42**: 392-394 [PMID: 27812642 DOI: 10.1590/S1806-37562016000000079]
14 **Lv GX**, Ge YP, Shen YN, Li M, Zhang X, Chen H, Deng S, de Hoog GS, Liu WD. Phaeohyphomycosis caused by a plant pathogen, Corynespora cassiicola. *Med Mycol* 2011; **49**: 657-661 [PMID: 21281061 DOI: 10.3109/13693786.2011.553635]
15 **Wang CH**, Chen WT, Ting SW, Sun PL. Subcutaneous Fungal Infection Caused by a Non-sporulating Strain of Corynespora cassiicola Successfully Treated with Terbinafine. *Mycopathologia* 2019; **184**: 691-697 [PMID: 31606812 DOI: 10.1007/s11046-019-00393-0]
16 **Huang HK**, Liu CE, Liou JH, Hsiue HC, Hsiao CH, Hsueh PR. Subcutaneous infection caused by Corynespora cassiicola, a plant pathogen. *J Infect* 2010; **60**: 188-190 [PMID: 19925826 DOI: 10.1016/j.jinf.2009.11.002]
17 **Drummond RA**, Lionakis MS. Mechanistic Insights into the Role of C-Type Lectin Receptor/CARD9 Signaling in Human Antifungal Immunity. *Front Cell Infect Microbiol* 2016; **6**: 39 [PMID: 27092298 DOI: 10.3389/fcimb.2016.00039]
18 **Drummond RA**, Saijo S, Iwakura Y, Brown GD. The role of Syk/CARD9 coupled C-type lectins in antifungal immunity. *Eur J Immunol* 2011; **41**: 276-281 [PMID: 21267996 DOI: 10.1002/eji.201041252]
19 **Vaezi A**, Fakhim H, Abtahian Z, Khodavaisy S, Geramishoar M, Alizadeh A, Meis JF, Badali H. Frequency and Geographic Distribution of *CARD9* Mutations in Patients With Severe Fungal Infections. *Front Microbiol* 2018; **9**: 2434 [PMID: 30369919 DOI: 10.3389/fmicb.2018.02434]
20 **Yan XX**, Yu CP, Fu XA, Bao FF, Du DH, Wang C, Wang N, Wang SF, Shi ZX, Zhou GZ, Tian HQ, Liu H, Zhang FR. CARD9 mutation linked to Corynespora cassiicola infection in a Chinese patient. *Br J Dermatol* 2016; **174**: 176-179 [PMID: 26440558 DOI: 10.1111/bjd.14082]

World Journal of Clinical Cases

Submit a Manuscript: https://www.f6publishing.com

World J Clin Cases 2022 April 16; 10(11): 3496-3504

DOI: 10.12998/wjcc.v10.i11.3496

ISSN 2307-8960 (online)

CASE REPORT

Preoperational diagnosis and management of breast ductal carcinoma *in situ* arising within fibroadenoma: Two case reports

Jun Wu, Ke-Wang Sun, Qiu-Ping Mo, Ze-Ran Yang, Yuan Chen, Miao-Chun Zhong

Specialty type: Medicine, research and experimental

Provenance and peer review: Unsolicited article; Externally peer reviewed.

Peer-review model: Single blind

Peer-review report's scientific quality classification

Grade A (Excellent): 0
Grade B (Very good): 0
Grade C (Good): C, C
Grade D (Fair): 0
Grade E (Poor): 0

P-Reviewer: Menendez-Menendez J, Spain; Serrano Uson Junior PL, United States

Received: August 9, 2021
Peer-review started: August 9, 2021
First decision: November 17, 2021
Revised: December 5, 2021
Accepted: February 27, 2022
Article in press: February 27, 2022
Published online: April 16, 2022

Jun Wu, Ke-Wang Sun, Qiu-Ping Mo, Miao-Chun Zhong, Department of Breast Surgery, Zhejiang Provincial People's Hospital, People's Hospital of Hangzhou Medical College, Hangzhou 310014, Zhejiang Province, China

Jun Wu, Ke-Wang Sun, Qiu-Ping Mo, Ze-Ran Yang, Yuan Chen, Miao-Chun Zhong, Cancer Center, Zhejiang Provincial People's Hospital, People's Hospital of Hangzhou Medical College, Hangzhou 310014, Zhejiang Province, China

Ze-Ran Yang, Yuan Chen, Department of Pathology, Zhejiang Provincial People's Hospital, People's Hospital of Hangzhou Medical College, Hangzhou 310014, Zhejiang Province, China

Corresponding author: Miao-Chun Zhong, MM, Surgeon, Department of Breast Surgery, Zhejiang Provincial People's Hospital, People's Hospital of Hangzhou Medical College, No. 158 Shangtang Road, Hangzhou 310014, Zhejiang Province, China. zhongmiaochun@126.com

Abstract

BACKGROUND

Ductal carcinoma *in situ* (DCIS) arising within fibroadenoma is a type of tumor that is rarely encountered in clinic, with only about 100 cases of carcinoma arising within a fibroadenoma reported in the literature. Here, we present two cases of breast DCIS arising within a fibroadenoma and discuss their clinical and imaging findings as well as treatment.

CASE SUMMARY

The patients did not have cancer-related personal and family histories. Case 1 (a 49-year-old woman) was diagnosed with a bilateral breast nodule in May 2018 and was followed (preoperative imaging data including ultrasound and mammography) for 3 years; she underwent an excisional biopsy to address an enlargement in nodule size. Case 2 (a 37-year-old woman) was diagnosed with a left breast nodule in June 2021 and consequently received vacuum-assisted biopsy of the tumor which appeared as "irregularly shaped" and "unevenly textured" tissue on ultrasound. The pathological diagnosis was clear in both cases. Both patients underwent breast-conserving surgery and sentinel lymph node biopsy. The two cases received or planned to receive radiotherapy as well as endocrine therapy (tamoxifen).

CONCLUSION

Breast DCIS arising within a fibroadenoma is rare, but patients treated with radiotherapy and endocrine therapy can have good prognosis.

Key Words: Fibroadenoma; Ductal carcinoma *in situ*; Vacuum-assisted biopsy; Excisional biopsy; Case report

Core Tip: Breast ductal carcinoma *in situ* arising within a fibroadenoma is a rare event. We present 2 such cases and discuss their clinical and imaging findings as well as treatment. Both patients underwent breast-conserving surgery and sentinel lymph node biopsy. The 2 cases received or planned to receive radiotherapy as well as endocrine therapy (tamoxifen). More sections are needed to reduce the missed rate. Complete follow-up data with preoperative imaging can help with decision-making during patient follow-up.

Citation: Wu J, Sun KW, Mo QP, Yang ZR, Chen Y, Zhong MC. Preoperational diagnosis and management of breast ductal carcinoma *in situ* arising within fibroadenoma: Two case reports. *World J Clin Cases* 2022; 10(11): 3496-3504
URL: https://www.wjgnet.com/2307-8960/full/v10/i11/3496.htm
DOI: https://dx.doi.org/10.12998/wjcc.v10.i11.3496

INTRODUCTION

Fibroadenoma is the most common breast tumor found in young women[1,2]. Ductal carcinoma *in situ* (DCIS) arising within a fibroadenoma is a specific pathological type of tumor that is rarely encountered in the clinic[3]. Its incidence ranges from 0.02% to 0.125%[4-6] and it is usually discovered by chance during pathological examination of fibroadenoma resected tissue. So far, approximately 100 cases for carcinoma arising within a fibroadenoma have been reported worldwide, including intraductal carcinoma, lobular carcinoma *in situ* and invasive carcinoma, most of which lack preoperative follow-up data. Herein, we present 2 cases of breast DCIS arising within a fibroadenoma and discuss their clinical and imaging findings as well as treatment.

CASE PRESENTATION

Chief complaints

Case 1: A 49-year-old woman was diagnosed with a bilateral breast nodule in May 2018 (Figure 1A). The first ultrasound diagnosis showed a breast nodule of 8 mm × 5 mm × 7 mm in size, located in the left breast at the one o'clock direction. The tissue was hypoechoic, with an internal visible bright spot that was about 4 mm in length. Mammography suggested coarse granular calcified nodules behind the left areola and small nodules in the upper quadrant of the right breast (Figure 2A). No palpable masses were noted in either breast. It was recommended that she undergo regular ultrasound review (which was performed again in March 2019 and June 2021) and received no interventional treatment. In March 2019, ultrasound (Figure 1B) and mammography (Figure 2B) of these breast nodules showed no differences compared with the previous diagnosis. Yet, in June 2021 the ultrasound suggested an increase in the size (11 mm × 6 mm × 11 mm) of the breast nodule behind the left areola at the one o'clock direction. Moreover, coarse calcification plaques about 4 mm in length with Breast Imaging Reporting and Data System (BIRADS) grade IVA were found in the interior of the nodule. Mammography findings were similar to those observed previously. The patient had no remarkable physical complaints.

Case 2: A 37-year-old woman was diagnosed with a left breast nodule in June 2021; yet, a specific size was not recorded. She was instructed to have regular ultrasound review, and no interventional treatment was given. The patient visited the outpatient clinic in July 2021 and underwent further ultrasound examination, which showed a nodule in the left breast at the five o'clock position. The nodule was approximately 15 mm × 9 mm × 11 mm in size with irregular morphology and uneven internal echogenicity but without calcification inside, and of BIRADS grade III. Mammography suggested no other abnormalities. During the history-taking, she revealed no remarkable physical complaints.

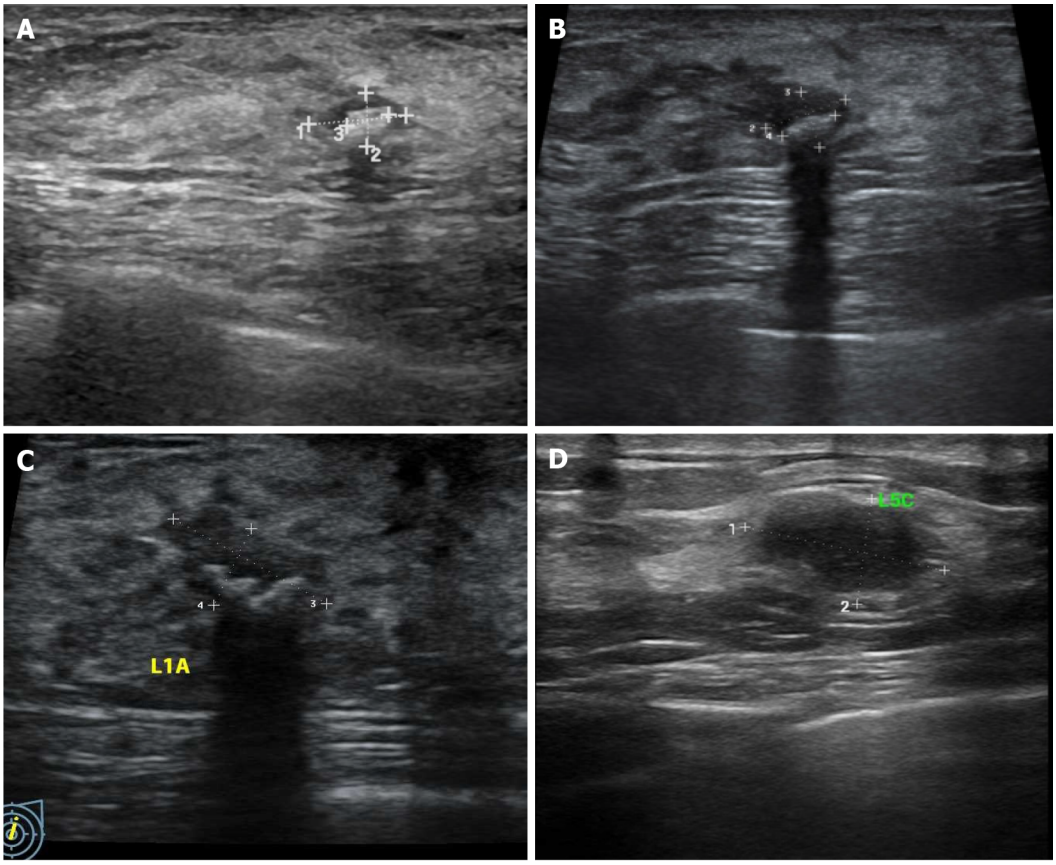

DOI: 10.12998/wjcc.v10.i11.3496

Figure 1 Left breast nodule ultrasonography of case 1 and case 2. A: May 2018 (case 1); B: March 2019 (case 1); C: June 2021 (case 1); D: Case 2.

History of present illness

Case 1 and case 2 have none present illness.

History of past illness

Case 1: The patient's previous medical history was unremarkable.

Case 2: The patient was diagnosed with depression for over 9 years. Oral paroxetine was used to control symptoms.

Personal and family history

Case 1 and case 2 had no personal or family histories of breast malignancy.

Physical examination

Case 1: Physical examination revealed the blood pressure to be 135/89 mmHg. No abnormalities were found in the cardiopulmonary and abdominal regions. The nipples were symmetrical, and the skin of both breasts was unremarkable, with no inversion of the nipple on either side and no significant nipple bleeding. No palpable masses were noted in either of the breasts, and no enlarged lymph nodes were palpable in the axilla and supraclavicular regions.

Case 2: Blood pressure was 122/79 mmHg. Physical examination of the cardiopulmonary and abdominal regions revealed no abnormalities. The nipples were symmetrical, and the skin of both breasts was unremarkable, with no inversion of the nipple on either side and no significant nipple bleeding. A nodule of about 15 mm × 10 mm in size with moderate texture, poorly defined borders, and smooth surface was palpable in the outer lower quadrant of the left breast. No palpable mass was detected in the right breast. No enlarged lymph nodes were palpable in the axilla and supraclavicular regions.

Laboratory examinations

Case 1: Sex hormone tests suggested estradiol < 10 pg/mL, follicle-stimulating hormone 24.86 IU/L and luteinizing hormone 15.19 IU/L. The levels of carcinoembryonic antigen, cancer antigen (CA) 125, CA153 and CA199 were within normal limits.

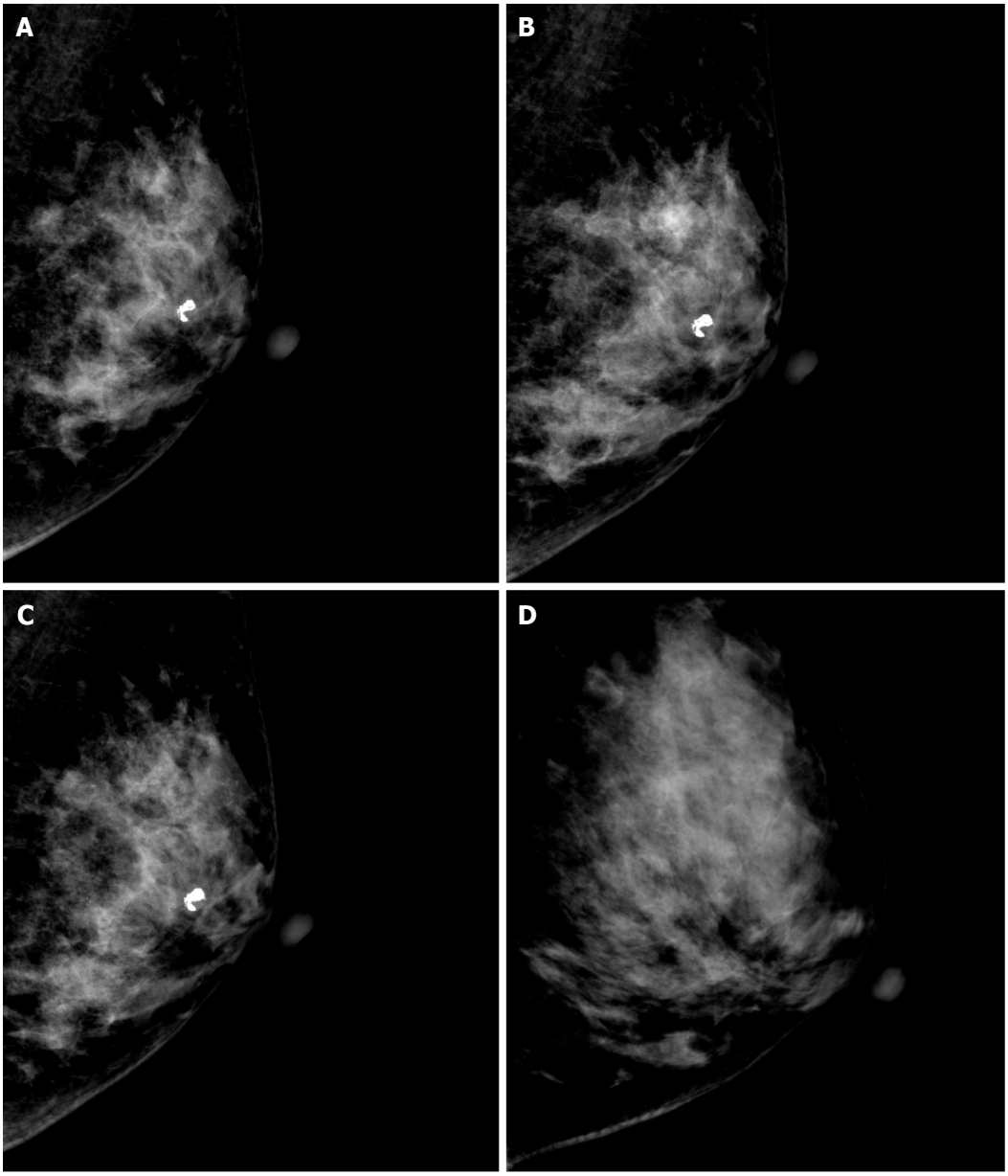

DOI: 10.12998/wjcc.v10.i11.3496

Figure 2 Left breast mammography of case 1 (mediolateral oblique view) and case 2. A: May 2018 (case 1); B: March 2019 (case 1); C: June 2021 (case 1); D: Case 2.

Case 2: Carcinoembryonic antigen and CA199 levels were within normal limits.

Imaging examinations

Case 1: Breast and axillary lymph node ultrasound showed the nodule behind the left areola at the one o'clock position of the left breast was 11 mm × 6 mm × 11 mm in size with coarse calcified plaques about 4 mm in length diameter and BIRADS grade IVA (Figure 1C). The remaining bilateral breast had multiple nodules and BIRADS grade II-III. Mammography suggested a coarse granular calcified nodule posterior to the left areola, BIRADS category 2 (Figure 2C). Dynamic contrast-enhanced magnetic resonance imaging of the breast showed a left posterior papillary nodule, approximately 7 mm × 6 mm in size with a clear border and slightly lobulated appearance, a type II pattern on enhancement curve and lipohyalinosis hypointense foci on T1-weight imaging and T2-weighted imaging with possible posterior calcification and BIRADS 4a. There were multiple small nodules (BIRADS 3) throughout both breasts (Figure 3).

Case 2: Breast and axillary lymph node ultrasound showed the nodule located at the five o'clock direction in the left breast. The nodule was approximately 15 mm × 9 mm × 11 mm in size with irregular morphology, uneven internal echogenicity, without calcification inside, and BIRADS grade III (Figure 1D). Mammography suggested mammary hyperplasia and BIRADS category 3 (Figure 2D).

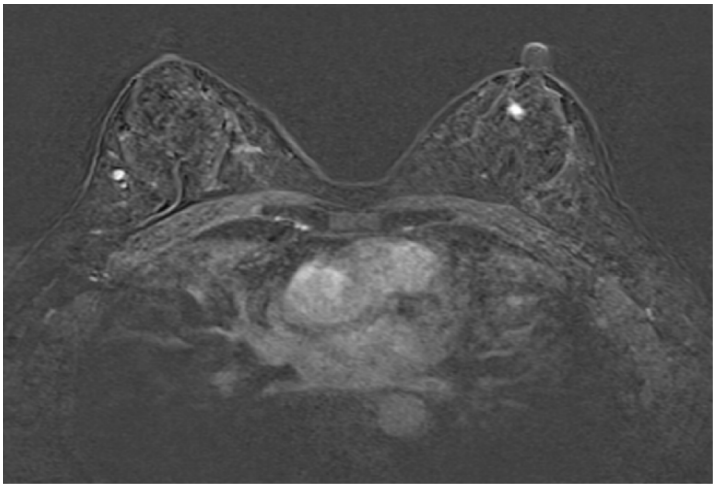

DOI: 10.12998/wjcc.v10.i11.3496

Figure 3 Dynamic contrast-enhanced magnetic resonance imaging of case 1.

Dynamic contrast-enhanced magnetic resonance examination of the mammary gland was not performed.

Pathological examination

Case 1: The left breast nodule of the patient was completely resected and sent for pathological examination. Intraoperative hematoxylin and eosin-stained frozen sections results are shown in Figures 4 and 4B; paraffin sections after operation are shown in Figures 5A and 5B. DCIS on a background of fibroadenomas (all surrounded by a fibroadenomatous component) in a nested pattern was well demonstrated on both frozen and paraffin sections.

Case 2: The patient's left breast nodule was excised by a vacuum-assisted biopsy system and then sent for pathological examination. Intraoperative hematoxylin and eosin-stained frozen section results are shown in Figure 4C and 4D and postoperative paraffin section findings in Figures 5C and 5D. The frozen section showed no dysplasia of the ductal epithelium within the fibroadenoma, either at low or medium magnification. In postoperative paraffin section analysis, a focal intraductal carcinoma component within a fibroadenoma was found.

FINAL DIAGNOSIS

The 2 patients were diagnosed with breast DCIS arising within fibroadenoma. Immunohistochemical examination suggested estrogen receptor positivity.

TREATMENT

Both patients underwent breast-conserving surgery and sentinel lymph node biopsy. During the operations, the negative margin of the resected specimen and negative sentinel lymph nodes were confirmed with frozen sections.

OUTCOME AND FOLLOW-UP

Both patients recovered well after the operation. One patient received radiotherapy, while the other prepared to start radiotherapy (she consulted a radiotherapy physician and received an appointment for radiotherapy). The recommendation to begin endocrine therapy with tamoxifen was given. The follow-up is ongoing.

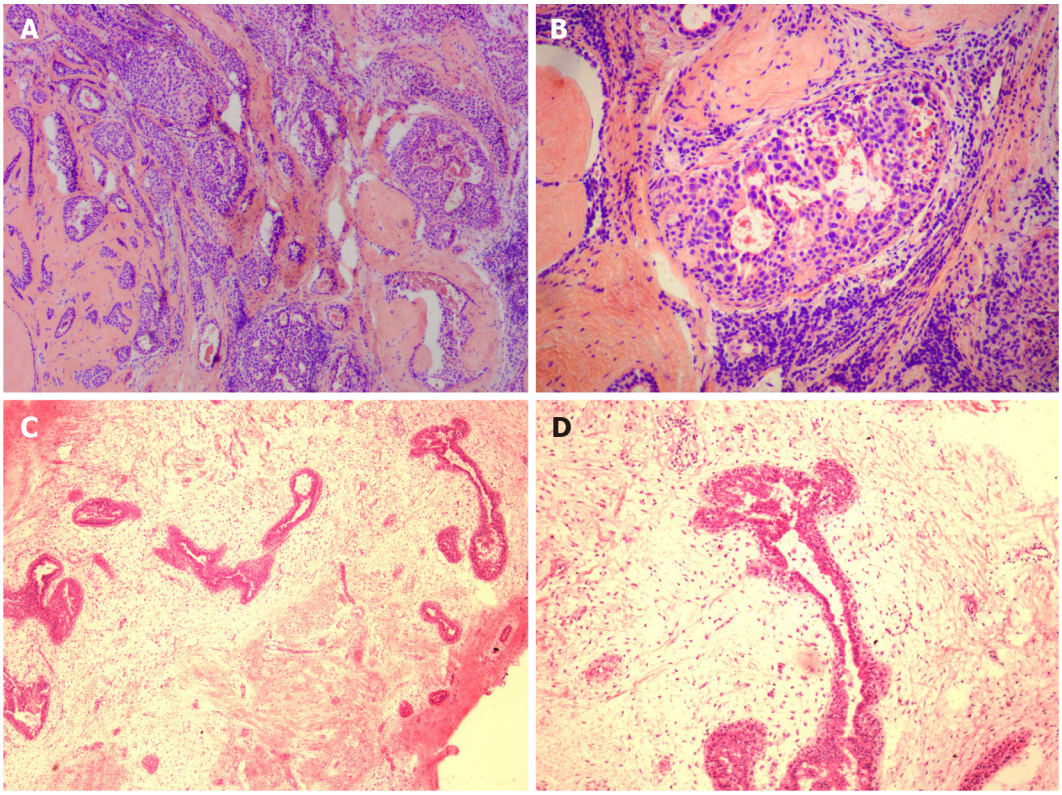

DOI: 10.12998/wjcc.v10.i11.3496

Figure 4 Intraoperative frozen section findings of case 1 and case 2. Sections were stained with hematoxylin and eosin. A: Low magnification image of case 1 (40 × magnification); B: Medium magnification image of case 1 (100 × magnification); C: Low magnification image of case 2 (40 × magnification); B: Medium magnification image of case 2 (100 × magnification).

DISCUSSION

To the best of our knowledge, this is the first study that reported imaging results of DCIS arising within fibroadenoma, which might gradually develop into a prediagnostic follow-up tool that could facilitate decisions on when to perform surgical biopsies for breast nodules with an apparently benign tumor observed at follow-up. Moreover, these data demonstrate the importance of adequate sampling, which can increase the accuracy of early diagnosis. In addition, our results verified the value of frozen and paraffin sections for diagnosing this particular cancer type, thus allowing for a definite diagnosis to be made.

Breast DCIS arising within a fibroadenoma is a rare occurrence. To our knowledge, there are no previous reports on imaging data (including ultrasound and mammography) during the longer preoperative follow-up for DCIS developing in fibroadenoma. Herein, we reported 2 cases of breast DCIS arising within fibroadenoma: 1 with a short medical history and 1 with more than 3 years of follow-up by ultrasound and mammography, subsequently confirmed by pathological examination.

Preoperative color Doppler sonography has a suggestive role in helping physicians make a correct diagnosis. In addition, longer preoperative follow-up imaging data allow us to review the developmental changes in this rare disease on imaging. Our data suggested that enlarged lesions with irregular margins, uneven texture, and concomitant calcifications could be important features for detecting this type of malignancy, which is consistent with previous studies[7,8].

Without adequate sampling and sectioning, a possibility of a missed diagnosis of intraductal carcinoma or even invasive carcinoma of such a focal location within a fibroadenoma increase. In addition, it is possible that the dysplastic ductal epithelium, or even carcinoma, could not be identified because frozen sections were only selected[9], although the ability of frozen sections for the diagnosis of this particular cancer type is adequate. In addition, some experts argue that invasive carcinomas arising in fibroadenomas could have similar prognostic features as intraductal carcinomas.

These 2 cases of breast DCIS arising within a fibroadenoma also clearly suggest that fibroadenomas should not be ignored and warrant close follow-up. Based on the course of the follow-up and diagnosis in the above cases and referring to the previous literature, a significantly enlarged mammary nodule with irregular morphology or uneven internal echogenicity under ultrasound may indicate the need for biopsy or surgical intervention[10].

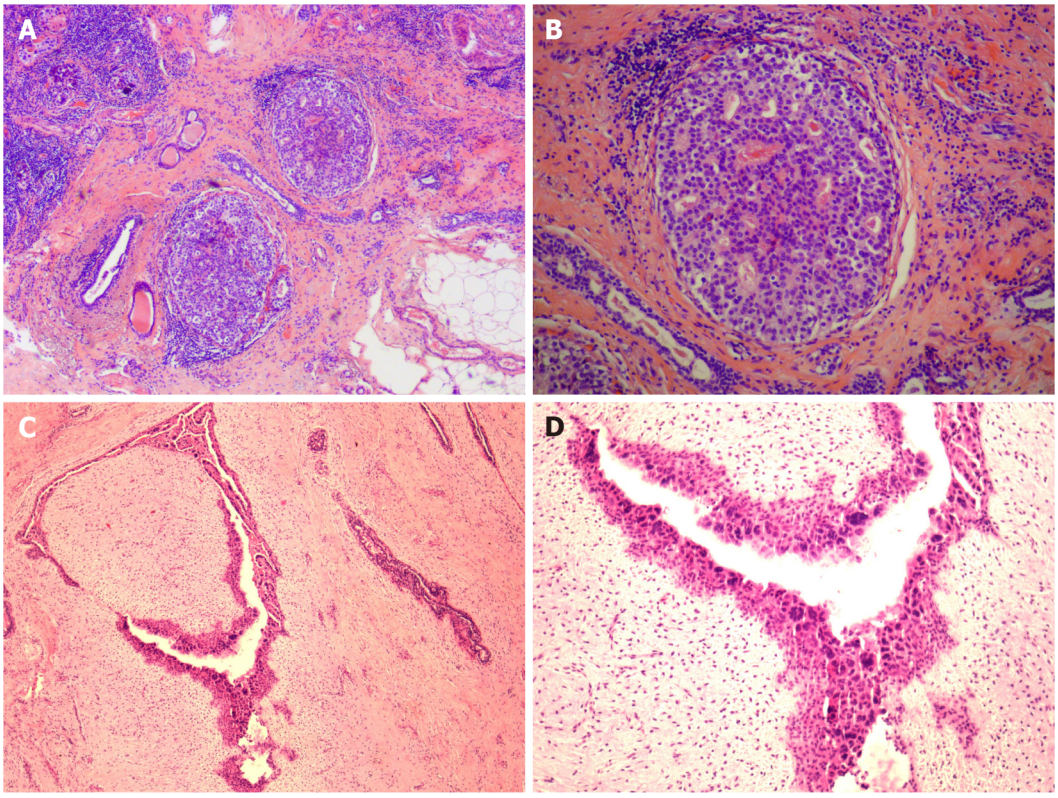

DOI: 10.12998/wjcc.v10.i11.3496

Figure 5 Paraffin section findings after operation of case 1 and case 2. Sections were stained with hematoxylin and eosin. A: Low magnification image of case 1 (40 × magnification); B: Medium magnification image of case 1 (100 × magnification); C: Low magnification image of case 2 (40 × magnification); D: Medium magnification image of case 2 (100 × magnification).

In general, the clinical and macroscopic features of DCIS arising within a fibroadenoma rarely differed from those of common DCIS[11]. Therefore, the treatment of this particular entity may be similar to the treatment of common DCIS. Based on the prognosis of carcinoma *in situ* within fibroadenomas, some scholars recommend breast-conserving surgery as the preferred treatment modality[11]. Only a small amount of adjacent breast tissue is usually included around the biopsy specimen. Therefore, biopsy is inadequate to assess adjacent mammary ducts. Re-excision is recommended. Mastectomy may also be performed if the patient wishes to approach "near-certain cure" [11]. In current National Comprehensive Cancer Network guidelines, patients suffering from DCIS treated with lumpectomy would be recommended to receive radiotherapy first, with the exception of those with lower recurrence risk factors. Whole breast radiation therapy with or without boost to tumor bed is the preferred method of radiotherapy (category I). The patients with DCIS without the high recurrence risk factors, such as age < 50 years, larger size, higher grade, palpable mass and close or involved margins, may be treated by excision alone. This propensity to excision alone would be stronger if they were estrogen receptor-positive because there are also endocrine therapies that can be used for treatment.

Despite the favorable prognosis, it remains unknown whether radiotherapy can be exempted after breast-conserving surgery in DCIS arising within a fibroadenoma. An analysis assessing 20-year mortality outcomes in patients with DCIS demonstrated no survival benefit to radiation, although it did reduce local recurrence risks significantly[12,13]. Relevant clinical studies could be designed but there are no recommendations in the current guidelines. In clinical practice, we may be more cautious in decisions about the treatment adopted for DCIS arising within a fibroadenoma. Referring to the recent guideline recommendations for common DCIS, age < 50 years was one of the recurrence risk factors. Therefore, the 2 patients received or will receive radiotherapy for treatment.

As recommended by National Comprehensive Cancer Network guidelines, DCIS patients are recommended routine genetics consultation. In addition to tumor type, age of cancer onset was also found to be a statistically significant indicator for germline referral[14]. The 2 cases involved in this report were both young patients, making genetic testing more valuable (*i.e.*, it may find BRCA1/2 mutations, *etc.*). Regrettably, neither patient accepted this recommendation.

Both of the patients showed estrogen receptor positivity. They were administered endocrine therapy with tamoxifen accordingly. As recommended by the recent National Comprehensive Cancer Network guidelines, endocrine therapy is considered the risk-reduction treatment of the ipsilateral breast after surgery in patients with DCIS undergoing breast-conserving surgery, especially in patients with

estrogen receptor-positive DCIS. Patients are treated with tamoxifen during the premenopausal period and with tamoxifen or an aromatase inhibitor during the postmenopausal period.

CONCLUSION

Breast DCIS arising within a fibroadenoma is rare. More sections are needed to reduce the missed rate. Complete follow-up data with preoperative imaging can help us make decisions during patient follow-up. Taken together, it remains uncertain whether a more conservative approach can be taken in the adjuvant setting for breast DCIS arising within a fibroadenoma.

ACKNOWLEDGEMENTS

The authors express special thanks to Dr Ke-Wang Sun who guided this work.

FOOTNOTES

Author contributions: Zhong MC designed the report; Sun KW, Mo QP, Yang ZR and Chen Y collected the patient's clinical data; Wu J and Zhong MC analyzed the data and wrote the paper.

Informed consent statement: The patients consented to submission of their anonymized cases and accompanying images.

Conflict-of-interest statement: The authors declare having no conflicts of interest.

CARE Checklist (2016) statement: The authors have read the CARE Checklist (2016), and the manuscript was prepared and revised according to the CARE Checklist (2016).

Country/Territory of origin: China

ORCID number: Jun Wu 0000-0002-6808-3207; Ke-Wang Sun 0000-0002-4839-477X; Qiu-Ping Mo 0000-0001-5667-5726; Ze-Ran Yang 0000-0003-0615-0256; Yuan Chen 0000-0002-9476-8816; Miao-Chun Zhong 0000-0003-2949-4967.

S-Editor: Wang JJ
L-Editor: A
P-Editor: Wang JJ

REFERENCES

1 **Carty NJ**, Carter C, Rubin C, Ravichandran D, Royle GT, Taylor I. Management of fibroadenoma of the breast. *Ann R Coll Surg Engl* 1995; **77**: 127-130 [PMID: 7793802 DOI: 10.1016/0960-9776(94)90010-8]
2 **Foster ME**, Garrahan N, Williams S. Fibroadenoma of the breast: a clinical and pathological study. *J R Coll Surg Edinb* 1988; **33**: 16-19 [PMID: 3418570 DOI: 10.18203/2349-2902.isj20212720]
3 **Fukuda M**, Nagao K, Nishimura R, Matsuda M, Baba K, Ueno Y, Morinaga H, Omachi H, Hamada T. Carcinoma arising in fibroadenoma of the breast--a case report and review of the literature. *Jpn J Surg* 1989; **19**: 593-596 [PMID: 2593394 DOI: 10.1007/bf02471669]
4 **Deschênes L**, Jacob S, Fabia J, Christen A. Beware of breast fibroadenomas in middle-aged women. *Can J Surg* 1985; **28**: 372-374 [PMID: 2990650 DOI: 10.1016/s0140-6736(83)90047-8]
5 **Dupont WD**, Page DL, Parl FF, Vnencak-Jones CL, Plummer WD Jr, Rados MS, Schuyler PA. Long-term risk of breast cancer in women with fibroadenoma. *N Engl J Med* 1994; **331**: 10-15 [PMID: 8202095 DOI: 10.1056/nejm199407073310103]
6 **Buzanowski-Konakry K**, Harrison EG Jr, Payne WS. Lobular carcinoma arising in fibroadenoma of the breast. *Cancer* 1975; **35**: 450-456 [PMID: 1111920 DOI: 10.1002/1097-0142(197502)35:2<450::aid-cncr2820350223>3.0.co;2-r]
7 **El-Essawy M**, Haidary A A, Khan A L. Ductal carcinoma in situ (DCIS) in breast fibroadenoma. *Egypt J Radiol Nuc M* 2020; **51**: 73 [DOI: 10.1186/s43055-020-00191-5]
8 **Ren Y**, Li P, Yang Y, Huang Y, Zhan D, Wen B. Imaging findings of ductal carcinoma in situ arising within fibroadenoma.

Breast J 2020; **26**: 1037-1038 [PMID: 31837072 DOI: 10.1111/tbj.13709]

9 **Hirano M**, Ueno E, Tanaka H, Aiyoshi Y, Soeda S. A case of ductal carcinoma arising in a fibroadenoma of the breast. *J STAGE* 1991; **52**: 1255-11258 [DOI: 10.3919/ringe1963.52.1255]

10 **Feliciano YZ**, Freire R, Net J, Yepes M. Ductal and lobular carcinoma in situ arising within an enlarging biopsy proven fibroadenoma. *BMJ Case Rep* 2021; **14** [PMID: 33468635 DOI: 10.1136/bcr-2020-237017]

11 **Diaz NM**, Palmer JO, McDivitt RW. Carcinoma arising within fibroadenomas of the breast. A clinicopathologic study of 105 patients. *Am J Clin Pathol* 1991; **95**: 614-622 [PMID: 1850948 DOI: 10.1093/ajcp/95.5.614]

12 **Lui SA**, Oh HB, Wang S, Chan CW. Ductal carcinoma in-situ arising within benign phyllodes tumours. *Ann R Coll Surg Engl* 2018; **100**: e97-e102 [PMID: 29484937 DOI: 10.1308/rcsann.2018.0024]

13 **Narod SA**, Iqbal J, Giannakeas V, Sopik V, Sun P. Breast Cancer Mortality After a Diagnosis of Ductal Carcinoma In Situ. *JAMA Oncol* 2015; **1**: 888-896 [PMID: 26291673 DOI: 10.1001/jamaoncol.2015.2510]

14 **Vlessis K**, Purington N, Chun N, Haraldsdottir S, Ford JM. Germline Testing for Patients With *BRCA1/2* Mutations on Somatic Tumor Testing. *JNCI Cancer Spectr* 2020; **4**: pkz095 [PMID: 32259017 DOI: 10.1093/jncics/pkz095]

World Journal of Clinical Cases

Submit a Manuscript: https://www.f6publishing.com

World J Clin Cases 2022 April 16; 10(11): 3505-3510

DOI: 10.12998/wjcc.v10.i11.3505

ISSN 2307-8960 (online)

CASE REPORT

Reconstruction of complex chest wall defects: A case report

Sheng-Chao Huang, Chun-Yan Chen, Pu Qiu, Ze-Ming Yan, Wei-Zhang Chen, Zhong-Zheng Liang, Kang-Wei Luo, Jian-Wen Li, Yuan-Qi Zhang, Bao-Yi Huang

Specialty type: Medicine, research and experimental

Provenance and peer review: Unsolicited article; Externally peer reviewed.

Peer-review model: Single blind

Peer-review report's scientific quality classification

Grade A (Excellent): A
Grade B (Very good): 0
Grade C (Good): C
Grade D (Fair): 0
Grade E (Poor): 0

P-Reviewer: Feizi A, Iran; Kapritsou M, Greece

Received: December 15, 2021
Peer-review started: December 15, 2021
First decision: January 26, 2022
Revised: February 3, 2022
Accepted: February 27, 2022
Article in press: February 27, 2022
Published online: April 16, 2022

Sheng-Chao Huang, Chun-Yan Chen, Pu Qiu, Ze-Ming Yan, Wei-Zhang Chen, Zhong-Zheng Liang, Kang-Wei Luo, Jian-Wen Li, Yuan-Qi Zhang, Bao-Yi Huang, Department of Vascular, Thyroid, and Breast Surgery, Affiliated Hospital of Guangdong Medical University, Zhanjiang 524000, Guangdong Province, China

Corresponding author: Yuan-Qi Zhang, PhD, Dean, Department of Vascular, Thyroid, and Breast Surgery, Affiliated Hospital of Guangdong Medical University, No. 57 Renmin Avenue South, Xiashan District, Zhanjiang 524000, Guangdong Province, China. 31428319@qq.com

Abstract

BACKGROUND

Chronic radiative chest wall ulcers are common in patients undergoing radiation therapy. If not treated early, then symptoms such as erosion, bleeding and infection will appear on the skin. In severe cases, ulcers invade the ribs and pleura, presenting a mortality risk. Small ulcers can be repaired with pedicle flaps. Because radioactive ulcers often invade the thorax, surgeons need to remove large areas of skin and muscle, and sometimes ribs. Repairing large chest wall defects are a challenge for surgeons.

CASE SUMMARY

A 74-year-old female patient was admitted to our department with chest wall skin ulceration after radiation therapy for left breast cancer. The patient was diagnosed with chronic radioactive ulceration. After multidisciplinary discussion, the authors performed expansive resection of the chest wall ulcers and repaired large chest wall defects using a deep inferior epigastric perforator (DIEP) flap combined with a high-density polyethylene (HDPE) patch. The patient was followed-up 6 mo after the operation. No pigmentation or edema was found in the flap.

CONCLUSION

DIEP flap plus HDPE patch is one of the better treatments for radiation-induced chest wall ulcers.

Key Words: Deep inferior epigastric perforator flap; High-density polyethylene patch; Breast cancer; Chest wall; Chronic radiation-induced ulcer; Case report

Core Tip: In recent years, with the development of microsurgical techniques and breast reconstruction techniques and the wide application of autologous flap transplantation, breast surgeons have provided new ideas for the treatment of chronic radiation-induced ulcers of the chest wall. Deep inferior epigastric perforator flap combined with a high-density polyethylene patch is a promising treatment for chronic radiation-induced ulcers of the chest wall.

Citation: Huang SC, Chen CY, Qiu P, Yan ZM, Chen WZ, Liang ZZ, Luo KW, Li JW, Zhang YQ, Huang BY. Reconstruction of complex chest wall defects: A case report. *World J Clin Cases* 2022; 10(11): 3505-3510
URL: https://www.wjgnet.com/2307-8960/full/v10/i11/3505.htm
DOI: https://dx.doi.org/10.12998/wjcc.v10.i11.3505

INTRODUCTION

The incidence of chest wall ulcers due to chronic radiation is about 25%-30%. The radiation dose, radiation time and patient's condition are the risk factors known to affect its occurrence. It has been reported that radiation doses exceeding 70 Gy/7 wk/30 fractions are prone to cause such ulcers[1]. Radiation-induced ulcers of the chest wall are secondary, progressive and irreversible, with a duration of as short as several months and as long as years or decades. Moreover, they can be classified as a special type of protracted wound. In addition, radiation can cause vascular contracture, reduce the amount of blood supplied to the skin, induce fibrosis of the skin, and directly impair the repair function of the skin tissue[2-5].

Chronic radiation-induced ulcers of the chest wall are often associated with infection and easily cause rib necrosis and osteomyelitis. This seriously affects the quality of life of patients and is a detriment to a patient's confidence in treating cancer. In the past, surgeons have tried to treat it with debridement and dressing change or skin grafting, but it is difficult to achieve the ideal therapeutic effect.At present, chest wall reconstruction includes two parts: Bone reconstruction of the chest wall, and soft tissue reconstruction of the chest wall. The former uses biological or artificial materials to restore stability of the chest wall, while the latter realizes the tightness of the chest wall by transferring its own tissue flap to cover the defect. In the repair of the chest wall, titanium alloy plates and high-density polyethylene (HDPE) patches are two commonly used materials. Some scholars have pointed out that HDPE patches have sufficient toughness and can better maintain the stability of the chest wall without interference with radiotherapy[6]. In terms of soft tissue repair, a banded myocutaneous flap is better to repair chest wall defects; however, the excessive muscle harvested during the surgery causes the patient sustains greater trauma, resulting in prolonged recovery time and affecting the subsequent treatment of patients. Due to the development of microsurgical techniques, the application of free flaps to repair chest wall defects has become a clinical hot spot.

In this report, the breast cancer patient suffered from a chronic radiation-induced ulcer of the chest wall combined with necrosis of the second to fifth ribs. The chest wall defect was repaired by deep inferior epigastric perforator (DIEP) flap combined with a HDPE patch, with good postoperative recovery.

CASE PRESENTATION

Chief complaints

A 74-year-old female patient was admitted for a radioactive ulcer on the chest wall for more than 4 mo.

History of present illness

The patient's chest wall ulcer occurred 1 wk after the 6th radiotherapy treatment and lasted about 4 mo. The area of the ulcer was 4 cm × 6 cm. The surface of the ulcer was dirty, and the basal granulation tissue was sparse. The ulcer surface bled easily, which indicated that it was closely attached to deep tissue. The ulcer was hard and surrounded by scar tissue.

History of past illness

The patient underwent modified radical mastectomy of the left breast in our department 5 mo prior. The patient did not have hypertension, diabetes or hyperlipidemia.

Personal and family history

Personal and family history was unremarkable.

Physical examination

An irregularly shaped ulcer was observed on the surface of the skin of the left chest wall and measuring 4 cm × 6 cm. It was accompanied by red coloration, fishy odor, and pus-like discharge. The skin around the ulcer was red and swollen, hard in consistency and tender (Figure 1A). No significantly enlarged lymph nodes were palpable in the left axilla or supraclavicular region.

Laboratory examinations

All laboratory tests were normal.

Imaging examinations

Chest computed tomography: Irregular subcutaneous soft tissue of the left anterior chest wall and multiple small nodular high-density shadows in the local area were observed. These were predicted to change after radiotherapy. Slightly disordered structure of the left axilla was also observed but no enlarged lymph nodes were found.

MULTIDISCIPLINARY EXPERT CONSULTATION

The consultation included specialists in breast surgery, thoracic surgery and radiology. After discussion by several specialists, the decision was made to perform an expanded excision of the ulcer on the chest wall of the patient, including the invaded muscle and ribs. Then, the thoracic defect would be repaired with a patch, and the chest wall defect would be covered with a free flap (Figure 1B).

FINAL DIAGNOSIS

Radiation-induced ulcer of the left chest wall (Figure 1C).

TREATMENT

DIEP flap combined with an HDPE patch was used to repair the chest wall ulcer (Figure 1D and E).

OUTCOME AND FOLLOW-UP

The patient was followed-up for 6 mo after the operation. The skin flap showed no pigmentation and no edema. The skin growth and healing of the donor site were acceptable. The donor site was not complicated with abdominal skin necrosis, abdominal bulge, abdominal weakness, nor abdominal hernia (Figure 1F).

DISCUSSION

Although radiotherapy equipment, technology and design have been developed to varying degrees in recent years, the occurrence of chronic radiation-induced ulcers of the chest wall are still common when radiation therapy is received after breast cancer surgery.

According to scholars, conservative treatment of radiation-induced ulcers using debridement, dressing change and antibiotics is ineffective for most patients[7]. Many clinicians have tried different methods to treat chronic radiation-induced ulcers of the chest wall. According to Nishimoto *et al*[8], an ideal therapeutic effect was observed in 4 patients upon transfusing platelet-rich plasma and simultaneous skin grafting. Other studies have reported that chronic radiation-induced ulcers of the chest wall have been cured by intravenous infusion of plasma-purified mannan-binding lectin to patients[9,10]. Researchers have also conducted an animal experiment (in guinea pigs) and administered arginine glutamate after artificially causing radiation-induced ulcers, and the therapeutic effect of the ulcers was adequate[10,11]. However, due to individual differences, the above treatment has not been widely promoted in clinical practice, and surgical treatment is still the main treatment.

Radiation injury causes soft tissue damage and leads to necrosis of the sternum and ribs. Surgical reconstruction of the chest wall includes two parts: Thoracic reconstruction and soft tissue repair. It is generally believed that if the anterolateral chest wall defect is less than 6 cm × 6 cm and the posterior chest wall defect is less than 10 cm × 10 cm, then generally no thoracic reconstruction is required[10,12]. Soft tissue coverage alone can eliminate the abnormal respiratory movement of the chest wall after

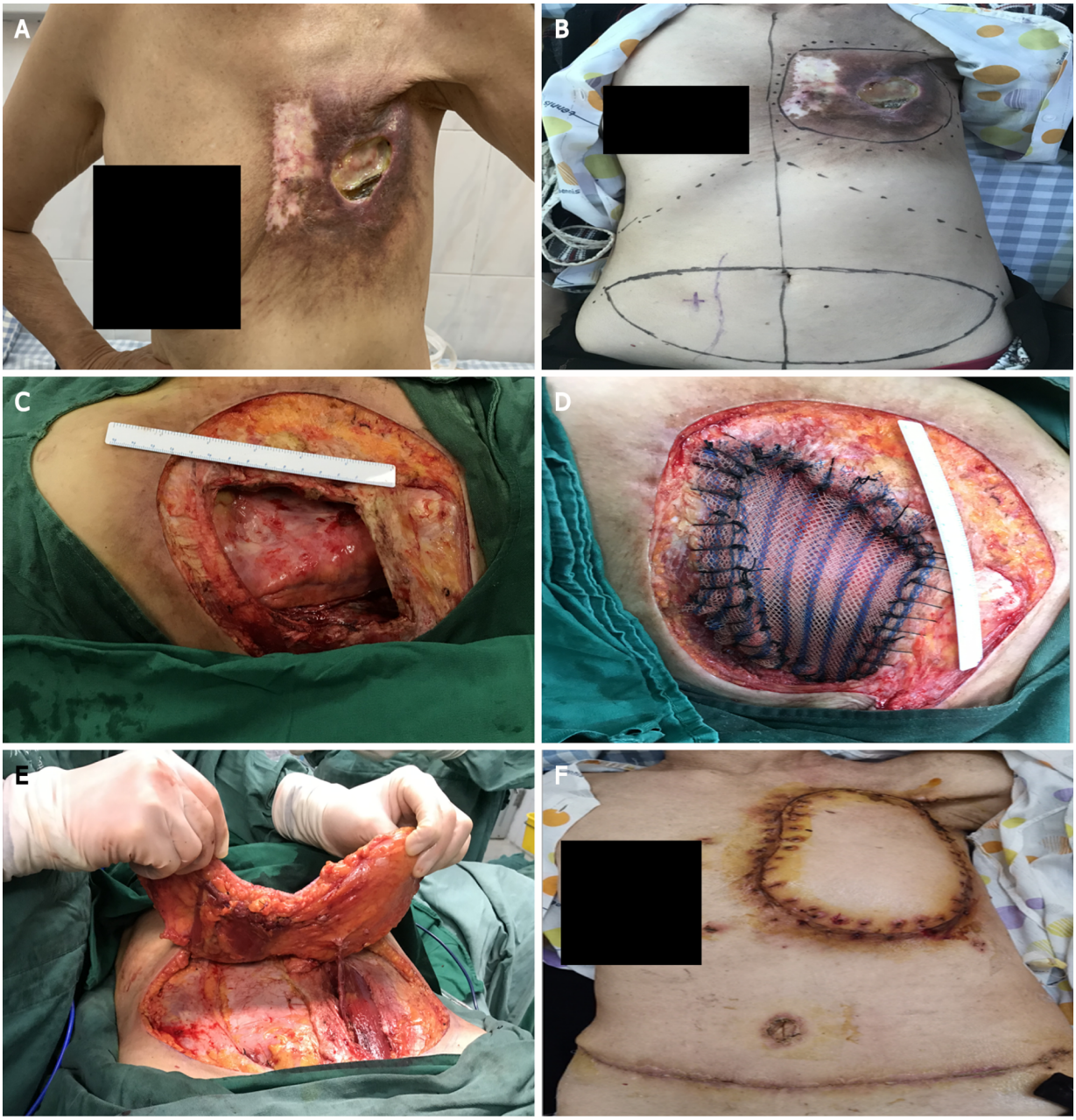

DOI: 10.12998/wjcc.v10.i11.3505

Figure 1 Physical examination and surgery. A: Chest wall ulcer; B: Preoperative design; C: Chest wall defect measurement; D: Bone thoracic repair; E: Flap acquisition; F: Skin flap shaping.

surgery. However, large defects require thoracic reconstruction to restore the firmness and stability of the thorax in order to protect the viscera and maintain normal respiration.

In the reconstruction of the bony chest wall, two kinds of synthetic materials titanium alloy plates and HDPE soft patch are mostly used. HDPE patches have good toughness and elicit minimal aseptic inflammatory response. In a short time, human tissue can grow on the patch and cover the cavity in the body, which is conducive to wound repair. In addition, the patch is easy to cut and use during surgery. However, compared with a titanium alloy plate, its hardness and support force are not satisfactory. Occasionally, when the patient breathes, the HDPE patch suture loosens, which results in deformation of the chest wall. However, HDPE patches do not interfere with subsequent radiation therapy.

Thorough debridement and myocutaneous flap coverage of the defect are the preferred methods for the surgical treatment of chest wall ulcers. When debridement of thoracic ulcers is performed, it is required to remove the injured skin and subcutaneous soft tissue, necrotic ribs, sternum, clavicle and surrounding muscle fibrous tissue as much as possible. The choice of myocutaneous flaps, such as latissimus dorsi flap, pectoralis major flap and rectus abdominis flap, is preferred[6]. These myocutaneous flaps have the advantages of rich tissue volume, stable vascular pedicle course, and easy operation. However, due to the harvesting of a large amount of autologous muscles from patients, they

cause greater trauma to individuals and result in a longer recovery time, which may delay the subsequent treatment time. In contrast, pedicle musculocutaneous flaps are difficult to cover large wounds due to their small incision area.

In this case, DIEP soft tissue was used to repair the chest wall defect. Without harvesting the muscle, there was a sufficient amount of tissue to cover the defect, which was less invasive to the patient and had less recovery time, that did not disrupt subsequent radiotherapy. However, compared with other myocutaneous flaps, DIEP has a relatively small amount of tissue and cannot be used to cover deeper or larger defects. Moreover, the operation of DIEP is relatively complex and requires knowledge and expertise in microvascular anastomosis surgery, which is difficult to promote in clinical practice.

The main characteristics of this case were: (1) Intraoperative use of DIEP does not cut the rectus abdominis muscle, making it less invasive to the patient and shortening the postoperative recovery time; and (2) Intraoperative use of HDPE patches can maintain stability of the chest wall and does not interfere with the patient's subsequent radiotherapy.

CONCLUSION

In summary, for patients with smaller chest wall defects accompanied by rib necrosis, DIEP combined with HDPE patch repair can be used to obtain satisfactory clinical efficacy and reduce the occurrence of postoperative complications. This may be a better way to treat large chest wall radiation-induced ulcers.

FOOTNOTES

Author contributions: Zhang YQ contributed to conception and design of the case report; Li JW contributed administrative support; Huang SC and Qiu P contributed to provision of study materials or patients; Liang ZZ, Yan ZM and Luo KW contributed to collection and assembly of data; Huang BY, Chen CY and Chen WZ contributed to data analysis and interpretation; Qiu P, Chen CY, Huang SC, Yan ZM, Chen WZ, Liang ZZ, Luo KW, Huang BY, Li JW and Zhang YQ contributed to manuscript writing and final approval of the manuscript.

Informed consent statement: The patient's consent was obtained for the anonymized release of the case data.

Conflict-of-interest statement: The authors declare no conflicts of interest.

CARE Checklist (2016) statement: The authors have read the CARE Checklist (2016), and the manuscript was prepared and revised according to the CARE Checklist (2016).

Country/Territory of origin: China

ORCID number: Sheng-Chao Huang 0000-0002-8713-8365; Chun-Yan Chen 0000-0002-7541-9784; Pu Qiu 0000-0003-0792-8808; Ze-Ming Yan 0000-0002-8473-7063; Wei-Zhang Chen 0000-0002-4668-6760; Zhong-Zheng Liang 0000-0002-6223-852X; Kang-Wei Luo 0000-0003-2742-5626; Jian-Wen Li 0000-0002-7657-1876; Yuan-Qi Zhang 0000-0002-7206-2353; Bao-Yi Huang 0000-0002-4282-2008.

S-Editor: Fan JR
L-Editor: A
P-Editor: Fan JR

REFERENCES

1 **Zhou Y**, Zhang Y. Single- versus 2-stage reconstruction for chronic post-radiation chest wall ulcer: A 10-year retrospective study of chronic radiation-induced ulcers. *Medicine (Baltimore)* 2019; **98**: e14567 [PMID: 30813173 DOI: 10.1097/MD.0000000000014567]
2 **Futran ND**, Trotti A, Gwede C. Pentoxifylline in the treatment of radiation-related soft tissue injury: preliminary observations. *Laryngoscope* 1997; **107**: 391-395 [PMID: 9121320 DOI: 10.1097/00005537-199703000-00022]
3 **Arnold PG**, Pairolero PC. Reconstruction of the radiation-damaged chest wall. *Surg Clin North Am* 1989; **69**: 1081-1089 [PMID: 2675349 DOI: 10.1016/s0039-6109(16)44939-x]
4 **Feldmeier JJ**. Hyperbaric oxygen therapy and delayed radiation injuries (soft tissue and bony necrosis): 2012 update. *Undersea Hyperb Med* 2012; **39**: 1121-1139 [PMID: 23342770 DOI: 10.1038/mtna.2012.47]

5 **Enomoto M**, Yagishita K, Okuma K, Oyaizu T, Kojima Y, Okubo A, Maeda T, Miyamoto S, Okawa A. Hyperbaric oxygen therapy for a refractory skin ulcer after radical mastectomy and radiation therapy: a case report. *J Med Case Rep* 2017; **11**: 5 [PMID: 28049509 DOI: 10.1186/s13256-016-1168-0]

6 **Hameed A**, Akhtar S, Naqvi A, Pervaiz Z. Reconstruction of complex chest wall defects by using polypropylene mesh and a pedicled latissimus dorsi flap: a 6-year experience. *J Plast Reconstr Aesthet Surg* 2008; **61**: 628-635 [PMID: 17656168 DOI: 10.1016/j.bjps.2007.04.011]

7 **Fujioka M**. Surgical Reconstruction of Radiation Injuries. *Adv Wound Care (New Rochelle)* 2014; **3**: 25-37 [PMID: 24761342 DOI: 10.1089/wound.2012.0405]

8 **Nishimoto S**, Fukuda K, Kawai K, Fujiwara T, Tsumano T, Fujita K, Kakibuchi M. Supplementation of bone marrow aspirate-derived platelet-rich plasma for treating radiation-induced ulcer after cardiac fluoroscopic procedures: A preliminary report. *Indian J Plast Surg* 2012; **45**: 109-114 [PMID: 22754164 DOI: 10.4103/0970-0358.96599]

9 **Maaløe N**, Bonde C, Laursen I, Christiansen M, Hölmich LR. Mannan-binding lectin and healing of a radiation-induced chronic ulcer--a case report on mannan-binding lectin replacement therapy. *J Plast Reconstr Aesthet Surg* 2011; **64**: e146-e148 [PMID: 21353657 DOI: 10.1016/j.bjps.2011.01.013]

10 **Zhou Y**, Guan X, Zhang Y. Staged repair of chronic chest wall radiation ulcer. *J Tissue Eng* 2014; **10**: 335-338 [DOI: 10.3969/j.issn.1673-0364.2014.06.009]

11 **Khalin I**, Kocherga G. Arginine glutamate improves healing of radiation-induced skin ulcers in guinea pigs. *Int J Radiat Biol* 2013; **89**: 1108-1115 [PMID: 23786463 DOI: 10.3109/09553002.2013.817698]

12 **Chang RR**, Mehrara BJ, Hu QY, Disa JJ, Cordeiro PG. Reconstruction of complex oncologic chest wall defects: a 10-year experience. *Ann Plast Surg* 2004; **52**: 471-9; discussion 479 [PMID: 15096930 DOI: 10.1097/01.sap.0000122653.09641.f8]

World Journal of Clinical Cases

Submit a Manuscript: https://www.f6publishing.com

World J Clin Cases 2022 April 16; 10(11): 3511-3517

DOI: 10.12998/wjcc.v10.i11.3511

ISSN 2307-8960 (online)

CASE REPORT

Young children with multidrug-resistant epilepsy and vagus nerve stimulation responding to perampanel: A case report

Hua Yang, Dan Yu

Specialty type: Medicine, research and experimental

Provenance and peer review: Unsolicited article; Externally peer reviewed.

Peer-review model: Single blind

Peer-review report's scientific quality classification

Grade A (Excellent): 0
Grade B (Very good): B, B
Grade C (Good): 0
Grade D (Fair): 0
Grade E (Poor): 0

P-Reviewer: Bazhanova ED, Russia; Hosoya S, Japan

Received: August 9, 2021
Peer-review started: August 9, 2021
First decision: November 6, 2021
Revised: November 23, 2021
Accepted: February 27, 2022
Article in press: February 27, 2022
Published online: April 16, 2022

Hua Yang, Dan Yu, Department of Pediatrics, West China Second University Hospital, Sichuan University, Chengdu 610041, Sichuan Province, China

Corresponding author: Dan Yu, MD, Doctor, Professor, Department of Pediatrics, West China Second University Hospital, Sichuan University, No. 20, Section 3, South Renmin Road, Chengdu 610041, Sichuan Province, China. yudan540@163.com

Abstract

BACKGROUND

Perampanel (PER), a third-generation antiepileptic drug, is a selective and noncompetitive α-amino-3-hydroxy-5-methyl-4-isoxazolepropionic acid receptor antagonist, and has been approved for the treatment of adults and adolescents with focal epilepsy. However, there are only a few studies about the efficacy and tolerability of PER in young children with multidrug-resistant epilepsy. In this case, we aimed to share our clinical experience in this group.

CASE SUMMARY

A 4-year-old boy without perinatal asphyxia and familial history of epilepsy began to have ictal seizures from age 14 mo, with jerky movement of four limbs and head nodding. Abnormal multifocal discharge and background activity were recorded through electroencephalography, and no pathogenic mutation was found in the whole exome sequencing for the patient and his parents. He had received valproate, levetiracetam, topiramate, oxcarbazepine, clonazepam and lacosamide sequentially at different times, but he still had frequent seizures even after vagus nerve stimulation (VNS) implantation. He was diagnosed with idiopathic multidrug-resistant epilepsy. However, his seizure frequency was significantly reduced after PER administration in a dose-dependent manner, and better cognitive behavior was observed. In addition, the adverse reactions of anger and aggression also appeared.

CONCLUSION

PER is effective as add-on therapy for young children with multidrug-resistant epilepsy who have previously undergone VNS implantation.

Key Words: Perampanel; Young children; Drug-resistant epilepsy; Vagus nerve stimulation; Case report

Core tip: We report a 4-year-old boy with multidrug-resistant epilepsy who still had frequent seizures after vagus nerve stimulation (VNS) implantation, and he showed significant response to perampanel (PER) as add-on in a dose-dependent manner. Considering its favorable cognitive profile and the similar efficacy and safety profile of PER in children aged < 12 years as in older people, we proposed that the use of PER as add-on could further reduce the seizure frequency for young children with drug-resistant epilepsy and even after VNS implantation, which may be attributed to its novel antiepileptic mechanism.

Citation: Yang H, Yu D. Young children with multidrug-resistant epilepsy and vagus nerve stimulation responding to perampanel: A case report. *World J Clin Cases* 2022; 10(11): 3511-3517
URL: https://www.wjgnet.com/2307-8960/full/v10/i11/3511.htm
DOI: https://dx.doi.org/10.12998/wjcc.v10.i11.3511

INTRODUCTION

About 10% of children with epilepsy have drug-resistant epilepsy[1]. The treatment of drug-resistant epilepsy can be challenging, including resective surgery, ketogenic diet, vagus nerve stimulation (VNS), and new antiepileptic drugs (AEDs). The anticonvulsant perampanel (PER), a selective and noncompetitive α-amino-3-hydroxy-5-methyl-4-isoxazolepropionic acid (AMPA) receptor antagonist, is a newly developed third-generation AED, possessing the completely different antiepileptic mechanisms with previous AEDs. Currently, PER is recommended by the American Academy of Neurology guideline as add-on therapy in treatment-resistant adult focal epilepsy to reduce epilepsy frequency (level A)[2]. However, only a few studies have reported the efficacy and safety of PER in children younger than 12 years old with drug-resistant epilepsy. In this paper, we present a 4-year-old child with multidrug-resistant epilepsy in whom the seizures were not well controlled after VNS implantation, and PER administration significantly reduced seizure frequency in a dose-dependent manner. We aimed to describe our experience about reducing the seizures in multidrug-resistant young children with PER.

CASE PRESENTATION

Chief complaints

A 19-mo-old boy presented with ictal seizures since age 14 mo, and was brought to our pediatric neurology department because of gradually increased seizure attack.

History of present illness

The history taken from the parents revealed that the patient began to have ictal seizures after age 14 mo, with jerky movement of four limbs and head nodding, and he experienced one seizure per week lasting for 1-2 s. His seizure frequency increased gradually, and when he was admitted to our department, he was experiencing 10-15 seizures per day lasting for 1-3 min each time, with hand raising and head nodding. The patient could speak only simple words, and could not communicate with others and understand instructions.

History of past illness

The patient had a free previous medical history.

Personal and family history

His parents reported that there was no consanguinity, and the patient was born at full term *via* vaginal delivery with a birth weight of 3100 g. He had no perinatal asphyxia, and his Apgar scores were 10 at 1, 5 and 10 min of life. He had no family history of epilepsy and other familial diseases.

Physical examination

Physical examination showed that the patient had normal consciousness but could not communicate with others and understand instructions. He showed normal appearance, and there was no abnormal skin mass or depigmentation. The muscle tension, strength and mobility of the limbs were normal.

Laboratory examinations

His laboratory examinations revealed nothing notable.

Imaging examinations

The cranial fluid-attenuated inversion recovery images showed patchy high-signal areas in the posterior part of bilateral lateral ventricle, and in the subcortical white matter of left occipital and temporal lobes (Figure 1).

FURTHER DIAGNOSTIC WORK-UP

Video-electroencephalography (vEEG) recordings showed irregular and slow background activity, as well as multifocal generalized sharp and (multi-) spike wave discharge (Figure 2A). The high-amplitude slow waves with high-frequency discharges were recorded in vEEG during a seizure (Figure 2B). To determine the underlying cause of epilepsy, we performed whole exome sequencing for the patient and his parents, however, no pathogenic mutation was found.

FINAL DIAGNOSIS

This patient had both focal and generalized seizures, and was later diagnosed as idiopathic multidrug-resistant epilepsy.

TREATMENT

Several AEDs were applied to this patient sequentially. Valproate sodium (VPA, maximum dose 50 mg/kg/d) was started at age 19 mo after hospitalization; however, it was ineffective at reducing seizure frequency. Levetiracetam (LEV, maximum dose 50 mg/kg/d) was add 1 mo later, and the seizures were reduced by 60% after the add-on of LEV. When he was aged 32 and 33 mo, topiramate (TPM, maximum dose 5 mg/kg/d) and oxcarbazepine (OXC, maximum dose 60 mg/kg/d) were added, and the seizure frequency was decreased gradually to five or six times per day. VPA was replaced with clonazepam (CLZ, maximum dose 0.1 mg/kg/d) at 3 years old; however, CLZ was discontinued after 3 mo due to ineffectiveness.

To further decrease seizure frequency, left VNS implantation was performed at age 39 mo, and the seizures were reduced by 50% to two per day, and he became responsive to calling. LEV, TPM and OXC were continued for 7 mo after the insertion of VNS, and OXC was gradually replaced with lacosamide (LCM, maximum dose 125 mg/d) in 3 mo after no improvement of seizure frequency. However, the seizures were still two per day and LCM was discontinued. PER was started at age 4 years and 3 mo at an initial dose of 2 mg/d (0.1 mg/kg/d, body weight 20 kg), and the seizures were significantly reduced to one every 1-2 d. Three months later his PER was up-titrated to 4 mg/d (0.2 mg/kg/d) and his seizure frequency was one seizure every 2-3 d. After 2 mo, PER was added to current dose of 6 mg/d (0.3 mg/kg/d), which improved his seizure frequency to one seizure every 3-4 d lasting for 1-2 min each time (Figure 3).

OUTCOME AND FOLLOW-UP

At the last follow-up visit, 7 mo after the add-on of PER, the follow-up vEEG showed a decrease in the frequency of multifocal discharges, and no seizure was observed during the monitoring (Figure 2C). Therefore, the improvements after the use of PER were both clinical and electrophysiological. The patient was responsive to calling, and could communicate with others and follow simple instructions, showing improved cognitive skills and language according to our observation and his parents' records. In addition, the adverse reactions of anger and aggressive behavior were noticed after the use of PER. Although the seizure-free status was not achieved in this patient after 7 mo treatment with PER, he was closely followed up to assess the long-term effect of PER oral treatment.

DISCUSSION

PER is the first AED targeting AMPA receptors, which was approved by the United States Food and Drug Administration (FDA) to treat partial-onset seizures with or without secondarily generalized seizures for adult patients with epilepsy in September 2018[2,3]. Its great cognitive profile, ease of use of the titration scheme and the once-daily oral regimen give it advantages over other AEDs. Although the FDA approved the use of PER in persons ≥ 4 years of age, according to the strategy that allows extrapolation of efficacy across populations[2], reports about the efficacy and safety of PER in children

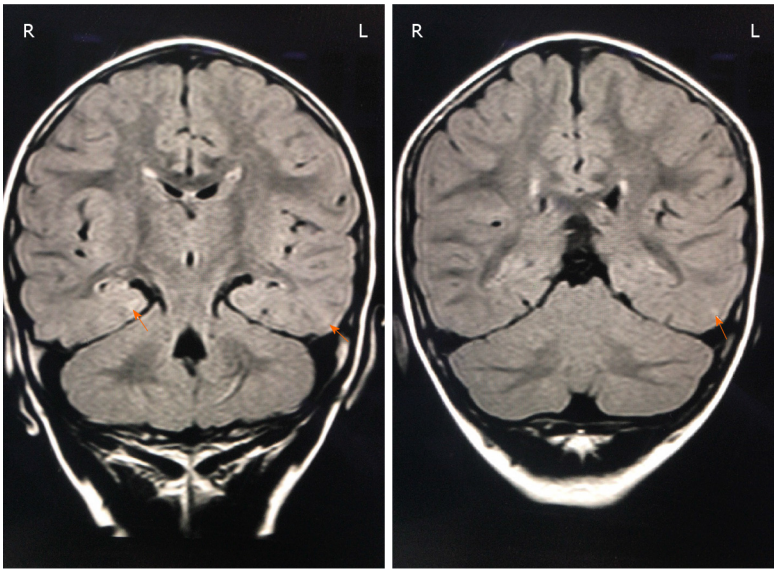

DOI: 10.12998/wjcc.v10.i11.3511

Figure 1 The patient's cranial magnetic resonance images. Fluid-attenuated inversion recovery showed patchy high-signal areas in the posterior part of bilateral lateral ventricle, and in the subcortical white matter of left occipital and temporal lobes (orange arrows).

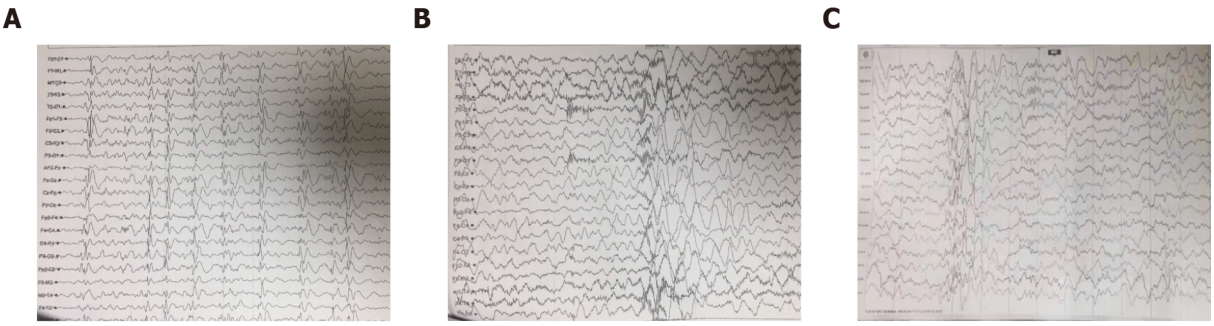

DOI: 10.12998/wjcc.v10.i11.3511

Figure 2 Video-electroencephalography recordings of this patient before and after perampanel treatment. A: Before treatment with perampanel (PER). The basic waves were irregular and slow, and multifocal generalized sharp and (multi-) spike wave discharges were frequent over the whole brain; B: Before treatment with PER. Seizures were observed during the monitoring, with 8-10 tics in each seizure, and the high-amplitude slow waves with high-frequency discharges were recorded in video-electroencephalography; C: During treatment with PER. The frequency of abnormal multifocal discharges was decreased, and no seizure was observed during the monitoring.

under 12 years old with drug-resistant epilepsy are still limited. In the present case, after the sequential use of six AEDs and left VNS implantation, the 4-year-old patient still had frequent seizure attacks, while seizures were significantly reduced by > 80% after adding PER in a dose-dependent manner. Hence, we believe that PER may be an effective and important add-on drug for treatment of multidrug-resistant epilepsy, especially in young children, which may be attributed to the novel antiepileptic mechanism of PER.

PER is a selective, noncompetitive antagonist of ionotropic AMPA glutamate receptor (AMPAR) that mediates the fast excitatory synaptic neurotransmission in the central nervous system (CNS). The AMPARs are expressed throughout the CNS, and are tetrameric complexes of four different types of subunits, including GluA1, GluA2, GluA3 and GluA4. The AMPAR subunits bind in pairs to form a variety of symmetric dimers, which next form functional ionic glutamate receptors surrounding a permeable cation channel of sodium (Na^+), potassium (K^+), and calcium (Ca^{2+}). Following the binding of glutamate to AMPARs, Na^+, K^+ and Ca^{2+} ions rapidly flow into the neurons, and depolarize the postsynaptic membranes from the resting potential[4]. The normal function of the human brain depends on the balance of excitatory and inhibitory activities of neural networks. Neurons antagonize excitatory activities by upregulating the aggregation of inhibitory -aminobutyric acid receptors (GABARs) on the postsynaptic membrane, so as to prevent excessive excitability of the neural network[5]. Abnormal changes in the composition, function and dynamic characteristics of AMPAR subunits lead to a large amount of Ca^{2+} influx into dendritic cells to overactivate the downstream pathway, inhibit the inhibitory GABARs function, and over-increase the excitability of neuronal networks, leading to the excitation/

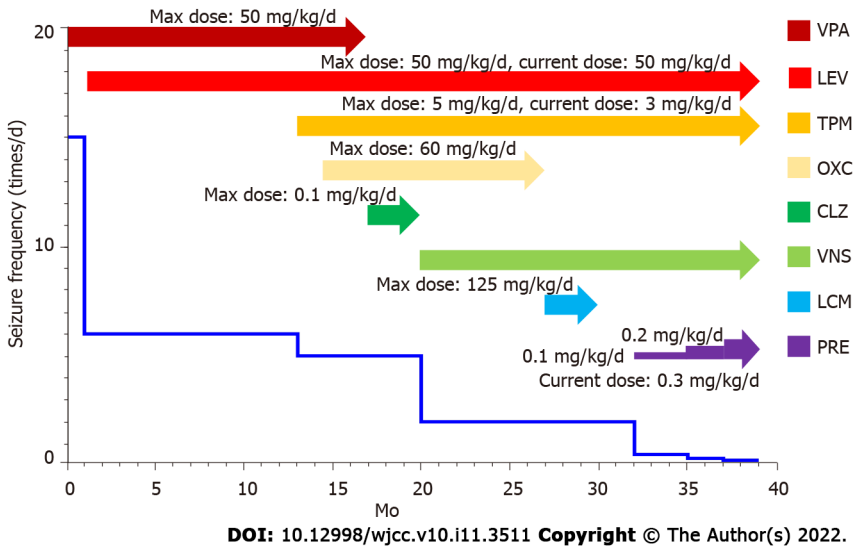

DOI: 10.12998/wjcc.v10.i11.3511

Figure 3 Clinical course of antiseizure drugs and seizure frequency since diagnosis (19 mo old). VPA: Valproate sodium; LEV: Levetiracetam; TPM: Topiramate; OXC: Oxcarbazepine; CLZ: Clonazepam; VNS: Vagus nerve stimulation; LCM: Lacosamide; PRE: Perampanel.

inhibition imbalance in brain, which may be the etiology and mechanism of epilepsy[6]. Up to now, there are only two AMPAR antagonists, talampanel and PER, which have entered clinical trials. However, development of talampanel was discontinued due to its short half-life, poor antiepileptic efficacy and serious adverse reactions in clinical trials. PER is the second AMPAR antagonist and is the only one approved for clinical use[6].

VNS is an adjuvant treatment approved by the FDA for patients ≥ 12 years of age with drug-resistant epilepsy, and was further approved for use in patients > 4 years of age in 2017. Nowadays, much evidence supports that VNS implantation as adjuvant therapy is possibly effective in pediatric (≤ 18 years old) drug-resistant epilepsy. The pooled prevalence estimates for 50% responder rate and seizure freedom at last follow-up (mean 2.54 years) were 56.4% and 11.6%, respectively[7], and VNS may have improved efficacy over time[8]. Davis Jones *et al*[9] reported that PER could further reduce the seizure frequency in some adult patients with drug-resistant epilepsy who still had seizures after their previous VNS implantation or resective surgery. However, no report was found about the use of PER in young children with drug-resistant epilepsy after VNS implantation. Our patient was a 4-year-old boy with multidrug-resistant epilepsy who still had frequent seizures after VNS implantation as adjuvant therapy, and he showed significant response to PER as add-on in a dose-dependent manner, with seizures reduced by > 80% after 7 mo treatment. Therefore, we propose that for young children with drug-resistant epilepsy who still have frequent seizures after VNS implantation, the use of PER as add-on could further reduce the seizure frequency.

Some studies have shown that PER may improve cognitive function in children patients. In a phase II randomized, double-blind, placebo-controlled study of 133 adolescent patients with uncontrolled partial-onset seizures, the systematic analysis of the Cognitive Drug Study revealed that PER may have favorable cognitive profile for adolescent population[10]. The increase of β-band in quantitative electroencephalogram (QEEG) is related to the improvement of attention and cognitive function, and the increase of α-band is related to the impairment of cognitive function[11]. In a QEEG study on patients treated with PER, PER increased the β-band in the occipital lobe region, without increasing the α-band, confirming the beneficial effect of PER on cognitive function, which may be mediated by its direct effect on the neurotransmission of glutamate[11]. In our case, although the quantitative scales were not evaluated in this patient before and after treatment with PER, he showed improved cognitive skills and language according to our observation and his parents' records, which suggested the favorable cognitive profile of PER in young children.

The adverse events (AEs) of AEDs are the key factors affecting drug selection, patients' quality of life and long-term drug retention. The AEs of PER mainly include dizziness, irritability, fatigue, aggressiveness, suicide, nausea and weight gain[2]. Dizziness and somnolence are the most common AEs[3]. Because of some severe mental and behavioral adverse reactions, including aggressiveness, irritability, homicidal behavior, and threats, PER was given a black box warning by the FDA when it was first approved[12]. The patient in our case developed irritability and aggressive behavior after treatment with PER, which were considered to be its adverse reactions. Irritability is the most common psychotic adverse reaction, with an incidence of 2.1%-17.9%[13]. Although the mechanism behind irritability and related aggressive behavior is unclear, serotonin, GABA, and especially glutamate (*via* the AMPAR) seems to play an important role[13]. The effects of glutamate on behavior are complex, and some animal studies have shown that blocking AMPARs can lead to increases or decreases in aggressive behavior.

This indicates that the AMPAR blockage may contribute to the emotion-related adverse reactions of PER [13]. The AEs of PER are dose-dependent, and may disappear after dose adjustment or drug withdrawal [14]. It is recommended to start PER with a low dose and titrate slowly, generally adding 2 mg every 2-4 wk. Slow titration can improve the long-term tolerance of PER and reduce the incidence and severity of AEs, including psychiatric symptoms. Adverse reactions of PER can be alleviated by taking the drug before bedtime[10].

In addition, we also searched the National Library of Medicine and the China National Knowledge Infrastructure between January 10 and 15, 2020, with the following keywords perampanel AND children. Only papers on the administration of PER for multidrug-resistant epilepsy were selected. We identified the data about the efficacy and safety profile of PER in children under 12 years old with drug-resistant epilepsy (summarized in Supplementary Table 1). From most previous researches, after 3-12 mo of treatment, nearly 40%-50% or more young children showed responses to PER, and some patients could reach seizure-free status using PER. For patients with various genetic causes, significant seizure reduction was also reached with treatment of PER. In children under 12 years old, the incidence of AEs ranged from 20% to 50%, including somnolence, behavioral deterioration, and emotional change, while no obvious AEs were demonstrated in most case reports. Furthermore, in most reported cohorts, PER possessed similar efficacy and safety profiles in children under 12 years old as in older people[15,16]. Together with this case, these results suggest that PER is an effective and broad-spectrum AED for children under 12 years old, who suffer from multidrug-resistant epilepsy, with acceptable safety profile.

CONCLUSION

In this study, we presented a 4-year-old boy with multidrug-resistant epilepsy who still had frequent seizures after VNS implantation, and he showed significant response to PER as add-on in a dose-dependent manner. We proposed that the use of PER as add-on could further reduce the seizure frequency for young children with drug-resistant epilepsy and even after VNS implantation, which may be attributed to its novel antiepileptic mechanism. Considering the similar efficacy and safety profile of PER in children < 12 years old as in older people, as well as its potential favorable cognitive profile and convenience of use, PER should be considered as an effective and important treatment for young children with multidrug-resistant epilepsy. Adverse reactions like irritability and aggressive behavior should be monitored during use.

ACKNOWLEDGMENTS

We thank the patient and his parents.

FOOTNOTES

Author contributions: Yang H wrote the manuscript; Yang H and Yu D collected the data and participated in patient care; Yu D reviewed and edited the manuscript.

Informed consent statement: Informed written consent was obtained from the patient for publication of this report and any accompanying images.

Conflict-of-interest statement: The authors declare that they have no conflict of interest.

CARE Checklist (2016) statement: The authors have read the CARE Checklist (2016), and the manuscript was prepared and revised according to the CARE Checklist (2016).

Country/Territory of origin: China

ORCID number: Hua Yang 0000-0001-5418-3605; Dan Yu 0000-0003-2859-5897.

S-Editor: Wang JJ
L-Editor: Kerr C

P-Editor: Wang JJ

REFERENCES

1 **Chang FM**, Fan PC, Weng WC, Chang CH, Lee WT. The efficacy of perampanel in young children with drug-resistant epilepsy. *Seizure* 2020; **75**: 82-86 [PMID: 31901668 DOI: 10.1016/j.seizure.2019.12.024]

2 **Kanner AM**, Ashman E, Gloss D, Harden C, Bourgeois B, Bautista JF, Abou-Khalil B, Burakgazi-Dalkilic E, Llanas Park E, Stern J, Hirtz D, Nespeca M, Gidal B, Faught E, French J. Practice guideline update summary: Efficacy and tolerability of the new antiepileptic drugs II: Treatment-resistant epilepsy: Report of the Guideline Development, Dissemination, and Implementation Subcommittee of the American Academy of Neurology and the American Epilepsy Society. *Neurology* 2018; **91**: 82-90 [PMID: 29898974 DOI: 10.1212/WNL.0000000000005756]

3 **Dozières-Puyravel B**, Auvin S. An Evidence-Based Review On The Use Of Perampanel For The Treatment Of Focal-Onset Seizures In Pediatric Patients. *Neuropsychiatr Dis Treat* 2019; **15**: 2789-2798 [PMID: 31576134 DOI: 10.2147/NDT.S178405]

4 **Hanada T**. Ionotropic Glutamate Receptors in Epilepsy: A Review Focusing on AMPA and NMDA Receptors. *Biomolecules* 2020; **10** [PMID: 32197322 DOI: 10.3390/biom10030464]

5 **Yuan CL**, Shi EY, Srinivasan J, Ptak CP, Oswald RE, Nowak LM. Modulation of AMPA Receptor Gating by the Anticonvulsant Drug, Perampanel. *ACS Med Chem Lett* 2019; **10**: 237-242 [PMID: 30891119 DOI: 10.1021/acsmedchemlett.8b00322]

6 **Charsouei S**, Jabalameli MR, Karimi-Moghadam A. Molecular insights into the role of AMPA receptors in the synaptic plasticity, pathogenesis and treatment of epilepsy: therapeutic potentials of perampanel and antisense oligonucleotide (ASO) technology. *Acta Neurol Belg* 2020; **120**: 531-544 [PMID: 32152997 DOI: 10.1007/s13760-020-01318-1]

7 **Jain P**, Arya R. Vagus Nerve Stimulation and Seizure Outcomes in Pediatric Refractory Epilepsy: Systematic Review and Meta-Analysis. *Neurology* 2021 [PMID: 33849993 DOI: 10.1212/wnl.0000000000012030]

8 **Morris GL 3rd**, Gloss D, Buchhalter J, Mack KJ, Nickels K, Harden C. Evidence-based guideline update: vagus nerve stimulation for the treatment of epilepsy: report of the Guideline Development Subcommittee of the American Academy of Neurology. *Neurology* 2013; **81**: 1453-1459 [PMID: 23986299 DOI: 10.1212/WNL.0b013e3182a393d1]

9 **Davis Jones G**, Stavropoulos I, Ibrahim K, Tristram M, Neale M, Jory C, Adcock J, Esposito M, Hamandi K, Shankar R, Rugg-Gunn F, Elwes R, Sen A. An evaluation of the effectiveness of perampanel in people with epilepsy who have previously undergone resective surgery and/or implantation of a vagal nerve stimulator. *Epilepsy Behav* 2021; **116**: 107738 [PMID: 33517199 DOI: 10.1016/j.yebeh.2020.107738]

10 **De Liso P**, Moavero R, Coppola G, Curatolo P, Cusmai R, De Sarro G, Franzoni E, Vigevano F, Verrotti A. Current role of perampanel in pediatric epilepsy. *Ital J Pediatr* 2017; **43**: 51 [PMID: 28577562 DOI: 10.1186/s13052-017-0368-6]

11 **Liguori C**, Spanetta M, Izzi F, Russo A, Guerra A, Mercuri NB, Placidi F. Perampanel Increases Cortical EEG Fast Activity in Child and Adult Patients Affected by Epilepsy: A Quantitative EEG Study. *Clin EEG Neurosci* 2021; **52**: 360-370 [PMID: 32762352 DOI: 10.1177/1550059420947936]

12 **Youn SE**, Kim SH, Ko A, Lee SH, Lee YM, Kang HC, Lee JS, Kim HD. Adverse Events During Perampanel Adjunctive Therapy in Intractable Epilepsy. *J Clin Neurol* 2018; **14**: 296-302 [PMID: 29971974 DOI: 10.3988/jcn.2018.14.3.296]

13 **Moraes JS**, Hepworth G, Ignatiadis S, Dharan A, Carne R, Seneviratne U, Cook MJ, D'Souza WJ. Improved irritability, mood, and quality of life following introduction of perampanel as late adjunctive treatment for epilepsy. *Epilepsy Behav* 2020; **104**: 106883 [PMID: 32045874 DOI: 10.1016/j.yebeh.2019.106883]

14 **Arzimanoglou A**, D'Cruz O, Nordli D, Shinnar S, Holmes GL; Pediatric Epilepsy Academic Consortium for Extrapolation (PEACE). A Review of the New Antiepileptic Drugs for Focal-Onset Seizures in Pediatrics: Role of Extrapolation. *Paediatr Drugs* 2018; **20**: 249-264 [PMID: 29616471 DOI: 10.1007/s40272-018-0286-0]

15 **Swiderska N**, Tan HJ, Rajai A, Silwal A, Desurkar A, Martland T. Effectiveness and tolerability of Perampanel in children, adolescents and young adults with refractory epilepsy: A UK national multicentre study. *Seizure* 2017; **52**: 63-70 [PMID: 28992560 DOI: 10.1016/j.seizure.2017.08.014]

16 **Ikemoto S**, Hamano SI, Hirata Y, Matsuura R, Koichihara R. Efficacy and serum concentrations of perampanel for treatment of drug-resistant epilepsy in children, adolescents, and young adults: comparison of patients younger and older than 12 years. *Seizure* 2019; **73**: 75-78 [PMID: 31759296 DOI: 10.1016/j.seizure.2019.10.023]

World Journal of Clinical Cases

Submit a Manuscript: https://www.f6publishing.com

World J Clin Cases 2022 April 16; 10(11): 3518-3526

DOI: 10.12998/wjcc.v10.i11.3518

ISSN 2307-8960 (online)

CASE REPORT

Intramedullary nailing for pathological fractures of the proximal humerus caused by multiple myeloma: A case report and review of literature

Guo-Qiang Xu, Gang Wang, Xiao-Dong Bai, Xin-Jia Wang

Specialty type: Orthopedics

Provenance and peer review: Unsolicited article; Externally peer reviewed.

Peer-review model: Single blind

Peer-review report's scientific quality classification

Grade A (Excellent): 0
Grade B (Very good): 0
Grade C (Good): C, C
Grade D (Fair): 0
Grade E (Poor): 0

P-Reviewer: Greco T, Italy; Solarino G, Italy

Received: September 3, 2021
Peer-review started: September 3, 2021
First decision: December 17, 2021
Revised: February 9, 2022
Accepted: February 27, 2022
Article in press: February 27, 2022
Published online: April 16, 2022

Guo-Qiang Xu, Gang Wang, Xiao-Dong Bai, Department of Orthopedics, Beijing Friendship Hospital, Capital Medical University, Beijing 100050, China

Xin-Jia Wang, Department of Pediatrics, Beijing Friendship Hospital, Capital Medical University, Beijing 100050, China

Corresponding author: Xin-Jia Wang, BMed, Doctor, Associate Chief Physician, Department of Pediatrics, Beijing Friendship Hospital, Capital Medical University, 95 Yonganlu, Xicheng District, Beijing 100050, China. docxjwang@163.com

Abstract

BACKGROUND

Multiple myeloma (MM) bone disease is indicative of MM, and reduces patient life quality. In addition to oncological, antineoplastic systemic therapy, surgical therapy in patients with MM is an essential treatment within the framework of supportive therapy measures and involves orthopedic tumor surgery. Nevertheless, there are few reports on intramedullary (IM) nailing in the treatment of MM-induced proximal humeral fracture to prevent fixation loss. We here describe a case of pathological fracture of the proximal humerus caused by MM successfully treated with IM nailing without removal of tumors and a review of the current literature.

CASE SUMMARY

A 64-year-old male patient complaining of serious left shoulder pain and limited movement was admitted. The patient was finally diagnosed with MM (IgAλ, IIIA/II). After treatment of the pathological fracture with IM nailing, the patient's function recovered and his pain was rapidly relieved. Histopathological examination demonstrated plasma cell myeloma. The patient received chemotherapy in the Hematology Department. The humeral fracture displayed good union during the 40-mo follow-up, with complete healing of the fracture, and the clinical outcome was satisfactory. At the most recent follow-up, the patient's function was assessed using the Musculoskeletal Tumor Society score, which was 29.

CONCLUSION

Early surgery should be performed for the fracture of the proximal humerus caused by MM. IM nailing can be used without removal of tumors. Bone cement

augmentation for bone defects and local adjuvant therapy can also be employed.

Key Words: Multiple myeloma; Bone disease; Pathological fractures; Intramedullary nailing; Surgical therapy; Case report

Core Tip: We report a case of a patient who was eventually diagnosed with multiple myeloma (MM). After treatment of the pathological fracture with intramedullary (IM) nailing and chemotherapy in the Hematology Department, the humeral fracture displayed good union during the 40-mo follow-up, with complete healing of the fracture, and the clinical outcome was satisfactory. This case report and review of the literature demonstrates early surgery should be performed for the fracture of the proximal humerus caused by MM. IM nailing can be used without removal of tumors. Bone cement augmentation for bone defects and local adjuvant therapy can also be employed.

Citation: Xu GQ, Wang G, Bai XD, Wang XJ. Intramedullary nailing for pathological fractures of the proximal humerus caused by multiple myeloma: A case report and review of literature. *World J Clin Cases* 2022; 10(11): 3518-3526
URL: https://www.wjgnet.com/2307-8960/full/v10/i11/3518.htm
DOI: https://dx.doi.org/10.12998/wjcc.v10.i11.3518

INTRODUCTION

Multiple myeloma (MM) is a type of plasma cell dyscrasia that is characterized by immortalized monoclonal plasma cell proliferation within the bone marrow. Different to bone metastasis, no new bone is formed in the osteolytic bone disease of MM[1]. Complications of osteolysis include fractures of the long bones, which often occur in the proximal humerus and femur, usually after minor trauma or can be atraumatic, and vertebral body fractures[2]. The clinical presentation and radiological features are non-specific, making it more difficult to diagnose. Therefore, some scholars have indicated that MM is an important disease that should not be ignored in the differential diagnosis of skeletal pain, even if no typical symptoms are identified initially, particularly in the elderly[3]. Intramedullary (IM) nailing is a technique used to treat humeral diaphysis fractures with minimal invasion, and it is advantageous in small lesions, reduces operation time, there is little soft tissue dissection, and results in early recovery [4]. However, there is controversy as to whether IM nailing should be used to treat proximal humeral fractures as it may lead to fixation loss[5]. As a result, IM nailing is currently restricted to the treatment of diaphyseal fractures[4,6-10]. To date, few studies have described the techniques applied in proximal humeral fractures, particularly if the skeletal defect is not augmented by the application of bone cement. We here describe a 64-year-old male patient suffering from MM bone disease (MMBD) in the proximal humerus. He received combined therapy with IM nailing and chemotherapy. Related reports of MMBD are also reviewed.

CASE PRESENTATION

Chief complaints

A 64-year-old man who came to our emergency department complaining of left shoulder pain.

History of present illness

He had mild left shoulder trauma due to accidental falling from the standing position while walking 3 h ago.

History of past illness

His past medical history included atrial fibrillation treated with aspirin enteric-coated tablets (Bayer SPA), metoprolol succinate sustained-release tablets (AstraZeneca AB), and chronic atrophic gastritis.

Personal and family history

The patient denied a history of smoking, alcohol consumption, drug intake, and a family history of pathological fracture or osteoporosis.

Physical examination

Physical examination demonstrated swelling of the left shoulder, localized tenderness, percussion pain on the proximal humerus, and limited shoulder motion. The muscular tone of the upper limb was normal with no hypoesthesia. Physiological reflexes were present without pathological reflexes.

Laboratory examinations

In contrast, routine laboratory evaluation on admission, with the exception of anemia, was unremarkable. Hematopoiesis accounted for 40%, the ratio of granulocytes to erythrocytes was approximately 2:1, and megakaryocytes were 2-7/high power field. Multifocal plasmacytoid cell aggregation was also observed. Immunochemistry showed CD38 (+), kappa (+), lambda (+); MPO (+), CD61 (+) and CK (-) (Figure 1).

Imaging examinations

Initial X-ray films of the left shoulder were obtained, which showed only a comminuted fracture and degenerative changes in the upper left humerus (Figure 2). Magnetic resonance imaging (MRI) was then performed and showed an abnormal signal intensity of the proximal humerus associated with a comminuted fracture, and multiple soft tissue masses around the fracture, ranging from 4.8 cm to 3.9 cm, which presented as hypointensity and isointensity, as well as hybrid hyperintensity on T1-weighted (T1-W) and T2-W images, respectively. The left humerus, glenoid, and clavicle had multiple sheet-like hyperintensity on T2-W images (Figure 2). A neoplastic lesion with radiological characteristics was highly suspected.

Further laboratory tests and imaging examinations were performed. Computed tomography (CT) scans and X-ray examinations revealed multiple areas of reduced bone density throughout the body. In addition, high 18-F-fluorodeoxyglucose metabolism was observed in several ribs on bone scans, and in the fifth lumbar vertebra (L5), and left proximal humerus (Figure 3).

FINAL DIAGNOSIS

Plasma cell myeloma was diagnosed following bone marrow aspirate and trephine.

TREATMENT

Following consultation with anesthesiologists and medical oncologists regarding the perioperative risks as well as the life expectancy of the patient, locked IM nailing (Sanatmetal Orthopaedic & Traumatologic Equipment Manufacturer Ltd.) was chosen for strong fixation of the humeral fracture *via* the trans-deltoid muscle approach. With the greater trochanter as the entry point, an IM nail was directly inserted into the humeral medullary cavity without the removal of tumors. The bone defect was not augmented with bone cement. No local adjuvant therapy was administered. We inserted the nail with great caution to avoid impingement of the acromion or rotator cuff tendons by the proximal end of the nail. We also inserted 3 proximal screws as well as 2 distal interlocking screws. On the day after surgery, the patient was encouraged to move his shoulder gently. One week after surgery, the patient was encouraged to perform passive stretching as well as gravity-resistance exercises.

OUTCOME AND FOLLOW-UP

After surgery, the patient achieved continuous pain relief and improved activity of the left upper limb, and no complications were reported. At 24 h postoperatively, the visual analog score declined by 7 points to 2. Histopathological examination of the sample revealed MM (IgAλ, IIIA/II). One week postoperatively, the patient received regular dexamethasone and bortezomib chemotherapy at the Department of Hematology. At the 40-mo follow-up, the humeral fracture showed favorable complete lesion healing (Figure 4), and the patient reported no pain. The Musculoskeletal Tumor Society score was 29[11]. In comparison with the contralateral shoulder, forward flexion, and abduction were limited at the terminal 10°, while complete external and internal adduction and rotation were achieved. No adverse events occurred.

DISCUSSION

MM accounts for 1% of cancer cases, and approximately 10% of hematologic cancer cases[12]. MM has a relatively higher morbidity in males than in females, and morbidity is two-fold higher in blacks than in

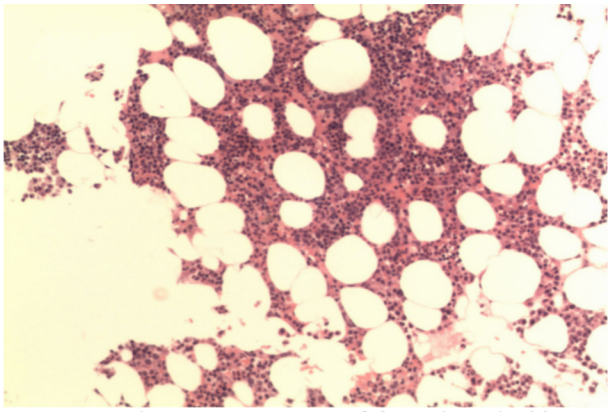

DOI: 10.12998/wjcc.v10.i11.3518

Figure 1 Plasma cell myeloma was diagnosed following bone marrow aspirate and trephine.

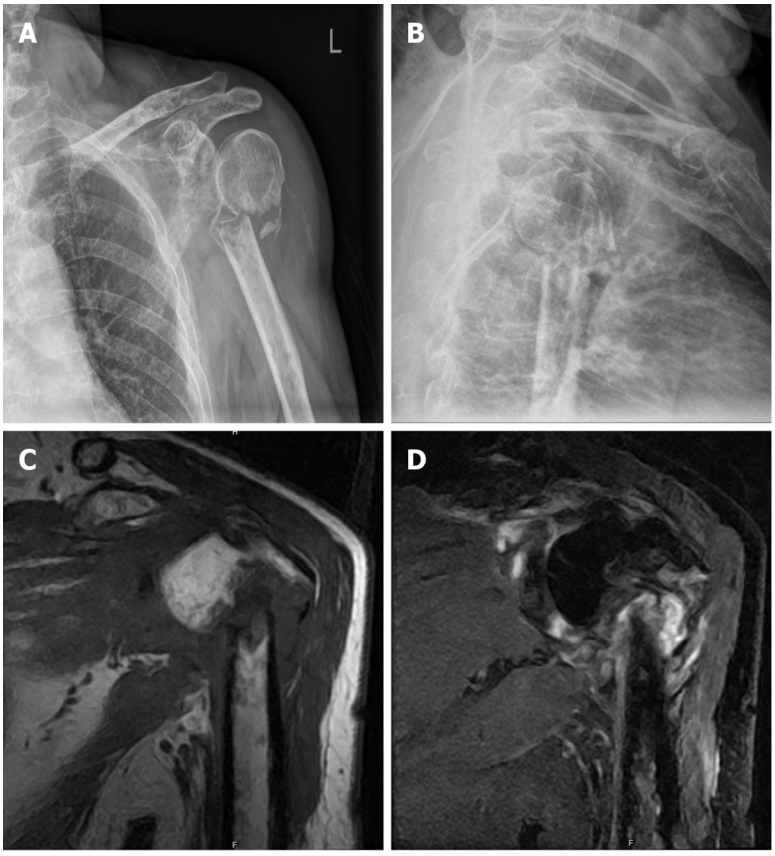

DOI: 10.12998/wjcc.v10.i11.3518

Figure 2 Preoperative X-ray films and magnetic resonance imaging. A, B: X-ray films (A, B) of the left shoulder revealed only a comminuted fracture and degenerative changes in the upper left humerus; C, D: Multiple soft tissue masses around the fracture presented as hypointensity and isointensity on T1 weighted (T1-W) images (C) and hybrid hyperintensity on T2-W images (D).

Caucasians[13,14]. MM affects the older population, and 70% of cases are diagnosed when they are 60 years and older[15]. MM is a type of plasma cell dyscrasia that is characterized by immortalized monoclonal plasma cell growth within the bone marrow. Nearly all MM cases progress from the asymptomatic monoclonal gammopathy of undetermined significance (MGUS) at the pre-malignant stage[16,17]. Moreover, MGUS will further develop into MM or associated cancers at an annual growth rate of 1%[18,19].

Bone lesions induced by MM are indicative of MM, and they reduce patient life quality. About 80% of cases have osteolytic bone disorders when diagnosed, which are linked to a higher risk of skeletal-related events (SREs) that increase morbidity and mortality[20]. Approximately 60% of MM cases develop fractures during the course of the disease[21]. The uncoupled bone-remodeling process lays the pathogenic foundation for bone disorders associated with myeloma. The myeloma cell-bone microenvir-

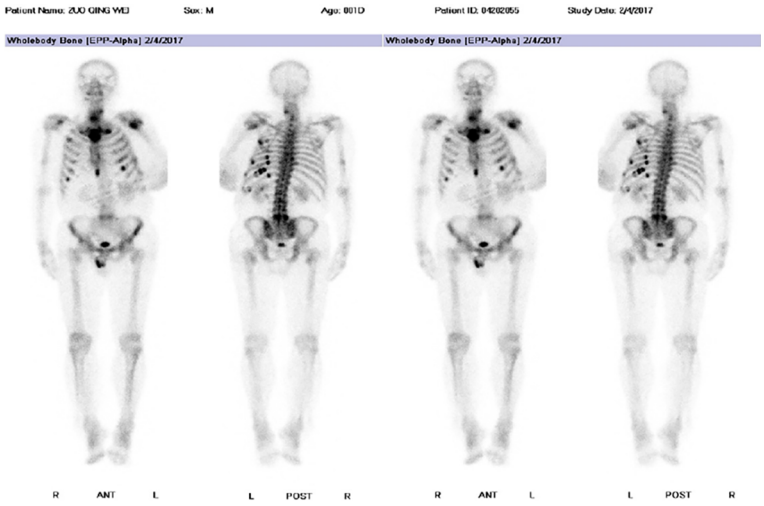

DOI: 10.12998/wjcc.v10.i11.3518

Figure 3 Bone scan showed high metabolism of 18-F fluorodeoxyglucose in multiple ribs, the fifth lumbar vertebra (L5), and left proximal humerus.

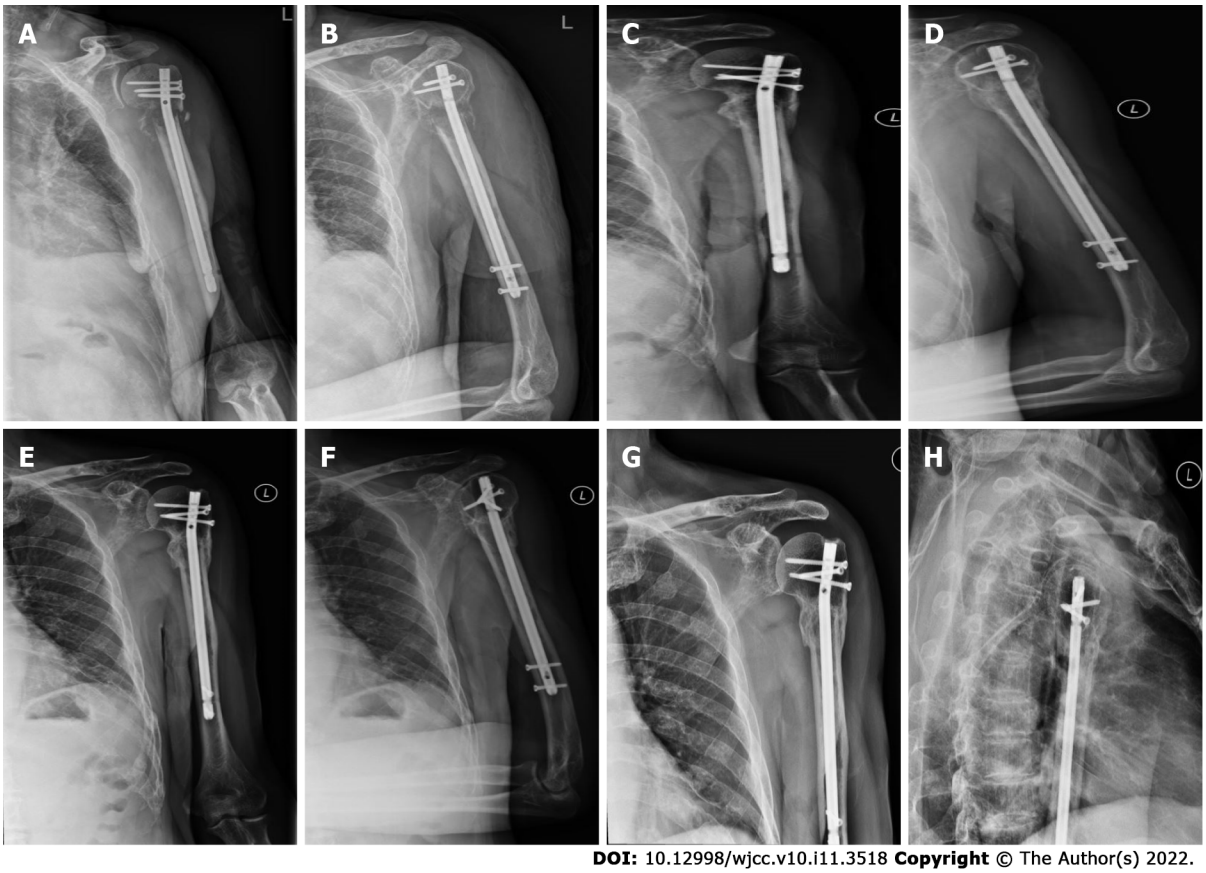

DOI: 10.12998/wjcc.v10.i11.3518

Figure 4 Postoperative X-ray films. A, B: Postoperative X-ray films of the left shoulder; C-H: Follow-up at 6 mo (C, D), 15 mo (E, F) and 40 mo (G, H) after surgery. The proximal humerus fracture eventually healed.

onment interaction will eventually activate osteoclasts while suppressing osteoblasts, giving rise to bone loss. Multiple intercellular, as well as intracellular signal transduction pathways, participate in the complicated course of MM. The crosstalk mediated by myeloma across diverse molecular pathways forms a forward feedback to maintain the survival of myeloma cells and the decomposition of bone, even after reaching the disease plateau[22].

MM is diagnosed when at least one myeloma defining event (MDE) and at least 10% clonal plasma cells are detected during bone marrow examinations or when plasmacytoma is detected in biopsy samples. MDEs are constituted by the recognized CRAB (hyperCalcaemia, Renal failure, Anaemia, Bony

lesions) characteristics and 3 representative biomarkers, including more than one focal lesion detected by MRI, ≥ 60% plasma cells in clonal bone marrow, as well as ≥100 free light chains (FLC) in serum[23]. In the case of suspected MM in the clinic, M protein testing is recommended by combining serum immunofixation, serum protein electrophoresis, as well as serum FLC assay[24]. About 2% of MM cases develop the non-secretory disorder with no M protein detected in the above-mentioned tests[25]. Positron emission tomography/computed tomography and low-dose whole-body CT scans are the best techniques for assessing bone disorder severity[24,26], which can show the changes in bones and soft tissues more clearly, and display the boundaries of the lesion. Plain radiographs are usually non-specific and can even underestimate the extent of the lesion, and are performed only when no other advanced imaging can be accessed. MRI is a particularly useful imaging technique of choice due to its noninvasive nature and greater anatomic detail, particularly when smoldering MM is suspected, to eliminate the risk of the focal lesion in the bone marrow observed before the occurrence of the actual osteolytic disorder. MRI also greatly contributes to the assessment of suspected cord compression and extramedullary disorder, and when it is necessary to visualize a certain symptomatic region. Although the diagnosis of MM is easy, based on blood and kidney tests and X-rays, in some cases an accurate diagnosis can only be made by pathology[27].

MM can result in progressive relapse. MM may recur with clinical symptoms or with biochemical disorders. Holistic and multidisciplinary treatment is needed for each MM patient[15]. Treatment involves multiple factors, which requires collaboration between radiotherapists, orthopedic surgeons, radiologists, hematologists, and anesthesiologists. In this regard, it is necessary to construct a prognostic model to predict disease stage, evaluate the patient's general condition, and determine underlying chronic disorders or possible adjuvant treatments[2]. To optimize the outcomes for individuals, elucidating the most suitable maintenance treatment or continuous therapy for the specific patient group is important. It is also important to consider the clinical safety, effectiveness, tolerability, life quality, convenience, feasibility, and long-time treatment burden in patients[23].

In addition to oncological and antineoplastic systemic therapy, surgical therapy in patients with MM is an essential treatment within the framework of supportive therapy measures and involves orthopedic tumor surgery. For SREs related to myeloma, surgery is mainly performed to maintain and restore skeletal function and recovery, reduce patient suffering such as pain, and improve patient mobility as well as life quality[28,29]. There is a need for surgical intervention not only for the care and treatment of stability-threatening bone lesions and pathological fractures but also for the treatment of tumor-related complications, such as neurological deficits, possible paraplegia, or in the case of conservative therapy, refractory bone pain. The surgical methods and timing of treatment should be decided individually depending on the risk and prognostic outcomes of myeloma cases[28]. Osteolysis of non-supporting skeletal sections such as the ribs, skull, or scapula does not usually require surgical treatment. The physical status grade established by the American Society of Anesthesiologists (ASA) has been extensively used to evaluate the patient's general condition or anesthesia tolerance. Ultrasound-guided intercostal brachial plexus block provides an alternative to general anesthesia for patients with pathologic humeral fractures caused by MM with systemic presentation and chest infections[30]. However, patients with < 2 mo survival or ASA = 4 will be treated using conservative methods instead of surgery[31].

Surgery is usually conducted to treat MM-induced proximal humeral fractures, to relieve patient suffering and recover bone function and mobility, as well as patient life quality. However, surgical strategies are complicated and demanding[32].

Shoulder pain and bone damage due to pathological fractures of the proximal humerus caused by MM can be treated using either the simple bone cement technique or percutaneous microwave ablation and cementoplasty[33].

Endoprosthetic reconstruction has been extensively used to treat proximal humeral fractures, but it does not achieve a satisfactory effect on impaired function. The prosthesis can be a good way of relieving pain and fixing the fracture, but it has poor functional recovery compared with other treatments[7,34-36]. In addition, more tendons and muscles are sacrificed during resection, which inevitably impairs function[35]. Also, plate fixation is associated with numerous drawbacks, such as short protection length, massive soft tissue stripping, and risk of nerve injury[9,37,38]. Local relapse may give rise to fixation loss or the need for a second operation[34,39]. As a result, plates are restricted in the treatment of metastasis.

IM nailing is thought to be unsuitable for treating proximal humeral fractures due to the bone defect and thin cortex following curettage[34]. Therefore, at present, IM nailing is restricted to the treatment of diaphyseal fractures[6]. Our results revealed that IM nailing is an efficient and robust method for treating proximal humeral fractures. IM nailing to fix proximal humeral fractures is advantageous due to its decreased operation time, can be used to treat small lesions, decreased soft tissue dissection, and early recovery.

In this case, we performed IM nailing to treat a proximal humeral fracture, without bone cement to augment the lesion. At follow-up visits, our patient had marked pain relief and improved shoulder function. At the 40-mo follow-up, the patient had a favorably healed humeral fracture, complete lesion healing was observed, and no pain was reported by the patient. In comparison with the contralateral shoulder, the forward flexion and abduction were limited at the terminal 10°, and complete external and

internal adduction and rotation were achieved.

Despite it being generally incurable, the long-time survival of MM patients is greatly improved as more treatments have recently been developed. In addition, improved survival is also associated with early treatment[40]. As suggested by randomized controlled trials which used modern treatments, MM has a median survival of about 6 years. An appropriate treatment for metastases is needed to prolong patient survival[41].

Although this technique achieved a satisfactory effect, few reports describe this method for the treatment of pathological fractures of the proximal humerus caused by MM. Therefore, it is necessary to conduct studies with a large sample size to further validate its efficacy and to identify the surgical indications and related complications.

Our patient was satisfied with his current functional recovery and treatment of the primary disease and agreed to publication of this report, in the hope that more patients suffering from the same disease may benefit.

CONCLUSION

When a pathological fracture of the proximal humerus caused by multiple myeloma occurs, early surgical treatment is indicated, which can effectively relieve pain and allow early movement. IM nailing can be performed for this type of fracture, without removal of tumors, bone cement augmentation for the bone defect, or local adjuvant therapy. Moreover, patients can receive combined therapy and have a good prognosis.

FOOTNOTES

Author contributions: Xu GQ wrote and edited the article; Wang G reviewed the literature; Bai XD collected information on the current case; Wang XJ revised the manuscript for important intellectual content; and All authors gave final approval of the version to be submitted.

Informed consent statement: The patient consented to the publication of this report. Written consent for publication was obtained for all potentially identifying data and accompanying images and these are available for review from the editor of this journal.

Conflict-of-interest statement: The authors declare that they have no competing interests.

CARE Checklist (2016) statement: The authors have read the CARE Checklist (2016), and the manuscript was prepared and revised according to the CARE Checklist (2016).

Country/Territory of origin: China

ORCID number: Guo-Qiang Xu 0000-0002-0452-806X; Gang Wang 0000-0002-7314-8693; Xiao-Dong Bai 0000-0002-6363-2764; Xin-Jia Wang 0000-0003-2190-3199.

S-Editor: Ma YJ
L-Editor: A
P-Editor: Ma YJ

REFERENCES

1 **Roodman GD**. Pathogenesis of myeloma bone disease. *Leukemia* 2009; **23**: 435-441 [PMID: 19039321 DOI: 10.1038/leu.2008.336]
2 **Guzik G**. Oncological and functional results of the surgical treatment of vertebral metastases in patients with multiple myeloma". *BMC Surg* 2017; **17**: 92 [PMID: 28830484 DOI: 10.1186/s12893-017-0288-9]
3 **Yilmaz E**. Presentation of multiple myeloma occurring in the humerus after strain: a case report. *Clin Rheumatol* 2021; **40**: 389-392 [PMID: 32613389 DOI: 10.1007/s10067-020-05256-4]
4 **Frassica FJ**, Frassica DA. Evaluation and treatment of metastases to the humerus. *Clin Orthop Relat Res* 2003; S212-S218 [PMID: 14600613 DOI: 10.1097/01.blo.0000093052.96273.a7]

5 **Weiss KR**, Bhumbra R, Biau DJ, Griffin AM, Deheshi B, Wunder JS, Ferguson PC. Fixation of pathological humeral fractures by the cemented plate technique. *J Bone Joint Surg Br* 2011; **93**: 1093-1097 [PMID: 21768635 DOI: 10.1302/0301-620X.93B8.26194]

6 **Laitinen M**, Nieminen J, Pakarinen TK. Treatment of pathological humerus shaft fractures with intramedullary nails with or without cement fixation. *Arch Orthop Trauma Surg* 2011; **131**: 503-508 [PMID: 20740287 DOI: 10.1007/s00402-010-1172-6]

7 **Camnasio F**, Scotti C, Peretti GM, Fontana F, Fraschini G. Prosthetic joint replacement for long bone metastases: analysis of 154 cases. *Arch Orthop Trauma Surg* 2008; **128**: 787-793 [PMID: 17922282 DOI: 10.1007/s00402-007-0464-y]

8 **Capanna R**, Campanacci DA. The treatment of metastases in the appendicular skeleton. *J Bone Joint Surg Br* 2001; **83**: 471-481 [PMID: 11380113 DOI: 10.1302/0301-620x.83b4.12202]

9 **Sarahrudi K**, Wolf H, Funovics P, Pajenda G, Hausmann JT, Vécsei V. Surgical treatment of pathological fractures of the shaft of the humerus. *J Trauma* 2009; **66**: 789-794 [PMID: 19276754 DOI: 10.1097/TA.0b013e3181692132]

10 **Atesok K**, Liebergall M, Sucher E, Temper M, Mosheiff R, Peyser A. Treatment of pathological humeral shaft fractures with unreamed humeral nail. *Ann Surg Oncol* 2007; **14**: 1493-1498 [PMID: 17211731 DOI: 10.1245/s10434-006-9257-8]

11 **Enneking WF**, Dunham W, Gebhardt MC, Malawar M, Pritchard DJ. A system for the functional evaluation of reconstructive procedures after surgical treatment of tumors of the musculoskeletal system. *Clin Orthop Relat Res* 1993; 241-246 [PMID: 8425352 DOI: 10.1007/978-1-4471-5451-8_128]

12 **Rajkumar SV**, Dimopoulos MA, Palumbo A, Blade J, Merlini G, Mateos MV, Kumar S, Hillengass J, Kastritis E, Richardson P, Landgren O, Paiva B, Dispenzieri A, Weiss B, LeLeu X, Zweegman S, Lonial S, Rosinol L, Zamagni E, Jagannath S, Sezer O, Kristinsson SY, Caers J, Usmani SZ, Lahuerta JJ, Johnsen HE, Beksac M, Cavo M, Goldschmidt H, Terpos E, Kyle RA, Anderson KC, Durie BG, Miguel JF. International Myeloma Working Group updated criteria for the diagnosis of multiple myeloma. *Lancet Oncol* 2014; **15**: e538-e548 [PMID: 25439696 DOI: 10.1016/S1470-2045(14)70442-5]

13 **Landgren O**, Weiss BM. Patterns of monoclonal gammopathy of undetermined significance and multiple myeloma in various ethnic/racial groups: support for genetic factors in pathogenesis. *Leukemia* 2009; **23**: 1691-1697 [PMID: 19587704 DOI: 10.1038/leu.2009.134]

14 **Landgren O**, Graubard BI, Katzmann JA, Kyle RA, Ahmadizadeh I, Clark R, Kumar SK, Dispenzieri A, Greenberg AJ, Therneau TM, Melton LJ 3rd, Caporaso N, Korde N, Roschewski M, Costello R, McQuillan GM, Rajkumar SV. Racial disparities in the prevalence of monoclonal gammopathies: a population-based study of 12,482 persons from the National Health and Nutritional Examination Survey. *Leukemia* 2014; **28**: 1537-1542 [PMID: 24441287 DOI: 10.1038/leu.2014.34]

15 **Chavda SJ**, Yong K. Multiple myeloma. *Br J Hosp Med (Lond)* 2017; **78**: C21-C27 [PMID: 28165783 DOI: 10.12968/hmed.2017.78.2.C21]

16 **Landgren O**, Kyle RA, Pfeiffer RM, Katzmann JA, Caporaso NE, Hayes RB, Dispenzieri A, Kumar S, Clark RJ, Baris D, Hoover R, Rajkumar SV. Monoclonal gammopathy of undetermined significance (MGUS) consistently precedes multiple myeloma: a prospective study. *Blood* 2009; **113**: 5412-5417 [PMID: 19179464 DOI: 10.1182/blood-2008-12-194241]

17 **Weiss BM**, Abadie J, Verma P, Howard RS, Kuehl WM. A monoclonal gammopathy precedes multiple myeloma in most patients. *Blood* 2009; **113**: 5418-5422 [PMID: 19234139 DOI: 10.1182/blood-2008-12-195008]

18 **Kyle RA**, Therneau TM, Rajkumar SV, Offord JR, Larson DR, Plevak MF, Melton LJ 3rd. A long-term study of prognosis in monoclonal gammopathy of undetermined significance. *N Engl J Med* 2002; **346**: 564-569 [PMID: 11856795 DOI: 10.1056/NEJMoa01133202]

19 **Kyle RA**, Larson DR, Therneau TM, Dispenzieri A, Kumar S, Cerhan JR, Rajkumar SV. Long-Term Follow-up of Monoclonal Gammopathy of Undetermined Significance. *N Engl J Med* 2018; **378**: 241-249 [PMID: 29342381 DOI: 10.1056/NEJMoa1709974]

20 **Terpos E**, Morgan G, Dimopoulos MA, Drake MT, Lentzsch S, Raje N, Sezer O, García-Sanz R, Shimizu K, Turesson I, Reiman T, Jurczyszyn A, Merlini G, Spencer A, Leleu X, Cavo M, Munshi N, Rajkumar SV, Durie BG, Roodman GD. International Myeloma Working Group recommendations for the treatment of multiple myeloma-related bone disease. *J Clin Oncol* 2013; **31**: 2347-2357 [PMID: 23690408 DOI: 10.1200/JCO.2012.47.7901]

21 **Terpos E**, Berenson J, Cook RJ, Lipton A, Coleman RE. Prognostic variables for survival and skeletal complications in patients with multiple myeloma osteolytic bone disease. *Leukemia* 2010; **24**: 1043-1049 [PMID: 20376081 DOI: 10.1038/leu.2010.62]

22 **Terpos E**, Ntanasis-Stathopoulos I, Gavriatopoulou M, Dimopoulos MA. Pathogenesis of bone disease in multiple myeloma: from bench to bedside. *Blood Cancer J* 2018; **8**: 7 [PMID: 29330358 DOI: 10.1038/s41408-017-0037-4]

23 **Dimopoulos MA**, Jakubowiak AJ, McCarthy PL, Orlowski RZ, Attal M, Bladé J, Goldschmidt H, Weisel KC, Ramasamy K, Zweegman S, Spencer A, Huang JSY, Lu J, Sunami K, Iida S, Chng WJ, Holstein SA, Rocci A, Skacel T, Labotka R, Palumbo A, Anderson KC. Developments in continuous therapy and maintenance treatment approaches for patients with newly diagnosed multiple myeloma. *Blood Cancer J* 2020; **10**: 17 [PMID: 32054831 DOI: 10.1038/s41408-020-0273-x]

24 **Lakshman A**, Paul S, Rajkumar SV, Ketterling RP, Greipp PT, Dispenzieri A, Gertz MA, Buadi FK, Lacy MQ, Dingli D, Fonder AL, Hayman SR, Hobbs MA, Gonsalves WI, Hwa YL, Kapoor P, Leung N, Go RS, Lin Y, Kourelis TV, Warsame R, Lust JA, Russell SJ, Zeldenrust SR, Kyle RA, Kumar SK. Prognostic significance of interphase FISH in monoclonal gammopathy of undetermined significance. *Leukemia* 2018; **32**: 1811-1815 [PMID: 29568092 DOI: 10.1038/s41375-018-0030-3]

25 **Chawla SS**, Kumar SK, Dispenzieri A, Greenberg AJ, Larson DR, Kyle RA, Lacy MQ, Gertz MA, Rajkumar SV. Clinical course and prognosis of non-secretory multiple myeloma. *Eur J Haematol* 2015; **95**: 57-64 [PMID: 25382589 DOI: 10.1111/ejh.12478]

26 **Hillengass J**, Usmani S, Rajkumar SV, Durie BGM, Mateos MV, Lonial S, Joao C, Anderson KC, García-Sanz R, Riva E, Du J, van de Donk N, Berdeja JG, Terpos E, Zamagni E, Kyle RA, San Miguel J, Goldschmidt H, Giralt S, Kumar S, Raje N, Ludwig H, Ocio E, Schots R, Einsele H, Schjesvold F, Chen WM, Abildgaard N, Lipe BC, Dytfeld D, Wirk BM, Drake M, Cavo M, Lahuerta JJ, Lentzsch S. International myeloma working group consensus recommendations on imaging in monoclonal plasma cell disorders. *Lancet Oncol* 2019; **20**: e302-e312 [PMID: 31162104 DOI:

10.1016/S1470-2045(19)30309-2]
27 **Alexa O**, Veliceasa B. Multiple myeloma with bilateral humerus location. Case report. *Rev Med Chir Soc Med Nat Iasi* 2013; **117**: 160-164 [PMID: 24505909 DOI: 10.1049/ic.2007.0836]
28 **Takei T**, Coles M. Treatment of pathologic fracture and surgical value of prognostic factors in multiple myeloma. *Int Surg* 1996; **81**: 403-406 [PMID: 9127806 DOI: 10.1016/S0901-5027(06)80042-1]
29 **Dürr HR**, Kühne JH, Hagena FW, Moser T, Refior HJ. Surgical treatment for myeloma of the bone. A retrospective analysis of 22 cases. *Arch Orthop Trauma Surg* 1997; **116**: 463-469 [PMID: 9352039 DOI: 10.1007/BF00387578]
30 **Hamal PK**, Lamichhane B, Pokhrel N, Singh J, Yadav RK. Ultrasound-Guided Interscalene Brachial Plexus Block for Pathological Humerus Fracture due to Multiple Myeloma with Systemic Manifestation: Useful Option for Management in Low-Income Countries. *Case Rep Anesthesiol* 2020; **2020**: 9892580 [PMID: 33123386 DOI: 10.1155/2020/9892580]
31 **Choi ES**, Han I, Cho HS, Park IW, Park JW, Kim HS. Intramedullary Nailing for Pathological Fractures of the Proximal Humerus. *Clin Orthop Surg* 2016; **8**: 458-464 [PMID: 27904730 DOI: 10.4055/cios.2016.8.4.458]
32 **Kehrer M**, Koob S, Kehrer A, Wirtz DC, Schmolders J. Multiple Myeloma - Current Standards in Surgical Treatment. *Z Orthop Unfall* 2019; **157**: 164-172 [PMID: 30064148 DOI: 10.1055/a-0639-5742]
33 **Deib G**, Deldar B, Hui F, Barr JS, Khan MA. Percutaneous Microwave Ablation and Cementoplasty: Clinical Utility in the Treatment of Painful Extraspinal Osseous Metastatic Disease and Myeloma. *AJR Am J Roentgenol* 2019; 1-8 [PMID: 30917019 DOI: 10.2214/AJR.18.20386]
34 **Siegel HJ**, Lopez-Ben R, Mann JP, Ponce BA. Pathological fractures of the proximal humerus treated with a proximal humeral locking plate and bone cement. *J Bone Joint Surg Br* 2010; **92**: 707-712 [PMID: 20436010 DOI: 10.1302/0301-620X.92B5.23246]
35 **Bickels J**, Kollender Y, Wittig JC, Meller I, Malawer MM. Function after resection of humeral metastases: analysis of 59 consecutive patients. *Clin Orthop Relat Res* 2005; 201-208 [PMID: 16056050 DOI: 10.1097/01.blo.0000165857.12676.00]
36 **Piccioli A**, Maccauro G, Rossi B, Scaramuzzo L, Frenos F, Capanna R. Surgical treatment of pathologic fractures of humerus. *Injury* 2010; **41**: 1112-1116 [PMID: 20828692 DOI: 10.1016/j.injury.2010.08.015]
37 **Karataglis D**, Stavridis SI, Petsatodis G, Papadopoulos P, Christodoulou A. New trends in fixation of proximal humeral fractures: a review. *Injury* 2011; **42**: 330-338 [PMID: 21093859 DOI: 10.1016/j.injury.2010.10.016]
38 **Young AA**, Hughes JS. Locked intramedullary nailing for treatment of displaced proximal humerus fractures. *Orthop Clin North Am* 2008; **39**: 417-428, v [PMID: 18803972 DOI: 10.1016/j.ocl.2008.05.001]
39 **Dijkstra S**, Stapert J, Boxma H, Wiggers T. Treatment of pathological fractures of the humeral shaft due to bone metastases: a comparison of intramedullary locking nail and plate osteosynthesis with adjunctive bone cement. *Eur J Surg Oncol* 1996; **22**: 621-626 [PMID: 9005151 DOI: 10.1016/s0748-7983(96)92450-6]
40 **Vaishya R**, Vijay V, Agarwal AK. Healing of pathological fracture in a case of multiple myeloma. *BMJ Case Rep* 2017; **2017** [PMID: 28073880 DOI: 10.1136/bcr-2016-218672]
41 **Thai DM**, Kitagawa Y, Choong PF. Outcome of surgical management of bony metastases to the humerus and shoulder girdle: a retrospective analysis of 93 patients. *Int Semin Surg Oncol* 2006; **3**: 5 [PMID: 16509975 DOI: 10.1186/1477-7800-3-5]

World Journal of Clinical Cases

Submit a Manuscript: https://www.f6publishing.com

World J Clin Cases 2022 April 16; 10(11): 3527-3532

DOI: 10.12998/wjcc.v10.i11.3527

ISSN 2307-8960 (online)

CASE REPORT

Double tracheal stents reduce side effects of progression of malignant tracheoesophageal fistula treated with immunotherapy: A case report

Chang-An Li, Wei-Xia Yu, Lin-Yang Wang, Hang Zou, Cheng-Jun Ban, Hong-Wu Wang

Specialty type: Medicine, general and internal

Provenance and peer review: Unsolicited article; Externally peer reviewed.

Peer-review model: Single blind

Peer-review report's scientific quality classification

Grade A (Excellent): 0
Grade B (Very good): 0
Grade C (Good): C, C
Grade D (Fair): 0
Grade E (Poor): 0

P-Reviewer: Covantsev S, Russia; Jabbarpour Z, Iran

Received: September 11, 2021
Peer-review started: September 11, 2021
First decision: January 25, 2022
Revised: January 31, 2022
Accepted: February 27, 2022
Article in press: February 27, 2022
Published online: April 16, 2022

Chang-An Li, Wei-Xia Yu, Lin-Yang Wang, Hang Zou, Cheng-Jun Ban, Hong-Wu Wang, Department of Respiratory, Beijing University of Chinese Medicine Affiliated Dongzhimen Hospital, Beijing 100700, China

Corresponding author: Cheng-Jun Ban, PhD, Assistant Professor, Department of Respiratory, Beijing University of Chinese Medicine Affiliated Dongzhimen Hospital, No. 5 Haihaicang, Dongcheng District, Beijing 100700, China. banchengjun3326@163.com

Abstract

BACKGROUND

The protective effect of tracheal stents is reported to relieve airway obstruction and reduce side effects of rapid progression of malignant tracheoesophageal fistula (MTEF) after immunotherapy in this case with 10 mo follow-up.

CASE SUMMARY

Two kinds of silicone stents were placed in the main airway of a 58-year-old male to relieve the airway obstruction caused by advanced esophageal carcinoma. The patient then received four doses of toripalimab. Subsequently, rapid, progressive deterioration of the original fistula was found. Although the fistula enlarged rapidly after immunotherapy, it remained covered completely, and likely because of this, his condition remained stable. Therefore, immunotherapy could be continued to treat the primary tumor. Despite these efforts, the patient died of the advancement of his esophageal cancer.

CONCLUSION

Appropriately-sized tracheal stent placement combined with immune checkpoint inhibitors may improve the quality of life and survival of patients with MTEF.

Key Words: Immunotherapy; Rapid progression; Malignant tracheoesophageal fistula; Esophagus carcinoma; Double tracheal stents; Case report

Core Tip: A 58-year-old male was diagnosed with advanced esophageal carcinoma and malignant tracheoesophageal fistula. For treatment, two kinds of silicone stents were placed in the main airway, followed by administration of four doses of toripalimab. Follow-up scans showed the original fistula to have rapidly increased in size between the upper trachea and esophagus. The fistula was still covered due to the appropriately-sized stents, which were likely protective, as no serious lung infections occurred and the patient remained stable. Accordingly, immunotherapy could be continued to treat the primary tumor. Unfortunately, however, the patient died of the esophageal cancer in February of 2021.

Citation: Li CA, Yu WX, Wang LY, Zou H, Ban CJ, Wang HW. Double tracheal stents reduce side effects of progression of malignant tracheoesophageal fistula treated with immunotherapy: A case report. *World J Clin Cases* 2022; 10(11): 3527-3532
URL: https://www.wjgnet.com/2307-8960/full/v10/i11/3527.htm
DOI: https://dx.doi.org/10.12998/wjcc.v10.i11.3527

INTRODUCTION

Malignant tracheoesophageal fistula (MTEF) is a devastating complication of esophageal cancer and tracheocarcinoma, which leads to a shorter life-span and decreased quality of life. MTEF develops in approximately 5%-15% of patients with an esophageal malignancy, with less than 1% of those having bronchogenic carcinoma[1,2]. Airway stent insertion provides an effective approach to improve symptoms and quality of life[3]. Toripalimab, a selective monoclonal antibody to the immune-checkpoint protein programmed cell death protein-1 (PD-1), is used for patients with advanced or metastatic esophageal squamous cell carcinoma[4].

In this report, we described the progression of MTEF in a patient caused by advanced esophagus squamous cell carcinoma invading the trachea, who was treated with toripalimab after tracheal stent placement.

CASE PRESENTATION

Chief complaints

A 58-year-old male presented with an 18-d history of choking after drinking and eating. He was hospitalized in Dongzhimen Hospital in Beijing on April 28, 2020.

History of present illness

The patient had previously been diagnosed with advanced esophageal squamous cell carcinoma (cT4bN0M1, stage 4B). The patient received radiation as the first-line therapy, without surgery or chemotherapy. He was then treated with afatinib for 4 d as a trial treatment. Subsequently, he began choking after drinking and eating, and developed dysphagia 18 d before admission. After anti-infective and nutritional support treatments, the patient's symptoms were not significantly relieved.

History of past illness

The patient had no remarkable disease history.

Personal and family history

The patient reported a personal history of smoking and drinking for more than 30 years. The patient reported his familial history did not include any tumors.

Physical examination

The patient's physical examination was unremarkable.

Laboratory examinations

Tests of peripheral blood tumor markers showed that pro-gastrin-releasing peptide (commonly known as pro-GRP) was 93.58 pg/mL and carcinoembryonic antigen (commonly known as CEA) was 5.6 ng/mL, both of which were higher than the normal range. All other markers tested were within normal range. White blood cell count was 3.8×10^9/L, hemoglobin was 125 g/L, and C-reactive protein was 4.69 mg/L.

Imaging examinations

Bronchoscopy and computer tomography imaging found a 5 mm malignant tracheoesophageal fistula in the main airway, located between the upper trachea and esophagus (Figure 1).

FINAL DIAGNOSIS

Malignant tracheoesophageal fistula

TREATMENT

Given that the airway was significantly obstructed by the tumor, and performance status and Eastern Cooperative Oncology Group (commonly known as ECOG) classification had worsened from 1 to 3-4, mechanical debulking was performed on the tumor arising from the membranous trachea. Initially, a Y-shaped silicone stent of 16 mm × 13 mm × 13 mm in diameter and 80 mm × 30 mm × 15 mm in length (Tracheobronxane™ Dumon® TD; Novatech SA, La Ciotat, France) was placed in the main trachea, with projections into both the left and right main bronchus by rigid bronchoscopy. However, the upper edge of the stent blocked the airway wall, so that the trachea was significantly narrowed. To open the trachea, a straight silicone stent 16 mm in diameter and 30-mm length, partially incised along the long axis, was sutured to reduce the lumen diameter and inserted into the Y-type Dumon stent in the form of a telescope (Figure 2). After placement of the stent, the fistula was completely enclosed, without significant stenosis of the trachea. One month after stenting, the patient received the first dose of toripalimab (240 mg, intravenous drip, every 3 wk). After the fourth dose of toripalimab, the patient presented with hemoptysis. Chest computed tomography and bronchoscopy revealed that the original malignant tracheoesophageal fistula between the upper trachea and esophagus had progressed rapidly in size, measuring 20-30 mm (Figure 3). However, the fistula was still completely covered by the silicone stents.

OUTCOME AND FOLLOW-UP

After palliative treatment for infection (piperacillin sodium and sulbactam sodium for injection, 3.75 g, intravenous drip, q8h) and hemostasis (haemocoagulase, 1 U, intravenous injection, q12h), the condition of the patient was stable. Immunotherapy was continued. During a 4-mo follow-up, no complications related to the stent placement were observed (Figure 4). However, after 7 mo total of toripalimab treatment, the patient died of esophageal cancer on February 16, 2021 (Figure 4B).

DISCUSSION

MTEF develops in approximately 5%-15% of patients with an esophageal malignancy, with less than 1% of those having bronchogenic carcinoma[1,2]. MTEF is a negative predictor of long-term survival, and those patients generally have a very poor prognosis and quality of life. Severe cough, frequent aspiration pneumonia, malnutrition, and life-threatening hemoptysis can lead to rapid deterioration of the patient, and most patients die within 3-4 mo.

MTEF is mostly caused by tumoral invasion or as a complication of cancer therapies. Esophageal cancer invades the trachea directly through its membranous wall or indirectly through metastases from the mediastinal lymph nodes. This leads to tumor necrosis, thus paving the path for MTEF formation[5].

Immediate management of MTEF involves nasogastric tube placement or gastrostomy, to minimize regurgitation. However, this palliative treatment does not improve the patient's quality of life, due its preclusion of oral eating. Radical resection of the MTEF has been reported but with minimal survival advantage[6] because of the advanced stage of the cancer and the consequent and ongoing nutritional depletion. Mesenchymal stem cell transplantation therapy for MTEF is most useful for smaller bronchopleural and distal fistulas, but the further research is required to gain an accurate understanding of the treatment's efficacy and safety profiles[7].

Insertion of a tracheal or esophageal stent, to cover the fistula, is also effective, as was the case with our patient. The stent placement relieved dyspnea for our patient, avoided chemical lung infections, and improved the quality of life, which enabled the patient to continue immunotherapy. Together, these factors likely contributed to the increased survival time for our patient, which was greater than the reported median survival time for MTEF (from stent insertion to death) of 163 d[3]. Although, it is important to note that the expanded stent may readily erode and enlarge the size of the fistula[5].

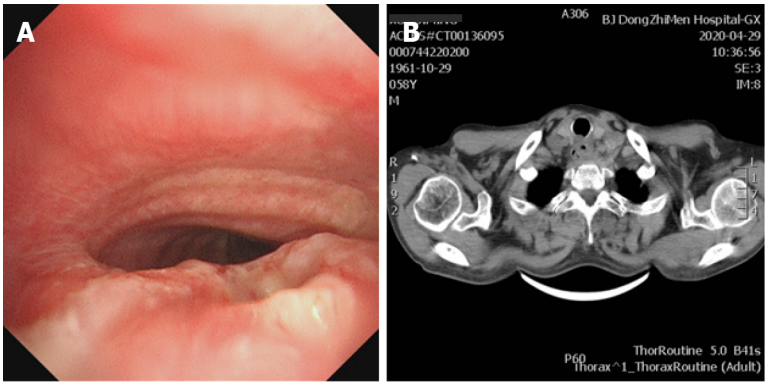

DOI: 10.12998/wjcc.v10.i11.3527

Figure 1 Tracheoesophageal fistula and narrowing of the main bronchus. A: Bronchoscopy image; B: Computed tomography image.

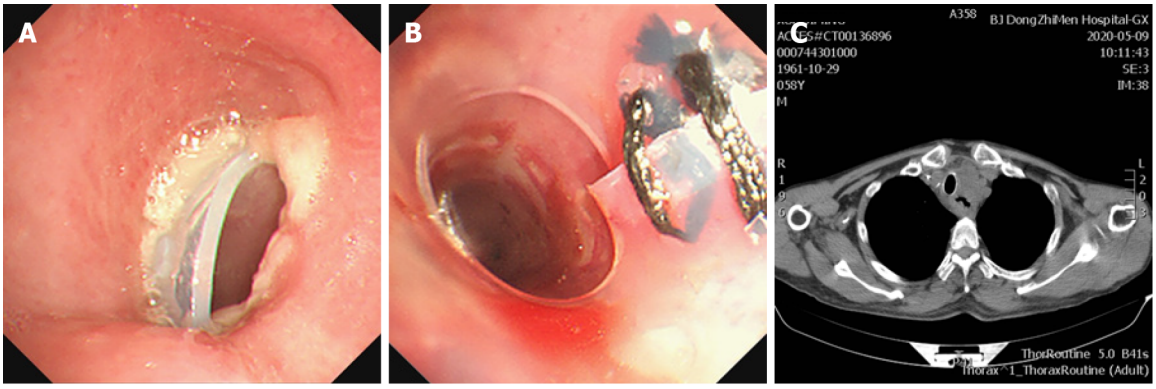

DOI: 10.12998/wjcc.v10.i11.3527

Figure 2 Fistula completely enclosed by a Y-shaped and modified straight silicone stent placed in the main trachea. A, B: Bronchoscopy image showing (A) the upper edge of Y-shaped silicone stent incarcerated the airway wall and (B) a Y-shaped silicone stent and a straight silicone stent placed after mechanical debulking of the tumor; C: Computed tomography image of B.

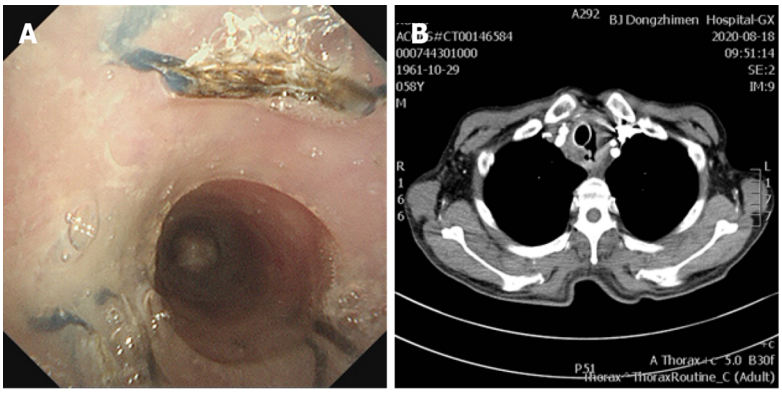

DOI: 10.12998/wjcc.v10.i11.3527

Figure 3 Original malignant tracheoesophageal fistula following rapid progression after the fourth dose of toripalimab. A: Bronchoscopy image; B: Computed tomography image showing the fistula having progressed.

Despite the increased survival time, the patient in the present report experienced rapid progression of MTEF after tracheal stent placement and treatment with toripalimab. Although several clinical studies have reported promising efficacies and manageable safety profiles of immune checkpoint inhibitors (ICIs) on advanced or metastatic esophageal squamous cell carcinoma[8,9], response rates to different anti-PD-1 antibodies in patients with previously treated advanced or metastatic esophageal squamous cell carcinoma were reported to be 14.3%-33.3%[10,11]. However, there have been no reports of immunotherapy and/or stenting increasing the size of the original fistula. Based on our case report, however, there is a potential risk of treating MTEF with immunotherapy and stenting. It is possible that

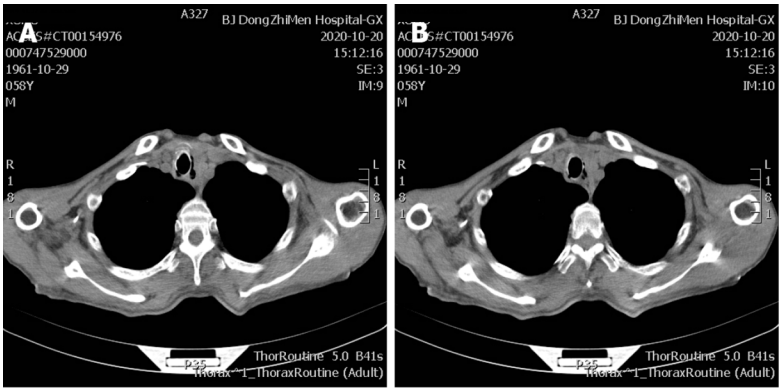

DOI: 10.12998/wjcc.v10.i11.3527

Figure 4 Computer tomography image showing the tracheoesophageal fistula after 4 mo of immunotherapy. A: The progressed fistula after 4 mo of immunotherapy; B: A different slice image.

immunotherapy may have hastened the development of a fistula by lysing the tumor. Although the fistula progressed rapidly after immunotherapy, the enlarged fistula remained completely covered, owing to the appropriate size of the stents; in addition, due to the dilation of the trachea by the stents, the airway remained open and protected against lung infections from either the cancer or the esophagobronchial fistula.

CONCLUSION

This rare case highlights the possibility that toripalimab might exacerbate the progress of a fistula in patients with MTEF. However, using an appropriately sized tracheal stent combined with ICIs therapy may improve the survival of patients with MTEF.

FOOTNOTES

Author contributions: Li CA, Ban CJ, and Wang HW designed the report; Yu WX, Wang LY, and Zou H collected the patient's clinical data; Li CA and Ban CJ wrote the paper.

Supported by National Natural Science Foundation of China, No. 81973784.

Informed consent statement: Written informed consent was obtained from the patient and his family for publication of this case report and any accompanying images.

Conflict-of-interest statement: The authors declare no conflicts of interest.

CARE Checklist (2016) statement: The authors have read the CARE Checklist (2016), and the manuscript was prepared and revised according to the CARE Checklist (2016).

Country/Territory of origin: China

ORCID number: Chang-An Li 0000-0001-9698-5585; Wei-Xia Yu 0000-0002-2749-6953; Lin-Yang Wang 0000-0003-2551-9506; Hang Zou 0000-0002-2570-7569; Cheng-Jun Ban 0000-0002-8468-3755; Hong-Wu Wang 0000-0003-1939-8795.

S-Editor: Ma YJ
L-Editor: A
P-Editor: Ma YJ

REFERENCES

1 **Chen YH**, Li SH, Chiu YC, Lu HI, Huang CH, Rau KM, Liu CT. Comparative study of esophageal stent and feeding gastrostomy/jejunostomy for tracheoesophageal fistula caused by esophageal squamous cell carcinoma. *PLoS One* 2012; **7**: e42766 [PMID: 22912737 DOI: 10.1371/journal.pone.0042766]

2 **Balazs A**, Kupcsulik PK, Galambos Z. Esophagorespiratory fistulas of tumorous origin. Non-operative management of 264 cases in a 20-year period. *Eur J Cardiothorac Surg* 2008; **34**: 1103-1107 [PMID: 18678504 DOI: 10.1016/j.ejcts.2008.06.025]

3 **Wang H**, Tao M, Zhang N, Li D, Zou H, Zhang J, Luo L, Ma H, Zhou Y. Airway Covered Metallic Stent Based on Different Fistula Location and Size in Malignant Tracheoesophageal Fistula. *Am J Med Sci* 2015; **350**: 364-368 [PMID: 26422803 DOI: 10.1097/MAJ.0000000000000565]

4 **Zheng Y**, Liu XB, Sun HB, Xu J, Shen S, Ba YF, Yan M, Qin Z, Liu BX, Wang ZF, Liu SL, Zhang RX, Chen PN, Liang GH, Yuan D, Li ZX, Liu Q, Wang HR, Li HM, Lv H, Ma X, Zhu J, Yu YK, Xing WQ; written on Henan Cancer Hospital Thoracic Oncology Group (HCHTOG). A phase III study on neoadjuvant chemotherapy versus neoadjuvant toripalimab plus chemotherapy for locally advanced esophageal squamous cell carcinoma: Henan Cancer Hospital Thoracic Oncology Group 1909 (HCHTOG1909). *Ann Transl Med* 2021; **9**: 73 [PMID: 33553366 DOI: 10.21037/atm-20-5404]

5 **Shamji FM**, Inculet R. Management of Malignant Tracheoesophageal Fistula. *Thorac Surg Clin* 2018; **28**: 393-402 [PMID: 30054077 DOI: 10.1016/j.thorsurg.2018.04.007]

6 **Davydov M**, Stilidi I, Bokhyan V, Arzykulov G. Surgical treatment of esophageal carcinoma complicated by fistulas. *Eur J Cardiothorac Surg* 2001; **20**: 405-408 [PMID: 11463565 DOI: 10.1016/s1010-7940(01)00796-5]

7 **Huang P**, Gao XL, Zhong ZC, Chen WF, Wang YC, Li J. [Bone marrow-derived mesenchymal stem-cell in treatment of bronchopleural fistula]. *Zhonghua Jie He He Hu Xi Za Zhi* 2019; **42**: 137-140 [PMID: 30704189 DOI: 10.3760/cma.j.issn.1001-0939.2019.02.013]

8 **Lin S**, Kato K, Kim SB, Ajani JA, Zhao K, He Z, Yu X, Shu Y, Luo Q, Wang J, Chen Z, Niu Z, Sun JM, Lin CY, Hara H, Pazo-Cid R, Borg C, Li L, Tao A, Van Cutsem E. RATIONALE 302: Randomized, phase 3 study of tislelizumab versus chemotherapy as second-line treatment for advanced unresectable/metastatic esophageal squamous cell carcinoma. *J Clin Oncol* 2021; **39**: 4012-4012 [DOI: 10.1200/JCO.2021.39.15_suppl.4012]

9 **Kojima T**, Shah MA, Muro K, Francois E, Adenis A, Hsu CH, Doi T, Moriwaki T, Kim SB, Lee SH, Bennouna J, Kato K, Shen L, Enzinger P, Qin SK, Ferreira P, Chen J, Girotto G, de la Fouchardiere C, Senellart H, Al-Rajabi R, Lordick F, Wang R, Suryawanshi S, Bhagia P, Kang SP, Metges JP; KEYNOTE-181 Investigators. Randomized Phase III KEYNOTE-181 Study of Pembrolizumab Versus Chemotherapy in Advanced Esophageal Cancer. *J Clin Oncol* 2020; **38**: 4138-4148 [PMID: 33026938 DOI: 10.1200/JCO.20.01888]

10 **Shah MA**, Kojima T, Hochhauser D, Enzinger P, Raimbourg J, Hollebecque A, Lordick F, Kim SB, Tajika M, Kim HT, Lockhart AC, Arkenau HT, El-Hajbi F, Gupta M, Pfeiffer P, Liu Q, Lunceford J, Kang SP, Bhagia P, Kato K. Efficacy and Safety of Pembrolizumab for Heavily Pretreated Patients With Advanced, Metastatic Adenocarcinoma or Squamous Cell Carcinoma of the Esophagus: The Phase 2 KEYNOTE-180 Study. *JAMA Oncol* 2019; **5**: 546-550 [PMID: 30570649 DOI: 10.1001/jamaoncol.2018.5441]

11 **Huang J**, Xu B, Mo H, Zhang W, Chen X, Wu D, Qu D, Wang X, Lan B, Yang B, Wang P, Zhang H, Yang Q, Jiao Y. Safety, Activity, and Biomarkers of SHR-1210, an Anti-PD-1 Antibody, for Patients with Advanced Esophageal Carcinoma. *Clin Cancer Res* 2018; **24**: 1296-1304 [PMID: 29358502 DOI: 10.1158/1078-0432.CCR-17-2439]

World Journal of Clinical Cases

Submit a Manuscript: https://www.f6publishing.com

World J Clin Cases 2022 April 16; 10(11): 3533-3540

DOI: 10.12998/wjcc.v10.i11.3533

ISSN 2307-8960 (online)

CASE REPORT

Ankylosing spondylitis complicated with andersson lesion in the lower cervical spine: A case report

Yu-Jian Peng, Zhuang Zhou, Qian-Liang Wang, Xiao-Feng Liu, Jun Yan

Specialty type: Orthopedics

Provenance and peer review: Unsolicited article; Externally peer reviewed.

Peer-review model: Single blind

Peer-review report's scientific quality classification

Grade A (Excellent): 0
Grade B (Very good): B
Grade C (Good): C
Grade D (Fair): 0
Grade E (Poor): 0

P-Reviewer: Cure E, Turkey; Hui Yang, China

Received: September 18, 2021
Peer-review started: September 18, 2021
First decision: December 10, 2021
Revised: December 18, 2021
Accepted: February 27, 2022
Article in press: February 27, 2022
Published online: April 16, 2022

Yu-Jian Peng, Qian-Liang Wang, Xiao-Feng Liu, Jun Yan, Department of Orthopedics, the Second Affiliated Hospital of Soochow University, Suzhou 215004, Jiangsu Province, China

Zhuang Zhou, Department of Pain, the Second Affiliated Hospital of Soochow University, Suzhou 215004, Jiangsu Province, China

Corresponding author: Jun Yan, MD, Chief Physician, Director, Department of Orthopedics, the Second Affiliated Hospital of Soochow University, No. 1055 San-Xiang Road, Suzhou 215004, Jiangsu Province, China. cxyanjun@hotmail.com

Abstract

BACKGROUND

Andersson lesion (AL) is an uncommon complication in ankylosing spondylitis (AS), which is characterized by nonneoplastic bone destruction and often appears as bone destruction and sclerosis in the vertebral body and/or the area involving the intervertebral disc. According to the literature, Andersson lesion commonly occur in the thoracic and lumbar spine and rarely in the cervical spine.

CASE SUMMARY

This case involved a 78-year-old man with a long history of AS who developed AL in the cervical spine (C5/6 and C6/7). One-stage anterior-posterior approach surgery was successfully performed. At the 6-month follow-up, the pain was significantly reduced, and the limb function was gradually improved.

CONCLUSION

AL uncharacteristically appears in the cervical spine and tends to be misdiagnosed as vertebral metastases or spinal tuberculosis. Posterior combined with anterior surgery achieves solid biological stabilization in the treatment of AL bone destruction.

Key Words: Andersson lesion; Ankylosing spondylitis; Cervical fracture; Case report

Core Tip: This case involved an Andersson lesion in the cervical spine that occurred in an ankylosing spondylitis patient and was very rare. The Andersson lesion was diagnosed based on orthopaedist clinical experience, imaging examinations and final pathology results. This case report provides a reference for the clinical diagnosis of such cases.

Citation: Peng YJ, Zhou Z, Wang QL, Liu XF, Yan J. Ankylosing spondylitis complicated with andersson lesion in the lower cervical spine: A case report. *World J Clin Cases* 2022; 10(11): 3533-3540
URL: https://www.wjgnet.com/2307-8960/full/v10/i11/3533.htm
DOI: https://dx.doi.org/10.12998/wjcc.v10.i11.3533

INTRODUCTION

Andersson lesion (AL) are characterized by nonneoplastic bone destruction, which is an uncommon phenomenon in late-stage ankylosing spondylitis (AS) and often appears as erosive focal changes with sclerosis widely distributed in the region of the vertebral end plate[1,2]. The prevalence of AL-complicating AS ranges from 1.5% to > 28%[3,4]. With the development of AL, these pathological and destructive changes of the spine may lead to progressive, localized and pain-intolerable kyphosis deformities and even neurological defects, which must be treated in severe cases[5,6]. AS is a chronic active nonunion state with unstable posterior column fractures or unfused facet joints associated with vertebral lesion[7]. Since nonspecific inflammation is the main pathological manifestation, Andersson lesion commonly occur in the region of the thoracic and lumbar spine but rarely in the cervical spine[8]. We successfully treated a patient with nonneoplastic and noninfectious bone destruction of the C6 vertebral body, who had a history of ankylosing spondylitis for decades, which resulted in nonunion involving the middle and posterior columns, characteristics of an Andersson lesion. To the best of our knowledge, this is the first report of unstable fractures of AS with C6 aggressive bone destruction and accumulation of three columns of the cervical spine.

CASE PRESENTATION

Chief complaints

A 78-year-old male farmer was admitted to our hospital with neck pain, worsened numbness and increased disability due to an accidental fall a month prior. He had neck pain and a limited range of motions, but he had no symptoms of fever, night sweats or increased nocturnal pain.

History of present illness

This patient had a history of AS and mobility impairments for decades. He had progressive symptoms of neck pain for 3 mo complicated with left upper limb pain and numbness without obvious cause.

History of past illness

He had no history of diabetes, tuberculosis or tumour. He had undergone thoracolumbar fracture surgery more than ten years ago.

Personal and family history

The patient denied family history.

Physical examination

Physical examination revealed a restricted cervical range of motion. The muscle power of the left upper limbs was grade IV with slightly decreased sensation. The Hoffman signs of both upper limbs were negative, and bilateral Babinski signs were negative in the lower extremities.

Laboratory examinations

Routine blood analysis revealed a slight increase in the neutrophil ratio (77.4%) with normal haematocrit and leukocyte counts. Prothrombin and partial thromboplastin times were almost normal, and d-dimers were increased at 1.56 μg/mL. Serum C-reactive protein was increased at 55.6 mg/dL (normal range < 10 mg/dL). The blood serum tumour marker analysis showed that ferroprotein increased at 516 ng/mL (normal range 30-400 ng/mL), and prostate-specific antigen marginally increased to 8.53 ng/mL (normal range < 4 ng/mL).

Imaging examinations

Radiography and computed tomography (CT) scans revealed typical ankylosing spondylitis in the entire spine, *i.e.*, bamboo-like changes; a pathological fracture changed from the C6 vertebra and accumulated at the upper and lower endplates to spinous processes (Figure 1). Magnetic resonance imaging (MRI) showed C6 new-onset vertebral compression fractures and oedema spread from the anterior region of the C6 spinal centrum to the spinous process and supraspinous ligaments, which were complicated by the degenerative cervical instability and compression of the spinal cord due to the injured cervical spinal stenosis (Figure 2).

FINAL DIAGNOSIS

The final diagnosis of the presented case was Andersson lesion in the lower cervical spine.

TREATMENT

The patient underwent surgery for instrumented stabilization through anterior combined posterior approaches. First, the patient's body temperature was normal throughout the examination. Second, he was convinced that he had no history of tuberculosis or malignant visceral tumours, and all tuberculosis-related laboratory tests or tumour markers were negative. To restore cervical stability, we performed a combined posterior and anterior fixation approach with pedicle screws under a C-arm perspective (Figure 3). In brief, after exposure of C4-T2 with a posterior midline incision, part of the C5 and C6 Laminae were removed using an ultrasonic osteotome; the structure in the spinal canal was exposed, and posterior spinal canal decompression was completed. Under the guidance of C-arm fluoroscopy, the lateral mass or pedicle screws (8 in total, brand: Medtronic) were placed after positioning, drilling and sounding on the side mass of C4, C5 and C7 and the pedicle of T2; a connecting rod (Brand: Medtronic) was used to connect the fixing screws. Next, anterior surgery in the supine position was performed to expose the C6 vertebral body. Under the microscope, the C6 vertebral body and the upper and lower endplates were scraped with a curette. Then, we removed the granulation tissue for pathological examination and bacterial culture, and a short titanium mesh (Brand: Medtronic) was used to support and fix between the C5 Lower endplate and the C6 residual vertebral body. Anterior cervical plates and screws (Brand: Medtronic) were placed in front of C4-T1. To prevent screw loosening caused by osteoporosis, we used bone cement to strengthen the nail channels.

OUTCOME AND FOLLOW-UP

The operation was very successful, and the pathology indicated hyperplastic and fibrous bone tissue with dead bone reaction with no indications of tumour cells and negative bacterial culture results (Figure 4). A postoperative double-check CT scan revealed that the internal fixation device was firm and reliable, and the stability of the cervical spine recovered well. Six months after the operation, the patient reported that the symptoms of pain and numbness were notably relieved and almost returned to normal. The follow-up X-ray images of the cervical spine AL showed that the balance of the coronal plane and sagittal plane recovered well (Figure 5).

DISCUSSION

Andersson first described the characteristics of destructive lesion of the vertebral body and/or intervertebral disc in patients with ankylosing spondylitis in 1937[8]. Since then, they have been known as Andersson lesion, spondylodiscitis, spinal pseudarthroses and destructive spondylopathy[9,10]. This uncertainty in the naming of AL is mainly due to the lack of consistency in the ethology and pathology of the characteristics of these lesions. To date, two mainstream possible mechanisms have been reported. First, these lesions are considered to have a chronic nonspecific inflammatory nature and are attributed to the disease characteristics of ankylosing spondylitis. The other explanation is that they originate from traumatic injury and are characterized by constitute mechanical stress fracture, spinal nonunion or pseudarthroses after trauma[11-13]. Generally, the entire spine of patients with ankylosing spondylitis is susceptible. However, clinically, the most common site of this lesion is the thoracic and lumbar spine, especially the thoracolumbar transition area, *i.e.*, T10-L2, possibly since this area is defined as the transition area of high stress in anatomy and biomechanics[14-16].

Previous reports on AL mainly involved the thoracic vertebrae and lumbar vertebrae regions, but there were almost no reports of AL in the cervical vertebrae. This is the first study to show nonneo-

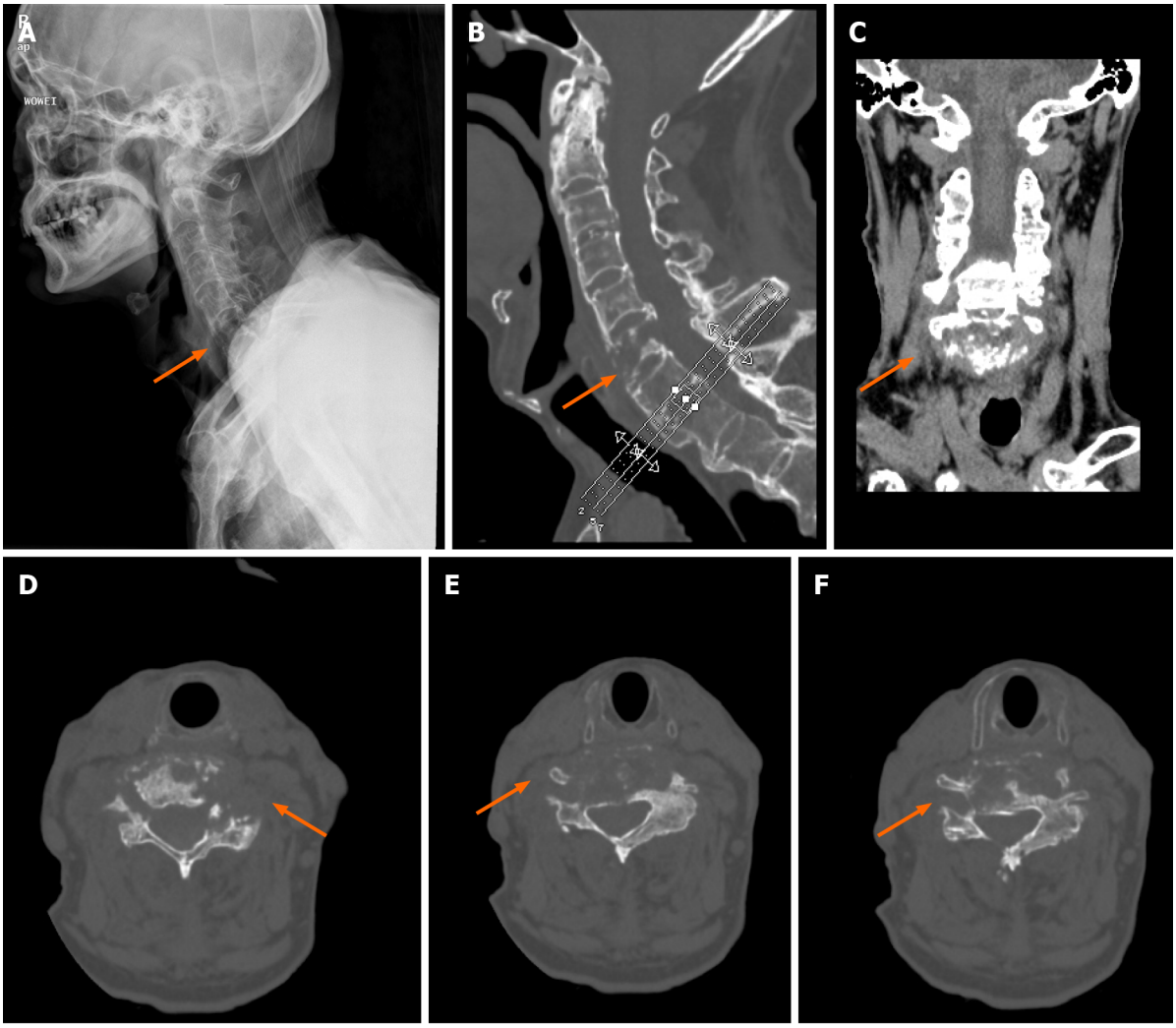

DOI: 10.12998/wjcc.v10.i11.3533

Figure 1 Preoperative X-ray and computed tomography. A: Lateral X-ray view, an arrow shows pathological fracture; B: CT sagittal image, an arrow shows pathological fracture; C: Computed tomography (CT) coronal image, an arrow shows pathological fracture; D-F: CT axial images at different slice levels, an arrow shows pathological fracture.

plastic destructive lesion in the lower cervical vertebrae and the induction of cervical trauma injury.

This patient had a recent history of trauma, and the destructive lesion in the C6 vertebra was almost consistent with the characteristics of imaging, pathology and biomechanics of the Andersson lesion (bone destruction caused by chronic compression). Thus, we suspected that these unstable lower cervical spine fractures resulted from trauma with Andersson lesion, although the location was different from that previously reported (mainly in the thoracic and lumbar vertebrae). Most AL patients have been middle-aged and elderly men with or without AS symptoms for decades. The common clinical manifestations are local intolerable and progressive pain of the thoracolumbar spine and local severe pain after mild trauma with dysfunction[12].

When combined with spinal cord nerve injury, some patients have serious symptoms such as numbness, muscle weakness, incomplete paralysis or even paraplegia. X-ray examination can preliminarily detect the degree of erosive bone destruction. Computed tomography is more accurate and stereoscopic than X-ray in displaying bone lesion, especially in assessing the location of spinal cord compression, the involvement of the spinal canal, the severity of vertebral destruction and the injury mechanism. In addition, MRI can provide information about the involvement of soft tissue around the spine, and the state of the spinal cord and nerve is clearer.

Based on the imaging findings for this patient, AL might be easily misdiagnosed for spinal tuberculosis or spinal metastasis because these conditions are mostly identified by bone destruction. In addition, both AL and spinal tuberculosis may be characterized by the narrowed intervertebral space, hyperosteogeny and late sclerosis[13]. Unlike AL, most patients with spinal tuberculosis have low fever, night sweats and other systemic symptoms in the early stage, and the anti-tuberculosis treatment is effective. Similarly, patients with spinal metastases often have symptoms in primary organs, such as gastrointestinal tumours and prostate cancer. Spinal metastases are common in the thoracolumbar spine, and cervical metastases are rarely reported. With detailed physical examination and previous AS

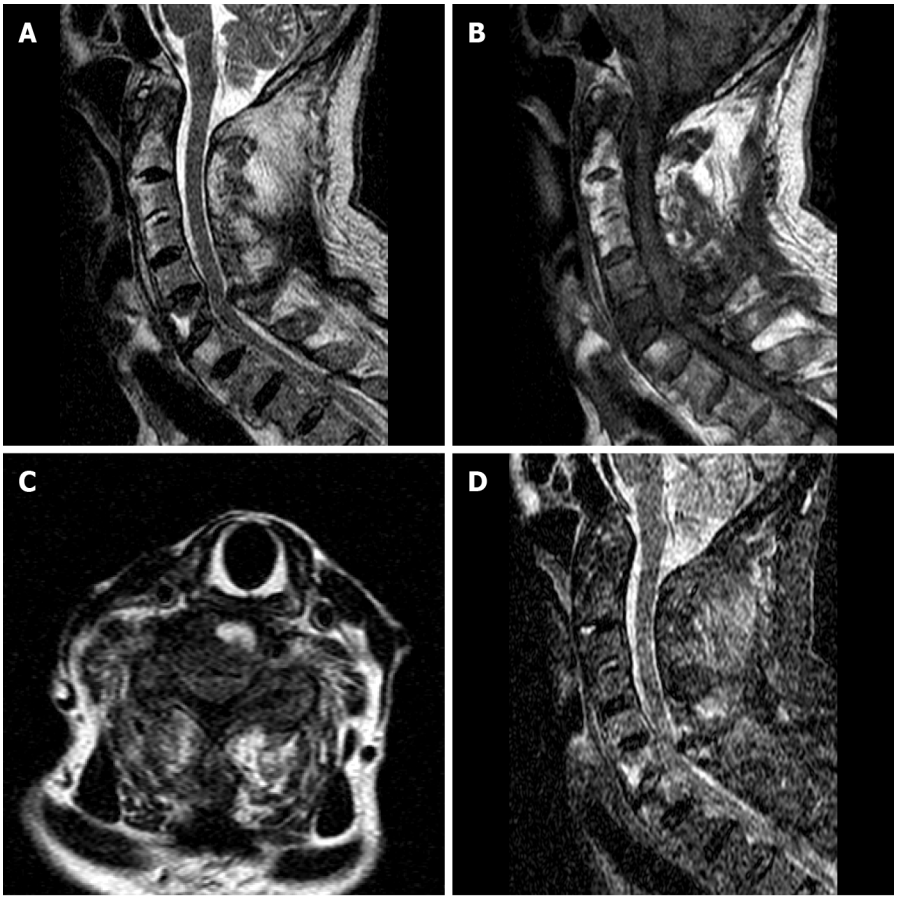

Figure 2 Preoperative magnetic resonance imaging. A: Sagittal T2-weighted image; B: Sagittal T1-weighted image; C: Axial T2-weighted image; D: Sagittal STIR image.

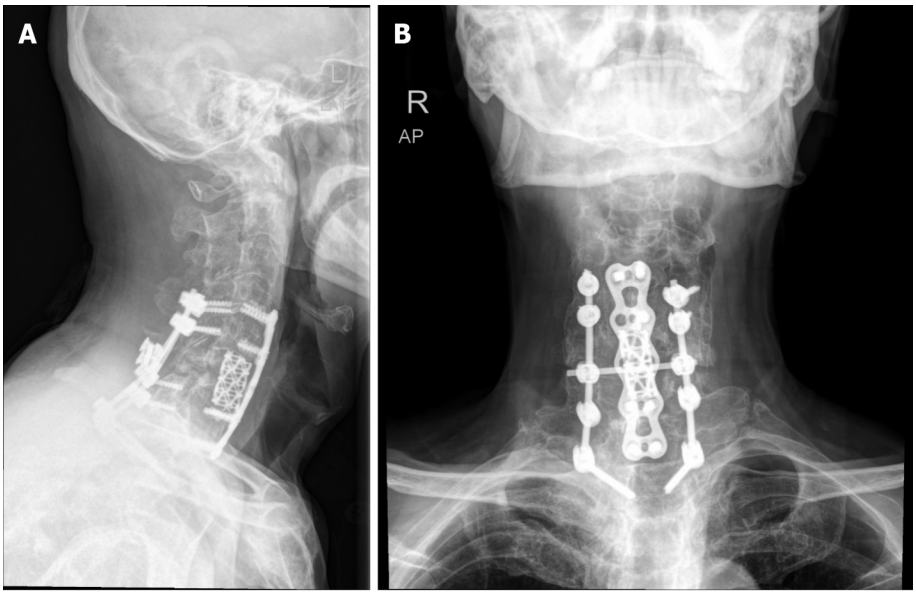

Figure 3 Postoperative X-ray. A: Lateral X-ray view; B: Anteroposterior X-ray view.

disease history, laboratory markers, X-ray, CT and magnetic resonance examination are vitally important for the diagnosis of AL.

To the best of our knowledge, there are no exact and consistent guidelines on how to systematically treat AL[17]. Conservative treatment, including NSAIDs and anti-TNF-α therapy, is often initially

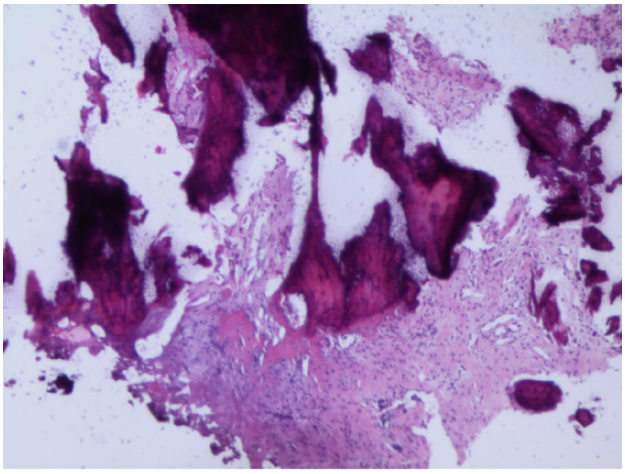

Figure 4 Pathology picture.

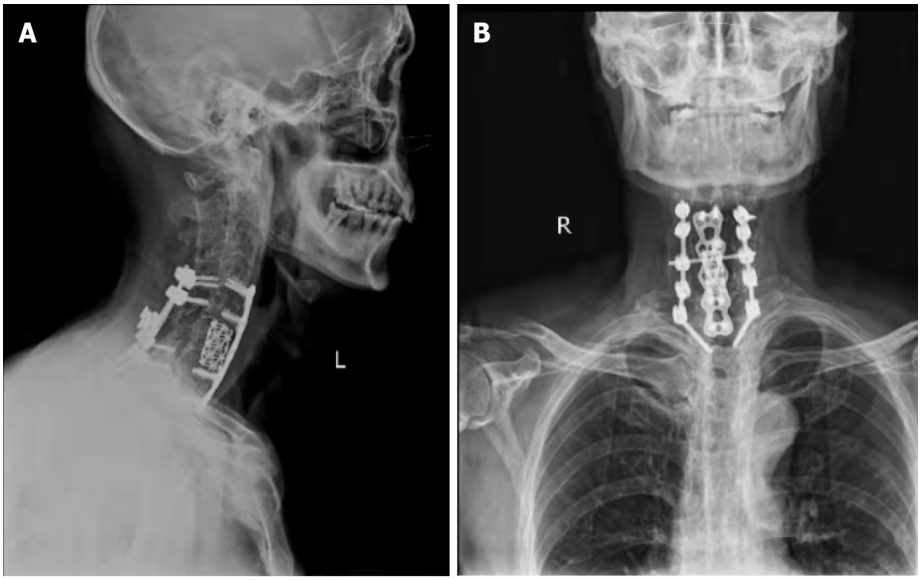

Figure 5 10 months postoperative X-ray. A: Lateral X-ray view; B: Anteroposterior X-ray view.

suggested, and some researchers have confirmed that conservative treatment is safe and effective[8]. Nevertheless, there is still no recognized evidence that these drugs can help the treatment of symptomatic AL, although they have been proven to be effective in patients with ankylosing spondylitis. Therefore, surgical treatment is recommended to reduce unbearable pain, kyphosis deformity, biomechanical instability or neurological deficits caused by trauma[18-21]. Our patient had a mild traumatic fracture involving three columns of the cervical spine secondary to Andersson lesion. To reconstruct the stability of the cervical spine and fully decompress the spinal canal, we chose the posterior with the anterior approach for surgery. According to our experience, successful interbody fusion through surgery (one-stage internal fixation) is the safest and most effective choice to treat AL.

CONCLUSION

In summary, AL constitutes a relatively infrequent nonneoplastic bone destruction in patients with AS. Our report provides a meaningful reference for the diagnosis, differential diagnosis, treatment and prognosis of AL. Surgery is a more reasonable choice to treat AL with unstable cervical fracture, especially for patients with kyphosis and dysfunction caused by nerve compression. Fusion is critical, and complete decompression is fundamental in the treatment of Andersson lesion.

FOOTNOTES

Author contributions: Peng YJ performed the study, collected data, and drafted the manuscript; Zhou Z and Wang QL collected data, performed literature searches and interpreted the data; Liu XF and Yan J made critical revisions to the manuscript; all authors have read and approved the version of the article presented for publication

Supported by the National Natural Science Foundation of China, No. 81902239 and the Natural Science Foundation of Jiangsu Province, No. BK20191169.

Informed consent statement: Written informed consent was obtained from the patient for the publication of this case report and the accompanying images.

Conflict-of-interest statement: The authors have no conflicts of interests to disclose.

CARE Checklist (2016) statement: The authors have read the CARE Checklist (2016), and the manuscript was prepared and revised according to the CARE Checklist (2016).

Country/Territory of origin: China

ORCID number: Yu-Jian Peng 0000-0001-6927-6599; Zhuang Zhou 0000-0002-9050-2578; Qian-Liang Wang 0000-0002-0785-2594; Xiao-Feng Liu 0000-0003-3405-1247; Jun Yan 0000-0003-3640-1714.

S-Editor: Ma YJ
L-Editor: A
P-Editor: Ma YJ

REFERENCES

1 **Wu M**, Yan F, Ping A, Lei J. Effects of Andersson lesion treatment in ankylosing spondylitis: A medical record review study focused on medium- to long-term outcomes. *Int J Rheum Dis* 2020; **23**: 753-762 [PMID: 32266777 DOI: 10.1111/1756-185X.13826]
2 **Ji X**, Su M, Chen J, Wang X, Cai X. A novel method for plastic particle sizing in suspension based on acoustic impedance spectrum. *Ultrasonics* 2017; **77**: 224-230 [PMID: 28260691 DOI: 10.1016/j.ultras.2017.01.024]
3 **Shao J**, Gao YZ, Gao K, Yu ZH. Ankylosing Spondylitis Complicated with Atlantoaxial Dislocation and Destruction of the Dens and Lateral Atlantoaxial Joint: A Case Report. *JBJS Case Connect* 2019; **9**: e0216 [PMID: 31833976 DOI: 10.2106/JBJS.CC.19.00216]
4 **Fu X**, Zhang Y, Jiang W, Monnot AD, Bates CA, Zheng W. Regulation of copper transport crossing brain barrier systems by Cu-ATPases: effect of manganese exposure. *Toxicol Sci* 2014; **139**: 432-451 [PMID: 24614235 DOI: 10.1093/toxsci/kfu048]
5 **Zhang X**, Wang Y, Wu B, Hu W, Zhang Z. Treatment of Andersson lesion-complicating ankylosing spondylitis *via* transpedicular subtraction and disc resection osteotomy, a retrospective study. *Eur Spine J* 2016; **25**: 2587-2595 [PMID: 26346847 DOI: 10.1007/s00586-015-4213-6]
6 **Barman A**, Sinha MK, Rao PB. Discovertebral (Andersson) lesion of the Ankylosing Spondylitis, a cause of autonomic dysreflexia in spinal cord injury. *Spinal Cord Ser Cases* 2016; **2**: 16008 [PMID: 28053752 DOI: 10.1038/scsandc.2016.8]
7 **Liang Y**, Tang X, Zhao Y, Wang Z. Posterior wedge osteotomy and debridement for Andersson lesion with severe kyphosis in ankylosing spondylitis. *J Orthop Surg Res* 2017; **12**: 54 [PMID: 28359323 DOI: 10.1186/s13018-017-0556-5]
8 **Wang HF**, Bi C, Chen ZQ. [Research progress on Andersson lesion in ankylosing spondylitis]. *Zhonghua Wai Ke Za Zhi* 2017; **55**: 798-800 [PMID: 29050182 DOI: 10.3760/cma.j.issn.0529-5815.2017.10.020]
9 **Van Royen BJ**, Kastelijns RC, Noske DP, Oner FC, Smit TH. Transpedicular wedge resection osteotomy for the treatment of a kyphotic Andersson lesion-complicating ankylosing spondylitis. *Eur Spine J* 2006; **15**: 246-252 [PMID: 16151717 DOI: 10.1007/s00586-005-1008-1]
10 **Obradov M**, Schönfeld DH, Franssen MJ, de Rooy DJ. Andersson lesion in ankylosing spondylitis. *JBR-BTR* 2001; **84**: 71 [PMID: 11374644]
11 **Queiro R**, Tejón P, Alonso S, Alperi M, Ballina J. Erosive discovertebral lesion (Andersson lesion) as the first sign of disease in axial psoriatic arthritis. *Scand J Rheumatol* 2013; **42**: 220-225 [PMID: 23311864 DOI: 10.3109/03009742.2012.739637]
12 **Dhakad U**, Das SK. Andersson lesion in ankylosing spondylitis. *BMJ Case Rep* 2013; **2013** [PMID: 23559648 DOI: 10.1136/bcr-2012-008404]
13 **Park YS**, Kim JH, Ryu JA, Kim TH. The Andersson lesion in ankylosing spondylitis: distinguishing between the inflammatory and traumatic subtypes. *J Bone Joint Surg Br* 2011; **93**: 961-966 [PMID: 21705571 DOI: 10.1302/0301-620X.93B7.26337]

14 **Wang G**, Zhuo N, Tian F, Wen Z, Li J. Andersson lesion in the lumbar spine of SAPHO syndrome. *Rheumatology (Oxford)* 2022; **61**: 877 [PMID: 33974076 DOI: 10.1093/rheumatology/keab417]

15 **Qin W**, Yang P, Zhou F, Mao H, Yang H. Andersson Lesion Occurring in the Lumbosacral Segment of a Young Man: A Case Report and Literature Review. *World Neurosurg* 2020; **143**: 419-422 [PMID: 32798782 DOI: 10.1016/j.wneu.2020.07.146]

16 **Hu X**, Kong Y, Li B. Andersson Lesion in the Thoracic Spine. *J Clin Rheumatol* 2021; **27**: e258 [PMID: 32398510 DOI: 10.1097/RHU.0000000000001402]

17 **Yang F**, Yang L, Ren E, Yang Y, Wang J, Kang X. Surgical Treatment of Ankylosing Spondylitis with Andersson Lesion. *J Coll Physicians Surg Pak* 2019; **29**: S135-S137 [PMID: 31779768 DOI: 10.29271/jcpsp.2019.12.S135]

18 **Dave BR**, Kulkarni M, Patidar V, Devanand D, Mayi S, Reddy C, Singh M, Rai RR, Krishnan A. Results of in situ fixation of Andersson lesion by posterior approach in 35 cases. *Musculoskelet Surg* 2021 [PMID: 34037925 DOI: 10.1007/s12306-021-00712-z]

19 **Ding K**, Zhu J, Chen H, Tian Y, Hao D. [Debridement and interbody fusion *via* posterior pedicle lateral approach for ankylosing spondylitis with thoracolumbar Andersson lesion]. *Zhongguo Xiu Fu Chong Jian Wai Ke Za Zhi* 2019; **33**: 1474-1479 [PMID: 31823543 DOI: 10.7507/1002-1892.201904068]

20 **Shaik I**, Bhojraj SY, Prasad G, Nagad PB, Patel PM, Kashikar AD, Kumar N. Management of Andersson Lesion in Ankylosing Spondylitis Using the Posterior-Only Approach: A Case Series of 18 Patients. *Asian Spine J* 2018; **12**: 1017-1027 [PMID: 30322255 DOI: 10.31616/asj.2018.12.6.1017]

21 **Rajoli SR**, Kanna RM, Aiyer SN, Shetty AP, Rajasekaran S. Circumferential Fusion through All-Posterior Approach in Andersson Lesion. *Asian Spine J* 2017; **11**: 444-453 [PMID: 28670413 DOI: 10.4184/asj.2017.11.3.444]

World Journal of Clinical Cases

Submit a Manuscript: https://www.f6publishing.com

World J Clin Cases 2022 April 16; 10(11): 3541-3546

DOI: 10.12998/wjcc.v10.i11.3541

ISSN 2307-8960 (online)

CASE REPORT

Severe gastric insufflation and consequent atelectasis caused by gas leakage using AIR-Q laryngeal mask airway: A case report

Yue Zhao, Ping Li, De-Wei Li, Gao-Feng Zhao, Xiang-Yu Li

Specialty type: Respiratory system

Provenance and peer review: Unsolicited article; Externally peer reviewed.

Peer-review model: Single blind

Peer-review report's scientific quality classification

Grade A (Excellent): 0
Grade B (Very good): B
Grade C (Good): C
Grade D (Fair): 0
Grade E (Poor): 0

P-Reviewer: Bairwa DBL, Chan SM

Received: December 7, 2021
Peer-review started: December 7, 2021
First decision: January 12, 2022
Revised: January 23, 2022
Accepted: February 23, 2022
Article in press: February 23, 2022
Published online: April 16, 2022

Yue Zhao, Ping Li, De-Wei Li, Gao-Feng Zhao, Xiang-Yu Li, Department of Anesthesiology, The Second Affiliated Hospital of Guangzhou University of Chinese Medicine, Guangdong Provincial Hospital of Chinese Medicine, Guangzhou 510120, Guangdong Province, China

Corresponding author: De-Wei Li, PhD, Doctor, Department of Anesthesiology, The Second Affiliated Hospital of Guangzhou University of Chinese Medicine, Guangdong Provincial Hospital of Chinese Medicine, No. 111 Dade Road, Guangzhou 510120, Guangdong Province, China. leedewei1123@sina.com

Abstract

BACKGROUND

The airways of patients undergoing awake craniotomy (AC) are considered "predicted difficult airways", inclined to be managed with supraglottic airway devices (SADs) to lower the risk of coughing or gagging. However, the special requirements of AC in the head and neck position may deteriorate SADs' seal performance, which increases the risks of ventilation failure, severe gastric insufflation, regurgitation, and aspiration.

CASE SUMMARY

A 41-year-old man scheduled for AC with the asleep–awake–asleep approach was anesthetized and ventilated with a size 3.5 AIR-Q intubating laryngeal mask airway (LMA). Air leak was noticed with adequate ventilation after head rotation for allowing scalp blockage. Twenty-five minutes later, the LMA was replaced by an endotracheal tube because of a change in the surgical plan. After surgery, the patient consistently showed low tidal volume and was diagnosed with gastric insufflation and atelectasis using computed tomography.

CONCLUSION

This case highlights head rotation may cause gas leakage, severe gastric insufflation, and consequent atelectasis during ventilation with an AIR-Q intubating laryngeal airway.

Key Words: Insufflation; Atelectasis; Laryngeal mask airway; Craniotomy; Case report

Core Tip: AIR-Q intubating laryngeal airway is a feasible airway management method for predicted difficult airways and has been proven to involve fewer complications and a shorter ventilation duration than fiberoptic intubation. This case highlights that head rotation during ventilation with an AIR-Q intubating laryngeal airway may lead to gas leakage, severe gastric insufflation, and consequent atelectasis; this indicates that physicians should pay attention to patient position changes when using laryngeal mask airway.

Citation: Zhao Y, Li P, Li DW, Zhao GF, Li XY. Severe gastric insufflation and consequent atelectasis caused by gas leakage using AIR-Q laryngeal mask airway: A case report. *World J Clin Cases* 2022; 10(11): 3541-3546
URL: https://www.wjgnet.com/2307-8960/full/v10/i11/3541.htm
DOI: https://dx.doi.org/10.12998/wjcc.v10.i11.3541

INTRODUCTION

The use of supraglottic airway devices (SADs) has been proven to be a feasible airway management method for awake craniotomy (AC) to lower the risk of coughing or gagging during the transition to the awake state[1]. Recently, a retrospective analysis of 30 cases of AC reported that patients receiving laryngeal mask airway (LMA) had fewer complications and a shorter ventilation duration than patients who underwent fiberoptic intubation[2]. Considering the requirements of craniotomy and scalp blocks, head rotation and neck flexion may influence the performance of SADs including oropharyngeal leak pressure, ventilation, and fiberoptic view[3,4]. Gastric insufflation and regurgitation were also reported by studies using SADs[3,5,6]. There are no clinical data on gastric insufflation and regurgitation in AC, and the current reviews do not provide suggestions to prevent these complications[1,7,8]. Here, we report a case of severe gastric insufflation and consequent atelectasis caused by gas leakage using AIR-Q LMA during preparation for craniotomy.

CASE PRESENTATION

Chief complaints

A 41-year-old man was admitted for paroxysmal unconsciousness for 7 d.

History of present illness

Written informed consent was obtained from the patient for the publication of this report and any accompanying images. A 41-year-old man (weight, 65 kg; height, 168 cm) was diagnosed with postoperative recurrence of a right frontotemporal glioma and was scheduled for AC with the asleep–awake–asleep approach[1] on July 24, 2020.

Preoperative medication included daily doses of phenobarbitone 120 mg and carbamazepine 600 mg. He did not receive premedication and fasted for longer than 8 h on the day of surgery. After attaching the monitors and securing peripheral venous access, pre-oxygenation was performed to reach an exhaled oxygen concentration > 90%. Anesthesia was induced with a bolus injection of propofol (2 mg/kg) and sufentanil (0.2 μg/kg). Bag-mask ventilation with the head-tilt-chin lift, jaw-thrust maneuver was applied and rated Grade 1 using Han's grading scale for mask ventilation[9]. At EEG stage D, a size 3.5 AIR-Q intubating laryngeal airway (Cookgas® company) was promptly inserted following a standard insertion technique. The sealing pressure was optimized by inflating the cuff until the cessation of the air leak sound from the mouth[10].

Large chest elevation amplitude, normal pulmonary auscultation, no epigastric audible sound, and standard end-tidal CO_2 ($ETCO_2$) curve were achieved. Volume-control ventilation was adopted with the following breath parameters: 500 mL/L O_2, gas flow 3 L/min, V_T 6 mL/kg, I:E 1:2, positive end-expiratory pressure (PEEP) = 0 cmH_2O, and peak inspiratory pressure (PIP) = 18 cmH_2O. The respiratory rate was adjusted to maintain $ETCO_2$ between 35 and 40 mmHg. Sevoflurane inhalation and target-controlled infusion of remifentanil were administered to maintain anesthesia. Scalp nerve block was performed using 20 mL ropivacaine 500 mg/L. To facilitate ultrasound-guided bilateral greater and lesser occipital nerve blocks, the patient's head was rotated approximately 45° to the left and right, respectively. Air leak sound from the mouth with obvious chest expansion and increased PIP (23 cmH_2O) was noticed and assessed as "adequate" ventilation using a three-point ventilation score[11]. After approximately 25 min of administering the scalp block, the anesthesia provider was informed that the surgical plan would change to craniotomy under general anesthesia. After administering an induction dose of cisatracurium (0.15 mg/kg), the LMA was withdrawn, and an endotracheal tube (ID 7.5) was successfully inserted using a video laryngoscope at the first attempt. Ventilation parameters remained

unchanged, except for PEEP 5 cmH_2O and PIP 22 cmH_2O. The length of surgery was 460 min. At the completion of the surgery, sevoflurane was stopped, and remifentanil was adjusted to 2 μg/mL. Patient consciousness and spontaneous breathing were restored in 13 min. However, V_T was consistently low (160-200 mL) even after a standard lung recruitment maneuver (RM).

History of past illness

The patient had no history of any medical illness other than the diagnosis from the previous surgery.

Personal and family history

This patient is with no family history.

Physical examination

Breath sounds decreased bilaterally.

Laboratory examinations

Intraoperative PO_2 of arterial blood gas was between 214 and 225 mmHg.

Imaging examinations

A lung computed tomography (CT) scan was performed in the hybrid operating room. Before gastric decompression, gastric insufflation (Figure 1A, asterisk) and atelectasis with air bronchogram (Figure 1B, asterisk) were observed. In contrast, after gastric decompression and RM, the stomach was deflated (Figure 1C, asterisk), and the atelectatic lung tissue (Figure 1D, asterisk) was re-aerated.

FINAL DIAGNOSIS

Abdominal and chest CT scans revealed severe gastric insufflation (Figure 1A), elevation of the bilateral diaphragm dome to the lower edge of the seventh thoracic vertebral body, and atelectasis of the bilateral lower lobes (Figure 1B).

TREATMENT

A nasogastric tube was promptly inserted, through which a large amount of gas was released. After another RM, V_T was restored to 300 mL. The second CT scan showed gastric deflation (Figure 1C), descent of the bilateral diaphragm dome to the lower edge of the ninth thoracic vertebral body, and a great reduction in the atelectasis region (Figure 1D).

OUTCOME AND FOLLOW-UP

The patient was transferred to the neurological intensive care unit, extubated after 48 h of synchronized intermittent mandatory ventilation without other pulmonary complications, and discharged from the hospital on the 7th postoperative day.

DISCUSSION

This is the first report to describe severe gastric insufflation and consequent atelectasis during mechanical ventilation with an AIR-Q LMA. Contrary to the endotracheal tube, SADs enable effective ventilation with risks of gastric insufflation, consequent regurgitation, and pulmonary aspiration[8]. These risks may increase upon changing the head and neck position, which is required for certain surgical and anesthetic procedures, such as AC and scalp block[1]. Neck flexion decreases longitudinal tension in the anterior pharyngeal muscles and reduces the pharyngeal anteroposterior diameter, resulting in significant impairment of ventilation and alignment between the SAD and glottis with increased oropharyngeal leak pressure. Conversely, neck extension increases the pharyngeal anteroposterior diameter by elevating the laryngeal inlet and reduces oropharyngeal leak pressure without impairing ventilation. A systematic review and meta-analysis reported that SAD performance was not significantly affected by the rotation of the head and neck, and the intracuff pressure of LMAs was standardized at 60 cmH_2O (5.9 kPa)[7]. In the present case, peak inspiratory pressure-guided intracuff pressure was applied to reduce postoperative pharyngolaryngeal complications[12]. This technique might have led to a lower intracuff pressure and cuff volume and consequently impaired seal performance of LMA as the head and neck positions changed. However, higher intracuff pressure does

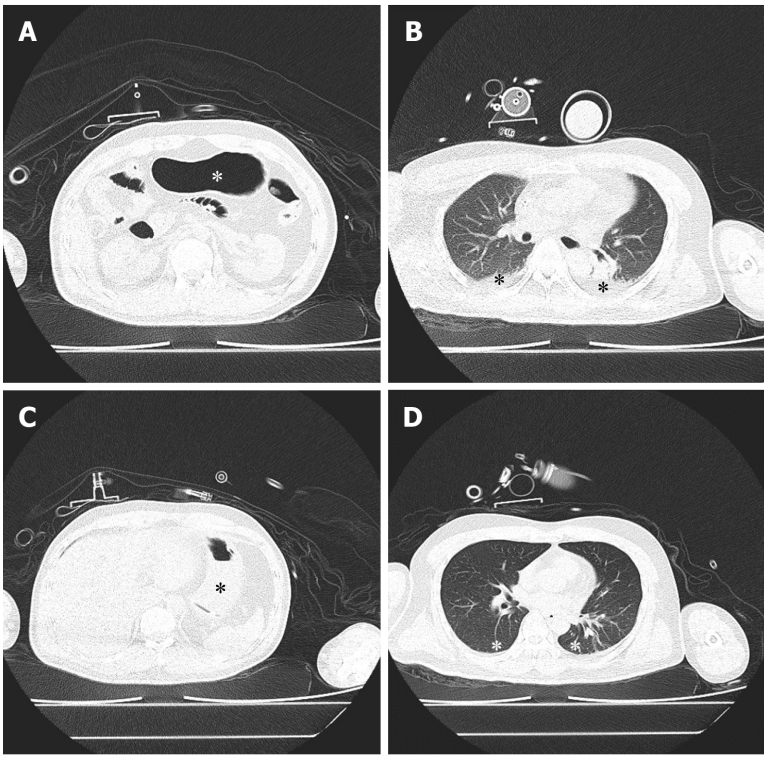

DOI: 10.12998/wjcc.v10.i11.3541

Figure 1 Patient's computed tomography of upper abdomen (A and C) and lung (B and D). Before gastric decompression, gastric insufflation (A, asterisk) and atelectasis with air bronchogram (B, asterisk) could be seen. After gastric decompression and standard lung recruitment manoeuvre, the stomach was deflated (C, asterisk) and atelectatic lung tissue (D, asterisk) was re-aerated.

not necessarily improve sealing performance. A recent study reported that an intracuff pressure of 20 cmH_2O reduced the incidence of gastric insufflation to 35%, compared with that of 60 cmH_2O (48%)[6]. Moreover, gastric insufflation detected with ultrasonography[6] is reported to be significantly more frequent than that with epigastric auscultation[8]. Prolonged duration of surgery and mechanical ventilation lead to atelectasis and other pulmonary complications[13]. However, the difference in the outcomes between the first RM and the RM after gastric decompression indicated that gastric insufflation was an important factor aggravating atelectasis. Furthermore, by continuously stretching the diaphragm for approximately 10 h, gastric insufflation might have led to diaphragmatic dysfunction, decreasing the patient's postoperative V_T[14].

Because of immobilization of the patient's head and limited access of the anesthetist to the patient, airway management in AC should be treated as a predicted difficult airway. Therefore, gastric insufflation with SAD ventilation, which may lead to regurgitation and aspiration, should be prevented, detected, and addressed early. An alternative solution may be ventilation with a SAD embedding a channel for orogastric tube placement, insertion of an orogastric tube, and careful titration of intracuff pressure for various head and neck positions during the asleep period. Further, the orogastric tube can be removed at the beginning of the transition to the awake period and reinserted if a SAD is replaced in the post-awake phase. If available, ultrasonography for early detection of gastric insufflation and measurement of gastric volume is significantly superior to epigastric auscultation. Moreover, ultrasonography may help monitor the development of atelectasis[15] and diaphragm function[16].

CONCLUSION

Our report suggests that head rotation may lead to gas leakage, severe gastric insufflation, and consequent atelectasis during ventilation with an AIR-Q intubating laryngeal airway.

FOOTNOTES

Author contributions: Zhao Y and Li DW reviewed the literature and contributed to manuscript drafting; Li P and Li XY were responsible for project administration and data curation; Zhao GF was responsible for the revision of the manuscript for important intellectual content; all authors issued final approval for the version to be submitted.

Informed consent statement: Informed written consent was obtained from the patient for publication of this report and any accompanying images.

Conflict-of-interest statement: The authors declare that they have no conflict of interest.

CARE Checklist (2016) statement: The authors have read the CARE Checklist (2016), and the manuscript was prepared and revised according to the CARE Checklist (2016).

Country/Territory of origin: China

ORCID number: Yue Zhao 0000-0001-7637-5464; Ping Li 0000-0002-1857-5203; De-Wei Li 0000-0002-5924-0565; Gao-Feng Zhao 0000-0001-7322-8493; Xiang-Yu Li 0000-0002-2438-5780.

S-Editor: Gong ZM
L-Editor: A
P-Editor: Gong ZM

REFERENCES

1 **Meng L**, McDonagh DL, Berger MS, Gelb AW. Anesthesia for awake craniotomy: a how-to guide for the occasional practitioner. *Can J Anaesth* 2017; **64**: 517-529 [PMID: 28181184 DOI: 10.1007/s12630-017-0840-1]
2 **Grabert J**, Klaschik S, Güresir Á, Jakobs P, Soehle M, Vatter H, Hilbert T, Güresir E, Velten M. Supraglottic devices for airway management in awake craniotomy. *Medicine (Baltimore)* 2019; **98**: e17473 [PMID: 31577780 DOI: 10.1097/MD.0000000000017473]
3 **Park SH**, Han SH, Do SH, Kim JW, Kim JH. The influence of head and neck position on the oropharyngeal leak pressure and cuff position of three supraglottic airway devices. *Anesth Analg* 2009; **108**: 112-117 [PMID: 19095838 DOI: 10.1213/ane.0b013e318192376f]
4 **Kim MS**, Park JH, Lee KY, Choi SH, Jung HH, Kim JH, Lee B. Influence of head and neck position on the performance of supraglottic airway devices: A systematic review and meta-analysis. *PLoS One* 2019; **14**: e0216673 [PMID: 31071171 DOI: 10.1371/journal.pone.0216673]
5 **Qamarul Hoda M**, Samad K, Ullah H. ProSeal versus Classic laryngeal mask airway (LMA) for positive pressure ventilation in adults undergoing elective surgery. *Cochrane Database Syst Rev* 2017; **7**: CD009026 [PMID: 28727896 DOI: 10.1002/14651858.CD009026.pub2]
6 **Hell J**, Pohl H, Spaeth J, Baar W, Buerkle H, Schumann S, Schmutz A. Incidence of gastric insufflation at high compared with low laryngeal mask cuff pressure: A randomised controlled cross-over trial. *Eur J Anaesthesiol* 2021; **38**: 146-156 [PMID: 32740320 DOI: 10.1097/EJA.0000000000001269]
7 **Kulikov A**, Lubnin A. Anesthesia for awake craniotomy. *Curr Opin Anaesthesiol* 2018; **31**: 506-510 [PMID: 29994938 DOI: 10.1097/ACO.0000000000000625]
8 **Potters JW**, Klimek M. Awake craniotomy: improving the patient's experience. *Curr Opin Anaesthesiol* 2015; **28**: 511-516 [PMID: 26263121 DOI: 10.1097/ACO.0000000000000231]
9 **Han R**, Tremper KK, Kheterpal S, O'Reilly M. Grading scale for mask ventilation. *Anesthesiology* 2004; **101**: 267 [PMID: 15220820 DOI: 10.1097/00000542-200407000-00059]
10 **Ali A**, Canturk S, Turkmen A, Turgut N, Altan A. Comparison of the laryngeal mask airway Supreme and laryngeal mask airway Classic in adults. *Eur J Anaesthesiol* 2009; **26**: 1010-1014 [PMID: 19707148 DOI: 10.1097/EJA.0b013e3283313fdd]
11 **Keller C**, Brimacombe JR, Keller K, Morris R. Comparison of four methods for assessing airway sealing pressure with the laryngeal mask airway in adult patients. *Br J Anaesth* 1999; **82**: 286-287 [PMID: 10365012 DOI: 10.1093/bja/82.2.286]
12 **Wang MH**, Zhang DS, Zhou W, Tian SP, Zhou TQ, Sui W, Zhang Z. Effects of Peak Inspiratory Pressure-Guided Setting of Intracuff Pressure for Laryngeal Mask Airway Supreme™ Use during Laparoscopic Cholecystectomy: A Randomized Controlled Trial. *J Invest Surg* 2021; **34**: 1137-1144 [PMID: 32354298 DOI: 10.1080/08941939.2020.1761487]
13 **Canet J**, Gallart L, Gomar C, Paluzie G, Vallès J, Castillo J, Sabaté S, Mazo V, Briones Z, Sanchis J; ARISCAT Group. Prediction of postoperative pulmonary complications in a population-based surgical cohort. *Anesthesiology* 2010; **113**: 1338-1350 [PMID: 21045639 DOI: 10.1097/ALN.0b013e3181fc6e0a]
14 **Goligher EC**, Brochard LJ, Reid WD, Fan E, Saarela O, Slutsky AS, Kavanagh BP, Rubenfeld GD, Ferguson ND. Diaphragmatic myotrauma: a mediator of prolonged ventilation and poor patient outcomes in acute respiratory failure. *Lancet Respir Med* 2019; **7**: 90-98 [PMID: 30455078 DOI: 10.1016/S2213-2600(18)30366-7]
15 **Frassanito L**, Sonnino C, Pitoni S, Zanfini BA, Catarci S, Gonnella GL, Germini P, Vizzielli G, Scambia G, Draisci G. Lung ultrasound to monitor the development of pulmonary atelectasis in gynecologic oncologic surgery. *Minerva Anestesiol* 2020; **86**: 1287-1295 [PMID: 33174404 DOI: 10.23736/S0375-9393.20.14687-X]

16 **Fossé Q**, Poulard T, Niérat MC, Virolle S, Morawiec E, Hogrel JY, Similowski T, Demoule A, Gennisson JL, Bachasson D, Dres M. Ultrasound shear wave elastography for assessing diaphragm function in mechanically ventilated patients: a breath-by-breath analysis. *Crit Care* 2020; **24**: 669 [PMID: 33246478 DOI: 10.1186/s13054-020-03338-y]

World Journal of Clinical Cases

Submit a Manuscript: https://www.f6publishing.com

World J Clin Cases 2022 April 16; 10(11): 3547-3552

DOI: 10.12998/wjcc.v10.i11.3547

ISSN 2307-8960 (online)

CASE REPORT

Hypereosinophilic syndrome presenting as acute ischemic stroke, myocardial infarction, and arterial involvement: A case report

Ran-Ran Sun, Tuan-Zhi Chen, Min Meng

Specialty type: Cardiac and cardiovascular systems

Provenance and peer review: Unsolicited article; Externally peer reviewed.

Peer-review model: Single blind

Peer-review report's scientific quality classification

Grade A (Excellent): 0
Grade B (Very good): B
Grade C (Good): C
Grade D (Fair): 0
Grade E (Poor): 0

P-Reviewer: Lakusic N, Croatia; Shariati MBH, Iran

Received: October 30, 2021
Peer-review started: October 30, 2021
First decision: December 27, 2021
Revised: January 6, 2022
Accepted: February 27, 2022
Article in press: February 27, 2022
Published online: April 16, 2022

Ran-Ran Sun, Tuan-Zhi Chen, Department of Neurology, Liaocheng People's Hospital, Liaocheng 252000, Shandong Province, China

Min Meng, Department of Central Laboratory, Liaocheng People's Hospital, Liaocheng 252000, Shandong Province, China

Corresponding author: Min Meng, MS, Doctor, Department of Central Laboratory, Liaocheng People's Hospital, No. 67 Dongchang West Road, Liaocheng 252000, Shandong Province, China. mengmin2011@126.com

Abstract

BACKGROUND

Simultaneous cerebral and myocardial infarction with arterial involvement has not been reported in hypereosinophilic syndrome (HES). Here, we report a patient with HES that was also associated with acute ischemic stroke, myocardial infarction, and arterial involvement of the left common carotid artery, vertebral arteries, posterior cerebral artery, and coronary artery.

CASE SUMMARY

A 64-year-old male patient was admitted with headache and right lower extremity weakness. Laboratory tests indicated eosinophilia. Brain magnetic resonance imaging (MRI) showed bilateral and multiple acute infarcts in the border zones. Electrocardiography revealed that T wave was inverted and that the concentration of troponin I was significantly elevated above normal levels. Cardiac echocardiography showed an ejection fraction of 69% with mitral and tricuspid mild regurgitation. Computed tomography angiography detected multiple and localized instances of mild stenosis in the left common carotid artery bifurcation, bilateral vertebral arteries (V5 segment), and the posterior cerebral artery (P2 segment). These were observed together with multiple non-calcified and mixed plaques as well as luminal stenosis in the left circumflex artery, left anterior descending artery, and right coronary artery. The patient was treated with oral methylprednisolone and clopidogrel, after which the absolute eosinophil count fell rapidly to a normal level. After one month, a second brain MRI showed a partial reduction in the size and number of the lesions.

CONCLUSION

HES can masquerade as ischemic stroke, myocardial infarction, and arterial vascular involvement. The patient reported here recovered very quickly when his eosinophil blood count returned to normal. Early diagnosis and rapid reduction of

eosinophils may lead to a good prognosis.

Key Words: Hypereosinophilic syndrome; Ischemic stroke; Myocardial infarction; Arterial involvement; Case report

Core Tip: Hypereosinophilic syndrome (HES) is characterized by unexplained eosinophilia in the blood and tissues. Neurologic and cardiac involvement in patients with HES is common and variable. Eosinophil-mediated arterial vascular involvement is a rare manifestation of HES. This rare case of HES was accompanied by acute ischemic stroke, myocardial infarction and arterial vascular involvement. Early diagnosis and rapid reduction of eosinophils may lead to a good prognosis.

Citation: Sun RR, Chen TZ, Meng M. Hypereosinophilic syndrome presenting as acute ischemic stroke, myocardial infarction, and arterial involvement: A case report. *World J Clin Cases* 2022; 10(11): 3547-3552
URL: https://www.wjgnet.com/2307-8960/full/v10/i11/3547.htm
DOI: https://dx.doi.org/10.12998/wjcc.v10.i11.3547

INTRODUCTION

Hypereosinophilic syndrome (HES) is characterized by unexplained eosinophilia in the blood and tissues, and is associated with a variety of clinical manifestations[1]. It has long been thought that HES is associated with multiple organ dysfunctions, ranging from minor skin involvement to serious and even life-threatening cardiovascular, hematologic, and neurologic manifestations[2]. Neurologic involvement in patients with HES is common and highly variable, and includes the occurrence of peripheral neuropathy, encephalopathy, and stroke[3]. Cardiac involvement may lead to the development of thrombi, resulting a transient ischemic attack or embolic stroke with associated sequelae[4]. However, eosinophil-mediated arterial vascular involvement is a rare manifestation of HES. Most HES patients present with organ involvement showed normal cranial computed tomography angiogram (CTA) or magnetic resonance angiography[3,5,6]. Here, we report a rare case of HES accompanied by the simultaneous occurrence of acute ischemic stroke and myocardial infarction (MI), as well as arterial vascular involvement of the left common carotid artery, vertebral arteries, posterior cerebral artery, and coronary artery.

CASE PRESENTATION

Chief complaints

A 64-year-old male patient without any cerebrovascular risk factors was admitted to our hospital with a headache and right lower extremity weakness that lasted for two days.

History of present illness

The patient had a history of toothache, smoking, and alcohol consumption.

History of past illness

Until hospitalization, the patient was not burdened with any significant cardiovascular comorbidity.

Personal and family history

The patient had no pertinent family history of heart disease or other illnesses.

Physical examination

The results of a physical examination showed right lower extremity weakness (4-/5 strength) and dystaxia.

Laboratory examinations

Routine laboratory tests revealed significant leucocytosis (12.36 × 10^9/L) and an elevated eosinophil count (6.89 × 10^9/L, 55.7% of leukocytes) in the peripheral blood. The results of a blood clotting test, urine and stool routine examination, virus screening, liver and renal function examination, and

immunological function examination were normal. The antinuclear antibodies, anti-neutrophil cytoplasmic antibodies, and tumor markers were also negative. Molecular genetic analysis of fusion gene mutation (Fip1-like 1-platelet-derived growth factor receptor alpha) was also negative. Bone marrow aspirate results were compatible with HES, showing no sign of myelodysplasia, hemoparasite, or atypical cells. Cerebrospinal fluid analysis revealed that the levels of white blood cells, proteins, and glucose were normal. Acid-fast staining and India ink staining of cerebrospinal fluid were negative. Electrocardiography (ECG) revealed that the T wave was inverted and the concentration of troponin I (0.644 ng/mL) was significantly elevated. The clinical history and examination results of this patient showed no sign of parasitic infection, neoplasm, vasculitis, or allergy.

Imaging examinations

A CT scan of the chest was normal. Abdominal ultrasound revealed multiple hepatic cysts. Brain magnetic resonance imaging (MRI) detected bilateral and multiple acute infarcts in the border zones, which were located in the cortical and subcortical areas (Figure 1A-C). CTA of the head and neck revealed multiple and localized mild instances of stenosis in the left common carotid artery bifurcation, bilateral vertebral arteries (V5 segment), and posterior cerebral artery (P2 segment) (Figure 1D-F). Cardiac echocardiography showed an ejection fraction of 69% with mitral and tricuspid mild regurgitation. Coronary CTA showed multiple non-calcified, mixed plaques and luminal stenoses in the left circumflex artery, left anterior descending artery, and right coronary artery (Figure 1G-I). The results of cardiac examination supported the diagnosis of non-ST-elevated MI.

FINAL DIAGNOSIS

The patient was diagnosed with HES, accompanied with multiple cerebral infarctions and acute MI.

TREATMENT

The patient was treated with oral methylprednisolone (1 mg/kg/d) and clopidogrel (75 mg/d) for 7 d, and responded well to the treatment. The absolute eosinophil count (0.18×10^9/L, 1.8% of leukocytes) fell to a normal level within 7 d.

OUTCOME AND FOLLOW-UP

The patient was discharged after two weeks and continued taking low-dose prednisone. The ECG at discharge showed a normal T wave. The troponin I was 0.455 ng/mL during hospitalization and 0.012 ng/mL at discharge. After one month, a second brain MRI showed a partial reduction in the size and number of the lesions (Figure 2A-C). After one year, another brain MRI showed cerebromalacia in multiple areas of the lesions (Figure 2D-F). The follow-up of this patient was satisfactory in that he remained asymptomatic while on low-dose prednisone.

DISCUSSION

HES comprises a group of disorders characterized by the abnormal accumulation of eosinophils in the peripheral tissues or blood, independent of known secondary causes of eosinophilia (*e.g.*, parasitic infection)[4]. In 2010, new diagnostic criteria of HES were proposed: An absolute eosinophil count of more than 1500/mm^3 on at least two occasions or marked blood eosinophilia and prominent tissue eosinophilia associated with symptoms; exclusion of secondary causes of eosinophilia, such as neoplasms, hypoadrenalism, chemical- or drug-induced eosinophilia, allergic diseases, and viral or parasitic infection. Advances in diagnostic and therapeutic approaches have prompted a re-evaluation of the definition and classification of HES[7]. More than half of the patients with HES in one study (27 of 52) had neurologic dysfunction[8]. Stroke represents the most devastating neurological consequence of HES, which is characterized by a distinct pattern of both internal and external border zone infarcts[2].

In the patient reported here, eosinophilic involvement resulted in multiple cerebral infarctions and acute MI. Acute cerebral infarctions in the border zones were the first presenting symptom in this case. Meanwhile, the patient suffered from ischemic ECG changes, troponin I elevation, and mild valve regurgitation in echocardiography, which supported the diagnosis of MI. As a rare complication of HES, MI occurs as the result of endomyocardial fibrosis[9]. CTA of the head and neck, as well as the coronary artery showed multiple arterial stenoses in this case. Single arterial stenosis or occlusion has been only occasionally reported in patients with HES. Chang *et al*[10] reported a 43-year-old male patient with

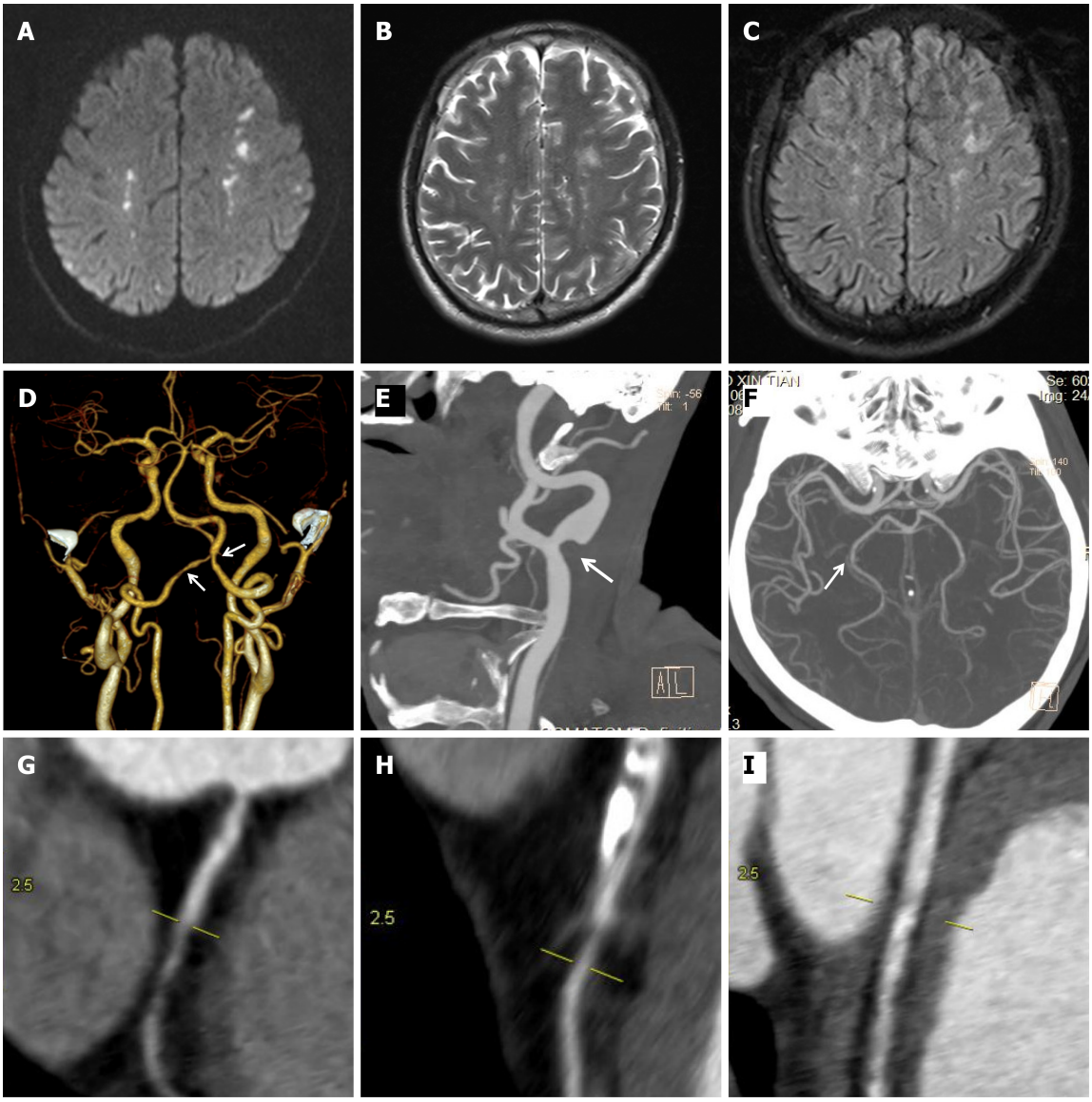

DOI: 10.12998/wjcc.v10.i11.3547

Figure 1 Brain magnetic resonance imaging and computed tomography angiography at admission. A: Diffusion-weighted magnetic resonance imaging (MRI); B: T2-weighted MRI; C: Fluid-attenuated inversion recovery revealed multiple acute infarcts in the bilateral border zones; D-I: Computed tomography angiogram (CTA) of the head and neck revealed mild stenosis in the (D) bilateral vertebral arteries, (E) left common carotid artery bifurcation, and (F) the posterior cerebral artery. Coronary CTA showed mild stenosis in the (G) right coronary artery, (H) left anterior descending artery, and (I) the left circumflex artery.

HES presenting with ischemic stroke and segmental stenosis of the right posterior cerebral artery resulting from direct eosinophilic toxicity. Li *et al*[11] described a middle-aged woman with idiopathic HES presenting with bilateral middle cerebral artery occlusion and progressive multiple cerebral infarction. Our patient suffered from multiple arterial vascular damage involving the left common carotid artery, vertebral arteries, posterior cerebral artery, and coronary artery. Eosinophilic toxicity to the vascular wall, *via* either arterial or venous vessels, was considered the pathological consequence of eosinophil accumulation[10]. Eosinophils have direct cytotoxic activity through the local release of toxic substances, including pro-inflammatory cytokines, reactive oxygen species, enzymes, arachidonic acid-derived factors, and cationic proteins[10,12].

The mechanism of eosinophilia-associated stroke remains unknown. The major etiology is cardiac embolism. More than half of cases with HES show a sign of cardiac involvement in echocardiography, which is a common source of thromboembolism with thrombi formation in damaged endocardium[13,14]. With the development of thromboembolism, patients with HES may experience a transient ischemic attack or embolic stroke as the initial presenting symptom[15]. Eosinophilia may damage the myocardium and endocardium, and therefore contribute to cardiac embolism by releasing eosinophilic granule contents, such as eosinophilic cationic protein and major basic protein[14]. Generally, eosinophilic myocarditis can be divided into three stages, which may occur simultaneously: (1) Acute necrosis/myocarditis stage-eosinophilic infiltration of the myocardium associated with myocardial necrosis due to the release of toxic cationic proteins from degranulated eosinophils; (2) thrombosis

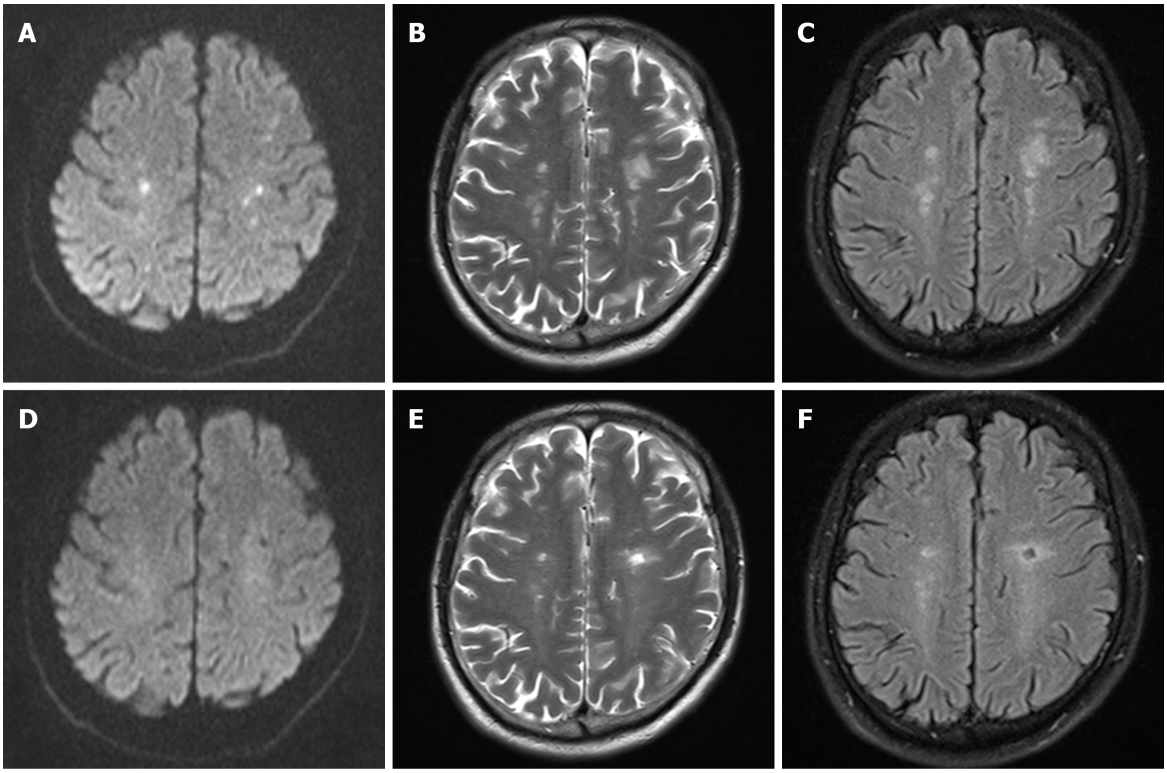

DOI: 10.12998/wjcc.v10.i11.3547

Figure 2 Brain magnetic resonance imaging during follow-up. A-C: Brain magnetic resonance imaging (MRI) at one month of follow-up showed a reduced size and number of lesions compared with the results at admission; D-F: Brain MRI at one year of follow-up showed cerebromalacia in multiple areas of the lesions.

stage-thrombosis at both ventricles where the ventricular outflow tract and subvalvular regions are associated with a significant risk of embolic complications; and (3) fibrotic stage-fibrosis replaces the thrombus formed on denuded myocardium and often requires surgical intervention[9,16]. The clinical records and laboratory tests of this case indicated that eosinophilia-induced cardioembolism and vascular wall damage may have been the main cause of cerebral infarction. Unfortunately, cardiac MRI and endocardial biopsy were not performed. Despite advances in noninvasive imaging methods (*e.g.*, echocardiography and cardiac MRI), endomyocardial biopsy remains the gold standard for the diagnosis of HES, especially in patients at the early stages of myocardial infiltration.

Corticosteroids are the most widely used medication to reduce eosinophil levels in patients with HES. If the patient presents with significant end-organ damage, corticosteroid treatment should be initiated immediately. An antiplatelet agent was used to reduce the risk of embolization in this case, however, the use of antiplatelet agents or anticoagulants alone is not recommended. The rapid reduction of eosinophil count is essential for preventing thromboembolic events and end-organ damage in patients at risk.

CONCLUSION

In conclusion, neurologic and cardiac complications occurred almost simultaneously in this case. Thus, the early diagnosis and treatment of HES are crucial for the prevention of widespread cardioembolism and subsequent irreversible, life-threatening cerebrovascular complications. Long-term follow-up and ongoing surveillance are important for monitoring the progression of the disease. Clinicians should be cognizant of HES patients presenting with cerebral infarction in the border zone. Early diagnosis and prompt treatment with corticosteroids are required.

FOOTNOTES

Author contributions: Sun RR and Chen TZ evaluated and managed the patient; Sun RR and Meng M prepared the figures; Meng M wrote and edited the manuscript; all authors read and approved the final manuscript.

Informed consent statement: Informed written consent was obtained from the patients for the publication of this

report and any accompanying images.

Conflict-of-interest statement: The authors declare that they have no conflict of interest.

CARE Checklist (2016) statement: The authors have read the CARE Checklist (2016), and the manuscript was prepared and revised according to the CARE Checklist (2016).

Country/Territory of origin: China

ORCID number: Ran-Ran Sun 0000-0002-1678-4917; Tuan-Zhi Chen 0000-0001-9866-9885; Min Meng 0000-0002-3055-7948.

S-Editor: Chen YL
L-Editor: A
P-Editor: Chen YL

REFERENCES

1 **Kahn JE**, Groh M, Lefèvre G. (A Critical Appraisal of) Classification of Hypereosinophilic Disorders. *Front Med (Lausanne)* 2017; **4**: 216 [PMID: 29259972 DOI: 10.3389/fmed.2017.00216]
2 **Rosenberg J**, Aamodt W, Takvorian S, Mullen M. Clinical Reasoning: A young woman with symmetric weakness and behavioral disturbance. *Neurology* 2018; **90**: e1442-e1447 [PMID: 29661906 DOI: 10.1212/WNL.0000000000005335]
3 **Chen H**, Raza HK, Jing J, Shen D, Xu P, Zhou S, Zu J, Yang X, Zhang W, Zhang S, Hua F, Cui G. Hypereosinophilic syndrome with central nervous system involvement: Two case reports and literature review. *Brain Inj* 2017; **31**: 1695-1700 [PMID: 28945486 DOI: 10.1080/02699052.2017.1357835]
4 **Curtis C**, Ogbogu P. Hypereosinophilic Syndrome. *Clin Rev Allergy Immunol* 2016; **50**: 240-251 [PMID: 26475367 DOI: 10.1007/s12016-015-8506-7]
5 **Psychogios K**, Evmorfiadis I, Dragomanovits S, Stavridis A, Takis K, Kaklamanis L, Stathis P. ANCA-Negative Churg-Strauss Syndrome Presenting as Acute Multiple Cerebral Infarcts: A Case Report. *J Stroke Cerebrovasc Dis* 2017; **26**: e47-e49 [PMID: 28065613 DOI: 10.1016/j.jstrokecerebrovasdis.2016.12.009]
6 **Rohmer J**, Groh M, Samson M, London J, Jachiet M, Rouzaud D, Paule R, Suarez F, Lefèvre G, Cohen F, Lambotte O, Perlat A, Bielefeld P, Guillevin L, Kahn JE, Terrier B; French Vasculitis Study Group (FVSG). Distal ischemia as the initial presentation of hypereosinophilic syndrome-related arterial involvement: A case study and literature review. *Autoimmun Rev* 2019; **18**: 828-830 [PMID: 31176876 DOI: 10.1016/j.autrev.2019.06.004]
7 **Simon HU**, Rothenberg ME, Bochner BS, Weller PF, Wardlaw AJ, Wechsler ME, Rosenwasser LJ, Roufosse F, Gleich GJ, Klion AD. Refining the definition of hypereosinophilic syndrome. *J Allergy Clin Immunol* 2010; **126**: 45-49 [PMID: 20639008 DOI: 10.1016/j.jaci.2010.03.042]
8 **Moore PM**, Harley JB, Fauci AS. Neurologic dysfunction in the idiopathic hypereosinophilic syndrome. *Ann Intern Med* 1985; **102**: 109-114 [PMID: 2981493 DOI: 10.7326/0003-4819-102-1-109]
9 **Ogbogu PU**, Rosing DR, Horne MK 3rd. Cardiovascular manifestations of hypereosinophilic syndromes. *Immunol Allergy Clin North Am* 2007; **27**: 457-475 [PMID: 17868859 DOI: 10.1016/j.iac.2007.07.001]
10 **Chang WL**, Lin HJ, Cheng HH. Hypereosinophilic syndrome with recurrent strokes: a case report. *Acta Neurol Taiwan* 2008; **17**: 184-188 [PMID: 18975525]
11 **Li QF**, Zhang Q, Huang YF, Zhang ZX. Acute progressive stroke with middle cerebral artery occlusion caused by idiopathic hypereosinophilic syndrome: a case report. *BMC Neurol* 2020; **20**: 361 [PMID: 33003998 DOI: 10.1186/s12883-020-01941-8]
12 **Roufosse F**, Cogan E, Goldman M. The hypereosinophilic syndrome revisited. *Annu Rev Med* 2003; **54**: 169-184 [PMID: 12525672 DOI: 10.1146/annurev.med.54.101601.152431]
13 **Ommen SR**, Seward JB, Tajik AJ. Clinical and echocardiographic features of hypereosinophilic syndromes. *Am J Cardiol* 2000; **86**: 110-113 [PMID: 10867107 DOI: 10.1016/s0002-9149(00)00841-9]
14 **Rezaizadeh H**, Sanchez-Ross M, Kaluski E, Klapholz M, Haider B, Gerula C. Acute eosinophilic myocarditis: diagnosis and treatment. *Acute Card Care* 2010; **12**: 31-36 [PMID: 20201659 DOI: 10.3109/17482940903578998]
15 **Spry CJ**, Davies J, Tai PC, Olsen EG, Oakley CM, Goodwin JF. Clinical features of fifteen patients with the hypereosinophilic syndrome. *Q J Med* 1983; **52**: 1-22 [PMID: 6878618]
16 **Cheung CC**, Constantine M, Ahmadi A, Shiau C, Chen LYC. Eosinophilic Myocarditis. *Am J Med Sci* 2017; **354**: 486-492 [PMID: 29173361 DOI: 10.1016/j.amjms.2017.04.002]

World Journal of Clinical Cases

Submit a Manuscript: https://www.f6publishing.com

World J Clin Cases 2022 April 16; 10(11): 3553-3560

DOI: 10.12998/wjcc.v10.i11.3553

ISSN 2307-8960 (online)

CASE REPORT

Cytochrome P450 family 17 subfamily A member 1 mutation causes severe pseudohermaphroditism: A case report

Yu Gong, Fang Qin, Wen-Jia Li, Le-Yu Li, Ping He, Xing-Jian Zhou

Specialty type: Medicine, research and experimental

Provenance and peer review: Unsolicited article; Externally peer reviewed.

Peer-review model: Single blind

Peer-review report's scientific quality classification

Grade A (Excellent): 0
Grade B (Very good): 0
Grade C (Good): C, C
Grade D (Fair): 0
Grade E (Poor): 0

P-Reviewer: Son TQ, Viet Nam; Velázquez-Saornil J, Spain

Received: November 5, 2021
Peer-review started: November 5, 2021
First decision: December 27, 2021
Revised: January 29, 2022
Accepted: February 27, 2022
Article in press: February 27, 2022
Published online: April 16, 2022

Yu Gong, Fang Qin, Wen-Jia Li, Le-Yu Li, Ping He, Xing-Jian Zhou, Department of Endocrine and Metabolism, Xiangyang No. 1 People's Hospital, Hubei University of Medicine, Xiangyang 441000, Hubei Province, China

Corresponding author: Xing-Jian Zhou, MD, Chief Doctor, Department of Endocrine and Metabolism, Xiangyang No. 1 People's Hospital, Hubei University of Medicine, No. 15 Jiefang Road, Fancheng District, Xiangyang 441000, Hubei Province, China. hazck147@163.com

Abstract

BACKGROUND

17α-Hydroxylase deficiency (17-OHD) is a rare form of congenital adrenal hyperplasia, characterized by hypertension, hypokalemia, and gonadal dysplasia. However, due to the lack of a comprehensive understanding of this disease, it is prone to misdiagnosis and missed diagnosis, and there is no complete cure.

CASE SUMMARY

We report a female patient with 17-OHD. The patient was admitted to the Department of Neurology of our hospital due to limb weakness. During treatment, it was found that the patient's condition was difficult to correct except for hypokalemia, and her blood pressure was difficult to control with various antihypertensive drugs. She was then transferred to our department for further treatment. On physical examination, the patient's gonadal development was found to be abnormal, and chromosome analysis demonstrated karyotype 46,XY. Considering the possibility of 17-OHD, the cytochrome P450 family 17 subfamily A member 1 (*CYP17A1*) test was performed to confirm the diagnosis.

CONCLUSION

The clinical manifestations of 17-OHD are complex. Hormone determination, imaging examination, chromosome determination and *CYP17A1* gene test are helpful for early diagnosis.

Key Words: Congenital adrenal cortex hyperplasia; Cytochrome P450 family 17 subfamily A member 1; 17α-Hydroxylase deficiency; Pseudohermaphroditism; Case report

Core Tip: 17α-Hydroxylase deficiency (17-OHD) is a rare form of congenital adrenal hyperplasia, characterized by hypertension, hypokalemia, and gonadal dysplasia. We report a case of 17-OHD admitted to our hospital due to limb weakness. The patient's blood pressure was difficult to control with various antihypertensive drugs. Her gonadal development was found to be abnormal, and chromosome analysis demonstrated karyotype 46,XY. The diagnosis was confirmed by the cytochrome P450 family 17 subfamily A member 1 (*CYP17A1*) test. The clinical manifestations of 17-OHD are complex. Hormone determination, imaging examination, chromosome determination and *CYP17A1* gene detection are helpful for early diagnosis.

Citation: Gong Y, Qin F, Li WJ, Li LY, He P, Zhou XJ. Cytochrome P450 family 17 subfamily A member 1 mutation causes severe pseudohermaphroditism: A case report. *World J Clin Cases* 2022; 10(11): 3553-3560
URL: https://www.wjgnet.com/2307-8960/full/v10/i11/3553.htm
DOI: https://dx.doi.org/10.12998/wjcc.v10.i11.3553

INTRODUCTION

17α-Hydroxylase deficiency (17-OHD) is a rare type of congenital adrenal hyperplasia (CAH), which is caused by mutations in the cytochrome P450 family 17 subfamily A member 1 (*CYP17A1*) gene, and the incidence of this disorder is approximately 1 in 50000[1]. In 1966, Biglieri *et al*[2] reported the first case of 17-OHD. To date, about 200 cases have been reported at worldwide[3-5]. At present, there is no unified standard for the diagnosis of 17-OHD, which is mainly based on the clinical manifestations, laboratory and imaging examinations, *etc*., and the diagnosis depends on the detection of gene *CYP17A1*[6]. We here report a patient with 17-OHD admitted to our hospital, and review the literature on the pathogenesis, clinical characteristics, diagnosis and treatment of the disease.

CASE PRESENTATION

Chief complaints

A 29-year-old female was admitted to the Department of Neurology in our hospital due to limb weakness for 1 d.

History of present illness

The patient had a history of syncope on several occasions, which lasted approximately 1 min and could be relieved without treatment.

History of past illness

She denied other medical history such as hypertension or coronary heart disease and had no history of smoking or alcohol consumption.

Personal and family history

Upon further investigation, the patient had primary amenorrhea and was unmarried and childless. Her parents were first cousins and her older brother was healthy.

Physical examination

At admission, her temperature was 36.5 °C, respiration rate was 23 breaths/min, pulse rate was 114 bpm, blood pressure was 184/127 mmHg, height was 180 cm, weight was 69 kg, and body mass index was 21.3 kg/m^2. The patient's breast development had only progressed to Tanner stage 1, and her vulva was similar to that of a female infant. The patient's pubic and axillary hair was undeveloped, and her Adam's apple was small. Pathological reflexes were not elicited (Figure 1).

Laboratory examinations

After admission, low serum potassium levels (2.26 mmol/L) were observed and appeared to be uncorrected after potassium supplementation. In addition, the patient had constant high blood pressure, with a maximum reading of 184/127 mmHg.

Imaging examinations

The results of the patient's biochemical and imaging examinations are shown in Figure 2 and Tables 1 and 2. Genetic analysis (Figure 3) showed homozygous mutations in the CYP17A1 gene (NM_000102.3:

Table 1 The biochemical examinations of the patient

Projects	Results	Reference range
Potassium (mmol/L)	2.26	3.5-5.5
Renin (mIU/L)	< 0.5	2.8-39.9
Aldosterone (ng/dL)	3.69	0-23.6
Angiotension II (pg/ml)	39.1	25-129
FSH (mIU/mL)	38.97	Follicular phase: 3.03-8.08; Ovulatory phase: 2.55-16.69; Luteal phase: 0.9-16.69; Postmenopausal: 26.7-133.4
LH (mIU/mL)	14.49	Follicular phase: 1.8-11.78; Ovulatory phase: 7.59-89.08; Luteal phase: 0.56-14; Postmenopausal: 5.16-61.99
Progesterone (ng/mL)	5.5	Follicular phase: < 0.1-0.3; Luteal phase: 1.20-15.9; Postmenopausal: < 0.1-0.2
Estradiol (pg/mL)	< 10	Follicular phase: 21-251; Luteal phase: 38-649; Postmenopausal: 21-312
Testosterone (ng/dL)	0.18	Male (21-49 yr): 2.4-8.71; Female (21-49 yr): 0.14-0.53
Cortisol (nmol/L)		
0 a.m.	83.46	45-135
8 a.m.	170.11	120-660
4 p.m.	106.01	55-200
ACTH (pmol/L)		
0 a.m.	8.54	0.4-4.0
8 a.m.	112.85	1.5-14.1
4 p.m.	27.15	0.95-9.5
Dehydroepiandrosterone-S (μg/dL)	17.80	95-510
GH (ng/mL)	0.648	< 8
Urine cortisol for 24 h (μg/24 h)	17.33	19.30-317.50
Urinary potassium 24 h (mmol/24 h)	204.5	25-100
Karyotype	46,*XY*	

FSH: Follicle-stimulating hormone; LH: Luteinizing hormone; ACTH: Aadreno-cortico-tropic-hormone; GH: Growth hormone.

Table 2 The imaging examinations of the patient

Projects	Results
Plain CT scan of adrenal	Bilateral multiple adrenal lesions were considered to be multiple myeloid lipomas or diffuse adrenal hyperplasia
Enhanced CT scan of adrenal	Bilateral multiple adrenal lesions were considered to be multiple myeloid lipomas
Plain MRI scan of pituitary gland	Normal
X-ray examination of both hands	The epiphyses of the fingers, metacarpal and distal ulna and radius of both hands were not healed
Ultrasonography of the pelvis	No obvious uterine echo was observed
Plain MRI scan of the pelvis	No obvious cryptorchidism and uterine accessory tissues were observed

CT: Computed tomography; MRI: Magnetic resonance imaging.

c.81C>A (p. Tyr27*)). These genetic variations have been reported by Müssig *et al*[7] and Keskin *et al*[8]. Genetic analysis of the patient showed a heterozygous mutation (c.81C>A). Unfortunately, we were unable to perform a genetic analysis of the patient's older brother, as he was unavailable at the time of testing.

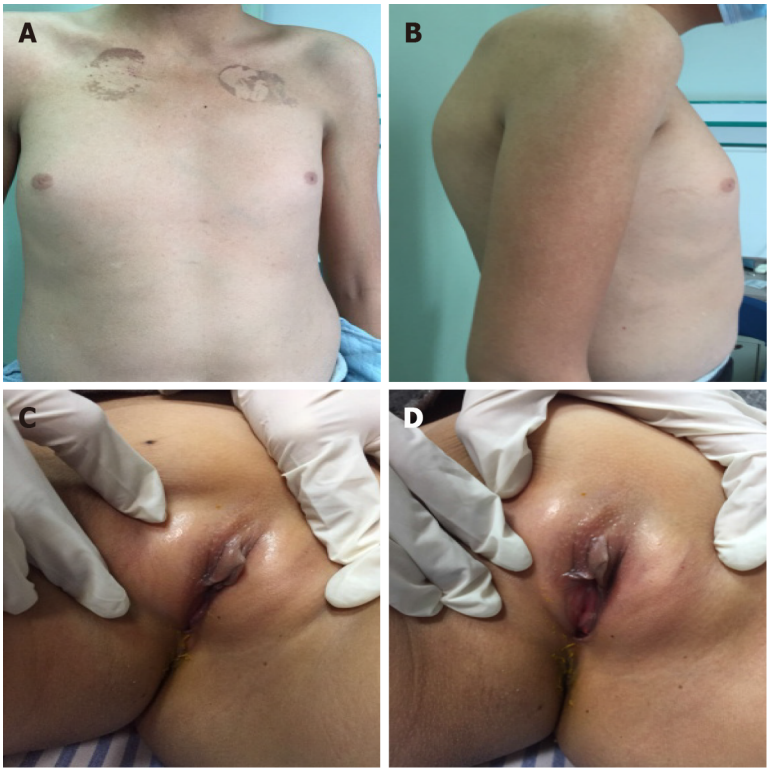

DOI: 10.12998/wjcc.v10.i11.3553

Figure 1 Physical examinations. A and B: The patient showed absence of breast development and axillary hair; C and D: The patient's vulva was similar to that of a female infant and had no pubic hair.

FINAL DIAGNOSIS

The clinical manifestations of this patient combined with the results of various auxiliary examinations, resulted in a final diagnosis of 17-OHD associated with multiple myeloid lipomas of the adrenal gland.

TREATMENT

Following the diagnosis of 17-OHD, the patient started on oral dexamethasone (0.75 mg/d), which will be a lifelong medication. When her blood pressure and potassium level had returned to normal, she was discharged from the hospital.

OUTCOME AND FOLLOW-UP

One year later, the patient's electrolytes (serum potassium level 4.6 mmol/L) and blood pressure (130/75 mmHg) were normal on re-examination.

DISCUSSION

CAH is an autosomal recessive disorder caused by mutations in the genes encoding essential enzymes for the synthesis of corticosteroids. As a result of the imbalance between glucocorticoids and mineralocorticoids, this leads to metabolic disorders, and thus morbidity and mortality in these patients are very high[9]. The enzymes involved include 21-hydroxylase, 11β-hydroxylase, 17α-hydroxylase, 3β-hydroxysteroid dehydrogenase/isomerase *etc*. These enzyme defects (reduced or absent activity) can lead to CAH, but with different clinical manifestations[10]. Of these enzymes, 21-hydroxylase deficiency is the most common, accounting for more than 95% of cases[11], followed by 11β-hydroxylase deficiency. 17-OHD accounts for about 1% of all CAH cases, with an estimated incidence of 1 in 50000 to 100000[12,13].

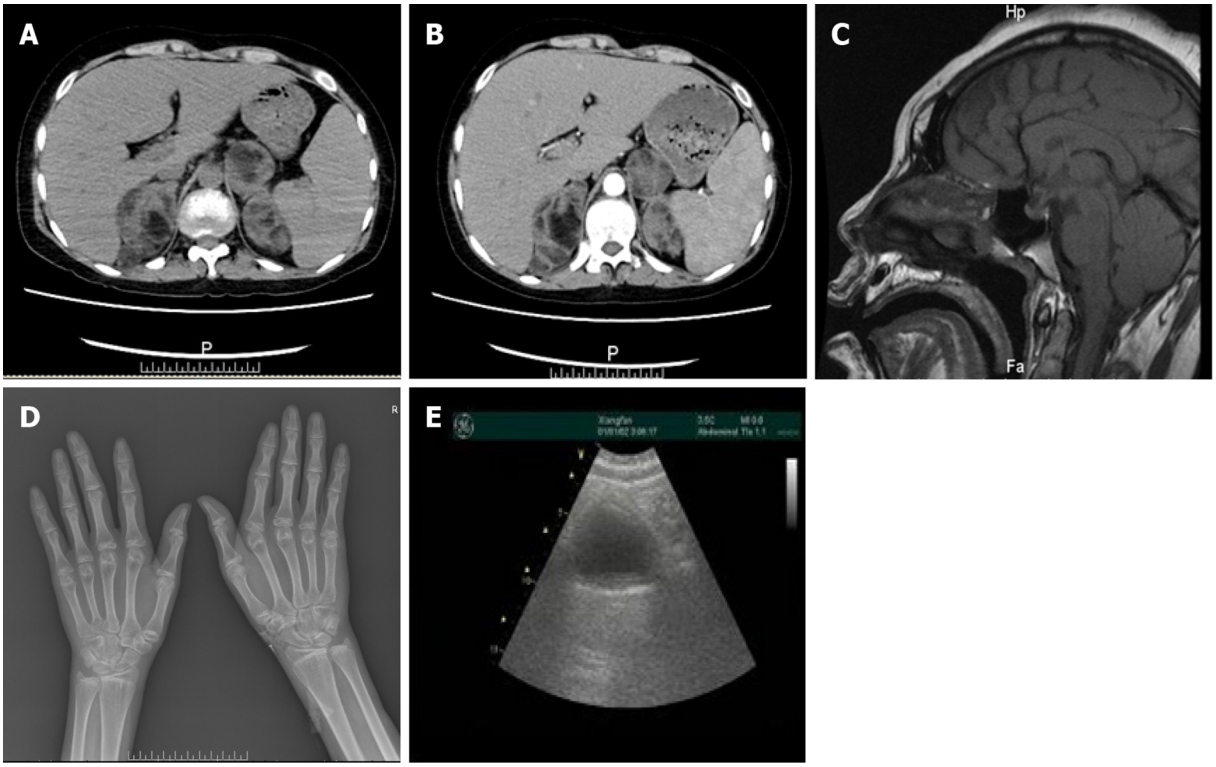

DOI: 10.12998/wjcc.v10.i11.3553

Figure 2 Imaging examinations. A: Plain computed tomography (CT) scan of adrenals; B: Enhanced CT scan of adrenals; C: Plain magnetic resonance imaging scan of the pituitary gland; D: X-ray examination of both hands; E: Ultrasonography of the pelvis.

17-OHD mainly manifests as hypertension, hypokalemia and abnormal sexual development. *CYP17A1* encodes an enzyme with 17a-hydroxylase and 17,20-lyase activities, which is essential for the normal production of adrenal and gonadal glands[14]. When it is deficient, pregnenolone cannot translate into 17-hydroxyprogesterone and 17-hydroxylpregnenolone, resulting in the impairment of cortisol and gonadal hormones (including testosterone and estrogen)[13]. Cortisol synthesis disorders lead to an increase in adrenocorticotropic hormone (ACTH) feedback, which further activates the 17-deoxy pathway of the zona fasciculata, producing overstimulation of this pathway and increasing progesterone, corticosterone and deoxycorticosterone (DOC) synthesis. The excessive levels of these hormones then lead to hypertension, and hypokalemia. Deficiency of gonadal hormones causes primary amenorrhea in women[15] and feminization of external genitalia in men[16]. Sexual dysplasia[6] in male patients mostly manifests as pseudohermaphroditism, with infantile female genitalia and a blind end vagina, while the internal genitalia is of the male type with small testicles and dysplasia, and external genitals are difficult to distinguish, such as small penis or mammary gland development. Female patients can be normal at birth, but do not develop secondary sexual signs with primary amenorrhea. There is no pubic or axillary hair growth in both men and women. After puberty, both follicle-stimulating hormone and luteinizing hormone are significantly increased. Due to the lag in bone age, the patient's height continues to increase slowly after reaching adulthood. The bone age of our patient was below the actual age, but she was tall (180.0 cm). In addition, some patients are prone to fatigue, infection, different degrees of skin pigmentation[17] and osteoporosis. The diversity of clinical manifestations in 17-OHD patients is due to the different mutation sites on the gene encoding the enzyme and different effects on the enzyme function. Therefore, in the clinic, the existence of hypertension, and hypokalemia accompanied by sexual dysplasia, should be considered as possible 17-OHD. This deficiency should be distinguished from several other diseases, such as 5α-reductase deficiency, androgen insensitivity syndrome and 3β-hydroxysteroid dehydrogenase deficiency. However, both 5α-reductase deficiency and androgen insensitivity syndrome are generally not accompanied by hypertension and hypokalemia[18,19], and the clinical manifestations in this case did not meet the criteria for 3 β-hydroxysteroid dehydrogenase deficiency[20]. Hence, we were able to rule out these diseases.

There is no complete cure for 17-OHD, and treatment mainly consists of appropriate glucocorticoid and sex steroid hormone supplementation, social sex selection and psychological interventions. Low-dose glucocorticoid (dexamethasone or prednisolone) replacement therapy is administered in order to decrease and normalize the blood levels of 11-DOC and ACTH, which can normalize blood pressure and electrolyte imbalances[21]. However, due to the need to avoid high-dose glucocorticoid therapy and complete inhibition of the hypothalamic–pituitary–adrenal axis, DOC cannot be completely suppressed,

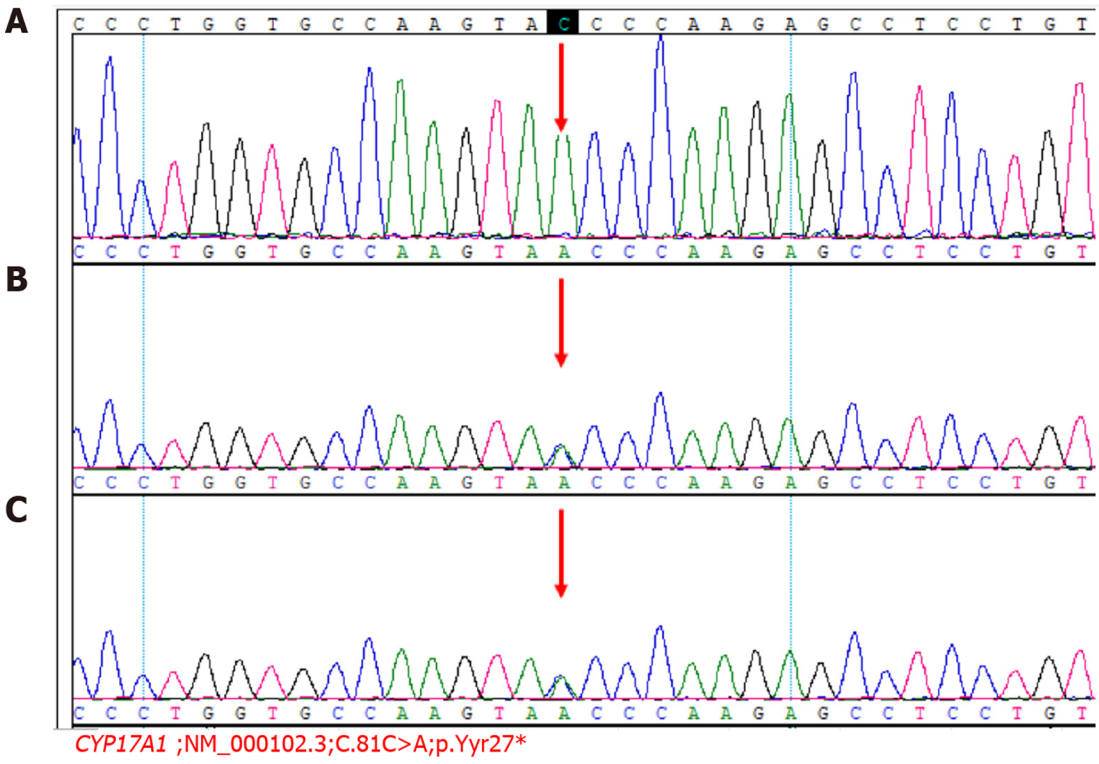

DOI: 10.12998/wjcc.v10.i11.3553

Figure 3 Cytochrome P450 family 17 subfamily A member 1 gene analysis. A: The patient; B: Her father; C: Her mother.

and many patients will eventually become hypertensive, and corticosteroid receptor antagonists or calcium channel blockers can be used to control blood pressure[11]. Therefore, during treatment, spironolactone and nifedipine sustained release tablets are given to control blood pressure. In addition, sex hormone replacement is required for breast and uterus development and to maintain female sexual characteristics. Patients require estrogen and progestin circulation therapy to induce circulatory arrest bleeding and prevent endometrial hyperplasia. If the patient decides to be considered male, androgen replacement therapy may be given, and extensive genital reconstructive surgery may be performed, such as gonadectomy, to avoid malignant degeneration of the testes within the abdomen[13]. In this case, after full communication with the patient and her family, she decided to temporarily discontinue sex hormones and surgical treatment.

CONCLUSION

In summary, 17-OHD is extremely rare in clinical practice, and is prone to misdiagnosis and missed diagnosis. For patients with abnormal development of hypertension and hypokalemia, attention should be paid to the differentiation of this disease. Chromosome karyotype analysis and gene sequencing can help in diagnosis. Hormone replacement and antihypertensive treatment should be given as soon as possible after diagnosis. In addition, the psychological state of patients should be closely monitored.

FOOTNOTES

Author contributions: Gong Y and Qin F treated the patient; Zhou XJ drafted the manuscript; Li WJ and Li LY participated in the analysis and the interpretation of the data; He P critically revised the manuscript; all authors approved the final manuscript as submitted and agree to be accountable for all aspects of the work.

Informed consent statement: Informed written consent was obtained from the patient for publication of this report and any accompanying images.

Conflict-of-interest statement: The authors declare that they have no conflict of interest.

CARE Checklist (2016) statement: The authors have read the CARE Checklist (2016), and the manuscript was prepared and revised according to the CARE Checklist (2016).

Country/Territory of origin: China

ORCID number: Yu Gong 0000-0001-7246-0637; Fang Qin 0000-0003-1173-2592; Wen-Jia Li 0000-0001-9609-968X; Le-Yu Li 0000-0002-4500-932X; Ping He 0000-0002-8060-6840; Xing-Jian Zhou 0000-0001-9432-111X.

S-Editor: Gao CC
L-Editor: A
P-Editor: Gao CC

REFERENCES

1 **Zhou Y**, Xue X, Shi P, Lu Q, Lv S. Multidisciplinary team management of 46,XY 17α-hydroxylase deficiency: a case report and literature review. *J Int Med Res* 2021; **49**: 300060521993965 [PMID: 33761789 DOI: 10.1177/0300060521993965]
2 **Biglieri EG**, Herron MA, Brust N. 17-hydroxylation deficiency in man. *J Clin Invest* 1966; **45**: 1946-1954 [PMID: 4288776 DOI: 10.1172/JCI105499]
3 **Fontenele R**, Costa-Santos M, Kater CE. 17α-hydroxylase deficiency is an underdiagnosed disease: high frequency of misdiagnoses in a large cohort of Brazilian patients. *Endocr Pract* 2018; **24**: 170-178 [PMID: 29144824 DOI: 10.4158/EP171987.OR]
4 **Hannah-Shmouni F**, Chen W, Merke DP. Genetics of Congenital Adrenal Hyperplasia. *Endocrinol Metab Clin North Am* 2017; **46**: 435-458 [PMID: 28476231 DOI: 10.1016/j.ecl.2017.01.008]
5 **Carvalho LC**, Brito VN, Martin RM, Zamboni AM, Gomes LG, Inácio M, Mermejo LM, Coeli-Lacchini F, Teixeira VR, Gonçalves FT, Carrilho AJ, Del Toro Camargo KY, Finkielstain GP, Taboada GF, Frade Costa EM, Domenice S, Mendonca BB. Clinical, hormonal, ovarian, and genetic aspects of 46,XX patients with congenital adrenal hyperplasia due to CYP17A1 defects. *Fertil Steril* 2016; **105**: 1612-1619 [PMID: 26920256 DOI: 10.1016/j.fertnstert.2016.02.008]
6 **Beştaş A**, Bolu S, Unal E, Aktar Karakaya A, Eröz R, Tekin M, Haspolat YK. A rare cause of delayed puberty and primary amenorrhea: 17α-hydroxylase enzyme deficiency. *Endocrine* 2021 [PMID: 34724156 DOI: 10.1007/s12020-021-02914-8]
7 **Müssig K**, Kaltenbach S, Machicao F, Maser-Gluth C, Hartmann MF, Wudy SA, Schnauder G, Häring HU, Seif FJ, Gallwitz B: 17alpha-hydroxylase/17, 20-lyase deficiency caused by a novel homozygous mutation (Y27Stop) in the cytochrome CYP17 gene. *J Pediatr Endocrinol Metab* 2005; **90**: 4362-4365 [PMID: 15811924 DOI: 10.1210/jc.2005-0136]
8 **Keskin M**, Uğurlu AK, Savaş-Erdeve Ş, Sağsak E, Akyüz SG, Çetinkaya S, Aycan Z: 17α-Hydroylase/17, 20-lyase deficiency related to P. Y27*(c.81C>A) mutation in CYP17A1 gene. *J Pediatr Endocrinol Metab* 2015; **28**: 919-921 [PMID: 25719302 DOI: 10.1515/jpem-2014-0444]
9 **Espinosa-Herrera F**, Espín E, Tito-Álvarez AM, Beltrán LJ, Gómez-Correa D, Burgos G, Llamos A, Zurita C, Rojas S, Dueñas-Espín I, Cueva-Ludeña K, Salazar-Vega J, Pinto-Basto J. A report of congenital adrenal hyperplasia due to 17α-hydroxylase deficiency in two 46,XX sisters. *Gynecol Endocrinol* 2020; **36**: 24-29 [PMID: 31464148 DOI: 10.1080/09513590.2019.1650342]
10 **Chatziaggelou A**, Sakkas EG, Votino R, Papagianni M, Mastorakos G. Assisted Reproduction in Congenital Adrenal Hyperplasia. *Front Endocrinol (Lausanne)* 2019; **10**: 723 [PMID: 31708872 DOI: 10.3389/fendo.2019.00723]
11 **El-Maouche D**, Arlt W, Merke DP. Congenital adrenal hyperplasia. *Lancet* 2017; **390**: 2194-2210 [PMID: 28576284 DOI: 10.1016/S0140-6736(17)31431-9]
12 **Fleming L**, Van Riper M, Knafl K. Management of Childhood Congenital Adrenal Hyperplasia-An Integrative Review of the Literature. *J Pediatr Health Care* 2017; **31**: 560-577 [PMID: 28416079 DOI: 10.1016/j.pedhc.2017.02.004]
13 **Xu S**, Hu S, Yu X, Zhang M, Yang Y. 17αhydroxylase/17,20lyase deficiency in congenital adrenal hyperplasia: A case report. *Mol Med Rep* 2017; **15**: 339-344 [PMID: 27959413 DOI: 10.3892/mmr.2016.6029]
14 **Xia Y**, Shi P, Xia J, Zhang H, Xu L, Kong X. Novel mutations of the CYP17A1 gene in four Chinese 46,XX cases with partial 17a-hydroxylase/17,20-lyase deficiency. *Steroids* 2021; **173**: 108873 [PMID: 34097983 DOI: 10.1016/j.steroids.2021.108873]
15 **Kim SM**, Rhee JH. A case of 17 alpha-hydroxylase deficiency. *Clin Exp Reprod Med* 2015; **42**: 72-76 [PMID: 26161337 DOI: 10.5653/cerm.2015.42.2.72]
16 **Auchus RJ**. Steroid 17-hydroxylase and 17,20-lyase deficiencies, genetic and pharmacologic. *J Steroid Biochem Mol Biol* 2017; **165**: 71-78 [PMID: 26862015 DOI: 10.1016/j.jsbmb.2016.02.002]
17 **Oh YK**, Ryoo U, Kim D, Cho SY, Jin DK, Yoon BK, Lee DY, Choi D. 17α-hydroxlyase/17, 20-lyase deficiency in three siblings with primary amenorrhea and absence of secondary sexual development. *J Pediatr Adolesc Gynecol* 2012; **25**: e103-e105 [PMID: 22841373 DOI: 10.1016/j.jpag.2012.05.008]
18 **Han B**, Cheng T, Zhu H, Yu J, Zhu WJ, Song HD, Yao H, Qiao J. Genetic Analysis of 25 Patients with 5α-Reductase Deficiency in Chinese Population. *Biomed Res Int* 2020; **2020**: 1789514 [PMID: 32596280 DOI: 10.1155/2020/1789514]
19 **Tyutyusheva N**, Mancini I, Baroncelli GI, D'Elios S, Peroni D, Meriggiola MC, Bertelloni S. Complete Androgen

Insensitivity Syndrome: From Bench to Bed. *Int J Mol Sci* 2021; **22** [PMID: 33514065 DOI: 10.3390/ijms22031264]

20 **Guran T**, Kara C, Yildiz M, Bitkin EC, Haklar G, Lin JC, Keskin M, Barnard L, Anik A, Catli G, Guven A, Kirel B, Tutunculer F, Onal H, Turan S, Akcay T, Atay Z, Yilmaz GC, Mamadova J, Akbarzade A, Sirikci O, Storbeck KH, Baris T, Chung BC, Bereket A. Revisiting Classical 3β-hydroxysteroid Dehydrogenase 2 Deficiency: Lessons from 31 Pediatric Cases. *J Clin Endocrinol Metab* 2020; **105** [PMID: 31950145 DOI: 10.1210/clinem/dgaa022]

21 **Soveid M Md**, Rais-Jalali GA Md. Seventeen Alpha-Hydroxylase Deficiency Associated with Absent Gonads and Myelolipoma: A Case Report and Review of Literature. *Iran J Med Sci* 2016; **41**: 543-547 [PMID: 27853336]

World Journal of Clinical Cases

Submit a Manuscript: https://www.f6publishing.com

World J Clin Cases 2022 April 16; 10(11): 3561-3572

DOI: 10.12998/wjcc.v10.i11.3561

ISSN 2307-8960 (online)

CASE REPORT

Patellar dislocation following distal femoral replacement after extra-articular knee resection for bone sarcoma: A case report

Yuta Kubota, Kazuhiro Tanaka, Masashi Hirakawa, Tatsuya Iwasaki, Masanori Kawano, Ichiro Itonaga, Hiroshi Tsumura

Specialty type: Orthopedics

Provenance and peer review: Unsolicited article; Externally peer reviewed.

Peer-review model: Single blind

Peer-review report's scientific quality classification

Grade A (Excellent): A
Grade B (Very good): B
Grade C (Good): 0
Grade D (Fair): 0
Grade E (Poor): 0

P-Reviewer: Ghimire R, Nepal; Wang YJ, China

Received: November 8, 2021
Peer-review started: November 8, 2021
First decision: December 27, 2021
Revised: January 9, 2022
Accepted: February 27, 2022
Article in press: February 27, 2022
Published online: April 16, 2022

Yuta Kubota, Kazuhiro Tanaka, Masashi Hirakawa, Tatsuya Iwasaki, Masanori Kawano, Ichiro Itonaga, Hiroshi Tsumura, Orthopaedic Surgery, Oita University, Yufu City 879-5593, Oita, Japan

Corresponding author: Kazuhiro Tanaka, MD, Associate Professor, Orthopaedic Surgery, Oita University, 1-1 Idaigaoka, Hasama, Yufu City 879-5593, Oita, Japan. ktanaka@oita-u.ac.jp

Abstract

BACKGROUND

For the treatment of bone sarcoma in the distal femur, wide-margin resection and knee reconstruction with tumor endoprosthesis are standard therapies. Extra-articular knee resection is required in cases of tumor invasion of the knee joint; however, the incidence of complications, such as aseptic loosening, prosthesis infection, and implant failure, is higher than that following intra-articular knee resection. To the best of our knowledge, there are three reports of patellar dislocations after replacement of a tumor endoprosthesis.

CASE SUMMARY

A 36-year-old man with no significant past medical history was admitted to our institution with continuous pain in his left knee for 4 mo. An open biopsy was performed, and the patient was diagnosed with a left distal femoral malignant bone tumor. Extra-articular knee resection and knee reconstruction with a tumor endoprosthesis were performed. Although the alignment of the tumor prosthesis was acceptable, knee instability was noticed postoperatively. The axial radiographic view of the patellar and computed tomography showed lateral patellar dislocation at 4 wk postoperatively. The patient had to undergo a lateral release and proximal realignment. He could perform his daily activities at 9 mo postoperatively. Radiography revealed no patellar re-dislocation.

CONCLUSION

Proximal realignment may be considered during primary surgery if there is an imbalance in the forces controlling the patellar tracking.

Key Words: Bone tumor; Distal femoral replacement; Lateral release; Patellar dislocation; Proximal realignment; Case report

Core Tip: Extra-articular knee resection is required in cases of tumor invasion of the knee joint. To the best of our knowledge, there are three reports of patellar dislocations after replacement of tumor endoprosthesis. We report a case of patellar dislocation after extra-articular knee resection and knee reconstruction with a tumor endoprosthesis without its malalignment. When distal femoral replacement with extra-articular knee resection is planned and the quadriceps muscle is assumed to be resected asymmetrically, proximal realignment may be considered during primary surgery if there is concern regarding an imbalance in the forces controlling the patellar tracking.

Citation: Kubota Y, Tanaka K, Hirakawa M, Iwasaki T, Kawano M, Itonaga I, Tsumura H. Patellar dislocation following distal femoral replacement after extra-articular knee resection for bone sarcoma: A case report. *World J Clin Cases* 2022; 10(11): 3561-3572
URL: https://www.wjgnet.com/2307-8960/full/v10/i11/3561.htm
DOI: https://dx.doi.org/10.12998/wjcc.v10.i11.3561

INTRODUCTION

Bone tumors often arise around the knee, especially in the distal femur[1]. Bone sarcomas, such as osteosarcoma, also frequently originate in the distal femur[2]. Standard therapies for bone sarcoma in the distal femur include wide-margin resection and knee reconstruction with tumor endoprosthesis, which is thought to be an effective surgery to control local tumors and restore knee function. However, in cases of tumor invasion extending into the knee joint, extra-articular knee resection is required, which leads to wider resection and functional disorders. Moreover, the incidence of complications, such as aseptic loosening, prosthesis infection, and implant failure, is higher with extra-articular knee resection than with intra-articular knee resection. Initially, a fixed-hinge knee prosthesis was used in these cases; however, aseptic loosening was sometimes noted. Since the introduction of the kinematic rotating hinge prosthesis, the prosthesis survival rate improved considerably. In 2010, Kinkel *et al*[3] reported that the five-year implant survival rate was 57%, and the local recurrence rate of primary malignant tumors around the knee was 3%. Eight reports that have ascertained the outcome and complications after extra-articular knee resection and knee reconstruction appear in Table 1[3-10]. In summary, following extra-articular knee resection, the endoprosthesis complication rate is higher than that following intra-articular knee resection.

Patellar dislocations are rare complications in these patients. We could find three reports of patellar dislocations after replacement of a tumor endoprosthesis[11-13], but there are no such reports that particularly focus on extra-articular knee resection. Herein, we report a case of patellar dislocation after extra-articular knee resection of a malignant bone tumor in the femur and knee reconstruction with a tumor endoprosthesis without its malalignment. The patient underwent proximal realignment and had an uneventful course.

CASE PRESENTATION

Chief complaints

A 36-year-old man with no significant past medical history was admitted to our institution with continuous pain in his left knee for 4 mo.

History of present illness

On physical examination, tenderness was observed over the left femoral medial epicondyle without any swelling, redness, or warmth around the joint. Radiological examination and computed tomography (CT) revealed an osteolytic lesion over the femoral medial epicondyle without a sclerotic rim, periosteal reaction, or calcification (Figure 1). Magnetic resonance imaging (MRI) showed a bone tumor. An open biopsy was performed, and reverse transcription-polymerase chain reaction (RT-PCR) and direct sequencing revealed the *EWSR1/ATF1* fusion gene in the tumor specimens[14]. No other signs of metastasis were found on whole-body CT and positron emission tomography/CT. Extra-articular knee resection and knee reconstruction with a tumor endoprosthesis were performed.

The patient was placed in a supine position. A longitudinal incision was made starting distally, medial to the patellar tendon, and progressing proximally towards the lateral aspect. Medially, the distal end of the vastus medialis was resected. Resection was performed at approximately 2 cm from the distal end of the intermuscular septum. Subsequently, the medial head of the gastrocnemius muscle and the semimembranosus muscle attachment was resected. The distal femur was resected at a distance of 12 cm. Patellar osteotomy was performed, preserving the articular capsule of the knee. After dissecting

Table 1 Complications of distal femoral replacement

Ref.	Total cases	Age (yr)[1]	Average follow-up (mo)[1]	Extra-articular cases	Implant type	Overall survival	Disease-free survival	Local recurr-ence	Limb salvage	Implant survival (without re-opera-tion)	Function score[1]	Total compli-cation	Infection	Aseptic loose-ning	Implant failure	Peri-prosth-etic fracture	Other compli-cationsl	Revision
Kendall *et al*[4], 2000	12 (3 died who were excluded from their case matched study)	32.7 (20-64)	18 (6-56)	9 cases	Rotating hinge: 8 cases; fixed hinge: One case	9/12 (75%)	5/12 (42%; 1 case had a local and 3 had systemic recurr-ences)	1 case	Amputa-tion/disa-rticulati-on: 2 cases	Revision of compo-nents: 0 case; amputa-tion/ disarticu-lation: 2 cases	Musculo-skeletal Tumour Society (%): 56.14; Knee Society (points), 130.14	12 cases (including amputa-tion and recurre-nce)	Superficia l, 2 cases; deep, 2 cases	NA	NA	NA	Disloca-tion of compo-nent: 1 case	Rebush-ing: 1
Sim *et al* [5], 2007	50	40.5 (13-79)	24.5 (2-124)	NA (all cases: Wide *en bloc* resection)	Rotating hinge	Median: 9.5 mo (metasta-tic bone tumor) and 23.5 mo (primary maligna-ncy). Eight docume-nted deaths	77% (39 patients were initially metastasis -free, 9 subseq-uently develo-ped metasta-sis) metastatic disease	0 case	Amputa-tion: 3 cases	5 patients required endopros-thetic revision, 3 patients underw-ent subseq-uent amputa-tion	NA	17 (34%)	Superfic-ial, 4 cases; deep, 6 cases	1 case	Mecha-nical wear: 2 cases	2 cases	Nerve palsies, 5 cases	5 patients require endopros-thetic revision (10%)
Kinkel *et al*[3], 2010	77	38 (11–78)	46 (3–128)	EAR, 31 cases Intraar-ticular resection, 46 cases	Rotating hinge	NA	97% (primary malignant tumor)	4 cases	92% (both 5 and 10 yr)	57% after 5 yr	Enneking score, 73%	64 complic-ations occurred (46 patients) -	11 cases	13 cases (17%)	Locking mechani-sm failure, 15 cases	3 cases	Reduced ROM, 5 cases; rupture of the patellar tendon, 1 case	70 surgical revisions in 45 patients (58%)
Zwolak *et al*[6], 2011	11	39.8 (15-79)	37.5 (14-80)	11	Rotating hinge 1 case; not mentio-ned in others	9/11 (81.8%)	7/11 (6 patients develo-ped metasta-sis)	1 case	100 %	100%	NA	NA	NA	NA	No complic-ations were associated with the extensor mechan-ism of the	NA	NA	0 case

														patellar, specifically no patellar fracture was detected			
Capanna *et al*[7], 2011	14	34.9 (17-68)	54 (12-144)	13	Rotating hinge in some cases	10/14 (71.4%)	8/14 (57.4%)	3 cases	100%	1 patient with an intercalary arthrodesing prosthesis (Megasystem C, Waldemar Link)	MSTS-ISOLS score, 83% (67- 90)	10 patients	Deep infection, 2 cases	0 case	1 case	0 case	Rupture of the patellar tendon, 2 cases	Infection, 2 cases; failure of the grafted patellar tendon, 2 cases
Hardes *et al*[8], 2013	59	33 (11-74)	56.4 (1-204)	55 (93%) underwent splitting of the patellar in the coronal plane; 4 (7%) underwent patellectomy	Rotating hinge	53/59 (89.3%)	49/59 (83%)	2 cases (3%)	76% at 151 mo	48% at 2 yr and 31% at 5 yr postoperatively	The mean MSTS functional score: 22 (10-29); the mean OKS score: 32 (10-48)	NA	22 patients (37%)	10 cases (17%)	Failure of the joint mechanism (wear or breakage), 12 patients (20%)	6 patients (10%)	Delayed healing, 18 patients (31%)	A total of 110 revision procedures were carried out
Ieguchi *et al*[9], 2014	14	EAR, 44.4 (23-65)	EAR, 82.8 (24-176)	EAR, 6 patients	Rotating hinge, 5 cases; semi-rotating hinge, 1 case	5/6 (83.3%)	3/6 (50.0%)	0	5/6 (83.3%, 1 case of amputation)	5-yr survival rate of the prostheses without re-operation was 33.3%	In the extra-articular group, the mean total MSTS functional score, 21 (18-26)	NA	2 cases	0 case	Avulsion fractures of the patellar ligament, 2 cases (no data regarding how many cases occurred in the EAR group	Detachment of the patellar component, 1 case (no data regarding how many cases occurred in the EAR group	NA	2 cases (1 required amputation)
Shahid *et al*[10] , 2017	76	32 (9-74) EAR: 33 (11-73)	64 (12-195)	EAR: 42 cases (55%)	NA	5-yr survival 60%	NA	12/42 (29%); 5-yr survival, 69%	Amputation, 0 case	EAR: 5- and 10-yr reconstruction survival, 65% and	MSTS 26 (24-30)	NA	NA	NA	NA	NA	NA	NA

							59%, respecti-vely

[1]Data are presented as median (range).

CI: Confidence interval; EAR: Extra-articular resection; MSTS: Musculoskeletal Tumor Society; ISOLS: International Symposium on Limb Salvage; NA: Not available; OKS: The Oxford knee score; PE: Polyethylene; ROM: Range of motion.

the patellar tendon, leaving an infrapatellar fat pad over the specimen, the 1-cm proximal tibia was cut above the tibial tuberosity (TT). The resected specimen was removed. The tumor prosthesis was implanted with patellar resurfacing (Figure 2A-C). The vastus medialis and vastus lateralis muscles were attached to the prosthesis. A medial gastrocnemius flap was used for the prosthesis coverage. When subcuticular closure was performed, there was no abnormal patellar position.

The patient wore a knee brace, which constrained knee extension, from the first postoperative day and began walking with full-body weight-bearing. After walking rehabilitation for six postoperative days, knee instability was noticed. Radiography showed a lateral subluxation of the patellar (Figure 2D and E). However, because the knee subluxation did not progress to dislocation, walking rehabilitation continued. Although a range of motion (ROM) of 30° was allowed during passive motion at 2 wk postoperatively, radiographs revealed no progression of subluxation. However, the axial radiographic view of the patellar (Figure 2F) and CT showed lateral patellar dislocation at 4 wk postoperatively.

History of past illness

The patient had no significant past medical history.

Personal and family history

The patient and his family had no significant past medical history.

Physical examination

The ROM of the patient was restricted to be between 0° and 60° without pain, swelling, and local heat.

Laboratory examinations

Laboratory tests revealed: Erythrocytes 5.05 × 10^{12}/L (reference range, 4.35 × 10^{12}-5.55 × 10^{12}/L), hemoglobin 126 g/L (reference range, 137-168 g/L), leukocytes 5.27 × 10^{9}/L (reference range, 3.3 × 10^{9}-8.6 × 10^{9}/L), eosinophils 3.2%, basophils 0.9%, neutrophils 54.6%, lymphocytes 36.6%, monocytes 4.7%, C-reactive protein 0.7 mg/L (reference range, 0-1.4 mg/L), total protein 69.3 g/L (reference range, 66.0-81.0 g/L), aspartate aminotransferase 28.8 U/L (reference range, 13.0-30.0 U/L), alanine aminotransferase 42.2 U/L (reference range, 10.0-42.0 U/L), blood urea nitrogen 23 mg/dL (reference range, 8-20 mg/dL), creatinine 1.12 mg/dL (reference range, 0.65-1.07 mg/dL), creatine phosphokinase 299 U/L (reference range, 59-248 U/L).

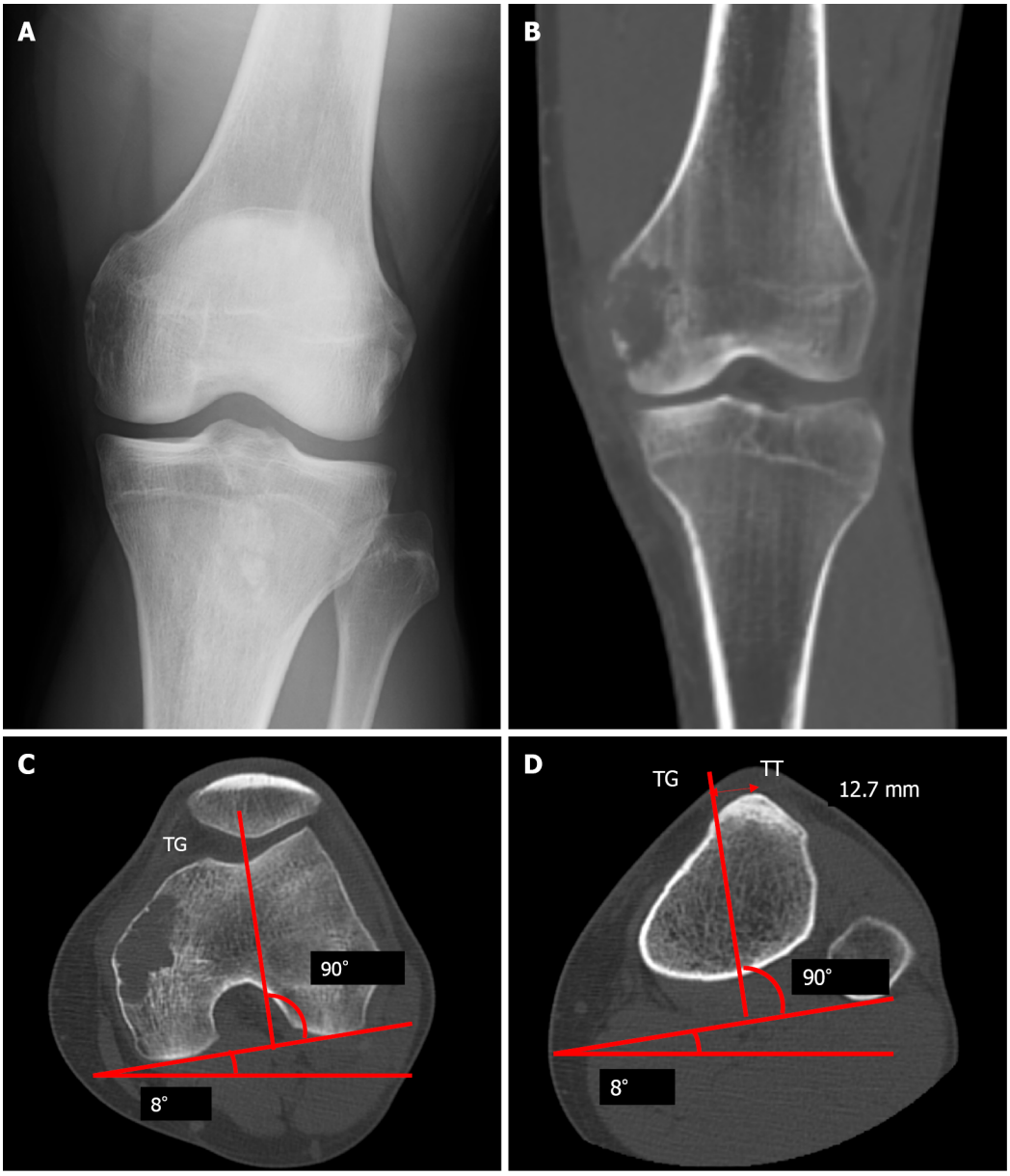

DOI: 10.12998/wjcc.v10.i11.3561

Figure 1 Images before the primary surgery. A: Radiograph showing osteolytic lesion in the left distal femur; B: Computed tomography scan also showing the lesion; C and D: The axial radiographic view of computed tomography before the primary operation, line from the middle of the tibial tuberosity (TT) to the bottom of the trochlear groove (TG) is drawn parallel to the posterior condyle line,and the distance between TT and TG is 12.7 mm. TT: Tibial tuberosity; TG: Trochlear groove.

Imaging examinations

Based on the findings of studies by Kim *et al*[15] and Fang *et al*[16], the postoperative radiographs showed good results. The angle between the distal portion of the femoral component and the femoral anatomical axis was 96°, and the angle between the proximal portion of the tibial component and the tibial anatomical axis was 91° (Figure 2D). A lateral radiograph also showed good results, with a postoperative femoral sagittal alignment of 3° and a postoperative tibial sagittal alignment of 2° (Figure 2E). The measurement of the patellar position Insall-Salvati ratio was 1.15, and the length of the patellar tendon (LT)/height of the patellar tendon insertion (HI) ratio was 1.27, which implied a good patellar location (Figure 4A and B) according to the report by Schwab *et al*[11]. Consequently, we considered that the tumor prosthesis was implanted precisely in terms of the alignment and position.

After the patient noticed knee instability for six postoperative days, radiography showed a lateral subluxation of the patellar (Figure 2D and E). The axial radiographic view of the patellar (Figure 2F) and CT showed lateral patellar dislocation at 4 wk postoperatively.

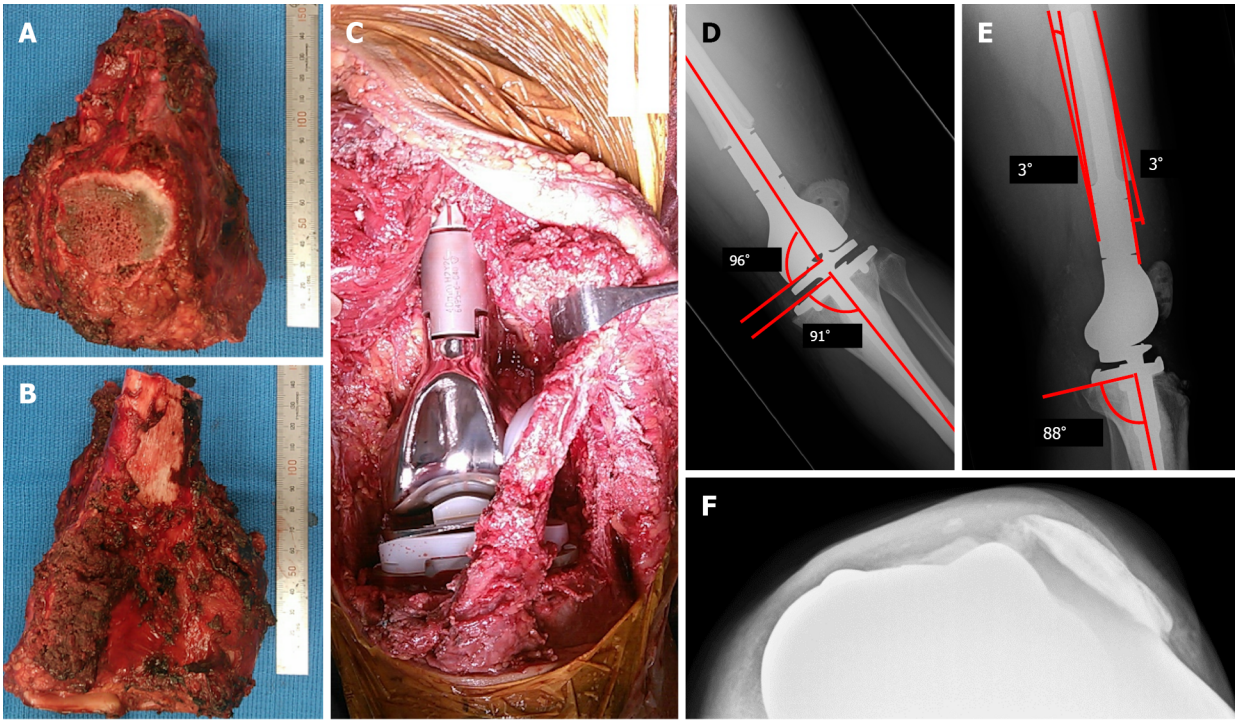

DOI: 10.12998/wjcc.v10.i11.3561

Figure 2 Photographic images during the primary surgery, and radiograph postoperatively. A: The anterior view of the resected specimen and the longitudinally split patellar are shown; B: The posterior view of the resected specimen; C: After removal of the tumor, a tumor endoprosthesis was implanted; D and E: Patellar subluxation is found in radiograph at 1 wk postoperatively. The radiograph of the left knee shows the measurement of the coronal alignment of the femoral and tibial components. The overall anatomical alignment is defined as the angle between the femoral anatomical axis and the tibial anatomical axis (D); the lateral radiograph of the left knee shows the measurement of the sagittal alignment of the femoral and tibial components (E); F: The radiograph shows lateral luxation of the patellar at 1 mo postoperatively.

FINAL DIAGNOSIS

The final diagnosis was patellar dislocation following distal femoral replacement after extra-articular knee resection for bone sarcoma.

TREATMENT

It was impossible to treat the patellar dislocation with closed reduction; therefore, open reduction was performed. Dejour *et al*[17] reported that a large distance between the natural TT and the trochlear groove (TG) induce lateral patellar tracking, resulting in patellar instability. These indices can be measured simply using CT, and they are defined as the distance between the middle of the TT to the bottom of the TG. The ideal TT-TG distance is within a range of 10 to 15 mm[17]; TT-TG, in this case, was 12.7 mm (Figure 1C and D).

We also measured the rotation of the tibial and femoral components using CT. Before the secondary surgery, the post-primary operative rotational alignment of the femoral component was defined as the angle subtended by the line tangent to the condyles and the axis of the femoral neck. The angle was 20°, which was equal to that of the native alignment (20°) (Figure 3A-D). Moreover, the external axial rotation of the tibial component in relation to the posterior margins of the tibial plateau and the tibial bearing was 5°, which was a good result (Figure 3E).

The secondary surgery consisted of lateral release and proximal realignment and was performed 1 mo postoperatively. Under anesthesia, it was impossible to treat the lateral patellar dislocation of the left knee with a closed reduction and passive ROM of 0°-30°. A skin incision was made which followed the previous skin incision. There was abundant thick scar tissue on the lateral side of the patellar and the vastus lateralis muscle. A lateral release was performed from the tibial component to 20 cm proximally, and scar adhesion between the vastus lateralis muscle and the femur was also released. Although patellar dislocation could be reduced, the ROM was still 30°. We concluded that scar formation of the quadriceps muscle was the reason for the flexion contracture.

The pie crust technique was applied to the quadriceps muscle along with a longitudinal split of the scar of the vastus lateralis muscle. The removal of scar tissue in the vastus intermedius muscle increased the ROM to 60°. The distal end of the vastus medialis had already been resected and was loosely and

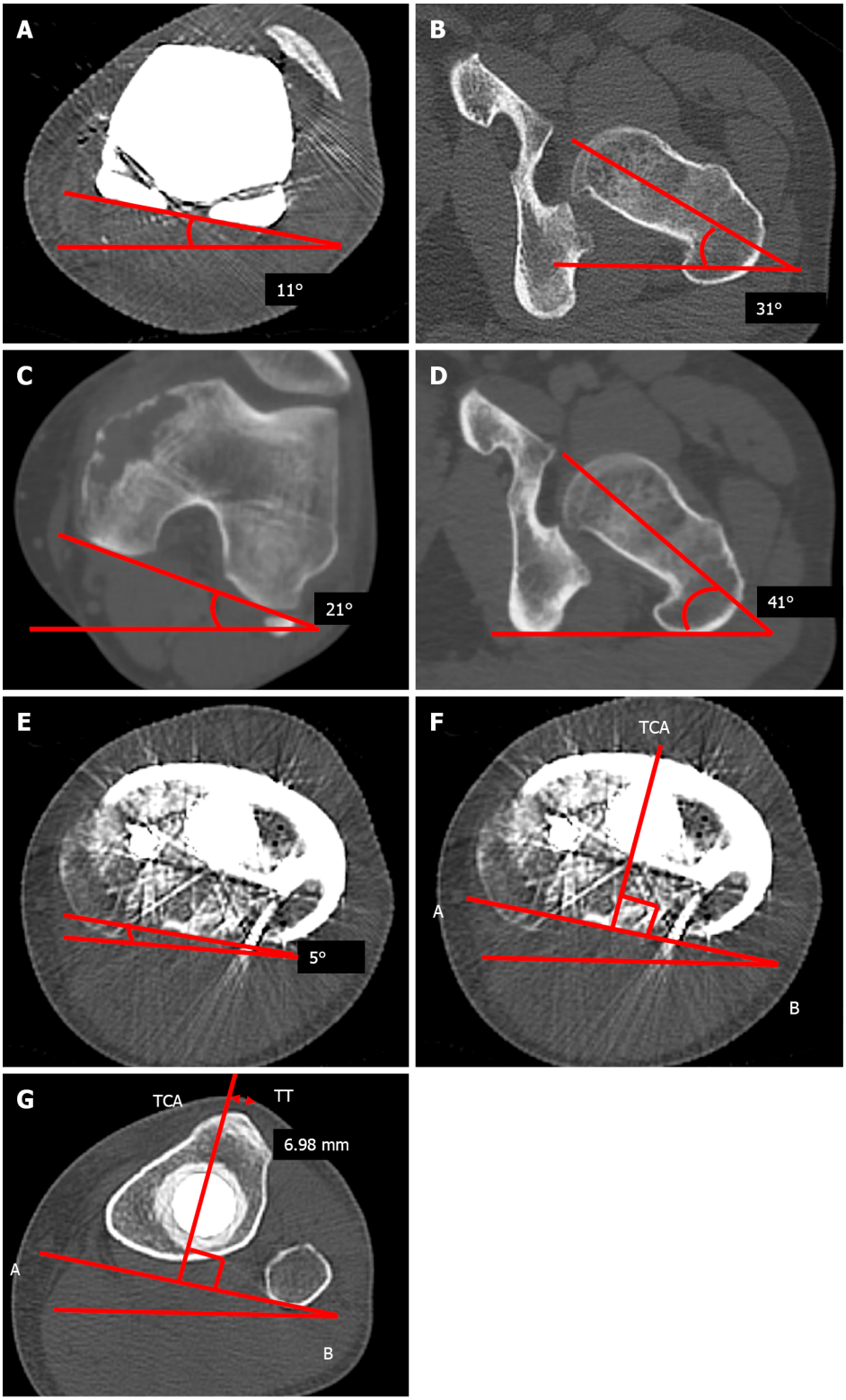

DOI: 10.12998/wjcc.v10.i11.3561

Figure 3 The computed tomography of a femoral axial and tibial axial view after or before the primary operation. A-D: The computed tomography (CT) imaging of a femoral axial after (A and B) and before (C and D) the primary operation, which shows that the postoperative angle between the femoral component and the femoral neck axis (A and B) is equal to the preoperative angle between the femoral posterior condylar axis and femoral neck axis (C and D); E-G: A CT scan shows the axial rotation of the tibial component in relation to the posterior margins of the tibial plateau and the tibial bearing after the primary operation. The line AB is drawn along the posterior margin of the tibial tray. The tibial component axis (TCA) is perpendicular to line AB (E and F); the perpendicular distance from the TCA to the tip of the tibial tuberosity is 6.98 mm (G). TCA: Tibial component axis; TT: Tibial tuberosity.

indirectly attached to the patellar *via* the scar tissue. After the vastus medialis obliquus and scar tissues were separated from the patellar, they were advanced over the tendon of the quadriceps muscle and sutured, using the baseball suture technique with polyblend polyethylene suture. Polybutylate-coated

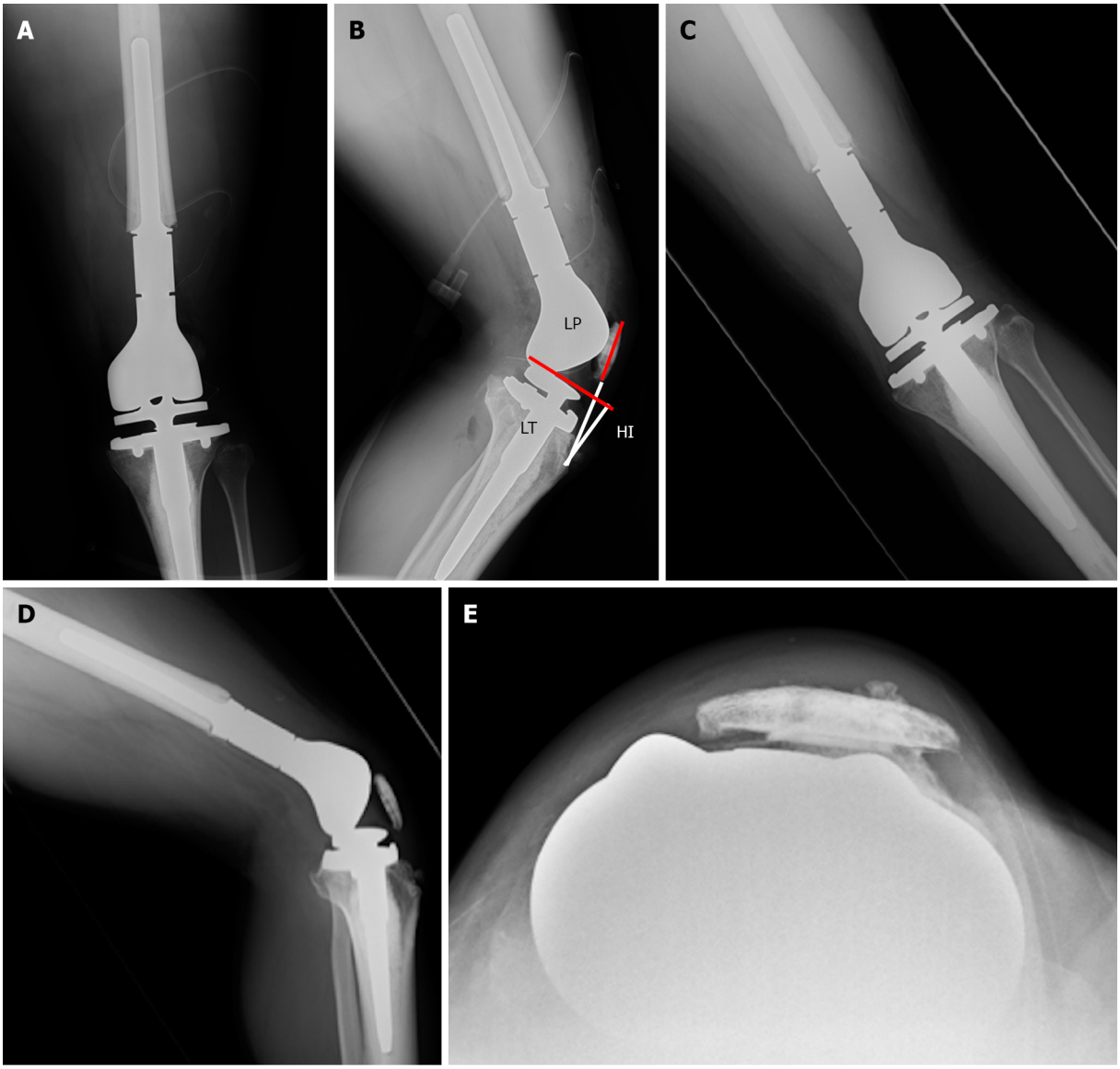

DOI: 10.12998/wjcc.v10.i11.3561

Figure 4 Radiographs after the secondary operation. A and B: Anteroposterior (AP) view (A) and (B) lateral view which show that the measurement of the patellar position Insall-Salvati ratio is 1.15, and the length of the patellar tendon (LT)/height of the patellar tendon insertion (HI) ratio is 1.27; C-E: Radiograph 9 mo after the proximal realignment operation which shows no patellar dislocation. LP: Length of the patellar; HI: Height of the insertion; LT: Length of the tendon.

braided polyester suture material was also used to reinforce the sutures. We confirmed that 45° flexion of the knee did not tear the sutures or cause patellar dislocation and subsequently closed the surgical wound.

From the first postoperative day, the patient began non-weight-bearing exercises. The ROM exercises were limited to up to 30°. After confirming wound healing at 2 wk postoperatively, full-weight bearing with bilateral crutches and limited ROM exercise up to 60° was allowed. Unlimited ROM exercise was started 3 wk postoperatively. The patient could walk with a lateral crutch and the ROM was 0°-90° at discharge and 4 wk postoperatively.

OUTCOME AND FOLLOW-UP

At the time of the outpatient consultation, the patient was able to walk stably without crutches, and the ROM was 0°-100°. The patient could perform his daily activities at 9 mo postoperatively. Radiography revealed no patellar re-dislocation (Figure 4C-E).

DISCUSSION

The most common site where bone tumors arise is the distal femur[1,2]. The current standard therapy for malignant bone tumors is wide margin resection and knee reconstruction using a tumor endoprosthesis. Extra-articular knee resection is required if the tumor invades the knee joint. As shown in Table 1, extra-articular knee resection results in various complications. However, extended survival of the salvaged limb can be achieved by taking care of each complication.

Several studies have reported that patellar dislocations occur after treatment with a tumor endoprosthesis. We could only find three reports on the cause of patellar dislocation and patellar impingement following distal femur replacement in the English literature[11-13]. Among them, only one report included extra-articular tumor resection[12]. Schwab *et al*[11] reported three features of distal femoral replacement. First, patellar tendon devascularization may cause scar formation, which leads to patellar baja. Second, if some parts of the extensor musculature are removed, the patellar offset can be increased. This action increases stress on the patellar, which may lead to patellar complications. Finally, knee mobilization can be delayed or insufficient because of fascia deficiency, marginal necrosis, and chemotherapy. The authors also reported that when the Insall-Salvati ratio was > 0.8 and < 1.2, the ROM was usually > 100°. The mean LT/HI ratio of patellar impingement cases was 0.9 and the mean LT/HI ratio without impingement was 1.4 (P = 0.07).

Akiyama *et al*[12] also reported patellar dislocation following distal femoral replacement after extra-articular tumor resection. The authors enumerated the following reasons for patellar dislocation after reconstruction: unconscious femoral rotation, usage of semi-rotating hinge endoprosthesis, insufficient balancing of soft tissues at the time of closure, and scarring of the tightened lateral soft tissues. They also mentioned that it was very difficult to predict good postoperative patellar tracking, even if intraoperative patellar tracking was normal. In their case, the modified Merkow's realignment procedure of the patellar was implemented with medial plication and lateral release, and no patellar dislocation occurred during the postoperative course.

We used a rotating hinge endoprosthesis, as recommended by Akiyama *et al*[12]. In addition, the alignment was favorable according to the abovementioned points and the criteria suggested by Kim *et al*[15]. The authors suggested placing the knee components in the position with the overall anatomical knee alignment at an angle of 3.0°-7.5° valgus, femoral component alignment at 2°-8° valgus, femoral sagittal alignment at 0°-3°, tibial coronal alignment at 90°, and tibial sagittal alignment at 0°-7°. In our case, each alignment was 7° valgus, 6° valgus, 3°, 91°, and 2°, respectively (Figure 2D and E).

Usually, to measure the femoral rotational alignment during total knee arthroplasty (TKA), the posterior condylar angle formed by the line tangent to the posterior condyles and the trans-epicondylar axis is used[15]. It was impossible to apply this procedure to our patient because of a distal femur replacement. Therefore, we measured the preoperative TT-TG (12.7 mm), which was within the ideal range (10-15 mm) (Figure 1C and D). We confirmed that the preoperative angle, subtended by the line tangent to the condyles and the axis of the femoral neck, was equal to that of the postoperative angle (Figure 3A-D).

With regard to the tibial rotational alignment, we measured 5° on the axial rotation of the tibial component in relation to the posterior margins of the tibial plateau and the tibial bearing (Figure 3E). The external rotation was within 2°-5°, which could be considered a precise alignment[15]. Furthermore, a more accurate measurement procedure for tibial rotational alignment, as described by Saffi *et al*[18], was also applied. The two-dimensional axial CT of the center of the tibial tray to the tip of the tibial tubercle was 6.98 mm. It was outside the cut-off values of < 6 mm and > 10 mm, and we confirmed that the tibial rotational alignment was preferable (Figure 3G). The causes of patellar dislocation reported in earlier cases were not present in our patient, and the implant alignment was favorable. However, the patient still experienced patellar dislocation.

The question remains whether extra-articular knee resection could be a cause of patellar dislocation. Compared to intra-articular knee resection, extra-articular knee resection requires a wider margin of resection, including quadriceps muscle resection, which can cause patellar instability. In this case, the reason for patellar dislocation was considered to be an imbalance in the forces controlling patellar tracking. The resection of the distal vastus medialis and the scarring of the distal vastus lateralis could be contributing factors. The resection of the distal vastus medialis reduces the ability to control the patellar medially. It was assumed that scarring of the distal vastus lateralis shortened its length, and the patellar was pulled laterally, although it is unknown how the scar developed.

There are four main treatment procedures for patellar dislocation after TKA: proximal realignment [19], medial patellofemoral ligament (MPFL) reconstruction[20-22], distal realignment including tibial tuberosity osteotomy (TTO)[23], and lateral retinaculum release[24]. When any procedure is performed, Gennip *et al*[21], and Goto *et al*[25] suggested that alignment of the implant should be assessed first, to determine whether it is within the normal range of alignment. Gennip *et al*[21] stated that it is better to consider distal realignment if the TT-TG value is outside the normal range, or if it is not possible to improve patellar mal-tracking with both lateral release and MPFL reconstruction despite a normal TT-TG value. Nevertheless, because the present case underwent extra-articular knee resection and distal femoral replacement, there was no point for anchoring a graft on the femoral side, and the anchor point of the thin patellar could be fractured. Therefore, we chose proximal realignments of the quadriceps as

the best procedure. Matar *et al*[19] reported that patellar proximal realignment for patellar dislocation after TKA is effective.

As Piedade *et al*[26] stated, TTO should not be performed preferentially because of the risk of skin necrosis and fracture of the tibial tubercle. If extra-articular knee resection is performed, further complications, such as skin necrosis and fracture of the tibial tubercle, could also develop. Hence, in cases similar to the present case, TTO should be avoided. Therefore, lateral release and proximal realignment were performed. No patellar dislocation occurred over the 9-mo postoperative follow-up period (Figure 4C-E).

CONCLUSION

To the best of our knowledge, this is the first report showing that extra-articular knee resection can cause patellar dislocation after distal femoral replacement without malalignment of the prosthesis. Lateral release and proximal realignment are the most effective procedures. As in the present case, when distal femoral replacement with extra-articular knee resection is planned, and the quadriceps muscle is assumed to be resected asymmetrically, proximal realignment may be taken into consideration during the primary surgery if the forces controlling patellar tracking are imbalanced.

FOOTNOTES

Author contributions: Kubota Y, Tanaka K and Tsumura H conceived the study; Kubota Y and Tanaka K reviewed the literature and contributed to manuscript drafting; Kubota Y, Tanaka K, Iwasaki T and Kawano M contributed data analysis and interpretation; Hirakawa M, Itonaga I and Tsumura H were responsible for the critical revision of the manuscript for important intellectual content; all authors have read and approved the final version of the manuscript.

Informed consent statement: Informed written consent was obtained from the patients for the publication of this report and any accompanying images.

Conflict-of-interest statement: The authors declare that they have no conflict of interest.

CARE Checklist (2016) statement: The authors have read the CARE Checklist (2016), and the manuscript was prepared and revised according to the CARE Checklist (2016).

Country/Territory of origin: Japan

ORCID number: Yuta Kubota 0000-0003-1426-148; Kazuhiro Tanaka 0000-0002-5138-8952; Masashi Hirakawa 0000-0002-0045-6214; Tatsuya Iwasaki 0000-0002-9407-3547; Masanori Kawano 0000-0002-1497-8689; Ichiro Itonaga 0000-0003-3071-711X; Hiroshi Tsumura 0000-0002-5384-822X.

S-Editor: Chen YL
L-Editor: A
P-Editor: Chen YL

REFERENCES

1 **Bergovec M**, Kubat O, Smerdelj M, Seiwerth S, Bonevski A, Orlic D. Epidemiology of musculoskeletal tumors in a national referral orthopedic department. A study of 3482 cases. *Cancer Epidemiol* 2015; **39**: 298-302 [PMID: 25703268 DOI: 10.1016/j.canep.2015.01.015]
2 **Öztürk R**, Arıkan ŞM, Bulut EK, Kekeç AF, Çelebi F, Güngör BŞ. Distribution and evaluation of bone and soft tissue tumors operated in a tertiary care center. *Acta Orthop Traumatol Turc* 2019; **53**: 189-194 [PMID: 30982757 DOI: 10.1016/j.aott.2019.03.008]
3 **Kinkel S**, Lehner B, Kleinhans JA, Jakubowitz E, Ewerbeck V, Heisel C. Medium to long-term results after reconstruction of bone defects at the knee with tumor endoprostheses. *J Surg Oncol* 2010; **101**: 166-169 [PMID: 19924724 DOI: 10.1002/jso.21441]
4 **Kendall SJ**, Singer GC, Briggs TW, Cannon SR. A functional analysis of massive knee replacement after extra-articular resections of primary bone tumors. *J Arthroplasty* 2000; **15**: 754-760 [PMID: 11021451 DOI: 10.1054/arth.2000.8104]

5 **Sim IW**, Tse LF, Ek ET, Powell GJ, Choong PF. Salvaging the limb salvage: management of complications following endoprosthetic reconstruction for tumours around the knee. *Eur J Surg Oncol* 2007; **33**: 796-802 [PMID: 17291709 DOI: 10.1016/j.ejso.2006.10.007]

6 **Zwolak P**, Kühnel SP, Fuchs B. Extraarticular knee resection for sarcomas with preservation of the extensor mechanism: surgical technique and review of cases. *Clin Orthop Relat Res* 2011; **469**: 251-256 [PMID: 20419485 DOI: 10.1007/s11999-010-1359-8]

7 **Capanna R**, Scoccianti G, Campanacci DA, Beltrami G, De Biase P. Surgical technique: extraarticular knee resection with prosthesis-proximal tibia-extensor apparatus allograft for tumors invading the knee. *Clin Orthop Relat Res* 2011; **469**: 2905-2914 [PMID: 21484473 DOI: 10.1007/s11999-011-1882-2]

8 **Hardes J**, Henrichs MP, Gosheger G, Gebert C, Höll S, Dieckmann R, Hauschild G, Streitbürger A. Endoprosthetic replacement after extra-articular resection of bone and soft-tissue tumours around the knee. *Bone Joint J* 2013; **95-B**: 1425-1431 [PMID: 24078544 DOI: 10.1302/0301-620X.95B10.31740]

9 **Ieguchi M**, Hoshi M, Aono M, Takada J, Ohebisu N, Kudawara I, Nakamura H. Knee reconstruction with endoprosthesis after extra-articular and intra-articular resection of osteosarcoma. *Jpn J Clin Oncol* 2014; **44**: 812-817 [PMID: 25057091 DOI: 10.1093/jjco/hyu093]

10 **Shahid M**, Albergo N, Purvis T, Heron K, Gaston L, Carter S, Grimer R, Jeys L. Management of sarcomas possibly involving the knee joint when to perform extra-articular resection of the knee joint and is it safe? *Eur J Surg Oncol* 2017; **43**: 175-180 [PMID: 27266818 DOI: 10.1016/j.ejso.2016.05.018]

11 **Schwab JH**, Agarwal P, Boland PJ, Kennedy JG, Healey JH. Patellar complications following distal femoral replacement after bone tumor resection. *J Bone Joint Surg Am* 2006; **88**: 2225-2230 [PMID: 17015600 DOI: 10.2106/JBJS.E.01279]

12 **Akiyama T**, Kanda S, Maeda A, Endo M, Saita K. Patella dislocation following distal femoral replacement after bone tumour resection. *BMJ Case Rep* 2014; **2014** [PMID: 25073529 DOI: 10.1136/bcr-2014-205006]

13 **Etchebehere M**, Lin PP, Bird JE, Satcher RL, Moon BS, Yu J, Li L, Lewis VO. Patellar Resurfacing: Does It Affect Outcomes of Distal Femoral Replacement After Distal Femoral Resection? *J Bone Joint Surg Am* 2016; **98**: 544-551 [PMID: 27053582 DOI: 10.2106/JBJS.O.00633]

14 **Kubota Y**, Tanaka K, Hisaoka M, Daa T, Iwasaki T, Kawano M, Itonaga I, Tsumura H. Primary clear cell sarcoma of the femur: a unique case with RT-PCR and direct sequencing confirmation of *EWSR1/ATF1* fusion gene. *BMC Musculoskelet Disord* 2021; **22**: 99 [PMID: 33478436 DOI: 10.1186/s12891-021-03969-4]

15 **Kim YH**, Park JW, Kim JS, Park SD. The relationship between the survival of total knee arthroplasty and postoperative coronal, sagittal and rotational alignment of knee prosthesis. *Int Orthop* 2014; **38**: 379-385 [PMID: 24173677 DOI: 10.1007/s00264-013-2097-9]

16 **Fang DM**, Ritter MA, Davis KE. Coronal alignment in total knee arthroplasty: just how important is it? *J Arthroplasty* 2009; **24**: 39-43 [PMID: 19553073 DOI: 10.1016/j.arth.2009.04.034]

17 **Dejour DH**, Mesnard G, Giovannetti de Sanctis E. Updated treatment guidelines for patellar instability: "un menu à la carte". *J Exp Orthop* 2021; **8**: 109 [PMID: 34837157 DOI: 10.1186/s40634-021-00430-2]

18 **Saffi M**, Spangehl MJ, Clarke HD, Young SW. Measuring Tibial Component Rotation Following Total Knee Arthroplasty: What Is the Best Method? *J Arthroplasty* 2019; **34**: S355-S360 [PMID: 30473230 DOI: 10.1016/j.arth.2018.10.022]

19 **Matar HE**, Illanes FL, Gollish JD. Extensive Proximal Extensor Mechanism Realignment for Chronic Patella Dislocations in Revision Knee Arthroplasty: Surgical Technique. *Knee* 2020; **27**: 1821-1832 [PMID: 33197822 DOI: 10.1016/j.knee.2020.09.018]

20 **Asada S**, Akagi M, Mori S, Hamanishi C. Medial patellofemoral ligament reconstruction for recurrent patellar dislocation after total knee arthroplasty. *J Orthop Sci* 2008; **13**: 255-258 [PMID: 18528660 DOI: 10.1007/s00776-007-1219-x]

21 **van Gennip S**, Schimmel JJ, van Hellemondt GG, Defoort KC, Wymenga AB. Medial patellofemoral ligament reconstruction for patellar maltracking following total knee arthroplasty is effective. *Knee Surg Sports Traumatol Arthrosc* 2014; **22**: 2569-2573 [PMID: 23108684 DOI: 10.1007/s00167-012-2269-y]

22 **Lamotte A**, Neri T, Kawaye A, Boyer B, Farizon F, Philippot R. Medial patellofemoral ligament reconstruction for patellar instability following total knee arthroplasty: A review of 6 cases. *Orthop Traumatol Surg Res* 2016; **102**: 607-610 [PMID: 27317639 DOI: 10.1016/j.otsr.2016.03.018]

23 **Putman S**, Boureau F, Girard J, Migaud H, Pasquier G. Patellar complications after total knee arthroplasty. *Orthop Traumatol Surg Res* 2019; **105**: S43-S51 [PMID: 29990602 DOI: 10.1016/j.otsr.2018.04.028]

24 **Maniar RN**, Singhi T, Rathi SS, Baviskar JV, Nayak RM. Surgical technique: Lateral retinaculum release in knee arthroplasty using a stepwise, outside-in technique. *Clin Orthop Relat Res* 2012; **470**: 2854-2863 [PMID: 22707069 DOI: 10.1007/s11999-012-2420-6]

25 **Goto T**, Hamada D, Iwame T, Suzue N, Takeuchi M, Egawa H, Sairyo K. Medial patellofemoral ligament reconstruction for patellar dislocation due to rupture of the medial structures after total knee arthroplasty: a case report and review of the literature. *J Med Invest* 2014; **61**: 409-412 [PMID: 25264063 DOI: 10.2152/jmi.61.409]

26 **Piedade SR**, Pinaroli A, Servien E, Neyret P. Tibial tubercle osteotomy in primary total knee arthroplasty: a safe procedure or not? *Knee* 2008; **15**: 439-446 [PMID: 18771928 DOI: 10.1016/j.knee.2008.06.006]

World Journal of Clinical Cases

Submit a Manuscript: https://www.f6publishing.com

World J Clin Cases 2022 April 16; 10(11): 3573-3578

DOI: 10.12998/wjcc.v10.i11.3573

ISSN 2307-8960 (online)

CASE REPORT

Qingchang decoction retention enema may induce clinical and mucosal remission in left-sided ulcerative colitis: A case report

Pei-Han Li, Yu Tang, Hong-Zhu Wen

Specialty type: Gastroenterology and hepatology

Provenance and peer review: Unsolicited article; Externally peer reviewed.

Peer-review model: Single blind

Peer-review report's scientific quality classification

Grade A (Excellent): 0
Grade B (Very good): B
Grade C (Good): C
Grade D (Fair): 0
Grade E (Poor): 0

P-Reviewer: Cheng TH, Taiwan; Salimi M, Iran

Received: November 8, 2021
Peer-review started: November 8, 2021
First decision: December 27, 2021
Revised: January 8, 2022
Accepted: February 27, 2022
Article in press: February 27, 2022
Published online: April 16, 2022

Pei-Han Li, Hong-Zhu Wen, Department of Gastroenterology, Longhua Hospital Affiliated to Shanghai University of Traditional Chinese Medicine, Shanghai 200032, China

Yu Tang, Department of Basic Medicine, Fudan University, Shanghai 200032, China

Corresponding author: Hong-Zhu Wen, MD, Attending Doctor, Department of Gastroenterology, Longhua Hospital Affiliated to Shanghai University of Traditional Chinese Medicine, No. 725 South Wanping Road, Shanghai 200032, China. ellawhz@sina.com

Abstract

BACKGROUND

Ulcerative colitis (UC) is a chronic autoimmune disease characterized by relapsing-remitting abdominal pain, diarrhea, mucopurulent discharge and rectal bleeding. To date, the etiology of the disease remains unknown; therefore, medical therapy is not yet available. Left-sided UC is mainly treated with oral and topical mesalazine. However, due to its modest clinical effect, endoscopic mucosal remission is not achieved in all patients.

CASE SUMMARY

A 44-year-old man presented to Longhua Hospital with a history of left-sided UC for more than 6 years and slight bloody diarrhea over time. Endoscopy suggested hyperemia, edema, and erosive mucosa involving the rectum and sigmoid colon. The Traditional Chinese medicine Qingchang decoction (QCD) enema treatment was initiated once a day combined with a previous standard dose of mesalazine for 8 wk, and rectal bleeding ceased after 4 wk of treatment. Another QCD enema treatment was provided after symptom relapse due to drug withdrawal for nearly 6 mo. At the 2-mo follow-up, the colonoscopy results indicated mucosal healing with no erosion or ulcers.

CONCLUSION

The Chinese formula QCD retention enema represents a potential treatment for left-sided UC with predominant rectal bleeding to achieve clinical and mucosal remission.

Key Words: Ulcerative colitis; Chinese formulas; Qingchang decoction enema; Qingchang suppository; Case report

Core Tip: We present a case of a 44-year-old man with mildly active left-sided ulcerative colitis (UC) for 6 years in whom mesalazine treatment failed but clinical and mucosal remission was achieved following Chinese formula Qingchang decoction (QCD) retention enema treatment combined with oral mesalazine. Thus, a QCD enema may be an effective treatment modality for patients with left-sided UC.

Citation: Li PH, Tang Y, Wen HZ. Qingchang decoction retention enema may induce clinical and mucosal remission in left-sided ulcerative colitis: A case report. *World J Clin Cases* 2022; 10(11): 3573-3578
URL: https://www.wjgnet.com/2307-8960/full/v10/i11/3573.htm
DOI: https://dx.doi.org/10.12998/wjcc.v10.i11.3573

INTRODUCTION

Ulcerative colitis (UC) is a chronic autoimmune disease characterized by relapsing-remitting abdominal pain, diarrhea, mucopurulent discharge, and rectal bleeding. Its lesions mainly involve the mucous membrane and submucosa of the colon. UC can be divided into proctitis, rectal-sigmoid colitis and extensive colitis[1], corresponding to 14.8%, 26.4% and 25.0% of all UC cases, respectively[2]. Left-sided colitis refers to colitis involving the lower part of the descending colon. The proportion of left-sided colitis in China exceeds 50%. The precise pathogenesis of UC remains unknown; therefore, medical therapy to cure the disease is not yet available. Therapeutic drugs include sulfasalazine, mesalazine, corticosteroids, immunosuppressants, and biological agents[3]. However, not all patients benefit from basic mesalazine and amino-salicylic acid treatment for left-sided UC. We report herein a case of a 44-year-old man with left-sided UC in whom standard oral and topical doses of mesalazine failed but clinical remission and mucosal healing were eventually achieved with the Chinese formula Qingchang decoction (QCD) enema. This publication reports and discusses the effects of QCD enema treatment on left-sided UC.

CASE PRESENTATION

Chief complaints

A 44-year-old Chinese man presented to Longhua Hospital with a history of left-sided UC for more than 6 years. He received oral treatment with mesalazine at a dose of 3 g/d (occasionally 2 g/d due to forgetting to take the medicine). Bowel movements were maintained 2-3 times a day, with a small amount of blood and mucus in the stool less than half of the time. Mesalazine suppository therapy and glucocorticoid enema were also administered briefly during this period, but the symptoms were not relieved. In the previous 6 years, colonoscopy was repeated annually, with results revealing a Mayo endoscopic score of 2 (erosion of the rectum and sigmoid colon covered with purulent secretions).

History of present illness

The patient suffered from recurrent bloody mucous stool. After another colonoscopy was conducted at a local hospital on October 30, 2019 (Figure 1), which suggested a diagnosis of active left-sided UC, he was admitted to our department on November 09, 2019. He reported bowel movements twice a day; mild, dull pain in the left lower abdomen that was relieved after a bowel movement; relapsing mucous discharge; and rectal bleeding when he was fatigued. We observed his tongue to be red with light yellow fur and a thin pulse.

History of past illness

The patient had no significant previous medical history.

Personal and family history

The patient had no significant family history.

Physical examination

Physical examination showed no obvious abnormalities, except for slight tenderness in the left lower abdomen.

Laboratory examinations

No sign of inflammation was found in the blood analysis, and the leukocyte level was low, at 3.55×10^9 /L, with predominant neutrophils (67.1%) and normal hemoglobin and platelet counts. The

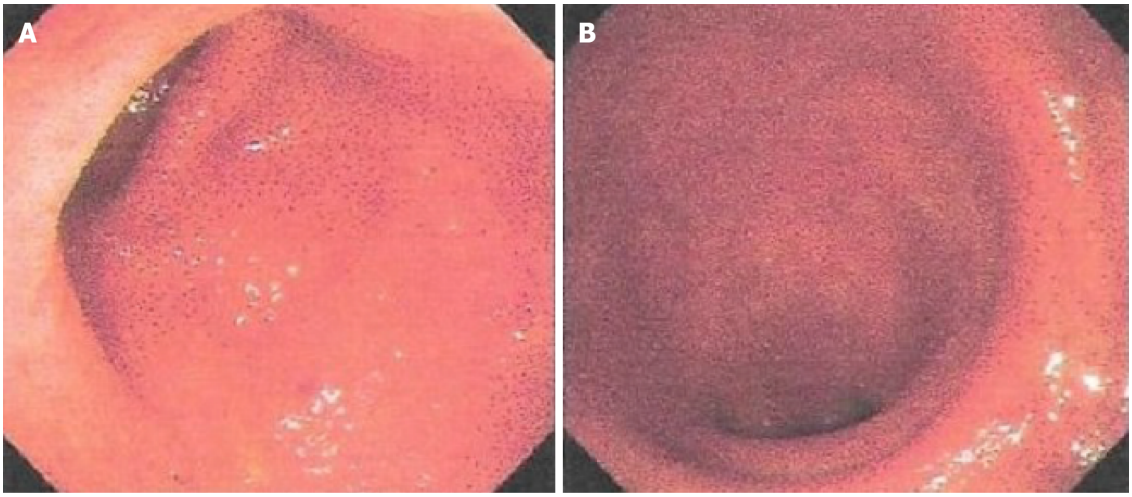

DOI: 10.12998/wjcc.v10.i11.3573

Figure 1 Endoscopic images before Qingchang decoction retention enema treatment. A: Colonoscopy image showing hyperemia, edema, erosions, and friability in the sigmoid colon; B: Colonoscopy image showing hyperemia, edema, erosions, and friability in the rectum.

prothrombin level, partial thromboplastin times, and d-dimer levels were normal. The serum C-reactive protein level was also within normal limits, and the erythrocyte sedimentation rate was 2 mm/h. The blood biochemistry and urine analyses were normal. The ECG results were also normal.

Imaging examinations

Mild inflammation, characterized by hyperemia, edema, erosions and friability was detected in the sigmoid colon (Figure 1A) and rectum (Figure 1B), 20 cm from the anus. Normal mucosa was noted in the remaining colon.

FINAL DIAGNOSIS

The patient was diagnosed with UC subtyped as left-sided colitis based on endoscopy of the rectum and colon (Figure 1) and histology of the biopsy. His condition was mild in severity with an active persistent phase. The relevant Traditional Chinese medicine (TCM) syndrome was spleen deficiency and the accumulation of dampness and heat.

TREATMENT

Treatment with QCD enema was administered to the patient at a dose of 180 mL once a night, combined with oral mesalazine at a dose of 3 g/d. Rectal bleeding ceased after 4 wk of treatment, and after 8 wk of treatment, the patient had one or two bowel movements per day, and no mucous or bloody discharge was observed. Due to the satisfactory effect, the dose of oral mesalazine was reduced to 2 g/d, and enema therapy was stopped without a consultation. At the end of June 2020, relapsing mucous and bloody discharge 3 to 4 times a day occurred. On June 22, 2020, the patient came to our ward for further treatment with QCD enema. The stool frequency was reduced to 2 to 3 times a day, with no mucus or blood present after 4 wk of treatment.

OUTCOME AND FOLLOW-UP

The patient received a total of 12 wk of QCD retention enema treatment combined with oral mesalazine. After the second episode of QCD treatment, on August 07, 2020, a colonoscopy was performed again. Normal mucosa was seen in the sigmoid colon (Figure 2A), and relative healing with patchy hyperemia was detected in the rectum (Figure 2B). The endoscopic Mayo score was evaluated as 1, which indicated that the integrated treatment induced both clinical and endoscopic remission. Subsequently, oral mesalazine was continued at a dose of 2 g/d with a QCD retention enema twice a week. The patient was last followed up on September 28, 2021, and he had no abdominal pain, nor bloody stool with mucus.

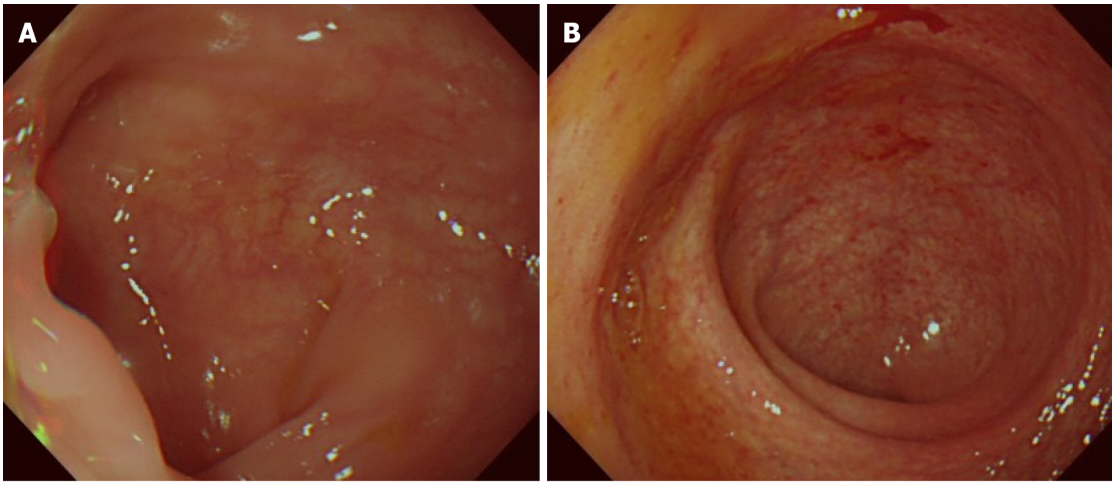

DOI: 10.12998/wjcc.v10.i11.3573

Figure 2 Endoscopic images after Qingchang decoction retention enema treatment. A: Colonoscopy image showing normal mucosa in the sigmoid colon; B: Colonoscopy image showing patchy hyperemia in the rectum.

DISCUSSION

As a subtype of inflammatory bowel disease (IBD), UC is characterized by chronic inflammation of the colonic mucosa and recurrent attack. The exact etiology and pathogenesis of UC remain unclear, and treatment options are limited. For long-standing UC, typically 8 or 10 years after disease onset, there is a defined risk of dysplasia and colorectal cancer caused by persistent large-scale colonic inflammation[4]. A targeted therapy that focuses on endoscopic mucosal healing rather than mere symptom remission has emerged as a new preferred concept in the management approach of IBD[5]. Mucosal healing refers to the resolution of inflammatory changes (Mayo endoscopic subscore of 0 or 1)[5]. It is essential to manage UC in the remission phase with the minimum category or dose of medicine due to the limited choice of medications.

The guidelines recommend oral mesalazine at a dose of ≥ 2.4 g/d combined with an amino-salicylic acid preparation enema ≥ 1 g/d as a first-line treatment for mild to moderate left-sided UC[3]. The guidelines also indicate that the local effect of mesalazine is better than that of topical corticosteroids. However, not all patients benefit from this treatment. For instance, the study by Marteau *et al*[6] showed that the remission rate of UC treated with mesalazine at a dose of 4 g/d combined with 1 g/d enema was 64%. A randomized controlled trial (RCT) by Hartmann *et al*[7] used mesalazine or budesonide enema therapy for patients with mild to moderate left-sided UC. The proportion of these patients in whom endoscopic remission (defined as an endoscopic score < 2) was achieved was 71.7% (76/106) and 68.0% (76/103), respectively. Bokemeyer *et al*[8] reported that 78.8%-84.4% of left-sided UC patients were assigned an endoscopic score of 0 or 1 (0 = normal or inactive disease; 1= mild disease, erythema, decreased vascular pattern, and mild friability) after 12 mo of oral mesalazine at a dose of 2 g/d. In conclusion, oral mesalazine and/or enema therapy is ineffective for approximately 20% to 30% of patients with left-sided UC. The guidelines[5] recommend using systemic corticosteroid therapy, but a large portion of patients in practice are unwilling to receive oral or intravenous corticosteroid therapy due to their side effects. For patients with poor outcomes with mesalazine treatment and who are unwilling to accept systemic corticosteroid treatment, TCM therapy is an effective option, which is also documented in China's IBD guidelines[1].

Although UC has no corresponding disease name in TCM, it has long been recorded throughout history and is well understood. According to the description of the clinical manifestations of "changpi", "Xiali", "chronic dysentery", and "recurrent dysentery" in the medical documents of the previous dynasties, it is not difficult to connect these diseases with UC. According to TCM theory, UC is located in the large intestine, and the main pathogenesis lies in dampness and heat accumulation. The stagnation of qi and blood with dampness and heat thus leads to the formation of pus. Heat toxicity also burns intestinal collaterals, causing blood perfusion outside of the collaterals. These pathological processes induce symptoms such as abdominal pain, diarrhea, and mucopurulent bloody stools. In the mid-1980s, Gui-Tong Ma, a renowned doctor at Longhua Hospital, developed the Qingchang suppository (QCS), which was the first suppository for rectal administration composed of pure Chinese herbs in China. QCS exerts its effect of clearing heat and dampness, promoting blood circulation and removing blood stasis by targeting four major pathogenic factors, namely, dampness, heat, toxicity, and blood stasis.

The QCS (Z05170722) consists of *Indigo naturalis* (IN), *Radix notoginseng*, *Gallnut*, *Herba portulacae* and *Borneol*[9]. As the most essential component of QCS, IN is a commonly used Chinese herb to cure UC by

reducing inflammation and rectal bleeding. A randomized, placebo-controlled trial conducted by Japanese researchers demonstrated that 8 wk of IN administration (0.5-2.0 g per day) induced a clinical response and mucosal healing in patients with active UC[10]. IN includes indigo and indirubin molecules[11], which act as representative human aryl hydrocarbon receptor (AHR) ligands. AHR signaling stimulates the production of interleukin-22 in mucosal type 3 innate lymphocytes, thus inducing the production of tight junction molecules and antimicrobial peptides, which contribute to mucosal healing[12]. IN also has an anti-inflammatory role by downregulating proinflammatory factors such as IL-1α, IL-6, IL-1β, IL-8 and TNF-α[13].

The mechanism of QCS has also been fully investigated. Sun *et al*[9] used QCS and sulfasalazine suppository (SASP) to treat rats with dextran sulfate sodium-induced colitis and normal control rats. The levels of the proinflammatory factors TNF-α and IL-6 were suppressed with both treatments, suggesting that QCS has anti-inflammatory effects. Moreover, the production of vascular endothelial growth factor (VEGF), hypoxia-inducible factor (HIF)-1α, and inducible NO synthase (iNOS) was also inhibited in the QCS- and SASP-treated groups, suggesting that QCS can restrain colonic vascular permeability and promote epithelial integrity and colonic hypoxia. Lu *et al*[14] administered low, medium, and high doses of QCS and SASP to rats with trinitro-benzene-sulfonic acid (TNBS)-induced colitis and observed the expression of F-actin protein, which is a major component of the cytoskeleton, through immunofluorescence. The study revealed that QCS can improve F-actin protein content based on reduction after modeling, which suggested that it can reduce the damage of UC to the mucosal cytoskeleton and protect the integrity of the intestinal barrier. These studies support the notion that QCS can effectively alleviate colonic inflammation in UC.

The clinical effect of QCS has been fully investigated. However, clinical trials aiming to identify the effect of QCD enema have not yet been conducted. A previous multicenter RCT demonstrated that an efficacy rate of 91.49% 8 wks after the initiation of QCS treatment at a dose of 2 g/d was achieved in patients with mild to moderate proctitis compared with 87.23% in the SASP treatment group ($P > 0.05$) [15]. Complete efficacy was defined as the basic disappearance of clinical symptoms and mild mucosal inflammation or the formation of pseudopolyps found by colonoscopy. The outcome of this study also demonstrated that QCS has more advantages in relieving symptoms such as abdominal pain and distention, tenesmus, mucopurulent stool, and burning anal pain. After a one-year follow-up of the QCS group (9.3%), the recurrence rate was significantly lower than that of the SASP group (26.83%). These results indicated that QCS is effective in inducing and maintaining clinical and mucosal remission.

Considering that the suppository application location is mainly limited to the rectum while an enema can reach the descending colon, a QCD enema was thus developed according to the components of QCS for the treatment of left-sided UC. In the case reported here, the patient with active left-sided UC suffered for 6 years after standard oral therapy with mesalazine and intermittent topical treatment. Based on oral mesalazine maintenance treatment, an additional QCD enema at a dose of 180 mL/d successfully induced endoscopic mucosal healing. Although this is a case report, it provides preliminary evidence for the treatment of active left-sided UC. In the future, we will continue to follow up with this patient and collect more cases of QCD treatment for UC to provide more evidence for its treatment effect in left-sided UC.

CONCLUSION

The case described herein demonstrates that the Chinese formula QCD retention enema can effectively reduce both the clinical and mucosal remission of left-sided UC, thus providing another effective therapy other than mesalazine. This finding provides a new understanding of the treatment of left-sided UC and a basis for further studies to determine the underlying mechanism of the QCD treatment effects.

FOOTNOTES

Author contributions: Li PH interpreted and reviewed the literature; Tang Y contributed to manuscript drafting and revision; Wen HZ was the patient's attending doctor and was responsible for revising the manuscript for important intellectual content; all authors issued final approval of the version to be submitted.

Supported by National Natural Science Foundation of China, No. 81703986.

Informed consent statement: Informed written consent was obtained from the patients for the publication of this report and any accompanying images.

Conflict-of-interest statement: The authors declare that they have no conflict of interest.

CARE Checklist (2016) statement: The authors have read the CARE Checklist (2016), and the manuscript was prepared and revised according to the CARE Checklist (2016).

Country/Territory of origin: China

ORCID number: Pei-Han Li 0000-0003-3084-7280; Yu Tang 0000-0003-3181-2987; Hong-Zhu Wen 0000-0002-6203-4869.

S-Editor: Chen YL
L-Editor: A
P-Editor: Chen YL

REFERENCES

1 **Inflammatory Bowel Disease Group**; Chinese Society of Gastroenterology (CSG), Chinese Medical Association. A consensus view on the diagnosis and treatment of inflammatory bowel disease (IBD). *Zhonghua Xiaohua Zazhi* 2018; **38**: 292-311 [DOI: 10.3760/cma.j.issn.0254-1432.2018.05.002]
2 **Chinese inflammatory bowel disease cooperative group**. Retrospective analysis of 3100 hospitalized cases of ulcerative colitis. *Zhonghua Xiaohua Zazhi* 2006; **26**: 368-372 [DOI: 10.3760/j.issn:0254-1432.2006.06.003]
3 **Harbord M**, Eliakim R, Bettenworth D, Karmiris K, Katsanos K, Kopylov U, Kucharzik T, Molnár T, Raine T, Sebastian S, de Sousa HT, Dignass A, Carbonnel F; European Crohn's and Colitis Organisation [ECCO]. Third European Evidence-based Consensus on Diagnosis and Management of Ulcerative Colitis. Part 2: Current Management. *J Crohns Colitis* 2017; **11**: 769-784 [PMID: 28513805 DOI: 10.1093/ecco-jcc/jjx009]
4 **Yashiro M**. Ulcerative colitis-associated colorectal cancer. *World J Gastroenterol* 2014; **20**: 16389-16397 [PMID: 25469007 DOI: 10.3748/wjg.v20.i44.16389]
5 **Rubin DT**, Ananthakrishnan AN, Siegel CA, Sauer BG, Long MD. ACG Clinical Guideline: Ulcerative Colitis in Adults. *Am J Gastroenterol* 2019; **114**: 384-413 [PMID: 30840605 DOI: 10.14309/ajg.0000000000000152]
6 **Marteau P**, Probert CS, Lindgren S, Gassul M, Tan TG, Dignass A, Befrits R, Midhagen G, Rademaker J, Foldager M. Combined oral and enema treatment with Pentasa (mesalazine) is superior to oral therapy alone in patients with extensive mild/moderate active ulcerative colitis: a randomised, double blind, placebo controlled study. *Gut* 2005; **54**: 960-965 [PMID: 15951542 DOI: 10.1136/gut.2004.060103]
7 **Hartmann F**, Stein J; BudMesa-Study Group. Clinical trial: controlled, open, randomized multicentre study comparing the effects of treatment on quality of life, safety and efficacy of budesonide or mesalazine enemas in active left-sided ulcerative colitis. *Aliment Pharmacol Ther* 2010; **32**: 368-376 [PMID: 20491741 DOI: 10.1111/j.1365-2036.2010.04354.x]
8 **Bokemeyer B**, Hommes D, Gill I, Broberg P, Dignass A. Mesalazine in left-sided ulcerative colitis: efficacy analyses from the PODIUM trial on maintenance of remission and mucosal healing. *J Crohns Colitis* 2012; **6**: 476-482 [PMID: 22398060 DOI: 10.1016/j.crohns.2011.10.006]
9 **Sun B**, Yuan J, Wang S, Lin J, Zhang W, Shao J, Wang R, Shi B, Hu H. Qingchang Suppository Ameliorates Colonic Vascular Permeability in Dextran-Sulfate-Sodium-Induced Colitis. *Front Pharmacol* 2018; **9**: 1235 [PMID: 30429788 DOI: 10.3389/fphar.2018.01235]
10 **Naganuma M**, Sugimoto S, Mitsuyama K, Kobayashi T, Yoshimura N, Ohi H, Tanaka S, Andoh A, Ohmiya N, Saigusa K, Yamamoto T, Morohoshi Y, Ichikawa H, Matsuoka K, Hisamatsu T, Watanabe K, Mizuno S, Suda W, Hattori M, Fukuda S, Hirayama A, Abe T, Watanabe M, Hibi T, Suzuki Y, Kanai T; INDIGO Study Group. Efficacy of Indigo Naturalis in a Multicenter Randomized Controlled Trial of Patients With Ulcerative Colitis. *Gastroenterology* 2018; **154**: 935-947 [PMID: 29174928 DOI: 10.1053/j.gastro.2017.11.024]
11 **Plitzko I**, Mohn T, Sedlacek N, Hamburger M. Composition of Indigo naturalis. *Planta Med* 2009; **75**: 860-863 [PMID: 19296433 DOI: 10.1055/s-0029-1185447]
12 **Sugimoto S**, Naganuma M, Kanai T. Indole compounds may be promising medicines for ulcerative colitis. *J Gastroenterol* 2016; **51**: 853-861 [PMID: 27160749 DOI: 10.1007/s00535-016-1220-2]
13 **Wang Y**, Liu L, Guo Y, Mao T, Shi R, Li J. Effects of indigo naturalis on colonic mucosal injuries and inflammation in rats with dextran sodium sulphate-induced ulcerative colitis. *Exp Ther Med* 2017; **14**: 1327-1336 [PMID: 28781623 DOI: 10.3892/etm.2017.4701]
14 **Lu L**, Xie JQ, Yuan JY, Qiu SK. Effect of Qingchang Suppository on fibroactin of colonic mucosa in rats with ulcerative colitis. *Zhongguo Zhongxiyi Jiehe Xiaohua Zazhi* 2012; **20**: 485-488 [DOI: 10.3969/j.issn.1671-038X.2012.11.002]
15 **Gong YP**, Liu W, Ma GT, Hu HY, Xie JQ, Tang ZP, Hao WW, Bian H, Zhu LY, Wu HP, Randomized controlled study of Qingchang Suppository in the treatment of ulcerative colitis. *Shanghai Zhongyiyao Daxue Xuebao* 2007; 33-36 [DOI: 10.3969/j.issn.1008-861X.2007.06.010]

World Journal of Clinical Cases

Submit a Manuscript: https://www.f6publishing.com

World J Clin Cases 2022 April 16; 10(11): 3579-3586

DOI: 10.12998/wjcc.v10.i11.3579

ISSN 2307-8960 (online)

CASE REPORT

Anti-nuclear matrix protein 2+ juvenile dermatomyositis with severe skin ulcer and infection: A case report and literature review

Ya-Ting Wang, Yu Zhang, Tao Tang, Chong Luo, Ming-Yue Liu, Li Xu, Li Wang, Xue-Mei Tang

Specialty type: Pediatrics

Provenance and peer review: Unsolicited manuscript; Externally peer reviewed.

Peer-review model: Single blind

Peer-review report's scientific quality classification

Grade A (Excellent): 0
Grade B (Very good): 0
Grade C (Good): C, C
Grade D (Fair): 0
Grade E (Poor): 0

P-Reviewer: Poddighe D, Kazakhstan; Wang CR, Taiwan

Received: December 7, 2021
Peer-review started: December 7, 2021
First decision: January 25, 2022
Revised: February 7, 2022
Accepted: February 27, 2022
Article in press: February 27, 2022
Published online: April 16, 2022

Ya-Ting Wang, Yu Zhang, Tao Tang, Chong Luo, Ming-Yue Liu, Li Xu, Li Wang, Xue-Mei Tang, Department of Rheumatology and Immunology; Ministry of Education Key Laboratory of Child Development and Disorders; National Clinical Research Center for Child Health and Disorders (Chongqing); China International Science and Technology Cooperation base of Child Development and Critical Disorders; Children's Hospital of Chongqing Medical University, Chongqing 400014, China

Ya-Ting Wang, Yu Zhang, Tao Tang, Chong Luo, Ming-Yue Liu, Li Xu, Li Wang, Xue-Mei Tang, Chongqing Key Laboratory of Child Infection and Immunity, Children's Hospital of Chongqing Medical University, Chongqing 400014, China

Corresponding author: Xue-Mei Tang, PhD, Chief Doctor, Department of Rheumatology and Immunology; Ministry of Education Key Laboratory of Child Development and Disorders; National Clinical Research Center for Child Health and Disorders (Chongqing); China International Science and Technology Cooperation base of Child Development and Critical Disorders; Children's Hospital of Chongqing Medical University, No. 136 Zhongshan 2nd Road, Yuzhong District, Chongqing 400014, China. tangxuemei2008@163.com

Abstract

BACKGROUND

Juvenile dermatomyositis (JDM) is an idiopathic inflammatory myopathy that occurs in childhood. It is characterized by muscle weakness and a characteristic rash. Previous literature reports have rarely described JDM with severe skin ulcers and infections.

CASE SUMMARY

Herein, we describe a case of a 2-year-old female patient who suffered from JDM, whose myositis-specific autoantibodies were positive for anti-nuclear matrix protein 2 antibody, with progressively worsening skin ulcers and severe infections. The patient was treated with glucocorticoids and various immunosuppressants. Nevertheless, further progression of the disease and the combination of primary disease and severe infection in the later period were fatal.

CONCLUSION

In children, anti-nuclear matrix protein 2+ JDM combined with skin ulcers often indicates severe disease. In such cases, personalized treatment for the primary disease and infection prevention and control are essential.

Key Words: Juvenile dermatomyositis; Skin ulcer; Anti-nuclear matrix protein 2 antibody; Case report

Core Tip: Juvenile dermatomyositis (JDM) is a rare systemic autoimmune disease characterized by specific skin lesions, chronic muscle inflammation, and systemic vasculitis. We report a very rare case of JDM with severe skin ulcers and infections. By reporting the disease development and treatment of this case of a patient positive for anti-nuclear matrix protein 2 (NXP2) antibody combined with skin ulcers and performing a comprehensive literature review, we summarize JDM with skin ulcers, the clinical characteristics of JDM combined with positivity for anti-NXP2 antibody, and treatment measures for severe JDM.

Citation: Wang YT, Zhang Y, Tang T, Luo C, Liu MY, Xu L, Wang L, Tang XM. Anti-nuclear matrix protein 2+ juvenile dermatomyositis with severe skin ulcer and infection: A case report and literature review. *World J Clin Cases* 2022; 10(11): 3579-3586
URL: https://www.wjgnet.com/2307-8960/full/v10/i11/3579.htm
DOI: https://dx.doi.org/10.12998/wjcc.v10.i11.3579

INTRODUCTION

Juvenile dermatomyositis (JDM) is a rare systemic autoimmune disease characterized by vascular disease that mainly affects muscles and skin, as well as the lungs, intestines, heart, and other organs[1-3]. JDM can also lead to macrophage activation syndrome, which is a potentially fatal complication of a number of rheumatological conditions[4]. JDM is the most common inflammatory myopathy in children and has been reported to affect 1.9 individuals per million children in the United Kingdom and 2.4-4.1 individuals per million children in the United States[5,6]. Skin ulcers are one of the severe manifestations of childhood dermatomyositis; however, cases of severe skin ulcers with infections are rarely reported. Here, we report a single case of a 2-year-old female patient who suffered from JDM and whose myositis-specific autoantibodies (MSAs) were positive for anti-nuclear matrix protein 2 antibody, with progressively worsening skin ulcers and severe infections.

CASE PRESENTATION

Chief complaints

A 2-year-old Chinese girl came to the Department of Rheumatology and Immunology with a heliotrope rash for 1 mo and muscle weakness for 10 d.

History of present illness

This patient developed a heliotrope rash, periorbital edema, and nailfold capillary changes within 1 mo, with symmetric proximal muscle weakness. There was no fever, cough, hoarseness, or sensory disturbance.

History of past illness

The patient had no significant medical or surgical history.

Personal and family history

The child was born at full term. Her parents and other family members had no family history of autoimmune or other diseases.

Physical examination

After admission, the patient's weight was 14 kg. There were heliotrope rashes on her face, periorbital edema, changes in nailfold capillaries, Gottron papules on the dorsal surface of the proximal interdigital (PIP), symmetric proximal muscle weakness of arms and legs, no erythema butterfly, and arthritis.

Laboratory examinations

Investigations revealed elevated creatine kinase of 12647 U/L (reference range, 50-220 U/L), lactate dehydrogenase (LDH) of 1358 U/L (reference range, 80-300 U/L), erythrocyte sedimentation rate (ESR) of 79 mm/h (reference range, 0-20 mm/h), and ferritin of 726 ng/mL (reference range, 10-120 ng/mL).

The autoantibody, immunoglobulin, and complement profiles were normal. Anti-nuclear matrix protein 2 (NXP-2) antibody was positive in the myositis spectrum, as determined by the dot-ELISA method, and no other myositis-associated autoantibodies were present (Table 1).

Imaging examinations

Magnetic resonance imaging (MRI) of the bilateral thighs revealed inflammatory changes in the musculature and subcutaneous fat layer of the thigh muscles on both sides, which were also characteristic of dermatomyositis. Electromyography (EMG) showed that the motor unit potential amplitude of the tibialis anterior and rectus femoris muscle was reduced, and the duration was shortened, thus suggesting myogenic abnormalities.

FINAL DIAGNOSIS

Characteristic skin lesions, proximal muscle weakness, elevated serum muscle enzyme levels, EMG myopathic abnormalities, and changes in muscle MRI findings confirmed the diagnosis of juvenile dermatomyositis.

TREATMENT

When the patient was diagnosed with anti-nuclear matrix protein 2 (NXP2)+ juvenile dermatomyositis, she initially received intravenous immunoglobulin (IVIG; 1 g/kg) for 2 d and high-dose glucocorticoids (GC; 15 mg/kg) for 3 d, after which she was treated with oral methylprednisolone (1.15 mg/kg.d), intravenous cyclophosphamide (IV CYC; 0.1 g/kg) for 2 d, methotrexate (MTX; 7.5 mg qw), hydroxychloroquine (0.05 g qd), and other symptomatic and supportive treatment. Following these treatments, the child's rash and edema basically disappeared, and her muscle strength improved.

In the following 8 mo, the girl was hospitalized 9 times, and she received IVIG 9 times (1 g/kg for 2 d each time) and IV CYC 6 times, replacing MTX and hydroxychloroquine with mycophenolate mofetil (MMF) and thalidomide. From the 4th month of the illness, she was treated with tofacitinib (2.5 mg bid). In the first three months after diagnosis, the child developed livedo reticularis on the skin of the extremities (Figure 1A) and ulcers on the buttock and left upper arm, while the ulcerated surfaces gradually increased. In the 6th month, yellow necrotic fascia was visible on the left buttock (Figure 1B). After she received proper wound care, anti-infection, and adjustment of immunosuppressants, the ulcers improved (in the 8th month), showing gradual scabbing. Nonetheless, her mother discontinued the patient's hospitalization. One month later, the patient suffered fatigue, anorexia, and multiple ulcers on the whole body again, which were worse than before. She never showed calcinosis during the whole course of the disease. After rehospitalization, she was given tocilizumab (12 mg/kg). However, when she received 20% of the infusion, the patient developed irritability, and her heart rate increased; thus, the administration of tocilizumab was stopped.

In the 10th month after diagnosis, the child was hospitalized for the last time because of bloody stools, fever, anorexia, listlessness, and multiple painful skin ulcers throughout the whole body (Figure 1C and D). The patient could not move on the bed by herself because of low muscle strength. Laboratory examinations revealed CK of 289 U/L, LDH of 689 U/L, and ESR of 92 mm/hr. Skin tissue biopsy of the left upper arm and left neck suggested epidermal necrosis, hyperplasia of subepidermal fibers and fatty tissues, visible vitreous and mucous changes, multifocal necrosis of the subepidermis and dermis, and focal chronic inflammatory cell infiltration. We used ceftazidime to fight infections and added vancomycin after 2 d. Pathogen detection in the pus from the buttock suggested *Escherichia coli*. Accordingly, the antibiotics were adjusted to vancomycin and meropenem; however, the ulcers further deepened (Figure 2A and B). After 9 d, re-examination of the culture revealed *Pseudomonas aeruginosa* and *Staphylococcus epidermidis*. Based on susceptibility testing, the antibiotics were changed to amikacin and ciprofloxacin. Other treatments included adjusting oral methylprednisolone at 6 mg qd (0.5 mg/kg·d) to intravenous methylprednisolone at 10 mg bid (2 mg/kg·d). During this period, the systemic dressing was changed at least 3 times per week, while IVIG, human albumin, component blood transfusion, and other symptomatic and supportive treatments were intermittently given.

OUTCOME AND FOLLOW-UP

On the 48th day after admission, gastrointestinal bleeding and shock occurred, after which the girl was transferred to the ICU. She was discharged 6 d later and died a few days after leaving the hospital.

Table 1 Laboratory examinations at the first hospital admission

Laboratory examinations	
CBC	WBC: 6.71 × 10^9/L, PLT: 165 × 10^9/L, L: 0.37, N: 0.54, Hb: 120 g/L, CRP < 8 mg/L
Biochemical examination	CK: 12647 U/L, LDH: 1358 U/L, ALT: 116.6 U/L, AST: 359.5 U/L
ESR	79 mm/h
Ferritin	726 ng/mL
Autoantibody profile	Negative
Immunoglobulins	Normal
Complements	Normal
MSA	Anti-nuclear matrix protein 2 antibody positive

ALT: Alanine aminotransferase; AST: Aspartate transaminase; CBC: Complete blood count; CK: Creatine kinase; ESR: Erythrocyte sedimentation rate; LDH: Lactate dehydrogenase; MSA: Myositis-specific autoantibody.

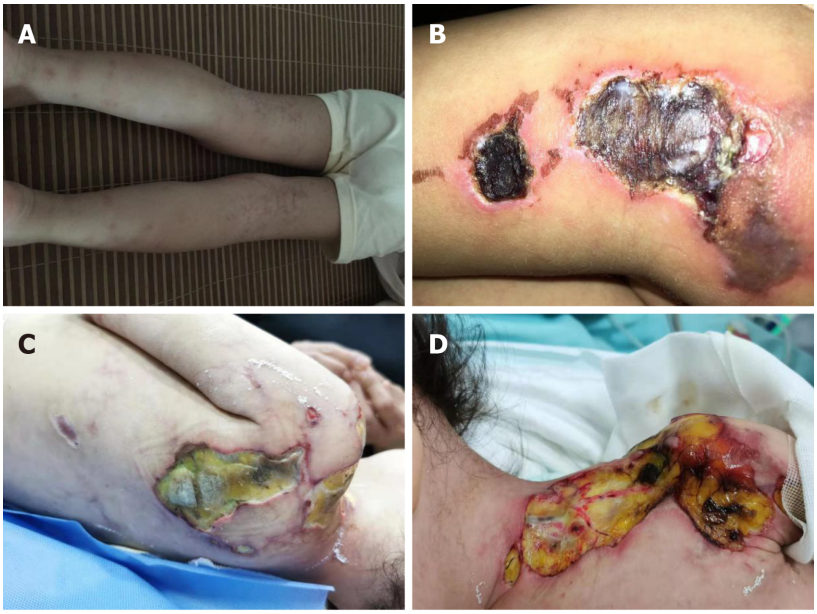

DOI: 10.12998/wjcc.v10.i11.3579

Figure 1 Clinal examination 3, 6, and 10 mo after diagnosis. A: 3 mo, livedo reticularis; B: 6 mo, ulcers in the buttock; C and D: 10 mo, ulcers in the back (C) and left (D) shoulder.

DISCUSSION

JDM is a rheumatic disease that occurs in childhood, with a mortality rate reaching approximately < 4%, which is second only to systemic lupus erythematosus[7,8]. With early treatment, 30%-50% of patients are likely to achieve remission within 2-3 years from the onset of the disease. In addition to the characteristic skin lesions, other criteria include symmetric proximal muscle weakness, elevated serum muscle enzyme levels, myopathic changes on electromyogram, and typical muscle biopsy results[9].

An ulcer is one of the most serious skin manifestations of JDM and is widely regarded as an indication for more intensive treatment[10]. In different cohorts, the incidence of JDM skin ulcers has been reported to range from 2.6%-23%[7,11,12]. Rare cases have shown such severe skin ulceration with multiple pathogenic infections. Cutaneous ulceration may occur on any soft tissue in JDM, especially the armpits, elbows, or pressure points. Although rare, gluteal ulcers are more likely to worsen due to irritation caused by stool, urine, friction, and maceration, especially in infants and young children[13]. In our case, the child's gluteal ulcer had a protracted condition that gradually expanded and deepened and was accompanied by refractory bacterial infection. Infection and JDM promote each other, which increases the difficulty of treatment and leads to prolonged and unhealed ulcers. A case of JDM in an infant with gluteal ulcer has been reported in Japan. After treatment with high-dose glucocorticoids with cyclophosphamide and MTX, the ulcer gradually healed[13]; however, this case was not

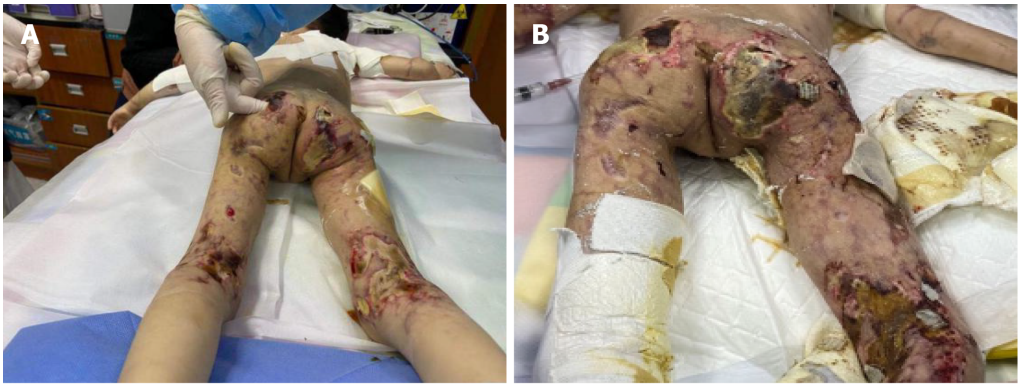

DOI: 10.12998/wjcc.v10.i11.3579

Figure 2 Deepening of the ulcers after treatment (A and B).

accompanied by serious infection. To prevent infection and promote ulcer healing, topical treatments and routine care for skin ulcers are necessary. In 2020, guidelines for skin ulcers related to connective tissue diseases were published in Japan, which in detail described systemic and local medication, nursing, and other treatment methods for skin ulcers and for different connective tissue diseases[14].

Persistent progression of skin ulcers has also been associated with neglected assessment of skin manifestations and severity of JDM. An expert group recommends that the follow-up of patients with JDM should focus more on the evaluation of the skin, including the use of multiple scales[8].The Cutaneous Dermatomyositis Disease Activity and Severity Index(CDASI) and the Cutaneous Assessment Tool (CAT)have good interrater reliability and correlation with other measures of activity and damage in children with JDM[15]. The child in our case had prominent skin damage in the later stage. Early assessment of skin may help with follow-up treatment. Additional assessment tools can be used in clinical practice to more comprehensively assess disease activity[16].

In recent years, JDM combined with different MSAs has received extensive clinical attention. Different MSAs have been associated with different clinical phenotypes, prognoses, and risks of associated malignancy. In United States and European cohorts, MSAs were reported to be present in approximately 70% of JDM cases[17,18].

NXP2 is a protein involved in transcription and RNA metabolism regulation[19]. The autoantibody was first identified in 1997 in childhood myositis and was considered a key biomarker for the diagnosis of idiopathic inflammatory myopathy[20]. Clinically, anti-NXP2+ JDM often manifests as obvious skin rash, muscle weakness, dysphagia, calcinosis, limb edema, younger age of onset and less remission at 2 years[16]. The incidence of anti-NXP2+ JDM is 20%-25% among JDM cases, making anti-NXP2 a common type of antibody[19]. Two different studies in China have revealed detection rates of anti-NXP2 antibodies in JDM of 30.6% and 20%[21,22]. Albayda *et al*[23] found that NXP2+ dermatomyositis with limb weakness and neck muscle weakness were more serious than NXP2- dermatomyositis; accordingly, as our patient showed severe weakness. Another feature of NXP2+ JDM is calcinosis, although this was not present in our case. Early diagnosis and treatment of JDM can prevent the occurrence of calcinosis[24]. As there is no definitive treatment for severe calcinosis, surgical treatment is often necessary; however, there is still the possibility of recurrence[25]. Although most NXP2+ JDM patients are sensitive to GC, some patients are prone to severe and refractory JDM manifestations.

Immediately after the diagnosis of JDM was made, we treated this patient with corticosteroids and immunosuppressants. Systemic corticosteroids are the gold-standard initial treatment for JDM. However, they should not be used as monotherapy because this approach is frequently ineffective and associated with the development of unacceptable long-term adverse effects[26]. Immunosuppressants have steroid protection and are recommended even for mild cases to minimize the adverse effects of long-term GC treatment. Treatments used for refractory disease include IVIG, cyclophosphamide, cyclosporine, azathioprine, MMF, hydroxychloroquine, tacrolimus, rituximab, infliximab, and autologous stem cell transplantation[8]. Some studies suggest that treatment with GC and cyclophosphamide combined with calcineurin inhibitors is very important for dermatomyositis patients with skin ulcers or other severe manifestations[27]. A JAK-inhibitor (JAKi) can be used to treat JDM and has been reported to be partially effective for interstitial lung disease and cutaneous dermatomyositis[28,29]. However, in the present case, a JAKi did not stop the progression of the disease. For NXP2+ JDM and severe JDM, many studies have reported a favorable therapeutic effect of rituximab[19,30], which can reduce disease activity and reduce GC use. Additionally, rituximab can ameliorate the skin symptoms of refractory JDM and is effective for skin ulcers of JDM[19]. However, because the skin ulcers in this case were accompanied by severe infection, we were worried that the use of rituximab would further aggravate the infection, so it was not used. We tried tocilizumab, but the patient could not tolerate it. Plasmapheresis can be considered for the treatment of cases refractory to immunosuppressants[8].

For JDM-related skin ulcers, steroids and immunosuppressants should be first used to control the primary disease. However, if skin ulcers are complicated by infections, this type of treatment may exacerbate the ulcers due to the increased susceptibility of the patient to infection[14]. Therefore, in such cases, it is necessary to treat the primary disease and the infection simultaneously. According to the pathogenic examination and drug susceptibility results of the site of infection, appropriate antibacterial drugs were chosen, and the use of IVIG was considered. Due to the refractory nature of cutaneous vasculitis in JDM, case studies suggest that nifedipine, sildenafil, intravenous prostaglandins, and bosentan should be added as early adjuncts[26,31].

In the present case, after high-dose GC treatment, IVIG, MTX, MMF, hydroxychloroquine, a JAKi, thalidomide, and tocilizumab were given to the patient, and improvement was observed; however, the disease was not completely prevented. Further progression of the disease and the combination of primary disease and severe infection in the later period were fatal. It remains unknown whether the early use of vasodilatory agents and rituximab or plasmapheresis at the proper time could save patients' lives, which future studies should address.

CONCLUSION

Only scarce reports of JDM with severe ulcers accompanied by infection have been reported. Skin ulcer-complicated and anti-NXP2+ JDM usually represent severe cases, and it is important to actively prevent the occurrence of infection while GC and appropriate immunosuppressive therapy are used. According to the different clinical manifestations and immunological indicators of JDM patients, appropriate assessment tools should be used to comprehensively assess the condition of JDM patients at an early stage, and individualized treatment plans should be customized.

FOOTNOTES

Author contributions: Tang XM conceived and designed the study and revised the manuscript; Wang YT collected medical records and wrote the manuscript; Zhang Y collected medical records and participated in its design; Tang T collected medical records and provided pictures; Luo C participated in study design and coordination; Liu MY, Xu L, and Wang L collected and organized the literature; All authors read and approved the final manuscript.

Informed consent statement: All study participants, or their legal guardian, provided informed written consent prior to study enrollment.

Conflict-of-interest statement: The authors declare that they have no conflict of interest.

CARE Checklist (2016) statement: The authors have read the CARE Checklist (2016), and the manuscript was prepared and revised according to the CARE Checklist (2016).

Country/Territory of origin: China

ORCID number: Ya-Ting Wang 0000-0003-3498-6181; Yu Zhang 0000-0003-1124-6543; Tao Tang 0000-0002-6467-0922; Chong Luo 0000-0002-7271-3064; Ming-Yue Liu 0000-0002-1934-778X; Li Xu 0000-0002-7288-1607; Li Wang 0000-0003-4663-102X; Xue-Mei Tang 0000-0002-6658-8084.

S-Editor: Gong ZM
L-Editor: A
P-Editor: Gong ZM

REFERENCES

1 **Rider LG**, Lidsley CB, Miller FW. Juvenile dermatomyositis. In: Petty RE, Laxer RM, Lindsey CB, Wedderburn LR, editors. Textbook of pediatric rheumatology, 7th ed. Philadelphia: Elsevier Saunder; 2016: 351-384
2 **Feldman BM**, Rider LG, Reed AM, Pachman LM. Juvenile dermatomyositis and other idiopathic inflammatory myopathies of childhood. *Lancet* 2008; **371**: 2201-2212 [PMID: 18586175 DOI: 10.1016/S0140-6736(08)60955-1]
3 **Varnier GC**, Pilkington CA, Wedderburn LR. Juvenile dermatomyositis: novel treatment approaches and outcomes. *Curr*

Opin Rheumatol 2018; **30**: 650-654 [PMID: 30124602 DOI: 10.1097/BOR.0000000000000538]
4 **Poddighe D**, Dauyey K. Macrophage activation syndrome in juvenile dermatomyositis: a systematic review. *Rheumatol Int* 2020; **40**: 695-702 [PMID: 31529231 DOI: 10.1007/s00296-019-04442-1]
5 **Mendez EP**, Lipton R, Ramsey-Goldman R, Roettcher P, Bowyer S, Dyer A, Pachman LM; NIAMS Juvenile DM Registry Physician Referral Group. US incidence of juvenile dermatomyositis, 1995-1998: results from the National Institute of Arthritis and Musculoskeletal and Skin Diseases Registry. *Arthritis Rheum* 2003; **49**: 300-305 [PMID: 12794783 DOI: 10.1002/art.11122]
6 **Gowdie PJ**, Allen RC, Kornberg AJ, Akikusa JD. Clinical features and disease course of patients with juvenile dermatomyositis. *Int J Rheum Dis* 2013; **16**: 561-567 [PMID: 24164844 DOI: 10.1111/1756-185X.12107]
7 **Mathiesen PR**, Zak M, Herlin T, Nielsen SM. Clinical features and outcome in a Danish cohort of juvenile dermatomyositis patients. *Clin Exp Rheumatol* 2010; **28**: 782-789 [PMID: 21029565]
8 **Bellutti Enders F**, Bader-Meunier B, Baildam E, Constantin T, Dolezalova P, Feldman BM, Lahdenne P, Magnusson B, Nistala K, Ozen S, Pilkington C, Ravelli A, Russo R, Uziel Y, van Brussel M, van der Net J, Vastert S, Wedderburn LR, Wulffraat N, McCann LJ, van Royen-Kerkhof A. Consensus-based recommendations for the management of juvenile dermatomyositis. *Ann Rheum Dis* 2017; **76**: 329-340 [PMID: 27515057 DOI: 10.1136/annrheumdis-2016-209247]
9 **Bohan A**, Peter JB. Polymyositis and dermatomyositis (first of two parts). *N Engl J Med* 1975; **292**: 344-347 [PMID: 1090839 DOI: 10.1056/NEJM197502132920706]
10 **Martin N**, Krol P, Smith S, Beard L, Pilkington CA, Davidson J, Wedderburn LR; Juvenile Dermatomyositis Research Group (JDRG). Comparison of children with onset of juvenile dermatomyositis symptoms before or after their fifth birthday in a UK and Ireland juvenile dermatomyositis cohort study. *Arthritis Care Res (Hoboken)* 2012; **64**: 1665-1672 [PMID: 22674907 DOI: 10.1002/acr.21753]
11 **Sun C**, Lee JH, Yang YH, Yu HH, Wang LC, Lin YT, Chiang BL. Juvenile dermatomyositis: a 20-year retrospective analysis of treatment and clinical outcomes. *Pediatr Neonatol* 2015; **56**: 31-39 [PMID: 24985888 DOI: 10.1016/j.pedneo.2014.02.006]
12 **Sag E**, Demir S, Bilginer Y, Talim B, Haliloglu G, Topaloglu H, Ozen S. Clinical features, muscle biopsy scores, myositis specific antibody profiles and outcome in juvenile dermatomyositis. *Semin Arthritis Rheum* 2021; **51**: 95-100 [PMID: 33360233 DOI: 10.1016/j.semarthrit.2020.10.007]
13 **Wakiguchi H**, Takei S, Imanaka H, Hiraki T, Higashi M, Yamatou T, Yamasaki Y, Kubota T, Kawano Y. Severe gluteal skin ulcers in an infant with juvenile dermatomyositis. *Eur J Dermatol* 2016; **26**: 192-193 [PMID: 26712099 DOI: 10.1684/ejd.2015.2701]
14 **Fujimoto M**, Asai J, Asano Y, Ishii T, Iwata Y, Kawakami T, Kodera M, Abe M, Amano M, Ikegami R, Isei T, Isogai Z, Ito T, Inoue Y, Irisawa R, Ohtsuka M, Omoto Y, Kato H, Kadono T, Kaneko S, Kanoh H, Kawaguchi M, Kukino R, Kono T, Koga M, Sakai K, Sakurai E, Sarayama Y, Shintani Y, Tanioka M, Tanizaki H, Tsujita J, Doi N, Nakanishi T, Hashimoto A, Hasegawa M, Hayashi M, Hirosaki K, Fujita H, Fujiwara H, Maekawa T, Matsuo K, Madokoro N, Motegi SI, Yatsushiro H, Yamasaki O, Yoshino Y, Pavoux AJL, Tachibana T, Ihn H; Japanese Dermatological Association Guidelines. Wound, pressure ulcer and burn guidelines - 4: Guidelines for the management of connective tissue disease/vasculitis-associated skin ulcers. *J Dermatol* 2020; **47**: 1071-1109 [PMID: 31960490 DOI: 10.1111/1346-8138.15186]
15 **Tiao J**, Feng R, Berger EM, Brandsema JF, Coughlin CC, Khan N, Kichula EA, Lerman MA, Lvovich S, McMahon PJ, Rider LG, Rubin AI, Scalzi LV, Smith DM, Taxter AJ, Treat JR, Williams RP, Yum SW, Okawa J, Werth VP. Evaluation of the reliability of the Cutaneous Dermatomyositis Disease Area and Severity Index and the Cutaneous Assessment Tool-Binary Method in juvenile dermatomyositis among paediatric dermatologists, rheumatologists and neurologists. *Br J Dermatol* 2017; **177**: 1086-1092 [PMID: 28421601 DOI: 10.1111/bjd.15596]
16 **Kim H**, Huber AM, Kim S. Updates on Juvenile Dermatomyositis from the Last Decade: Classification to Outcomes. *Rheum Dis Clin North Am* 2021; **47**: 669-690 [PMID: 34635298 DOI: 10.1016/j.rdc.2021.07.003]
17 **Tansley SL**, Betteridge ZE, Gunawardena H, Jacques TS, Owens CM, Pilkington C, Arnold K, Yasin S, Moraitis E, Wedderburn LR, McHugh NJ; UK Juvenile Dermatomyositis Research Group. Anti-MDA5 autoantibodies in juvenile dermatomyositis identify a distinct clinical phenotype: a prospective cohort study. *Arthritis Res Ther* 2014; **16**: R138 [PMID: 24989778 DOI: 10.1186/ar4600]
18 **Rider LG**, Nistala K. The juvenile idiopathic inflammatory myopathies: pathogenesis, clinical and autoantibody phenotypes, and outcomes. *J Intern Med* 2016; **280**: 24-38 [PMID: 27028907 DOI: 10.1111/joim.12444]
19 **Aggarwal R**, Loganathan P, Koontz D, Qi Z, Reed AM, Oddis CV. Cutaneous improvement in refractory adult and juvenile dermatomyositis after treatment with rituximab. *Rheumatology (Oxford)* 2017; **56**: 247-254 [PMID: 27837048 DOI: 10.1093/rheumatology/kew396]
20 **Oddis CV**, Fertig N, Goel A, Espada G, Confalone Gregorian M, Cocco JAM, Londino AV. Clinical and serological characterization of the anti-MJ antibody in childhood myositis. *Arthritis Rheum* 1997; **40**: S139
21 **Wang X**, Ding Y, Zhou Z, Hou J, Xu Y, Li J. Clinical characteristics and poor predictors of anti-NXP2 antibody-associated Chinese JDM children. *Pediatr Rheumatol Online J* 2021; **19**: 6 [PMID: 33407621 DOI: 10.1186/s12969-020-00492-z]
22 **Li DM**, Wang L, Liu MY, Xu L, Tang XM. [The analysis of clinical phenotypes and autoantibodies in juvenile dermatomyositis]. *Zhonghua Er Ke Za Zhi* 2020; **58**: 966-972 [PMID: 33256317 DOI: 10.3760/cma.j.cn112140-20200724-00751]
23 **Albayda J**, Pinal-Fernandez I, Huang W, Parks C, Paik J, Casciola-Rosen L, Danoff SK, Johnson C, Christopher-Stine L, Mammen AL. Antinuclear Matrix Protein 2 Autoantibodies and Edema, Muscle Disease, and Malignancy Risk in Dermatomyositis Patients. *Arthritis Care Res (Hoboken)* 2017; **69**: 1771-1776 [PMID: 28085235 DOI: 10.1002/acr.23188]
24 **Hoeltzel MF**, Oberle EJ, Robinson AB, Agarwal A, Rider LG. The presentation, assessment, pathogenesis, and treatment of calcinosis in juvenile dermatomyositis. *Curr Rheumatol Rep* 2014; **16**: 467 [PMID: 25366934 DOI: 10.1007/s11926-014-0467-y]
25 **Kobayashi I**, Akioka S, Kobayashi N, Iwata N, Takezaki S, Nakaseko H, Sato S, Nishida Y, Nozawa T, Yamasaki Y, Yamazaki K, Arai S, Nishino I, Mori M. Clinical practice guidance for juvenile dermatomyositis (JDM) 2018-Update. *Mod*

Rheumatol 2020; **30**: 411-423 [PMID: 31955618 DOI: 10.1080/14397595.2020.1718866]

26 **Waldman R**, DeWane ME, Lu J. Dermatomyositis: Diagnosis and treatment. *J Am Acad Dermatol* 2020; **82**: 283-296 [PMID: 31279813 DOI: 10.1016/j.jaad.2019.05.105]

27 **Ishigaki K**, Maruyama J, Hagino N, Murota A, Takizawa Y, Nakashima R, Mimori T, Setoguchi K. Skin ulcer is a predictive and prognostic factor of acute or subacute interstitial lung disease in dermatomyositis. *Rheumatol Int* 2013; **33**: 2381-2389 [PMID: 23553518 DOI: 10.1007/s00296-013-2735-y]

28 **Kurasawa K**, Arai S, Namiki Y, Tanaka A, Takamura Y, Owada T, Arima M, Maezawa R. Tofacitinib for refractory interstitial lung diseases in anti-melanoma differentiation-associated 5 gene antibody-positive dermatomyositis. *Rheumatology (Oxford)* 2018; **57**: 2114-2119 [PMID: 30060040 DOI: 10.1093/rheumatology/key188]

29 **Moghadam-Kia S**, Charlton D, Aggarwal R, Oddis CV. Management of refractory cutaneous dermatomyositis: potential role of Janus kinase inhibition with tofacitinib. *Rheumatology (Oxford)* 2019; **58**: 1011-1015 [PMID: 30608616 DOI: 10.1093/rheumatology/key366]

30 **Oddis CV**, Reed AM, Aggarwal R, Rider LG, Ascherman DP, Levesque MC, Barohn RJ, Feldman BM, Harris-Love MO, Koontz DC, Fertig N, Kelley SS, Pryber SL, Miller FW, Rockette HE; RIM Study Group. Rituximab in the treatment of refractory adult and juvenile dermatomyositis and adult polymyositis: a randomized, placebo-phase trial. *Arthritis Rheum* 2013; **65**: 314-324 [PMID: 23124935 DOI: 10.1002/art.37754]

31 **Combalia A**, Giavedoni P, Tamez L, Grau-Junyent JM, Mascaró JM Jr. Bosentan for Cutaneous Ulcers in Anti-MDA5 Dermatomyositis. *JAMA Dermatol* 2018; **154**: 371-373 [PMID: 29344607 DOI: 10.1001/jamadermatol.2017.5462]

World Journal of Clinical Cases

Submit a Manuscript: https://www.f6publishing.com

World J Clin Cases 2022 April 16; 10(11): 3587-3592

DOI: 10.12998/wjcc.v10.i11.3587

ISSN 2307-8960 (online)

CASE REPORT

Ultrasound-guided local ethanol injection for fertility-preserving cervical pregnancy accompanied by fetal heartbeat: Two case reports

Toshiyuki Kakinuma, Kaoru Kakinuma, Yoshio Matsuda, Michitaka Ohwada, Kaoru Yanagida, Hirotsune Kaijima

Specialty type: Obstetrics and gynecology

Provenance and peer review: Unsolicited article; Externally peer reviewed.

Peer-review model: Single blind

Peer-review report's scientific quality classification

Grade A (Excellent): 0
Grade B (Very good): 0
Grade C (Good): C, C
Grade D (Fair): 0
Grade E (Poor): 0

P-Reviewer: Feng J, China; Zhao Q, China

Received: December 1, 2021
Peer-review started: December 1, 2021
First decision: January 22, 2022
Revised: February 7, 2022
Accepted: February 27, 2022
Article in press: February 27, 2022
Published online: April 16, 2022

Toshiyuki Kakinuma, Kaoru Kakinuma, Yoshio Matsuda, Michitaka Ohwada, Kaoru Yanagida, Department of Obstetrics and Gynecology, International University of Health and Welfare Hospital, Nasushiobara 329-2763, Japan

Hirotsune Kaijima, Minatomirai Yume Clinic, Yokohama 220-0012, Japan

Corresponding author: Toshiyuki Kakinuma, MD, PhD, Professor, Department of Obstetrics and Gynecology, International University of Health and Welfare Hospital, 537-3, Iguchi, Nasushiobara 329-2763, Japan. kakinuma@iuhw.ac.jp

Abstract

BACKGROUND

The incidence of cervical pregnancy is increasing due to the recent widespread application of assisted reproductive technology. Although hysterectomy has been a treatment option, high-sensitivity human chorionic gonadotropin testing and improved accuracy of transvaginal ultrasound imaging have increased possibility of uterine preservation. Dilation and curettage with methotrexate therapy and uterine artery embolization have been reported as treatments with fertility preservation; however, certain disadvantages limit their use.

CASE SUMMARY

In our two reported cases, we avoided massive bleeding and immediately resumed infertility treatment using ultrasound-guided local ethanol injection for cervical pregnancies with fetal heartbeats.

CONCLUSION

This treatment may be a new fertility-preserving option for cervical pregnancy.

Key Words: Ultrasonography; Ethanol; Infertility; Fertility preservation; Methotrexate; Case report

Core Tip: We describe the use of transvaginal ultrasound-guided local injection of absolute ethanol as a new treatment method for cervical pregnancy that preserves fertility. In both cases, the patients had developed cervical pregnancy through assisted reproductive technology and sought fertility-preserving treatment. A local injection of absolute ethanol allowed resumption of menstruation 2 mo after treatment and early resumption of infertility treatment without any complications. We suggest that local injection of absolute ethanol for cervical pregnancy could be a safe and effective new treatment method.

Citation: Kakinuma T, Kakinuma K, Matsuda Y, Ohwada M, Yanagida K, Kaijima H. Ultrasound-guided local ethanol injection for fertility-preserving cervical pregnancy accompanied by fetal heartbeat: Two case reports. *World J Clin Cases* 2022; 10(11): 3587-3592
URL: https://www.wjgnet.com/2307-8960/full/v10/i11/3587.htm
DOI: https://dx.doi.org/10.12998/wjcc.v10.i11.3587

INTRODUCTION

Cervical pregnancies occur in approximately 1 in 9000 pregnancies[1,2]. They are believed to be more common in those with a history of abortion or cesarean delivery, and are more common with assisted reproductive technology than with natural pregnancies[3]. The cervix contains very little smooth muscle, and it is thought that the villi easily infiltrate the muscular layer and form a high degree of placenta accreta. Furthermore, careless intracervical curettage for cervical pregnancy may cause complicated massive bleeding. Therefore, hysterectomy should be considered for treatment.

However, the recent development of high-sensitivity human chorionic gonadotropin (hCG) testing and improved accuracy of transvaginal ultrasound imaging have allowed asymptomatic diagnosis and increased fertility preservation due to early intervention. Dilation and curettage with methotrexate (MTX) therapy[4] and uterine artery embolization (UAE)[5] have been reported as treatments for the preservation of fertility. However, in patients who wish to preserve fertility, MTX therapy poses problems that may include ovarian dysfunction and a delay in resumption of infertility treatment due to the washout period[6]. Furthermore, there are many reported cases of unsuccessful MTX administration in cases accompanied by fetal heartbeat or blood hCG concentration of ≥ 10000 mIU/mL[7]. Moreover, with UAE, the rate of preterm birth in subsequent pregnancies may increase, and placenta accreta may occur[8].

There have been reports on the efficacy and safety of ultrasound-guided local ethanol injection as an alternative to topical MTX therapy in ectopic pregnancy[9,10]. This therapy has the potential to become a treatment option, as it does not require a washout period and has fewer complications than UAE therapy. Nevertheless, reports on this topic are scarce. In this report, we present two cases of cervical pregnancy with fetal heartbeat and elevated blood hCG concentration, in which fertility was preserved using local ethanol therapy.

CASE PRESENTATION

Chief complaints

Case 1: A 39-year-old nulliparous woman achieved pregnancy *via in vitro* fertilization-embryo transfer (IVF-ET). Ultrasonographic images at 6 wk 2 d of gestation suggested cervical pregnancy; therefore, she was referred to our hospital for detailed examination and treatment.

Case 2: A 33-year-old woman, gravida 2, para 1 had achieved pregnancy *via* IVF-ET. Ultrasound imaging results at 7 wk 6 d of gestation suggested cervical pregnancy; therefore, she was referred to our hospital for further examination and treatment.

History of present illness

Cases 1 and 2: The patients were asymptomatic aside from the ultrasonographic images suggesting cervical pregnancy.

History of past illness

Cases 1 and 2: The patients reported no notable past illness.

Personal and family history

Cases 1 and 2: No notable personal or family medical history.

Physical examination

Case 1: Findings upon presentation included blood pressure of 128/72 mmHg, pulse rate of 72 beats/min, and body temperature of 36.8 ℃.

Case 2: Findings upon presentation included a blood pressure of 104/79 mmHg, pulse rate of 78 beats/min, and body temperature of 36.9 ℃.

Laboratory examinations

Case 1: Blood testing revealed an elevated hCG concentration of 16346 mIU/mL and no other abnormalities noted.

Case 2: Blood testing revealed an elevated hCG concentration of 26930 mIU/mL and no other noteworthy abnormalities.

Imaging examinations

Case 1: Transvaginal ultrasonography revealed no gestational sac (GS) within the uterine body; however, a 21-mm GS-like mass with a fetal heartbeat was found within the cervix (Figure 1).

Case 2: Transvaginal ultrasonography revealed a 30 mm cervical GS with fetal heartbeat, and blood flow was noted around the GS by color Doppler imaging (Figure 2).

FINAL DIAGNOSIS

In both cases, based on the findings, cervical pregnancy was diagnosed.

TREATMENT

Case 1

MTX therapy was offered as a treatment option because of the patient's desire to preserve fertility. The patient declined MTX therapy after learning that side effects may include ovarian dysfunction and that a course of contraception was required during MTX washout. Dilation and curettage with UAE were also presented as options; however, the patient declined these after understanding that UAE may affect subsequent pregnancies. As such, the patient sought other fertility-preserving therapies. Therefore, we offered transvaginal ultrasound-guided local absolute ethanol injection because it allows early resumption of infertility treatment and has little effect on ovarian function and subsequent pregnancy. We also emphasized its efficacy and safety in patients with ectopic pregnancies. We explained that the use of local absolute ethanol injection for cervical pregnancy is an off-label and unestablished treatment at this time. Upon explaining the above, the patient and her family chose this treatment.

The treatment involved local injection of 2.5 mL absolute ethanol around the cervical GS using a 23-gauge percutaneous transhepatic cholangiography (PTC) needle under transvaginal ultrasonic guidance (Hakko Co., Ltd., Nagano, Japan). The blood hCG concentration 2 h after treatment was decreased by 20% from the pretreatment value; therefore, the therapeutic effect was confirmed. However, the blood hCG concentration increased the next day to 18087 mIU/mL; therefore, 2.5 mL absolute ethanol was injected again in the same manner. Thereafter, the blood hCG concentration decreased steadily, and spontaneous passage of the GS was observed 7 d after the second local injection of absolute ethanol. Histopathological examination revealed decidua and chorionic villi.

Case 2

The patient and her family sought fertility-preserving treatment. As in Case 1, the patient chose transvaginal ultrasound-guided local absolute ethanol injection among the available fertility-preserving treatments.

Using a 23-gauge PTC needle, 4.0 mL absolute ethanol was locally injected around the cervical GS under transvaginal ultrasonic guidance (Hakko Co., Ltd.). The blood hCG concentration 2 h after treatment was 20% less than the pretreatment value, verifying the therapeutic effect. Thereafter, the blood hCG concentration decreased steadily, and the GS spontaneously passed 6 d after the local injection of absolute ethanol. Histopathological examination revealed decidua and chorionic villi.

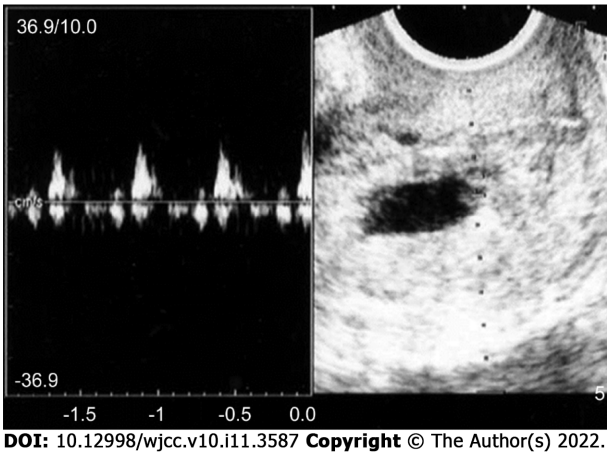

DOI: 10.12998/wjcc.v10.i11.3587

Figure 1 Transvaginal ultrasound findings in Case 1. A gestational sac with fetal heartbeat was found in the cervix.

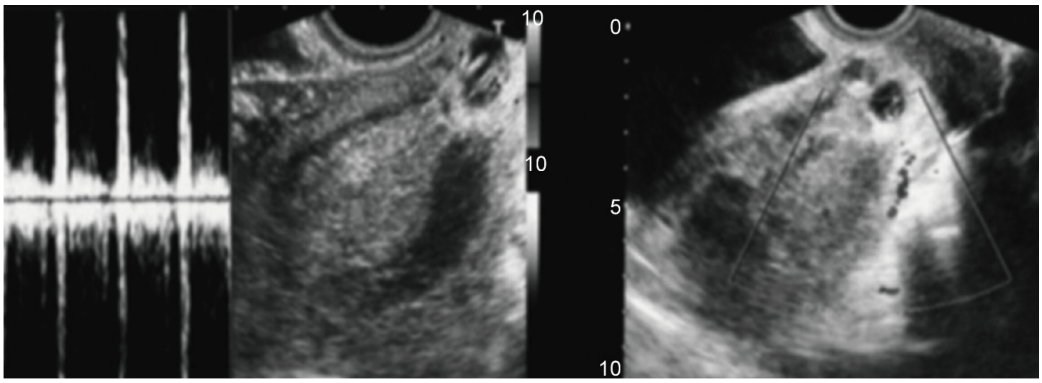

DOI: 10.12998/wjcc.v10.i11.3587

Figure 2 Transvaginal ultrasound findings in Case 2. A 30 mm gestational sac with fetal heartbeat was found in the cervix, and blood flow was noted around the sac by color Doppler imaging.

OUTCOME AND FOLLOW-UP

Case 1

On day 17, the blood hCG concentration had decreased to 198 mIU/mL, and no complications due to local ethanol injection were observed during follow-up. Two months after local ethanol therapy, menstruation had resumed, and infertility treatment was re-initiated.

Case 2

On day 10, the blood hCG concentration had decreased to 116 mIU/mL, and only a small amount of vaginal bleeding was noted during follow-up. In addition, no complications due to local ethanol injection were noted. Two months after local ethanol therapy, menstruation had resumed, and infertility treatment was re-initiated.

DISCUSSION

The patients in this report developed cervical pregnancy through assisted reproductive technology. Under these circumstances, many patients wish to preserve their fertility. Such patients often choose MTX therapy or UAE, both of which have high rates of treatment success[4,5] and postoperative pregnancy[11]. However, MTX therapy and UAE also have disadvantages for patients who desire fertility preservation. In a study of 35 patients with a history of MTX treatment for cervical pregnancy, oocyte yields during *in vitro* fertilization were 10.1 ± 3.9 before treatment and 7.8 ± 3.6 after treatment, suggesting that MTX therapy caused a decrease in the number of oocytes. It has been reported that a decrease in oocyte count leads to a decrease in the number of collected eggs[6], and because MTX therapy affects the ovaries, it may also affect fertility preservation. Furthermore, when MTX is used, a 4–6-mo contraception period is required after surgery for washout[12,13], which delays the resumption

of fertility treatment. Because patients under infertility treatment are becoming older, the best treatment method should allow early resumption of infertility treatment.

In UAE, postoperative fever is the most common complication, and pain, endometritis, intrauterine adhesions, uterine necrosis, and ovarian dysfunction may also occur[14-16]. According to Hardeman *et al*[17], 14 of 53 patients who underwent UAE for obstetrical bleeding desired subsequent pregnancy (all gelatin embolization cases), and 12 of these patients conceived and had successful delivery. These results indicate relatively high rates of postoperative fertility. However, in post-UAE pregnancies, there have been reports of significant increases in miscarriage rate, postpartum bleeding, preterm birth rate, and fetal position abnormalities, and there have been case reports of intrauterine growth restriction[8]. This emphasizes the need for strict perinatal management in post-UAE pregnancies.

In this report, transvaginal ultrasound-guided local injection of absolute ethanol was performed as a new treatment method replacing MTX therapy and UAE. Previously, we reported the efficacy and safety of transvaginal ultrasound-guided local absolute ethanol injection in ectopic pregnancies[9,10]. This treatment method involves the local injection of absolute ethanol around the implantation site under ultrasonic guidance. Its therapeutic effect can be determined earlier than in MTX therapy since a 10%-30% decrease in blood hCG concentration can be confirmed within 2 h of injection. We believe that absolute ethanol dehydrates and denatures the villous tissue, and that acute tissue changes reduce the blood hCG concentration within a short period of time. Therefore, we believe that these mechanisms are effective in patients such as ours, who had high blood hCG concentrations and fetal heartbeats—factors associated with unsuccessful MTX therapy. Furthermore, because no massive bleeding was observed after local injection of absolute ethanol, we believe that these mechanisms are hemostatic and may also be an effective treatment for cervical pregnancy accompanied by genital bleeding in patients who desire fertility preservation.

Absolute ethanol administration may also be effective in other transvaginal procedures, as there is a low possibility of iatrogenic infection. The therapy requires no anesthesia because the small needles cause less bleeding and pain, and the procedure is also more affordable than MTX therapy. This mitigates the physical and financial burdens of patients. In addition, when repeated administration is required for persistent ectopic pregnancy, side effects of anticancer drugs, such as MTX, also become a problem. However, injection of absolute ethanol causes only a local effect, which means that it can be repeated for persistent ectopic pregnancies. In Case 1, two local injections of absolute ethanol were administered for persistent ectopic pregnancy; however, no side effects were observed with this treatment.

In our two reported cases, blood hCG concentration was high and fetal heartbeat was present, which are risk factors for unsuccessful MTX therapy. However, the local injection of absolute ethanol was still able to preserve fertility. In both cases, local injection of absolute ethanol allowed resumption of menstruation 2 mo after treatment and early resumption of infertility treatment without any complications. Based on these results, we suggest that local injection of absolute ethanol for cervical pregnancy could be a safe and effective new treatment method.

CONCLUSION

In this report, we presented two cases of cervical pregnancy with elevated blood hCG concentrations and fetal heartbeats. Each underwent fertility-preserving treatment with local ethanol injection. The outcomes suggested that this treatment method may avoid the complications of MTX therapy and UAE and may be an option for patients who desire fertility preservation.

FOOTNOTES

Author contributions: Kakinuma T designed the research study and wrote the manuscript; Kakinuma T, Kakinuma K, Ohwada M and Yanagida K performed the research; Matsuda Y and Kaijima H provided help and advice on the study protocol; All authors read and approved the final manuscript.

Informed consent statement: The study was approved by the Ethics Committee of the International University of Health and Welfare Hospital (Approval date: July 21, 2021; Approval number 21-B-8). The patients provided consent after receiving written and verbal explanation of the study protocol.

Conflict-of-interest statement: The authors declare no competing interests.

CARE Checklist (2016) statement: The authors have read the CARE Checklist (2016), and the manuscript was prepared and revised according to the CARE Checklist (2016).

Country/Territory of origin: Japan

ORCID number: Toshiyuki Kakinuma 0000-0001-7853-4860; Kaoru Kakinuma 0000-0003-4647-9582; Yoshio Matsuda 0000-0002-2890-2802; Michitaka Ohwada 0000-0002-0396-6228; Kaoru Yanagida 0000-0002-5348-3603; Hirotsune Kaijima 0000-0002-1932-4780.

S-Editor: Gong ZM
L-Editor: A
P-Editor: Gong ZM

REFERENCES

1 **Ushakov FB**, Elchalal U, Aceman PJ, Schenker JG. Cervical pregnancy: past and future. *Obstet Gynecol Surv* 1997; **52**: 45-59 [PMID: 8994238 DOI: 10.1097/00006254-199701000-00023]
2 **Vela G**, Tulandi T. Cervical pregnancy: the importance of early diagnosis and treatment. *J Minim Invasive Gynecol* 2007; **14**: 481-484 [PMID: 17630167 DOI: 10.1016/j.jmig.2006.11.012]
3 **American College of Obstetricians and Gynecologists**. ACOG Practice Bulletin No.94: Medical management of ectopic pregnancy. *Obstet Gynecol* 2008; **111**: 1479-1485 [PMID: 18515537 DOI: 10.1097/AOG.0b013e31817d201e]
4 **Adabi K**, Nekuie S, Rezaeei Z, Rahimi-Sharbaf F, Banifatemi S, Salimi S. Conservative management of cervical ectopic pregnancy: systemic methotrexate followed by curettage. *Arch Gynecol Obstet* 2013; **288**: 687-689 [PMID: 23525594 DOI: 10.1007/s00404-013-2807-y]
5 **Martinelli P**, Maruotti GM, Oppedisano R, Agangi A, Mazzarelli LL, Votino C, Quarantelli M, Iaccarino V. Is uterine artery embolization for cervical ectopic pregnancy always safe? *J Minim Invasive Gynecol* 2007; **14**: 758-763 [PMID: 17980340 DOI: 10.1016/j.jmig.2007.05.017]
6 **McLaren JF**, Burney RO, Milki AA, Westphal LM, Dahan MH, Lathi RB. Effect of methotrexate exposure on subsequent fertility in women undergoing controlled ovarian stimulation. *Fertil Steril* 2009; **92**: 515-519 [PMID: 18829004 DOI: 10.1016/j.fertnstert.2008.07.009]
7 **Kirk E**, Condous G, Haider Z, Syed A, Ojha K, Bourne T. The conservative management of cervical ectopic pregnancies. *Ultrasound Obstet Gynecol* 2006; **27**: 430-437 [PMID: 16514619 DOI: 10.1002/uog.2693]
8 **Goldberg J**, Pereira L, Berghella V. Pregnancy after uterine artery embolization. *Obstet Gynecol* 2002; **100**: 869-872 [PMID: 12423843 DOI: 10.1016/s0029-7844(02)02347-5]
9 **Kaijima H**, Osada H, Kato K, Segawa T, Takehara Y, Teramoto S, Kato O. The efficacy and safety of managing ectopic pregnancies with transvaginal ultrasound-guided local injections of absolute ethanol. *J Assist Reprod Genet* 2006; **23**: 293-298 [PMID: 16832599 DOI: 10.1007/s10815-006-9037-1]
10 **Kakinumaa T**, Kakinumaa K, Kaijima H. The Efficacy and Safety of Managing Interstitial Pregnancies with Transvaginal Ultrasound-Guided Local Injections of Absolute Ethanol. *Annal Cas Rep Rev* 2020; ACRR-152 [DOI: 10.39127/2574-5747/ACRR:1000152]
11 **Ornan D**, White R, Pollak J, Tal M. Pelvic embolization for intractable postpartum hemorrhage: long-term follow-up and implications for fertility. *Obstet Gynecol* 2003; **102**: 904-910 [PMID: 14672461 DOI: 10.1016/s0029-7844(03)00769-5]
12 **Gougeon A**. Dynamics of follicular growth in the human: a model from preliminary results. *Hum Reprod* 1986; **1**: 81-87 [PMID: 3558758 DOI: 10.1093/oxfordjournals.humrep.a136365]
13 **Strauss J**, Barbieri R, Gargiulo A. The ovarian life cycle. In: Strauss JF, Barbieri RL, editors. Yen and Jaffe's reproductive endocrinology: physiology, pathophysiology, and clinical management. 5th ed. Philadelphia: Elsevier Saunders, 2004: 213 [DOI: 10.1016/j.fertnstert.2004.09.010]
14 **Badawy SZ**, Etman A, Singh M, Murphy K, Mayelli T, Philadelphia M. Uterine artery embolization: the role in obstetrics and gynecology. *Clin Imaging* 2001; **25**: 288-295 [PMID: 11566093 DOI: 10.1016/s0899-7071(01)00307-2]
15 **Vegas G**, Illescas T, Muñoz M, Pérez-Piñar A. Selective pelvic arterial embolization in the management of obstetric hemorrhage. *Eur J Obstet Gynecol Reprod Biol* 2006; **127**: 68-72 [PMID: 16229935 DOI: 10.1016/j.ejogrb.2005.09.008]
16 **Hong TM**, Tseng HS, Lee RC, Wang JH, Chang CY. Uterine artery embolization: an effective treatment for intractable obstetric haemorrhage. *Clin Radiol* 2004; **59**: 96-101 [PMID: 14697382 DOI: 10.1016/j.crad.2003.08.007]
17 **Hardeman S**, Decroisette E, Marin B, Vincelot A, Aubard Y, Pouquet M, Maubon A. Fertility after embolization of the uterine arteries to treat obstetrical hemorrhage: a review of 53 cases. *Fertil Steril* 2010; **94**: 2574-2579 [PMID: 20381035 DOI: 10.1016/j.fertnstert.2010.02.052]

World Journal of Clinical Cases

Submit a Manuscript: https://www.f6publishing.com

World J Clin Cases 2022 April 16; 10(11): 3593-3600

DOI: 10.12998/wjcc.v10.i11.3593

ISSN 2307-8960 (online)

CASE REPORT

Successful apatinib treatment for advanced clear cell renal carcinoma as a first-line palliative treatment: A case report

Hang-Ping Wei, Jie Mao, Zu-Liang Hu

Specialty type: Medicine, research and experimental

Provenance and peer review: Unsolicited article; Externally peer reviewed.

Peer-review model: Single blind

Peer-review report's scientific quality classification

Grade A (Excellent): 0
Grade B (Very good): 0
Grade C (Good): C, C
Grade D (Fair): 0
Grade E (Poor): 0

P-Reviewer: Maurea S, Italy; Rioja Viera PE, Peru

Received: December 6, 2021
Peer-review started: December 6, 2021
First decision: January 18, 2022
Revised: January 26, 2022
Accepted: February 27, 2022
Article in press: February 27, 2022
Published online: April 16, 2022

Hang-Ping Wei, Zu-Liang Hu, Department of Medical Oncology, Dongyang Hospital Affiliated to Wenzhou Medical University, Dongyang 322100, Zhejiang Province, China

Jie Mao, Department of Radiology, Dongyang Hospital Affiliated to Wenzhou Medical University, Dongyang 322100, Zhejiang Province, China

Corresponding author: Zu-Liang Hu, Doctor, Deputy Director, Department of Medical Oncology, Dongyang Hospital Affiliated to Wenzhou Medical University, No. 60 West Wuning Road, Dongyang 322100, Zhejiang Province, China. applewhp1988@163.com

Abstract

BACKGROUND

Apatinib is an orally bioavailable small-molecule receptor tyrosine kinase inhibitor. In December 2014, the China Food and Drug Administration made it the first anti-angiogenic therapy to be approved for treating metastatic gastric cancer. It was specifically designated as a third-line or later treatment for metastatic gastric cancer.

CASE SUMMARY

Here, we present a case of advanced renal cell carcinoma (RCC) with multiple metastases (Stage IV) in a 48-year-old male with an extremely poor general status (Karnofsky 30%). He was initially given pazopanib as a targeted therapeutic. However, he experienced severe adverse reactions within two weeks, including grade IV oral mucositis. We, thus, tried switching his targeted treatment to an apatinib dose of 250 mg once daily since April 2018. The patient demonstrated striking benefits from this switch to the apatinib palliative treatment. Nearly one month later, his pain and other associated symptoms were alleviated. The patient was able to move freely and had an excellent general status (Karnofsky 90%). His progress has been followed up with regularly, allowing for a documented progression-free survival interval of approximately 32 mo.

CONCLUSION

This case suggests that, like other multi-target drugs, apatinib may be a useful first-line therapeutic drug for advanced RCC. It may be a particularly helpful curative option when patients are found to be intolerant of other targeted drugs.

Key Words: Apatinib; Renal cell carcinoma; Targeted therapy; Palliative treatment; Case report

Core Tip: Apatinib, an orally bioavailable small-molecule receptor tyrosine kinase inhibitor, is typically used in the treatment of partial solid tumours. Here, we report a case of advanced renal cell carcinoma (RCC) with multiple metastases (Stage IV) in a 48-year-old man with an extremely poor general status (Karnofsky 30%). Due to his intolerance to pazopanib (patient developed oral mucositis), we attempted targeted treatment with apatinib, at a dose of 250 mg once daily (from April 2018). This led to an excellent recovery response, realising an approximately 32 mo progression-free survival. This case suggests that apatinib, like other multi-target drugs, may be used as a first-line therapeutic treatment for advanced RCC.

Citation: Wei HP, Mao J, Hu ZL. Successful apatinib treatment for advanced clear cell renal carcinoma as a first-line palliative treatment: A case report. *World J Clin Cases* 2022; 10(11): 3593-3600
URL: https://www.wjgnet.com/2307-8960/full/v10/i11/3593.htm
DOI: https://dx.doi.org/10.12998/wjcc.v10.i11.3593

INTRODUCTION

Renal cell carcinoma (RCC) derives from malignant tumours originating in the renal parenchymal urotubular epithelium. Although it only accounts for approximately 2% of all malignant tumours, its morbidity and mortality rates are increasing annually[1,2]. Clear cell RCC (ccRCC) is the most common subtype of RCC, accounting for 80% of all cases[3]. Although surgical excision can cure localised RCC, recurrence is common. In addition, many RCC patients do not present clinical symptoms until they have developed unresectable, locally progressive, or metastatic lesions. Consequently, many patients miss the window for surgery. Moreover, RCC is unresponsive to standard radiotherapy and chemotherapy, and its incidence and mortality rates are increasing with each passing year. Thus, targeted therapy is the most effective treatment for ccRCC patients. Currently, the main targeted drugs for ccRCC include sorafenib, sunitinib, pazopanib, and cabozantinib; all of which achieve anti-tumour effects by impacting vascular endothelial growth factor receptor (VEGFR) expression and inhibiting blood pressure angiogenesis and cell proliferation[2,4].

Apatinib (Hengrui Pharmaceutical Co, Ltd, Shanghai, China) is a highly selective inhibitor of VEGFR-2 tyrosine kinase. In December 2014, it became the first China Food and Drug Administration approved anti-angiogenic therapy for treating metastatic gastric cancer. Its official approved use was as a third-line or later treatment[5]. It acts to specifically inhibit the VEGFR tyrosine kinase activity, thereby inhibiting tumour angiogenesis. Since its approval, given its effectiveness in treating gastric cancer, it has also been used to treat other tumours. Hence, apatinib has shown to be a strikingly effective new option against multifarious malignancies, including advanced non-small cell lung cancer, metastatic triple-negative breast cancer, angiosarcoma, desmoplastic small round cell tumour, advanced intrahepatic cholangiocarcinoma, and myxoid/round cell liposarcoma[6-10].

However, to the best of our knowledge, cases have yet to be reported regarding apatinib's usefulness in both the treatment of RCC and controlling tumour growth. Thus, in the current report, we present an advanced ccRCC case with multiple metastases (Stage IV) in a 48-year-old male with an extremely poor general status (Karnofsky 30%).

CASE PRESENTATION

Chief complaints

In March 2010, a middle-aged (48-year-old) man was admitted to Dongyang Hospital Affiliated to Wenzhou Medical University complaining of soreness and swelling on his waist and back.

History of present illness

The patient's symptoms of persistent pain had started one year prior. However, two weeks before admission, it had worsened to the point that he could not lie down on his back at night. Oral analgesics did not control his pain, which he reported suffering from in frequent bouts.

History of past illness

In May 2017, the patient was admitted to the Fourth Affiliated Hospital of Zhejiang University's Medical College. Urinary system and bladder ultrasounds showed the presence of a parenchymal space-occupying tumour of the left kidney. Chest and abdomen computed tomography (CT) scans suggested

that the tumour had triggered implantation metastasis at multiple sites, including parapyloric nodules, lumbar areas, multiple nodules in both lungs, left pleura, left breast, and the abdominal wall. Realising the seriousness of his condition, the patient immediately visited the Cancer Hospital affiliated with Fudan University, where he was advised to undergo a left nephrectomy, followed by adjuvant therapy. However, the patient was resistant and refused the suggested treatment. Instead, he consumed traditional Chinese medicine orally at home. Unfortunately, by March 2018, the tumours had progressed and the mass on his back had grown more.

Personal and family history

The patient had no history of smoking or drinking alcohol. There was no relevant family history.

Physical examination

The patient's vital signs were stable in March 2018. However, the clinical examination showed tenderness in the lower back and localised skin swelling.

Laboratory examinations

Blood tests showed increased leukocytes and tumour markers. The neutrophil, hemoglobin, platelets and biochemistry was normal.

Imaging examinations

Lumbar CT scans, taken on March 5, 2018, showed that the patient's lumbar spinous process level space had been blocked by the deterioration and absorption of lumbar 2 appendages and the invasion of the spinal canal (Figure 1).

Further diagnostic work-up

Considering the medical history and follow-up treatments in this case, a puncture biopsy of the mass was recommended. Thus, on March 17, 2018, a puncture biopsy was performed on the back tumour, with guided colour Doppler ultrasound. The observed malignant tumours were consistent with ccRCC according to their morphology and histology; CK+, CK7−, CK20−, cam5.2+, CD10+, EMA+, 34beta E12−, Ki-67+ (10%) (Figure 2).

MULTIDISCIPLINARY EXPERT CONSULTATION

This patient had a clear diagnosis of ccRCC with multiple metastases (Stage IV; IMDC mid-risk). Given the multiple metastases, surgery was not advisable. Instead, medical treatment was considered.

FINAL DIAGNOSIS

The patient was diagnosed with ccRCC with multiple metastases (Stage IV; IMDC mid-risk) in various organs, including the lungs (contralateral), bones, pleura, abdominal cavities, and lymph nodes. The patient had an extremely poor general status (Karnofsky 30%) and was informed on his poor prognosis.

TREATMENT

Initially, the patient was administered pazopanib targeted treatment. However, two weeks later he experienced severe adverse reactions in the form of grade IV oral mucositis. Considering his intolerance to pazopanib, we attempted targeted treatment with apatinib, at a dose of 250 mg daily since April 2018. There were no grade III or higher adverse reactions during apatinib treatment.

OUTCOME AND FOLLOW-UP

In response to apatinib treatment, the lump in his back shrank after one week. The patient was thus able to lie down, and his pain in so doing was alleviated. He was able to move freely and his performance status improved drastically (Karnofsky 90%). CT taken on July 26, 2018, revealed left inferior pole RCC (diameter: 4.5 cm), L2 spinous process metastatic bone tumours secondary to corresponding plane spinal stenosis, and multiple metastatic tumours in both the lungs (both the length and diameter of the lesion were approximately 1.0 cm), and he had a stable disease (SD), according to the RECIST 1.1 criteria (Figure 3). After several months, a follow-up CT taken on October 20, 2018, and compared with the prior scan (July 26, 2018), suggested that the left inferior pole RCC had reduced in size (diameter: 3.9 cm).

DOI: 10.12998/wjcc.v10.i11.3593

Figure 1 Lumbar computed tomography was taken on March 5, 2018, which showed lumbar spinous process level occupied space with destruction and absorption of lumbar 2 appendages and invasion of the spinal canal. A: Sagittal sections of the masses; B: Coronal sections of the masses (red arrow).

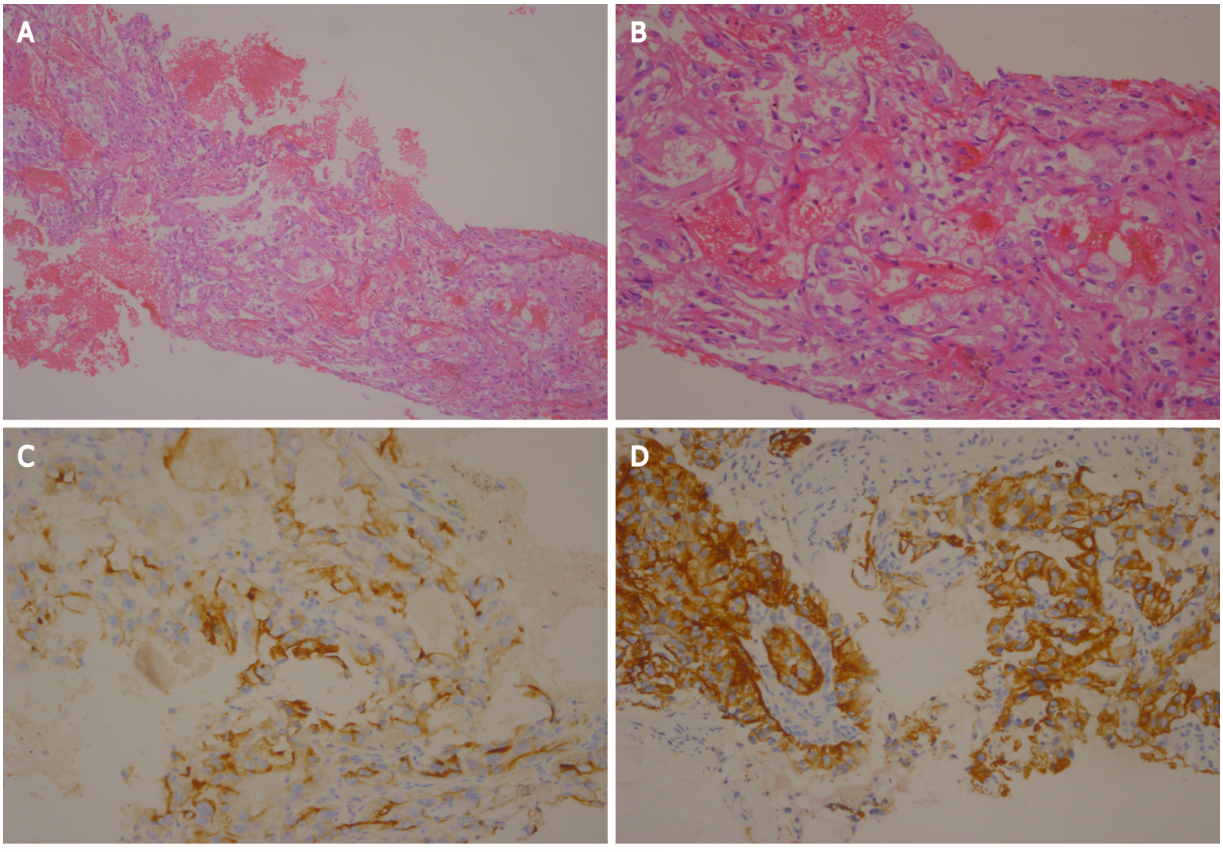

DOI: 10.12998/wjcc.v10.i11.3593

Figure 2 Haematoxylin and eosin staining of a tumour section. A: Under × 10 times microscope; B: Under × 40 times microscope. Immunohistochemical staining of a tumour section; C: It showed that CD10 was postive; D: It showed that CD20 was negtive.

Moreover, the rest of the metastatic tumours did not demonstrate any noticeable change (in terms of growth) (Figure 3). Furthermore, the patient showed a SD, according to the RECIST 1.1 criteria. The follow-up CT taken on March 5, 2019 showed that the left inferior pole RCC had enlarged (diameter: Approximately 4.7 cm). However, the progression was slow, according to the RECIST 1.1 criteria

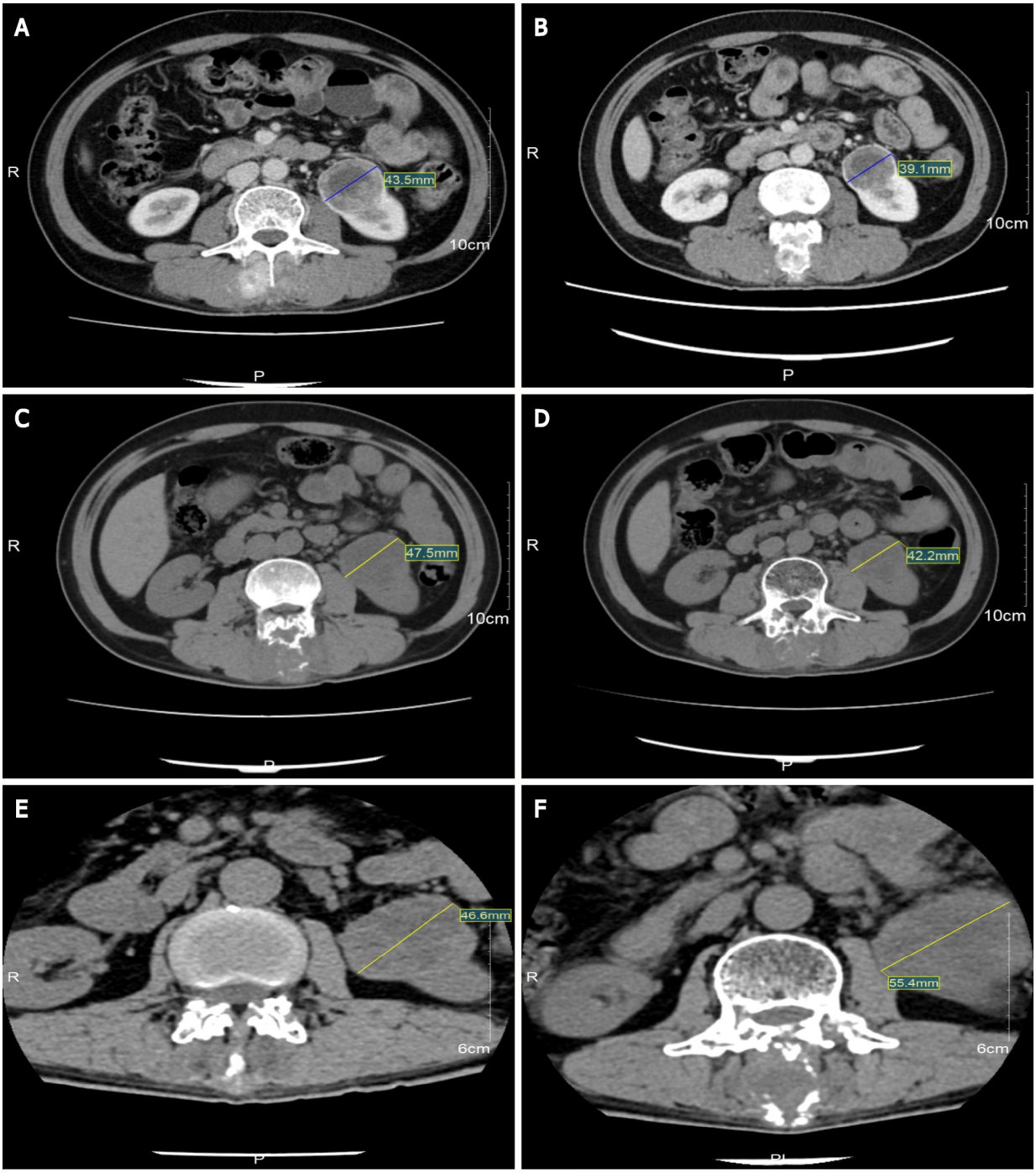

DOI: 10.12998/wjcc.v10.i11.3593

Figure 3 Computed tomography images during treatment showing the changes of the mass. A: Computed tomography (CT) images obtained on July 26, 2018; B: CT images obtained on October 20, 2018; C: CT images obtained on March 5, 2019; D: CT images obtained on December 24, 2019; E: CT images obtained on October 5, 2020; F: CT images obtained on December 14, 2020.

(Figure 3). During this period, combination immunotherapy was recommended due to the increase in tumour size. However, the patient rejected it for economic reasons. Thereafter, he was followed up with several times and was reported to be stable till December 2020. The follow-up CT, taken on December 14, 2020, showed that the left inferior pole RCC had increased in size (diameter: Approximately 5.5 cm). Considered together with the other lesions, this indicated that the disease had resumed progression (Figure 3). Strikingly, until this point, the patient had experienced 32 mo of progression-free survival (PFS).

DISCUSSION

RCC is considered a serious disease worldwide because of the extent to which it endangers human life and health. It demonstrates insidious onset, low survival rate, and high morbidity and mortality. RCC is the second most common urinary tumour, accounting for 2%–3% of all adult malignant tumours[2]. Currently, the best treatment for RCC is surgical resection. In 2010, radical nephrectomy was proposed as a viable option for advanced RCC patients in sufficiently good general condition such that they could tolerate surgery[11]. However, approximately one third of RCC patients demonstrate distant metastasis at the time of initial diagnosis. Thus, they have missed the window for surgery. Statistically, RCC patients showing a 2-year survival rate amount to less than 20% of all cases, whereas the 5-year survival rate is approximately 10%[2]. Therefore, pursuit of medical treatment for RCC is also extremely important. Luckily, over the past decade, a range of therapeutic options have been approved for mRCC, including the targeted, immune checkpoint, and combined immune checkpoint treatments[12]. In the mid to late 2000s, targeted therapies, including inhibitors of VEGF and the mammalian target of rapamycin pathway have entered into the clinical toolkit, thus expanding the range of standard ccRCC therapy options[13]. Consequently, the 5-year survival rate for advanced RCC has increased to nearly 20%[2]. Recent studies have shown that immunotherapy and target therapy combined with immunotherapy have led to positive results in the PFS of advanced RCC patients[14,15].

Researchers have shown that targeted therapies, such as bevacizumab, sunitinib, and axitinib, have a 25%–35% overall response rate among treatment-naive patients, a disease control rate of 45%–80%, and a median PFS ranging from 6.5–11 mo[16]. Currently, immunotherapy has also been used as a first-line treatment[17]. The median PFS for advanced first-line RCC immunotherapy is between 11.2 and 15.1 mo [18-20]. However, immunotherapy, being very expensive and not yet insured, is not an economic first-line RCC treatment[21].

Apatinib is an orally bioavailable small-molecule VEGFR2 tyrosine kinase inhibitor. It inhibits VEGF-mediated endothelial cell migration and proliferation, thereby arresting angiogenesis in tumours[22]. In addition, this agent mildly inhibits c-Kit and c-Src tyrosine kinases. Studies have shown that apatinib can arrest the growth of tumour cells in advanced gastric cancer patients. It has been shown to similarly affect advanced epithelial ovarian cancer, recurrent malignant glioma, and metastatic breast cancer[5,6,8,23,24].

In the present case, the patient was diagnosed with ccRCC with multiple metastases (Stage IV) and was in deplorable physical condition. Therefore, targeted therapy was recommended. Given the patient's intolerance to pazopanib and our uncertainty with regards to his response to sunitinib, we chose apatinib as this drug had been reported to be successful in treating various malignancies. The patient showed a positive clinical response to apatinib. His general status improved drastically, and nearly 32 mo of PFS was realised, which was longer than any previously reported case. Although, the patient showed a slow disease progression, apatinib was still effective in reversing disease severity. Thus, we posit an ideal treatment combination of apatinib and immunotherapy. Unfortunately, the patient did not receive immunotherapy concurrently for financial reasons.

However, this study has some limitations. Because case reports cannot replace randomised controlled trials, it is unclear whether apatinib is suitable for all RCC patients. Further prospective studies are required to optimise the use of apatinib in the treatment of RCC and identify patients that can benefit from this agent.

CONCLUSION

In conclusion, this case report indicates that apatinib significantly augmented the quality of life for an RCC patient. It also markedly improved his PFS. Thus, apatinib, like other multi-target drugs, may be useful as a first-line therapeutic drug for advanced RCC. It may be a particularly helpful curative option when patients are found to be intolerant of other targeted drugs.

FOOTNOTES

Author contributions: Hu ZL and Wei HP were medical oncologist of the patients, who consulted the literature and participated in the drafting of the manuscript; Mao J was responsible for the imaging data of patients; all authors have approved the final version of the manuscript to be submitted.

Informed consent statement: Informed written consent was obtained from the patient for publication of this report and any accompanying images.

Conflict-of-interest statement: The authors declare that they have no conflict of interest.

CARE Checklist (2016) statement: The authors have read the CARE Checklist (2016), and the manuscript was

prepared and revised according to the CARE Checklist (2016).

Country/Territory of origin: China

ORCID number: Hang-Ping Wei 0000-0002-2904-7086; Jie Mao 0000-0002-6723-072X; Zhu-Liang Hu 0000-0002-9032-6471.

S-Editor: Fan JR
L-Editor: A
P-Editor: Fan JR

REFERENCES

1 **Hsieh JJ**, Purdue MP, Signoretti S, Swanton C, Albiges L, Schmidinger M, Heng DY, Larkin J, Ficarra V. Renal cell carcinoma. *Nat Rev Dis Primers* 2017; **3**: 17009 [PMID: 28276433 DOI: 10.1038/nrdp.2017.9]
2 **Xia L**, Song YY, Hao RM. Current status and drug development consideration of treatment for advanced renal cell carcinoma. *Chin J Clin Pharmacol* 2020; **318**: 2571-2577
3 **Siegel RL**, Miller KD, Jemal A. Cancer statistics, 2019. *CA Cancer J Clin* 2019; **69**: 7-34 [PMID: 30620402 DOI: 10.3322/caac.21551]
4 **Singh D**. Current updates and future perspectives on the management of renal cell carcinoma. *Life Sci* 2021; **264**: 118632 [PMID: 33115605 DOI: 10.1016/j.lfs.2020.118632]
5 **Li J**, Qin S, Xu J, Xiong J, Wu C, Bai Y, Liu W, Tong J, Liu Y, Xu R, Wang Z, Wang Q, Ouyang X, Yang Y, Ba Y, Liang J, Lin X, Luo D, Zheng R, Wang X, Sun G, Wang L, Zheng L, Guo H, Wu J, Xu N, Yang J, Zhang H, Cheng Y, Wang N, Chen L, Fan Z, Sun P, Yu H. Randomized, Double-Blind, Placebo-Controlled Phase III Trial of Apatinib in Patients With Chemotherapy-Refractory Advanced or Metastatic Adenocarcinoma of the Stomach or Gastroesophageal Junction. *J Clin Oncol* 2016; **34**: 1448-1454 [PMID: 26884585 DOI: 10.1200/JCO.2015.63.5995]
6 **Deng L**, Wang Y, Lu W, Liu Q, Wu J, Jin J. Apatinib treatment combined with chemotherapy for advanced epithelial ovarian cancer: a case report. *Onco Targets Ther* 2017; **10**: 1521-1525 [PMID: 28352185 DOI: 10.2147/OTT.S126471]
7 **Du Z**, Yu Y, Wu D, Zhang G, Wang Y, He L, Meng R. Apatinib for salvage treatment of advanced malignant pleural mesothelioma: A case report. *Medicine (Baltimore)* 2018; **97**: e13105 [PMID: 30407323 DOI: 10.1097/MD.0000000000013105]
8 **Fang SC**, Zhang HT, Zhang YM, Xie WP. Apatinib as post second-line therapy in EGFR wild-type and ALK-negative advanced lung adenocarcinoma. *Onco Targets Ther* 2017; **10**: 447-452 [PMID: 28176910 DOI: 10.2147/OTT.S126613]
9 **Kou P**, Zhang Y, Shao W, Zhu H, Zhang J, Wang H, Kong L, Yu J. Significant efficacy and well safety of apatinib in an advanced liver cancer patient: a case report and literature review. *Oncotarget* 2017; **8**: 20510-20515 [PMID: 28103584 DOI: 10.18632/oncotarget.14724]
10 **Wang LY**, Gong S, Gao LP, Hou LX, He W. Apatinib for treating advanced intrahepatic cholangiocarcinoma after failed chemotherapy: A case report and literature review. *Medicine (Baltimore)* 2018; **97**: e13372 [PMID: 30544406 DOI: 10.1097/MD.0000000000013372]
11 **Yang F**, Zhou X, Du S, Zhao Y, Ren W, Deng Q, Wang F, Yuan J. LIM and SH3 domain protein 1 (LASP-1) overexpression was associated with aggressive phenotype and poor prognosis in clear cell renal cell cancer. *PLoS One* 2014; **9**: e100557 [PMID: 24955835 DOI: 10.1371/journal.pone.0100557]
12 **Ghatalia P**, Zibelman MR, Geynisman DM, Plimack ER. Evolving landscape of the treatment of metastatic clear cell renal cell carcinoma. *Clin Adv Hematol Oncol* 2018; **16**: 677-686 [PMID: 30543598]
13 **Lee CH**, Chung J, Kwak C, Jeong CW, Seo SI, Kang M, Hong SH, Song C, Park JY, Hwang EC, Lee H, Ku JY, Seo WI, Choi SH, Ha HK; Korean Renal Cancer Study Group. Targeted therapy response in early versus late recurrence of renal cell carcinoma after surgical treatment: A propensity score-matched study using the Korean Renal Cancer Study Group database. *Int J Urol* 2021; **28**: 417-423 [PMID: 33527588 DOI: 10.1111/iju.14485]
14 **Perego G**, Barzaghi P, Vavassori I, Petrelli F. Treating metastatic clear-cell renal cell carcinoma: beyond immunotherapy. *Med Oncol* 2020; **37**: 81 [PMID: 32767163 DOI: 10.1007/s12032-020-01408-3]
15 **Caruso M**, Romeo V, Stanzione A, Buonerba C, Di-Lorenzo G, Maurea S. Current imaging evaluation of tumor response to advanced medical treatment in metastatic renal-cell carcinoma: Clinical implications. *Applied Sciences* 2021; **11**: 6930 [DOI: 10.3390/app11156930]
16 **Choueiri TK**, Halabi S, Sanford BL, Hahn O, Michaelson MD, Walsh MK, Feldman DR, Olencki T, Picus J, Small EJ, Dakhil S, George DJ, Morris MJ. Cabozantinib Versus Sunitinib As Initial Targeted Therapy for Patients With Metastatic Renal Cell Carcinoma of Poor or Intermediate Risk: The Alliance A031203 CABOSUN Trial. *J Clin Oncol* 2017; **35**: 591-597 [PMID: 28199818 DOI: 10.1200/JCO.2016.70.7398]
17 **Bando Y**, Furukawa J, Terakawa T, Harada K, Hinata N, Nakano Y, Fujisawa M. Treatment outcomes of molecular targeted therapy following nivolumab in metastatic renal cell carcinoma. *Jpn J Clin Oncol* 2021; **51**: 1313-1318 [PMID: 33954587 DOI: 10.1093/jjco/hyab068]

18 **Rini BI**, Plimack ER, Stus V, Gafanov R, Hawkins R, Nosov D, Pouliot F, Alekseev B, Soulières D, Melichar B, Vynnychenko I, Kryzhanivska A, Bondarenko I, Azevedo SJ, Borchiellini D, Szczylik C, Markus M, McDermott RS, Bedke J, Tartas S, Chang YH, Tamada S, Shou Q, Perini RF, Chen M, Atkins MB, Powles T; KEYNOTE-426 Investigators. Pembrolizumab plus Axitinib versus Sunitinib for Advanced Renal-Cell Carcinoma. *N Engl J Med* 2019; **380**: 1116-1127 [PMID: 30779529 DOI: 10.1056/NEJMoa1816714]

19 **Motzer RJ**, Penkov K, Haanen J, Rini B, Albiges L, Campbell MT, Venugopal B, Kollmannsberger C, Negrier S, Uemura M, Lee JL, Vasiliev A, Miller WH Jr, Gurney H, Schmidinger M, Larkin J, Atkins MB, Bedke J, Alekseev B, Wang J, Mariani M, Robbins PB, Chudnovsky A, Fowst C, Hariharan S, Huang B, di Pietro A, Choueiri TK. Avelumab plus Axitinib versus Sunitinib for Advanced Renal-Cell Carcinoma. *N Engl J Med* 2019; **380**: 1103-1115 [PMID: 30779531 DOI: 10.1056/NEJMoa1816047]

20 **Motzer RJ**, Tannir NM, McDermott DF, Arén Frontera O, Melichar B, Choueiri TK, Plimack ER, Barthélémy P, Porta C, George S, Powles T, Donskov F, Neiman V, Kollmannsberger CK, Salman P, Gurney H, Hawkins R, Ravaud A, Grimm MO, Bracarda S, Barrios CH, Tomita Y, Castellano D, Rini BI, Chen AC, Mekan S, McHenry MB, Wind-Rotolo M, Doan J, Sharma P, Hammers HJ, Escudier B; CheckMate 214 Investigators. Nivolumab plus Ipilimumab versus Sunitinib in Advanced Renal-Cell Carcinoma. *N Engl J Med* 2018; **378**: 1277-1290 [PMID: 29562145 DOI: 10.1056/NEJMoa1712126]

21 **Pipitone S**, Vitale MG, Baldessari C, Dominici M, Sabbatini R. Long survival of a young patient with Xp11.2 translocation metastatic clear cell renal carcinoma: case report. *Tumori* 2021; **107**: NP131-NP135 [PMID: 34696653 DOI: 10.1177/03008916211049275]

22 **Tian S**, Quan H, Xie C, Guo H, Lü F, Xu Y, Li J, Lou L. YN968D1 is a novel and selective inhibitor of vascular endothelial growth factor receptor-2 tyrosine kinase with potent activity in vitro and in vivo. *Cancer Sci* 2011; **102**: 1374-1380 [PMID: 21443688 DOI: 10.1111/j.1349-7006.2011.01939.x]

23 **Lin Y**, Wang C, Gao W, Cui R, Liang J. Overwhelming rapid metabolic and structural response to apatinib in radioiodine refractory differentiated thyroid cancer. *Oncotarget* 2017; **8**: 42252-42261 [PMID: 28178685 DOI: 10.18632/oncotarget.15036]

24 **Zhang H**, Chen F, Wang Z, Wu S. Successful treatment with apatinib for refractory recurrent malignant gliomas: a case series. *Onco Targets Ther* 2017; **10**: 837-845 [PMID: 28243119 DOI: 10.2147/OTT.S119129]

World Journal of Clinical Cases

Submit a Manuscript: https://www.f6publishing.com

World J Clin Cases 2022 April 16; 10(11): 3601-3608

DOI: 10.12998/wjcc.v10.i11.3601

ISSN 2307-8960 (online)

CASE REPORT

Del(5q) and inv(3) in myelodysplastic syndrome: A rare case report

Hai-Ping Liang, Xing-Chun Luo, Ya-Li Zhang, Bei Liu

Specialty type: Hematology

Provenance and peer review: Unsolicited article; Externally peer reviewed.

Peer-review model: Single blind

Peer-review report's scientific quality classification

Grade A (Excellent): 0
Grade B (Very good): B, B
Grade C (Good): 0
Grade D (Fair): 0
Grade E (Poor): 0

P-Reviewer: Fazilat-Panah D, Iran; Papadopoulos VP, Greece

Received: December 6, 2021
Peer-review started: December 6, 2021
First decision: January 25, 2022
Revised: February 3, 2022
Accepted: February 27, 2022
Article in press: February 27, 2022
Published online: April 16, 2022

Hai-Ping Liang, Xing-Chun Luo, Ya-Li Zhang, The First Clinical Medical College, Lanzhou University, Lanzhou 730000, Gansu Province, China

Bei Liu, Department of Hematology, The First Affiliated Hospital, Lanzhou University, Lanzhou 730000, Gansu Province, China

Corresponding author: Bei Liu, MD, PhD, Professor, Department of Hematology, The First Affiliated Hospital, Lanzhou University, No. 1 Donggangxi Road, Chengguan District, Lanzhou 730000, Gansu Province, China. liubeiff@163.com

Abstract

BACKGROUND

Del(5q) is the most common molecular event in myelodysplastic syndrome (MDS), accounting for 10%-15% of cases. Inv(3) is an adverse cytogenetic abnormality observed in less than 1% of MDS patients. Few studies have reported the coexistence of del(5q) and inv(3) in MDS. Therefore, the pathological mechanism, treatment strategy and prognosis of this subtype need to be elucidated.

CASE SUMMARY

A 66-year-old woman was admitted to the hospital due to chest tightness and shortness of breath. Combining clinical assessments with laboratory examinations, the patient was diagnosed with MDS containing both del(5q) and inv(3). Considering the deletion of chromosome 5q, we first treated the patient with lenalidomide. When drug resistance arose, we tried azacitidine, and the patient had a short remission. Finally, the patient refused treatment with haematopoietic stem cell transplantation and died of severe infection four months later.

CONCLUSION

MDS patients with del(5) and inv(3) have a poor prognosis. Azacitidine may achieve short-term remission for such patients.

Key Words: Myelodysplastic syndrome; Del(5q); Inv(3); Lenalidomide; Azacitidine; Case report

Core Tip: We report a rare case of myelodysplastic syndrome (MDS) with two chromosomal structural abnormalities, del(5q) and inv(3). The patient evolved from the initial del(5q) to inv(3) combined with del(5q). Considering the deletion of chromosome 5q, we first treated the patient with lenalidomide. When drug resistance arose, we tried azacitidine, and the patient had a short remission. Finally, the patient refused treatment with haematopoietic stem cell transplantation (HSCT), and her condition gradually deteriorated until she was discharged from the hospital. In this rare and contradictory situation, we found that MDS patients with coexisting del(5q) and inv(3) may have a poor prognosis. However, azacitidine may play a role to some extent in MDS with del(5q) and inv(3), and HSCT may be the only way to cure the disease.

Citation: Liang HP, Luo XC, Zhang YL, Liu B. Del(5q) and inv(3) in myelodysplastic syndrome: A rare case report. *World J Clin Cases* 2022; 10(11): 3601-3608
URL: https://www.wjgnet.com/2307-8960/full/v10/i11/3601.htm
DOI: https://dx.doi.org/10.12998/wjcc.v10.i11.3601

INTRODUCTION

Myelodysplastic syndrome (MDS) is defined as a typical heterogeneous group of clonal haematopoietic disorders characterized by dysplastic and ineffective haematopoiesis, and approximately 30% of patients progress to acute myeloid leukaemia (AML)[1,2]. The incidence of MDS is associated with age, especially in people 60 years older, and males are more susceptible than females[3]. MDS patients generally have poor outcomes, with a median overall survival of 5 years[2]. According to the International Prognostic Scoring System (IPSS) and revised International Prognostic Scoring System (IPSS-R), cytogenetic abnormalities, especially certain unbalanced abnormalities, have a profound impact on the prognosis of MDS patients[4]. Unbalanced chromosomal abnormalities caused by partial acquisition or deletion of chromosomes are common in MDS[5]. These abnormalities often occur during tumorigenesis and play a crucial role in MDS progression.

Here, we report a case of an MDS patient with clonal progression from del(5q) to inv(3) and del(5q), who was treated with azacitidine after lenalidomide resistance. Furthermore, we will summarize the genetic abnormalities and treatment strategies to add a corresponding contribution to the treatment and prognosis of these patients.

CASE PRESENTATION

Chief complaints

In September 2020, a 66-year-old woman was admitted to our hospital for progressive chest tightness and shortness of breath.

History of present illness

One year prior, the patient had been admitted to the hospital with severe anaemia and thrombocytosis. Physical examination showed that the patient had an anaemic appearance. The results of peripheral blood examination were as follows: red blood cell (RBC) count, 1.0×10^{12}/L; platelet (PLT) count, 409×10^{9}/L; haemoglobin (HB), 36 g/L; creatinine, 0.55 mg/dL; and lactate dehydrogenase (LDH), 418 U/L. Bone marrow trephine biopsy revealed more than 10% abnormal megakaryocytes (single round nuclei and cytosolic lobulated micronuclei) (Figure 1A). Fluorescence in situ hybridization (FISH) indicated deletion of the *EGR1* (5q31) gene (Figure 1B). Furthermore, the karyotype was described as 46, XX, del(5)(q13q31) by G band staining (Figure 1C). Based on clinical manifestations and laboratory tests, the patient was diagnosed with low-risk MDS (low risk, IPSS-R = 2.5). The endothelial activation and stress index (EASIX) was 0.56. EASIX is an independent prognostic factor for lower-risk MDS patents that was calculated by the following formula: LDH (U/L) × creatinine (mg/dL)/PLT (nL)[6]. The patient was advised to be treated with lenalidomide. The dosing schedule was 10 mg/d or 21 d in a 28-d cycle. After three cycles of treatment, peripheral blood examination showed HB 97 g/L and PLT 341×10^{9}/L.

History of past illness

The patient was previously healthy. There was no disease history in other systems.

Personal and family history

No contributory personal history or similar family history.

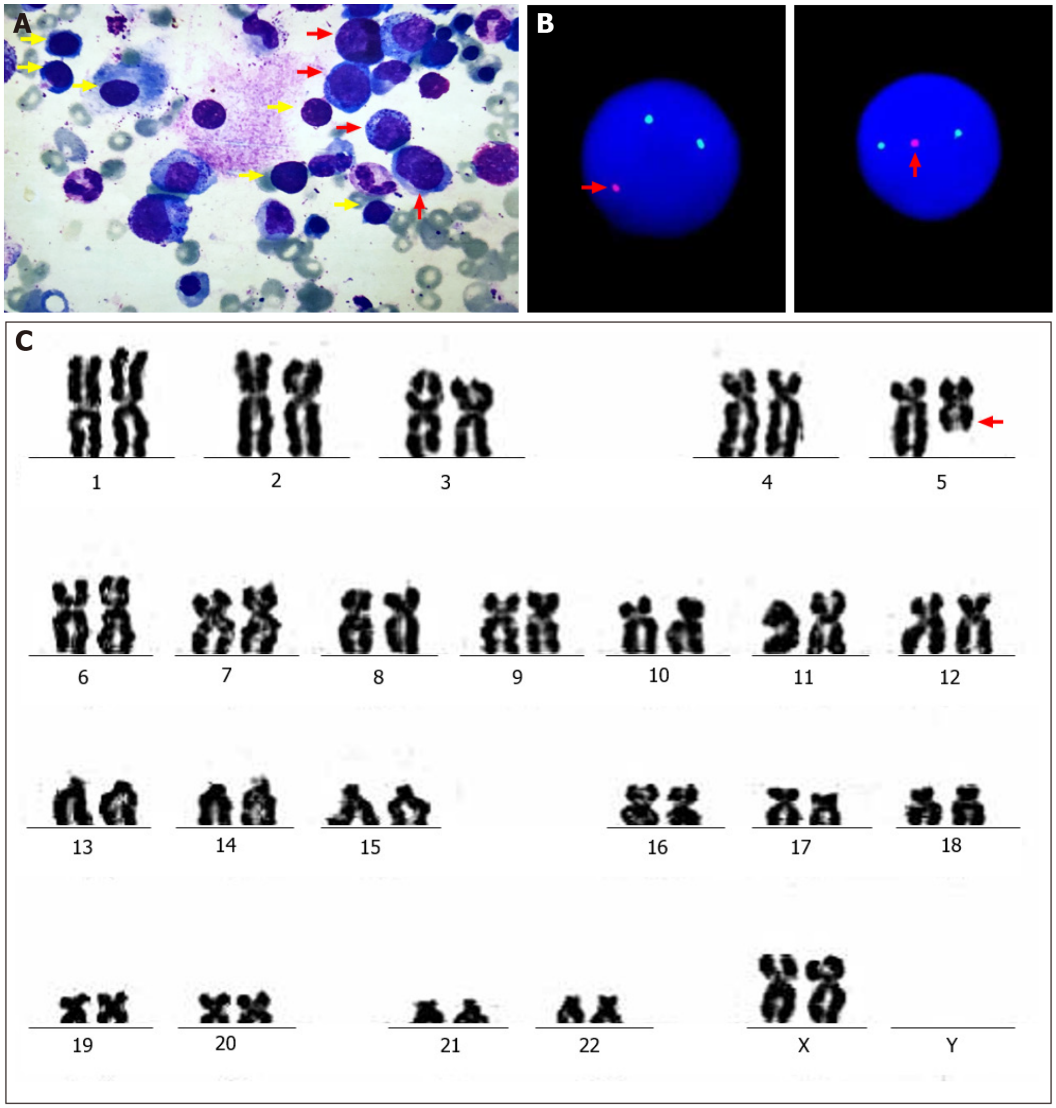

DOI: 10.12998/wjcc.v10.i11.3601

Figure 1 Bone marrow aspiration biopsy, karyotype and fluorescence *in situ* hybridization assay at first diagnosis. A: Representative image of May Grunwald-Giemsa staining of bone marrow specimen. It is showed that more than 5% blast cell and more than 10% abnormal megakaryocytes, including unicellular megakaryocytes (panel A red arrow) and lymphatic-like small megakaryocytes (yellow arrow). B: EGR(5q31) gene was detected by fluorescence in situ hybridization. Each signal mode was detected as follows :2G1R 50%,2G2R 50%. EGR(5q31) probe was labeled with red fluorescence, D5S23 and D5S721(5p15.2) probe was labeled with green fluorescence. C: G-band bone marrow karyotype. Arrows indicate the del(5)(q13q31).

Physical examination

Physical examination showed that the patient had a moderate anaemic appearance. Her vital signs were stable, with no other positive findings.

Laboratory examinations

The results of the peripheral blood examination were as follows: RBC, 2.27 × 10^{12}/L; WBC, 1.93 × 10^{9}/L; PLT, 114 × 10^{9}/L; and HB, 58 g/L.

Further diagnostic work-up

Bone marrow aspirate smears showed hypercellularity with marked myeloid and erythroid hypoplasia and a blast cell count of 16% (Figure 2A). Another karyotype examination revealed 46, XX, inv(3)(q21q26), and del(5)(q13q31) (Figure 2B). qRT–PCR showed that the EVI1 expression level was 90.63%, which was classified as high expression.

FINAL DIAGNOSIS

According to the IPSS-R, the patient's diagnosis was revised to high-risk MDS (very high risk, IPSS-R =

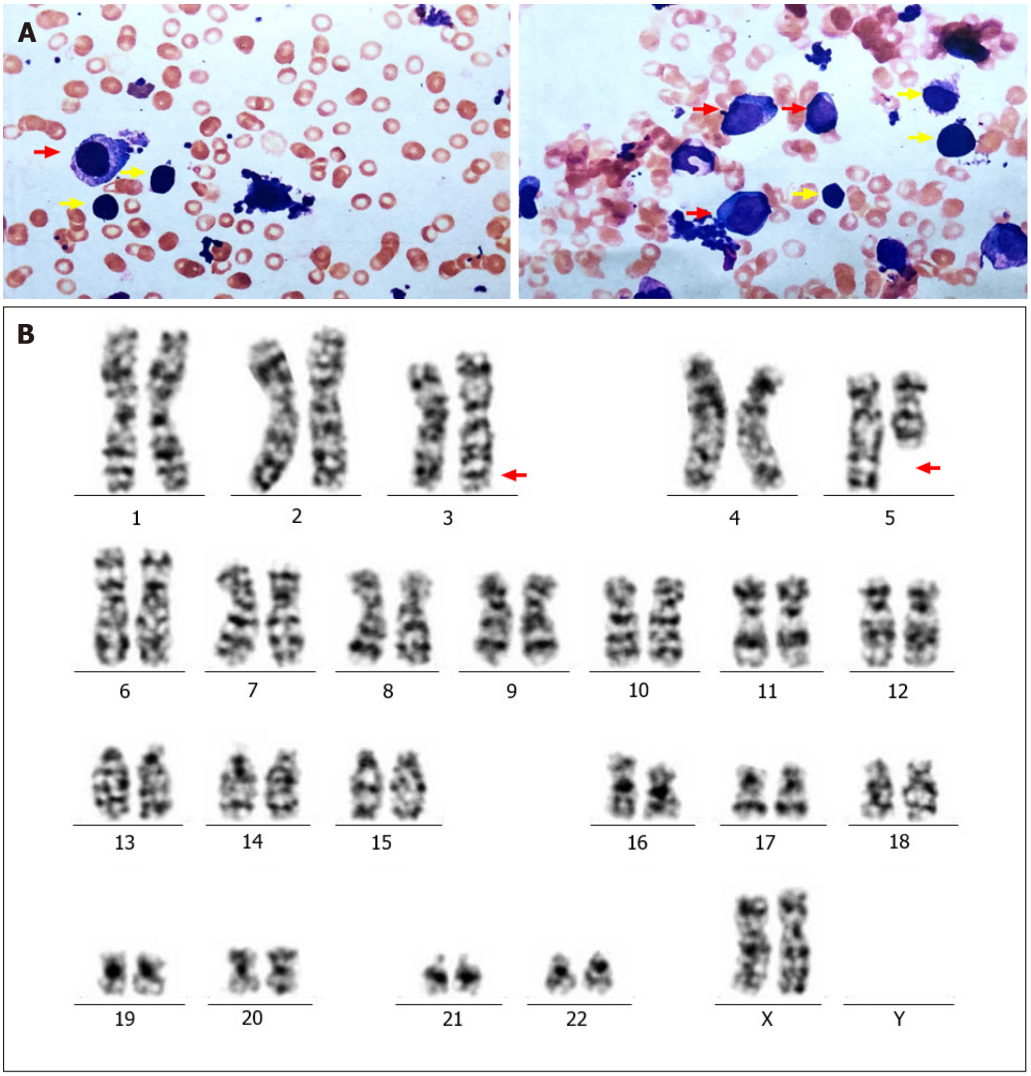

DOI: 10.12998/wjcc.v10.i11.3601

Figure 2 Bone marrow aspiration biopsy and karyotype analysis after lenalidomide resistances. A: Bone marrow aspiration smear showing blast cell counted 16% and Hypercellularity with marked myeloid and erythroid hypoplasia. Abnormal megakaryocytes including unicellular megakaryocytes (red arrow) and lymphatic-like small megakaryocytes (yellow arrow) could still be observed. B: karyotype analysis depicting 46, XX, inv(3)(q21q26),del(5)(q13q31) (Red arrow).

7.5).

TREATMENT

We continued to treat the patient with lenalidomide. In less than one treatment cycle, the patient rapidly developed resistance to the drug. Subsequently, we tried azacitidine as a treatment and administered 75 mg/m^2/d intravenously for 7 consecutive days every 28 d. After two courses, haematology showed HB 70 g/L and PLT 56 × 10^9/L. After the fourth cycle, peripheral blood examination revealed HB 40 g/L and PLT 14 × 10^9/L. Bone morrow aspirate smears revealed that nucleated cells accounted for 6% of the cell population. A mutation of the *ASXL1* gene [NM 015338:c.4232_4233delinsA(p. W1411*) exon 12] with a variant allele frequency of 33.1% was detected. Subsequently, her medical condition gradually deteriorated. In view of the present situation, we recommended HSCT.

OUTCOME AND FOLLOW-UP

The patient was discharged and wilfully refused HSCT. After four months, the patient died of the infection.

DISCUSSION

We report a rare case of MDS with clonal evolution from del(5q) to inv(3) (Figure 3). MDS with del(5q), also known as 5q-syndrome, is a specific type of MDS that has a better prognosis than other subtypes of MDS. The median expected survival time of this syndrome is approximately 58 mo[7]. Deletion of chromosome arm 5q results in the deletion of genes located on this chromosome, including SPARC, EGR1, CTNNA1, APC and NPM1[8]. Based on this, we used LSI EGR1 and D5S23 and a D5S721 dual colour probe to detect del(5q). MDS with inv(3)/t(3) is considered to be a rare event (< 1%); it is an invasive disease with a high risk of developing AML. Furthermore, high expression of EVI1 was observed with chromosome 3 abnormalities in our case. EVI1 is an oncogenic transcriptional regulator that may be involved in the proliferation and maintenance of haematopoietic stem cells, and its abnormally high expression often promotes disease progression[9]. In addition, ASXL1 mutations that frequently occur in MDS were detected in our case and predict an adverse outcome[10]. Therefore, the patient in our report contained "dominant" karyotypes [del(5q)], "inferior" karyotypes [inv(3)] and harmful ASXL1 mutations. However, the prognostic tendency of these patients remains elusive.

Combining bone marrow cytogenetics, the percentage of bone marrow blasts and cytopenia, our patient was classified as low risk according to the IPSS-R at primary diagnosis. In recent years, cardiovascular disease has been considered to be the second most common cause of death among patients with low-risk MDS after haematological complications[11]. Therefore, we used EASIX to assess the patient's cardiovascular risk, which was 0.56[6]. Because the patient had no previous history of cardiovascular disease and the cardiovascular examination results were negative at admission, we alleviated the patient's cardiovascular disease concerns. Considering the IPSS-R and EASIX, we preliminarily evaluated the patient had a good prognosis.

Lenalidomide therapy is initially recommended based on age, general conditions, and cytogenetic abnormalities. Since 2005, the Food and Drug Administration of the United States has approved the use of lenalidomide for the treatment of transfusion-dependent low-risk MDS with or without del(5q), and it has been indicated that lenalidomide could reduce transfusion requirements and reverse cytogenetic abnormalities[12]. Lenalidomide is the first and only treatment for cytogenetically defined subsets of MDS disease, especially MDS with del(5q). However, not all patients achieve a long-term response. It was reported that approximately half of patients with del(5q) lost response or progression after 2-3 years of treatment[13]. Indeed, lenalidomide resistance has become a common event in the treatment of MDS.

In our case, lenalidomide treatment initially showed a good response in the patient, but the patient rapidly developed drug resistance after the first remission. Based on the available data, we found that the occurrence of primary resistance to lenalidomide in MDS is mainly related to TP53 mutations. We reviewed the role of TP53 mutations and abnormal p53 pathway activation in myeloid malignant tumours. In del (5q) patients who had a high mutation rate of TP53, the cytogenetic complete remission rate was less than 12% after treatment with lenalidomide[7]. Therefore, it is plausible that there is a high correlation between TP53 mutations and lenalidomide resistance. In addition, lenalidomide upregulates RUNX1 expression in a CRBN- and TP53 -dependent manner in del (5q) MDS, and RUNX1 induces megakaryocyte differentiation and apoptosis assisted by GATA2. As a result, lenalidomide resistance occurs when RUNX1 is mutated or downregulated[14]. The secondary or acquired resistance to lenalidomide is associated with the overexpression of PP2A. The overexpression of PP2A leads to the degradation of p53 in red blood cell precursors and the instability of β-catenin, which is more conducive to the evolution of del(5q) clones[15]. However, TP53 and RUNX1 mutations were not detected in our case. The acquired resistance of our patients to lenalidomide may be related to PP2A abnormalities, but further sufficient data is required for further exploration.

After the lenalidomide treatment failed, inv(3) with EVI1 overexpression and ASXL1 mutations occurred in the patient. Based on clinical assessments and laboratory examination, the patient's diagnosis was revised to high-risk MDS. We then tried to treat the patient with azacytidine, which is a demethylation drug. Demethylation drugs mainly include azacitidine and decitabine, both of which can inhibit DNA methylation by binding to DNA. Interestingly, azacitidine also binds to RNA to inhibit RNA synthesis and protein metabolism[16]. Sallman *et al*[16] reported a study about the response to azacitidine in del(5q) MDS patients after lenalidomide resistance. Among 18 del(5q) MDS patients treated with azacytidine, the overall response rate was 56%, including a complete response rate of 5.6%, a marrow complete response rate of 11.1%, and a haematological improvement rate of 38.9%. Azacitidine had the same effect in del(5q) and non-del(5q) patients[17]. In the study by Wanquet *et al* [18], 157 AML/MDS patients with chromosome 3q abnormalities and 27 patients with isolated EVI1 overexpression were treated with azacitidine. The overall response rate was 50%, including a complete remission rate of 29%, and the median overall survival time was 10.6 mo. AML/MDS with 3q abnormalities has a special response to azacitidine, and azacitidine is an appropriate choice before the patient receives allohaematopoietic stem cell transplantation[18]. To date, there have been a few reports on the treatment of MDS with decitabine[3]. Therefore, we believe that azacitidine is a reasonable option for the treatment of MDS after the failure of lenalidomide. Our patient experienced a short-term improvement after 2 courses of azacitidine treatment.

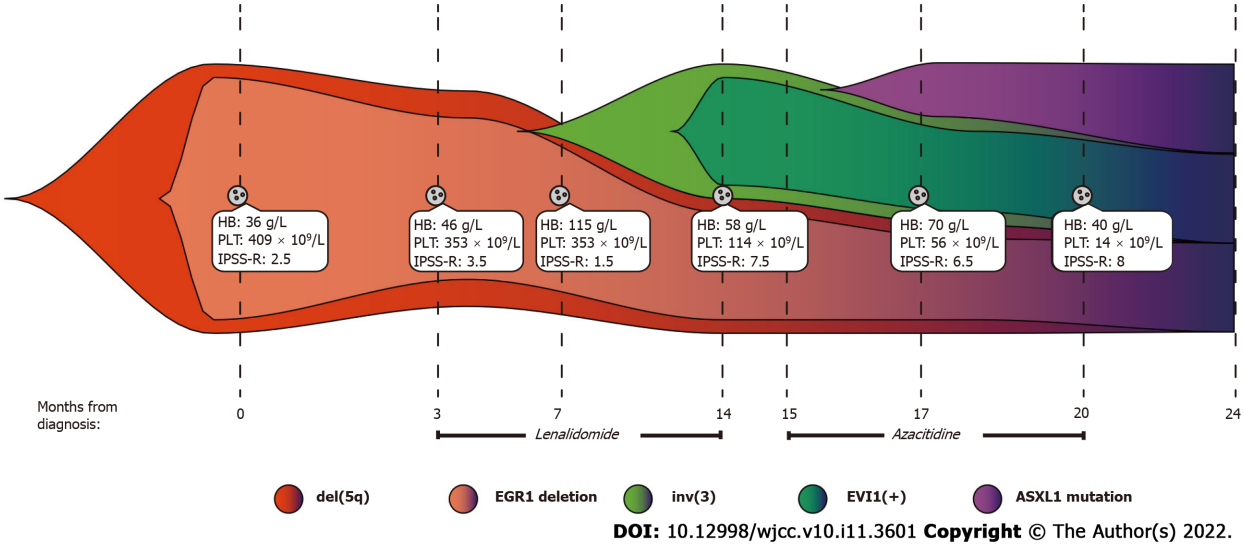

DOI: 10.12998/wjcc.v10.i11.3601

Figure 3 Clonal evolution architecture of the patient. The patient was initially found to have del(5q) with EGR1 gene deletion, so she was diagnosed with MDS (low risk). Following lenalidomide treatment, the patient developed inv(3) with overexpression of EVI1. At that time, the patient's diagnosis was revised to MDS (very high risk). In addition, the patient also had ASXL1 mutations. The revised international prognostic scoring system (IPSS-R) for myelodysplastic syndrome was calculated according to a previously reported method[24], and the details can be found in Supplementary Table 1. HB: Haemoglobin; PLT: Platelet; IPSS-R: Revised International Prognostic Scoring System.

The condition of our patient worsened again after a short period of time, and we considered HSCT. At present, for both low-risk and high-risk MDS patients, HSCT is still the only curative treatment[19]. Patients under 65 years of age and suitable healthy elderly patients should be strongly recommended for HSCT with a suitable donor with the same human leukocyte antigen[20]. Among high-risk MDS patients undergoing HSCT, 40-50% of patients have achieved a prolonged disease-free survival and have improved over the years[21]. However, the optimal timing of HSCT and the specific chemical regimen before HSCT treatment is still a controversial issue. It is generally believed that an increase in the percentage of bone marrow blasts, especially if it is greater than 10%, is associated with a higher risk of recurrence[22]. In addition, the existence of poor prognostic mutations, especially mutations in TP53, ASXL1 and RUNX1, should be considered for the use of HSCT to reduce the risk of recurrence[23]. However, in our case, when we recommended that the patient undergo HSCT, the patient rejected the recommendation for unknown reasons. Subsequently, the patient chose to leave the hospital voluntarily, and we learned during follow-up that the patient died of serious infection after four months.

CONCLUSION

In summary, we report a rare case of MDS with clonal evolution from del(5) to inv(3). Although lenalidomide and azacitidine provided temporary remission to the patient, the patient inevitably has a poor prognosis. The complex and heterogeneous pathophysiology of MDS is still the main reason for the limited effectiveness of current treatments; thus, emerging therapeutic strategies are still urgently needed.

FOOTNOTES

Author contributions: Liang HP designed the study and wrote the manuscript; Luo XC collected and analyzed the data; Zhang YL prepared figures; Liu B was in charge of patient treatment and designed the paper; all authors read and approved the final manuscript.

Informed consent statement: Informed written consent was obtained from the patient for publication of this report and any accompanying images.

Conflict-of-interest statement: The authors declare that they have no conflict of interest.

CARE Checklist (2016) statement: The authors have read the CARE Checklist (2016), and the manuscript was prepared and revised according to the CARE Checklist (2016).

Country/Territory of origin: China

ORCID number: Hai-Ping Liang 0000-0001-7537-278X; Xing-Chun Luo 0000-0002-4576-9011; Ya-Li Zhang 0000-0002-4176-9129; Bei Liu 0000-0003-4331-2138.

S-Editor: Gong ZM
L-Editor: A
P-Editor: Gong ZM

REFERENCES

1 **Gorshein E**, Weber UM, Gore S. Higher-risk myelodysplastic syndromes with del(5q): does the del(5q) matter? *Expert Rev Hematol* 2020; **13**: 233-239 [PMID: 32067540 DOI: 10.1080/17474086.2020.1730806]
2 **Menssen AJ**, Walter MJ. Genetics of progression from MDS to secondary leukemia. *Blood* 2020; **136**: 50-60 [PMID: 32430504 DOI: 10.1182/blood.2019000942]
3 **Garcia-Manero G**, Chien KS, Montalban-Bravo G. Myelodysplastic syndromes: 2021 update on diagnosis, risk stratification and management. *Am J Hematol* 2020; **95**: 1399-1420 [PMID: 32744763 DOI: 10.1002/ajh.25950]
4 **Hosono N**. Genetic abnormalities and pathophysiology of MDS. *Int J Clin Oncol* 2019; **24**: 885-892 [PMID: 31093808 DOI: 10.1007/s10147-019-01462-6]
5 **Ogawa S**. Genetics of MDS. *Blood* 2019; **133**: 1049-1059 [PMID: 30670442 DOI: 10.1182/blood-2018-10-844621]
6 **Merz A**, Germing U, Kobbe G, Kaivers J, Jauch A, Radujkovic A, Hummel M, Benner A, Merz M, Dreger P, Luft T. EASIX for prediction of survival in lower-risk myelodysplastic syndromes. *Blood Cancer J* 2019; **9**: 85 [PMID: 31712595 DOI: 10.1038/s41408-019-0247-z]
7 **Lee JH**, List A, Sallman DA. Molecular pathogenesis of myelodysplastic syndromes with deletion 5q. *Eur J Haematol* 2019; **102**: 203-209 [PMID: 30578738 DOI: 10.1111/ejh.13207]
8 **Jädersten M**, Karsan A. Clonal evolution in myelodysplastic syndromes with isolated del(5q): the importance of genetic monitoring. *Haematologica* 2011; **96**: 177-180 [PMID: 21282717 DOI: 10.3324/haematol.2010.038281]
9 **Birdwell C**, Fiskus W, Kadia TM, DiNardo CD, Mill CP, Bhalla KN. EVI1 dysregulation: impact on biology and therapy of myeloid malignancies. *Blood Cancer J* 2021; **11**: 64 [PMID: 33753715 DOI: 10.1038/s41408-021-00457-9]
10 **Thol F**, Friesen I, Damm F, Yun H, Weissinger EM, Krauter J, Wagner K, Chaturvedi A, Sharma A, Wichmann M, Göhring G, Schumann C, Bug G, Ottmann O, Hofmann WK, Schlegelberger B, Heuser M, Ganser A. Prognostic significance of ASXL1 mutations in patients with myelodysplastic syndromes. *J Clin Oncol* 2011; **29**: 2499-2506 [PMID: 21576631 DOI: 10.1200/JCO.2010.33.4938]
11 **Jaiswal S**, Natarajan P, Silver AJ, Gibson CJ, Bick AG, Shvartz E, McConkey M, Gupta N, Gabriel S, Ardissino D, Baber U, Mehran R, Fuster V, Danesh J, Frossard P, Saleheen D, Melander O, Sukhova GK, Neuberg D, Libby P, Kathiresan S, Ebert BL. Clonal Hematopoiesis and Risk of Atherosclerotic Cardiovascular Disease. *N Engl J Med* 2017; **377**: 111-121 [PMID: 28636844 DOI: 10.1056/NEJMoa1701719]
12 **List A**, Dewald G, Bennett J, Giagounidis A, Raza A, Feldman E, Powell B, Greenberg P, Thomas D, Stone R, Reeder C, Wride K, Patin J, Schmidt M, Zeldis J, Knight R; Myelodysplastic Syndrome-003 Study Investigators. Lenalidomide in the myelodysplastic syndrome with chromosome 5q deletion. *N Engl J Med* 2006; **355**: 1456-1465 [PMID: 17021321 DOI: 10.1056/NEJMoa061292]
13 **Talati C**, Sallman D, List AF. SOHO State of the Art and Next Questions: Management of Myelodysplastic Syndromes With Deletion 5q. *Clin Lymphoma Myeloma Leuk* 2018; **18**: 629-635 [PMID: 30097406 DOI: 10.1016/j.clml.2018.07.293]
14 **Martinez-Høyer S**, Deng Y, Parker J, Jiang J, Mo A, Docking TR, Gharaee N, Li J, Umlandt P, Fuller M, Jädersten M, Kulasekararaj A, Malcovati L, List AF, Hellström-Lindberg E, Platzbecker U, Karsan A. Loss of lenalidomide-induced megakaryocytic differentiation leads to therapy resistance in del(5q) myelodysplastic syndrome. *Nat Cell Biol* 2020; **22**: 526-533 [PMID: 32251398 DOI: 10.1038/s41556-020-0497-9]
15 **Sallman DA**, Wei S, List A. PP2A: The Achilles Heal in MDS with 5q Deletion. *Front Oncol* 2014; **4**: 264 [PMID: 25295231 DOI: 10.3389/fonc.2014.00264]
16 **Sallman DA**, Barnard J, Al Ali NH, Garcia-Manero G, Sekeres MA, DeZern A, Steensma DP, Roboz G, Jabbour E, Maciejewski JP, Pierce S, Padron E, Lancet JE, Kantarjian H, List AF, Komrokji RS. Hypomethylating Agent Therapy in Myelodysplastic Syndromes With Chromosome 3 Abnormalities. *Clin Lymphoma Myeloma Leuk* 2020; **20**: e597-e605 [PMID: 32303488 DOI: 10.1016/j.clml.2020.03.005]
17 **Iizuka H**, Yoshimi A, Yamamoto G, Masuda A, Nannya Y, Ichikawa M, Yatomi Y, Kurokawa M. Effective azacitidine treatment for myelodysplastic syndrome transformed from essential thrombocythemia. *Rinsho Ketsueki* 2013; **54**: 468-472 [PMID: 23727686]
18 **Wanquet A**, Prebet T, Berthon C, Sebert M, Roux C, Kulasekararaj A, Micol JB, Esterni B, Itzykson R, Thepot S, Recher C, Delaunay J, Dreyfus F, Mufti G, Fenaux P, Vey N. Azacitidine treatment for patients with myelodysplastic syndrome and acute myeloid leukemia with chromosome 3q abnormalities. *Am J Hematol* 2015; **90**: 859-863 [PMID: 26113240 DOI:

10.1002/ajh.24099]

19 **Garderet L**, Ziagkos D, van Biezen A, Iacobelli S, Finke J, Maertens J, Volin L, Ljungman P, Chevallier P, Passweg J, Schaap N, Beelen D, Nagler A, Blaise D, Poiré X, Yakoub-Agha I, Lenhoff S, Craddock C, Schots R, Rambaldi A, Sanz J, Jindra P, Mufti GJ, Robin M, Kröger N. Allogeneic Stem Cell Transplantation for Myelodysplastic Syndrome Patients with a 5q Deletion. *Biol Blood Marrow Transplant* 2018; **24**: 507-513 [PMID: 29196078 DOI: 10.1016/j.bbmt.2017.11.017]

20 **Fenaux P**, Haase D, Santini V, Sanz GF, Platzbecker U, Mey U; ESMO Guidelines Committee. Myelodysplastic syndromes: ESMO Clinical Practice Guidelines for diagnosis, treatment and follow-up†☆. *Ann Oncol* 2021; **32**: 142-156 [PMID: 33221366 DOI: 10.1016/j.annonc.2020.11.002]

21 **de Witte T**, Bowen D, Robin M, Malcovati L, Niederwieser D, Yakoub-Agha I, Mufti GJ, Fenaux P, Sanz G, Martino R, Alessandrino EP, Onida F, Symeonidis A, Passweg J, Kobbe G, Ganser A, Platzbecker U, Finke J, van Gelder M, van de Loosdrecht AA, Ljungman P, Stauder R, Volin L, Deeg HJ, Cutler C, Saber W, Champlin R, Giralt S, Anasetti C, Kröger N. Allogeneic hematopoietic stem cell transplantation for MDS and CMML: recommendations from an international expert panel. *Blood* 2017; **129**: 1753-1762 [PMID: 28096091 DOI: 10.1182/blood-2016-06-724500]

22 **Fenaux P**, Platzbecker U, Ades L. How we manage adults with myelodysplastic syndrome. *Br J Haematol* 2020; **189**: 1016-1027 [PMID: 31568568 DOI: 10.1111/bjh.16206]

23 **Della Porta MG**, Gallì A, Bacigalupo A, Zibellini S, Bernardi M, Rizzo E, Allione B, van Lint MT, Pioltelli P, Marenco P, Bosi A, Voso MT, Sica S, Cuzzola M, Angelucci E, Rossi M, Ubezio M, Malovini A, Limongelli I, Ferretti VV, Spinelli O, Tresoldi C, Pozzi S, Luchetti S, Pezzetti L, Catricalà S, Milanesi C, Riva A, Bruno B, Ciceri F, Bonifazi F, Bellazzi R, Papaemmanuil E, Santoro A, Alessandrino EP, Rambaldi A, Cazzola M. Clinical Effects of Driver Somatic Mutations on the Outcomes of Patients With Myelodysplastic Syndromes Treated With Allogeneic Hematopoietic Stem-Cell Transplantation. *J Clin Oncol* 2016; **34**: 3627-3637 [PMID: 27601546 DOI: 10.1200/JCO.2016.67.3616]

24 **Greenberg PL**, Tuechler H, Schanz J, Sanz G, Garcia-Manero G, Solé F, Bennett JM, Bowen D, Fenaux P, Dreyfus F, Kantarjian H, Kuendgen A, Levis A, Malcovati L, Cazzola M, Cermak J, Fonatsch C, Le Beau MM, Slovak ML, Krieger O, Luebbert M, Maciejewski J, Magalhaes SM, Miyazaki Y, Pfeilstöcker M, Sekeres M, Sperr WR, Stauder R, Tauro S, Valent P, Vallespi T, van de Loosdrecht AA, Germing U, Haase D. Revised international prognostic scoring system for myelodysplastic syndromes. *Blood* 2012; **120**: 2454-2465 [PMID: 22740453]

World Journal of Clinical Cases

Submit a Manuscript: https://www.f6publishing.com

World J Clin Cases 2022 April 16; 10(11): 3609-3614

DOI: 10.12998/wjcc.v10.i11.3609

ISSN 2307-8960 (online)

CASE REPORT

Papillary thyroid microcarcinoma with contralateral lymphatic skip metastasis and breast cancer: A case report

Min Ding, Ya-Hui Kong, Jian-Hua Gu, Rong-Li Xie, Jian Fei

Specialty type: Oncology

Provenance and peer review: Unsolicited article; Externally peer reviewed.

Peer-review model: Single blind

Peer-review report's scientific quality classification

Grade A (Excellent): 0
Grade B (Very good): 0
Grade C (Good): C, C
Grade D (Fair): 0
Grade E (Poor): 0

P-Reviewer: Gassler N, Raiter A

Received: December 29, 2021
Peer-review started: December 29, 2021
First decision: January 25, 2022
Revised: February 3, 2022
Accepted: February 23, 2022
Article in press: February 23, 2022
Published online: April 16, 2022

Min Ding, Jian Fei, Department of General Surgery, Ruijin Hospital, Shanghai Jiao Tong University School of Medicine, Shanghai 200025, China

Ya-Hui Kong, Department of General Surgery, Shanghai Changhang Hospital, Shanghai 200122, China

Jian-Hua Gu, Department of General Surgery, Shanghai Ruijin Rehabilitation Hospital, Shanghai 200023, China

Rong-Li Xie, Department of General Surgery, Ruijin Hospital Luwan Branch, Shanghai Jiao Tong University School of Medicine, Shanghai 200020, China

Corresponding author: Jian Fei, MD, PhD, Chief Doctor, Department of General Surgery, Ruijin Hospital, Shanghai Jiao Tong University School of Medicine, No. 197 Second Ruijin Road, Huangpu District, Shanghai 200025, China. fj10777@rjh.com.cn

Abstract

BACKGROUND

The recognized pattern of cervical lymph node metastasis (CLNM) of papillary thyroid carcinoma involves a stepwise route. Contralateral lymph node skip metastasis is very rare. In addition, the patient in our case report also suffered from a breast carcinoma accompanied by left supraclavicular lymphadenopathy, which made it difficult to distinguish the origin of the CLNM. Based on this case, we recommended that more detailed physical and imaging examinations are needed for patients with uncommon cervical lymphatic metastasis of primary cancer.

CASE SUMMARY

A 53-year-old women was admitted to the hospital for a neck mass in the left cervical region that had existed for 2 mo. The neck mass was suspected to be an enlarged lateral LN originating from papillary thyroid microcarcinoma of the contralateral thyroid lobe, according to ultrasound and ultrasound-guided fine needle aspiration biopsy. The patient underwent total thyroidectomy and radical cervical LN dissection. Postoperative pathology confirmed the diagnosis of papillary thyroid microcarcinoma with contralateral lymphatic skip metastasis. Unfortunately, a breast cancer was discovered 4 mo later, which was accompanied by ipsilateral supraclavicular LN metastasis. She accepted neoadjuvant chemotherapy and subsequent left modified radical mastectomy for treatment. The patient is currently receiving postoperative radiotherapy, and no local

recurrence was observed in the 6-mo follow-up after surgery.

CONCLUSION
We present a rare case of papillary thyroid microcarcinoma with contralateral lymphatic skip metastasis and breast cancer with supraclavicular lymphatic metastasis.

Key Words: Thyroid cancer; Papillary; Breast neoplasms; Lymphatic metastasis; Skip metastasis; Contralateral metastasis; Case report

Core Tip: The recognized pattern of cervical lymph node metastasis (CLNM) of papillary thyroid carcinoma involves a stepwise route. Contralateral lymph node skip metastasis is very rare. In addition, the patient in our case report also suffered from a breast carcinoma accompanied by left supraclavicular lymphadenopathy, which made it difficult to distinguish the origin of the CLNM. Based on this case, we recommended that more detailed physical and imaging examinations are needed for patients with uncommon cervical lymphatic metastasis of primary cancer.

Citation: Ding M, Kong YH, Gu JH, Xie RL, Fei J. Papillary thyroid microcarcinoma with contralateral lymphatic skip metastasis and breast cancer: A case report. *World J Clin Cases* 2022; 10(11): 3609-3614
URL: https://www.wjgnet.com/2307-8960/full/v10/i11/3609.htm
DOI: https://dx.doi.org/10.12998/wjcc.v10.i11.3609

INTRODUCTION

Thyroid cancer and breast cancer (BC) are very common in women[1] and both can involve cervical lymph node metastasis (CLNM). The most common type of thyroid cancer is papillary carcinoma, and papillary thyroid microcarcinoma (PTMC) accounts for the majority of cases. When it comes to multiple primary cancers, such as PTMC and BC, the origin of CLNM needs to be distinguished. CLNM in PTMC is usually related to a relatively poor prognosis, especially for lateral CLNM. The recognized pattern of CLNM of PTMC involves a stepwise route. The first site involved is the central compartment, followed by the ipsilateral lateral lymph node (LN) compartment. The contralateral and the mediastinal LN compartments then follow suit[2,3]. Contralateral LN skip metastasis is very rare. CLNM in BC is usually indicative of a terminal stage.

Here, we report a rare case of PTMC with contralateral lymphatic skip metastasis and BC with supraclavicular lymphatic metastasis.

CASE PRESENTATION

Chief complaints

A 53-year-old woman presented to the hospital with a neck mass in her left lateral cervical region.

History of present illness

The patient's symptom started 2 mo prior and she had not received any treatment in that period.

History of past illness

The patient had a free medical history.

Personal and family history

The patient denied any relevant personal family history, particularly for thyroid issues.

Physical examination

A nodule of approximately 0.8 cm in diameter was found in the right lobe of the thyroid gland. It was not tender and easily moved upward and downward when she swallowed. A firm mass of roughly 1.0 cm was palpated in the left lateral cervical region.

Laboratory examinations

Thyroid function and autoimmune antibody were all in normal ranges, except for the anti-thyroid peroxidase (TPO) antibody (787.40 IU/mL; normal range: 0-9 IU/mL). Routine blood indexes were all within normal range. Tests for serum tumor markers, including carcinoembryonic antigen, alpha-fetoprotein, carbohydrate antigen 19-9, CA242, cytokeratin 19 fragment and squamous cell carcinoma antigen, were all negative.

Imaging examinations

Ultrasound (US) examination showed a 7.8 mm × 7.4 mm heterogeneous hypoechoic nodule in the right lobe of the thyroid gland (Thyroid Imaging Reporting and Data System category 4B). In addition, several abnormal LNs were detected in level V; the biggest one being approximately 14.0 mm × 7.0 mm in size (Figure 1).

Further diagnostic follow-up

US-guided fine needle aspiration biopsy was taken for further evaluation. It indicated that the nodule in the right lobe was PTMC, and the LN was malignant. We preliminarily concluded that this patient suffered from PTMC accompanied by CLNM.

The patient underwent total thyroidectomy and radical cervical neck dissection (bilateral central LN and left lateral LN). Postoperative pathology found isolated PTMC in the right lobe, which was also supported by the findings of immunohistochemical analysis [CD56 (partly positive), HBME-1 (negative), galectin-3 (positive), CK19 (partly positive), TPO (negative), Ki67 index (1%)]. Surprisingly, the bilateral central cervical LNs (n = 16) were all disease-free. Metastasis was found, involving one LN in the left level V and one LN in levels III and IV (Figure 2). Immunohistochemical analysis of the metastatic LN in left levels III and IV were positive for galectin-3 and CK19, and were negative for CD56, HBME-1 and TPO. The Ki-67 index of 1% indicted that the left lateral CLNM in levels III and IV had originated from the thyroid.

No local relapse was found by US at the next 3-mo follow-up. The patient intended to receive iodine-131 therapy; however, she was admitted to our hospital for a large mass in her left breast 1 mo later. Mammography showed a mass of approximately 3.7 cm ´ 2.6 cm in the left breast, which was highly suspicious of malignancy (Breast Imaging Reporting and Data System 5). US also showed several abnormally enlarged LNs in the left axillary, supraclavicular and level V. US-guided core needle biopsy was taken for the breast mass, which revealed infiltrative carcinoma originating from the breast by pathology and immunohistochemical analysis. US-guided fine needle aspiration biopsy was taken for the suspicious LNs, including the left axillary, supraclavicular and level V, which were all determined to be malignant. It was unknown whether the CLNM in the supraclavicular and level V area originated from the thyroid or breast. The patient underwent another thyroid US. Several hypoechogenic structures could be detected in levels IV and V with irregular shape, obscure boundary and unclear lymphatic hilus. The findings were highly suspicious of metastatic LNs, and we first considered origination from the breast (Figure 3). No distant metastasis was found upon further examination.

FINAL DIAGNOSIS

PTMC with contralateral lymphatic skip metastasis and BC with supraclavicular lymphatic metastasis.

TREATMENT

Given that the BC was in an advanced stage (cT2N3M0), the patient underwent four cycles of neoadjuvant chemotherapy with epirubicin (145 mg/m^2) and cyclophosphamide (900 mg/m^2), followed by four cycles with docetaxel (150 mg/m^2). Clinical responses in the breast and LNs were assessed by US after the neoadjuvant chemotherapy treatment, and she was determined to have achieved partial remission. Then, she underwent a left modified radical mastectomy. Postoperative pathology of the breast revealed invasive ductal carcinoma accompanied by a few invasive micropapillary carcinomas and intermediate grade ductal carcinoma *in situ*. In addition, three of the seventeen LNs were metastatic. The immunohistochemistry profile of the specimen was as follows: estrogen receptor (+, strong, 95%); progesterone receptor (+, strong, 80%); human epidermal growth factor receptor-2 (1+); Ki-67 (15%); androgen receptor (60%); E-cadherin (+); GATA3 (+); mucin (+); cytokeratin 5/6 (-); epidermal growth factor receptor (-); D2-40 (-); and P63 (-).

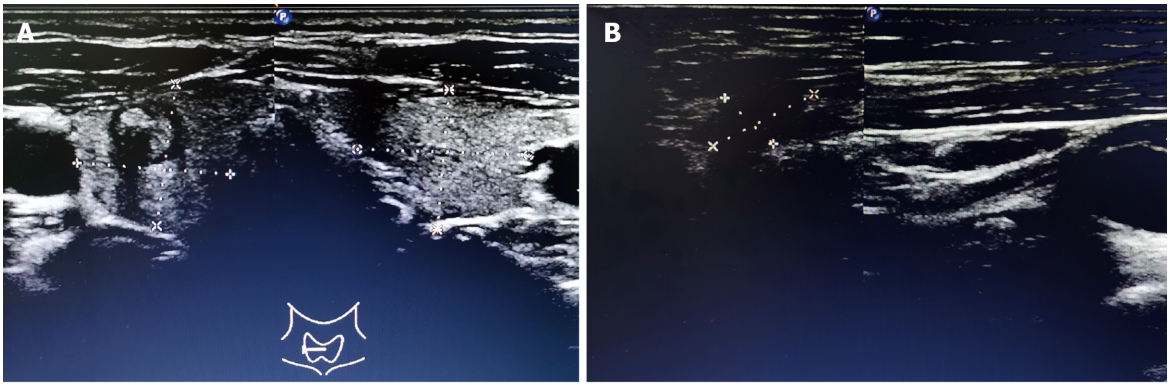

DOI: 10.12998/wjcc.v10.i11.3609

Figure 1 Ultrasound showed a nodule in the right thyroid lobe and an abnormal lymph node in left level V. A: A 7.8 mm × 7.4 mm heterogeneous hypoechoic nodule with obscure boundary and hyperechoic punctuations was observed in the middle and upper part of the right lobe of the thyroid gland; B: A hypoechogenic structure could be detected in level V, which was approximately 14.0 mm × 7.0 mm in size, with irregular shape, obscure boundary, heterogeneous echo, and unclear lymphatic hilus.

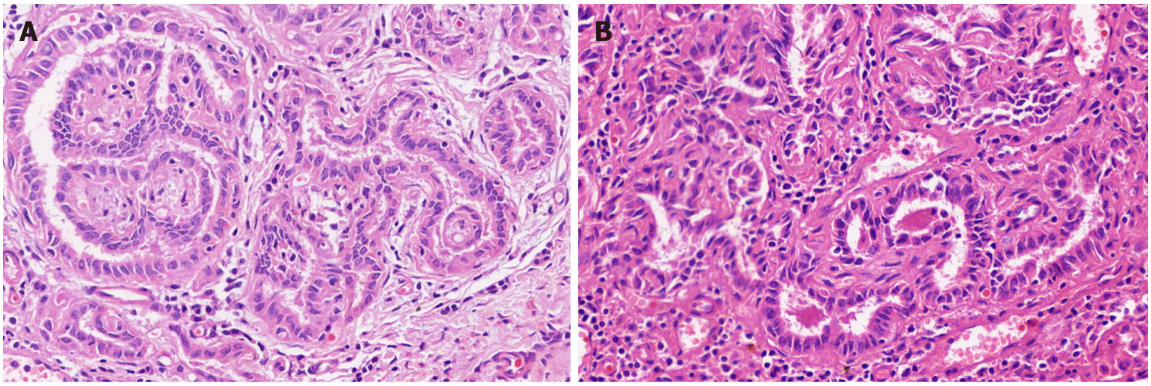

DOI: 10.12998/wjcc.v10.i11.3609

Figure 2 Hematoxylin and eosin staining of the right thyroid nodule and lymph node in left levels III and IV. A: Papillary thyroid microcarcinoma in the right thyroid lobe; B: Lymph node metastasis in left levels III and IV. Magnification: 800 ×.

OUTCOME AND FOLLOW-UP

The patient is currently receiving postoperative radiotherapy for control of the metastatic lesions. At the 6-mo follow-up, US assessment revealed no local recurrence.

DISCUSSION

We have reported, here, the first case of a rare contralateral LN skip metastasis of PTMC accompanied by BC. Bruno *et al*[4] reported a similar case of contralateral LN skip metastasis in Germany. However, those authors identified the unusual pathway of CLNM, mainly *via* the detection of high thyroglobulin levels in the wash-out liquid of fine-needly aspiration biopsy. In our case, it was mainly based on the postoperative immunohistochemical findings.

We raised two hypotheses for this kind of phenomenon. First, there may be unknown cervical LN drainage pathways. Second, there may be occult PTMC in the left lobe. A previous study reported cases of occult PTMC without detection of the primary tumor[5,6]. In one, Yamashita *et al*[5] hypothesized that the primary tumor was PTMC of less than 5 mm, as it was difficult to prepare slices of pathological specimens thinner than 5 mm.

Our patient, described herein, had developed cancers of PTMC and BC. However, the US-fine needle aspiration biopsy of LNs in the supraclavicular and level V areas failed to show the origin of her metastasis, which was crucial information. We hypothesized that they had originated from the BC instead of PTMC, for the following reasons. First, the most common sites of lateral CLNM in PTMC are levels II to IV. CLNM in level V is comparatively rare[7,8]. Second, the metastatic LNs of PTMC may show specific features, such as microcalcifications and cystic appearance, on US[9], which was not

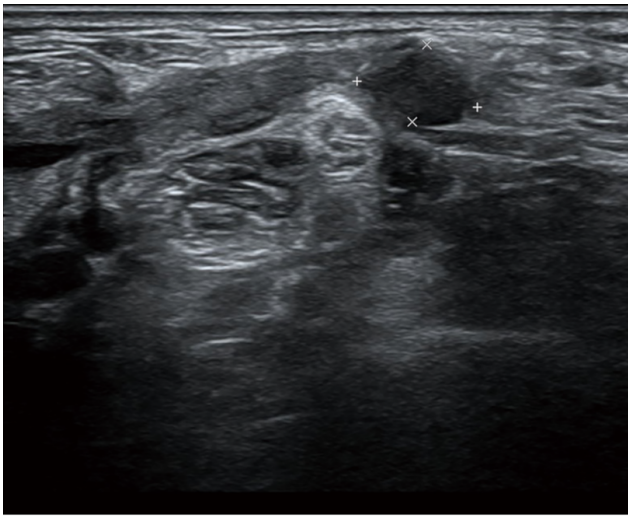

DOI: 10.12998/wjcc.v10.i11.3609

Figure 3 Ultrasound for the abnormal lymph nodes in the left supraclavicular and level V areas. Several hypoechogenic structure were detected in the left supraclavicular and level V areas, one of which was approximately 10.1 mm × 6.5 mm in size with unclear lymphatic hilus.

observed in our patient. Third, the size of the metastatic cervical LNs obviously decreased after neoadjuvant chemotherapy for BC.

Although most PTMC diagnoses have an excellent prognosis due to its indolent nature, some tend to be aggressive and are related to a poor prognosis[10]. The PTMC in our patient was T1aN1bM0 (IVa) stage according to the American Joint Committee on Cancer/Union for International Cancer Control TNM staging system[11]. Therefore, radical therapy was recommended. Because PTMC usually has a high incidence of multifocality and the presence of contralateral abnormal LNs[10], we could not exclude the existence of occult PTMC in the left lobe preoperatively. The patient underwent total thyroidectomy instead of lobectomy for complete resection of malignant tumors that allowed subsequent radiotherapy. Furthermore, prophylactic central compartment bilateral neck dissection was conducted for the presence of clinically involved lateral LNs (cN1b) as recommended by the 2015 American Thyroid Association guidelines[11]. However, a longer follow-up time was needed to learn the long-term prognosis of this patient. The BC was in a terminal stage as soon as it was discovered. In fact, it may have been discovered earlier if a more detailed examination had been performed at her first visit. The level V metastatic LNs discovered in the first surgery were not evaluated by further immunohistochemistry and were assumed to also be contralateral skip metastatic LNs. However, we cannot exclude that it may have originated from BC.

CONCLUSION

Here, we describe a case of PTMC with contralateral lymphatic skip metastasis and BC with supraclavicular lymphatic metastasis, which has rarely been reported in the literature. Both thyroid cancer and BC may involve CLNM. The characteristics of US, more detailed immunohistochemistry examination findings, and knowledge of the sites of CLNM may help to distinguish the origin of CLNM. In addition, when it comes to uncommon CLNM of the primary cancer, a more detailed examination such as by head-neck computed tomography, chest computed tomography and physical examination is strongly recommended.

ACKNOWLEDGEMENTS

We would like to thank Liu-Shu Jiang and Jun Liu for assisting with data collection.

FOOTNOTES

Author contributions: Ding M reviewed the literature and contributed to data analysis and manuscript drafting; Kong YH and Xie RL were responsible for data collection; Fei J and Gu JH were responsible for the revision of the manuscript, considering and providing important intellectual content; All authors issued final approval for the version to be submitted.

Supported by The Project of Shanghai Municipal Health Commission, No. 20214Y0223.

Informed consent statement: Informed written consent (surgical operation) was obtained from the patient.

Conflict-of-interest statement: The authors declare that they have no conflicts of interest.

CARE Checklist (2016) statement: The authors have read the CARE Checklist (2016), and the manuscript was prepared and revised according to the CARE Checklist (2016).

Country/Territory of origin: China

ORCID number: Min Ding 0000-0001-5444-9397; Ya-Hui Kong 0000-0002-6708-6297; Jian-Hua Gu 0000-0002-3501-7692; Rong-Li Xie 0000-0002-5266-383X; Jian Fei 0000-0001-7159-8562.

Corresponding Author's Membership in Professional Societies: Shanghai Association of Chinese Integrative Medicine Thyroid Professional Committee.

S-Editor: Gong ZM
L-Editor: A
P-Editor: Gong ZM

REFERENCES

1 **Siegel RL**, Miller KD, Jemal A. Cancer statistics, 2020. *CA Cancer J Clin* 2020; **70**: 7-30 [PMID: 31912902 DOI: 10.3322/caac.21590]
2 **Attard A**, Paladino NC, Lo Monte AI, Falco N, Melfa G, Rotolo G, Rizzuto S, Gulotta E, Salamone G, Bonventre S, Scerrino G, Cocorullo G. Skip metastases to lateral cervical lymph nodes in differentiated thyroid cancer: a systematic review. *BMC Surg* 2019; **18**: 112 [PMID: 31074393 DOI: 10.1186/s12893-018-0435-y]
3 **Park JH**, Lee YS, Kim BW, Chang HS, Park CS. Skip lateral neck node metastases in papillary thyroid carcinoma. *World J Surg* 2012; **36**: 743-747 [PMID: 22354485 DOI: 10.1007/s00268-012-1476-5]
4 **Bruno R**, Giannasio P, Chiarella R, Capula C, Russo D, Filetti S, Costante G. Identification of a neck lump as a lymph node metastasis from an occult contralateral papillary microcarcinoma of the thyroid: key role of thyroglobulin assay in the fine-needle aspirate. *Thyroid* 2009; **19**: 531-533 [PMID: 19416000 DOI: 10.1089/thy.2009.0049]
5 **Yamashita G**, Kondo T, Okimura A, Nakatsugawa M, Hirano H, Takeda A, Kikawada N, Aihara Y, Chiba Y, Ogawa Y, Tsukahara K. Occult Papillary Thyroid Carcinoma without Detection of the Primary Tumor on Preoperative Ultrasonography or Postoperative Pathological Examination: A Case Report. *Case Rep Oncol* 2020; **13**: 105-112 [PMID: 32231531 DOI: 10.1159/000505831]
6 **Liu H**, Lv L, Yang K. Occult thyroid carcinoma: a rare case report and review of literature. *Int J Clin Exp Pathol* 2014; **7**: 5210-5214 [PMID: 25197399]
7 **Gong Y**, Yang J, Yan S, Su A, Liu F, Gong R, Zhu J, Li Z. Pattern of and clinicopathologic risk factors for lateral lymph node metastases in papillary thyroid carcinoma patients with lateral cervical lymphadenopathy. *Medicine (Baltimore)* 2018; **97**: e12263 [PMID: 30200164 DOI: 10.1097/MD.0000000000012263]
8 **Caron NR**, Tan YY, Ogilvie JB, Triponez F, Reiff ES, Kebebew E, Duh QY, Clark OH. Selective modified radical neck dissection for papillary thyroid cancer-is level I, II and V dissection always necessary? *World J Surg* 2006; **30**: 833-840 [PMID: 16555024 DOI: 10.1007/s00268-005-0358-5]
9 **Leboulleux S**, Girard E, Rose M, Travagli JP, Sabbah N, Caillou B, Hartl DM, Lassau N, Baudin E, Schlumberger M. Ultrasound criteria of malignancy for cervical lymph nodes in patients followed up for differentiated thyroid cancer. *J Clin Endocrinol Metab* 2007; **92**: 3590-3594 [PMID: 17609301 DOI: 10.1210/jc.2007-0444]
10 **Yu XM**, Lloyd R, Chen H. Current treatment of papillary thyroid microcarcinoma. *Adv Surg* 2012; **46**: 191-203 [PMID: 22873040 DOI: 10.1016/j.yasu.2012.03.002]
11 **Haugen BR**, Alexander EK, Bible KC, Doherty GM, Mandel SJ, Nikiforov YE, Pacini F, Randolph GW, Sawka AM, Schlumberger M, Schuff KG, Sherman SI, Sosa JA, Steward DL, Tuttle RM, Wartofsky L. 2015 American Thyroid Association Management Guidelines for Adult Patients with Thyroid Nodules and Differentiated Thyroid Cancer: The American Thyroid Association Guidelines Task Force on Thyroid Nodules and Differentiated Thyroid Cancer. *Thyroid* 2016; **26**: 1-133 [PMID: 26462967 DOI: 10.1089/thy.2015.0020]

World Journal of Clinical Cases

Submit a Manuscript: https://www.f6publishing.com

World J Clin Cases 2022 April 16; 10(11): 3615-3623

DOI: 10.12998/wjcc.v10.i11.3615

ISSN 2307-8960 (online)

CASE REPORT

Contrast-enhanced ultrasound manifestations of synchronous combined hepatocellular-cholangiocarcinoma and hepatocellular carcinoma: A case report

Ling Gao, Jia-Yan Huang, Zi-Jian Lu, Qiang Lu

Specialty type: Medicine, research and experimental

Provenance and peer review: Unsolicited article; Externally peer reviewed.

Peer-review model: Single blind

Peer-review report's scientific quality classification
Grade A (Excellent): 0
Grade B (Very good): B
Grade C (Good): 0
Grade D (Fair): D
Grade E (Poor): 0

P-Reviewer: Caiati C, Sintusek P

Received: December 12, 2021
Peer-review started: December 12, 2021
First decision: January 26, 2022
Revised: February 8, 2022
Accepted: February 23, 2022
Article in press: February 23, 2022
Published online: April 16, 2022

Ling Gao, Jia-Yan Huang, Qiang Lu, Department of Ultrasound, West China Hospital, Sichuan University, Chengdu 610041, Sichuan Province, China

Ling Gao, Department of Ultrasound, Chengdu BOE hospital, Chengdu 610219, Sichuan Province, China

Zi-Jian Lu, Department of Pathology, West China Hospital, Sichuan University, Chengdu 610041, Sichuan Province, China

Corresponding author: Qiang Lu, MD, Chief Doctor, Department of Ultrasound, West China Hospital, Sichuan University, No. 37 Guo Xue Xiang, Chengdu 610041, Sichuan Province, China. luqiang@scu.edu.cn

Abstract

BACKGROUND

Synchronous combined hepatocellular-cholangiocarcinoma (CHC) and hepatocellular carcinoma (HCC) is very rare, with few literature reports and poor clinical outcomes associated with the disorder. Surgical resection is the main treatment, which makes the preoperative diagnosis very important. However, due to imaging manifestations overlapping with HCC, diagnosis of this type of synchronous cancer is challenging and it tends to be misdiagnosed as multiple HCC. Herein, we report the contrast-enhanced ultrasound (CEUS) manifestations of a case of synchronous CHC and HCC, aiming at adding to the understanding of this disease. CEUS displayed exquisite vascularity and tissue perfusion in real time with good spatial and temporal resolution and more accurately reflect tumor washin and washout times than contrast-enhanced computed tomography (CT) in this case.

CASE SUMMARY

The patient was a 69-year-old female with a 20-year history of chronic hepatitis B. Due to months of epigastric pain and anorexia, she reffered to our hospital for treatment. Five days before hospitalization, abdominal magnetic resonance imaging performed at another hospital detected a space-occupying lesion in the liver. After her hospitalization, laboratory tests showed elevated alpha-fetoprotein and carbohydrate antigen 19-9 level. Two suspicious liver lesions located in S4 and S6, respectively, were identified in a cirrhotic background by abdominal

contrast-enhanced CT (CECT). Furthermore, the lesion in S4 and S6 were detected by CEUS and assigned to CEUS LI-RADS 5 and M categories, respectively. The patient underwent tumor radical resections. Post-operative pathology confirmed the S4 and S6 lesions to be HCC and CHC, respectively. A newly-found suspicious liver nodule with potential malignancy was detected in liver S1 by both CEUS and CECT 7 mo after operation.

CONCLUSION

The CEUS characteristics of CHC and HCC are different. CEUS features in combination with clinical information could help in effective diagnosis, clinical decision-making and better prognosis.

Key Words: Contrast-enhanced ultrasound; Synchronous dual primary malignancies of liver; Combined hepatocellular and cholangiocarcinoma; Hepatocellular carcinoma; Case report

Core Tip: Synchronous hepatocellular-cholangiocarcinoma (CHC) and hepatocellular carcinoma (HCC) is rare and tend to be misdiagnosed as multiple HCC in clinical settings. Patients afflicted with this disorder generally have poor prognosis, moreover, preoperative imaging diagnosis is often challenging. This paper introduces contrast-enhanced ultrasound (CEUS) manifestations of a case of synchronous CHC and HCC, which showed different imaging features on CEUS images. Overall, the combination of CEUS characteristics with clinical information could help in effective diagnosis of synchronous CHC and HCC, as well as clinical decision-making and patients' prognosis.

Citation: Gao L, Huang JY, Lu ZJ, Lu Q. Contrast-enhanced ultrasound manifestations of synchronous combined hepatocellular-cholangiocarcinoma and hepatocellular carcinoma: A case report. *World J Clin Cases* 2022; 10(11): 3615-3623

URL: https://www.wjgnet.com/2307-8960/full/v10/i11/3615.htm

DOI: https://dx.doi.org/10.12998/wjcc.v10.i11.3615

INTRODUCTION

Liver cancer is predicted to be the sixth most commonly diagnosed cancer and the fourth leading cause of cancer death worldwide in 2018[1]. Approximately half of primary liver cancers exhibit multifocal origins[2]. According to different origins, multifocal liver cancer can be divided into primary liver cancer with intrahepatic metastasis and liver cancer with a multicentric origin[3,4]. Synchronous combined hepatocellular-cholangiocarcinoma (CHC) and hepatocellular carcinoma (HCC) is rare in multicentric liver cancer, and it is often misdiagnosed as multiple HCC and has a poor prognosis[5,6]. Moreover, the treatment strategies and outcomes of the two diseases are different. When CHC and HCC occur synchronously, due to the unique fiber components of intrahepatic cholangiocarcinoma (ICC) contained in CHC, treatments typically used for multiple HCC, *e.g.* transcatheterial arterial chemoembolization (TACE) and chemotherapy, provide limited benefits[6]. Therefore, an accurate preoperative diagnosis is very important.

CASE PRESENTATION

Chief complaints

A 69-year-old female referred to our hospital due to months of epigastric pain and anorexia.

History of present illness

Epigastric pain and anorexia were presented. No nausea, vomiting, acid regurgitation, belching, chills, fever, hematemesis, melena or jaundice (among other symptoms) were observed.

History of past illness

The patient had a 20-years history of chronic hepatitis B and did not receive standardized treatments.

Personal and family history

The patient had a > 20-year history of alcoholism (approximately 50 mL liquor *per* day) and did not have a smoking history, nor did she have a travel history to pastoral areas or epidemic areas.

Physical examination

The patient's height and weight were 155 cm and 59 kg, respectively, with a body mass index of 24.6 kg/m^2. No swollen lymph nodes were found. The abdomen was soft without rebound tenderness, and the liver and spleen were not palpable under the ribs. There was no percussion pain in the liver area. Mobility dullness was negative, and bowel sounds were normal.

Laboratory examinations

Platelet count: 93 × 10^9/L; white blood cell count: 2.65 × 10^9/L; red blood cell count: 3.99 × 10^{12}/L; hemoglobin: 124 g/L; albumin: 42.2 g/L (normal range: 40.0-55.0 g/L); globulin: 23.1 g/L (normal range: 20.0-40.0 g/L); total bilirubin: 10.3 μmol/L (normal range: 5.0-28.0 μmol/L); direct bilirubin: 3.4 μmol/L (normal range: < 8.8 μmol/L); alanine aminotransferase (ALT): 50 IU/L (normal range: < 40.0 IU/L); aspartate aminotransferase (AST): 61 IU/L (normal range: < 35.0 IU/L); alkaline phosphatase (ALP): 126 IU/L (normal range: 50.0-135.0 IU/L); hepatitis B surface antigen (+); hepatitis B e antibody (+); hepatitis B core antibody (+); hepatitis C antibody (-); HBV DNA level: 6.32 × 10^5 IU/Ml (normal range: < 1.0 × 10^2 IU/mL); Serum bio-marker analysis showed elevated alpha-fetoprotein (AFP): 219.00 ng/mL (normal range: < 7 ng/mL), serum carbohydrate antigen 19-9 (CA19-9): 38.40 U/mL (normal range: < 30 U/mL) and protein induced by vitamin K absence or antagonist-II (PIVKA-II): 54.00 mAU/mL (normal range: 6.0-32.5 mAU/mL); carcinoembryonic antigen (CEA) and serum carbohydrate antigen 125 (CA-125) were both normal.

Imaging examinations

CT showed a slightly enlarged spleen. S4 showed a hypoattenuating mass (Figure 1A) (approximately 2.1 cm × 2.0 cm), which presented with marked enhancement in the arterial phase (Figure 1B) and isoenhancement in the portal venous phase (Figure 1C). S6 revealed a hypoattenuating mass (Figure 2A) (an area of approximately 3.0 cm × 2.7 cm), which presented with an annular weak enhancement in the arterial phase (Figure 2B) and mild hypoenhancement in the portal venous phase (Figure 2C). The diagnosis was considered to be cirrhosis with a malignant tumor of the liver. Ultrasound indicated that the liver parenchyma was thickened and uneven. A quasicircular hypoechoic nodule with a size of approximately 2.1 cm × 2.0 cm was found in S4 alongside the gallbladder (Figure 1D); it had a clear boundary and a regular shape and pushed and squeezed the gallbladder. The gallbladder wall was continuous and complete, and a mild blood flow signal was observed inside of the nodule (Figure 1E). S6 indicated a hypoechoic nodule with a size of approximately 3.9 cm × 3.5 cm (Figure 2D), with an irregular shape and an unclear boundary. The nodule protruded outward and pushed and squeezed the right kidney. The capsule of the right kidney was intact. Additionally, short-line blood flow signals could be observed inside of the nodule (Figure 2E). No enlarged lymph nodes were found in the abdominal cavity. On contrast-enhanced ultrasound (CEUS) (Sonazoid 0.6 mL bolus injection, Philips EPIQ7, and C5-1 convex array probe), the S4 nodule showed rapid hyperenhancement in the arterial phase (Figure 1F), mild hyperenhancement in the portal venous phase (Figure 1G) and mild hypoenhancement in the post vascular phase (Figure 1H). The S6 nodule indicated rim hyperenhancement in the arterial phase (Figure 2F); in addition, washing out began in the late arterial phase (27 s) (Figure 2G), the portal phase showed hypoenhancement, and the post vascular phase showed marked hypoenhancement (Figure 2H). The ultrasound suggested liver cirrhosis; additionally, the S4 hypoechoic nodule was considered to be HCC, and the S6 hypoechoic nodule was considered to be a malignant liver tumor (the ultrasound manifestations of the two intrahepatic nodules are shown in Table 1).

FINAL DIAGNOSIS

Synchronous CHC and HCC.

TREATMENT

The patient underwent a complex liver cancer resection, cholecystectomy and partial resection of the right adrenal gland.

Table 1 Ultrasound manifestation of the two intrahepatic nodules

Nodules	Location	Size (cm)	Boundary	Arterial phase	Portal phase	Post-vascular phase
HCC	S4	2.1 × 2.0	Clear	Hyperenhancement	Hyperenhancement	Mild hypoenhancement
CHC	S6	3.0 × 2.7	Unclear	Rim enhancement	Marked hypoenhancement	Marked hypoenhancement

HCC: Hepatocellular carcinoma; CHC: Hepatocellular-cholangiocarcinoma.

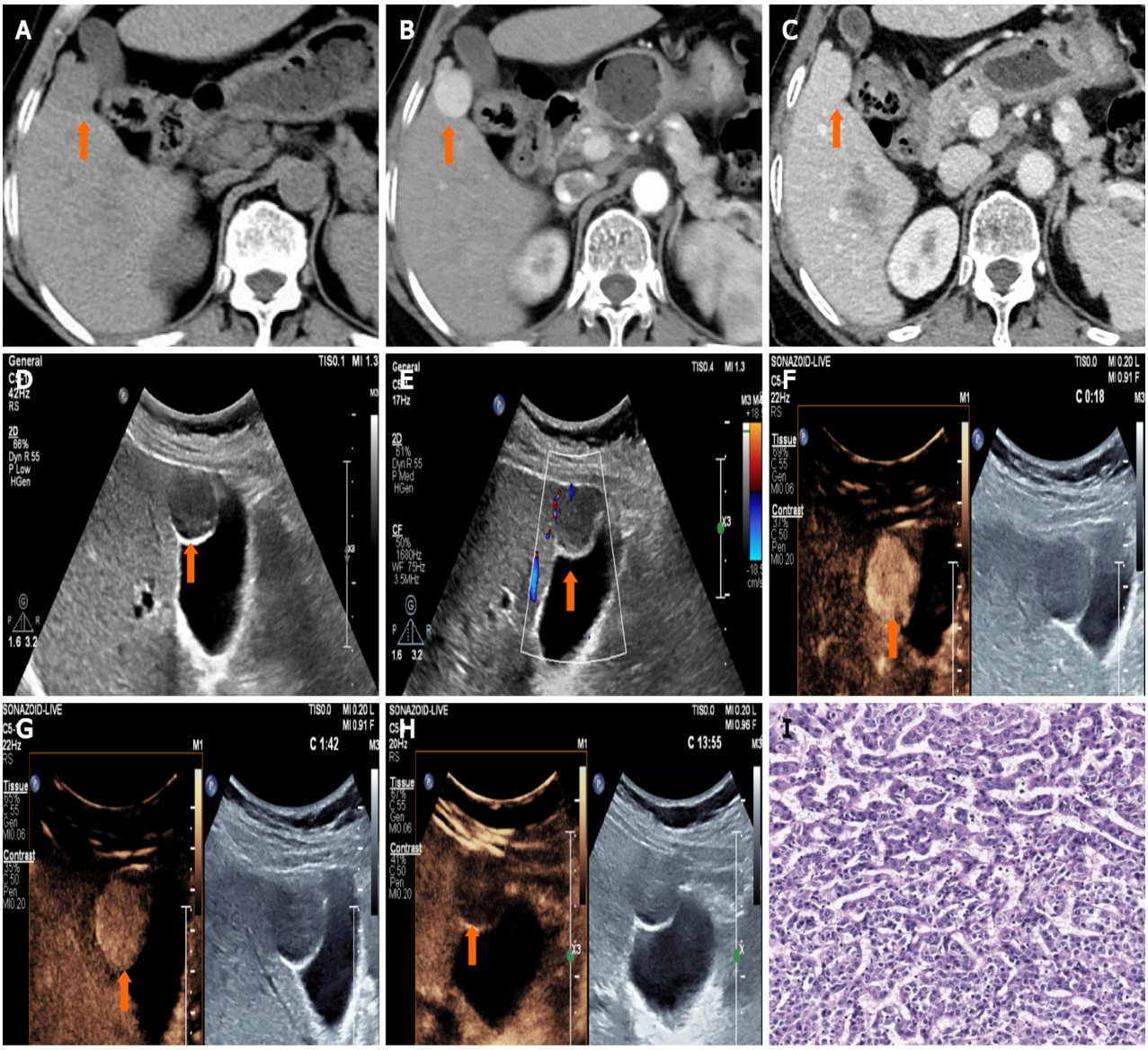

DOI: 10.12998/wjcc.v10.i11.3615

Figure 1 Contrast enhanced computed tomography and ultrasound images of a liver lesion in S4. A: A slightly low-density nodule measuring 2.1 cm × 2.0 cm was detected in liver S4 (A, arrow) on unenhanced computed tomography; B and C: The nodule showed marked enhancement in the arterial phase (B, arrow) followed by isoenhancement in the portal venous phase (C, arrow); D and E: The nodule presented a hypoechoic lesion with a clear boundary and regular shape (D, arrow) on conventional ultrasound; the color Doppler showed punctate blood flow signal (E, arrow) in the peripheral area of the lesion; F-H: On contrast enhaned ultrasound, the lesion manefested homogeneous hyperenhancement (F, arrow), followed by mild hyperenhancement in the portal venous phase (G, arrow) and hypoenhancement in the late phase (H, arrow); I: Postoperative pathology confirmed this lesion as being a poorly differentiated hepatocellular carcinoma (hematoxylin-eosin staining).

OUTCOME AND FOLLOW-UP

Postoperative pathology

Postoperative pathology confirmed the S4 nodule a HCC (Figure 1I) and the S6 nodule a CHC

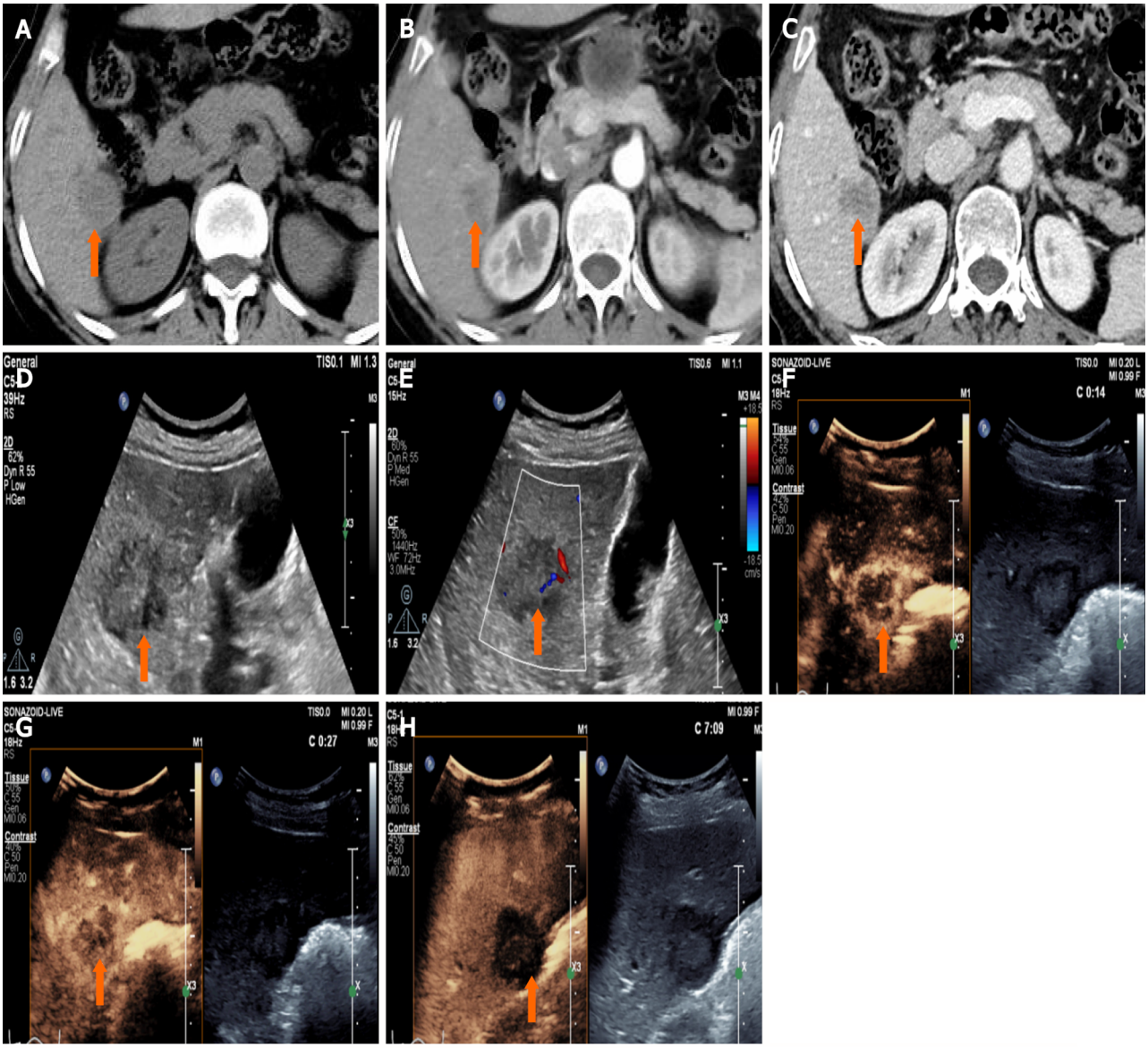

DOI: 10.12998/wjcc.v10.i11.3615

Figure 2 Contrast enhanced computed tomography and ultrasound images of a liver lesion in S6. A: A low-density nodule measuring 3.0 cm × 2.7 cm was detected in liver S6 (A, arrow) on unenhanced computed tomography (CT); B and C: The lesion showed rim hyperenhancement in the arterial phase (B, arrow) followed by hypoenhancement (C, arrow) in the portal venous phase on contrast enhanced CT; D and E: The lesion presented a hypoechoic nodue with an unclear boundary and irregular shape (D, arrow); a sparse of blood flow was detected by color Doppler (E, arrow); F-H: The lesion manefested rapid rim hyperenhancement (F, arrow) and early washout (G, arrow) in the arterial phase, followed by marked washout in the late phase on contrast enhanced ultrasound.

(Figure 3). As to the S6 lesion, positive expression of Arginase 1 (Arg 1) (Figure 4A) and Glypican-3 (GPC-3) (Figure 4B) in the hepatocellular carcinoma component, and Cytokeratin 7 (CK7) (Figure 4C) and Cytokeratin 19 (CK19) (Figure 4D) in the cholangiolocarcinoma components were confirmed by immunohistochemical analysis. No metastasis was found in the gallbladder or in the right adrenal gland.

Examination results

The patient underwent follow-up examinations at 7 mo after the operation. A newly found liver lesion located in S1 showing internal hypoenhancement and mild peripheral hyperenhancement was detected by contrast-enhanced computed tomography (CECT) (Figure 5A). The lesion manifested peripherial hyperenhancement (Figure 5B) in the arterial phase followed by early washout in the portal venous phase (Figure 5C) on CEUS. Both CECT and CEUS considered this lesion a malignancy.

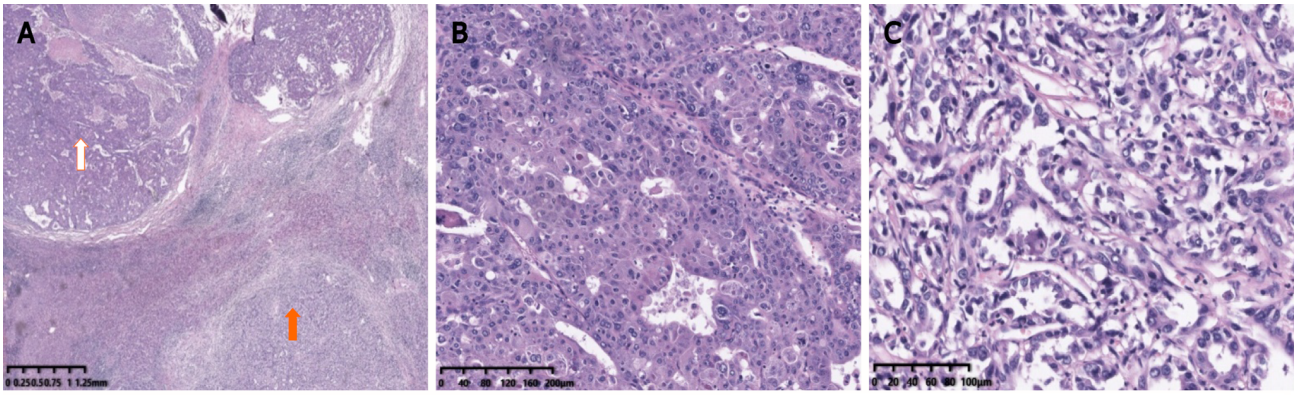

DOI: 10.12998/wjcc.v10.i11.3615 **Copyright** © The Author(s) 2022.

Figure 3 The nodule in liver S6 confirmed to be a combined hepatocellular-cholangiolocarcinoma by pathology. A: A distinct transitional zone was observed between the hepatocellular carcinoma (white arrow) and cholangiolocarcinoma (orange arrow) tissues (original magnification); B: Hepatocellular carcinoma cells huddled between the trabecular in disarray; C: Cholangiolocarcinoma consisted of neoplastic cells with marked pleomorphism.

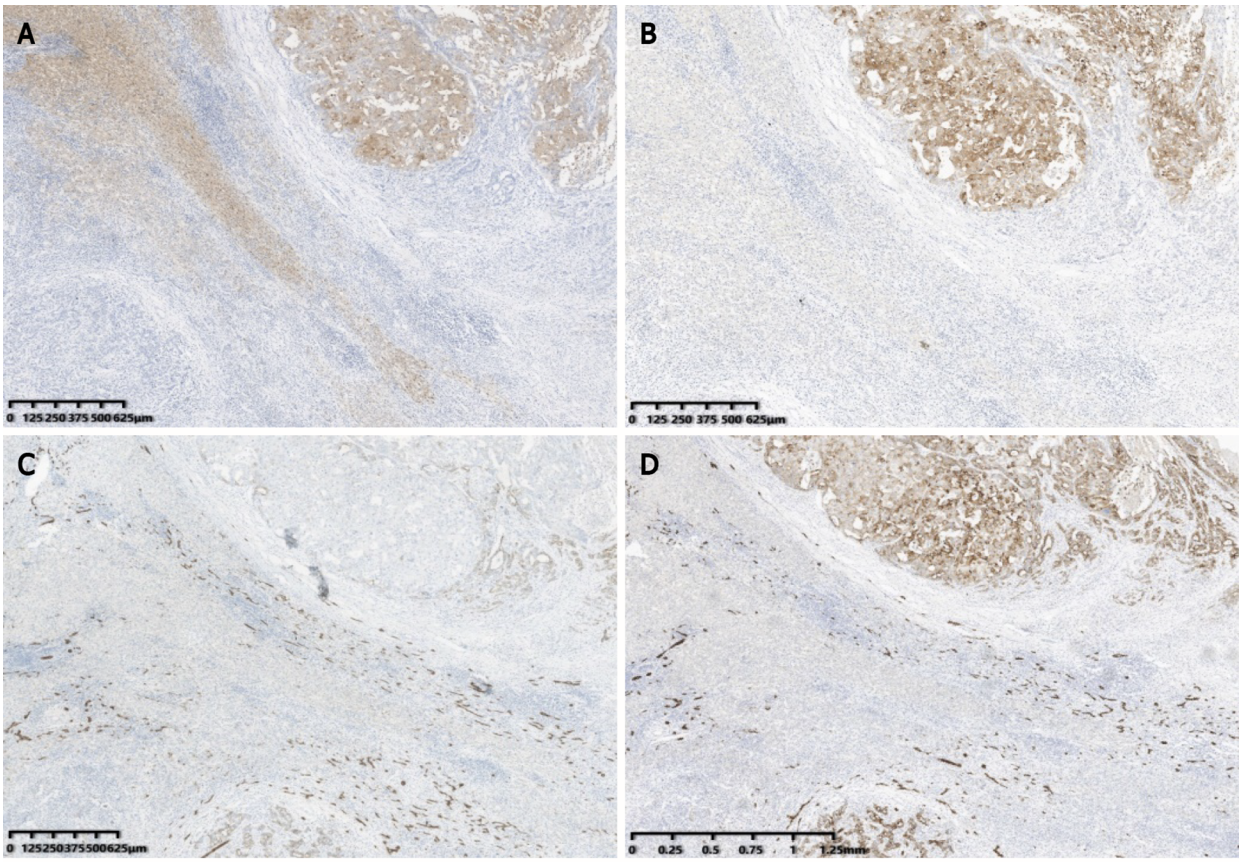

DOI: 10.12998/wjcc.v10.i11.3615 **Copyright** © The Author(s) 2022.

Figure 4 Immunohistochemical analysis of the nodule in liver S6. A and B: Arg (A) and GPC-3 (B) were highly expressed in hepatocellular carcinoma tissues; C and D: CK7 (C) and CK19 (D) were expressed in Cholangiolocarcinoma tissues, respectively.

DISCUSSION

Synchronous CHC and HCC is an uncommon condition that very few literatures had reported previously. Though rarely occurs, this disorder typically has a poor prognosis. Because of overlapping imaging features with HCC and atypical clinical manifestation, effective diagnosis of this disease can be challenging[6]. Patients afflicted with synchronous CHC and HCC has little or no response to therapeutic drugs due to unique fiber components of ICC in CHC. Therefore, a series of local treatments, including TACE and chemotherapy, cannot significantly benefit these patients[6]. Previous studies showed that the survival rate of patients with CHC, who underwent liver transplantation showed inferior survival in comparison to those with HCC alone, and the role and indications of liver

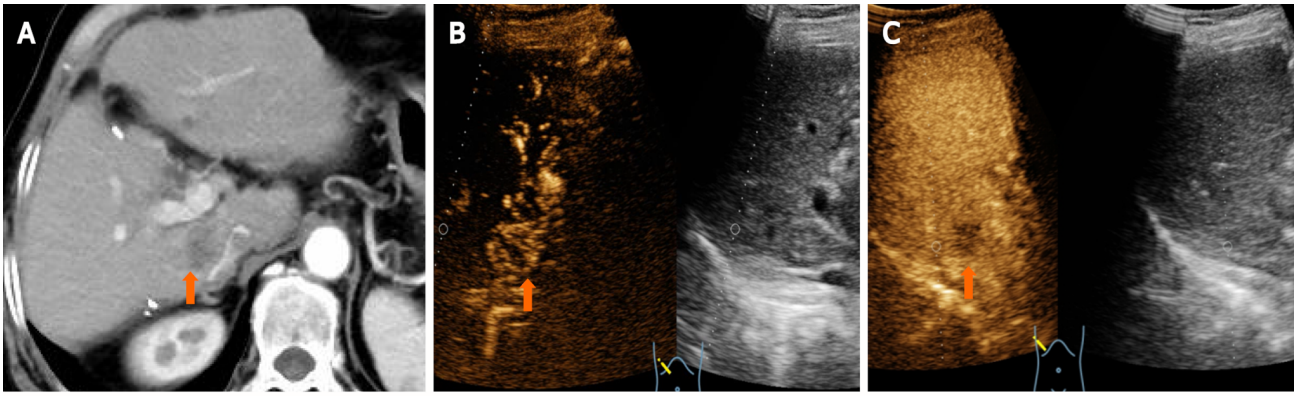

DOI: 10.12998/wjcc.v10.i11.3615

Figure 5 A recurrent tumor in liver S1 was found by contrast enhanced imaging modalities 7 mo after operation. A: The nodule showed mild annular enhancement on contrast enhanced computed tomography; B and C: The lesion manifested peripherial hyperenhancement (B, arrow) in the arterial phase and hypoenhancement in the portal venous phase (C, arrow) on contrast enhanced ultraound.

transplantation in combined tumor have yet to be defined[7-9]. Therefore, surgery is currently the best treatment choice, but the prognosis is poor due to a high incidence of vascular invasion and lymph node metastasis; additionally, the average relapse time after radical resection is only 5.4 mo[10,11]. Thus, an accurate preoperative diagnosis is of great significance for clinical decision-making and good prognosis.

Although the CEUS features of CHC partially overlap with those of HCC and ICC, CHC still possesses its own clinical characteristics. HCC usually occurs in patients with chronic hepatitis B or cirrhosis. On CEUS images, rapid arterial phase hyperenhancement (APHE) resulted from the formation of neoangiogenesis, and washout during postarterial phases due to reduced or absent of normal structure of portal triads, are identified as characterics of HCC[12]. According to the criteria of CEUS LI-RADS V2017 and related research[13,14], typical HCC is characterized by APHE (in whole or in part, not rim or peripheral discontinuous globular enhancement) with mild and late washout (> 60 s). Rim-like hyperenhancement, early (< 60 s) washout and marked washout within 120 s are specific enhancement patterns of ICC on CEUS. Arterial rim hyperenhancement pattern of ICC is associated with a high degree of malignant cell proliferation in the periphery while necrosis or fibrosis in the center of the tumor on pathology[15,16]. The ultrasound manifestations of CHC are related to the proportion of HCC and ICC components in the mass. The enhancement pattern of HCC-dominant lesions is similar to that of HCC, whereas those of ICC-dominant lesions is similar to that of ICC. The amount of the HCC component may be the main determinant of radiologic LI-RADS categories of hepatocellular-cholangiocarcinoma; tumors of LR-4 or LR-5 categories were associated with a larger proportion of the HCC component and smaller or none proportion of the cholangiocarcinomas component[17]. According to the CEUS LI-RADS criteria, most CHCs are diagnosed as LR-M, and studies have showed that the disease-free survival rate of these patients is low[18-20]. The enhancement pattern of CHC on CEUS is also associated with nodule size. When the nodule is smaller than or equal to 3 cm, the enhancement pattern is similar to that of HCC; when the nodule is larger than 3 cm, the enhancement mode is similar to that of ICC. With an increase in lesion diameter, the manifestations of CHC in enhanced images change from HCC-like to ICC-like[21]. On CECT, CHC commonly shows central delayed enhancement in the delayed phase, whereas it shows marked washout on CEUS images. This heterogeneity rarely appears in HCC, which is helpful in distinguishing between the two entities. In our case, the S4 nodule showed rapid and hyperenhancement in the arterial phase followed by mild and late washout in the delayed phase, a typical manifestation of CEUS LR-5 category. The S6 nodule displayed peripheral rim-like hyperenhancement in the arterial phase, followed by early washout, which should be classified as a LR-M nodule. Both of the nodules were differ in enhancement pattern, and onset and degree of washout. The discrepancy between the simultaneously elevated level of AFP and CA19-9 and the CEUS patterns (*i.e.*, the CEUS mode of ICC presents upon the increase in AFP and the CEUS mode of HCC presents upon the increase in CA19-9) have been reported to be the diagnostic criteria that can improve the accurate diagnostic rate of CHC[22]. Although some of the previously described features can help us distinguish CHC from HCC, accurate diagnosis of some cases remained tough before operations. Alternatively, ultrasound-guided puncture biopsy is necessary in such circumstances.

CONCLUSION

In summary, the CEUS manifestations of HCC and CHC are different. CEUS combined with clinical information (history of chronic hepatitis B and the synchronously elevated level of AFP and CA19-9) may indicate synchronous CHC and HCC, which help in effective diagnosis, clinical decision-making

and better prognosis.

FOOTNOTES

Author contributions: Gao L reviewed the literature and drafted the article; Lu Q conceived the article; Lu Q and Huang JY provided critical revision to the manuscript; Lu ZJ contributed pathological data; and all authors issued final approval for the version to be submit.

Informed consent statement: Informed written consent was obtained from the patient's daughter for publication of this report and any accompanying images.

Conflict-of-interest statement: The authors declare that they have no conflict of interest.

CARE Checklist (2016) statement: The authors have read the CARE Checklist (2016), and the manuscript was prepared and revised according to the CARE Checklist (2016).

Country/Territory of origin: China

ORCID number: Ling Gao 0000-0003-3683-2207; Jia-Yan Huang 0000-0002-1918-2874; Zi-Jian Lu 0000-0001-9660-9002; Qiang Lu 0000-0002-4057-1997.

S-Editor: Fan JR
L-Editor: A
P-Editor: Fan JR

REFERENCES

1 **Bray F**, Ferlay J, Soerjomataram I, Siegel RL, Torre LA, Jemal A. Global cancer statistics 2018: GLOBOCAN estimates of incidence and mortality worldwide for 36 cancers in 185 countries. *CA Cancer J Clin* 2018; **68**: 394-424 [PMID: 30207593 DOI: 10.3322/caac.21492]
2 **Xie DY**, Fan HK, Ren ZG, Fan J, Gao Q. Identifying Clonal Origin of Multifocal Hepatocellular Carcinoma and Its Clinical Implications. *Clin Transl Gastroenterol* 2019; **10**: e00006 [PMID: 30829920 DOI: 10.14309/ctg.0000000000000006]
3 **Matsumoto Y**, Fujii H, Matsuda M, Kono H. Multicentric occurrence of hepatocellular carcinoma: diagnosis and clinical significance. *J Hepatobiliary Pancreat Surg* 2001; **8**: 435-440 [PMID: 11702253 DOI: 10.1007/s005340100006]
4 **Feo F**, Pascale RM. Multifocal hepatocellular carcinoma: intrahepatic metastasis or multicentric carcinogenesis? *Ann Transl Med* 2015; **3**: 4 [PMID: 25705636 DOI: 10.3978/j.issn.2305-5839.2014.12.08]
5 **Ide R**, Oshita A, Nishisaka T, Nakahara H, Aimitsu S, Itamoto T. Primary biliary cholangitis metachronously complicated with combined hepatocellular carcinoma-cholangiocellular carcinoma and hepatocellular carcinoma. *World J Hepatol* 2017; **9**: 1378-1384 [PMID: 29359023 DOI: 10.4254/wjh.v9.i36.1378]
6 **Connell LC**, Harding JJ, Shia J, Abou-Alfa GK. Combined intrahepatic cholangiocarcinoma and hepatocellular carcinoma. *Chin Clin Oncol* 2016; **5**: 66 [PMID: 27829279 DOI: 10.21037/cco.2016.10.02]
7 **Garancini M**, Goffredo P, Pagni F, Romano F, Roman S, Sosa JA, Giardini V. Combined hepatocellular-cholangiocarcinoma: a population-level analysis of an uncommon primary liver tumor. *Liver Transpl* 2014; **20**: 952-959 [PMID: 24777610 DOI: 10.1002/lt.23897]
8 **Song S**, Moon HH, Lee S, Kim TS, Shin M, Kim JM, Park JB, Kwon CH, Kim SJ, Lee SK, Joh JW. Comparison between resection and transplantation in combined hepatocellular and cholangiocarcinoma. *Transplant Proc* 2013; **45**: 3041-3046 [PMID: 24157032 DOI: 10.1016/j.transproceed.2013.08.064]
9 **Magistri P**, Tarantino G, Serra V, Guidetti C, Ballarin R, Di Benedetto F. Liver transplantation and combined hepatocellular-cholangiocarcinoma: Feasibility and outcomes. *Dig Liver Dis* 2017; **49**: 467-470 [PMID: 28258929 DOI: 10.1016/j.dld.2017.01.166]
10 **Kim SH**, Park YN, Lim JH, Choi GH, Choi JS, Kim KS. Characteristics of combined hepatocelluar-cholangiocarcinoma and comparison with intrahepatic cholangiocarcinoma. *Eur J Surg Oncol* 2014; **40**: 976-981 [PMID: 24909336 DOI: 10.1016/j.ejso.2014.04.016]
11 **Stavraka C**, Rush H, Ross P. Combined hepatocellular cholangiocarcinoma (cHCC-CC): an update of genetics, molecular biology, and therapeutic interventions. *J Hepatocell Carcinoma* 2019; **6**: 11-21 [PMID: 30643759 DOI: 10.2147/JHC.S159805]
12 **Fowler KJ**, Burgoyne A, Fraum TJ, Hosseini M, Ichikawa S, Kim S, Kitao A, Lee JM, Paradis V, Taouli B, Theise ND, Vilgrain V, Wang J, Sirlin CB, Chernyak V. Pathologic, Molecular, and Prognostic Radiologic Features of Hepatocellular Carcinoma. *Radiographics* 2021; **41**: 1611-1631 [PMID: 34597222 DOI: 10.1148/rg.2021210009]

13 **Kono Y**, Lyshchik A, Cosgrove D, Dietrich CF, Jang HJ, Kim TK, Piscaglia F, Willmann JK, Wilson SR, Santillan C, Kambadakone A, Mitchell D, Vezeridis A, Sirlin CB. Contrast Enhanced Ultrasound (CEUS) Liver Imaging Reporting and Data System (LI-RADS®): the official version by the American College of Radiology (ACR). *Ultraschall Med* 2017; **38**: 85-86 [PMID: 28249328 DOI: 10.1055/s-0042-124369]

14 **Sugimoto K**, Kakegawa T, Takahashi H, Tomita Y, Abe M, Yoshimasu Y, Takeuchi H, Kasai Y, Itoi T. Usefulness of Modified CEUS LI-RADS for the Diagnosis of Hepatocellular Carcinoma Using Sonazoid. *Diagnostics (Basel)* 2020; **10** [PMID: 33076435 DOI: 10.3390/diagnostics10100828]

15 **Xu HX**, Chen LD, Liu LN, Zhang YF, Guo LH, Liu C. Contrast-enhanced ultrasound of intrahepatic cholangiocarcinoma: correlation with pathological examination. *Br J Radiol* 2012; **85**: 1029-1037 [PMID: 22374276 DOI: 10.1259/bjr/21653786]

16 **Li R**, Yuan MX, Ma KS, Li XW, Tang CL, Zhang XH, Guo DY, Yan XC. Detailed analysis of temporal features on contrast enhanced ultrasound may help differentiate intrahepatic cholangiocarcinoma from hepatocellular carcinoma in cirrhosis. *PLoS One* 2014; **9**: e98612 [PMID: 24874413 DOI: 10.1371/journal.pone.0098612]

17 **Choi SH**, Jeon SK, Lee SS, Lee JM, Hur BY, Kang HJ, Kim H, Park Y. Radio-pathologic correlation of biphenotypic primary liver cancer (combined hepatocellular cholangiocarcinoma): changes in the 2019 WHO classification and impact on LI-RADS classification at liver MRI. *Eur Radiol* 2021; **31**: 9479-9488 [PMID: 34037829 DOI: 10.1007/s00330-021-07984-w]

18 **Yang J**, Huang JY, Chen X, Ling WW, Luo Y, Shi YJ, Liu JB, Lu Q, Lyshchik A. Combined hepatocellular-cholangiocarcinoma: can we use contrast-enhanced ultrasound Liver Imaging Reporting and Data System (LI-RADS) to predict the patient's survival? *Eur Radiol* 2021; **31**: 6397-6405 [PMID: 33492470 DOI: 10.1007/s00330-020-07656-1]

19 **Jeon SK**, Joo I, Lee DH, Lee SM, Kang HJ, Lee KB, Lee JM. Combined hepatocellular cholangiocarcinoma: LI-RADS v2017 categorisation for differential diagnosis and prognostication on gadoxetic acid-enhanced MR imaging. *Eur Radiol* 2019; **29**: 373-382 [PMID: 29955948 DOI: 10.1007/s00330-018-5605-x]

20 **Zhang HC**, Zhu T, Hu RF, Wu L. Contrast-enhanced ultrasound imaging features and clinical characteristics of combined hepatocellular cholangiocarcinoma: comparison with hepatocellular carcinoma and cholangiocarcinoma. *Ultrasonography* 2020; **39**: 356-366 [PMID: 32407611 DOI: 10.14366/usg.19093]

21 **Zhou Y**, Li D, Long L, Ding JM, Wang FM, Wang YD, Zhou HY, Jing X. Analysis of enhancement patterns and combined diagnosis of combined hepatocellular-cholangiocarcinoma: CEUS, CECT/MRI and tumor markers. *Chin J Ultrasonogr* 2020; **29**: 754-760 [DOI: 10.3760/cma.j.cn131148-20200317-00196]

22 **Sagrini E**, Iavarone M, Stefanini F, Tovoli F, Vavassori S, Maggioni M, Renzulli M, Salvatore V, Stefanescu H, Colombo M, Bolondi L, Piscaglia F. Imaging of combined hepatocellular-cholangiocarcinoma in cirrhosis and risk of false diagnosis of hepatocellular carcinoma. *United European Gastroenterol J* 2019; **7**: 69-77 [PMID: 30788118 DOI: 10.1177/2050640618815378]

World Journal of Clinical Cases

Submit a Manuscript: https://www.f6publishing.com

World J Clin Cases 2022 April 16; 10(11): 3624-3629

DOI: 10.12998/wjcc.v10.i11.3624

ISSN 2307-8960 (online)

CASE REPORT

Thyrotoxicosis after a massive levothyroxine ingestion: A case report

Fang Du, Shi-Wei Liu, Hua Yang, Rui-Xue Duan, Wen-Xia Ren

Specialty type: Endocrinology and metabolism

Provenance and peer review: Unsolicited article; Externally peer reviewed.

Peer-review model: Single blind

Peer-review report's scientific quality classification
Grade A (Excellent): 0
Grade B (Very good): B
Grade C (Good): C
Grade D (Fair): 0
Grade E (Poor): 0

P-Reviewer: Kaur M, Notsu M

Received: December 30, 2021
Peer-review started: December 30, 2021
First decision: January 25, 2022
Revised: February 1, 2022
Accepted: February 23, 2022
Article in press: February 23, 2022
Published online: April 16, 2022

Fang Du, Department of Endocrinology, Taiyuan Central Hospital of Shanxi Medical University, Taiyuan 030009, Shanxi Province, China

Fang Du, Department of Endocrinology and Metabolism, West China Hospital, Sichuan University, Chengdu 610041, Sichuan Province, China

Shi-Wei Liu, Hua Yang, Rui-Xue Duan, Wen-Xia Ren, Department of Endocrinology, Shanxi Bethune Hospital, Shanxi Academy of Medical Sciences, Taiyuan 030032, Shanxi Province, China

Corresponding author: Shi-Wei Liu, MD, Professor, Chief, Department of Endocrinology, Shanxi Bethune Hospital, Shanxi Academy of Medical Sciences, No. 99 Longcheng Street, Xiaodian District, Taiyuan 030032, Shanxi Province, China. lswspring6@aliyun.com

Abstract

BACKGROUND

The literature on thyrotoxicosis caused by excessive ingestion of exogenous thyroid hormone is limited, and most cases reported have involved pediatric clinical studies.

CASE SUMMARY

A 21-year-old woman initially presented with palpitation and chest tightness after an overdose of levothyroxine (10 mg). The patient transiently lost consciousness and developed atrial fibrillation during hospitalization. We used propylthiouracil to decrease the peripheral conversion of T4 to T3 and inhibit the synthesis of endogenous thyroxine, propranolol to control heart rate, hydrocortisone to correct severe thyrotoxicosis, and hemoperfusion to increase levothyroxine clearance. The patient recovered and was discharged.

CONCLUSION

For patients with thyrotoxicosis after taking excess levothyroxine, it is critical to monitor vital signs and initiate effective treatment.

Key Words: Levothyroxine; Overdose; Thyrotoxicosis; Thyroid crisis; Treatment; Case report

Core Tip: The literature on thyrotoxicosis caused by excessive ingestion of exogenous thyroid hormone is limited. We report a 21-year-old woman who presented with thyroid crisis after an overdose of levothyroxine. For patients with thyrotoxicosis or even thyroid storm after an overdose of levothyroxine, it is critical to monitor vital signs and symptoms and initiate effective treatment.

Citation: Du F, Liu SW, Yang H, Duan RX, Ren WX. Thyrotoxicosis after a massive levothyroxine ingestion: A case report. *World J Clin Cases* 2022; 10(11): 3624-3629
URL: https://www.wjgnet.com/2307-8960/full/v10/i11/3624.htm
DOI: https://dx.doi.org/10.12998/wjcc.v10.i11.3624

INTRODUCTION

Levothyroxine is a commonly used medication for hypothyroidism. Although many patients with hypothyroidism use levothyroxine as an alternative treatment, few cases of acute overdosage have been reported worldwide[1], and a large proportion of them have involved pediatric patients. Most reported levothyroxine intoxication symptoms have been mild[2,3], but severe manifestations including hyperthermia[3], vomiting[4], cardiac arrhythmias[5], seizures[6], coma[7], and thyroid storm[7,8] have been reported to occur after massive levothyroxine overdosage.

We report herein a case of a 21-year-old woman with a history of hypothyroidism and depression who took 200 tablets of levothyroxine, more than 10 tablets of clonazepam, and 20 tablets of zolpidem after mental stimulation. She ultimately developed symptoms of thyrotoxicosis, such as arrhythmia, dyspnea, dizziness, and coma.

CASE PRESENTATION

Chief complaints

A 21-year-old woman was admitted to the emergency department with palpitations and chest tightness.

History of present illness

Fifteen hours earlier, the patient had ingested 200 levothyroxine tablets (10 mg), more than 10 clonazepam tablets (20 mg), and 20 zolpidem tablets (200 mg), after mental stimulation.

History of past illness

The patient's parents reported that she had been diagnosed with hypothyroidism due to fatigue 3 years ago and was being treated with levothyroxine (12.5-25.0 μg/d) without thyroid function monitoring. In addition, she was diagnosed with depression 2 years previously and was taking clonazepam and zolpidem for intermittent treatment.

Personal and family history

Her family history included maternal hypothyroidism.

Physical examination

On admission, the patient was conscious, presenting with palpitations, dyspnea, dizziness, fatigue, and sweating but with no nausea, vomiting, abdominal pain, nor diarrhea. Her vital signs were a temperature of 37.3 ºC, heart rate of 103 beats/min, blood pressure of 100/73 mmHg, respiratory rate of 27 breaths/min, and oxygen saturation of 95% while breathing room air. The thyroid gland was I degree swollen, tough, and without tenderness.

Laboratory examinations

The patient's thyroxine (T4) level was > 320 nmol/L, free thyroxine (FT4) level was > 100 pmol/L, triiodothyronine (T3) level was 6.27 nmol/L, free triiodothyronine (FT3) level was 27.96 pmol/L, thyroid stimulating hormone (TSH) level was < 0.01 mIU/mL, thyroglobulin antibody (TGAb) level was 583.4 IU/mL, thyroid peroxidase antibody (TPOAb) level was 30.8 IU/mL, and thyrotropin receptor antibody (TRAb) level was < 0.3 IU/L (Table 1). Chemistries were within normal limits, except for an alanine aminotransferase level of 74.3 U/L (normal range: 7-40 U/L).

Imaging examinations

There was no imaging examination.

Table 1 Laboratory results after levothyroxine ingestion

Result	Day 1	Day 2	Day 4	Day 8	Day 14	Reference range
FT3 (pmol/L)	27.96	17.5	10	6.18	3.41	3.11-8.53
FT4 (pmol/L)	> 100	> 100	53.29	34.02	16.35	9.11-25.70
T3 (nmol/L)	6.27	3.46	4.84	–	–	1.3-3.1
T4 (nmol/L)	> 320	> 320	236.58	–	–	66-181
TSH (mIU/mL)	< 0.01	< 0.01	< 0.01	< 0.01	< 0.01	0.3-5.0
TGAb (IU/mL)	583.4	–	–	–	–	< 115
TPOAb (IU/mL)	30.8	–	–	–	–	< 34
TRAb (IU/L)	< 0.3	–	–	–	–	< 1.75

FT3: Free triiodothyronine; FT4: Free thyroxine; T3: Triiodothyronine; T4: Thyroxine; TSH: Thyroid stimulating hormone; TGAb: Thyroglobulin antibody; TPOAb: Thyroid peroxidase antibody; TRAb: Thyrotropin receptor antibody.

FINAL DIAGNOSIS

Thyrotoxicosis caused by excessive intake of levothyroxine.

TREATMENT

After fluid rehydration, supplemental oxygen, and emergency hemoperfusion, the patient was transferred to our department. Continuous cardiorespiratory monitoring was begun, propylthiouracil (150 mg 3 times per day) was given to reduce the conversion of T4 to T3 and inhibit the synthesis of endogenous thyroxine, propranolol (20 mg every 6 h) to control the heart rate, and intermittent hemoperfusion to increase levothyroxine clearance. Treatment was supplemented with liver protection, adequate energy intake, and other support measures.

On day 3 after admission, the patient lost consciousness without inducement, along with excessive sweating, and without nausea, vomiting, or gatism. Her pupils were sensitive to light, the body temperature was 37.1 ºC, the electrocardiogram showed sinus tachycardia, heart rate fluctuations of 120-150 beats/min, blood pressure fluctuations from 90-110/76-94 mmHg, and an oxygen saturation of 94%-96% with a nasal catheter flow of 2 L/min and 40-50 breaths/min. Considering that the patient was in thyroid crisis, intravenous hydrocortisone 100 mg was given and an emergency hemoperfusion was performed. The patient regained consciousness 1 h later.

On day 7 after admission, the patient developed atrial fibrillation, with a heart rate of 100-110 beats/min after emotional agitation; after about 1 h, the patient spontaneously shifted to sinus rhythm. The patient continued to improve and was discharged on day 15.

OUTCOME AND FOLLOW-UP

The patient had no discomfort after discharge, and thyroid function gradually returned to normal.

DISCUSSION

Thyrotoxicosis involves an excess of circulating thyroid hormone that has a number of causes and eventually leads to sympathetic nerve excitation and hypermetabolic syndrome. The symptoms are diverse and include fever, irritability, tachycardia, diarrhea, and seizures. The most common causes of thyrotoxicosis are Graves' disease, toxic multinodular goiter, and thyroiditis. An excess dose of exogenous thyroid hormones can also lead to thyrotoxicosis, but the published literature on levothyroxine intoxication is limited and most of the described cases are pediatric clinical reports. Cases of adults ingesting overdose levothyroxine are extremely rare, and adults who ingest massive doses of levothyroxine nearly always have mental disorders and other relevant medical histories[2]. Our case occurred in a woman who presented with severe symptoms of thyrotoxicosis after taking a massive levothyroxine dose. As she took the medication after mental stimulation, it may have been related to her history of depression.

Our patient developed clinical symptoms 15 h after an overdose of levothyroxine, improved with treatment, and was discharged 15 d after admission. Golightly *et al*[9] studied levothyroxine ingestion in 41 children who accidentally ingested levothyroxine sodium. The patients were managed by a standard protocol based on the reported amount of ingested levothyroxine, which ranged from 0.05-13 mg. The onset of symptoms ranged from 12 h to 11 d, and all symptoms resolved by 14 d after ingestion. Levothyroxine is a synthetic T4 preparation that needs to be converted to T3 *in vivo* to exert its effects, and has a long half-life of approximately 7 d. Therefore, the symptoms of levothyroxine overdose may be delayed and may last for several days.

Thyroid storm, also known as thyroid crisis, is a serious clinical manifestation of thyrotoxicosis and is characterized by high fever, sweating, tachycardia, arrhythmia, loss of consciousness, and other symptoms that may be life threatening. Prompt diagnosis and active treatment are essential. The Burch and Wartofsky scoring system[10], based on abnormalities of thermoregulation and the central nervous system, gastrointestinal, and cardiovascular systems can be used to help determine whether a patient is experiencing a thyroid storm. This patient had a total score of 55 points, 30 for disturbance of consciousness and 25 for tachycardia, which met the diagnostic criteria for thyroid storm. Thyroid storm can occur a few days after an overdose of levothyroxine. In the cases reported by Wong *et al*[7] and Schottstaedt and Smoller[11], the thyroid storm occurred 3 d after ingestion. The delayed occurrence of the thyroid storm can be attributed to the onset of levothyroxine action, which occurs 3–5 d after oral administration.

Alternative treatments of levothyroxine overdose

Conservative monitoring: This is recommended if the patient is asymptomatic or only mildly symptomatic.

Gastrointestinal decontamination: There are no standard criteria for when to perform gastrointestinal decontamination. Ritowitz and White[12] studied 78 children who were all about 12 years of age and had accidentally ingested levothyroxine. They recommended that children with ingestion of ≤ 0.5 mg should not be treated by gastrointestinal purification, those ingesting 0.5–3.0 mg can be treated by ipecac-induced emesis at home, and those ingesting > 3.0 mg should be treated by ipecac-induced emesis followed by activated charcoal. Tunget *et al*[13] recommend that children who ingest > 5.0 mg of levothyroxine be given activated charcoal, as it can reduce systemic absorption if given within 1 h of the levothyroxine. Bouchard[14] recommended that adults with a levothyroxine intake of > 5.0 mg be given activated charcoal. There is a limited role for gastric lavage in this setting, except very soon after a massive overdose (*e.g.*, > 10 mg).

Symptomatic treatment: Pay close attention to the patient's vital signs and symptoms, and deal with them promptly. Beta-blockers are recommended for symptomatic treatment of patients with sympathetic overexcitation, such as tachycardia, and propranolol is the first choice. In addition to cardiac benefits, propranolol also reduces the conversion of FT4 to FT3 in peripheral blood. Our patient had palpitations and a heart rate of more than 100 beats/min, so propranolol was given to control the heart rate. Physical cooling and acetaminophen are recommended for patients with fever. Benzodiazepines can be considered if the patient is severely agitated and irritable[14], and antiepileptic drugs, such as phenobarbital, may be considered for patients with seizures[2].

Decrease peripheral conversion of T4 to T3: Propylthiouracil can reduce the peripheral conversion of T4 to T3 and inhibit the synthesis of endogenous thyroxine. Dexamethasone[15], prednisone[16], and hydrocortisone[17] can be useful in severe thyrotoxicosis because they also reduce T4 to T3 conversion. Kirstie *et al*[1] recommend the use of corticosteroids in patients with an overdose of levothyroxine (> 10.0 mg), especially when the initial FT4 Level is above the upper limit, or in any patient with associated adrenal insufficiency. In our case, we used propylthiouracil upon admission and we also used hydrocortisone when the patient developed a coma. If necessary, sodium ipodate can also be used because it inhibits type I iodothyronine 5′-monodeiodinase, which catalyzes the T4 to T3 conversion[3].

Increase thyroid hormone clearance: It has been reported that hemoperfusion[17,18] and plasmapheresis[17] remove levothyroxine from serum and can be used to treat acute and severe thyrotoxicosis. Our patient had taken a high dose of thyroxine and thyroid storm was considered, so hemoperfusion was used. Levothyroxine has a high rate of binding to specific transporters of about 99.97%, and plasmapheresis seems to be more effective than hemoperfusion for the clearance of T4. In addition, patients can be given cholestyramine, which reduces thyroid hormone levels by decreasing levothyroxine enterohepatic recycling and enhancing elimination[19].

CONCLUSION

Although most patients with levothyroxine overdose are asymptomatic or have only mild symptoms, severe cases and delayed symptoms have also been reported. Levothyroxine overdose can usually be

diagnosed by the patient's history and examination results. Treatment of a thyroxine overdose should be based on the levothyroxine dose and the patient's clinical symptoms and signs.

ACKNOWLEDGEMENTS

We are grateful to the patient for allowing publication of this case report.

FOOTNOTES

Author contributions: Du F managed the patient and drafted the manuscript; Liu SW supervised the manuscript writing; Yang H and Ren WX developed the treatment strategies for the patient; Duan RX was responsible for the care of the patient; All authors read and approved the final manuscript.

Informed consent statement: The patient agreed to the related test, and simultaneously signed a written informed consent form for publication of her case details.

Conflict-of-interest statement: The authors declare that they have no conflicting interests.

CARE Checklist (2016) statement: The authors have read the CARE Checklist (2016), and the manuscript was prepared and revised according to the CARE Checklist (2016).

Country/Territory of origin: China

ORCID number: Fang Du 0000-0001-8941-6747; Shi-Wei Liu 0000-0002-7816-3091; Hua Yang 0000-0002-8766-9705; Rui-Xue Duan 0000-0001-6896-252X; Wen-Xia Ren 0000-0003-2866-8865.

S-Editor: Gong ZM
L-Editor: A
P-Editor: Gong ZM

REFERENCES

1 **Allen KM**, Crawford VB, Conaglen JV, Elston MS. Case report: clues to the diagnosis of an unsuspected massive levothyroxine overdose. *CJEM* 2015; **17**: 692-698 [PMID: 25824846 DOI: 10.1017/cem.2014.75]
2 **Xue J**, Zhang L, Qin Z, Li R, Wang Y, Zhu K, Li X, Gao X, Zhang J. No obvious sympathetic excitation after massive levothyroxine overdose: A case report. *Medicine (Baltimore)* 2018; **97**: e10909 [PMID: 29879029 DOI: 10.1097/MD.0000000000010909]
3 **Ioos V**, Das V, Maury E, Baudel JL, Guéchot J, Guidet B, Offenstadt G. A thyrotoxicosis outbreak due to dietary pills in Paris. *Ther Clin Risk Manag* 2008; **4**: 1375-1379 [PMID: 19337445 DOI: 10.2147/tcrm.s4110]
4 **Hays HL**, Jolliff HA, Casavant MJ. Thyrotoxicosis after a massive levothyroxine ingestion in a 3-year-old patient. *Pediatr Emerg Care* 2013; **29**: 1217-1219 [PMID: 24196094 DOI: 10.1097/PEC.0b013e3182aa4714]
5 **Kumar SH**, Ramesh H. Cavitary pulmonary tuberculosis mimicking congenital cystic adenomatoid malformation in an infant. *Indian Pediatr* 2014; **51**: 840 [PMID: 25362024 DOI: 10.1007/s12098-014-1462-z]
6 **Tsutaoka BT**, Kim S, Santucci S. Seizure in a child after an acute ingestion of levothyroxine. *Pediatr Emerg Care* 2005; **21**: 857-859 [PMID: 16340765 DOI: 10.1097/01.pec.0000190240.81222.9a]
7 **Wong O**, Wong A, Greene S, Graudins A. Prolonged coma resulting from massive levothyroxine overdose and the utility of N-terminal prohormone brain natriuretic peptide (NT-proBNP). *Clin Toxicol (Phila)* 2019; **57**: 415-417 [PMID: 30484711 DOI: 10.1080/15563650.2018.1533639]
8 **Majlesi N**, Greller HA, McGuigan MA, Caraccio T, Su MK, Chan GM. Thyroid storm after pediatric levothyroxine ingestion. *Pediatrics* 2010; **126**: e470-e473 [PMID: 20643722 DOI: 10.1542/peds.2009-2138]
9 **Golightly LK**, Smolinske SC, Kulig KW, Wruk KM, Gelman CJ, Rumack BH, Linden CH. Clinical effects of accidental levothyroxine ingestion in children. *Am J Dis Child* 1987; **141**: 1025-1027 [PMID: 2887106 DOI: 10.1001/archpedi.1987.04460090102039]
10 **Burch HB**, Wartofsky L. Life-threatening thyrotoxicosis. Thyroid storm. *Endocrinol Metab Clin North Am* 1993; **22**: 263-277 [PMID: 8325286]
11 **Schottstaedt ES**, Smoller M. "Thyroid storm" produced by acute thyroid hormone poisoning. *Ann Intern Med* 1966; **64**: 847-849 [PMID: 23841204 DOI: 10.7326/0003-4819-64-4-847]

12 **Litovitz TL**, White JD. Levothyroxine ingestions in children: an analysis of 78 cases. *Am J Emerg Med* 1985; **3**: 297-300 [PMID: 2860910 DOI: 10.1016/0735-6757(85)90050-6]

13 **Tunget CL**, Clark RF, Turchen SG, Manoguerra AS. Raising the decontamination level for thyroid hormone ingestions. *Am J Emerg Med* 1995; **13**: 9-13 [PMID: 7832964 DOI: 10.1016/0735-6757(95)90231-7]

14 **Bouchard NC**. Thyroid and Antithyroid Medications. In: Nelson L, Lewin NA, Howland M, Hoffman RS, Goldfrank LR, Flomenbaum NE (eds.), Goldfrank's Toxicological Emergencies, 9th ed. New York: McGraw-Hill; 2011

15 **Shilo L**, Kovatz S, Hadari R, Weiss E, Nabriski D, Shenkman L. Massive thyroid hormone overdose: kinetics, clinical manifestations and management. *Isr Med Assoc J* 2002; **4**: 298-299 [PMID: 12001709]

16 **Lehrner LM**, Weir MR. Acute ingestions of thyroid hormones. *Pediatrics* 1984; **73**: 313-317 [PMID: 6701055]

17 **Binimelis J**, Bassas L, Marruecos L, Rodriguez J, Domingo ML, Madoz P, Armengol S, Mangues MA, de Leiva A. Massive thyroxine intoxication: evaluation of plasma extraction. *Intensive Care Med* 1987; **13**: 33-38 [PMID: 3558934 DOI: 10.1007/BF00263555]

18 **Kreisner E**, Lutzky M, Gross JL. Charcoal hemoperfusion in the treatment of levothyroxine intoxication. *Thyroid* 2010; **20**: 209-212 [PMID: 20151829 DOI: 10.1089/thy.2009.0054]

19 **de Luis DA**, Dueñas A, Martin J, Abad L, Cuellar L, Aller R. Light symptoms following a high-dose intentional L-thyroxine ingestion treated with cholestyramine. *Horm Res* 2002; **57**: 61-63 [PMID: 12006723 DOI: 10.1159/000057950]

World Journal of Clinical Cases

Submit a Manuscript: https://www.f6publishing.com

World J Clin Cases 2022 April 16; 10(11): 3630-3638

DOI: 10.12998/wjcc.v10.i11.3630

ISSN 2307-8960 (online)

CASE REPORT

Pleomorphic adenoma of the left lacrimal gland recurred and transformed into myoepithelial carcinoma after multiple operations: A case report

Wen-Peng Huang, Li-Ming Li, Jian-Bo Gao

Specialty type: Medicine, research and experimental

Provenance and peer review: Unsolicited article; Externally peer reviewed.

Peer-review model: Single blind

Peer-review report's scientific quality classification

Grade A (Excellent): 0
Grade B (Very good): 0
Grade C (Good): C, C
Grade D (Fair): 0
Grade E (Poor): 0

P-Reviewer: Ding J, China; Mohey NM, Egypt

Received: December 14, 2021
Peer-review started: December 14, 2021
First decision: January 25, 2022
Revised: February 2, 2022
Accepted: February 27, 2022
Article in press: February 27, 2022
Published online: April 16, 2022

Wen-Peng Huang, Li-Ming Li, Jian-Bo Gao, Department of Radiology, The First Affiliated Hospital of Zhengzhou University, Zhengzhou 450052, Henan Province, China

Corresponding author: Jian-Bo Gao, PhD, Academic Research, Chairman, Chief Doctor, Instructor, Department of Radiology, The First Affiliated Hospital of Zhengzhou University, No. 1 East Jianshe Road, Zhengzhou 450052, Henan Province, China.
jianbogaochina@163.com

Abstract

BACKGROUND

Myoepithelial carcinoma (MC) is a clinically rare malignancy, there is controversy regarding its etiology and its biological behavior is not fully elucidated. Extensive surgical resection is the main treatment method. We describe a case of pleomorphic adenoma (PA) with multiple postoperative recurrences after malignant transformation, and the history of the disease in this patient was more than 20 years. Complete resection during the first surgery of PA and long-term postoperative follow-up is necessary.

CASE SUMMARY

A 34-year-old male with PA and a history of 5 postoperative recurrences over 21 years, each surgically removed, presented 15 d ago with headache, nasal congestion, protrusion of the right eyeball and loss of vision in the right eye, with progressively worsening symptoms. The patient underwent surgery, and MC was confirmed by pathology examination. A small PA component was locally visible under light microscope. The patient had a recurrence of the tumor 2 mo after surgery and underwent surgical resection.

CONCLUSION

During the first operation for PA, care should be taken not to rupture the envelope to prevent tumor cell implantation, and when complete resection is not possible due to the anatomical site, postoperative radiotherapy is necessary to control the lesion and prevent infiltration and malignant transformation of the tumor to MC. Computed tomography and magnetic resonance imaging is important for establishing diagnosis and developing a treatment plan.

Key Words: Myoepithelial carcinoma; Pleomorphic adenoma; Magnetic resonance

imaging; Treatment; X-ray computed tomography; Case report

Core Tip: This case illustrates that pleomorphic adenoma should be completely removed during the first operation to prevent capsule rupture and tumor cell implantation. When complete resection is not possible due to the anatomical site, postoperative radiotherapy should be performed to control the lesion and prevent infiltration and malignant transformation to myoepithelial carcinoma. Postoperative follow-up, especially long-term follow-up for recurrent cases, is necessary and systemic examination should be undertaken to prevent distant metastasis.

Citation: Huang WP, Li LM, Gao JB. Pleomorphic adenoma of the left lacrimal gland recurred and transformed into myoepithelial carcinoma after multiple operations: A case report. *World J Clin Cases* 2022; 10(11): 3630-3638

URL: https://www.wjgnet.com/2307-8960/full/v10/i11/3630.htm

DOI: https://dx.doi.org/10.12998/wjcc.v10.i11.3630

INTRODUCTION

Myoepithelial carcinoma (MC) is a rare malignant tumor with a low incidence[1]. The mechanism of myoepithelial carcinogenesis is still controversial and the biological behavior is not yet fully elucidated. Some scholars believe that the tumor may occur independently, while some believe that the tumor is a malignant transformation from pleomorphic adenoma (PA) or benign myoepithelial tumor[2]. Here, we present a rare case of PA which recurred many times after surgery and finally transformed into MC.

CASE PRESENTATION

Chief complaints

A 34-year-old male patient presented to our hospital 15 d ago with headache, nasal congestion, protrusion of the right eyeball and loss of vision in the right eye, with progressively worsening symptoms.

History of present illness

The patient had undergone resection of a left lacrimal gland tumor 21 years ago, and postoperative pathology showed PA. The tumor recurred at 19 years, 12 years, 9 years, and 2 years, respectively, and was surgically removed. He came to our hospital for medical treatment. He had normal spirit, appetite, sleep, defecation and urination, and no weight loss.

History of past illness

The patient had no previous history of hypertension or heart disease, no history of diabetes mellitus or cerebrovascular allergy, no history of infectious diseases or drug allergy.

Personal and family history

The patient had no family history of hereditary diseases.

Physical examination

On admission, he had old surgical incisions on the left frontotemporal and periorbital areas, partial depression of the surface, muscle atrophy, protrusion of the right eye, and normal movement of the right eye in multiple directions.

Laboratory examinations

Laboratory test results showed that the white blood cell count was 13.11 × 10^9/L (normal range, 3.50–9.50 × 10^9/L), lymphocyte count was 0.80 × 10^9/L (normal range, 1.10–3.20 × 10^9/L), red blood cell count was 2.67 × 10^{12}/L (normal values range, 4.30–5.80 × 10^{12}/L), neutrophil count was 11.84 × 10^9/L (normal range, 1.80–6.30 × 10^9/L), and hemoglobin was 82.1 g/L (normal range, 130–175 g/L).

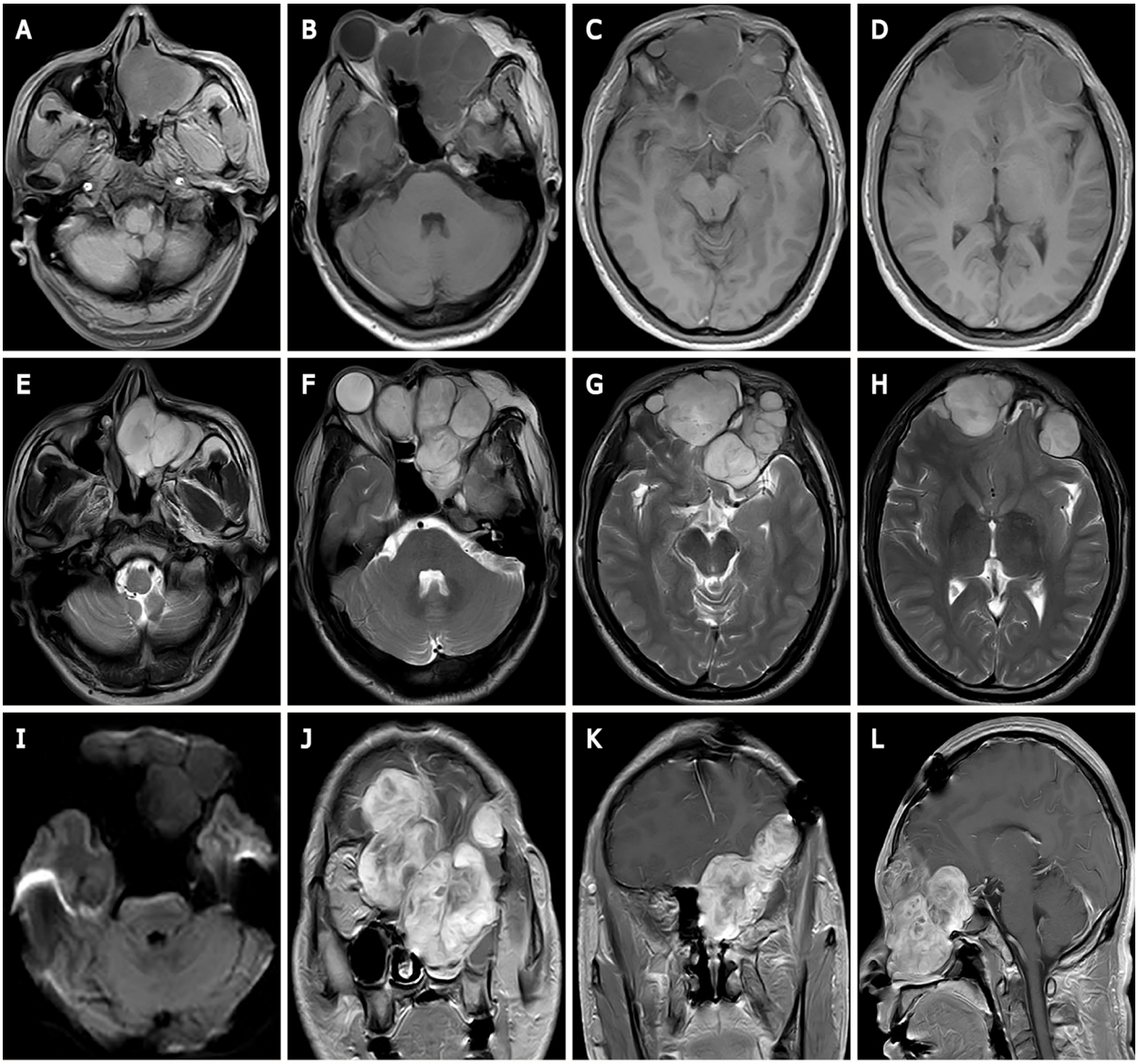

DOI: 10.12998/wjcc.v10.i11.3630

Figure 1 The first preoperative Magnetic resonance imaging findings. A-I: Magnetic resonance imaging shows multiple masses with T1 weighted imaging (WI) inhomogeneous low signals (A-D) and T2WI inhomogeneous high signals (E-H) in the bilateral frontal, bilateral septal sinuses, bilateral frontal sinuses, left orbit, left nasal cavity, left pterygoid sinus and left maxillary sinus, the lesion showed equal or slightly lower signals on diffusion WI with poorly defined borders (I); J-L: Bilateral frontal lobe and right orbital compression resulted in a localized left shift of the frontal midline, and right shift of the nasal cavity. After enhancement, the lesion showed significant heterogeneous progressive enhancement.

Imaging examinations

Ultrasound showed multiple solid hypoechoic masses with poorly defined borders and uneven internal echogenicity in the bilateral orbits, and dotted line blood flow signals were detected on color Doppler flow imaging. Computed tomography (CT) revealed multiple round-like soft tissue masses in the left maxillary sinus, pterygoid sinus, bilateral septal sinuses, nasal tract and bilateral intraorbital, frontal sinus, and bilateral frontal lobes, with swelling, resorption destruction and compression displacement of the surrounding adjacent bones, and anterior convexity of the right eyeball with compression, with no obvious invasion of the right optic nerve. Magnetic resonance imaging (MRI) displayed multiple masses with inhomogeneous low signals on T1 weighted imaging (T1WI) and inhomogeneous high signals on T2WI in the bilateral frontal, bilateral septal sinuses, bilateral frontal sinuses, left orbit, left nasal cavity, left pterygoid sinus and left maxillary sinus, the lesion showed an equal or slightly lower signal on diffusion WI (DWI) with poorly defined borders. Bilateral frontal lobe and right orbital compression resulted in a localized left shift of the frontal midline, and right shift of the nasal cavity. After enhancement, the lesion showed significant heterogeneous progressive enhancement (Figure 1) of approximately 7.3 cm × 7.8 cm × 8.4 cm (AP × LR × SI). Bilateral frontal dura mater was visible as linear enhancement.

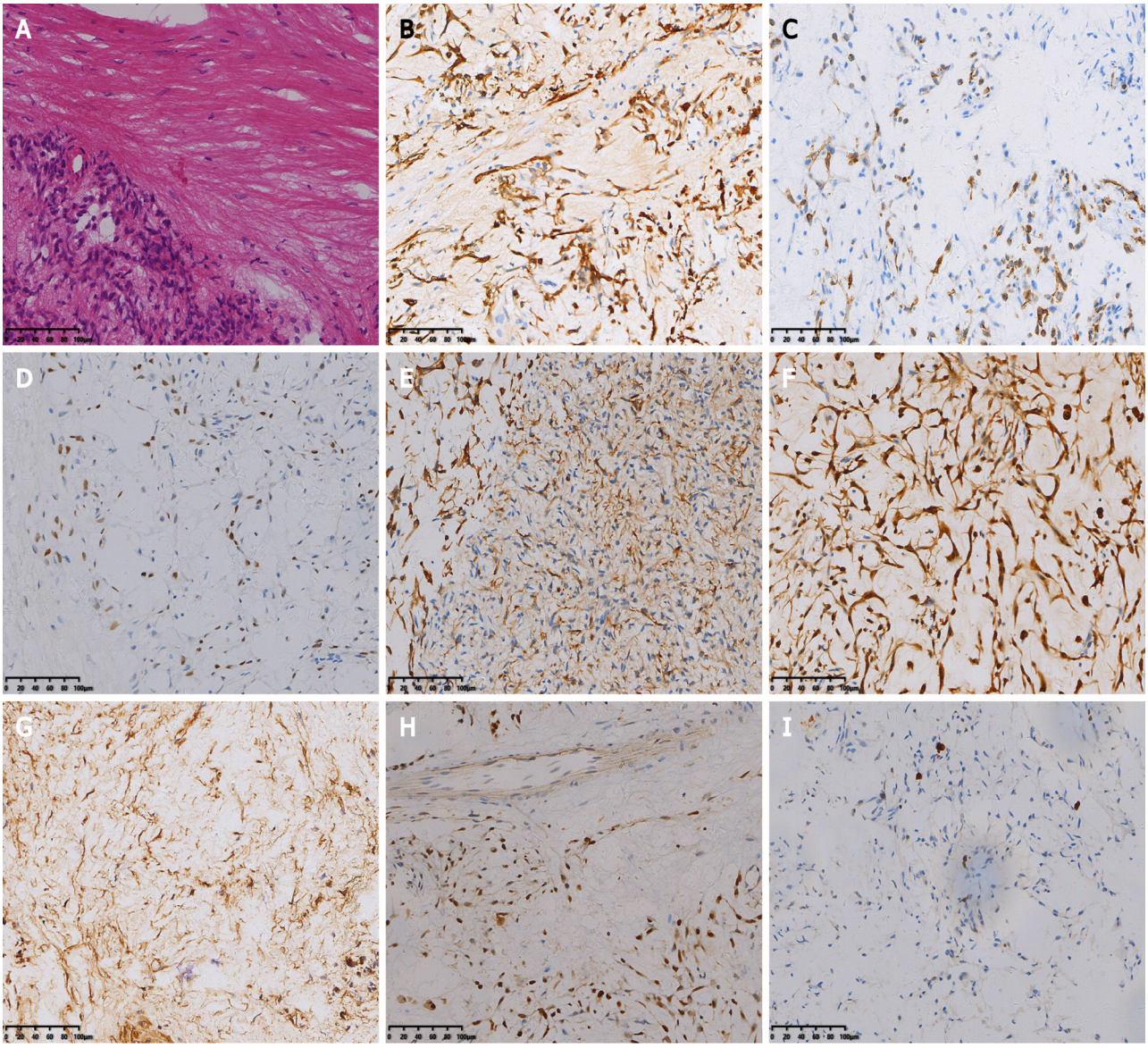

DOI: 10.12998/wjcc.v10.i11.3630

Figure 2 The first postoperative immunohistochemistry results. A: Hematoxylin-eosin staining shows spindle-shaped tumor cells, mucinous mesenchyme and foci of necrosis, with nuclear schizophrenia and marked nuclear anisotropy, and a small localized pleomorphic adenomatous component in the tumor (magnification × 200); B-I: Immunohistochemistry showed that the tumor cells were positive for CK (B), CK7 (C), P63 (D), Calponin (E), S-100 (F), SMA (G), SOX-10 (H) and 5% of cells were positive for Ki-67 (I) [Envision (B-I) × 200].

FINAL DIAGNOSIS

Postoperative pathology combined with morphology and immunohistochemistry findings were consistent with PA transformation to MC.

TREATMENT

The patient underwent the fifth surgical resection of the tumor. Intraoperatively, the tumor tissue was located outside the dura mater, grayish yellow and grayish red in color, with a hard texture and rich blood supply, and the tumor had an envelope, which was lobulated and locally invaded the dura mater. A small amount of cerebrospinal fluid leaked out during resection of the tumor and its envelope. The fifth postoperative pathology showed spindle-shaped tumor cells, mucinous mesenchyme and foci of necrosis, with nuclear schizophrenia and marked nuclear anisotropy, and a small localized pleomorphic adenomatous component of the tumor (Figure 2). Immunohistochemistry findings were as follows: CK (+), EMA (-), S-100 (+), SSTR-2 (-), Ki-67 (5%+), CD34 (-), CD68 (-), SMA (+), SOX -10 (+), P63 (+), Calponin (+), and CK7 (+).

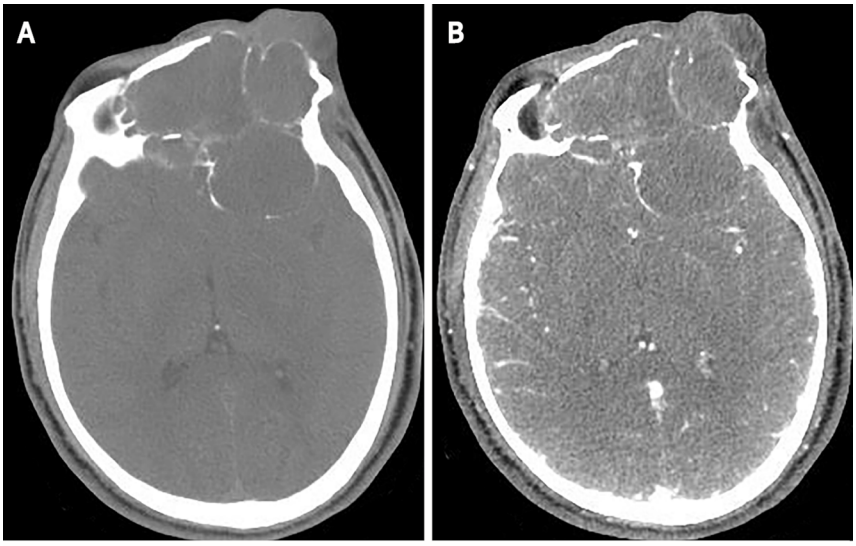

DOI: 10.12998/wjcc.v10.i11.3630

Figure 3 The second preoperative computed tomography findings. A: Computed tomography (CT) scan shows large lamellar soft tissue density masses in the left orbit, bilateral frontal areas, bilateral septal sinuses, pterygoid sinuses, left maxillary sinus, and anterior skull base, with CT attenuation of approximately 22 Hounsfield units (HU), peripheral multiple osteolytic destruction of bone; B: Arterial phase shows moderate enhancement of the lesion, with CT attenuation of approximately 58 HU.

After surgery, the patient was given symptomatic supportive treatment such as anti-infection, dehydration, and pain relief. The patient did not receive adjuvant therapy.

OUTCOME AND FOLLOW-UP

Two months later the patient developed dizziness. Combined head and neck CT angiography showed posterior displacement of the left internal carotid artery due to compression, slightly dilated lumen of the cavernous sinus segment, slender right vertebral artery, bilateral internal carotid arteries with calcium shifts and mixed plaque shadow, and moderate lumen narrowing. A large lamellar soft tissue density shadow was seen in the left orbit, bilateral frontal areas, bilateral septal sinuses, pterygoid sinus, left maxillary sinus, and anterior skull base, with CT attenuation of about 37 Hounsfield units (HU) and multiple surrounding osteolytic destruction of bone, and CT attenuation of about 58 HU in the arterial phase (Figure 3). The patient underwent MRI, which showed multiple abnormal signals in the left orbit, bilateral frontal areas, bilateral septal sinuses, pterygoid sinuses, left maxillary sinus, and anterior skull base with significant enhancement (Figure 4), and tumor recurrence was considered. The patient underwent the sixth surgical resection again, and intraoperatively, grayish-white tumor tissue was seen in the anterior skull base epidural with a general blood supply, eroding the bone of the bilateral supraorbital wall, brow arch and anterior skull base, and growing into the anterior skull base, sieve sinus and nasal cavity on both sides. The bone of the bilateral supraorbital wall was eroded by the tumor, and the bone was thin, with localized worm-like changes of bone hyperplasia and partial defects in the eroded bone. The tumor had an envelope, with relative boundaries to the surrounding tissues but abnormally tight adhesions, and separation-like changes were seen within the tumor. The tumor, part of the tumor envelope, and the bone of the anterior skull base and supraorbital wall eroded by the tumor were removed microscopically in pieces. The sixth postoperative pathology showed diffuse distribution of spindle-shaped tumor cells, and immunohistochemistry findings were as follows: CK (+), CK7 (+), P63 (+), Calponin (+), CK5/6 (+), SOX-10 (+), S-100 (+), SMA (-), Des (-), CD99 (±), ERG (-), Ki-67 (8%+), and SSTR -2 (+). A postoperative pathological diagnosis of MC recurrence was made (Figure 5). The patient is still being followed up.

DISCUSSION

PA is one of the most common salivary gland tumors, and is mostly located in the parotid gland, followed by the submandibular gland and sublingual gland, with easy recurrence after surgery, histologically it originates from epithelial cells with multidirectional differentiation potential and complex composition, containing mucus, adeno-duct-like structures and cartilage-like tissue, molecular characters such as TERT promoter mutation, high PD-L1 expression, and t(3;8) chromosomal

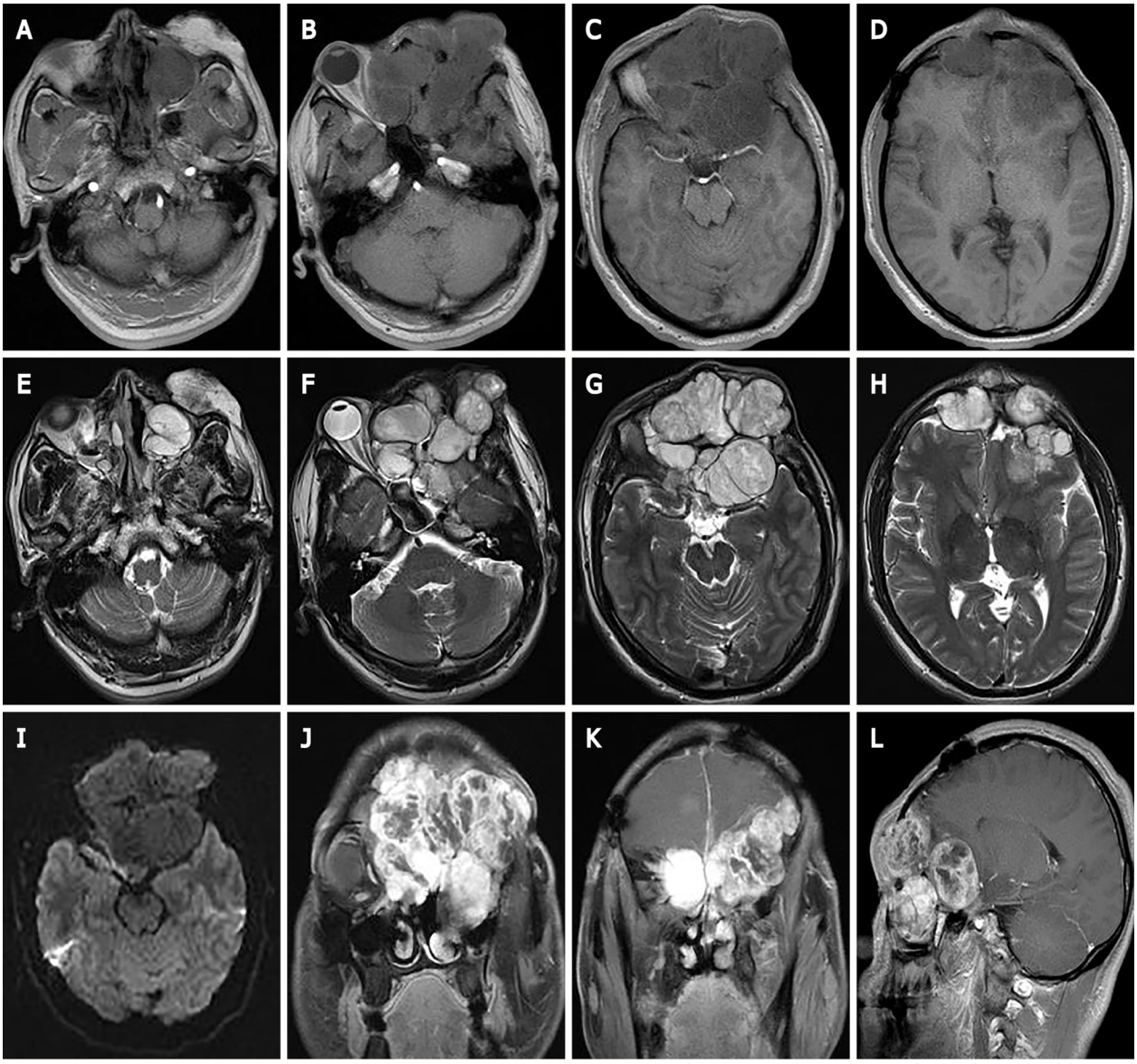

DOI: 10.12998/wjcc.v10.i11.3630

Figure 4 The second preoperative magnetic resonance imaging findings. A-H: Magnetic resonance imaging shows multiple masses of T1 weighted imaging (WI) low signals (A-D) and T2WI inhomogeneous high signals (E-H) in the left orbit, bilateral frontal areas, bilateral septal sinuses, pterygoid sinuses, left maxillary sinus, and anterior skull base; I: Slightly lower signals on diffusion WI, and lesion borders were not well defined; J-L: After enhancement, the lesion showed significant heterogeneous enhancement.

abnormality[3,4]. Because PA has a recurrent and infiltrative envelope, it is clinically classified as a junctional tumor, *i.e.*, a tumor that is intermediate between benign and malignant. The WHO has classified malignant PAs into three categories: (1) Carcinoma ex pleomorphic adenoma (CXPA), which refers to the presence of cancerous components in an existing PA, with high invasiveness and metastasis, the origin of which is still uncertain, and the cancerous components are diverse, mostly salivary gland ductal carcinoma, non-specific adenocarcinoma, a few are MC, epithelial-MC, undifferentiated carcinoma, and adenoid cystic carcinoma[5]; (2) Carcinosarcoma (CS), in which the epithelial component is often in the form of ductal carcinoma and the mesenchymal component is in the form of chondrosarcoma-like changes; and (3) Metastasizing pleomorphic adenoma, in which the risk of malignant transformation to CXPA is about 12% in patients who develop recurrence after surgical excision of PA[6]. In particular, if the mass is long-standing and appears to increase rapidly over a short period of time, the possibility of PA malignancy to CXPA should be highly suspected, and if the tumor infiltrates the nerves and surrounding tissues, it may be accompanied by facial palsy, skin infiltration, pain, and restricted mouth opening. The long course and rapid growth of the tumor are the important features in the present case. The patient had a typical clinical course of PA appearing malignant, and recurrence may have been due to incomplete surgical resection of tumor cells breaking through the envelope to infiltrate normal tissues, or to rupture of the tumor leading to implantation of tumor cells and recurrence. This patient has undergone five surgeries and has a disease history of more than 20

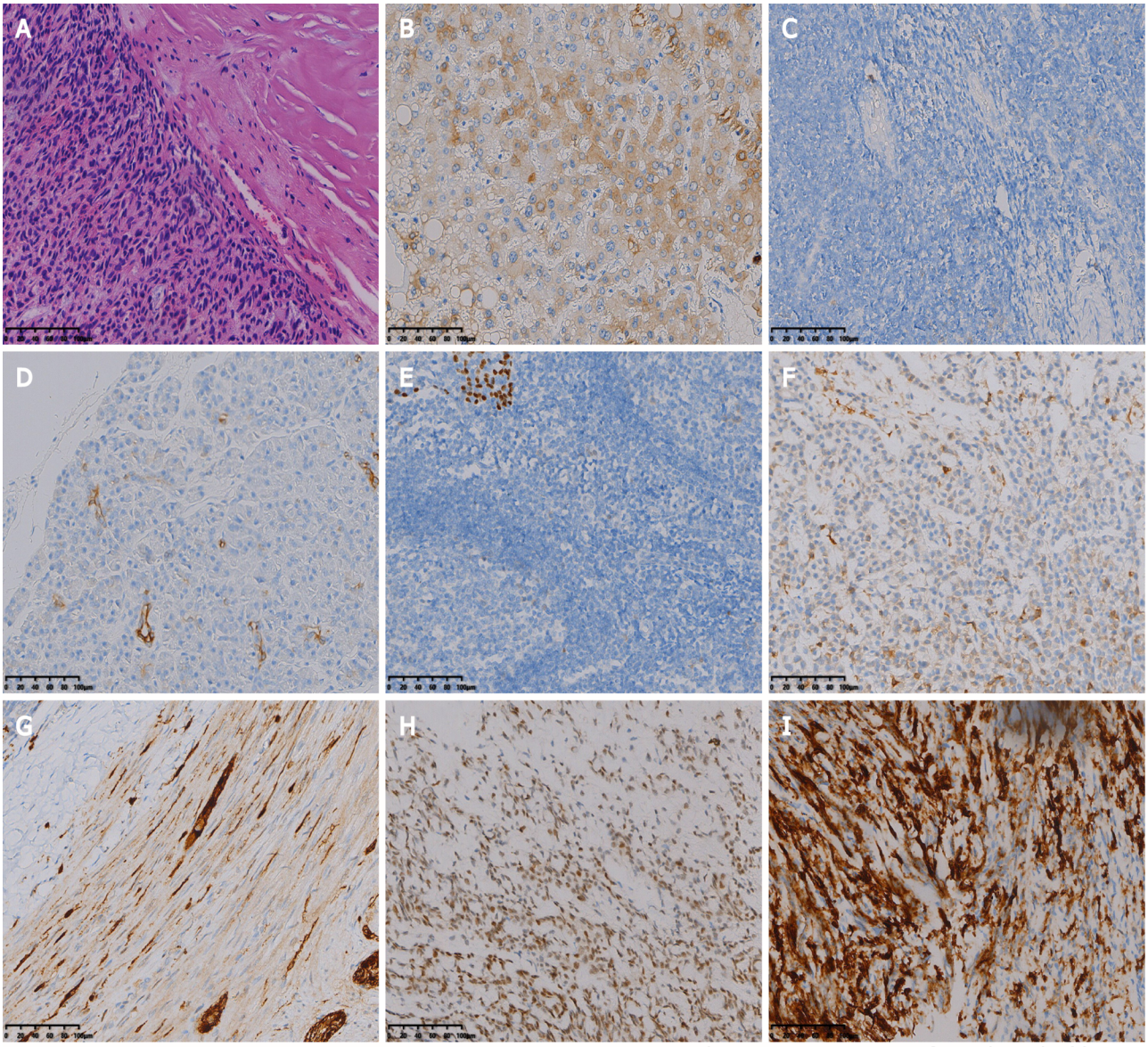

DOI: 10.12998/wjcc.v10.i11.3630

Figure 5 The second postoperative immunohistochemistry results. A: Hematoxylin-eosin staining shows diffuse distribution of spindle-shaped tumor cells (magnification × 200); B-I: Immunohistochemistry showed that the tumor cells were positive for CK (B), CK5/6 (C), CK7 (D), P63 (E), Calponin (F), S-100 (G), SOX-10 (H) and SSTR2 (I) [Envision (B-I) × 200].

years, with associated malignancy. Early symptoms are atypical due to the hidden anatomical location of the orbital region and clinicians should be particularly alert to this disease. Depending on the degree of infiltration of cancer cells into surrounding tissues, CXPA can be divided into three subtypes: Non-invasive, minimally invasive (invading surrounding tissues to a depth of ≤ 1.5 mm), and invasive (invading surrounding tissues to a depth of > 1.5 mm)[7]. In the present case, infiltration into the surrounding tissue was deep, and it was an invasive CXPA with tight adhesion to the surrounding tissue, and hemorrhagic necrosis and cystic changes were seen on the cut surface.

Preoperative confirmation of the diagnosis of CXPA relies on highly accurate fine needle aspiration cytopathology. However, the large size of this patient's tumor, the high number of malignant components, and the small proportion of residual PA components made the cytocentrifugal diagnosis very difficult. In this patient, the combination of mass morphology, immunohistochemical findings, and medical history was consistent with a PA carcinoma with a malignant type of MC.

In this case, the lesion was located in the eye, was large in size, had swelling and invasive growth, involved many complex structures, and had an incomplete envelope, which is now generally considered not to be a true tissue envelope, but a fibrous package formed by the reaction of the surrounding tissues caused by the tumor growth process. The density on CT was similar to that of the adjacent muscles, and the border was poorly defined, and CT clearly showed the details of the bone changes. Due to the thin structure of the orbital area tissue, this caused compression, resorption, and osteolytic destruction of the surrounding bone. MRI showed the relationship between internal tumor structures and adjacent

structures. In this case, the signal was heterogeneous on T1WI and T2WI, which was related to its diverse pathological composition. Some of the lesions showed equal or slightly lower signals on DWI, which was related to the sparseness of pathological structures and the amount of interstitial stroma, and some of the lesion centers showed more hypointense or obvious T1WI low signals and T2WI high signal cystic areas. Pathology mostly demonstrated a large number of proliferating tiny arteries and trophoblastic vessels, which showed marked enhancement, and the progressive enhancement pattern may have been related to the prolonged residence time of the contrast medium and slow contouring due to mucus and adenoid-like structures in CXPA. CT can show the location, size and density of the tumor, and is the preferred examination method for showing bony lesions. MRI has better resolution of soft tissues than CT, and can clearly show the histological features of the tumor and its relationship with surrounding tissues, and is currently considered the most valuable imaging method for diagnosing ocular lesions.

Current treatment is wide surgical excision to ensure adequate safety margins, with the surgical route and approach depending on the tumor site and size. Miccio *et al*[8] showed that adjuvant radiotherapy prolongs the survival of patients with grade III and IV MC. Polymorphic adenomas are prone to recurrence after surgery, and the cause of recurrence is related to the first inappropriate surgical approach. Avoidance of preoperative biopsy and intraoperative compression and clamping of the tumor, together with complete excision of the mass with the envelope may reduce the recurrence rate. When rupture of the tumor envelope occurs during surgery, tumor cells can easily spread into the adjacent tissues leading to recurrence. As the lymph node metastasis rate of this tumor is not high, selective cervical lymphatic dissection can be considered in principle. In the present case, recurrence and malignancy occurred 21 years after surgery and the disease was of long duration; therefore, postoperative follow-up, especially long-term follow-up in recurrent cases, is necessary and systemic examination may be performed to prevent distant metastases. CT and MRI can show features such as lesion morphology, size, blood supply, and growth characteristics, which are important for selection of the surgical modality and follow-up review.

CONCLUSION

In summary, we report a patient with PA that recurred multiple times after surgery and finally transformed to MC. During the first operation for PA, care should be taken not to rupture the envelope to prevent implantation of tumor cells, and when complete resection is not possible due to the anatomical site, postoperative radiotherapy should be performed to control the lesion and prevent infiltration and malignant transformation to MC. CT and MRI can provide accurate visualization and aid decision making for the surgical approach, which is important for clarifying clinical diagnosis and developing a treatment plan.

FOOTNOTES

Author contributions: Huang WP contributed to the acquisition and analysis of the work, drafted the manuscript, imaging data collection and analysis; Li LM contributed to the manuscript editing; Gao JB wrote the review and editing; all authors met the requirements for authorship for the submitted version and agreed to its submission.

Informed consent statement: Participant gave written consent to participate in the study.

Conflict-of-interest statement: The authors declare that they have no competing interests.

CARE Checklist (2016) statement: The authors have read the CARE Checklist (2016), and the manuscript was prepared and revised according to the CARE Checklist (2016).

Country/Territory of origin: China

ORCID number: Wen-Peng Huang 0000-0002-9104-1494; Li-Ming Li 0000-0002-2910-9742; Jian-Bo Gao 0000-0003-2621-3701.

S-Editor: Fan JR
L-Editor: A
P-Editor: Fan JR

REFERENCES

1 **Xu B**, Mneimneh W, Torrence DE, Higgins K, Klimstra D, Ghossein R, Katabi N. Misinterpreted Myoepithelial Carcinoma of Salivary Gland: A Challenging and Potentially Significant Pitfall. *Am J Surg Pathol* 2019; **43**: 601-609 [PMID: 30789358 DOI: 10.1097/PAS.0000000000001218]

2 **Petersson F**, Chao SS, Ng SB. Anaplastic myoepithelial carcinoma of the sinonasal tract: an underrecognized salivary-type tumor among the sinonasal small round blue cell malignancies? *Head Neck Pathol* 2011; **5**: 144-153 [PMID: 21104210 DOI: 10.1007/s12105-010-0226-y]

3 **Erickson LA**. Pleomorphic Adenoma in the Parotid Gland. *Mayo Clin Proc* 2017; **92**: e55-e56 [PMID: 28259235 DOI: 10.1016/j.mayocp.2017.01.006]

4 **Hernandez-Prera JC**, Skálová A, Franchi A, Rinaldo A, Vander Poorten V, Zbären P, Ferlito A, Wenig BM. Pleomorphic adenoma: the great mimicker of malignancy. *Histopathology* 2021; **79**: 279-290 [PMID: 33368685 DOI: 10.1111/his.14322]

5 **Lewis JE**, Olsen KD, Sebo TJ. Carcinoma ex pleomorphic adenoma: pathologic analysis of 73 cases. *Hum Pathol* 2001; **32**: 596-604 [PMID: 11431714 DOI: 10.1053/hupa.2001.25000]

6 **Yin LX**, Van Abel KM, Rooker SA, Nagelschneider AA, Olsen KD, Price DL, Janus JR, Kasperbauer JL, Moore EJ. Risk factors for carcinoma ex pleomorphic adenoma in patients presenting with recurrence after resection of pleomorphic adenoma. *Head Neck* 2021; **43**: 419-427 [PMID: 33043539 DOI: 10.1002/hed.26489]

7 **Hu Y**, Xia L, Zhang C, Xia R, Tian Z, Li J. Clinicopathologic Features and Prognostic Factors of Widely Invasive Carcinoma Ex Pleomorphic Adenoma of Parotid Gland: A Clinicopathologic Analysis of 126 Cases in a Chinese Population. *J Oral Maxillofac Surg* 2020; **78**: 2247-2257 [PMID: 32649893 DOI: 10.1016/j.joms.2020.06.013]

8 **Miccio JA**, Oladeru OT, Yang J, Xue Y, Hoda ST, Ryu S, Stessin AM, Parker RI. Myoepithelial Carcinoma: The Role of Radiation Therapy. A Case Report and Analysis of Data From the Surveillance, Epidemiology, and End Results (SEER) Registry. *J Pediatr Hematol Oncol* 2016; **38**: 274-278 [PMID: 26886377 DOI: 10.1097/MPH.0000000000000508]

Published by **Baishideng Publishing Group Inc**
7041 Koll Center Parkway, Suite 160, Pleasanton, CA 94566, USA
Telephone: +1-925-3991568
E-mail: bpgoffice@wjgnet.com
Help Desk: https://www.f6publishing.com/helpdesk
https://www.wjgnet.com